

Dottorato in
DINAMICA INTERNA DEI SISTEMI VULCANICI E RISCHI
IDROGEOLOGICO-AMBIENTALI

PhD in
INTERNAL DYNAMICS OF VOLCANIC SYSTEMS and
HYDROGEOLOGICAL-ENVIRONMENTAL RISKS
XXVI CICLO
Ph. D. Thesis

Investigation on Pollution Level in Surface Sediments of
Coastal Area, the Case of Naples and Salerno Gulfs, and *in*
***situ* Laboratory Raman Researches**

Wang Menghan

Advisors:

Prof. Benedetto De Vivo (Università di Naples “Federico II”, Naples, Italy)

Prof. Wanjun Lu (China University of Geosciences, Wuhan, China)

March 31st, 2014

Acknowledgement

Abstract

Chapter 1

Overview

Chapter 2

Environmental geochemistry study of Campania region in Italy: in land and in the sea.

Section 2.1

A case of compositional analysis and pollution impact estimation: Naples and Salerno Gulfs

Section 2.2

OCPs and PAHs in the Naples and Salerno Gulfs and ecological risk assessment of organic pollutants

Section 2.3

Polycyclic aromatic hydrocarbons in the soils of a densely populated region and associated human health risks: the Campania Plain (Southern Italy) case study

Section 2.4

Investigation on Inorganic Pollution Level in Surface Sediments of Naples and Salerno Bay

Chapter 3

Laboratory Raman in situ researches of fluid systems and iron minerals changes

Section 3.1

In situ Raman spectroscopic study of diffusion coefficients of methane in liquid water under high pressure and wide temperatures

Section 3.2

Pressure and temperature dependence of the Raman peak intensity ratio of asymmetric stretching vibration (ν_3) and asymmetric bending overtone ($2\nu_2$) of methane

Section 3.3

The effects of CH_4 and CO_2 on the sulfidization of goethite and magnetite – an in-situ Raman spectroscopic study in the high-pressure capillary optical cells at room temperature

Chapter 4

Surface enhanced Raman scattering applied to in-situ geochemistry

Section 4.1

In situ extraction and SERS analysis of organic compounds

Section 4.2

Sensitive SERS Detection of Nitroaromatic Pollutants in Water

Appendix A

Maps of inorganic elements distribution in the Naples and Salerno Gulfs

Appendix B

Maps of PAH (Polycyclic Aromatic Hydrocarbons) distribution in the Naples and Salerno Gulfs

Appendix C

Maps of OCPs (Organochlorinated Pesticides) in the Naples and Salerno Gulfs

Acknowledgement

First of all, I would like to thank Prof. Benedetto De Vivo. Prof. De Vivo kindly enrolled me to his group and totally supports my proposal. Prof. De Vivo provides me this chance to study abroad, which deeply influences me. I am encouraged by Prof. De Vivo to purchase innovative aims from all the possibilities.

I must thank to Dr. Stefano Albanese. From the time I landed at Naples the first time, Dr. Albanese helped me not only academically but also helped me settled down in this city. Dr. Albanese guided me in the area of environmental geochemistry. Also I need to thank to Dr. Antonio Cosenza, Dr. Diego Civitillo, Dr. Rosario Esposito and Dr. Claudia Cannatelli. I have worked together with them joyfully and helpfully.

I also thank to Prof. Wanjun Lu, in China University of Geosciences (Wuhan). Prof. Lu is also my master tutor, and guided me in the area of Raman scattering and in situ experiments. Also thanks to him, I had the idea of SERS.

Thanks to Prof. Maurizio Muniz-Miranda, in University of Florence, I could realize my first trial of SERS. Prof. Muniz-Miranda taught me lots of knowledge concerns about SERS and relative techniques.

Thanks to Dr. Marco Sacchi and Dr. Flavia Molisso, from C.N.R geomare in Napoli, I received sediments of Naples and Salerno Gulfs, which are the basic material of my thesis. Also thanks to Prof. Shihua Qi, from China University of Geosciences, I can have organic analysis results.

In addition, I want to thank my friends here in Naples and in Wuhan, they have accompanied me for these three years.

Also I want to thank the city, Naples. *Lo amo Napoli.*

Last but not least, I want to express my deeply thanks to my family. They tolerate my caprice and also support my own decision. Thanks to my wife Ms. Na Zhao a lot. Finally, this thesis is dedicated to her and our coming baby.

ABSTRACT

Environmental geochemistry is a major branch of regional geochemistry. In this thesis are presented the environmental geochemical investigation of Campania Plain and Naples and Salerno Gulfs in South Italy, concerning potential toxic elements and organic compounds distribution. Multivariate and univariate analysis are used to illustrate distribution and sources of elements and organic compounds, both on land and in sea sediments for Naples and Salerno Gulfs. Different pollution impact factors and risk assessment factors are estimated for soils and sediments that easily comes to contact with human beings. The results suggest that Naples city territory, and Naples and Pozzuoli Gulfs are characterized by highly incremental lifetime cancer risk.

An attempt of applying in situ Raman spectroscopic detection of pollutants started with a series of laboratory experiments. With the help of capillary high pressure optical cell, following results are achieved: 1) methane diffusion coefficients in water under high pressure and wide temperature range, and the relationship of diffusion coefficients with temperature was established; 2) Raman intensity ratio of asymmetric stretching vibration (ν_3) and asymmetric bending overtone ($2\nu_2$) of methane were numerically described vs temperature, pressure and gas phase density; 3) reactions of goethite and magnetite with sulfide solutions under CH_4 and/or CO_2 atmospheres were monitored at room temperature. Pyrrhotite and mackinawite were observed in final products.

A demanding of innovative approach to detect organic contaminants encourages various researches to improve in-situ techniques. A new substrate embedding silver nanoparticles into siloxane polymer is used as the platform to generate Surface-Enhanced Raman Scattering (SERS). Polymer serves as supporting material of silver nanoparticles as well as a stationary phase. After a short period of extraction, certain partition of organic compounds from aqueous solution accumulates into polymer. When silver nanoparticles is in touch with organic compounds, enhanced Raman scattering is obtained with $10^4\sim 10^6$ orders of magnitude. Raman scattering is obtained. Because of these two-steps amplification, SERS, which is typical applied strictly at lab condition, could be compromised when applied for field survey.

Crystal violet (CV) is chosen to evaluate extraction properties of polymer. Color “transferring” indicates effective extraction of crystal violet into polymer. Intensive Raman bands include SERS effects and resonance scattering of CV. Low concentration of 4-nitrophenol (PNP) and 4-nitroaniline (PNA) in solution (as low as 10^{-7} M) are dropped onto substrate and generate SERS fingerprint. After subtracting Raman bands of polymer and silver salts, clear evidence indicates availability of macro SERS spectra. Micro SERS testifies compounds penetrating as depth as 200 μm from the surface.

CHAPTER 1

OVERVIEW

Introduction

Regional geochemistry is the study of the spatial variation in the chemical composition of materials at the surface of the Earth, on a scale of tens to thousands of kilometers, historically oriented towards mineral exploration (Garrett et al., 2008). Environmental geochemistry is a major branch of regional geochemistry, with similar study methods but more focusing on environmental and human health issues. Environmental geochemistry is assuming more relevance both at regional and local scale, because of the increasing concerns related to high pollution of different media (soil, water, vegetation).

Initial geochemical surveys dated back to several centuries ago for heavy minerals panning (Garrett et al., 2008). Until 1930s, Russian geologists firstly developed geographical investigation of elements (minerals), which was believed as the starts of modern regional geochemistry. Minerals were the initial target of survey, because gold (and other metals) rush (Hawkes and Webb, 1962) invoked the emergence and development of geochemistry survey.

Elements or oxides weights are measured for regional geochemistry studies. Concentrations are expressed in weight fraction (wt% or ppm) of sample's composition. All the elements could be divided into three groups: major (>1%), minor (0.1~1%) and trace (<0.1%). Trace elements distributions provide significant information of particular geological or environmental bodies (Hawkes, 1976). Potential Toxic Elements (PTSs) (eg. Hg, As) mainly belong to trace elements; their anomalies in the environment may cause major damage to human health (Adriano, 2001).

Differently from rock sample, environmental samples are generally taken at the surface. Soil, sediment and stream water are the major source of environmental geochemical samples (Manahan, 2005). The evolution of sample source implies a more concern on anthropogenic influence to regional geochemistry. In fact, majority of studies are concerned about pollutants in environment (Manahan, 2005). The concerning also invokes investigation of organic pollutants (Fu et al., 2003). Harmful organic compounds, as the inorganics ones, also exist in natural environment independently from human activities, but vast input has occurred since the industrial revolution. Most harmful compounds include Polycyclic Aromatic Hydrocarbons (PAHs), Polychlorinated Biphenyls (PCBs) and Organochlorine Pesticides (OCPs). The above compounds attract intensive studies mainly because they form a new category of pollutants: POPs (Persistent Organic Pollutants) (Jones and De Voogt, 1999). POPs exhibit following four characteristics: 1) high toxicity: small quantity of POPs

may cause severe damage; 2) persistency: POPs are resistant to photolysis, chemolysis and biolysis; 3) accumulation: POPs are hydrophobic and lipophilic, as a consequence they accumulate in soil, sediment and biological adipose tissue; 4) mobility: most POPs are semi-volatile and they easily migrate in the atmosphere (Kukkonen et al., 2003).

Extensions and applications of environmental geochemistry are interrelated with other subjects. Environmental (Albanese et al., 2007) and health (Albanese, 2008) issues are closely related to medical disciplines. Evaluation of contaminants source is another primary goal when anomalies of PTEs or POPs are found in the environment (De Vivo et al., 2004). Shape analysis of chemical distribution is useful for finding the sources (Lima et al., 2003). Other useful approaches include diagnostic ratio (Jiang et al., 2009; Soclo et al., 2000; Yunker et al., 2002), dynamic analysis and topological analysis. Risk assessment (CCME, 2002; Long et al., 1995) is more convincing when combined with geochemical distribution information. Other related subjects include medical issue (Martyn et al., 1989), remediation and environmental managements.

Geographic Information System (GIS) based approach is used to generate maps in different scales. The results of geochemical survey are commonly expressed in maps, dot maps or interpolation maps. Dot maps exhibit concentration locally strictly related to sampling sites. For interpolation maps, a numerical process is operated to generate new data points within the range of a discrete set of known data points. Filled contour maps with different colors are used to show concentration of elements (compounds) in different color pixel (McBratney et al., 2003).

Related geostatistical studies also attract global scientists (Davis, 1986; Reimann et al., 2011; Carranza, 2008) Factor and cluster analysis help to identify intrerelationships existing between different elements and controlling factors. Normality analysis is always run in the first step to evaluate the type of data distribution. When data distribution is not normal, a further transformation is needed. A branch of environmental geochemistry concerns about the rationality of data distribution and it try to solve problems with compositional analysis (Reimann et al., 2011). Raw data of geochemical sampling is expressed as concentration of elements, commonly expressed in compositional form, such as mg/kg or ppm. Such expression is consistent to the chemical analysis methodology and established by usage. However, compositional data is problematic to interpret because no single variable varies independently. Univariate analysis is doubtful when dealing with compositional data. Researches for solving compositional data problems have been developed for

almost three decades (Reimann et al., 2011). A satisfactory approach for statistician as well as geochemist is still on the way. Up to date, logratio transformation is the most admitted approach to cope with dependent variables. Three major expressions have been developed, which are, additive logratio transform, centered logratio transform and isometric logratio transform. But each of the expression introduces certain new problems. In some cases, transformed data covers useful information.

Improvements of environmental geochemistry also rely on the development of detection instruments. Concentration of POPs in soils, sediments and aqueous systems are commonly measured with proven technique, such as Gas Chromatography (GC). Samples are washed and then concentrated with stationary phase, such as hexane. Extracted POPs are heated and passed through a GC column, in which each gas moves through the column at a different rate. Combined with Mass Spectrometry (MS), different POPs can be determined quantitatively at the same time.

However, demanding of *in-situ* detection techniques requires advanced technologies to replace GC-MS. The next generation technology should be rapid, non-destructive and portable. Spectroscopic approaches, such as infrared absorption, Raman and fluorescence, which are the most suitable alternatives.

Raman spectroscopy allows the identification of different molecules on the basis of their vibrational bands, providing an unambiguous molecular fingerprint. However, the low sensitivity of Raman scattering, along with possible spectral interference due to fluorescence emission, impairs the use of this technique for the recognition of molecules in trace concentration.

In these cases can be used the Surface-Enhanced Raman Scattering (SERS) effect, which is able to enhance the Raman intensity of molecules adsorbed on metal substrates by many orders of magnitude and to promote a drastic quenching of fluorescence. Huge magnifications of the Raman signal are observed when a molecule adheres to nanostructured surfaces of metals with high optical reflectivity, such as Ag, Au and Cu. The SERS enhancement factors are generally up to 10^7 with respect to the Raman intensities of non-adsorbed molecules. By means of experimental procedures that combine microscopy and spectral observation beyond the light diffraction limit, 10^{14} - 10^{15} enhancement factors are reached, thus ensuring single-molecule detection. Thanks to its peculiar properties, SERS spectroscopy, since its discovery at the beginning of the seventies, has achieved a leading role in the analytical investigation of very low traces of contaminants, allowing the

spectroscopic detection at sub-picogram level.

Research aims

The scope of the PhD thesis includes two aspects: 1) illustration of geochemical distribution of PTEs and POPs in Campania region and nearby seas; 2) apply Raman techniques, including SERS, for geochemical detection of pollutants.

The first aim is achieved describing the inorganics and organics distribution in Naples and Salerno gulfs and in the soils of Naples and Caserta areas. This section of the study utilizes different geostatistical approaches to show the chemical distribution of both inorganic and organic pollutants patterns, with the purpose of pointing out geogenic from anthropogenic source. Among inorganic elements, the harmful ones for health, such as heavy metals, have been emphasized and evaluated in terms of relative risk assessment. After heavy metals, POPs have been also represented by mean of spatial analysis and evaluated in terms of risk assessment as well.

The second aim has been achieved investigating new detection approach for organic environmental contaminants. In this study, a combination of SERS with SPME (Solid Phase MicroExtraction) has been proposed as the final solution. Before applying advanced SERS techniques, a series Raman experiments has been conducted, obtaining results concerning CO₂ diffusion, methane peaks and iron sulfide minerals. Finally, by SERS technique experimental work, a prototype has been proposed able to detect 10⁻⁷ mol/L nitroaromatic compounds.

Articles in the PhD Thesis

1. *A case of compositional analysis and pollution impact estimation: Naples and Salerno Gulfs* by Wang M., Albanese S., Lima A., Lu W., Molisso F., Sacchi M. and De Vivo B. Paper submitted to *Journal of Geochemical Exploration*

Aim of the paper is to comprehensively present the elements distribution in Naples and Salerno Gulfs. Factor analysis was used to clarify selected 26 elements into three groups: geogenic, water dynamic and anthropogenic. Concentrations of elements were additively logratio transformed using concentration of aluminum as reference. Discussion of advantages and disadvantages of logratio transformation was included. Pollution impacts were executed based on surface average concentration of study area. The results indicate that Bagnoli coastal area is characterized by heavy

metals distribution potentially harmful for citizens.

2. OCPs and PAHs in the Naples and Salerno Gulfs and ecological risk assessment of organic pollutants by Wang M., Albanese S., Lima A., Lu W., Molisso F., Sacchi M. and De Vivo B. Paper submitted to *Environmental Geochemistry and Health*.

Aim of the paper is to illustrate distribution patterns of organic pollutants in the Naples and Salerno Gulfs. Ecological risk assessment is conducted for organic pollutants, taking into account the most advanced studies as guidelines. The results point out that Bagnoli coastal area is at highly risk compared with other sector of the investigated Gulfs. PAHs diagnostic ratio analysis indicates solid combustion as the primary source of PAHs in sediments.

3. Investigation on Inorganic Pollution Level in Surface Sediments of Naples and Salerno Bay, by Wang M., Albanese S., De Vivo B., Lima A., Lu W., Molisso F. and Sacchi M. Paper published in *Computational Water, Energy, and Environmental Engineering*, 2013, Volume 2, Pages 36-40.

The paper concerns the same topic of as the article #1. However, the compositional data was transformed with the centered log-ratio transformation. In this approach, the geometric mean value serves as denominator to generate ratio values.

4. Polycyclic aromatic hydrocarbons in the soils of a densely populated region and associated human health risks: the Campania Plain (Southern Italy) case study, by Albanese S., Fontaine B., Chen W., Lima A., Piccolo A., Qi S., Wang M. and De Vivo B. Paper accepted by *Environmental Geochemistry and Health* and in progress.

In this paper, the behavior and the distribution patterns of sixteen PAHs, listed as priority pollutants by the United States Environmental Protection Agency (USEPA), were evaluated in 119 soil samples collected in different areas of Campania region, Southern Italy. In accordance with the Italian environmental law (D. Lgs. 152/2006) some of the investigated areas should be considered potentially contaminated and not suitable for a residential use unless an environmental risk analysis does not demonstrate their safety.

5. In situ Raman spectroscopic study of diffusion coefficients of methane in liquid water under high pressure and wide temperatures, by Guo H., Chen Y., Lu W., Li L. and Wang M. Paper published in *Fluid Phase Equilibrium*, 2013, in Volume 360, Pages 274-278.

The aim of the research has been to apply in situ Raman for measuring diffusion coefficients of

methane. The results are obtained under elevated temperature and pressure which far expands the range resulting from previous studies.

6. *Pressure and temperature dependence of the Raman peak intensity ratio of asymmetric stretching vibration (ν_3) and asymmetric bending overtone ($2\nu_2$) of methane*, by Wang M., Lu W., Qiao S. and Li L. Paper accepted by *Applied Spectroscopy* (in press).

The aim of the paper is to illustrate numerical relations of a newly discovered methane Raman parameter. The Raman peak intensity ratio depends strictly on temperature and pressure of the system strictly. A numerical model was given to describe the relationships.

7. *The effects of CH_4 and CO_2 on the sulfidization of goethite and magnetite – an in-situ Raman spectroscopic study in the high-pressure capillary optical cells at room temperature*, by Wang M., Lu W., Chou IM. and De Vivo B. Paper submitted to *European Journal of Mineralogy*.

The aim of the paper is to describe the process of iron oxide minerals changing to iron sulfide minerals under high pressure. The study finds the significant role that CO_2 plays in the reaction. CO_2 initiates and accelerates minerals changes and also progresses dissolution of iron sulfide minerals. In addition, CO_2 in vapor phase urges the presence of thermodynamic stable iron sulfide minerals.

8. *Sensitive SERS Detection of Nitroaromatic Pollutants in Water*, by Wang M, Lu W., De Vivo B. and Muniz-Miranda M. Paper accepted by *Applied Spectroscopy* (in press).

The aim of the research was to apply the innovative SERS substrate to detect environment pollutants. The SERS active silver nanoparticles were successfully embedded into polymer matrix which could extract organics from aqueous solution. An application of the substrate to detect nitroaromatic compounds proves the limitation of detection could be lower than 10^{-7} .

ENVIRONMENTAL GEOCHEMISTRY STUDY OF CAMPANIA REGION, ITALY: IN LAND AND IN THE SEA

In the next paragraphs will be summarized the main results of environmental studies carried with geochemical investigations on sea (marine sediments) and land (soils), reported in the above listed papers n. 1, 2, 3 and 4. I summarize, first the content of the investigation on marine sea sediments (Papers n. 1, 2 and 3) and after the investigations on soils (Paper n. 4).

Summary of papers N. 1, 2 and 3.

Study area

Naples and Salerno Gulfs are located along the Eastern Tyrrhenian Sea, separated by Sorrento peninsula. Naples Gulf is semi-closed by Ischia and Procida islands in NW, Campi Fregrei and Campanian plain in NE, and Sorrento peninsula in SE, while Salerno Gulf locates on the coastal area offshore of Sele plain. Naples has second population density in Italy, in metropolitan area, around 4.4 million citizen habitat, while Salerno has a population of 140 thousand (Fig. 1).

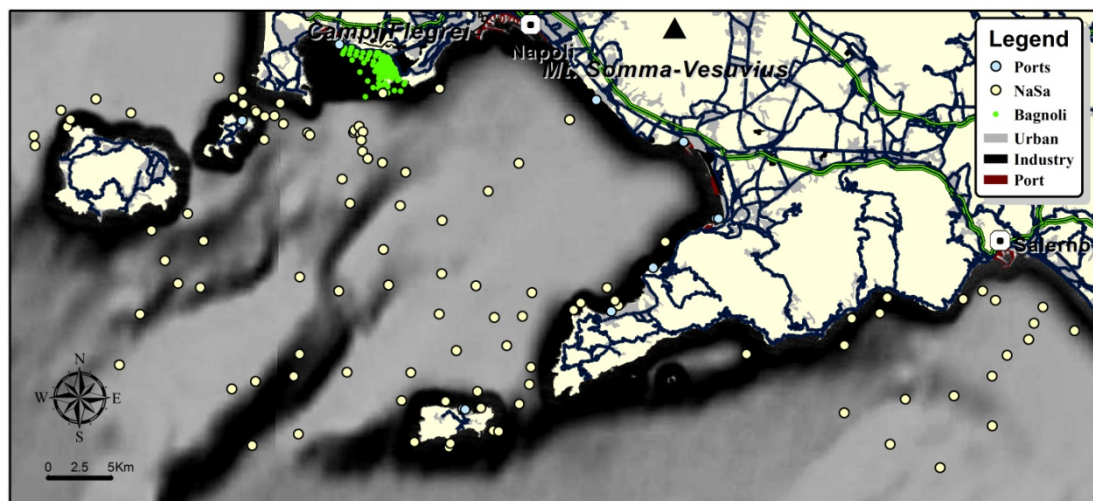


Figure 1. Study area and sampling sites of sediments

The Tyrrhenian Sea is the result of Miocene-Quaternary extension contemporaneously to

eastward accretion and anticlockwise rotation of the Apenninic fold and thrust belt during the roll-back of the subducting Adria plate. The Campanian Plain and Naples Gulf are an integral basin, as well as Sele Plain combined with Salerno Gulf, both of which are parts of half-graben basins developed in eastern Tyrrhenian margin.

Sea floor of Naples and Salerno Gulfs are covered by Plio-Quaternary sedimentary and pyroclastic fall deposits. Two small coalescent deltas, Sebeto delta and Sarno delta, characterize eastern depositional system of Naples Gulf (Insinga et al., 2008). Along Sorrento peninsula, Capri Island and Salerno Gulf, Mesozoic-Cenozoic carbonate units also influence the composition of surface sediment.

Volcanic process during the late Quaternary has significant influence on morphology and deposits in Naples Gulf. Several volcanic eruptions happened in Campania Plain (Campi Flegrei, Ischia and Mt Somma-Vesuvius) during Quaternary, producing among others, Campanian Ignimbrite 39 ka B.C (De Vivo et al., 2001) and Neapolitan Yellow Tuff 12 ka B.C. (De Vivo et al., 2010).

Naples and Salerno provinces are among the most touristic regions around Mediterranean Sea. The port of Naples is one of the most important port in Europe, and has one of the highest level of passengers flow in the Mediterranean sea. Naples is one of the most important transportation centers in south Italy, including railway, highway and various roads. Agriculture is still the basic income of economy, being recently partially replaced by service industries. Various stream system in Campania plain and Sele plain carry related products and fertilizers into the sea.

In Bagnoli area, a large industrial area (brownfield site) had been dismantled between 1990 and 2000. The area used to concentrate various industries, such as steel production, asbestos materials manufacturing, cement production and fertilizer production. Although it is going through remediation by Italian Government, industrial relicts still concentrate in soil, as well as sediment in Bagnoli bay (Albanese et al., 2010).

Material and methods

Sampling and sample preparation

Sediments from three field sampling activities are included in this study. General survey of sea sediments in Naples and Salerno Gulfs (NaSa) provided regional information. Geochemical surveys of Bagnoli site (BaSi) and ports around Naples Gulf (PoNa) were focused on concentration of

pollutants.

Sediment samples (following the directives of the national program for assessment of marine pollution of highly contaminated Italian coastal areas) were collected from 230 locations (Fig. 1). Differential global positioning system (DGPS) was used to identify each location precisely.

Among NaSa samples (May, 2000), 23 samples were collected using a box-corer with an inner diameter of 25 cm, of which superficial sediments were analyzed in this study and other 63 NaSa samples were collected by grab by *C.N.R. Istituto Geomare Sud, Naples*. BaSi samples (between November 2004 and March 2005) included surface sediments (0-20 cm) of 123 boreholes along the coastline. PoNa samples (2003) included surface sediments (0-20 cm) of 11 boreholes.

From May to July 2011, 186 samples (surface and bottom) had been subset in Geomare CNR Institute (Naples), including 35 box corer sediment samples and 80 grab sediment samples. Most of box corer samples were divided into two parts, surface (or subsurface) and bottom sediment, as well as some of grabbing samples. Each sample were subset into three parts, 30g for metal and inorganic analysis, 100g for organic analysis and rest were stored in Geomare as backup.

Chemical analysis

Inorganic Elements: 1) NaSa sediment samples were analyzed by Acme Analytical Laboratories Ltd. (Vancouver, Canada), through its Italian affiliate (Norwest Italia Srl, Naples) with Inductively Coupled Plasma Mass Spectrometry (ICP-MS) and Atomic Emission Spectrometry (ICP-AES). 2) Analyses of elements (Al, Sb, As, Be, Cd, Co, Cr, P, Hg, Ni, Pb, Cu, Se, Sn, V, Ta and Zn) on the ports of Naples sediment samples and metals (Al, As, Be, Cd, Co, Cr, Fe, Hg, Mn, Ni, Pb, Cu, Sn, V, and Zn) of Bagnoli site sediments were performed by ICRAM Laboratories with Inductively Coupled Plasma-Optical Emission Spectrometry (ICP-OES) and Atomic Absorption Spectroscopy (AAS).

Polycyclic Aromatic Hydrocarbons (PAHs) and Organochlorine Pesticides (OCPs): PAHs and OCPs in sediments were concentrated to 0.2 ml under a gentle nitrogen stream and analyzed by Gas Chromatography-Mass Spectrometry (GC-MS). The analysis was carried out in Key Laboratory of Biogeology and Environmental Geology of the Ministry of Education (Wuhan, P.R.C)

Numerical analysis

Background of PTEs (Potential Toxic Elements):

Background value of PTEs for risk assessment was determined based on NaSa samples. Multivariate analyses were applied to NaSa data to group elements to speculate about the sources. Risk assessments were focused on BaSi and PoNa samples. Univariate analysis was applied to eight most concerned heavy metals of entire dataset, as well as ERA (Ecological Risk Assessment).

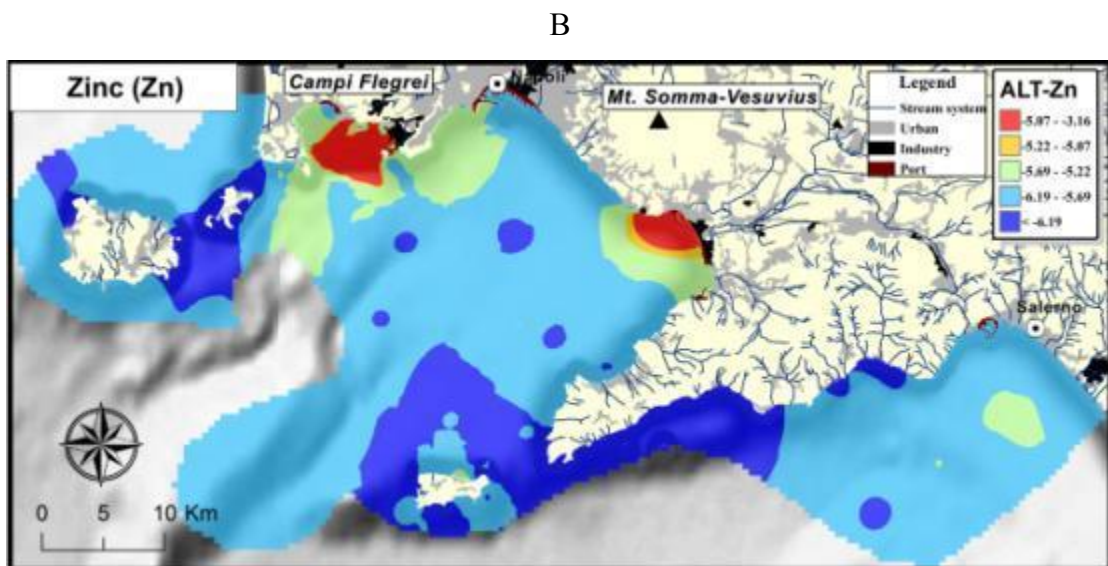
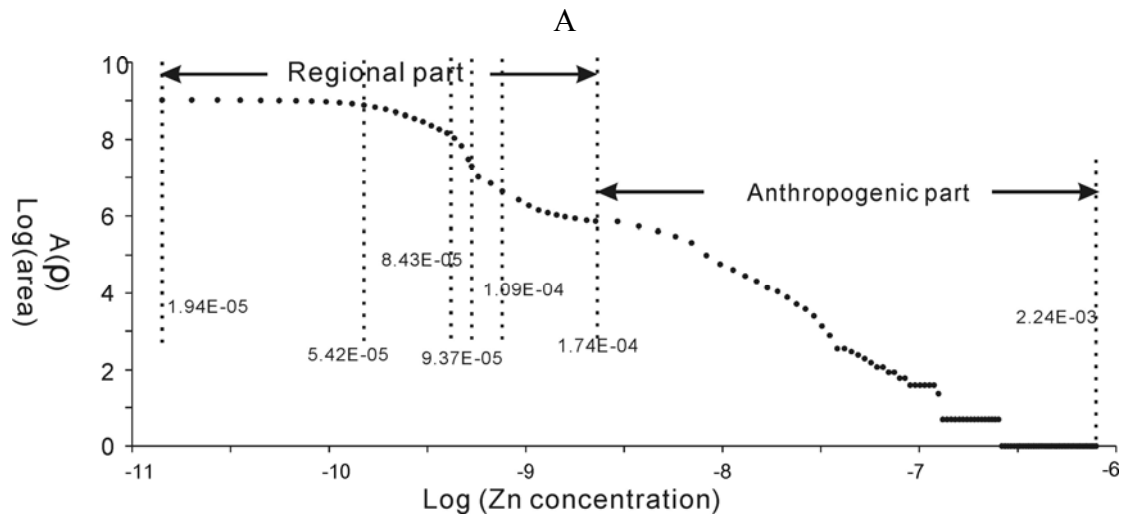
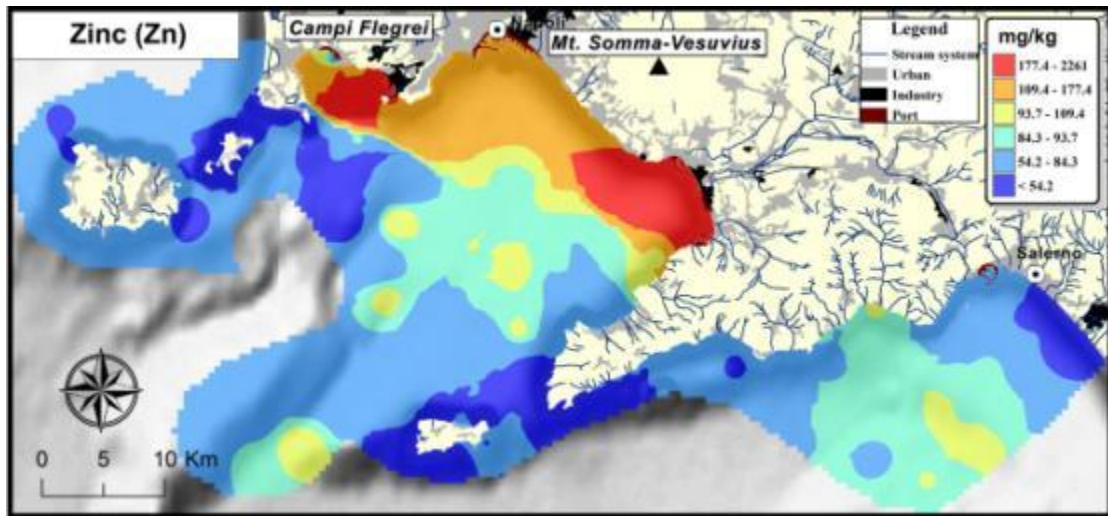
Geostatistical analysis and generation of interpolation maps

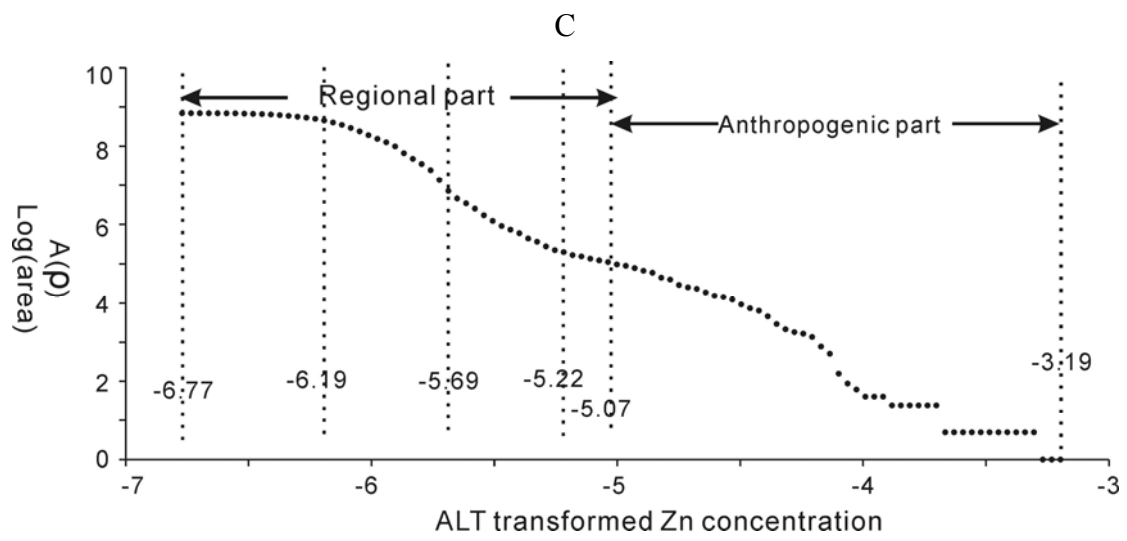
Factor analysis help to identify relationships between different elements and get informations on controlling factors. Additive Log-ratio Transformation (ALT) was used to solve the problems of dependences among elements compositions. The comparative results exhibited advantages and disadvantages of transformed data.

The production of geochemical maps for Naples and Salerno Gulf sediment results, using Arcgis and GeoDAS (Cheng, 2001), is described by presenting, as an example, a complete set of geochemical maps produced for Zn (Fig. 2A). The usefulness of this technique in environmental studies has already been demonstrated (Lima et al., 2003).

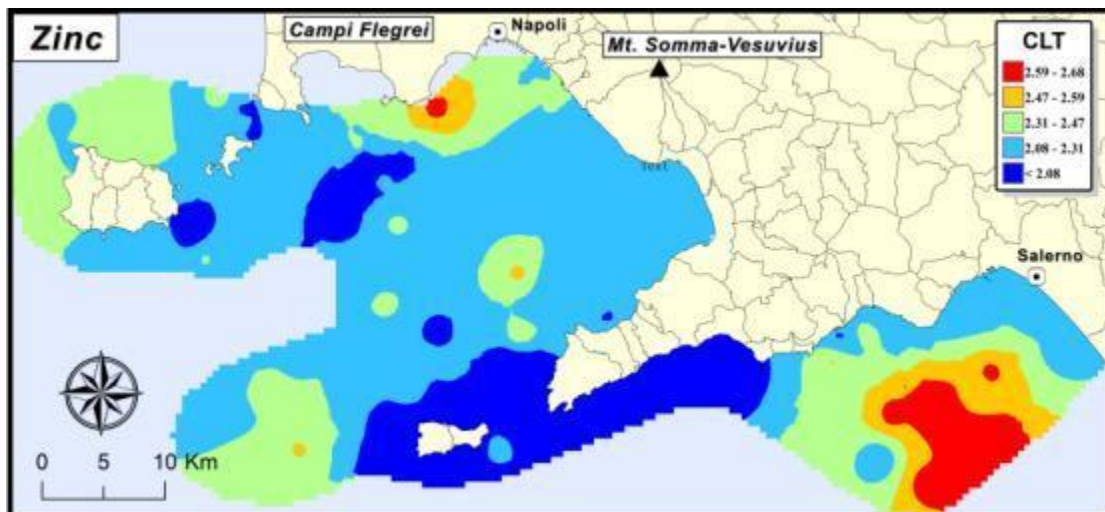
Both original concentration data, ALT and CLT (Centered Log-ratio Transformation) transformations were used to generate geochemical distribution maps with inverse distance weighted (IDW) algorithm as the interpolation method.

Concentration-area (C-A) plot (Fig. 2B, Fig. 2D and Fig. 2E) illustrates a fractal analysis of data distribution in the area. In this plot, the vertical axis represents log value of cumulative pixel areas $A(\rho)$. $A(\rho)$ means areas with element concentration greater than ρ . ρ is shown in horizontal axis in log value for unconverted data, while for ALT and CLT data ρ is shown as it is. The C-A plot is first divided into two parts for original concentration and ALT: regional concentration and anthropogenic concentration, divided by the maximum value of NaSa data. Regional part is consequently divided based on fractal analysis. Because CLT transformation only covered NaSa samples, the results were compared to regional part in the other two maps. Divisions of C-A plot are applied as classes on interpolation maps in color scale.





D



E

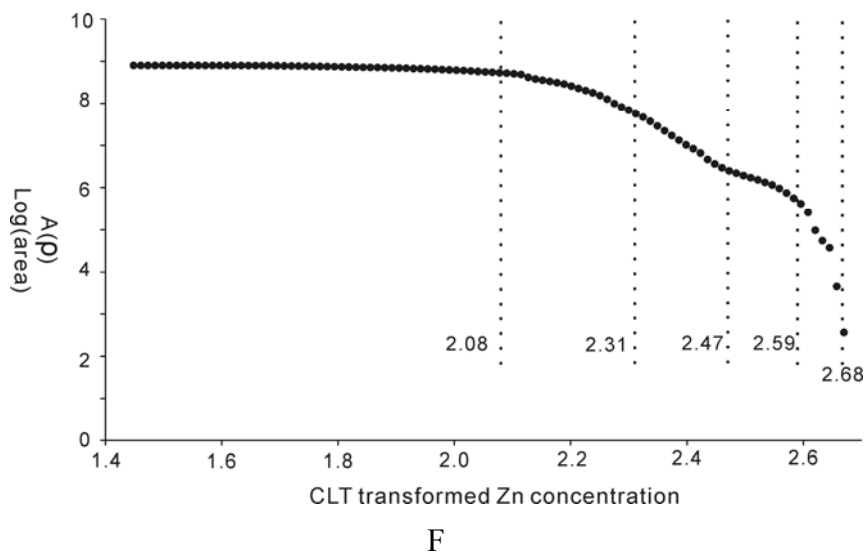


Figure 2. (A) Interpolation map of original Zn value in mg/kg. (B) Fractal concentration-area (C-A method) plot for Interpolation map of original Zn value in mg/kg. (C) Interpolation map of Additive Log-ratio Transformed (ALT) Zn value. (D) Fractal C-A plot for Interpolation map of ALT Zn value. (E) Interpolation map of Centered Log-ratio Transformed (CLT) Zn value. (F) Fractal C-A plot for Interpolation map of CLT Zn value.

Risk assessments

Background value estimation

Bagnoli area and ports exhibit very high concentration of PTEs. The investigation of entire region set an opportunity to estimate regional background. In this study, mean value of NaSa samples is used as reference background value (eliminate the outlier near Capo Posillipo, GRNN 4).

Estimation of pollutant impact

Numbers of factors (Abraham and Parker, 2008; Chapman and Wang, 2001; Harrison et al., 2003; Lu et al., 2009; Ridgway and Shimmield, 2002; Santos et al., 2005) have been put forward for quantifying the degree of metal enrichment in sediments. In this study, three PIA parameters are selected to study pollutant impact. Enrichment factor (**EF**), Geoaccumulation index (**I_{geo}**), Degree of contamination (**D_c**), Incremental Lifetime Cancer Risk (**ILCR**) and Percentage of risk samples (**P_r**) were estimated in this study.

PAHs diagnostic ratio:

Five PAHs diagnostic ratio were selected to infer the source of PAHs in the area: An/178, BaA/228, Fluo/Fluo+PY, IP/IP+Bghi and $\sum\text{COMB}/\sum\text{PAH}$.

Results

Compositional analysis

A debate on correctness of compositional data lasted for decades (Aitchison, 1982; Filzmoser et al., 2009; Reimann and Filzmoser, 2000). Comparing results of original data and transformed data are performed on interpolated maps of heavy metals in Naples and Salerno Gulfs. Transformed data theoretically fit to realistic elements distribution. Transformed maps limit some heavy metals to their sources, such as Cd, Cr, Pb and Zn; and enlarge risk area of some others, such as Hg and Ni. Statistical characteristics of transformed data are more regular than original data; this is helpful in determining better class division. However, transformed results also introduce certain difficulties for interpretation and in adapting them to environmental estimation indexes. If the investigation only analyzes certain elements other than entire elements analysis, the results are highly influenced by the choice of ratio-denominator.

PTEs distribution

R mode factor analysis points out three element associations attributed to different sources: geogenic contribution, finer deposits due to water dynamic decreasing and anthropogenic activities. Because extreme high concentration in Bagnoli site coastal area and ports around Naples Gulf, areas with concentrated PTEs due to geological process was concealed in interpolation maps of single elements. However, after ALT transformation, sub-high concentration centres of certain elements (eg., Cr, Ni and Cu) indicate the effect of water dynamic.

Organic pollutants distribution

In sea sediments, PAHs are generally concentrated in the area closer to Bagnoli brownfield site, formerly occupied by heavy steel and other industries (Albanese et al., 2010). OCPs concentrations in the area are less severe than the PAHs concentrations.

Risk assessment

In the sediments, Pb, Zn, Cd and Hg are shown as the most risky elements in the area. More than 40% samples exhibit moderate to high degree of contamination. When considering ERA, Pb is the most risky elements in the area. For organic pollutants, most of compounds in open sea are with

concentration below the ones indicated by criteria of adverse biological effects. However, in the area closer to Bagnoli brownfield, over 80% of samples are bonded to risk quantity of PAHs. Creatures in contact with 20% to 45% of samples in the area may have intense biological harms. Beach recreation in the Gulf of Pozzuoli and out of Capo Posillipo is potentially harmful due to ILCR estimation of skin cancer. Also beaches nearby the ports around Naples Gulf are at the risk for baseline increase of cancer incidence.

Summary of paper n. 4

Paper n. 4 - *Polycyclic aromatic hydrocarbons in the soils of a densely populated region and associated human health risks: the Campania Plain (Southern Italy) case study*, by Albanese S., Fontaine B., Chen W., Lima A., Piccolo A., Qi S., Wang M. and De Vivo B. Paper accepted by *Environmental Geochemistry and Health*.

Polycyclic aromatic hydrocarbons (PAHs) are a major class of environmental pollutants mainly arising from anthropogenic activities. In this paper, the behavior and the distribution patterns of sixteen PAHs, listed as priority pollutants by the United States Environmental Protection Agency (USEPA), were evaluated in 119 soil samples collected in different areas of Campania region in the southern Italy. The study area covers about 2,400 km², roughly corresponding to the Campanian Plain which is a wide coastal belt that goes from the Volturno River plain, in the north-west of the Campania region, to the Sarno River basin, southward of the volcanic complex of Mt. Vesuvius. The observation of the geochemical distribution patterns showed that both high (HMW-PAHs) and low molecular weight PAHs (LMW-PAHs) are mostly concentrated within the metropolitan area of Naples, the Agro Aversano area and, partly, the Sarno River basin. In accordance with the Italian environmental law (D. Lgs. 152/2006) these areas should be considered potentially contaminated and not suitable for a residential use unless an environmental risk analysis does not demonstrate their safety. As a consequence, a preliminary quantitative risk assessment (PQRA) enhanced by the use of GIS was run revealing the existence of an incremental lifetime cancer risk higher than 1×10^{-5} for the city of Naples and for some other populous areas.

The results obtained by the PQRA in this study together with the epidemiological evidence of an

increased incidence of some cancer types in Campania pose the need of developing a detailed and multi-media based geochemical characterization of the regional territory to define, at least at regional scale, a conceptual model considering all the exposure pathways followed by contaminants to reach the human target from the emitting source. Soil, water, air, food should be taken into account and concentrations of metals and organic compound, such as PAHs, should be determined within these media to allow the development of a environmental risk analysis based on the effective concentrations of contaminant likely to come into contact with humans.

Although, in case of an objective risk to human health, little could be done to clean up the soils of a territory covering more than 1,000 km², the location and the control of the sources of emission of contaminants could be of crucial importance to recover the environment in the long term and the results of a risk assessment could be used, at least, to establish a priority order in the implementation of safety measures and remediation plans consistent with the available resources.

LABORATORY RAMAN *IN SITU* RESEARCHES OF FLUID SYSTEMS AND IRON MINERALS CHANGES

In the next paragraphs will be summerized the main results of Laboratory studies carried with with Raman, reported in the above listedpapers n. 5, 6 and 7:

***In situ* researches apparatus**

Capillary high pressure optical cells (CHPOC) were used in this study to carry on *in situ* experiments and observation. CHPOC was constructed from square or round cross-sectioned fused silica-capillary tubing (I.D. is from 50 µm to 300 µm while O.D. is from 100 µm to 600 µm respectively) and a high pressure valve plus heating-cooling stage that allows *in situ* Raman studies at pressures up to 100 MPa and temperature ranges from -80 °C to 400 °C. The same study conditions may be achieved by diamond anvil cells (DAC) but in the need of a much more complicated device.

Several key features of this cell include: (1) The ability to directly load sample fluids and monitor pressure during investigation, (2) the lack of optical distortion, (3) the small cell volume suitable for samples of limited supply, (4) the high pressures that can be achieved, (5) the high-magnification, high-numerical wall of the capillary tube, (6) the heating-cooling stage that allowed for temperature controlling, and (7) the observation of metastable transition phase of reactions (Fig. 3).

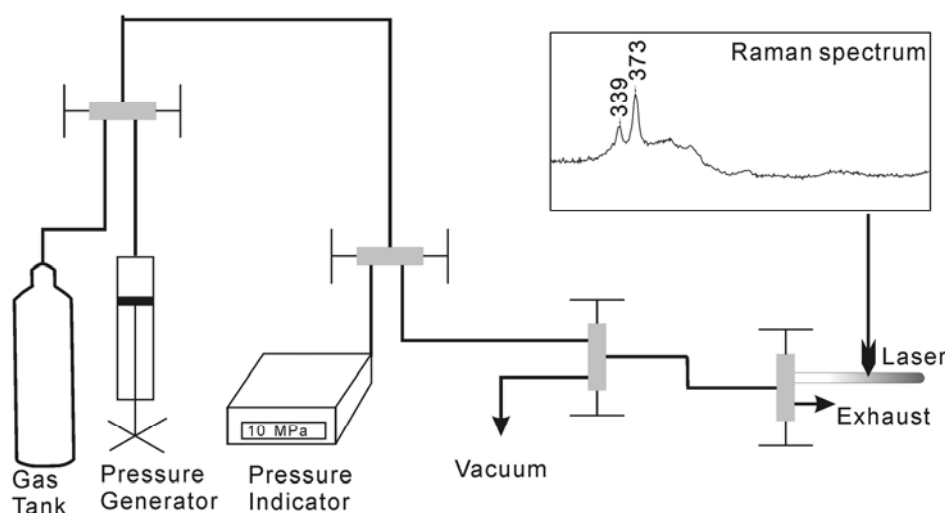


Figure 3. A schematic diagram of the experimental set up for collecting in situ Raman spectra of the sample in an CHPOC. The example Raman spectrum was derived from pyrrhotite.

Diffusion coefficients of methane in aqueous systems

Raman spectroscopy has been used for quantitative analysis for several decades. At constant temperature the concentration of dissolved methane is proportional to the Raman band intensity ratio of methane and water. Thus, we can use the quantitative Raman spectroscopic method to monitor in situ the concentration changes during methane diffusion in water under high pressure and elevated temperature. We have previously applied such quantitative Raman spectroscopic methods to determining the diffusion coefficients of methane in water at room temperature and under two pressures. In this study, the work was extended to the wider temperature and pressure ranges, from 273 to 473 K and from 5 to 40 MPa, to study the temperature and pressure effects on the diffusion coefficients of methane in water.

It is concluded that, diffusion coefficients of methane in water show Arrhenius behaviour only

at higher temperatures, the temperature dependence of the diffusion coefficients of methane in water can be fitted with Speedy – Angell power-law. The pressure effect is very small (Fig. 4).

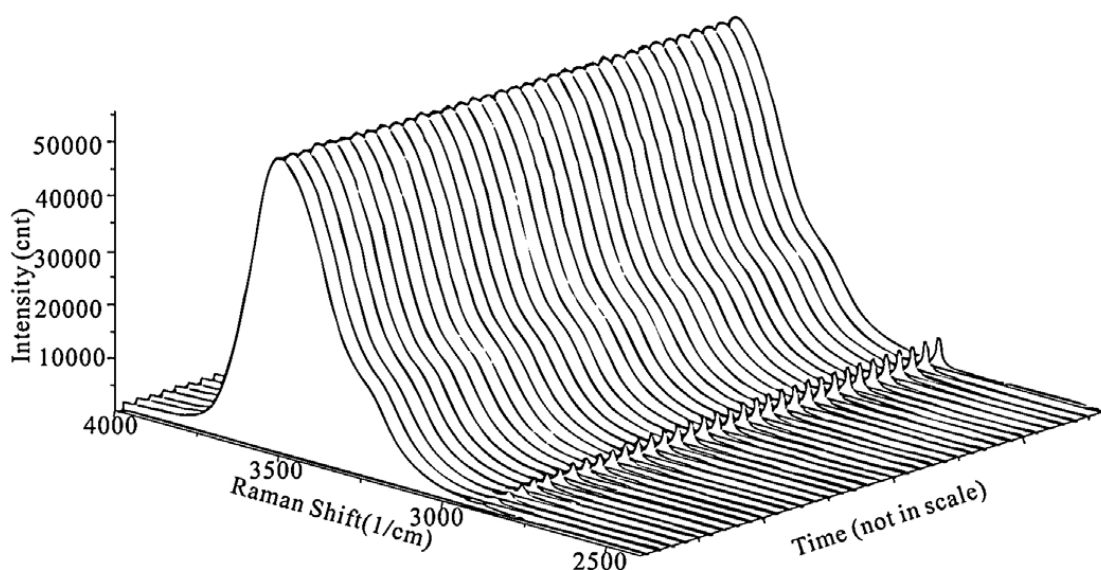


Figure 4. Time-dependent Raman spectra of dissolved methane (CH_4 , around 2910 cm^{-1}) and water (H_2O , around 3520 cm^{-1}) collected at the spot B (3.000 mm away from the spot A, and 14.911 mm away from the end of the tube), at different times after the after the water was pressurized by methane at 20 MPa and 473 K.

Asymmetric bands of methane dependences of temperature and pressure

Raman spectroscopy is also a powerful tool to study the properties of gas phase in fluid inclusions. Besides the most intensified C-H symmetric stretching band (ν_1), asymmetric stretching band (ν_3) and asymmetric bending band overtone ($2\nu_2$) are two primary bands with mediate intensity ($\sim 2\%$ intensity of ν_1). Peak intensity ratio (PIR) of ν_3 and $2\nu_2$ is found to systematically change with pressure at room temperature and the relationship between PIR and pressure seems to be independent to composition of natural gas. It is worthy to know how the relationship between the PIR and pressure is affected by temperature and the composition of the fluid samples, when we use PIR to accurately determine the pressure of methane-bearing fluid inclusion.

In this study, the PIR is studied for pure methane system at elevated pressures and temperatures. The relationship among peak intensity ratio, temperature, and pressure/density were derived with numerical equations. As a demonstration, the inner pressure and density of two methane inclusions were determined by Raman spectroscopic measurement of the peak intensity ratios of ν_3 and $2\nu_2$ (Fig. 5).

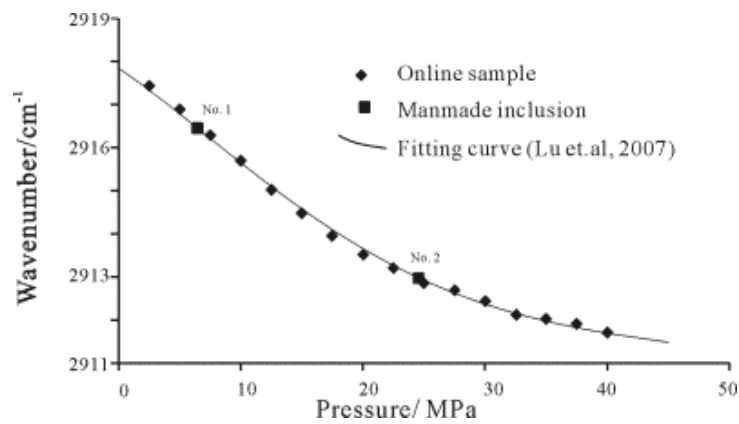


Figure 5. The fitting curve (solid line) followed the form of calculating methane vapor pressure with ν_1 peak position. Least square method is used to fit the laboratory standard ν_0 , which is determined as 2917.849 cm^{-1} . The corrected ν_1 peak position of manmade methane inclusions (solid squares) are 2916.456 cm^{-1} and 2912.972 cm^{-1} for No.1 and No.2 methane inclusion respectively. Followed Eq. 3, inner pressures of inclusions are 6.45 MPa and 24.54 MPa, respectively.

Sulfidation of iron minerals.

Various valences of iron sulfide minerals commonly appear at the transient depth between iron oxide reduction zone and sulfate reduction zone in marine sediments. Reactivity of iron oxide minerals towards sulfide is solely ascribed to various crystal structures. However, large discrepancy of reaction rate exists between different studies. The discrepancy is assumed as a result of different interstitial compositions and geochemical environments. For example, organoclastic related iron sulfides reflect concentrations of S and Fe in pore water (Haese et al., 1997), whereas methanotrophic source of iron sulfides indicate concentrations of methane and carbon dioxide in pore water.

Combined with high pressure optical cells, Raman spectroscopy shows advantages to monitor the evolution of minerals. Optical images and Raman spectra could demonstrate that under CH_4 atmosphere, pure Na_2S solution could coexist peacefully with iron oxide minerals. If CO_2 partially replaces CH_4 , intense reaction occurs not only to sulfide solution but also triggers iron oxide minerals sulfidation. The products in solution and vapor phase are different: in solution only appears iron monosulfide; in the vapor phase pyrrhotite is detected. The results serve as a possible explanation to anoxic environmental iron sulfide minerals.

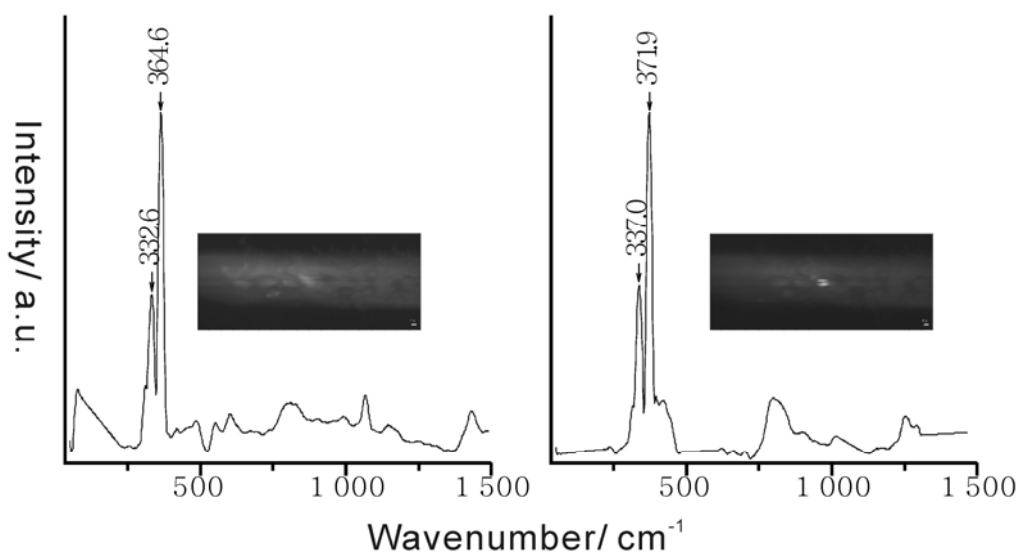


Figure 6. Raman spectra of iron sulfide minerals. Peaks at $\sim 333\text{ cm}^{-1}$ and $\sim 363\text{ cm}^{-1}$ (a), or 337 cm^{-1} and $\sim 372\text{ cm}^{-1}$ (b) indicate the occurrence of pyrrhotite. The white sample spot shined after excited by laser.

SURFACE ENHANCED RAMAN SCATTERING APPLIED TO *IN SITU* GEOCHEMISTRY

In the next paragraphs will be summarized the main results of Laboratory studies carried with with SERS, reported in the above listed paper n. 8:

Intense development of industries during last century has created thousands of synthetic organic compounds, such as plastics, lubricants, fuels, pesticides and etc. All of these compounds, along with organic byproducts and residues, constitute a new category of contaminants to natural environment. Among all the organic contaminants, persistent organic pollutants (POPs) are believed to be the most harmful compounds. POPs include variety of pesticides (OCPs), chlorobenzene species (PCBs and HCBs) and polyaromatic hydrocarbons (PAHs). POPs exhibit following four characteristics. 1) high toxicity: small quantity of POPs may cause severe damage; 2) persistency: POPs are resistant to photolysis, chemolysis and biolysis; 3) accumulation: POPs are hydrophobic and lipophilic, which helps POPs accumulate in soil, sediment and biological adipose tissue; 4) mobility: most POPs are semi volatile and easily migrate in the atmosphere.

Clean water, which is free from toxic chemicals, is essential to both human health and economic development, when considering its different uses, as (1) drinking water, (2) water for agriculture, (3) water for zoo-technique, (4) water for industrial systems. Moreover, the demand for pure water is continuously rising due to the global industrialization and the socio-economical growth of emerging countries. Unfortunately, aquifers as sources of drinking water can undergo pollution, due to (1) atmospheric contamination, (2) discharge of liquid contaminants and/or (3) percolation from contaminated soils. At the same time, water pollution can provoke soil contamination, by accumulating both heavy metals and toxic or carcinogenic compounds in marine and fluvial sediments. In marine waters, as well as in flow waters and aquifers, chemical compounds, usually used as herbicides, pesticides and antibacterial agents in agriculture and zoo-prophylaxis, can be present. Many of these have molecular structures similar to natural products and are degraded naturally or through their own chemical or photochemical instability. On the other hand, when these compounds are stable, they can alter the ecosystem, accumulating in living organisms or diffusing through the environment by volatilization, dissolution or percolation from contaminated soils. As a consequence, the effects of the pollution can manifest themselves very far from the original site.

Raman spectroscopy allows the identification of different molecules on the basis of their vibrational bands, providing an unambiguous molecular fingerprint. However, the low sensitivity of Raman scattering, along with possible spectral interference due to fluorescence emission, impairs the use of this technique for the recognition of molecular traces. In these cases one can use the SERS (Surface-Enhanced Raman Scattering) effect, which is able to enhance the Raman intensity of molecules adsorbed on metal substrates by many orders of magnitude and to promote a drastic quenching of fluorescence. Huge magnifications of the Raman signal are observed when a molecule adheres to nanostructured surfaces of metals with high optical reflectivity, such as Ag, Au and Cu. The SERS enhancement factors are generally up to 10^7 with respect to the Raman intensities of non-adsorbed molecules. By means of experimental procedures that combine microscopy and spectral observation beyond the light diffraction limit, 10^{14} - 10^{15} enhancement factors are reached, thus ensuring single-molecule detection. Thanks to its peculiar properties, SERS spectroscopy, since its discovery at the beginning of the seventies, has achieved a leading role in the analytical investigation of very low traces of contaminants, allowing the spectroscopic detection at subpicogram level. Actually, aromatic nitroderivatives could be identified by means of SERS spectroscopy when

adsorbed on silver nanoparticles, as demonstrated in the literature by observing strong enhancements of their Raman bands.

Determination of POPs and other organic contaminants in marine environment inspires the study of *in-situ* detection approaches. An intension of applying such advanced techniques into field survey is consistent with the object of environmental geochemistry. Integration of field survey, rapid analysis and geochemical mapping extends the future of geochemistry and serves effectively to governing and management.

In this study, an integrated approach of surface enhanced Raman scattering (SERS) and solid phase extraction (SPE) is considered. Organic pollutants were firstly concentrated into solid phase with silver nanoparticles embedded, and following micro (macro) Raman detection of SERS spectrum. Lower concentration of nitroaromatic compounds (lower than 10^{-6} M) is easily detected. Thanks to polymer layers, silver nanoparticles are protected, which extends the period of availability.

REFERNCES

- Abraham, G., Parker, R., 2008. Assessment of heavy metal enrichment factors and the degree of contamination in marine sediments from Tamaki Estuary, Auckland, New Zealand. *Environ Monit Assess*, 136, 227-238.
- Adriano, D.C., 2001. Trace elements in terrestrial environments: biogeochemistry, bioavailability, and risks of metals. Springer.
- Aitchison, J., 1982. The statistical analysis of compositional data. *Journal of the Royal Statistical Society. Series B (Methodological)*, 139-177.
- Albanese, S., 2008. Evaluation of the bioavailability of potentially harmful elements in urban soils through ammonium acetate-EDTA extraction: a case study in southern Italy. *Geochem-Explor Env Anal*, 8, 49-57.
- Albanese, S., De Vivo, B., Lima, A., Cicchella, D., 2007. Geochemical background and baseline values of toxic elements in stream sediments of Campania region (Italy). *Journal of Geochemical Exploration*, 93, 21-34.
- Albanese, S., De Vivo, B., Lima, A., Cicchella, D., Civitillo, D., Cosenza, A., 2010. Geochemical baselines and risk assessment of the Bagnoli brownfield site coastal sea sediments (Naples, Italy).

- Journal of Geochemical Exploration, 105, 19-33.
- CCME, 2002. Canadian sediment quality guidelines for the protection of aquatic life. Canadian Environmental Quality Guidelines, in: Environment, C.C.o.M.o.t. (Ed.). MB, Winnipeg.
- Chapman, P.M., Wang, F., 2001. Assessing sediment contamination in estuaries. *Environ Toxicol Chem*, 20, 3-22.
- Cheng, Q., 2001. Decomposition of Geochemical Map Patterns Using Scaling Properties to Separate Anomalies from Background. ISI.
- Carranza E.J.M., 2008. Geochemical anomaly and mineral prospectivity mapping in GIS. Elsevier. Pages: 368.
- Davis, J.C., 1986. Statistics and data analysis in geology. J. Wiley, Pages: 646.
- De Vivo, B., Lima, A., Albanese, S., Cicchella, D., Fedele, L., Frattini, P., 2004. Geochemical environmental maps of soils of Campania Region urban areas, Italy. *Geochim Cosmochim Acta*, 68, A535-A535.
- De Vivo, B., Rolandi, G., Gans, P.B., Calvert, A., Bohron, W.A., Spera, F.J., Belkin, H.E., 2001. New constraints on the pyroclastic eruptive history of the Campanian volcanic Plain (Italy). *Mineralogy and Petrology*, 73, 47-65.
- De Vivo, B., Petrosino, P., Lima, A., Rolandi, G., Belkin, H.E., 2010. Research progress in volcanology in the Neapolitan area, southern Italy: a review and some alternative views. *Miner Petrol*, 99, 1-28.
- Filzmoser, P., Hron, K., Reimann, C., Garrett, R., 2009. Robust factor analysis for compositional data. *Computers & Geosciences*, 35, 1854-1861.
- Fu, J., Mai, B., Sheng, G., Zhang, G., Wang, X., Peng, P., Xiao, X., Ran, R., Cheng, F., Peng, X., 2003. Persistent organic pollutants in environment of the Pearl River Delta, China: an overview. *Chemosphere*, 52, 1411-1422.
- Garrett, R.G., Reimann, C., Smith, D.B., Xie, X., 2008. From geochemical prospecting to international geochemical mapping: a historical overview. *Geochemistry: Exploration, Environment, Analysis*, 8, 205-217.
- Haese, R.R., Wallmann, K., Dahmke, A., Kretzmann, U., Muller, P.J., Schulz, H.D., 1997. Iron species determination to investigate early diagenetic reactivity in marine sediments. *Geochim Cosmochim Acta*, 61, 63-72.

- Harrison, R.M., Tilling, R., Callén Romero, M.a.S., Harrad, S., Jarvis, K., 2003. A study of trace metals and polycyclic aromatic hydrocarbons in the roadside environment. *Atmospheric Environment*, 37, 2391-2402.
- Hawkes, H., 1976. The early days of exploration geochemistry. *Journal of Geochemical Exploration*, 6, 1-11.
- Hawkes, H.E., Webb, J.S., 1962. *Geochemistry in mineral exploration*. Harper & Row, New York Evanston. pages: 409.
- Insinga, D., Molisso, F., Lubritto, C., Sacchi, M., Passariello, I., Morra, V., 2008. The proximal marine record of Somma-Vesuvius volcanic activity in the Naples and Salerno Gulfs, Eastern Tyrrhenian Sea, during the last 3 kyrs. *J Volcanol Geoth Res*, 177, 170-186.
- Jiang, Y.F., Wang, X.T., Wang, F., Jia, Y., Wu, M.H., Sheng, G.Y., Fu, J.M., 2009. Levels, composition profiles and sources of polycyclic aromatic hydrocarbons in urban soil of Shanghai, China. *Chemosphere*, 75, 1112-1118.
- Jones, K.C., De Voogt, P., 1999. Persistent organic pollutants (POPs): state of the science. *Environmental Pollution*, 100, 209-221.
- Kukkonen, J.V.K., Landrum, P.F., Mitra, S., Gossiaux, D.C., Gunnarsson, J., Weston, D., 2003. Sediment characteristics affecting desorption kinetics of select PAH and PCB congeners for seven laboratory spiked sediments. *Environ Sci Technol*, 37, 4656-4663.
- Lima, A., De Vivo, B., Cicchella, D., Cortini, M., Albanese, S., 2003. Multifractal IDW interpolation and fractal filtering method in environmental studies: an application on regional stream sediments of (Italy), Campania region. *Appl Geochem*, 18, 1853-1865.
- Long, E.R., Macdonald, D.D., Smith, S.L., Calder, F.D., 1995. Incidence of adverse biological effects within ranges of chemical concentrations in marine and estuarine sediments. *Environmental Management*, 19, 81-97.
- Lu, X., Wang, L., Lei, K., Huang, J., Zhai, Y., 2009. Contamination assessment of copper, lead, zinc, manganese and nickel in street dust of Baoji, NW China. *J Hazard Mater*, 161, 1058-1062.
- Manahan, S., 2005. *Environmental chemistry*. CRC press. ISBN-13: 978-1420059205.
- Martyn, C.N., Osmond, C., Edwardson, J.A., Barker, D.J.P., Harris, E.C., Lacey, R.F., 1989. Geographical relation between Alzheimer-disease and aluminum in drinking water. *Lancet*, 1, 59-62.

- McBratney, A.B., Mendonça Santos, M.L., Minasny, B., 2003. On digital soil mapping. *Geoderma* 117, 3-52.
- Reimann, C., Filzmoser, P., Garrett, R., Dutter, R., 2011. *Statistical data analysis explained: applied environmental statistics with R*. John Wiley & Sons. Pages: 362.
- Reimann, C., Filzmoser, P., 2000. Normal and lognormal data distribution in geochemistry: death of a myth. Consequences for the statistical treatment of geochemical and environmental data. *Environmental Geology*, 39, 1001-1014.
- Ridgway, J., Shimmield, G., 2002. Estuaries as repositories of historical contamination and their impact on shelf seas. *Estuarine, Coastal and Shelf Science*, 55, 903-928.
- Santos, I.R., Silva-Filho, E.V., Schaefer, C.E., Albuquerque-Filho, M.R., Campos, L.S., 2005. Heavy metal contamination in coastal sediments and soils near the Brazilian Antarctic Station, King George Island. *Mar Pollut Bull*, 50, 185-194
- Soclo, H.H., Garrigues, P., Ewald, M., 2000. Origin of polycyclic aromatic hydrocarbons (PAHs) in coastal marine sediments: Case studies in Cotonou (Benin) and Aquitaine (France) areas. *Mar Pollut Bull*, 40, 387-396.
- Yunker, M.B., Macdonald, R.W., Vingarzan, R., Mitchell, R.H., Goyette, D., Sylvestre, S., 2002. PAHs in the Fraser River basin: a critical appraisal of PAH ratios as indicators of PAH source and composition. *Org Geochem*, 33, 489-515.

CHAPTER 2

ENVIRONMENTAL GEOCHEMISTRY STUDY

OF CAMPANIA REGION IN ITALY: IN LAND

AND IN THE SEA

This chapter includes studies concerning inorganic elements and organic compounds distribution in the soil of Campania region and sediments in Gulfs of Naples and Salerno.

SECTION 2.1

**A case of compositional analysis and pollution impact estimation: Gulfs of Naples
and Salerno**

*Paper submitted to **Journal of Geochemical Exploration***

A case of compositional analysis and pollution impact estimation: Gulfs of Naples and Salerno

Wang Menghan¹, Albanese Stefano^{1*}, Lima Annamaria¹, Cannatelli Claudia¹, Cosenza Antonio¹, Esposito Rosario¹, Lu wanjun², Marco Sacchi³ and De Vivo Benedetto¹

¹Dipartimento di Scienze della Terra, dell'Ambiente e delle Risorse, Università di Naples "Federico II", Via Mezzocannone 8, 80134, Naples (Italy)

²State Key Laboratory of Geological Process and Mineral Resources, China University of Geosciences, 430074, Wuhan, People's Republic of China;

³C.N.R. Istituto Geomare Sud, Naples, Italy

*Corresponding author: Ph. +39 0812535059; Fax +39 0812535061; E-mail: stefano.albanese@unina.it

Abstract

In this paper the results of an environmental geochemical investigation on Naples and Salerno Gulfs, out of Campania plain (Southern Italy) are presented. Surface marine sediments samples were collected during three field activities: Naples and Salerno Gulfs investigation (NaSa); Bagnoli site coastal area investigation (BaSi); Ports around Naples Gulf investigation (PoNa).

Elemental concentrations were determined and their interpolated distribution maps were presented. Three geochemical sources were determined for elements by analyzing the results obtained from a R-mode factor analysis: geogenic contribution, finer deposits due to water dynamics decreasing and anthropogenic activities. This result partially was presented on the single element distributions of eight concerned potential toxic elements (PTEs). Additive log-ratio transformed elements distributions are also presented in the paper. Transformed data resolves inner dependences between variables and, theoretically, exhibited the actual distribution of each variable.

Local geochemical backgrounds of PTEs were determined from average value of NaSa samples. Based on these background values, pollution impact analysis was applied to both BaSi and PoNa samples to illustrate pollution levels in these areas. An ecological risk assessment was applied to entire database to evaluate the overall environmental condition of the area.

Keywords: *Naples and Salerno Gulfs, Compositional data, Potential toxic elements, Risk assessments*

1. Introduction

Environmental geochemistry illustrates the spatial variation of elements and compounds in the composition of Earth surface, and focuses on elements with ecological and human risks. Results of environmental geochemistry study could serve to clarify baseline values of elements (Albanese et al., 2007; Albanese et al., 2010), and consequently distinguish areas with potential harms to human beings (Albanese et al., 2013a). Interaction of environment and human beings are also investigated by environmental geochemists, such as risk assessments (Albanese et al., 2010; Albanese et al.,

2013b; De Vivo et al., 2013), pollution and remediation effects (De Vivo and Lima, 2008) and governmental management of environments (De Vivo and Lima, 2008; De Vivo et al., 2008).

Raw data of geochemical investigation is commonly expressed in compositional form, such as mg/kg. Such expression is consistent to chemical analysis methodology and was established by usage. However, compositional data are problematic to be interpreted because single variable do not varies independently; the common calculations based on Euclidean geometry are inappropriate to apply for compositional data (Aitchison, 1982; Filzmoser et al., 2009; Reimann et al., 2012).

Researches about compositional data have been developed for almost three decades (Aitchison, 1982). A satisfactory option for statisticians as well as for geochemists is still on the way. Up to date, log-ratio transformation (Aitchison, 1999; Aitchison et al., 2000; Egozcue et al., 2003; Martin-Fernandez et al., 2003) is the most admitted approach to cope with dependent variables. Three major expressions have been developed: additive log-ratio transform, centered log-ratio transform and isometric log-ratio transform. But each of them introduces certain new problems (Reimann et al., 2012), which determine a debate about the ideal solution to be adopted. Anyway there is a large consensus on the necessity of data transformation to better evaluate the significance of geochemical distribution of elements in the environment.

Public show, erroneously, more interests in the potential influence of hazardous elements other than statistical methodology. Pollution impact analysis (PIA) and ecological risk assessment (ERA) are two major approaches to evaluate harmfulness of elements and compounds. PIA (Abraham and Parker, 2008; Chapman and Wang, 2001; Harrison et al., 2003; Lu et al., 2009; Santos et al., 2005) is based on the comparison between studied samples to global or regional background concentration. Enrichment factor (EF), geoaccumulation index (I_{geo}) and degree of contamination (D_c) are three major parameters of PIA. ERA gives out biological adverse effect of pollutants. The initial step of ERA is to set a guideline for each element or compound. The determination of guideline is based on statistical relationship between material concentration and ratio of reported adverse biological effects. Up to date, US Environment Protection Agency (EPA) (Long et al., 1998; Long et al., 1995) and Canadian Council of Ministers of the Environment (CCME) (CCME, 2002) have set elaborate guidelines for potential toxic elements (PTEs) and persistent organic pollutants (POPs), as well as Italian government (D. M. Ambiente 260/2010).

A comprehensive study on PTEs distribution in Naples and Salerno Gulfs has been developed for

the purposes of the present study and additive log-ratio transformation (ALT) has been used to solve the compositional data problem. Background values are determined as the regional scale to serve as a reference for the application of PIA.

2. Study area

Naples and Salerno Gulfs are two marginal seas located along the Eastern Tyrrhenian Sea and separated by the Sorrento peninsula (Fig 1). Naples Gulf is semi-closed by Ischia and Procida islands in NW, Campi Fregrei and Campania plain in NE, and Sorrento peninsula in SE; Salerno Gulf is located on the coastal area offshore of the Sele river plain. Naples has the second highest population density in Italy and around 4.4 million citizens live in its metropolitan area; Salerno province has a population of 140 thousand inhabitants.

The Tyrrhenian Sea is the result of Miocene-Quaternary extension contemporaneously to eastward accretion and anticlockwise rotation of the Apenninic fold and thrust belt during the roll-back of the subducting Adria plate (Bruno et al., 2003; Insinga et al., 2008; Milia and Torrente, 1999; Sacchi et al., 2005). The Campanian Plain and Naples Gulfs, together with the Sele Plain and the Salerno Gulfs are parts of half-graben basins developed along the eastern Tyrrhenian margin (Sacchi et al., 2005).

Sea floor of Naples and Salerno Gulfs are covered by Plio-Quaternary sedimentary and pyroclastic fall deposits (Bruno et al., 2003). Two small coalescent deltas, Sebeto delta and Sarno delta, characterize eastern depositional system of Naples Gulf (Insinga et al., 2008). Along Sorrento peninsula, Capri Island and Salerno Gulf, Mesozoic-Cenozoic carbonate Units dominate the composition of surface sediment (Milia and Torrente, 2003).

Volcanic processes during the late Quaternary significantly influence morphology and deposits in Naples Gulf (Aiello et al., 2005; De Vivo et al., 2001; Milia and Torrente, 2007; Milia and Torrente, 1999, 2003). Several volcanic eruptions happened in Campania Plain (Campi Fregrei, Mt Somma-Vesuvius, Ischia, several Ignimbrite events, among which the Campanian Ignimbrite at 39 Ka B.C. (De Vivo et al., 2001).

Naples and Salerno provinces are among the most touristic regions around Mediterranean Sea: in 2008, 381,000 people visited this area. The port of Naples is one of the most important ports in Europe, and has the Mediterranean's second-highest level of passengers flow. Naples has one of the

largest transportation networks in south Italy, including railway, highway and various roads. Agriculture in Campania region still provides basic economical income. By an environmental point of view, the stream networks system in Campania plain and Sele plain is responsible for carrying fertilizers and related products into the sea (Albanese et al., 2007) (Fig. 1).

Bagnoli area is one of the largest brownfield sites in Italy. It has been dismissed in the early 1990's. The area used to concentrate various industries, such as steel factory, asbestos materials manufacturing, cement and fertilizer production factories. Although it has undergone t a large remediation programme funded by Italian Government, the area is still affected by high concentrations of toxic metals and organics (POPs, namely PAH, PCB and OCP) spreaded both in soil and in sea sediments of Pozzuoli Gulf (Albanese et al., 2010; De Vivo and Lima, 2008).

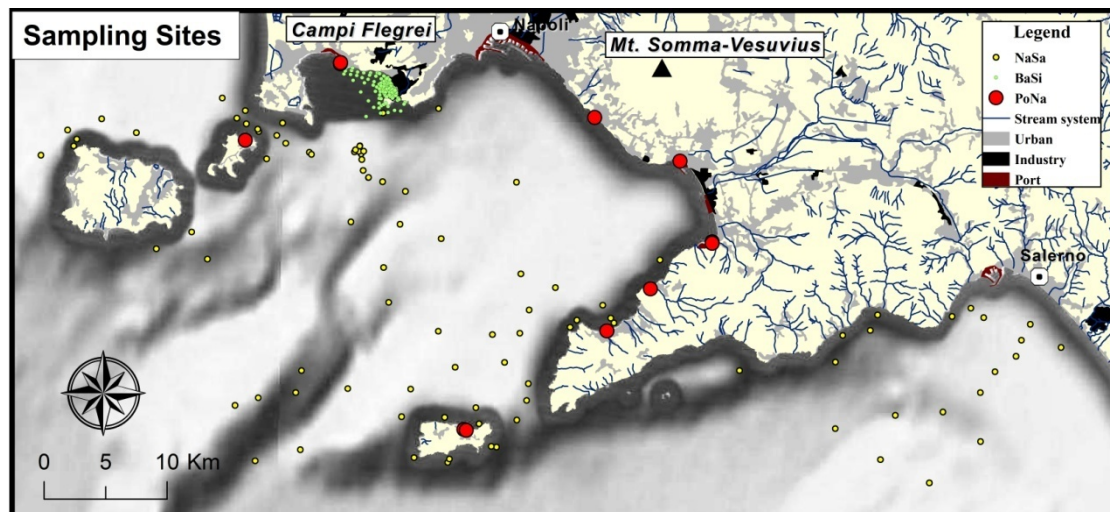


Figure 1 - Study area and sampling site locations

3. Material and methods

3.1 Sampling method

Sediments from three field sampling activities were included in this study. A general survey of sea sediments in Naples and Salerno Gulfs (NaSa) was used to provide regional geochemical information, whereas sea sediments surveys of Bagnoli site (BaSi) and Naples Gulf ports (Capri,

Castellammare, Pozzuoli, Procida, Sorrento, Torre Annunziata, Torre del Greco and Vico Equense) (PoNa) were focused on the concentration of PTEs (Fig. 1).

Sediment samples (following the directives of the national program for assessment of marine pollution of highly contaminated Italian coastal areas) were collected by C.N.R. Istituto Geomare Sud, Naples, from 96 locations (Fig. 1). Differential global positioning system (DGPS) was used to identify each location precisely.

Among NaSa samples, in May, 2000, 23 samples were collected using a box-corer with an inner diameter of 25 cm and 63 were collected by grab. BaSi samples (collected between November 2004 and March 2005) were sampled by ICRAM along the coastline by 123 boreholes at different depths. PoNa sediments were sampled by 11 boreholes at different depths by a Norwest Italia s.r.l. investigating different harbour area of Campania region during the 2003 summer. All the samples used for the purposes of these studies were collected in a depth range between 0 and 20 cm from the sea bed.

3.2 Chemical analyses and quality control

All the NaSa and PoNa sea sediments, after being air dried, were sieved and 30 g of the <150 µm fraction was retained for analysis of 53 elements. Analyses were carried out by ACME Analytical Laboratories Ltd. (Vancouver, Canada), through its Italian affiliate (Norwest Italia Srl, Naples). Each sample was digested in a modified aqua regia solution and analyzed by inductively coupled plasma–mass spectrometry (ICP-MS) and atomic emission spectrometry (ICP-AES). Specifically, a 15-g split of the pulp was digested in 45 ml of the aqua regia mixture (1 part concentrated hydrochloric acid to 1 part nitric acid to 1 part deionised water) at 90 °C for 1 h. The solution was taken to a final volume of 300 ml with 5% HCl. Aliquots of sample solution were aspirated into a Jarrel Ash Atomcomp 975 ICP-Emission Spectrometer and a Perkin Elmer Elan 6000 ICP-Mass Spectrometer.

Precision of the analysis was calculated using three in-house replicates, and two blind duplicates submitted by the authors. Accuracy was determined using ACME's in-house reference material, DS2 (HMTRI, 1997).

Analyses of elements (Al, As, Be, Cd, Co, Cr, Fe, Hg, Mn, Ni, Pb, Cu, Sn, V, and Zn) of BaSi sediments were performed by ICRAM Laboratories. Microwave assisted acid digestion for a total

decomposition of matrices was applied to sediment samples according to EPA Method 3052 (US-EPA, 1996). Each sample was digested in an HCl and HNO₃ (1:3) solution for 15 min. The sample was placed in an inert polymeric vessel, sealed and heated in a microwave system. A 4-step heating cycle was performed prior to adding HF to the cooled solution. After a second heating cycle, H₃BO₃ was added to the solution. Finally, the solution was filtered and brought to a final volume of 100 ml with the addition of ultrapure water. As, Cd, Cu, Pb and Zn were analyzed by ICP-OES (Inductively Coupled Plasma-Optical Emission Spectrometry), Hg (and other elements, if characterized by concentrations below the ICP-OES detection limits) were analyzed by AAS (Atomic Absorption Spectroscopy)

3.3 Geomathematic analysis

Statistical data elaboration performed on total of NaSa samples, covering the entire Naples and Salerno Gulfs, was used to obtain regional background information about distribution of all the elements. Multivariate analysis was applied to NaSa data in order to group elements and speculate about the sources of elements.

BaSi and PoNa samples were investigated mostly to focus on local (Bagnoli site and ports) potential impact of PTEs (As, Cd, Cr, Cu, Hg, Pb, Ni and Zn). PIA was applied to these locations, as well.

Univariate analysis and ERA were applied to the eight most concerned PTEs of entire dataset.

3.3.1 Factor analysis

Elemental distribution controlling factors has been evaluated by R-mode factor analysis. Such analysis has been carried out on 96 NaSa Gulfs samples, reducing the the number of evaluable elements to 26 out of the 53: in fact, some elements were rejected because of concentrations lower than the limit of detection (LOD) in most of the samples (e.g. Pd, Re and Pt) or because of their cumulative variances <0.5 (e.g. As, Mn and Fe). The 26 elements included in the final variables matrix are shown in Table 1. Variables matrix was varimax-rotated in order to facilitate the interpretation of results. Varimax rotation is an orthogonal rotation that minimizes the number of variables with high loadings on each factor. Three factors were obtained and they were studied and interpreted in accordance with their presumed origin (lithology background, water cynetics and

anthropogenic). The three-factor model, accounting for 84.88% of data variability, deemed appropriate for marine sediments, is shown in Table 1. The associations of the three-factor model are F1: K-La-Be-U-Th-Al-Tl-Na-Ti-V; F2: Ni-Sc-Co-Li-Cu-Cr-Zn-V; F3: Au-Hg-Sn-Ag-Pb-Bi-Zn- Cr (Table 1).

3.3.2 Compositional data log-ratio transformation

Univariate statistical analysis is performed to show the single element geochemical distribution. Elements concentration data is compositional which varies dependently. In such case a simple statistical approach can introduce faulty explanations. For example, elements concentration (e.g. Zn) difference also depends on concentrations of other elements. Directly concluded results could underestimate (overestimate) these differences (Filzmoser et al., 2009). In order to solve such problem in this study the raw data were normalized by means of a logratio-transformation.

Additive, centered and isometric log-ratio transformation approaches are the three major transformation processes to try to normalize compositional data (Aitchison, 1982; Aitchison, 1999; Aitchison, 2003). Log-ratio transformed variables are supposed to vary separately from other variables in data volume. Ideal transformation indicates a “real” variation and distribution, and relates geometry of original data directly to Euclidean geometry (Egozcue et al., 2003; Filzmoser et al., 2009).

The approach used in this study is the additive log-ratio transformation (ALT) (Table 2). Because the centered log-ratio transformation (CLT), which used geometric mean value of all the variables as denominator, was not applicable in our research. In fact, BaSi and PoNa dataset did not contain all the elements analysed in the dataset of NaSa.

For the ALT in this study, each variable was divided by the concentration of Al, followed by a log-transformation (Reimann et al., 2012). Al is the most abundant (Lutgens and Tarbuck, 1986) metallic elements on the Earth's surface, and third most of all elements (after oxygen and silicon). Variation of Al in sediments is generally geogenic and, as a matter of the fact, the regional distribution of Al, mostly along Neapolitan coastline, is mainly affected by the diffuse volcanism of the Neapolitan area (Vesuvius, Campi Flegrei, Ischia, Ignimbrites) (De Vivo et al., 2010). In addition, in the study area, Al concentrations have a good correlation with the geometric mean values of all 53 analysed elements (correlation coefficient: 0.863) of NaSa dataset, which indicates Al as a good

substitutive of the geomedian value for normalizing data distribution.

3.3.3 Generation of interpolated maps

The production of geochemical maps for Naples and Salerno Gulfs sediment results, using ESRI ARCGIS and GeoDAS (Cheng, 2001), is described by presenting, as an example, a complete set of geochemical maps produced for Zn (Fig. 2). The usefulness of this technique in environmental studies has already been demonstrated (Albanese et al., 2007; Lima et al., 2003).

Both original concentration and ALT transformed data were used to generate geochemical distribution maps with a multifractal inverse distance weighted (MIDW) algorithm as an interpolation method (Cheng, 1999).

Concentration-area (C-A) plot (Fig. 2B and Fig. 2D) illustrates the fractal analysis of data distribution in the area. In this plot, the vertical axis represents the log values of cumulative pixel areas $A(\rho)$. $A(\rho)$ infers areas with element concentration greater than ρ ; ρ is shown in horizontal axis in log values for unconverted data, while for ALT data ρ is shown as it is. The C-A plot was first divided into two parts (regional concentration and anthropogenic concentration) by means of the maximum value of NaSa data. Regional part was subsequently divided on the basis of a fractal filtering analysis. Divisions of C-A plot were then applied as classes on interpolation maps (Fig. 2A and Fig. 2C) in color scale.

In Fig. 5, the interpolated maps of PTEs (As, Cd, Cr, Cu, Ni, Pb, Hg and Zn) are presented. Interpolated elements associations (based on factor scores) resulting from R-mode factor analysis were also elaborated using the same procedure as above (Fig. 3).

3.3.4 Background value estimation

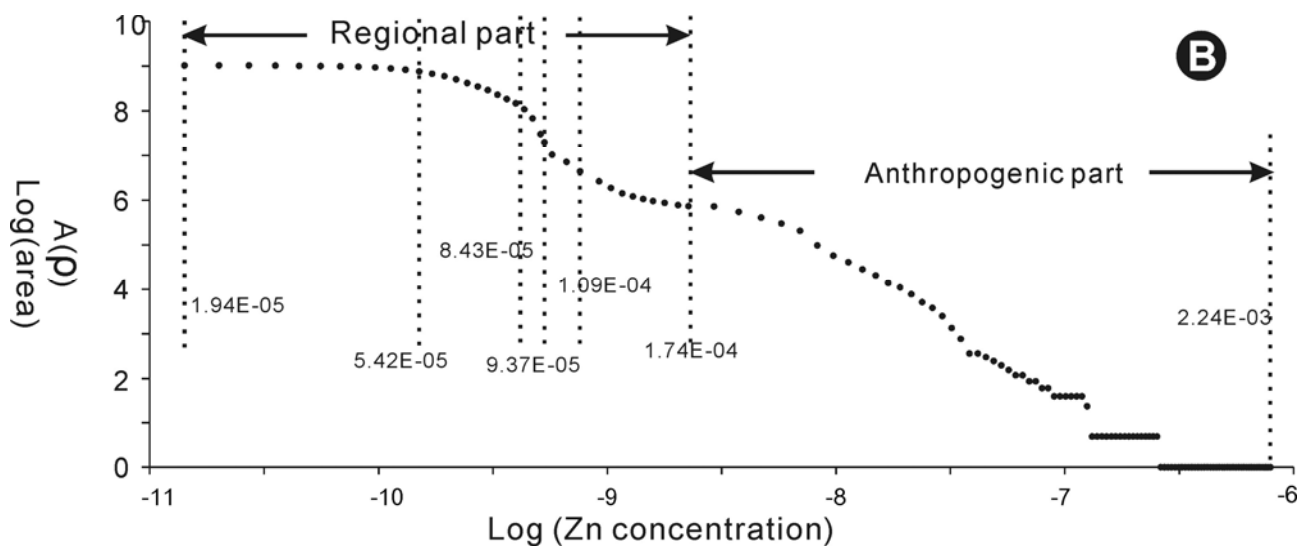
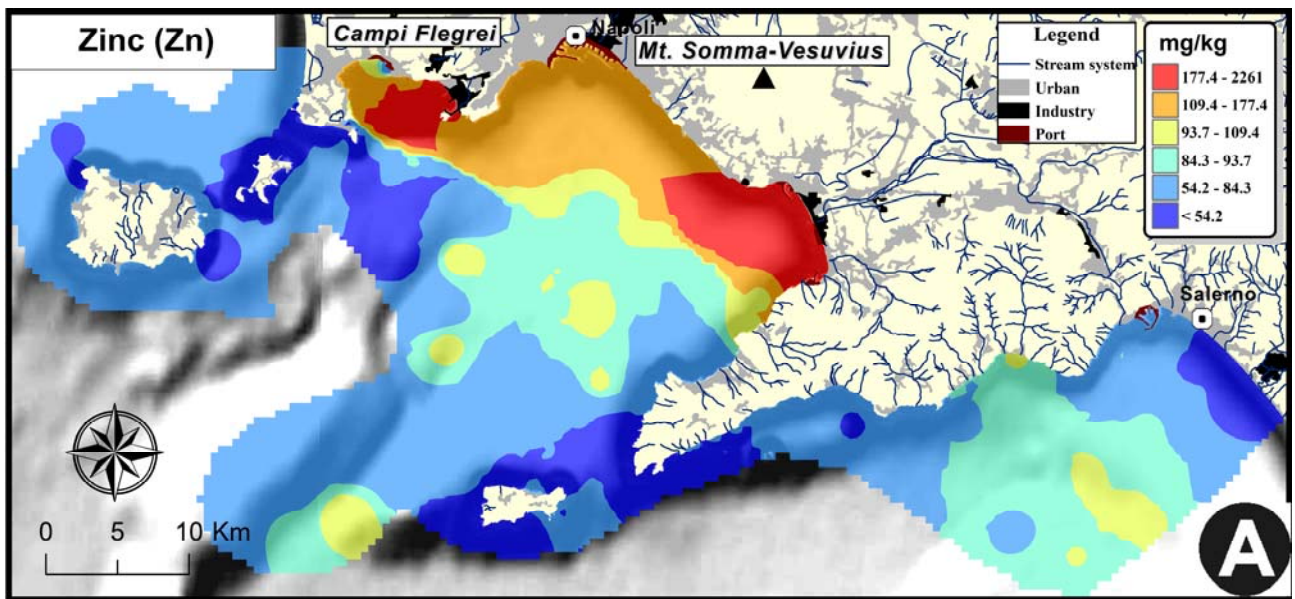
Bagnoli area and ports exhibit very high concentration of PTEs. The investigation on the entire NaSa dataset has been used to estimate regional background as reference value for the element concentrations in the sea sediments of Bagnoli (BaSi) and of different ports (PoNa). The knowledge of background values is in fact very important to evaluate the pollution levels of the elements in specific areas. Literature studies determine background values following two approaches: 1) considering as reference element global average values in similar environmental media; or 2) considering as reference element the concentrations in deep core samples.

Table 1 Varimax-rotated factor (three-factor model) for 23 selected elements of 96 NaSa samples. Bold entiers report loading values over 0.5; underlined entries report negative loadings below -0.5.

	Factors		
	F1	F2	F3
Data Variability	32.5%	27.4%	24.9%
Cu	0.424	0.786	0.345
Pb	0.392	0.299	0.788
Zn	0.251	0.655	0.676
Ag	-0.005	-0.141	0.838
Ni	-0.006	0.981	0.035
Co	0.167	0.92	0.063
U	0.884	-0.161	0.122
Au	0.105	-0.048	0.944
Th	0.853	0.307	0.147
Bi	0.126	0.408	0.781
V	0.609	0.541	0.163
La	0.894	-0.056	0.122
Cr	0.024	0.671	0.665
Ti	0.722	-0.309	0.015
Al	0.846	0.483	0.116
Na	0.808	0.196	0.147
K	0.916	0.133	0.134
Sc	-0.033	0.946	0.005
Tl	0.824	0.353	0.257
Hg	0.163	0.104	0.927
Sn	0.293	0.086	0.878
Be	0.891	0.279	0.207
Li	0.186	0.9	0.09

Table 2 Statistic parameter of original value and ALT transformed value

Elements	N	Concentration				Additive logratio transformation			
		Median	Skewness	Kurtosis	St.dev	Median	Skewness	Kurtosis	St.dev
Cu	230	2.99E-05	5.39	43.90	5.03E-05	-6.97	-0.13	0.78	0.82
Pb	230	7.14E-05	3.06	13.27	2.32E-04	-6.11	0.47	-0.69	0.97
Zn	230	1.36E-04	2.40	6.94	4.60E-04	-5.60	0.73	-0.49	1.04
Ni	230	2.52E-05	1.07	-0.24	4.55E-05	-7.03	-0.22	0.33	0.86
As	230	1.23E-05	2.94	13.54	9.15E-06	-7.78	-0.28	0.81	0.88
Cd	230	1.10E-07	4.09	22.11	8.75E-08	-12.32	0.38	0.33	1.25
Cr	230	1.55E-05	7.31	78.32	2.44E-05	-7.38	-0.40	-0.57	0.93
Hg	230	1.47E-07	3.19	11.71	5.63E-07	-12.33	-0.10	0.43	1.34



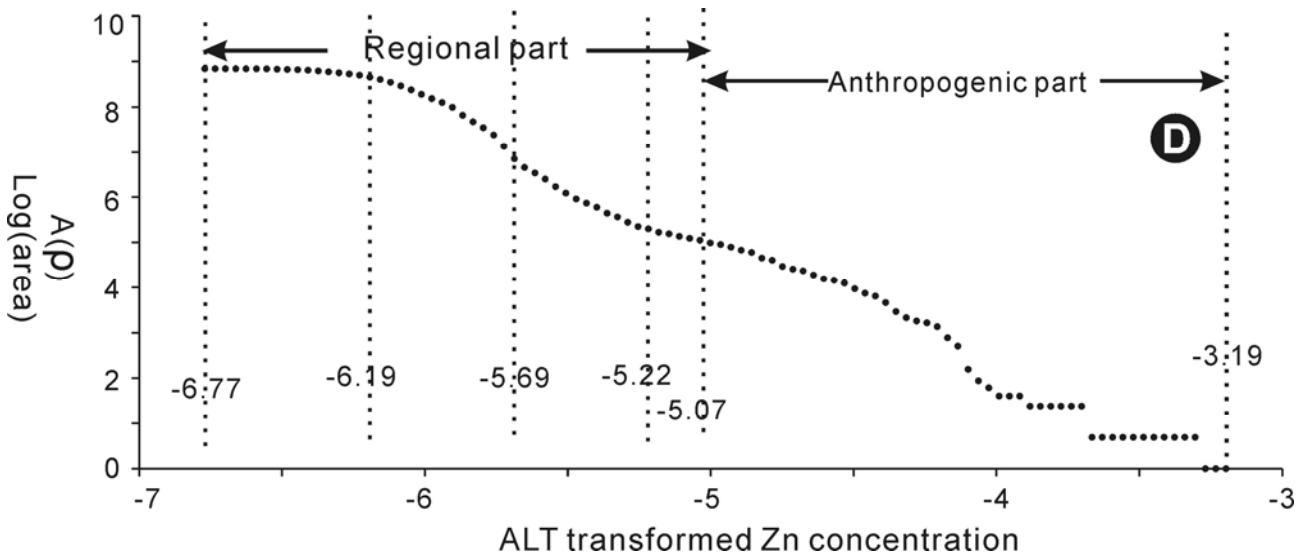
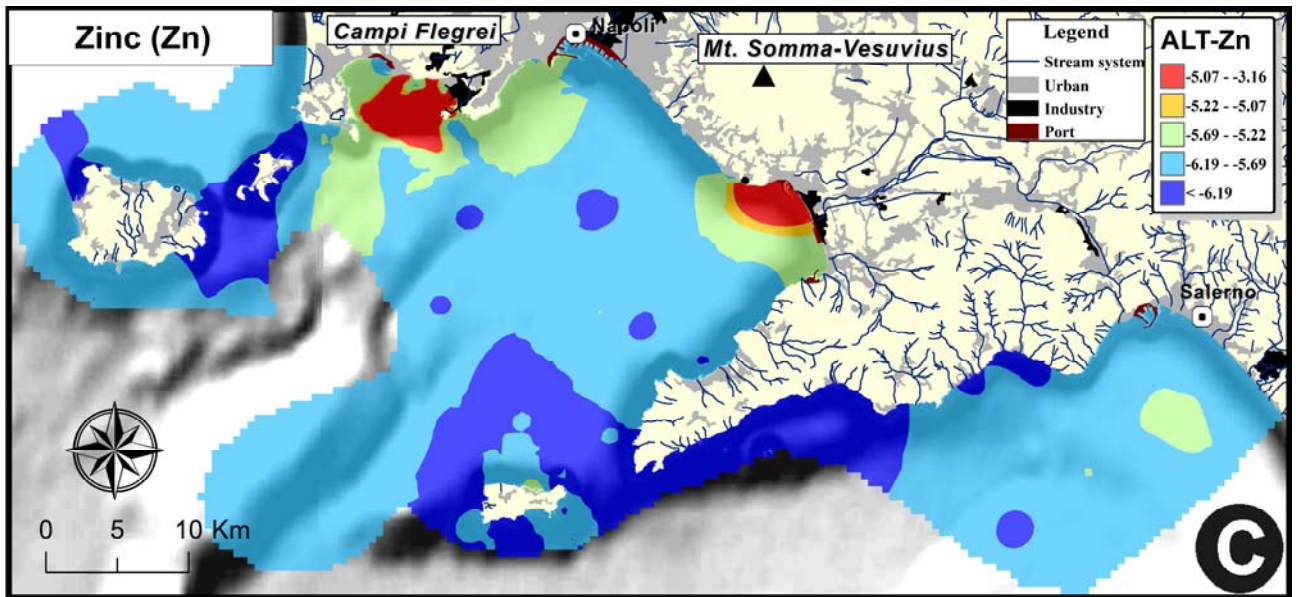
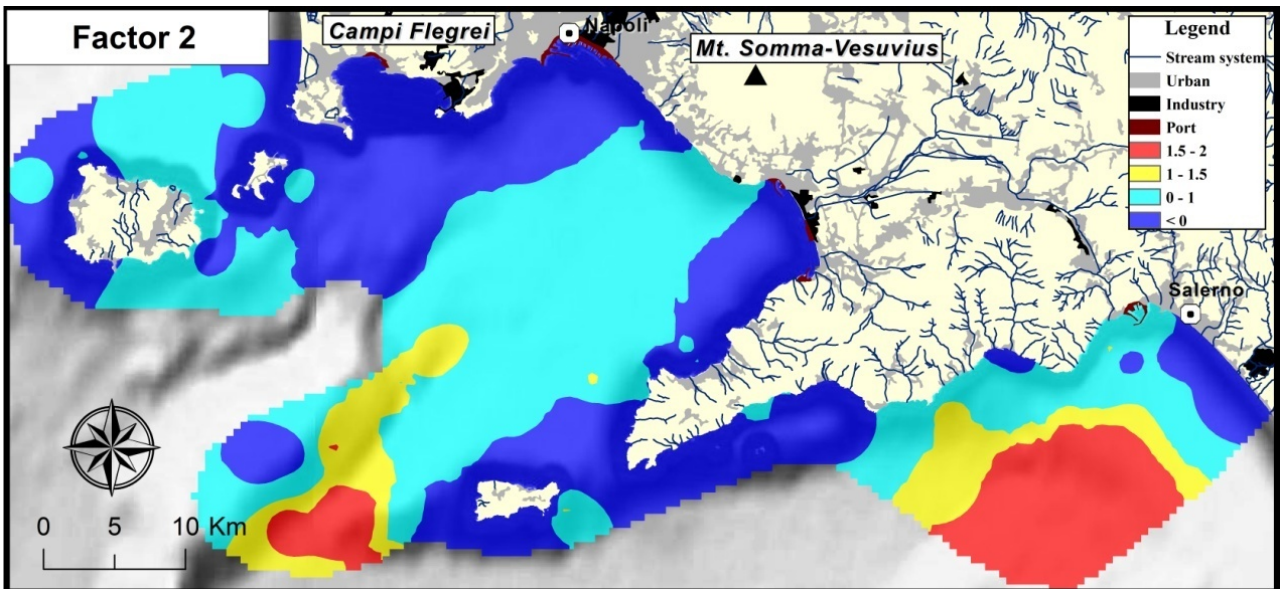
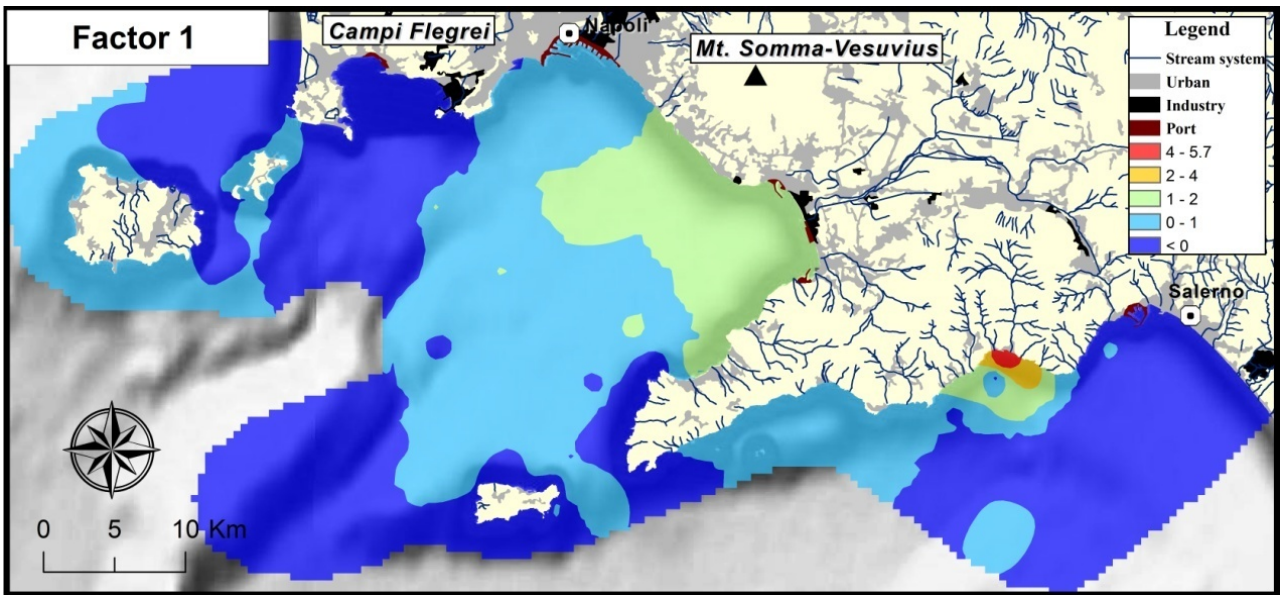


Figure 2. (A) Interpolation map of original Zn value in mg/kg. (B) Fractal concentration-area (C-A method) plot for Interpolation map of original Zn value in mg/kg. (C) Interpolation map of additive logratio transformed (ALT) Zn value. (D) Fractal C-A plot for Interpolation map of ALT Zn value.



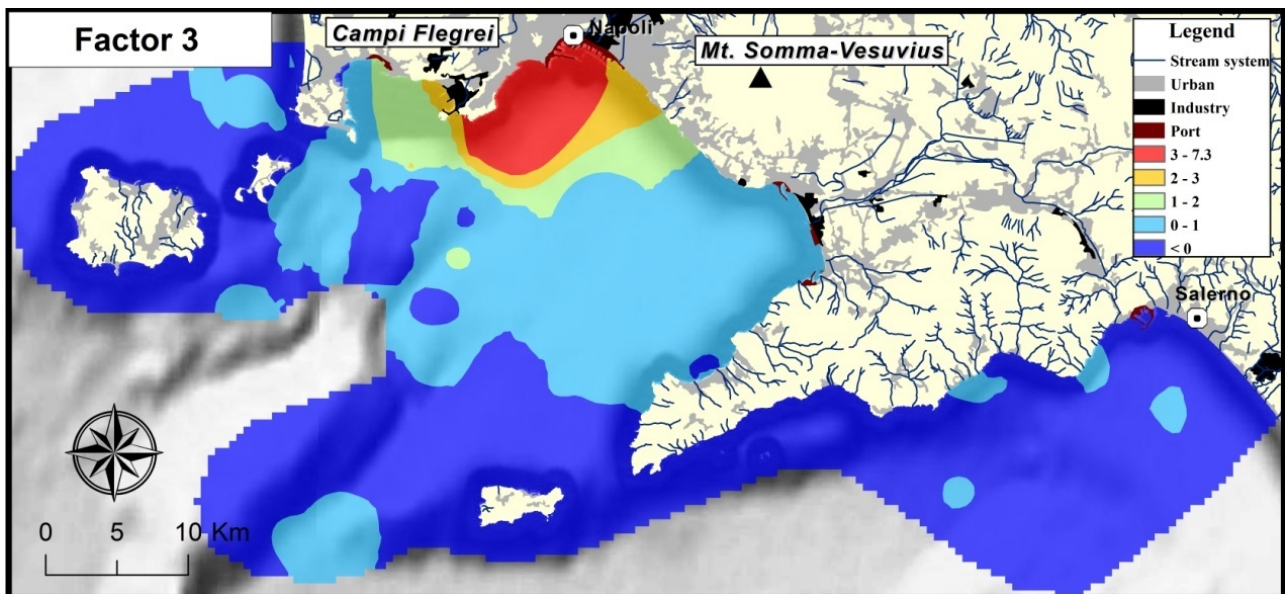


Figure 3. Interpolation maps of three factor associations. Grid pixels were classified with a colour scale using the fractal concentration–area plot (C-A method) that characterises image patterns and classifies them into different classes based on a C-A plot. Factor 1 is the association of K-La-Ba-U-Th-Al-Tl-Na-Ti-V; factor 2 is the association of Ni-Cu-Sc-Co-Li-Cr-Zn-V; factor 3 is the association of Au-Hg-Sn-Ag-Pb-Bi-Zn-Cr

The concentration values in our study are generally higher than the study of Adamo et al. (2005) and lower than the study of Damiani et al. (1987) using deep core values from Pozzuoli Gulf and Naples port. Furthermore, when compared with average continental crust (Hawkes and Webb, 1962), in our study area Pb, As and Hg are relatively enriched, whereas Ni is less than half of the average continental crust value.

Since the study area is thoroughly affected by volcanic eruption products which weakens the accuracy of background values generated from deep core, average values of metals in surface sediments were considered more representative of the to local sea bed conditions.

In this study, mean elemental values of NaSa samples is used as reference background value (eliminating the outlier near Capo Posillipo, GRNN 4, Table 3).

3.3.5 Estimation of pollutant impact

Numbers of factors (Abraham and Parker, 2008; Chapman and Wang, 2001; Harrison et al., 2003; Lu et al., 2009; Ridgway and Shimmield, 2002; Santos et al., 2005) have been put forward for

quantifying the degree of metal enrichment in sediments. In this study, four indexes are selected to study pollutant impact:

Table 3 Background values of harmful heavy metals from different studies.

Category	Elements							
	Cu	Pb	Zn	Ni	As	Cd	Cr	Hg
Average continental crust	25.00	14.80	65.00	56.00	1.70	0.10	126.00	40.00
Naples city port (Adamo et al., 2005)	21.10	22.70	56.60	-	15.80	0.20	21.60	-
Pozzuoli Gulf (Damiani et al., 1987)	20.00	60.00	80.00	20.00	-	-	30.00	250.00
This study	26.09	38.30	67.42	20.37	16.87	0.09	25.78	89.58

1) Enrichment factor (EF) is a normalized factor to estimate anthropogenic impact. The EF normalizes the measured heavy metal content with respect to reference elements, such as Al. The EF is calculated according to the following equation:

$$EF_x = \frac{[C_x/C_{Al}]_{\text{sample}}}{[C_x/C_{Al}]_{\text{background}}} \quad (1)$$

where C_x is the concentration of the element of interest, C_{Al} is the concentration of the Al. Five contamination categories are recognized on the basis of the enrichment factor (Table 4) (Lu et al., 2009).

2) Geoaccumulation index (I_{geo}): assesses the degree of metal pollution in terms of seven enrichment classes. The term is calculated as follows:

$$I_{geo} = \log_2 \left[\frac{C_{\text{sample}}}{1.5 C_{\text{background}}} \right] \quad (2)$$

The constant value 1.5 is introduced to minimize the effect of possible variations in the background values. The classification of I_{geo} is given in Table 4

3) Degree of contamination (D_c): D_c gives out average concentration level of pollutants of interest. The term is calculated as follows:

$$d_x = \frac{C_{\text{sample}}}{C_{\text{background}}} \quad (3)$$

$$D_c = \frac{\sum_1^n d_x}{n} \quad (4)$$

where d_x represents increasing level of single metal, n is the number of indicator metals.

Table 4 Categories of impact levels calculated from EF (enrichment factor), I_{geo} (geoaccumulation index), D_c (degree of contamination). The last column exhibits the calculated D_c in this study.

Class	Indication	Index			D_c in this study
		EF	I_{geo}	D_c	
A	unpolluted		<0	<1.5	26
B	slightly to moderately polluted	<2	0-1	1.5-2	9
C	moderately polluted	2-5	1-2	2-4	44
D	moderately to strongly polluted	5-20	2-3	4-8	37
E	strongly polluted		3-4	8-16	16
F	strongly to extremely polluted	20-40	4-5	16-32	3
G	extremely polluted	>40	>5	>32	0

4) Percentage of risk samples (P_r): P_r is a summation of samples that exceed environmental guidelines. The guideline is predetermined by national law. P_r is calculated according to following:

$$P_r = \frac{N_{\text{exceed}}}{N_{\text{total}}} \times 100\% \quad (5)$$

where N_{exceed} is the number of samples with concentration higher than guideline, and N_{total} is the number of samples acquired.

The first three above parameters are calculated with respect BaSi, PoNa and GRNN 4 of NaSa with background value generated with the general NaSa dataset. P_r is calculated with respect the entire database.

4 Results and discussion

4.1 Elemental distribution

In Naples and Salerno Gulfs, Al, which have been selected as normalizing element for the study

area, concentrated in the areas with essential volcanic influences, a strait area along coastline in front of Mt. Vesuvio. High concentration of Al also appears at both Pozzuoli and Amalfi Gulfs, as well.

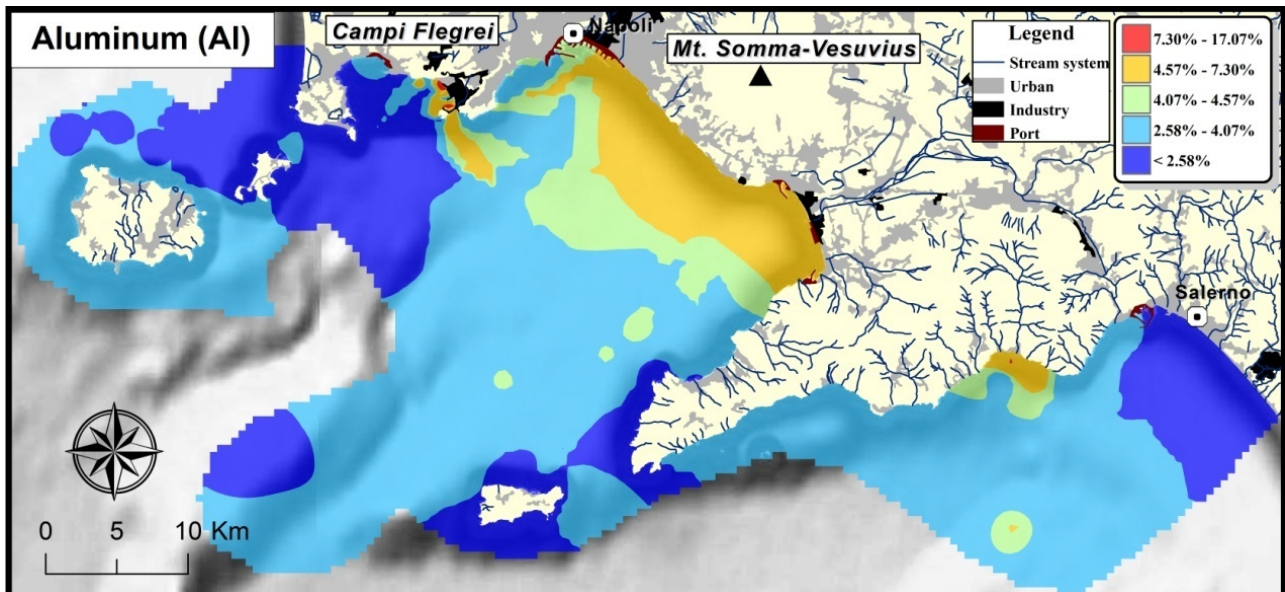


Figure 4. Interpolation map of Al in Naples and Salerno gulfs.

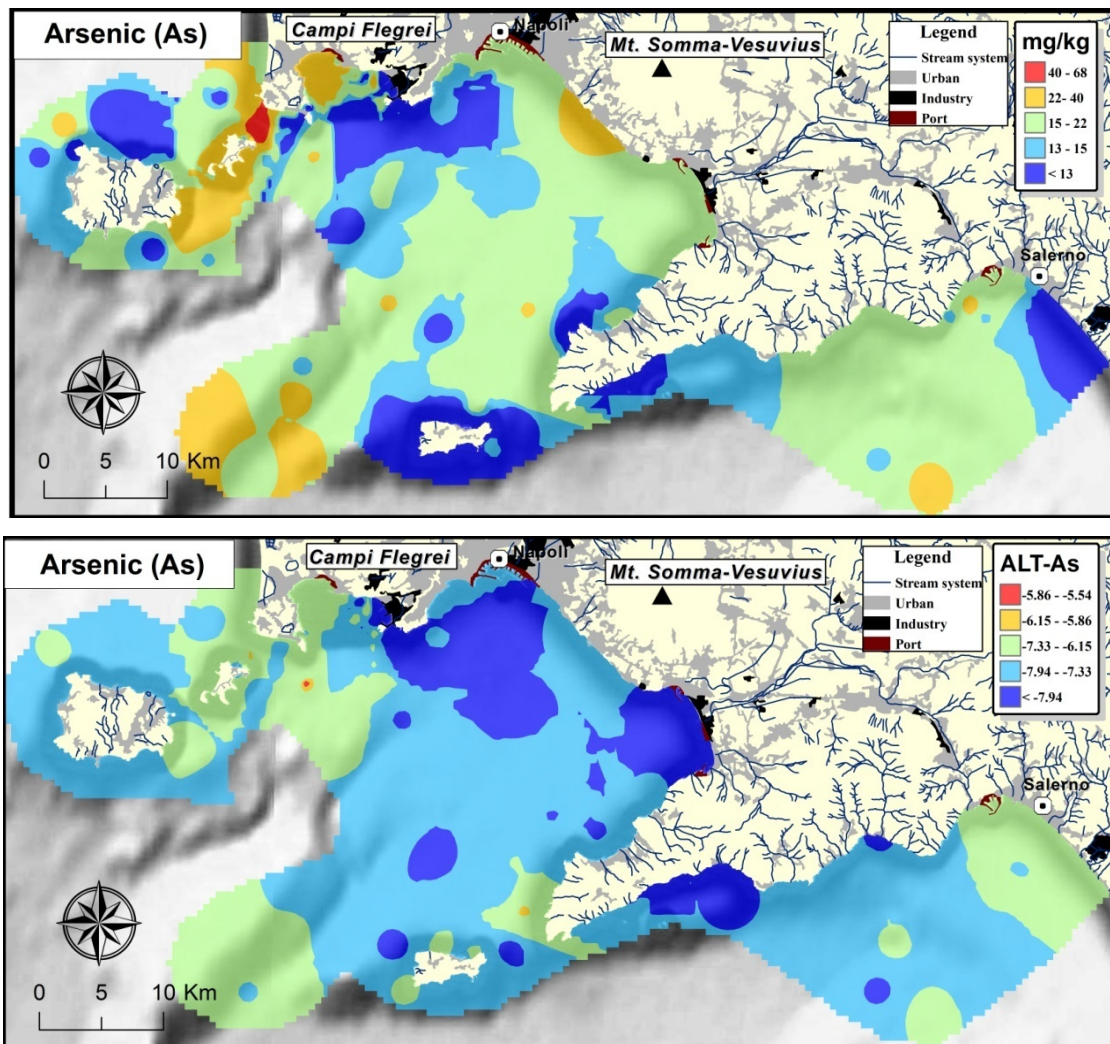
Most elements (As, Cu, Cd, Cr, Pb and Zn) are characterized by extreme-high concentrations spreaded across the whole study area, while Ni and Hg are only extremely concentrated in the Bagnoli area. After ALT transformation, four different changes occurred to interpolated maps: i) extreme-high concentrated areas of Hg and Ni were enlarged but still limited in the Bagnoli; ii) area with extreme-high Cu concentrations changed slightly; iii) other elements (Cd, Cr, Pb and Zn) high concentration patterns were limited at the Bagnoli and Sarno estuary and iv) As was smoothed due to its volcanic origin.

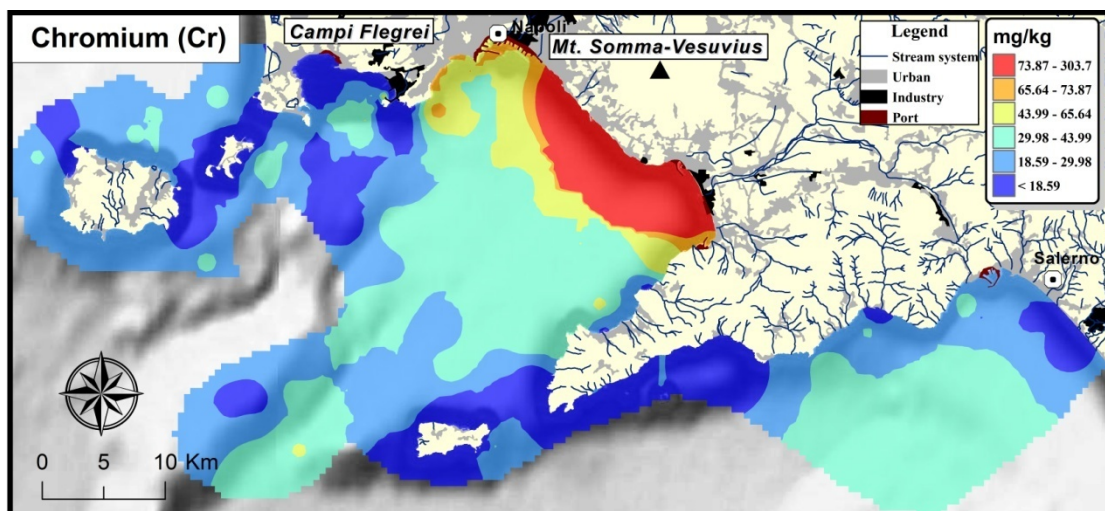
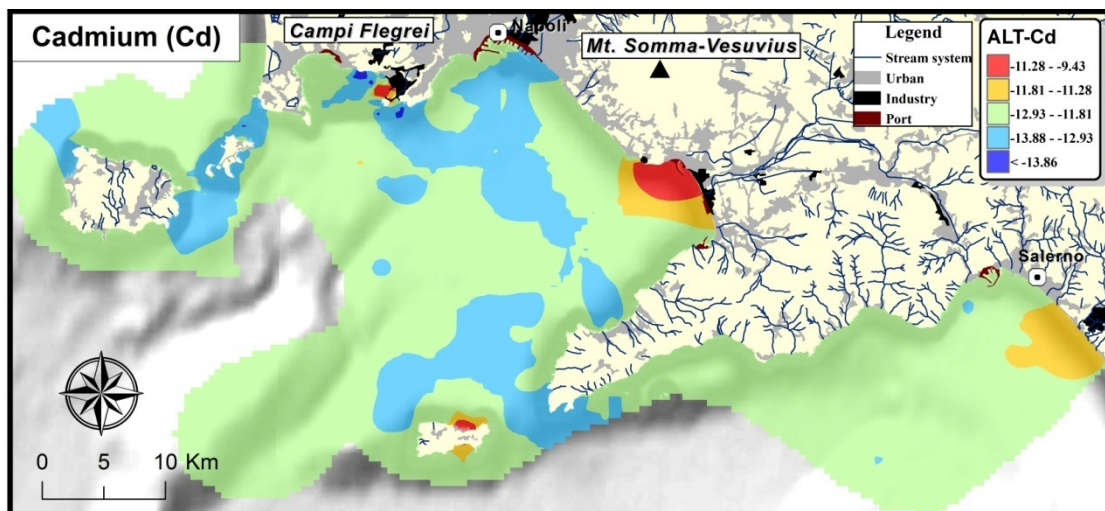
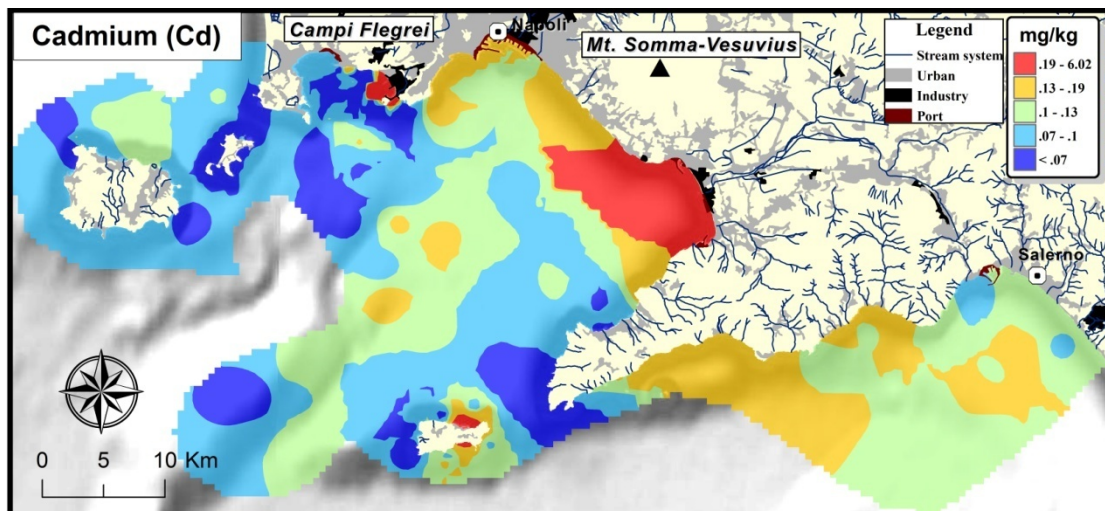
C-A plot was used to divide classes in the interpolated maps. The C-A plots of the original interpolated maps were commonly irregular (Fig. 2B) and their division in classes directly followed the fractal theory with some inaccuracies. The majority of the study area was covered with lower concentration spanned on a small range of the Y axis while a small area was, usually, characterized by higher concentrations spanned on a large range of the Y axis.. The highest value in NaSa samples set the boundary of regional and anthropogenic parts (Fig. 2). After ALT transformation, the C-A plots presented a more regular distribution and the new applied divisions resulted in a greater usefulness of the interpolated maps.

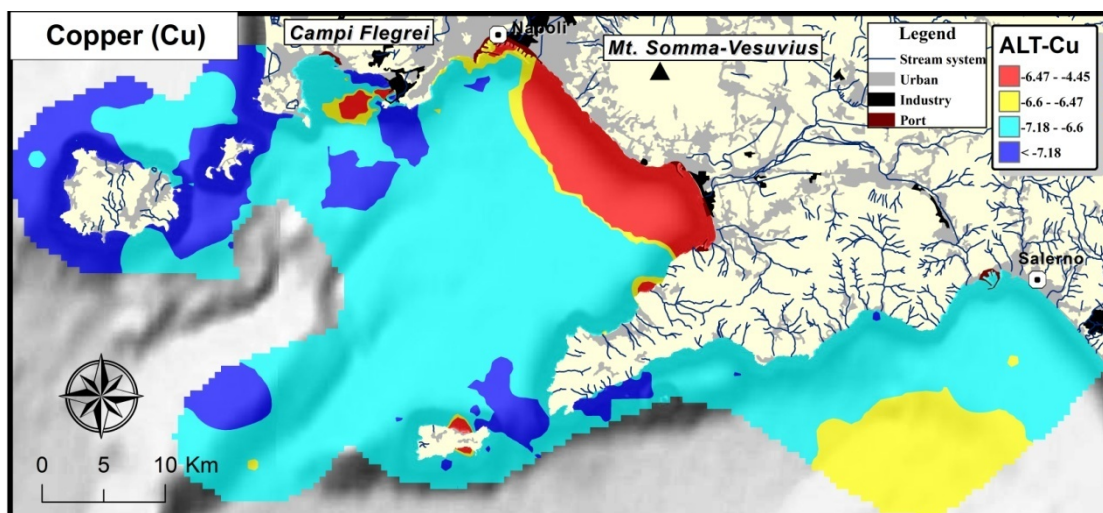
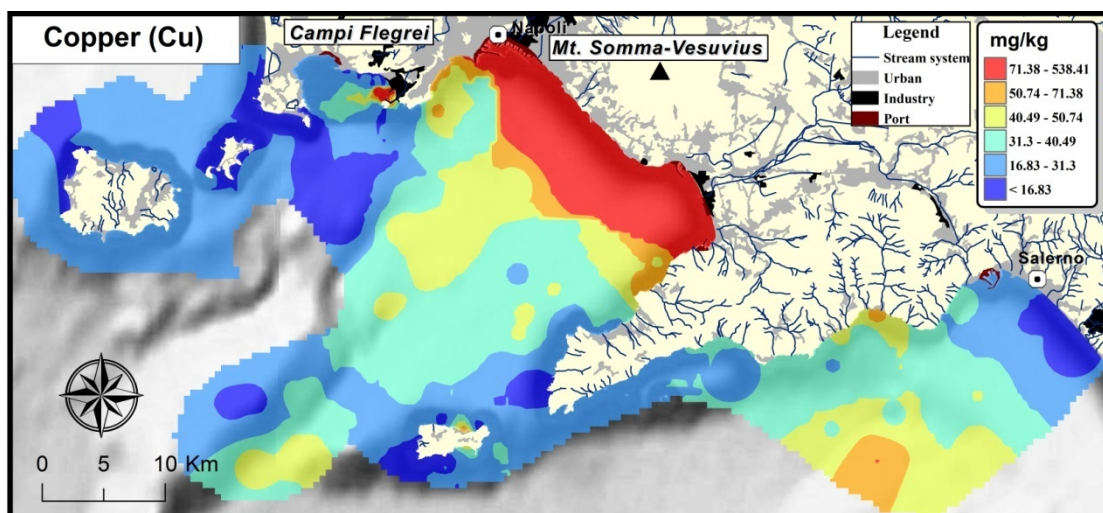
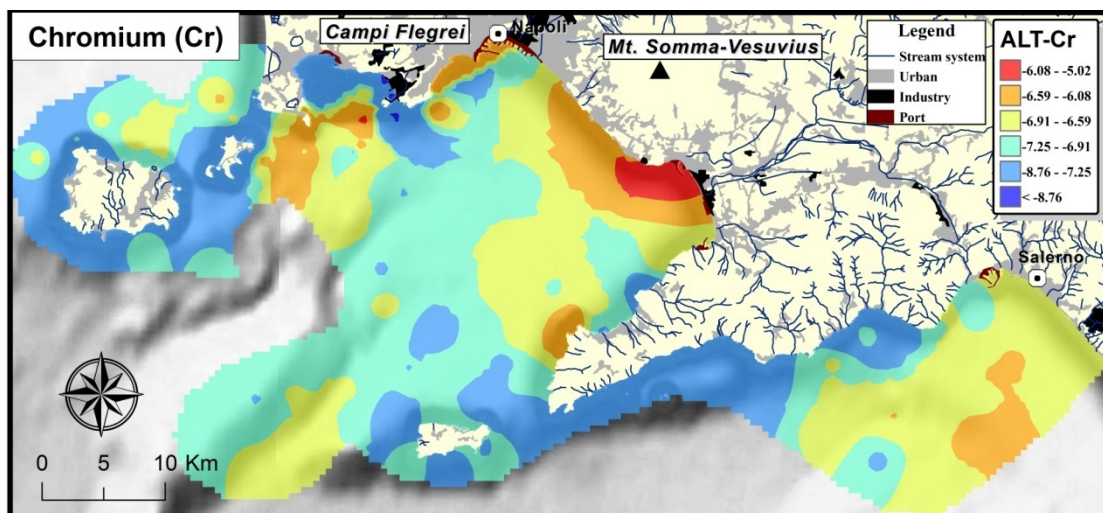
In fact, for Cd, Cr, Pb and Zn, the limited extreme-high concentrated area clearly indicates the prevailing source area of pollutants: the Bagnoli coastal area and the Sarno river estuary.

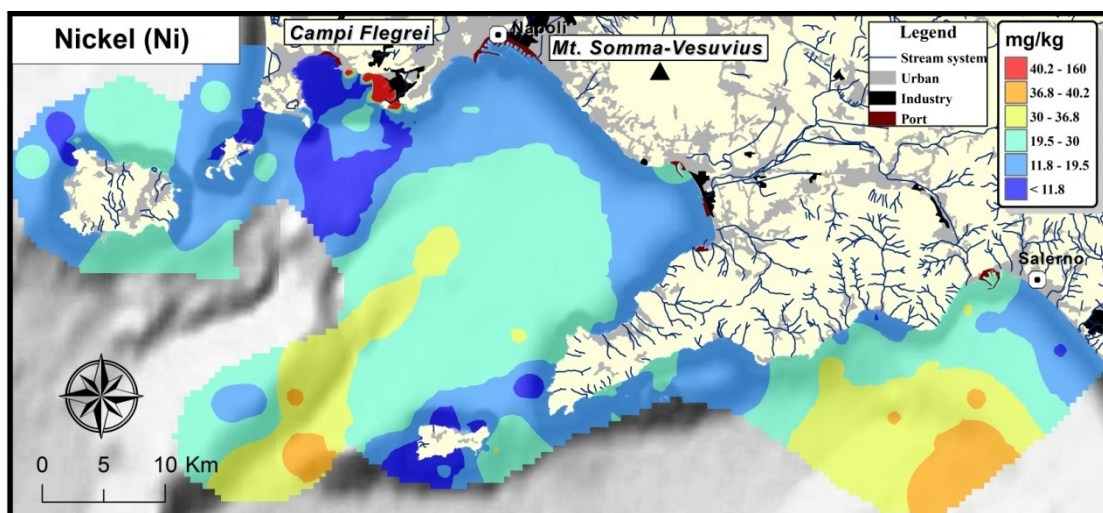
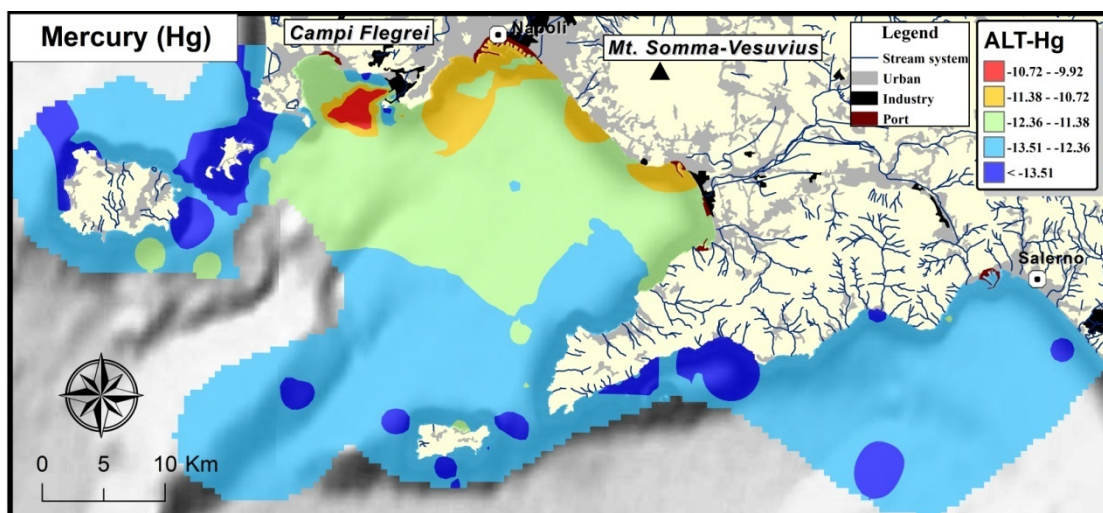
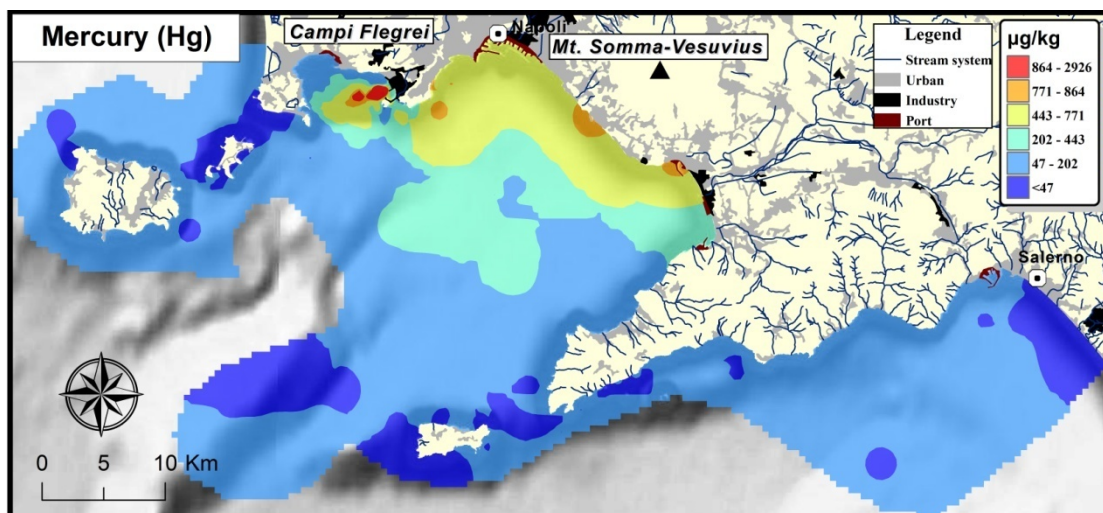
Specifically, areas with higher concentrated Cr and Ni were enlarged in outward, emphasizing the depositional centers and anthropogenic sources of Hg become more evident at the Bagnoli site. For As, geogenic source was confirmed because its distribution patterns were “flattened” by the AI normalization.

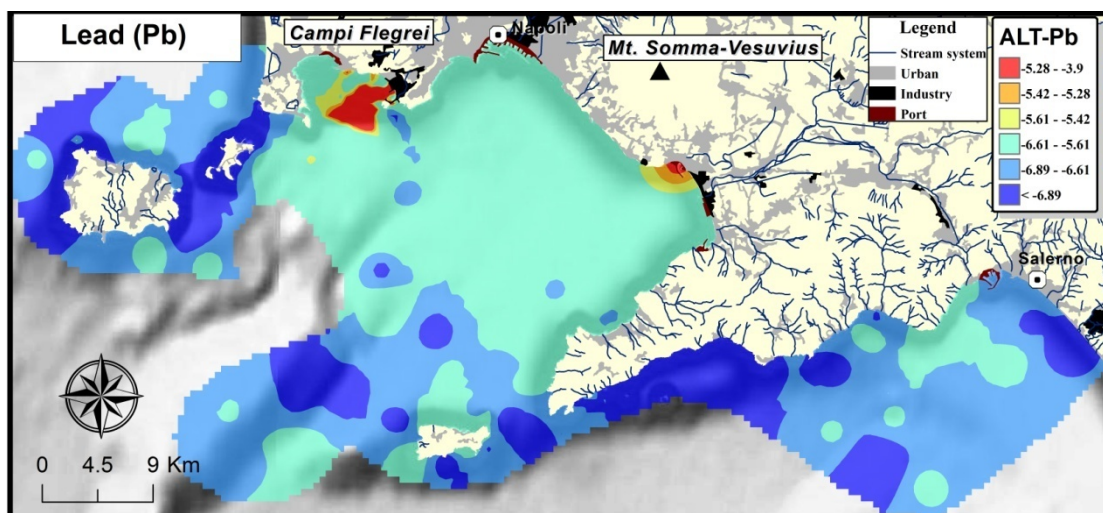
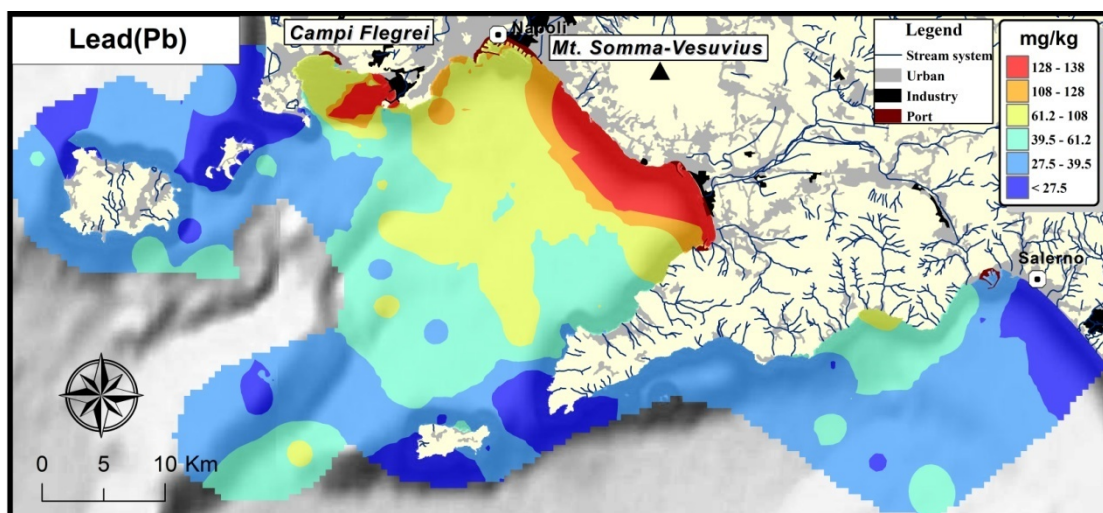
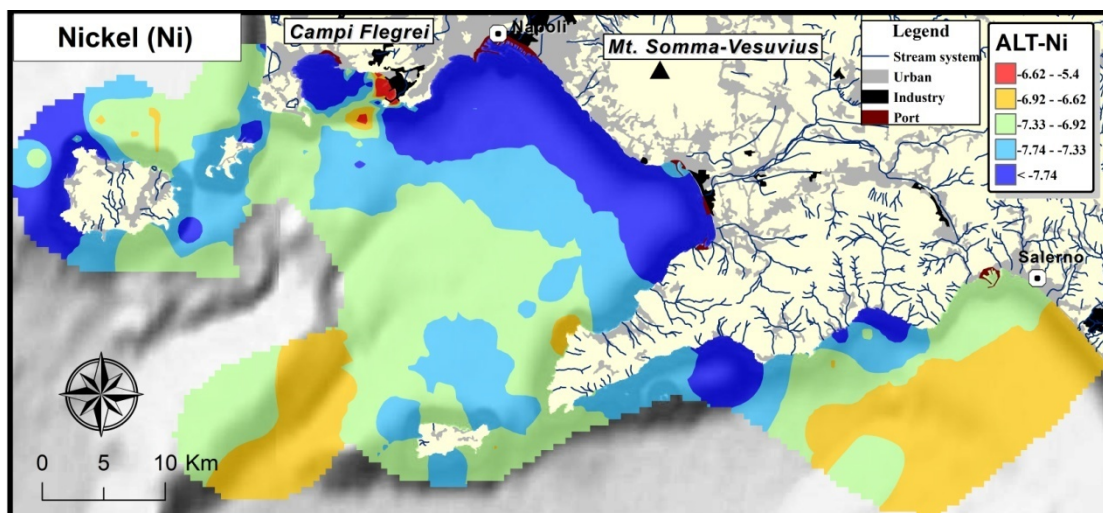
The changes obtained from ALT transformation found also a correspondence with the results of factor analysis presented below.











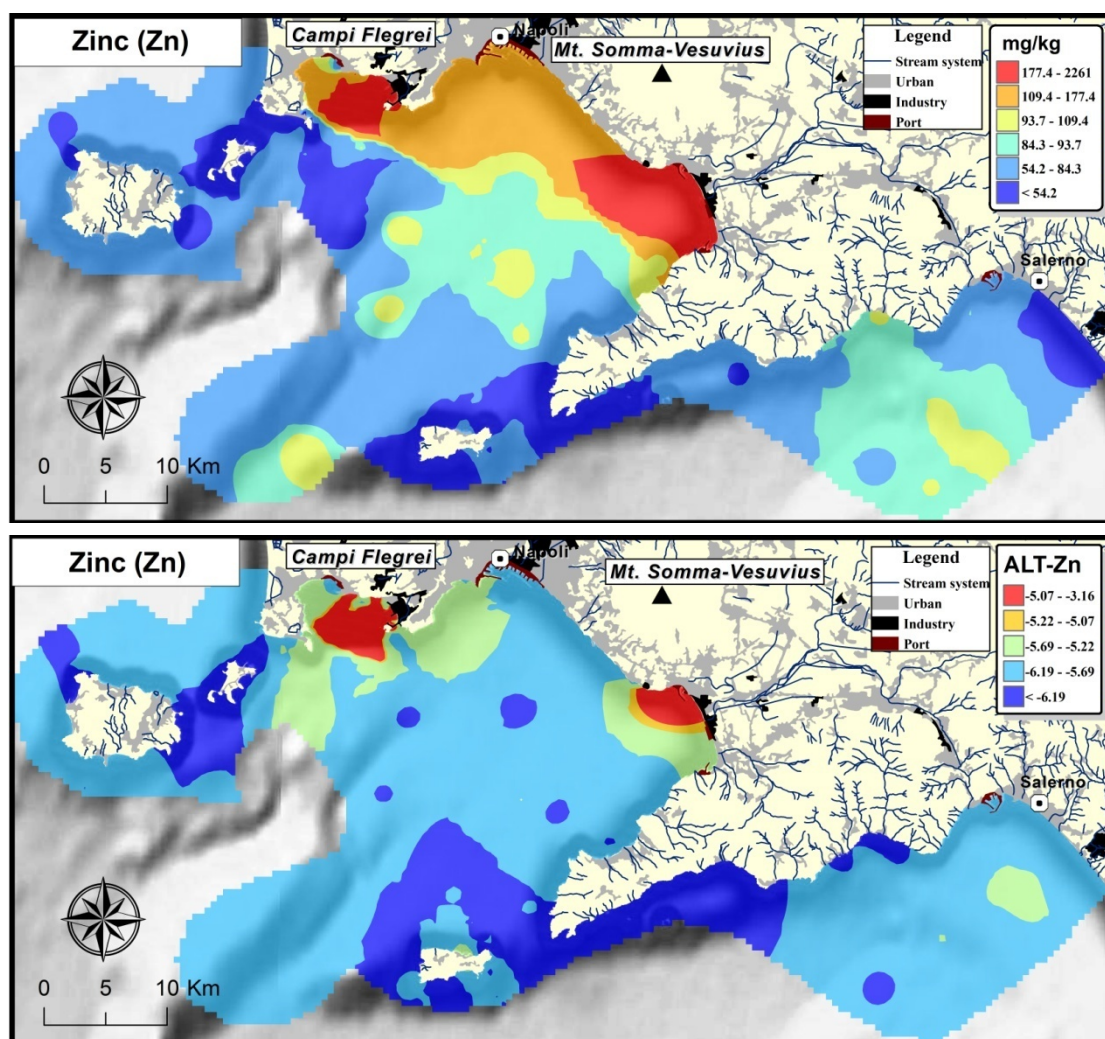
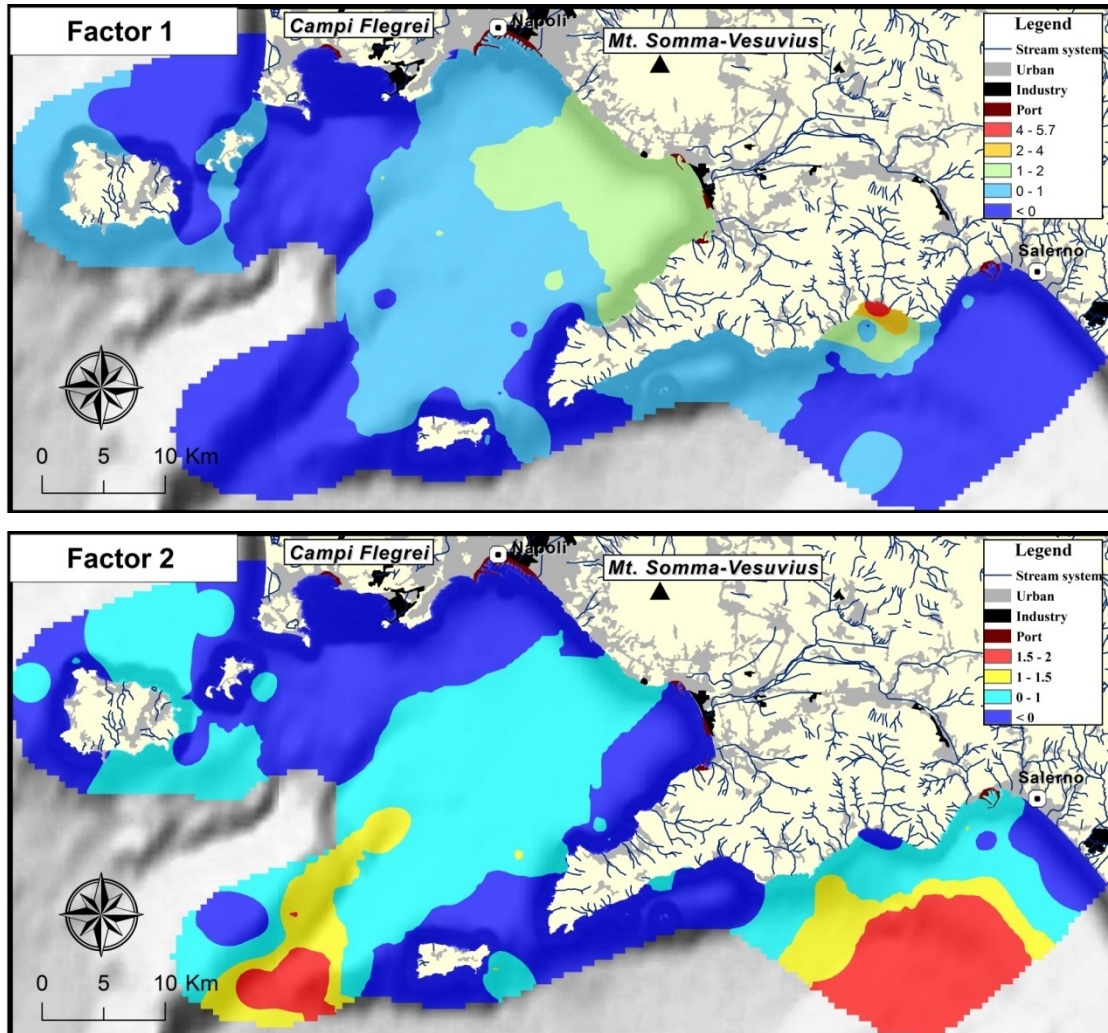


Figure 5. Interpolated maps of heavy metals/metalloids (As, Cd, Cr, Cu, Hg, Ni, Pb and Zn) in Naples and Salerno Gulfs. Elements were shown alphabetically, and marked at upleft of each map. Each element was shown in the order of origin data and ALT transformed data.

The element association of Factor 1 (F1: K-La-BE-U-Th-Al-Tl-Na-Ti-V) (Fig. 3) seems to be strongly controlled by alkali volcanic rocks, mainly outcropping in the southern sector of the Gulf of Naples (in front of the Mt. Somma-Vesuvius) and by pyroclastic sediments, mantling the carbonatic rocks outcropping along the whole coastline of the Sorrento Peninsula. In fact, these areas are characterized by factor scores ranging from 1 to 6 and factor scores of Factor 1 generally decrease from coastline toward the open sea.

The element association of Factor 2 (F2: Ni-Cu-Sc-Co-Li-Cr-Zn-V) (Fig. 3), seems to be strongly controlled by local marine cynetics. High factor scores (from 1 to 2) of Factor 2 occur mostly

far from the coastline, outward sea, where the energy of water is reduced and consequently finer sediments, generally enriched in heavy metals, deposit.



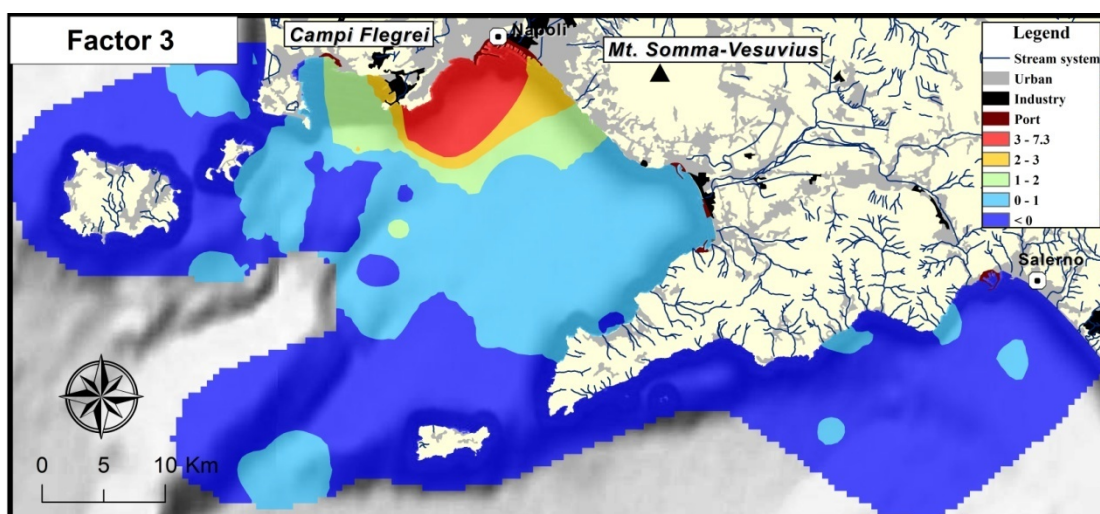


Figure 3. Interpolation maps of three factor associations. Grid pixels were classified with a colour scale using the fractal concentration–area plot (C-A method) that characterizes image patterns and classifies them into different classes based on a C-A plot. Factor 1 is the association of K-La-Ba-U-Th-Al-Tl-Na-Ti-V; factor 2 is the association of Ni-Cu-Sc-Co-Li-Cr-Zn-V; factor 3 is the association of Au-Hg-Sn-Ag-Pb-Bi-Zn-Cr

The element association of Factor 3 (F3: Au-Hg-Sn-Ag-Pb-Bi-Zn-Cr) (Fig. 3) reflects the anthropogenic contribution from the inland urban activities. In fact, factor scores, ranging from 1-7.5, is highly concentrated out of Capo Posillipo and Naples metropolitan area while the absence of high values in the Sarno estuary could be explained by the lack of sampling points in this sector.

4.3 Pollution impact

4.3.1 Pollution impact factors

Pollution impact factors were calculated for BaSi and PoNa dataset and for a single sample (GRNN 4) extracted from NaSa dataset due to it represented an outliers compared to rest of the samples.

The calculated enrichment Factor (EF) (Table 5) exhibits a general anthropogenic enrichment of heavy PTEs. (As, Cd, Cr, Cu, Hg, Ni, Pb and Zn). Pb, Zn, Cd and Hg are the most anomalous elements while only few samples show very high concentration values for Cd and Hg. I_{geo} is the most important index of pollution levels and, as shown in Table 6, only Pb, Zn and Cd are characterized by high value of this index.

D_c is a comprehensive index to estimate average pollution impact calculated from all eight

considered PTEs, and, as shown in the last column of Table 4, 81 samples show moderately to strongly degree of contamination. Sixteen samples are strongly polluted and three samples show strongly to extremely degree of contamination.

4.3.2 Pollution levels

Ecological risk assessment (ERA) is a process to evaluate the likelihood that adverse ecological effects may occur or are occurring as a result of exposure to one or more stressors (Long et al., 1995).

Italian law set guidelines for Ni, As, Cd, Hg, Cr and Pb. Among these elements, Pb in Naples and Salerno Gulfs sediments shows the highest risk (Table 7), whereas Cr shows the least risky heavy metal. Other elements show moderate risk (30% to 50%). Sediments with risky value for Ni, Cd and Hg mostly are located in Bagnoli coastal area, while sediments with As risk are distributed in the entire Naples and Salerno Gulfs.

Table 5 Sample classification according to EF. The last row exhibit the maximum EF in all samples

Class	Elements							
	Cu	Pb	Zn	Ni	As	Cd	Cr	Hg
A	101	40	39	74	128	70	128	59
B								
C	28	47	43	48	7	30	6	33
D	6	45	47	13	0	28	1	38
E	0	3	6	0	0	6	0	3
F								
G	0	0	0	0	0	1	0	2
Max EF	12.61	21.58	30.65	8.28	4.70	44.07	6.62	52.82

Table 6 Sample classification according to I_{geo} . The last row exhibit the maximum I_{geo} in all samples

Class	Elements							
	Cu	Pb	Zn	Ni	As	Cd	Cr	Hg
A	81	15	8	53	123	45	113	122
B	27	24	28	13	11	15	18	10
C	21	36	41	46	1	28	2	2
D	5	39	27	23	0	18	2	1
E	1	18	26	0	0	19	0	0
F	0	3	5	0	0	8	0	0
G	0	0	0	0	0	2	0	0
Max I_{geo}	3.78	4.95	4.81	2.57	1.11	5.70	2.97	4.68

Table 7 ERA results based on Italian law, percentage of samples that exceed guidelines of Italian law.

Element	Guideline (ppm)	Total	Naples and Salerno Gulf	Bagnoli coastal	Ports
Nickel	30	43.91%	19.59%	66.67%	0.00%
Arsenic	12	51.74%	75.26%	30.89%	75.00%
Cadmium	0.3	32.17%	0.00%	56.91%	33.33%
Mercury	0.3	31.74%	2.06%	54.47%	41.67%
Chromium	50	3.91%	2.06%	2.44%	41.67%
Lead	30	84.78%	64.95%	99.19%	91.67%

5. Conclusion

A debate on correctness of compositional data lasted for decades. In our case, the ALT transformed maps limited some heavy metals such as Cd, Cr, Pb and Zn, to their sources, enlarging the risk area of some others, such as Hg and Ni. Statistical characteristics of transformed data resulted to be more regular than original data, favoring a better class division of the distribution patters of elements. However, transformed results also introduced some difficulties into the interpretation process and they resulted to be not suitable for the estimation of to environmental pollution indexes. Furthermore, if the investigation only analyzes certain elements other than entire elements analysis, the results seems to be highly influenced by the choice of ratio-denominator.

Furthermore, the data distribution obtained from the ALT transformation resulted to be more consistent with the R mode factor analysis results.

Because ultra concentration in Bagnoli site coastal area and ports around Naples Gulf, factor 1 was concealed in single elements interpolation maps. However, after ALT transformation, sub-high concentration centre of certain elements (eg. Cr, Ni and Cu) indicate the effect of water cynetics.

Environmental impacts of heavy metals estimated with PIA and ERA indexes showed that Pb, Zn, Cd and Hg are among the most risk elements in the area.

REFERECES

- Abraham, G., Parker, R., 2008. Assessment of heavy metal enrichment factors and the degree of contamination in marine sediments from Tamaki Estuary, Auckland, New Zealand. *Environ Monit Assess* 136, 227-238.
- Adamo, P., Arienzo, M., Imperato, M., Naimo, D., Nardi, G., Stanzione, D., 2005. Distribution and partition of heavy metals in surface and sub-surface sediments of Naples city port. *Chemosphere*

61, 800-809.

- Aiello, G., Angelino, A., D'Argenici, B., Marsella, E., Pelosi, N., Ruggieri, S., Siniscalchi, A., 2005. Buried volcanic structures in the Gulf of Naples (Southern Tyrrhenian Sea, Italy) resulting from high resolution magnetic survey and seismic profiling. *Ann Geophys-Italy* 48, 883-897.
- Aitchison, J., 1982. The statistical analysis of compositional data. *Journal of the Royal Statistical Society. Series B (Methodological)*, 139-177.
- Aitchison, J., 1999. Logratios and natural laws in compositional data analysis. *Mathematical Geology* 31, 563-580.
- Aitchison, J., Barcelo-Vidal, C., Martin-Fernandez, J.A., Pawlowsky-Glahn, V., 2000. Logratio analysis and compositional distance. *Mathematical Geology* 32, 271-275.
- Aitchison, J., 2003. A concise guide to compositional data analysis, CDA Workshop, Girona.
- Albanese, S., De Vivo, B., Lima, A., Cicchella, D., 2007. Geochemical background and baseline values of toxic elements in stream sediments of Campania region (Italy). *Journal of Geochemical Exploration* 93, 21-34.
- Albanese, S., De Vivo, B., Lima, A., Cicchella, D., Civitillo, D., Cosenza, A., 2010. Geochemical baselines and risk assessment of the Bagnoli brownfield site coastal sea sediments (Naples, Italy). *Journal of Geochemical Exploration* 105, 19-33.
- Albanese, S., Iavazzo, P., Adamo, P., Lima, A., De Vivo, B., 2013a. Assessment of the environmental conditions of the Sarno river basin (south Italy): a stream sediment approach. *Environmental Geochemistry and Health* 35, 283-297.
- Albanese, S., Taiani, M.V.E., De Vivo, B., Lima, A., 2013b. An environmental epidemiological study based on the stream sediment geochemistry of the Salerno province (Campania region, Southern Italy). *Journal of Geochemical Exploration* 131, 59-66.
- Bruno, P.P.G., Rapolla, A., Di Fiore, V., 2003. Structural setting of the Bay of Naples (Italy) seismic reflection data: implications for Campanian volcanism. *Tectonophysics* 372, 193-213.
- Carranza, E.J.M., 2008. Geochemical anomaly and mineral prospectivity mapping in GIS. Elsevier.
- CCME, 2002. Canadian sediment quality guidelines for the protection of aquatic life. Canadian Environmental Quality Guidelines, in: Environment, C.C.o.M.o.t. (Ed.). MB, Winnipeg.
- Chapman, P.M., Wang, F., 2001. Assessing sediment contamination in estuaries. *Environ Toxicol Chem* 20, 3-22.
- Cheng, Q., 1999. Multifractality and spatial statistics. *Computers & Geosciences* 25, 949-961.
- Cheng, Q., 2001. Decomposition of Geochemical Map Patterns Using Scaling Properties to Separate Anomalies from Background. ISI.
- Damiani, V., Baudo, R., Rosa, S., Simone, R., Ferretti, O., Izzo, G., Serena, F., 1987. A case study: Bay of Pozzuoli (Gulf of Naples, Italy). *Hydrobiologia* 149, 201-211.
- Davis, J.C., Sampson, R.J., 2002. Statistics and data analysis in geology.
- De Vivo, B., Rolandi, G., Gans, P.B., Calvert, A., Bohrsen, W.A., Spera, F.J., Belkin, H.E., 2001. New constraints on the pyroclastic eruptive history of the Campanian volcanic Plain (Italy). *Mineralogy and Petrology* 73, 47-65.
- De Vivo, B., Lima, A., 2008. Characterization and remediation of a brownfield site: the Bagnoli case in Italy. *Environmental Geochemistry: Site Characterization, data Analysis and Case histories*. Elsevier, 355-385.
- De Vivo, B., Lima, A., Bove, M.A., Albanese, S., Cicchella, D., Sabatini, G., Di Lella, L.A., Protano, G., Riccobono, F., Frizzo, P., Raccagni, L., 2008. Environmental geochemical maps of Italy from the FOREGS database. *Geochem-Explor Env A* 8, 267-277.

- De Vivo, B., Petrosino, P., Lima, A., Rolandi, G., Belkin, H.E., 2010. Research progress in volcanology in the Neapolitan area, southern Italy: a review and some alternative views. *Miner Petrol* 99, 1-28.
- De Vivo, B., Albanese, S., Lima, A., Cicchella, D., Dinelli, E., Valera, P., Reimann, C., Birke, M., Demetriades, A., Team, G.P., 2013. GEMAS: The geochemical mapping of agricultural and grazing land soils of Europe, in: Pirrone, N. (Ed.), *Proceedings of the 16th International Conference on Heavy Metals in the Environment*.
- Egozcue, J.J., Pawlowsky-Glahn, V., Mateu-Figueras, G., Barcelo-Vidal, C., 2003. Isometric logratio transformations for compositional data analysis. *Mathematical Geology* 35, 279-300.
- Filzmoser, P., Hron, K., Reimann, C., 2009. Univariate statistical analysis of environmental (compositional) data: problems and possibilities. *Sci Total Environ* 407, 6100-6108.
- Harrison, R.M., Tilling, R., Callén Romero, M.a.S., Harrad, S., Jarvis, K., 2003. A study of trace metals and polycyclic aromatic hydrocarbons in the roadside environment. *Atmospheric Environment* 37, 2391-2402.
- Hawkes, H.E., Webb, J.S., 1962. *Geochemistry in mineral exploration*.
- Insinga, D., Molisso, F., Lubritto, C., Sacchi, M., Passariello, I., Morra, V., 2008. The proximal marine record of Somma-Vesuvius volcanic activity in the Naples and Salerno bays, Eastern Tyrrhenian Sea, during the last 3 kyrs. *J Volcanol Geoth Res* 177, 170-186.
- Lima, A., De Vivo, B., Cicchella, D., Cortini, M., Albanese, S., 2003. Multifractal IDW interpolation and fractal filtering method in environmental studies: an application on regional stream sediments of (Italy), Campania region. *Appl Geochem* 18, 1853-1865.
- Long, E.R., Macdonald, D.D., Smith, S.L., Calder, F.D., 1995. Incidence of adverse biological effects within ranges of chemical concentrations in marine and estuarine sediments. *Environmental Management* 19, 81-97.
- Long, E.R., Field, L.J., MacDonald, D.D., 1998. Predicting toxicity in marine sediments with numerical sediment quality guidelines. *Environmental Toxicology and Chemistry* 17, 714-727.
- Lu, X., Wang, L., Lei, K., Huang, J., Zhai, Y., 2009. Contamination assessment of copper, lead, zinc, manganese and nickel in street dust of Baoji, NW China. *J Hazard Mater* 161, 1058-1062.
- Lutgens, F.K., Tarbuck, E.J., 1986. *Essentials of geology*. Charles E. Merrill Publishing Company.
- Martin-Fernandez, J.A., Barcelo-Vidal, C., Pawlowsky-Glahn, V., 2003. Dealing with zeros and missing values in compositional data sets using nonparametric imputation. *Mathematical Geology* 35, 253-278.
- Milia, A., Torrente, M.M., 1999. Tectonics and stratigraphic architecture of a peri-Tyrrhenian half-graben (Bay of Naples, Italy). *Tectonophysics* 315, 301-318.
- Milia, A., Torrente, M.M., 2003. Late-Quaternary volcanism and transtensional tectonics in the Bay of Naples, Campanian continental margin, Italy. *Mineralogy and Petrology* 79, 49-65.
- Milia, A., Torrente, M.M., 2007. The influence of paleogeographic setting and crustal subsidence on the architecture of ignimbrites in the Bay of Naples (Italy). *Earth Planet Sc Lett* 263, 192-206.
- Reimann, C., Filzmoser, P., Garrett, R., Dutter, R., 2011. *Statistical data analysis explained: applied environmental statistics with R*. John Wiley & Sons.
- Reimann, C., Filzmoser, P., Fabian, K., Hron, K., Birke, M., Demetriades, A., Dinelli, E., Ladenberger, A., Team, G.P., 2012. The concept of compositional data analysis in practice - Total major element concentrations in agricultural and grazing land soils of Europe. *Sci Total Environ* 426, 196-210.
- Ridgway, J., Shimmield, G., 2002. Estuaries as repositories of historical contamination and their

- impact on shelf seas. *Estuarine, Coastal and Shelf Science* 55, 903-928.
- Sacchi, M., Insinga, D., Milia, A., Molisso, F., Raspini, A., Torrente, M.M., Conforti, A., 2005. Stratigraphic signature of the Vesuvius 79 AD event off the Sarno prodelta system, Naples Bay. *Marine Geology* 222, 443-469.
- Santos, I.R., Silva-Filho, E.V., Schaefer, C.E., Albuquerque-Filho, M.R., Campos, L.S., 2005. Heavy metal contamination in coastal sediments and soils near the Brazilian Antarctic Station, King George Island. *Mar Pollut Bull* 50, 185-194.
- Taylor, S.R., McLennan, S.M., McCulloch, M.T., 1983. Geochemistry of loess, continental crustal composition and crustal model ages. *Geochim Cosmochim Acta* 47, 1897-1905.
- USEPA, E., 1995. Method 3052: Microwave assisted acid digestion of siliceous and organically based matrices. *Test Methods for Evaluating Solid Waste*.

SECTION 2.2

OCPs and PAHs in the Gulf of Naples and Salerno and ecological risk assessment of organic pollutants

*Paper submitted to **Environmental Geochemistry and Health***

OCPs and PAHs in the Gulf of Naples and Salerno and ecological risk assessment of organic pollutants

Wang Menghan¹, Albanese Stefano^{1*}, Lima Annamaria¹, Cannatelli Claudia¹, Esposito Rosario¹, Lu Wanjun², Qi Shihua³, Flavia Molisso⁴, De Vivo Benedetto¹

¹Dipartimento di Scienze della Terra, dell'Ambiente e delle Risorse, Università degli Studi di Naples "Federico II", Via Mezzocannone 8, 80134, Naples (Italy)

²State Key Laboratory of Geological Process and Mineral Resources, China University of Geosciences, 430074, Wuhan, People's Republic of China;

³State Key Laboratory of Biogeology and Environmental Geology, China University of Geosciences, 430074, Wuhan, People's Republic of China;

⁴C.N.R. Istituto Geomare Sud, Naples, Italy

*Corresponding author: Ph. +39 0812535059; Fax +39 0812535061; E-mail: stefano.albanese@unina.it

Abstract

Coastal and estuary areas that concentrated with population commonly generated contaminated marine sediment. A comprehensive investigation of organic pollutants, PAHs and OCPs, are presented in Naples and Salerno Gulfs. PAHs as well as OCPs are generally concentrated close to Bagnoli field, while the situation of PAHs is more severe. Oppositely, sediments in the open sea (far from coastlines) are with concentration of congeners lower than criteria of adverse biological effects. Along the coastlines of Naples Gulf, especially in the Gulf of Pozzuoli, adverse biological effects are in highly risk. Incremental lifetime skin cancer risk assessment is applied to people who used to spend summer time in beaches around Naples and Salerno Gulfs. The results indicate Gulf of Pozzuoli and several locations close to ports are not suitable for beach recreation.

Keywords: PAHs and OCPs, Naples and Salerno Gulfs, risk assessment, incremental lifetime cancer risk, Bagnoli brownfield

Introduction

Intense industrial development during last century has created thousands of synthetic organic compounds, such as plastics, lubricants, fuels, pesticides and etc. All of these compounds, along with organic byproducts and residues, constitute a new category of contaminants to natural environment: persistent organic pollutants (POPs). Among all the organic contaminants, POPs are believed to be the most harmful compounds (Jones and De Voogt, 1999). POPs include variety of pesticides (OCPs), chlorobenzene species (PCBs and HCBs) and polyaromatic hydrocarbons (PAHs). POPs exhibit following four characteristics. 1) high toxicity: small quantity of POPs may cause severe damage, and

some of them are carcinogenic; 2) persistency: POPs are resistant to photolysis, chemolysis and biolysis; 3) accumulation: POPs are hydrophobic and lipophilic, which helps POPs accumulate in soil, sediment and biological adipose tissue; 4) mobility: most POPs are semi volatile and easily migrate in the atmosphere (Kukkonen et al., 2003).

Campania is the region with second-largest-population in Italy, as well as the most densely populated region in the country (Albanese et al., 2007). As primary receptors, Naples and Salerno Gulfs are undergone input of pollutants from runoff and as well by atmospheric deposition. Two sources of contaminants in sea sediments have been identified (De Vivo and Lima, 2008; De Vivo et al., 2004): 1) natural source related to the volcanic activity, which mainly contributes to high concentration of heavy metals; 2) anthropogenic source related to industrial, agricultural and municipal activities, which contributes to heavy metals and organic pollutants. Area in Bagnoli Bay with different type of factories has been affected by large industrialization process (Albanese et al., 2010). Although such factories were dismissed during the years 1990s, brownfield site still have an impact both on land and marine environment. The agrifood industry is one of the main pillars of Campania economy. The use of antycryptogamics, fungicides, and biological fertilizers may introduce quantity of organic contaminants and finally deposit them into marine sediment along with stream runoff. Burning illegally of woods and urban waste happened frequently in the lands facing the marine environment, producing a big impact in terms of pollution, whose entity still has to be properly quantified. This illegal burning has made the inland Naples area, infamously known as "Land of Fires" (Terra dei Fuochi). As a result of such illegal combustion, PAHs are widely distributed in the region included marine areas.

In this study, a general investigation of PAHs and OCPs distribution in Naples and Salerno Gulfs sea sediments is combined with researches concerned about the sediments in the Bagnoli Bay, facing the brownfield site and small ports in the Naples Gulf. Ecological risk assessments based on updated guidelines (EPA, 2005) are used to define pollution levels in concern areas. Skin cancer risk is estimated with respect to people who are used to recreate on coastline beaches along the Naples and Salerno Gulfs and Bagnoli Bay. Diagnostic ratios are applied to distinguish the PAHs source.

Study area

Naples and Salerno Gulfs are two marginal seas located along the Eastern Tyrrhenian Sea,

separated by Sorrento peninsula. Naples Gulf is semi-closed by Ischia-Procida islands in NW, Campi Flegrei and Campanian plain in NE, and Sorrento peninsula in SE, whereas Salerno Gulf locates on the coastal area offshore of Sele plain. Naples has second population density in Italy, in metropolitan arera, with about 4.4 million inhabitants, while Salerno province just has a population of 140 thousand inhabitants. Naples and Salerno provinces are among the most touristic regions around Mediterranean Sea. In 2008, 381,000 visitors visited in this area. The port of Naples is one of the most important ports in Europe, and has the Mediterranean's second-highest level of passengers flow. Naples is one of the largest transportation centers in south Italy, including railway, highway and various roads. Agriculture represents still the basic income of economy, partially replaced by service industries. Various stream system in Campania and Sele Plains carry related products and fertilizers into the Tyrrhenian Sea (Fig 1) (Di Donato et al., 2009; Romano et al., 2004).

In Bagnoli area, a large industrial area had been dismissed in the years 1990s. The area used to concentrate various industries, such as steel (Ilva) and asbestos materials manufacturing (Etenit) factories, cement (Cementir) and fertilizer (Fefderconsorzi) factories. Although such brownfield site has undergone remediation programmes funded by Italian Government, environmental pollution of both soil and sea sediments in the Bagnoli Gulf still represent a not solved problem (Albanese et al., 2010; De Vivo and Lima, 2008).

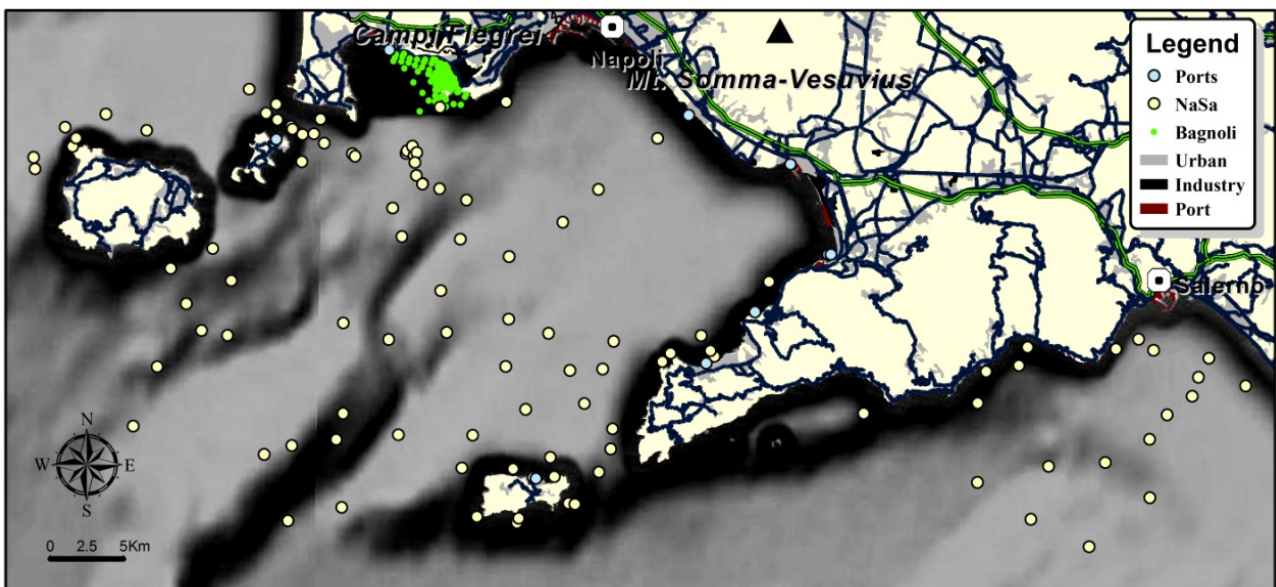


Figure 1. Study area and sampling locations

Methods

Sediments from three field sampling activities are included in this study. General survey of sea sediments in Naples and Salerno Gulfs (NaSa) provided regional information. Geochemical surveys of Bagnoli site (BaSi) and ports around Naples Gulf (BaPo) were focused on concentration of pollutants. (Fig 1)

Sampling

Sediment samples (following the directives of the national program for assessment of marine pollution of highly contaminated Italian coastal areas) were collected from 241 locations (Fig 1). Differential global positioning system (DGPS) was used to identify each location precisely.

Among NaSa samples (May, 2000), 33 samples were collected using a box-corer with an inner diameter of 25 cm, of which superficial sediments were analyzed in this study. Another 75 NaSa samples were collected by grab. Bagnoli samples (collected between November 2004 and March 2005) (Albanese et al., 2010) included surface sediments (0-20 cm) of 122 boreholes along the coastline. Samples from ports around Naples Gulf (2003) included surface sediments (0-20 cm) of 11 boreholes.

Chemical analysis

NaSa PAHs

The sediment samples were homogenized and frozen-dried. 10 g of dried sediments from each sample were spiked with 1000 ng ($5\mu\text{l}$ of 200 mg l^{-1}) of recovery surrogates (naphthalene-D8; acenaphthene-D10; phenanthrene-D10; chrysene-D12 and perylene-D12) and were Soxhlet-extracted (4-6 cycles/h) with dichloromethane for 24 h. Elemental S was removed by adding activated Cu granules to the collection flasks.

The sample extract was concentrated and solvent-exchanged to hexane and further reduced to 2-3 ml by a rotary evaporator (Heidolph4000). A 1:2 (v/v) alumina/silica gel column (both 3% deactivated with H_2O) was used to clean up the extract and PAHs were eluted with 30 ml of dichloromethane/hexane (3:7). The eluate was then concentrated to 0.2 ml under a gentle nitrogen stream. 1000 ng ($5\mu\text{l}$ of 200 mg l^{-1}) of hexamethylbenzene was added as an internal standard prior to gas chromatography- mass spectrometry (GC- MS) analysis.

PAHs were identified and quantified on a HP5972A GC-MSD following the QA/QC requirements of USEPA method 610. A standard mixture of 16 priority PAHs including naphthalene,

acenaphthylene, acenaphthene, fluorene, phenanthrene, anthracene, fluoranthene, pyrene, benzo(a)anthracene, chrysene, benzo(b)-fluoranthene, benzo(k)fluoranthene, benzo(a)pyrene, indeno(1,2,3-cd)pyrene, dibenzo(a,h)anthracene and benzo(ghi)perylene (Ultrascientific Co.) was used as a calibration solution. In the sample preparation, extracts and all fractions containing PAHs were concentrated to near dryness and constant weight for 24 hours and weighed. Prior to GC and GC-MSD injection, 2 µg of hexamethylbenzene were added to each sample as an internal standard. Detailed procedures of extraction, separation and analysis of PAHs in sediments can be found elsewhere (Chen et al., 2011).

BaPo PAHs

For PAHs determinations of BaPo samples, the description is available in Albanese et al. (2010).

NaSa OCPs

The sediment samples were homogenized and frozen-dried. Fifteen grams of dried material from each sample were spiked with 20 ng of TCmX and PCB209 as recovery surrogates and were Soxhlet-extracted with dichloromethane for 24 h. Elemental S was removed by adding activated Cu granules to the collection flasks.

The sample extract was concentrated and solvent exchanged to hexane and further reduced to 2–3 ml by a rotary evaporator (Heidolph 4000). A 1:2 (v/v) alumina/silica gel column (both 3% deactivated with H₂O) was used to clean up the extract and OCPs were eluted with 30 ml of dichloromethane/hexane (2:3). The eluate was then concentrated to 0.2 ml under a gentle nitrogen stream. Twenty nanograms (4 µl of 5 mg l⁻¹) PCNB was added as an internal standard prior to gas chromatography–electron capture detector (GC-ECD) analysis.

OCPs were identified and quantified on a HP6890 GC-MSD following the QA/QC requirements of China Geological Survey (DD2005-1 and DD2005-3). A standard mixture of 26 OCPs including *p,p'*-DDT, *o,p'*-DDT, *p,p'*-DDD, *o,p'*-DDD, *p,p'*-DDE, *o,p'*-DDE, α -HCH, β -HCH, γ -HCH, δ -HCH, HCB, aldrin, dieldrin, endrin, α -Endosulfan, β -Endosulfan, *Trans*-chlordane, *Cis*-chlordane, endosulfan sulfate, endrin aldehyde, endrin ketone, heptachlor, heptachlor epoxide, *Trans*-Nonachlor, *Cis*-Nonachlor and methoxychlor (Ultrascientific Co) was used as calibration solution. In the sample preparation, extracts and all fractions containing OCPs were concentrated to near dryness and

constant weight for 24 hours and weighed. Prior to GC and GC-MSD injection, Twenty nanograms (4 µl of 5 mg l⁻¹) PCNB were added to each sample as an internal standard. Detailed procedures of extraction, separation and analysis of OCPs in sediments can be found elsewhere (Chen et al., 2011).

Statistical analysis and geochemical mapping

In order to show the single-element geochemical distribution, a detailed univariate analysis was performed on each of produced databases. A value corresponding to 80% of the instrumental detection limit (IDL) was assigned to all data reported as below the IDL in order to allow their inclusion in the statistical analysis. Table 1 and Table 2 present all the calculated statistical parameters for each sampling sites.

Maps showing chemical data distributions were generated using the ArcGIS™ and GeoDas™ softwares (Cheng, 2001). The multifractal inverse distance weighted (MIDW) algorithm was used as the interpolation method to compile the geochemical maps and the C-A (Concentration-Area) method was used to define concentration intervals on maps (Cheng, 1999; Lima et al., 2003).

Risk assessment

Ecological risk assessment (ERA) is based on recently published sediment quality guidelines (SQG) for marine sediments. Most criteria are extracted from US-EPA (EPA, 2005) prediction based on researches of amphipods, which are the common targets for obtaining experimental data. Other sources of guidelines include Long et al. (1995), CCME (2002) and researches on Mediterranean ports (Gómez-Gutiérrez et al., 2007).

For ERA all the samples were classified into four categories: no adverse effect, slight adverse effect, mediate adverse effect and intense adverse effect. All the four categories represent the possibility of contaminants impact; intense adverse effects indicate a big possibility of biological adverse effects on creatures in touch with sediments.

Exposure to carcinogenic compounds potentially increases the risk of cancer for animals, including human beings. Incremental lifetime cancer risk (ILCR) is evaluated by multiplying total exposure with unit risk (cancer slope factor). ILCR of skin cancer was derived for recreational users in Naples and Salerno beaches as follow:

$$ILCR = \frac{SF_{\text{derm}} \times C_{\text{fine}} \times SA \times SL \times RAF_{\text{derm}} \times RT \times D_{\text{day}} \times D_{\text{year}}}{B_w \times LE}$$

where:

Table 1. Statistical parameters for PAHs in NaSa and BaPo sediments

Item	NaSa ($\mu\text{g}/\text{kg}$)			BaPo (mg/kg)		
	Max	Min	Mean	Max	Min	Mean
Naphthalence	110.89	0.03	5.98	632.570	0.000	16.965
Acenaphthylene	248.67	0.00	5.94			
Acenaphthene	25.73	0.00	1.24	109.490	0.000	3.155
Fluorene	229.24	0.03	7.48	89.880	0.000	3.189
Phenanthrene	1795.23	2.19	48.86	588.350	0.010	18.294
Anthracene	877.29	0.03	23.44	178.960	0.000	7.239
Fluoranthene	2989.10	0.03	100.99	623.880	0.010	27.926
Pyrene	1986.59	0.66	75.35	555.250	0.005	24.379
Benz(a)anthracene	1214.29	0.03	55.90	166.880	0.005	9.078
Chrysene	1550.28	0.03	90.75	160.130	0.005	9.180
Benzo(b)fluoranthene	1373.55	0.03	65.68	159.950	0.005	8.910
Benzo(k)fluoranthene	766.51	0.03	45.88	62.220	0.005	3.684
Benzo(a)pyrene	3506.01	0.03	125.37	166.760	0.005	8.968
Indeno(1,2,3-c,d)pyrene	4376.45	0.03	111.67	441.700	0.000	11.843
Dibenzo(a,h)anthracene	523.04	0.03	18.08	7.330	0.000	0.513
Benzo(ghi)perylene	2099.81	0.03	67.60	69.790	0.000	5.462
Total	18710.01	9.58	850.22	2947.440	0.005	152.327

ILCR (unitless) = Incremental lifetime cancer risk;

SF_{derm} ($\text{kg}\cdot\text{day}/\text{mg}$) = Dermal slope factor (chemical specific) = 25 $\text{kg}\cdot\text{day}/\text{mg}$ (Knafla et al., 2006);

C_{fine} (mg/kg) = BaP equivalence concentration in finer sediments;

SA (cm^2) = Surface area of entire body = 17640 cm^2 (Hussain et al., 1998; Richardson, 1997);

SL ($\text{kg}/\text{cm}^2\cdot\text{event}$) = Sediment loading rate to exposed skin = 0.35 kg/cm^2 (Marley et al., 2005; Shoaf et al., 2005);

RAF_{derm} (unitless) = Dermal relative adsorption factor = 0.148 (Moody et al., 2007);

RT (event) = Recreation times in beach sites per day = 1 (Hussain et al., 1998);

D_{day} (days) = Recreation days per year = 30 days (Hussain et al., 1998);

D_{year} (year) = Total of years with exposure = 30 years (Hussain et al., 1998);

B_w (kg) = Body weight of receptor = 70.7 kg (Richardson, 1997);

LE (years) = Life expectancy = 70 years (Richardson, 1997).

Table 2. Statistical parameters for OCPs in NaSa sediments

Item	Max	Min	Mean
α -HCH	0.32	0.00	0.07
β -HCH	18.18	0.00	0.62
γ -HCH	0.98	0.00	0.10
Δ -HCH	1.09	0.00	0.15
HCB	1.40	0.00	0.43
o,p`-DDE	13.53	0.00	0.23
p,p`-DDE	4.03	0.00	0.18
o,p`-DDD	6.42	0.00	0.12
p,p`-DDD	81.37	0.00	0.93
o,p`-DDT	6.06	0.00	0.29
p,p`-DDT	45.65	0.00	1.81
trans-Chlordan	0.60	0.00	0.04
cis-Chlordan	1.55	0.00	0.06
α -Endosulfan	2.35	0.00	0.09
Heptachlor	17.15	0.00	1.89
Aldrin	4.17	0.00	0.33
Hepte	0.41	0.00	0.01
trans-Nonachlor	3.06	0.00	0.07
Dieldrin	0.43	0.00	0.02
Endrin	28.95	0.00	0.44
β -Endosulfan	2.63	0.00	0.08
cis-Nonachlor	32.73	0.00	0.31
Endrin aldehyde	0.56	0.00	0.01
Endosulfan-sal	4.02	0.00	0.13
Endrin ketone	33.62	0.00	0.35
methoxychlor	13.00	0.00	1.18
Total HCH	19.06	0.00	0.94
Total DDE	17.57	0.00	0.41
Total DDD	82.01	0.00	1.05
Total DDT	45.65	0.00	2.10

When spending leisure time on beach site, usually finer sediments is more easily adsorbed by the skin. Concentration of contaminanst in finer sediments (clay + silt) was determined as total

concentration in sediments divided by the fraction of finer group (Hussain et al., 1998).

The concentrations of each PAH compound were converted to the corresponding BaP toxic equivalent concentrations by using the Toxic Equivalency Factor (TEF) (Nisbet and LaGoy, 1992) reported in Table 3 and for each sample the total PAHs concentration was determined by summing the BaP toxic equivalents calculated per each compound.

Table 3. PAHs toxic equivalency factors (TEFs) with respect to BaP (Nisbet and LaGoy, 1992)

Compound	TEFs
Benzo[a]anthracene	0.1
Benzo[a]pyrene	1
Benzo[b]fluoranthene	0.1
Benzo[k]fluoranthene	0.1
Benzo[g,h,i]perylene	0.1
Chrysene	0.01
Dibenzo[a,e]pyrene	1
Dibenzo[a,l]pyrene	100
Dibenzo[a,h]pyrene	1
Dibenzo[a,h]anthracene	1
Indeno[1,2,3-cd]pyrene	0.1
Pyrene	0.001

PAHs diagnostic ratio

Five PAHs diagnostic ratios were selected to infer the source of PAHs in the area: An/178, BaA/228, Fluo/Fluo+PY, IP/IP+Bghi (Jiang et al., 2009; Tobiszewski and Namiesnik, 2012; Yunker et al., 2002) and $\sum\text{COMB}/\sum\text{PAH}$ (Hwang et al., 2003). The source criteria are shown in Table 4.

Table 4. Diagnostic ratios used with their typically reported values for particular processes

	Petrogenic	Petroleum combustion	Solid combustion
An-178	<0.1	>0.1	>0.1
BaA-228	<0.2	[0.2,0.35](mixed)	>0.35(pyrolytic)
FyFl	<0.4	[0.4,0.5]	>0.5
IP	<0.2	[0.2,0.5]	>0.5
$\sum\text{COMB}/\sum\text{PAHs}$	<0.3	>0.3	>0.3

Results

Distribution in Naples and Salerno Gulfs

Concentration of Σ_{16} PAHs in both the NaSa samples and BaPo samples ranged from 0.1 to 18710.01 mg/kg. Mean Σ_{16} PAHs concentrations are 850.22 and 335.83 mg/kg in NaSa samples and BaPo samples respectively. The concentration of PAHs in NaSa samples mainly exceeded that of BaPo samples. The most concentrated congeners in NaSa samples was benzo(a)pyrene with mean value of 125.37 mg/kg. Following high concentration congeners were indeno(1,2,3-c,d)pyrene and fluoranthene. In BaPo samples, pyrene had the biggest mean concentration of 54.42 mg/kg, followed by benzo(b)fluoranthene, chrysene and benzo(a)pyrene. Among all priority congeners, only naphthalence and acenaphthene were more concentrated in BaPo samples than NaSa samples. (Table 1)

General distribution pattern of single congeners is similar to the distribution pattern of Σ_{16} PAHs. Highest concentration of PAHs mainly is distributed southeast of Posillipo Peninsula along the metropolitan area of Naples. Higher total PAHs occur out of Pozzuoli Gulf and ports out facing Mt. Vesuvius. Intermediate concentration occurs north of Capri Island and west of Sorrento Peninsula. (Fig 2)

Only five kinds of OCPs in the investigated areas exhibit ecological risks at different levels. Endrin and DDE are mostly concentrated in the sample GRNN 4, which is close to Posilippo. γ HCH also concentrates in the sample of GRNN 4, but with some sub concentration site in the central area of Naples Gulf. Two concentration centers of DDD locate out of Posilippo and Salerno port. DDT, the most risk OCP compound in the study area, exhibits similar distribution pattern as γ HCH.

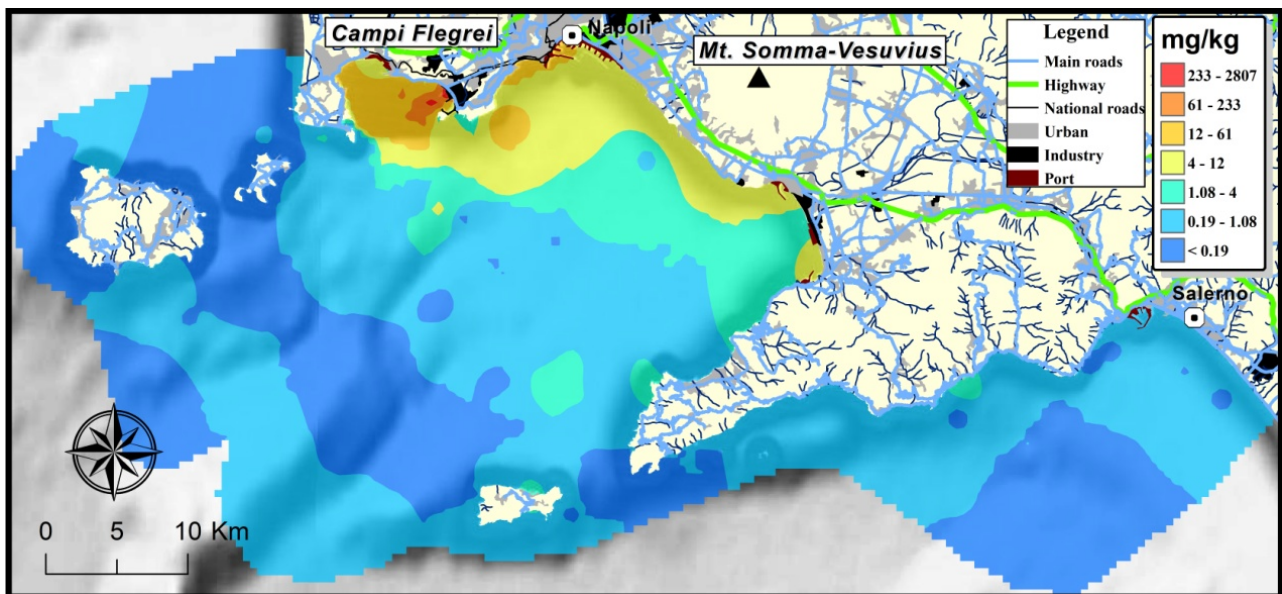


Figure 2. Total PAHs distribution in Naples and Salerno Gulfs

Risk assessment

In the frame of ERA, several criteria were refined based on region-specific effects and contaminant information. Most compounds guidelines used in this study were adopted from a recent EPA-NOAA report (EPA, 2005), because limited Mediterranean guidelines exist (Table 5).

Concentrations of certain POPs in sea sediments were entirely below the Threshold Effect Concentration (TEC) level. Among the POPs indicating probable risk, 70% to 90% samples show values below the TEC level in NaSa samples, indicating absence of obvious adverse biological effects. The fact that most concentrations were below the threshold values might indicate a lower contamination level of POPs in Naples and Salerno Gulfs sediments. POPs concentrations above Probable Effect Concentration (PEC) levels were calculated to range between 0% to 5.5% in NaSa samples. Only one sample (less than 1%) in NaSa samples exceeds the Extreme Effect Concentration (EEC) for indeno (1,2,3-c,d) pyrene; toxicity induced by chemicals in sample GRNN 4 is highly probable.

Table 5. Sediment quality guidelines (SQGs) (in $\text{ng}\cdot\text{g}^{-1}$ dry weight) considered for PAHs and OCPs in the marine environment

Item	T20/TEC	T50/PEC	T80/EEC
Acenaphthene	19	120	710
Acenaphthylene	14	140	1420
Anthracene	34	290	2490
Benz(a)anthracene	61	470	3530
Benzo(a)pyrene	69	520	3910
Benzo(b)fluoranthene	120	1110	9410
Benzo(g,h,i)perylene	67	500	3710
Benzo(k)fluoranthene	70	540	4120
Chrysene	82	650	5190
Dibenz(a,h)anthracene	19	110	690
Fluoranthene	120	1030	8950
Fluorene	19	110	660
Indeno(1,2,3-c,d)pyrene	68	490	3480
Naphthalene	30	220	1570
Perylene	74	450	2770
Phenanthrene	68	460	3060
Pyrene	120	930	6980
Total PAH	4022	44790	
DDT	1.3	7	143
DDE	2.4	55	460
DDD	1.8	15	100
HCB	n.d	22	230
Dieldrin	0.83	2.9	10
Lindane	0.32	0.99	
Endrin	2.67	62.4	
Heptachlor epoxide	0.6	2.74	
Chlordane	2.26	2.79	

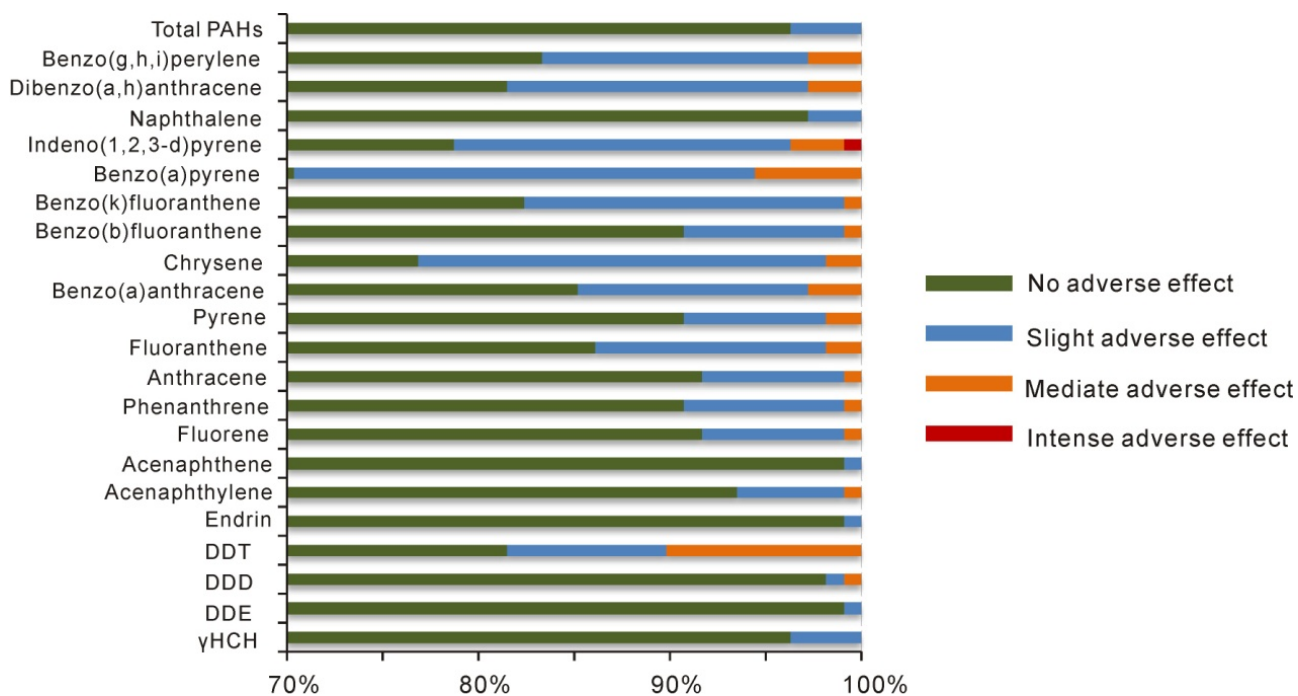


Figure 3. Percentage of NaSa samples with different level of ecological risks.

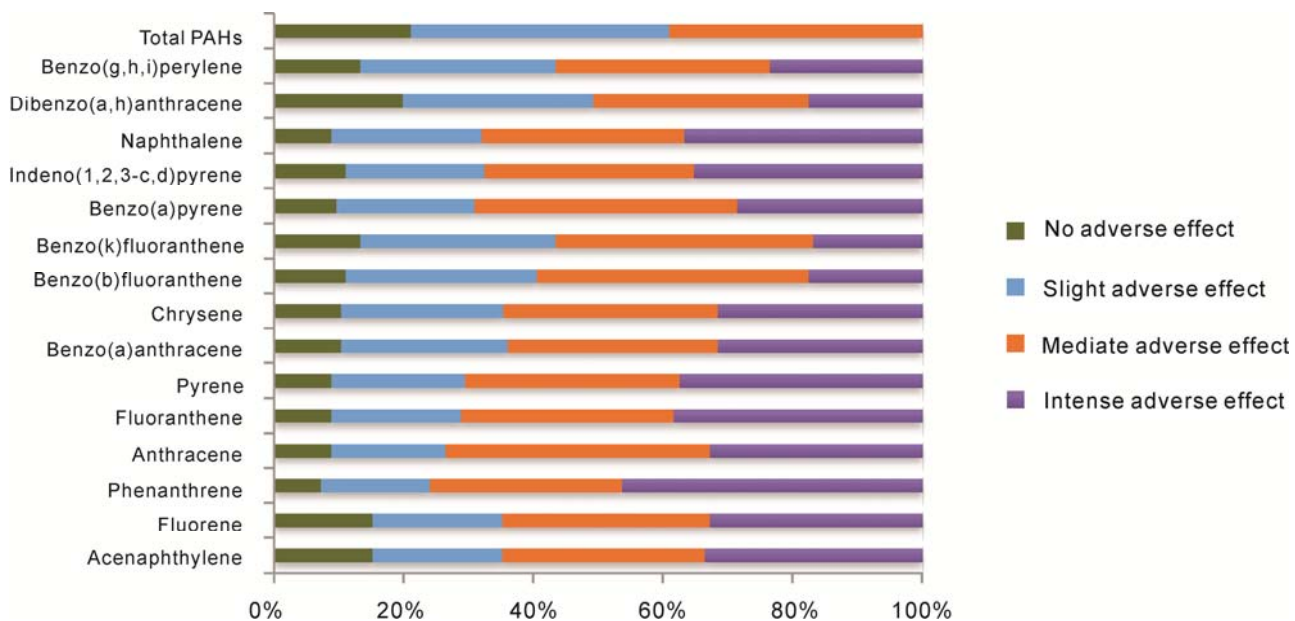


Figure 4. Percentage of BaPo samples with different level of ecological risks.

The percentage of samples with adverse biological effects is much larger (83% to 97%) in BaPo samples, mainly due to the highly pollution levels of Bagnoli site samples. Less than 20% of samples

indicate safety regarding PAHs concentration. One third of the remaining samples exceeds EEC criteria which indicates a high risk toxicity for the creatures in contact with such sediments (Fig 3 and Fig 4).

Naples and Salerno Gulfs are well-known for their recreation beach around Mediterranean Sea. Local citizens (4.4 millions) are attracted to sun bathing and swimming along the beach. The result ILCR estimation for people bathing and swimming along coastline indicates a high increase of getting skin cancer in areas close to Bagnoli brownfield site and out of Capo Posilipo (Fig 5A and Fig 5B). Beaches located close to certain ports (including Ischia, Procida and Capri islands) are also not suitable for recreation activities (Fig 5C and Fig 5D). However, skin cancer risk is also determined by sediment grain size distribution. For example, rocky shore in the Pozzuoli Gulf with high ILCR value (for example, center coastlines in Pozzuoli bay) poses little health risk because finer sediment fraction is limited being difficult to be adsorbed by skin.

PAH ratios and their indication of PAH sources

Five diagnostic PAHs ratios were selected following the stable properties of different congeners with same molecular weight. Combustion of fuels and solids results less stable PAHs congeners, whereas PAHs with petrogenic (associated with petroleum production) source congeners are more stable.

Most diagnostic PAHs ratios indicate mainly sources from solid combustion. The solid combustion PAHs sources occur both in NaSa and BaPo samples. However, value of BaA/228 ratio in NaSa Gulfs points out a three-divisions pattern: petrogenic, mixed and combustion. Similarly a petrogenic source explains Fl/PY values in BaPo areas, accompanied by an increased portion of petroleum fuel (Table 6).

a) Fluoranthene (Fl) to fluoranthene plus pyrene (Py) (Fig 7)

Fl/Py ratio could reflect specific fuel, solid or liquid. The Fl/Py ratio varied between 0.034 to 0.606 in NaSa areas and 0.04 to 0.98 in BaPo areas. The samples with value below 0.4 are ascribed as petrogenic sources, while those with value above 0.4 are ascribed as combustion sources. Within the latter, Fl/Py value exceeding 0.5 indicates a solid combustion and those between 0.4 and 0.5 are explained by petroleum combustion. The average of Fl/Py ratio in NaSa samples is 0.53, with most of the samples having values higher than 0.5; this suggests that most of the samples fall in the category

of solid combustion products. The average Fl/Py ratio in BaPo samples has a value of 0.48. Almost half of the samples fall in the category of solid combustion products, a quarter in the category of petroleum combustion sources and the rest quarter of samples in the category of petrogenic PAHs. Petrogenic sources PAHs widely spread along coastal area of Naples Gulf, as well surrounding Procida Island and Capri Island and out of Positano. The remaining area, mainly the open sea, is occupied by combustion source PAHs, with most in the category of solid fuel.

b) Indeno[1,2,3-cd]pyrene (IP) to IP plus benzo[ghi]perylene (IP+Bghi) (Fig 7)

The IP/IP+Bghi ratio varies between 0.02 to 0.72 in NaSa samples and 0.26 to 0.99 in BaPo samples. The samples with value below 0.2 are ascribed to the category of petrogenic sources, whereas those with values above 0.2 are ascribed to combustion sources. Within the category of combustion source, IP/IP+Bghi ratio values exceeding 0.5 indicate a solid combustion and those between 0.2 and 0.5 indicate petroleum combustion. The average of IP/IP+Bghi ratio in NaSa samples is 0.56, with most of samples having values higher than 0.5, suggesting that most of the samples belong to the category of solid combustion products. The same pattern is found in BaPo samples, with an average IP of 0.64. Petrogenic sources PAHs only are scattered distributed along Sorrento Peninsula and Capri Island. The remaining area is occupied by combustion source PAHs, with most in the category of solid fuel. Small areas, such as out of Bocca Grand, have values in the category of liquid fuel.

c) Benzo[a]anthracene (BaA) to BaA plus chrysene (228) (Fig 7)

The BaA/228 ratio generally varies between 0.10 to 0.56 in NaSa and 0.07 to 0.98 in BaPo, commonly ranging from 0.1 to 0.6. The average of BaA/228 ratio ratio is 0.3 and 0.46 for NaSa and BaPo samples respectively. The samples with values below 0.2 are ascribed to the category of petrogenic sources, whereas those with values above 0.35 are ascribed to combustion sources. The samples with values between 0.2 and 0.35 are ascribed to mixed sources. BaA/228 ratio in NaSa samples points out a three-divisions pattern: petrogenic, mixed and combustion. In BaPo samples, most indicate purely combustion sources, whereas 14% samples indicate mixed sources of 228 weight congeners. Area with petrogenic sources is larger than the ones indicated by other parameters, including areas northwest of Naples Gulf and open sea in Salerno Gulf. Combustion sources category occupied areas of open sea in Naples Gulf. .

d) Anthracene (An) to anthracene plus phenancerene (178) (Fig 7)

The An/178 ratio generally varies between 0.003 to 0.664 in NaSa and 0.1 to 0.8442 in BaPo. Most of samples have values above 0.1, being attributed to combustion sources category. NaSa samples are mainly distributed in two ranges, below 0.4 and above 0.5, while BaPo samples mainly have values below 0.4. The average of An/178 ratio is 0.28 and 0.33 for NaSa and BaPo samples respectively. Based on An/178, petrogenic source PAHs is mostly concentrated in Bagnoli site, out of Sarno estuary and outer area of Salerno Gulf.

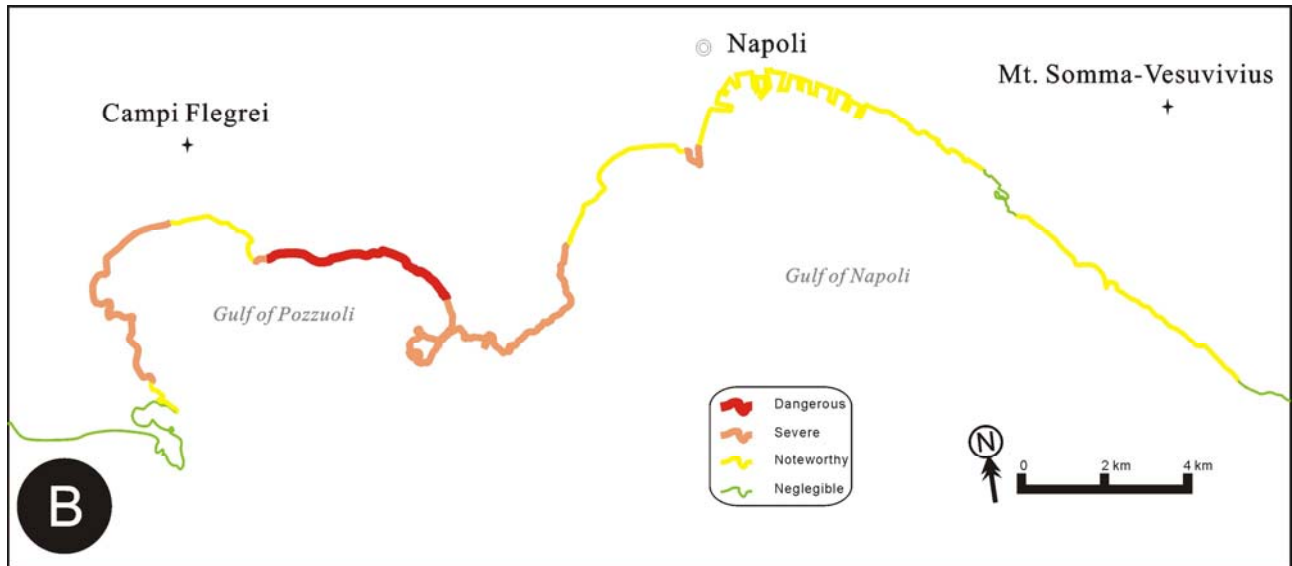
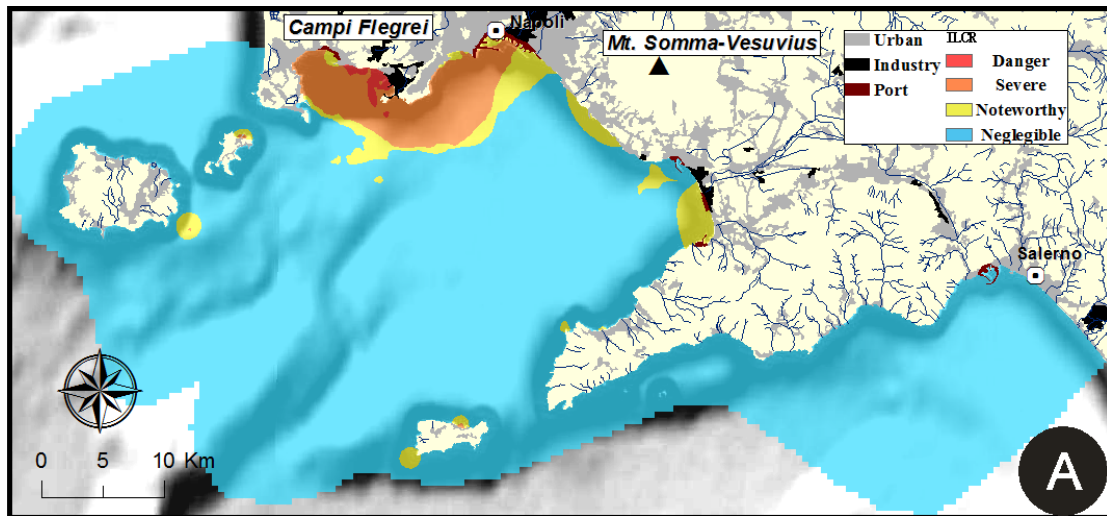
e) $\Sigma COMB / \Sigma PAH$ (Fig 7)

$\Sigma COMB$ represents the summation of combustion congeners including fluoranthene, pyrene, benzo(a)anthracene, chrysene, benzo(b)fluoranthene, benzo(k)fluoranthene, benzo(e)-pyrene, benzo(a)pyrene, indeno(1,2,3-cd)pyrene and benzo(g,h,i)perylene. The ratio of $\Sigma COMB$ vs ΣPAH represents a new proposed diagnostic ratio. PAHs in the combustion sources category have values greater than 0.3. The $\Sigma COMB$ ratio varies between 0.10 to 0.96 in NaSa samples and 0.09 to 0.93 in BaPo samples. The average of $\Sigma COMB$ ratio is 0.82 and 0.75 for NaSa and BaPo respectively.

Petrogenic sources category PAHs only occur areas surrounding Procida Island, out of Sarno estuary and Bagnoli site.

Table 6. Percentage of samples ascribed to different categories based on diagnostic ratio analysis

	NaSa				BaPo			
	combustion solid	liquid	mixed	petrogenic	combustion solid	liquid	mixed	petrogenic
An178	84.26%			15.74%	99.19%			0.81%
FIFIPy	91.67%	6.48%		1.85%	49.60%	24.00%		26.40%
BaA228	35.19%		36.11%	28.70%	83.09%		13.97%	2.94%
IIPBghi	81.48%	15.74%		2.78%	88.46%	11.54%		0.00%
COMB/TOTAL	98.15%			1.85%	96.00%			4.00%



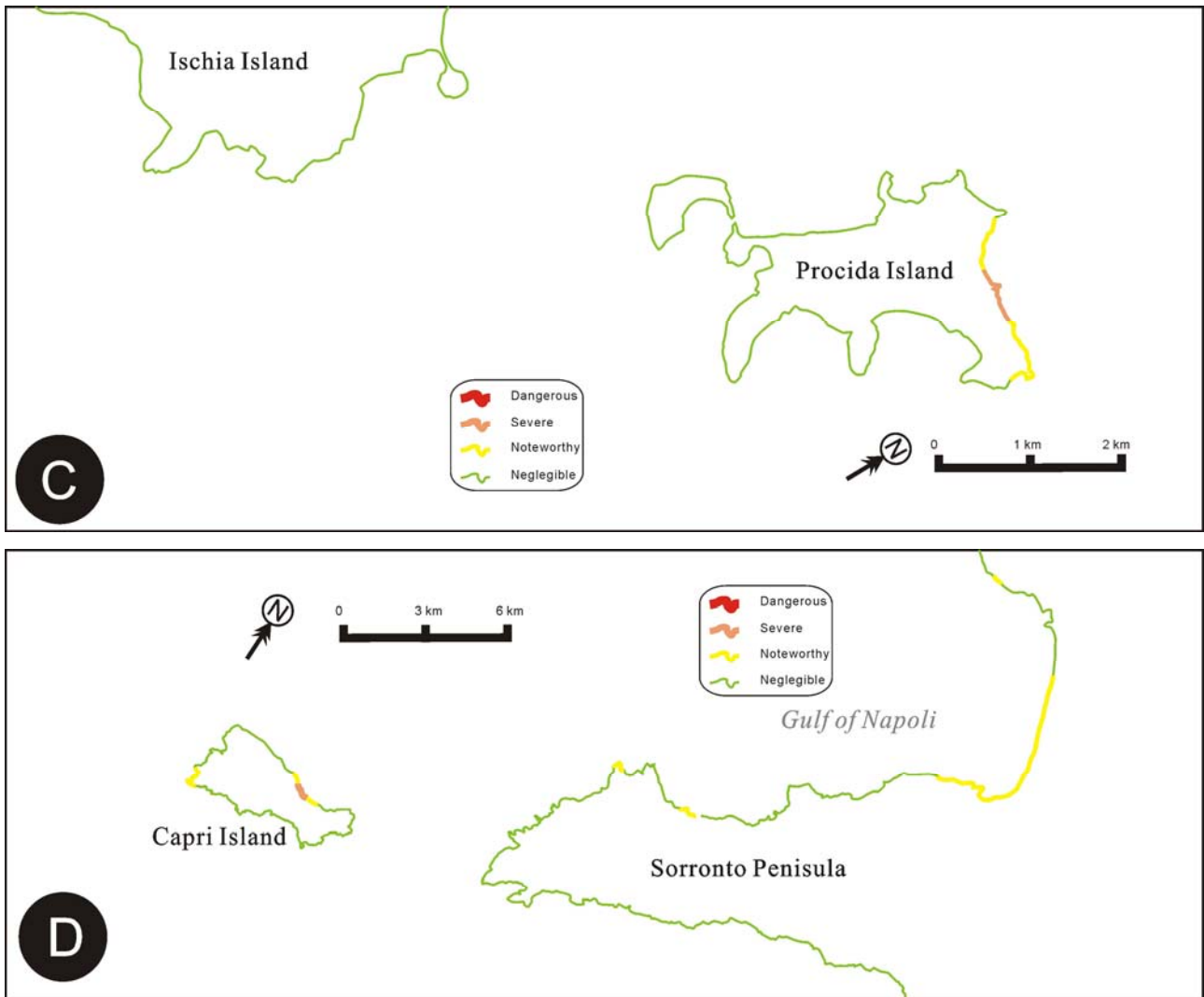


Figure 5. Incremental lifetime skin cancer risk assessment was calculated due to skin contact with finer sediment with PAHs. The areas with ILCR value lower than 1×10^{-5} were characterized as negligible area (blue areas in A and green areas in B to D). From 1×10^{-5} to 1×10^{-4} , ILCR was classified as Noteworthy (yellow); from 1×10^{-4} to 1×10^{-3} , ILCR was identified as Severe; Higher than 1×10^{-3} , ILCR was Dangerous to human beings. A is the general interpolation map of ILCR, while B (Gulfs of Pozzuoli and Naples), C (Islands Ischia and Procida) and D (Capri Island and Sorrento Peninsula) give out the specific description of coastlines with cancer risk.

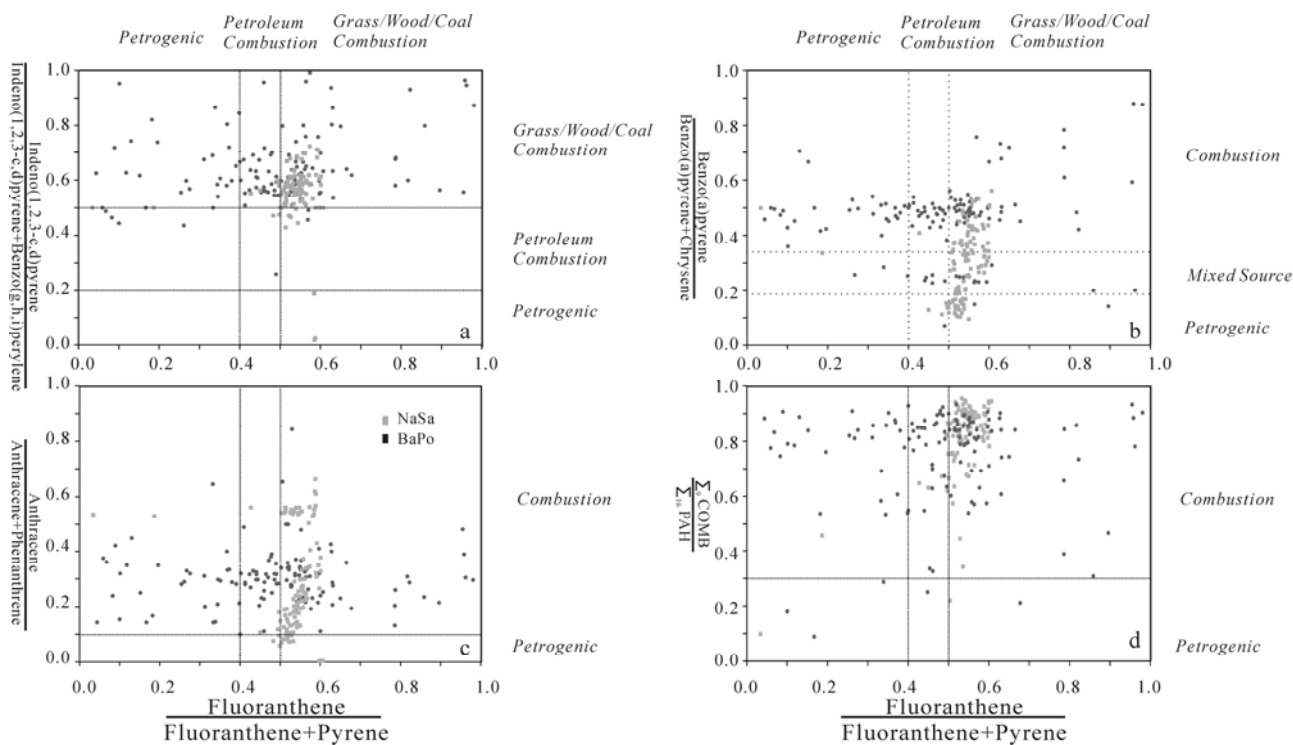
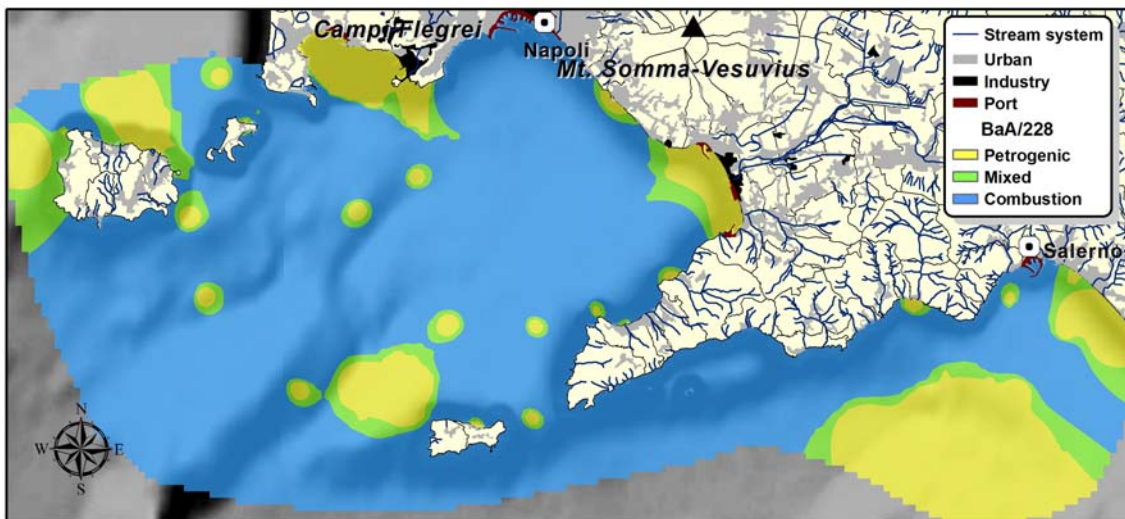
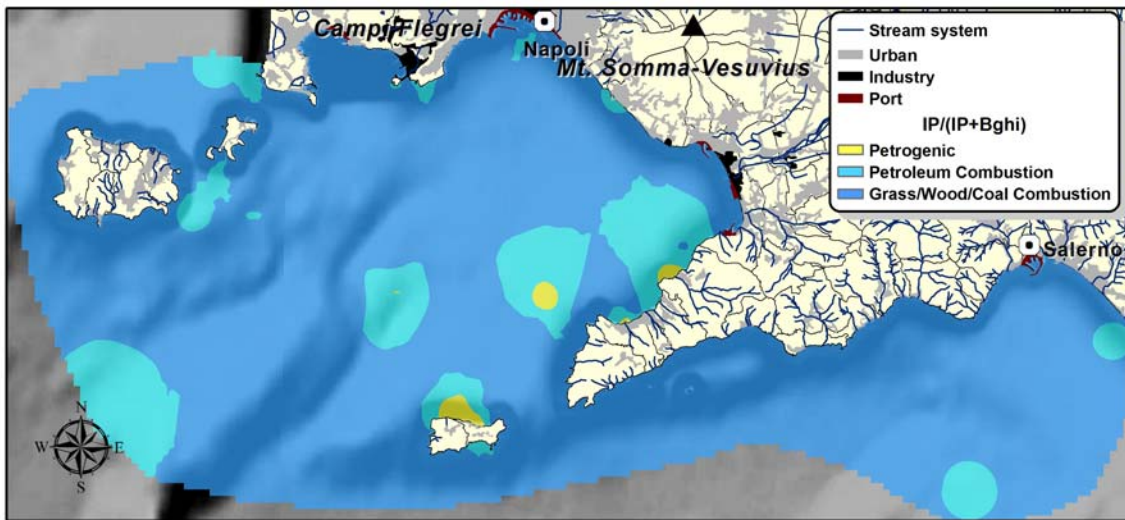
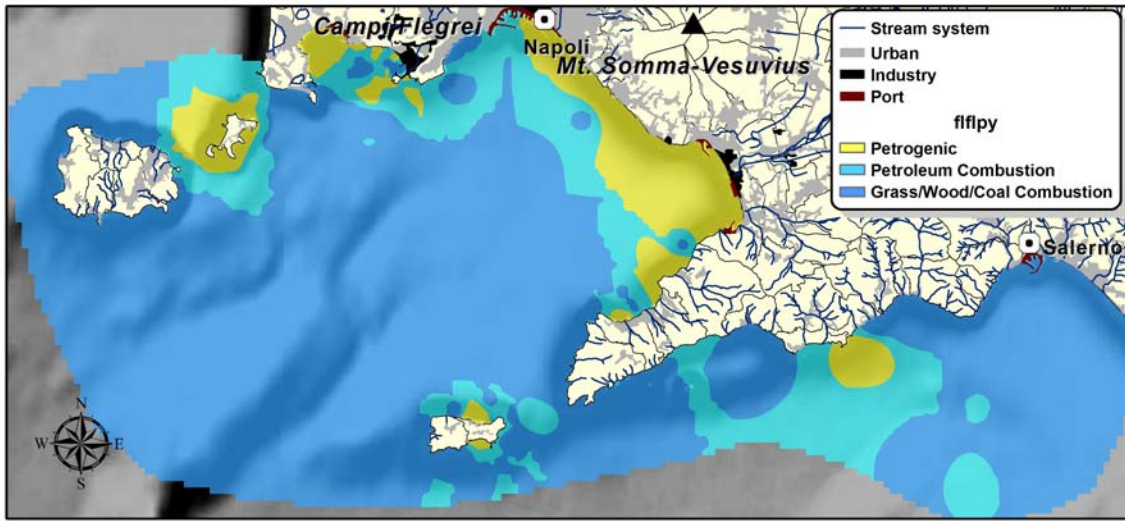


Figure 6. PAH cross plots for the ratio of (a) indeno[1,2,3-cd]pyrene (IP) to IP plus benzo[ghi]perylene (IP+Bghi), (b) anthracene (An) to anthracene plus phenanthrene (178), (c) benzo[a]anthracene (BaA) to BaA plus chrysene (228) and (d) summation of combustion generated congeners to the summation of total 16 priority PAHs vs. fluoranthene (Fl) to fluoranthene plus pyrene (Py). Combustion congeners included fluoranthene, pyrene, benzo(a)anthracene, chrysene, benzo(b)fluoranthene, benzo(k)fluoranthene, benzo(e)-pyrene, benzo(a)pyrene, indeno(1,2,3-cd)pyrene and benzo(g,h,i)perylene



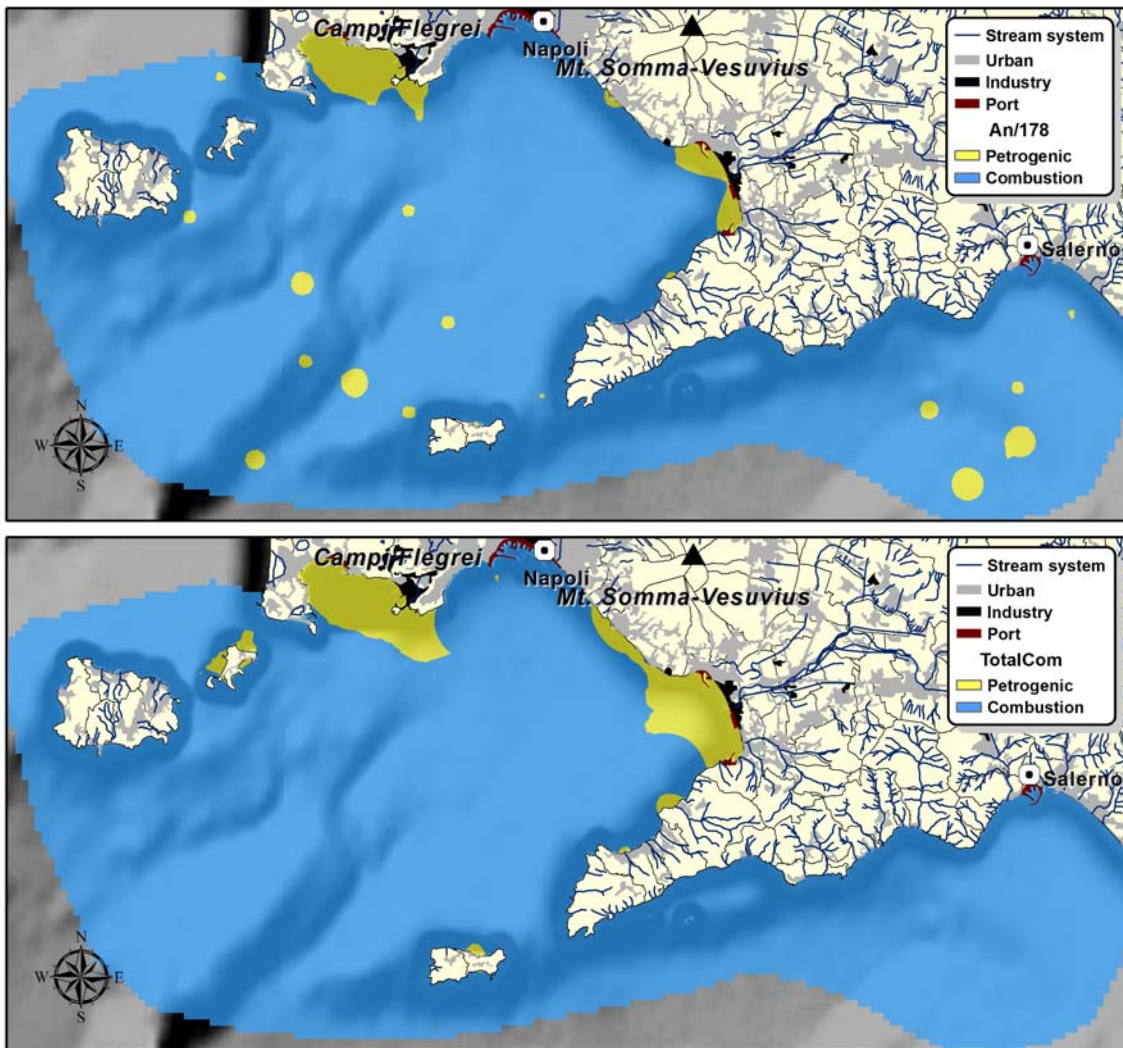


Figure 7 Interpolated value of PAHs diagnostic ratio values in Naples and Salerno Gulfs.

Conclusions

PAHs are generally concentrated in the area closed to Bagnoli field, where used to be occupied by developed industries. OCPs in the area are less severe than the situation of PAHs. Ecological risk assessments are used to classify the contaminants in the area based on most advanced sediment quality guidelines. Most of compounds in opensea are with concentration less than criteria of adverse biological effects. However, in the area closed to Bagnoli field, over 80% of samples are bonded to risk quantity of PAHs. Creatures in contact with 20% to 45% of samples in the area may have intense biological harms. Beach recreation in the Gulf of Pozzuoli and out of Capo Posillipo is potentially

harmful due to ILCR estimation of skin cancer. Also beaches vicinity to ports around Naples Gulf are in the risk of increase baseline of cancer incidence. According to results of PAHs diagnostic ratios, most of PAHs are generated from combustion process. Solid fuel combustion, such as wood, grass and coal produce the major section of PAHS.

An influence from dismantled industries in Bagnoli area still dominates regional environment. Intense anthropogenic activities, such as vehicles fuel, burning accidents and garbage disposal, are significant source of pollutants in the area.

References

- Albanese, S., De Vivo, B., Lima, A., and Cicchella, D. (2007): Geochemical background and baseline values of toxic elements in stream sediments of Campania region (Italy): *Journal of Geochemical Exploration*, 93, 1, 21-34.
- Albanese, S., De Vivo, B., Lima, A., Cicchella, D., Civitillo, D., and Cosenza, A. (2010): Geochemical baselines and risk assessment of the Bagnoli brownfield site coastal sea sediments (Naples, Italy): *Journal of Geochemical Exploration*, 105, 1-2, 19-33.
- CCME, 2002, Canadian sediment quality guidelines for the protection of aquatic life. *Canadian Environmental Quality Guidelines*, in *Environment*, C. C. o. M. o. t., ed.: Winnipeg, MB.
- Chen, W., Jing, M., Bu, J., Ellis Burnet, J., Qi, S., Song, Q., Ke, Y., Miao, J., Liu, M., and Yang, C. (2011): Organochlorine pesticides in the surface water and sediments from the Peacock River Drainage Basin in Xinjiang, China: a study of an arid zone in Central Asia: *Environmental monitoring and assessment*, 177, 1, 1-21.
- Cheng, Q. (1999): Multifractality and spatial statistics: *Computers & Geosciences*, 25, 9, 949-961. (2001): Decomposition of Geochemical Map Patterns Using Scaling Properties to Separate Anomalies from Background: ISI.
- De Vivo, B., and Lima, A. (2008): Characterization and remediation of a brownfield site: the Bagnoli case in Italy: *Environmental Geochemistry: Site Characterization, data Analysis and Case histories*. Elsevier, 355-385.
- De Vivo, B., Lima, A., Albanese, S., Cicchella, D., Fedele, L., and Frattini, P. (2004): Geochemical environmental maps of soils of Campania Region urban areas, Italy: *Geochim Cosmochim Acta*, 68, 11, A535-A535.
- Di Donato, V., Esposito, P., Garilli, V., Naimo, D., Buccheri, G., Caffau, M., Ciampo, G., Greco, A., and Stanzione, D. (2009): Surface-bottom relationships in the Gulf of Salerno (Tyrrhenian Sea) over the last 34 kyr: Compositional data analysis of palaeontological proxies and geochemical evidence: *Geobios-Lyon*, 42, 5, 561-579.
- EPA, U. S., 2005, Predicting Toxicity to Amphipods from Sediment Chemistry.
- Gómez-Gutiérrez, A., Garnacho, E., Bayona, J. M., and Albaigés, J. (2007): Screening ecological risk assessment of persistent organic pollutants in Mediterranean sea sediments: *Environ Int*, 33, 7, 867-876.
- Hussain, M., Rae, J., Gilman, A., and Kauss, P. (1998): Lifetime health risk assessment from exposure of recreational users to polycyclic aromatic hydrocarbons: *Archives of*

- Environmental Contamination and Toxicology, 35, 3, 527-531.
- Hwang, H. M., Wade, T. L., and Sericano, J. L. (2003): Concentrations and source characterization of polycyclic aromatic hydrocarbons in pine needles from Korea, Mexico, and United States: *Atmospheric Environment*, 37, 16, 2259-2267.
- Jiang, Y. F., Wang, X. T., Jia, Y., Wang, F., Wu, M. H., Sheng, G. Y., and Fu, J. M. (2009): Occurrence, distribution and possible sources of organochlorine pesticides in agricultural soil of Shanghai, China: *J Hazard Mater*, 170, 2-3, 989-997.
- Jones, K. C., and De Voogt, P. (1999): Persistent organic pollutants (POPs): state of the science: *Environmental Pollution*, 100, 1-3, 209-221.
- Knafla, A., Phillipps, K. A., Brecher, R. W., Petrovic, S., and Richardson, M. (2006): Development of a dermal cancer slope factor for benzo a pyrene: *Regulatory Toxicology and Pharmacology*, 45, 2, 159-168.
- Kukkonen, J. V. K., Landrum, P. F., Mitra, S., Gossiaux, D. C., Gunnarsson, J., and Weston, D. (2003): Sediment characteristics affecting desorption kinetics of select PAH and PCB congeners for seven laboratory spiked sediments: *Environ Sci Technol*, 37, 20, 4656-4663.
- Lima, A., De Vivo, B., Cicchella, D., Cortini, M., and Albanese, S. (2003): Multifractal IDW interpolation and fractal filtering method in environmental studies: an application on regional stream sediments of (Italy), Campania region: *Appl Geochem*, 18, 12, 1853-1865.
- Long, E. R., MacDonald, D. D., Smith, S. L., and Calder, F. D. (1995): Incidence of adverse biological effects within ranges of chemical concentrations in marine and estuarine sediments: *Environmental management*, 19, 1, 81-97.
- Marley, B. S., Jeffry, H. S., Golan, K., John, S., and John, C. K. (2005): Child dermal sediment loads following play in a tide flat: *Journal of Exposure Science and Environmental Epidemiology*, 15, 5, 407-412.
- Moody, R. P., Joncas, J., Richardson, M., and Chu, I. (2007): Contaminated Soils (I): In Vitro Dermal Absorption of Benzo[a]Pyrene in Human Skin: *Journal of Toxicology and Environmental Health, Part A*, 70, 21, 1858-1865.
- Nisbet, I. C. T., and LaGoy, P. K. (1992): Toxic equivalency factors (TEFs) for polycyclic aromatic hydrocarbons (PAHs): *Regulatory Toxicology and Pharmacology*, 16, 3, 290-300.
- Richardson, G. M., 1997, *Compendium of Canadian human exposure factors for risk assessment*: O'Connor Associates Environmental Inc.
- Romano, E., Ausili, A., Zharova, N., Magno, M. C., Pavoni, B., and Gabellini, M. (2004): Marine sediment contamination of an industrial site at Port of Bagnoli, Gulf of Naples, Southern Italy: *Mar Pollut Bull*, 49, 5-6, 487-495.
- Shoaf, M. B., Shirai, J. H., Kedan, G., Schaum, J., and Kissel, J. C. (2005): Adult dermal sediment loads following clam digging in tide flats: *Soil Sediment Contam*, 14, 5, 463-470.
- Tobiszewski, M., and Namiesnik, J. (2012): PAH diagnostic ratios for the identification of pollution emission sources: *Environ Pollut*, 162, 110-119.
- Yunker, M. B., Macdonald, R. W., Vingarzan, R., Mitchell, R. H., Goyette, D., and Sylvestre, S. (2002): PAHs in the Fraser River basin: a critical appraisal of PAH ratios as indicators of PAH source and composition: *Org Geochem*, 33, 4, 489-515.
- EPA, U.S., 2005. *Predicting Toxicity to Amphipods from Sediment Chemistry*, in: Agency, U.S.E.P. (Ed.), Washington, D.C.

SECTION 2.3

Polycyclic aromatic hydrocarbons in the soils of a densely populated region and associated human health risks: the Campania Plain (Southern Italy) case study

*Paper accepted by **Environmental Geochemistry and Health**
(in press)*

Polycyclic aromatic hydrocarbons in the soils of a densely populated region and associated human health risks: the Campania Plain (Southern Italy) case study.

Albanese Stefano^{1,*}, Fontaine Barbara², Chen Wei³, Lima Annamaria¹, Cannatelli Claudia¹, Piccolo Alessandro², Qi Shiua³, Wang Menghan¹, De Vivo Benedetto¹

¹Dipartimento di Scienze della Terra, dell'Ambiente e delle Risorse, Università degli Studi di Naples "Federico II", Via Mezzocannone 8, 80134, Naples (Italy)

²Dipartimento di Scienze del Suolo, della Pianta, dell'Ambiente e delle Produzioni Animali, Università degli Studi di Naples "Federico II", Via Università 100, 80055, Portici, Naples (Italy)

³State Key Laboratory of Biogeology and Environmental Geology, China University of Geosciences, 430074, Wuhan, People's Republic of China;

*Corresponding author: Ph. +39 0812535059; Fax +39 0812535061; E-mail: stefano.albanese@unina.it

Abstract

Polycyclic aromatic hydrocarbons (PAHs) are a major class of environmental pollutants mainly arising from anthropogenic activities. In this paper, the behavior and the distribution patterns of sixteen PAHs, listed as priority pollutants by the United States Environmental Protection Agency (USEPA), were evaluated in 119 soil samples collected in different areas of Campania region in the southern Italy. The study area covers about 2,400 km², roughly corresponding to the Campanian Plain which is a wide coastal belt that goes from the Volturno River plain, in the north-west of the Campania region, to the Sarno River basin, southward of the volcanic complex of Mt. Vesuvius. The observation of the geochemical distribution patterns showed that both high (HMW-PAHs) and low molecular weight PAHs (LMW-PAHs) are mostly concentrated within the metropolitan area of Naples, the Agro Aversano area and, partly, the Sarno River basin. In accordance with the Italian environmental law (D. Lgs. 152/2006) these areas should be considered potentially contaminated and not suitable for a residential use unless an environmental risk analysis does not demonstrate their safety. As a consequence, a preliminary quantitative risk assessment (PQRA) enhanced by the use of GIS was run revealing the existence of an incremental lifetime cancer risk higher than 1×10^{-5} for the city of Naples and for some other populous areas.

Keywords: Polycyclic aromatic hydrocarbons; soil pollution; geochemical mapping; health risk; Campania region.

1. Introduction

Polycyclic aromatic hydrocarbons (PAHs) are widespread contaminants in the environment. Once released they may remain in the environment for a long time and can undergo a long-range transportation (Sun et al. 2009). Some PAHs are receiving increasing attentions due to their

carcinogenic and mutagenic properties. (Enzminger and Ahlert 1987). Sixteen PAHs including naphthalene (Nap), acenaphthylene (Acy), acenaphthene (Ane), fluorene (Flo), phenanthrene (Phe), anthracene (Ant), fluoranthene (Fla), pyrene (Pyr), benzo[a]anthracene (BaA), chrysene (Chr), benzo[b]fluoranthene (BbF), benzo[k]fluoranthene (BkF), indeno[1,2,3-cd]pyrene (IcdP), dibenzo[a,h]anthracene (DahA), benzo[g,h,i]perylene (BghiP), and the well known carcinogenic PAH compound benzo[a]pyrene (BaP) have been listed as priority pollutants by the United States Environmental Protection Agency (USEPA 2013).

Although generated by natural combustion processes, such as volcanic eruptions, forest and grassland fires, PAHs are primarily emitted in urban environment by anthropogenic sources, such as vehicle emissions, fossil fuel power generation, petroleum refining, industrial processing, chemical manufacturing, oil spills and coal tars (Masih and Taneja 2006; Nam et al. 2003).

Soil is the most relevant environmental sink for PAHs; due to the high hydrophobicity and their stable chemical structure, PAHs are slightly or completely insoluble in water and they are adsorbed on soil particles, particularly on soil organic matter (Means et al. 1980). Hence, the physical-chemical properties of soils are responsible for the retention of PAHs in soil matrices. The organic carbon content, the hydrophobicity of soil organic matter and soil texture were estimated to be the most significant parameters controlling the environmental availability of PAHs (Weissenfels et al. 1992; Murphy et al. 1990; Conte et al. 2001). The more PAHs are bio-available, the more they may affect the biological and biochemical activity of soil (Shuttleworth and Cerniglia 1995). As PAHs in soils can be dispersed by both surface runoff and air dust production, soils can be also considered as the main secondary source of these compounds in air and sediments (Mai et al. 2003). Moreover, PAHs can be absorbed by plants and potentially transferred into animals and humans through the food chain (Froehner et al. 2011).

The main objective of this study was to determine the distribution patterns of these contaminants in the surface soils of a large coastal area of the Campania region (Italy), and hence to identify their possible emission sources.

2. Study area

A study area of about 2,400 km² roughly corresponds to the Campanian Plain which is a wide coastal belt that goes from the Volturno River plain, in the north-west of the region, to the Sarno River

basin, southward of the volcanic complex of Mt. Vesuvius (Fig. 1A).

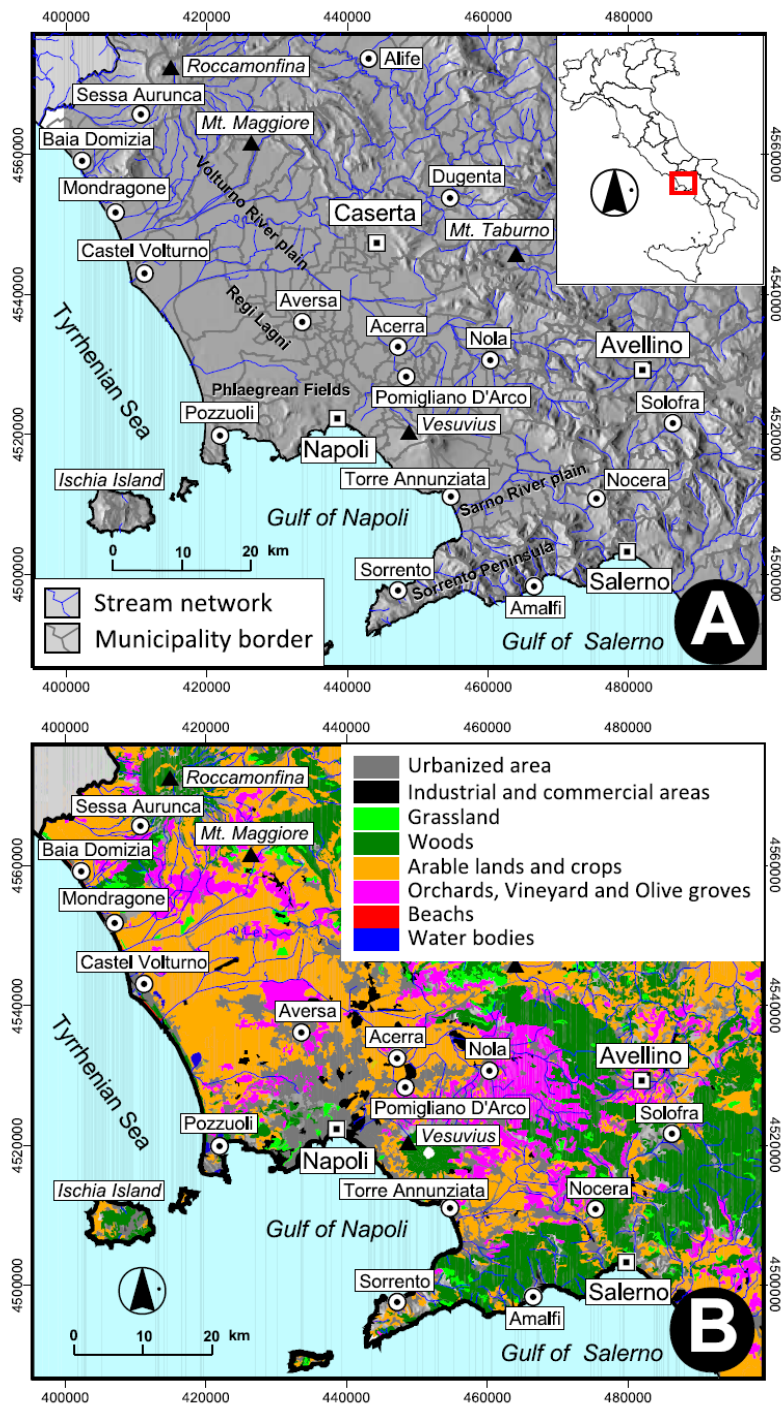


Fig. 1 - A) Study area; B) Land use map of the study area.

Specifically, the Campanian Plain is a huge graben formed during the Pliocene, collapsed

during the Quaternary, and filled by the volcanic products generated from a fissural activity which interested some neotectonic Appennine faults (De Vivo et al. 2001) from Mt. Roccamonfina, the Phlaegrean Fields and Mt. Vesuvius and by marine and alluvial deposits generated by the weathering and decay of both the pyroclastic deposits mantling and the carbonatic rocks forming the surrounding mountains.

Large urban settlements, densely populated and industrialized, and concomitant extensive areas devoted to agriculture, are located in the study area which could be separated in three ideal territorial units based on morphology (Fig. 1A) and on land use (Fig. 1B): the Domizio-Flegreo Littoral and Agro Aversano, the metropolitan area of Naples and the Sarno River basin and Sorrento Peninsula.

The Domizio-Flegreo Littoral and the Agro Aversano

The Domitizio-Flegreo Littoral and Agro Aversano (including the Volturno River plain, the Regi Lagni basin and the Phlegrean Fields volcanic area) has been declared as a National Interest Site (S.I.N.) by the Italian Government because of its wide contamination potential. Chemical industry, intensive agriculture and buffalo farms are the main productive activities in the Volturno River plain and in the Regi Lagni basin and they are likely the main heavy metals pollution source of both stream waters and soils (Grezzi et al. 2011; Bove et al. 2011). Automotive traffic is a relevant source of heavy metal contamination for the Phlegrean Fields area, especially in correspondence with the urbanized areas and the road network (Grezzi et al. 2011). Across the whole Domitizio-Flegreo Littoral and Agro Aversano, several illegal waste dumpings and the fall out of the soot produced by uncontrolled burning of agricultural and industrial wastes also contribute to the degradation process of overall environmental equilibrium.

Within the Agro Aversano territory, the Acerra-Marigliano conurbation, including the municipalities of Acerra, Pomigliano d'Arco, Castelcisterna, Mariglianella, Marigliano and Nola, is worth mentioning as it was named "The triangle of death", after Senior and Mazza (2004) demonstrated how the local abnormal rate of cancer mortality could be related to the presence of many illegal waste disposals buried under productive agricultural lands. The conurbation covers a total area of about 100 km² with an average population density of about 1600 inhabitants/km². In the southern sector of the conurbation, a branch factory of the Italian automotive industries FIAT is

present since the early 70's, and in the northern sector of the Acerra municipal territory the Montefibre factory, accused to be the main culprits of soil and groundwater pollution in the area, has been producing polyester fibers since the 80's. Furthermore, in the same area a power plant fueled by liquid biomass (palm oil) and an incinerator for urban waste treatment are present; the incinerator was inaugurated in 2009, close to the Montefibre site, and began to burn non-differentiated waste of the metropolitan area of Naples, that had been accumulated during the worldwide infamous waste crises of the Campania Region (2004, 2008-2009) . In the late years, the area have been also renamed by local media "the land of fires" since the daily occurrence across its territory of unauthorized fires burning agricultural wastes mixed with all kinds of industrial wastes of unknown origin.

The metropolitan area of Naples

The metropolitan area of Naples, extending from the Phlaegrean Fields to Mt. Vesuvius volcanic complex, is mostly occupied by urban and industrial settlements. In the eastern sector of Naples municipal area, which is in a condition of economic and social decline, important factories, especially chemical industries and refineries, are still operating and affect the air quality and the environment in general (De Vivo et al. 2006; Cicchella et al. 2005). In western sector of the city, the Bagnoli brownfield site still undergoes a never ending environmental reclamation to remove metals and hydrocarbons from soils and groundwater polluted by the former steelwork factory, decommissioned in the early 90's (Albanese et al. 2010; Albanese et al. 2011).

The Sarno River basin and the Sorrento Peninsula

The Sarno River basin, including the alluvial plain of the Sarno River (some 440 km²) and the Solofrana and Cavaioia tributaries basins, is a strongly urbanized (in some area the population density goes up to about 2,000 inhabitants/km²) (ISTAT 2011) and industrialized area in the southern sector of the study area. During decades, the river has been seriously polluted by the presence of both 160 tanning plants operating in its upper valley and of several tomato cannery industries. Nevertheless, its continuous use to supply water to the local intensive agriculture in its mid valley (Albanese et al. 2013a) and its frequent flooding, has contaminated many agricultural lands along its course. Moreover, several chemical-pharmaceutical, engineering and manufacturing industries were established in the lower valley of the river close to the coastal plain, thereby contributing to the final

pollution of sea waters and sediments. South-east of the the Sarno River basin the Sorrento Peninsula, named after its main town, Sorrento, is mostly mountainous with high coasts and small beaches attracting thousands of tourists generating an intense automotive traffic flow especially during the summer season.

3. Materials and methods

3.1 Field sampling and sample preparation

A total of 119 soil samples were collected for polycyclic aromatic hydrocarbons (PAHs) analyses during the months of April and May 2011 across the whole study area. Each sampling site was located at the center of the squared cells of an ideal grid superimposed to the study area (Fig. 2). The cells had variable dimension and sampling density varied accordingly from the 36 km² of the Domizio-Flegreo Littoral and Agro Aversano to the 4 km² of the Acerra-Marigliano conurbation. At each site a composite sample of 0.5 kg was collected, by joining together five aliquots taken at the center and at the corners of an ideal square with a side of 5 m. Every 20 sampling site, a duplicate sample was collected in the same cell of the 20th sample in order to allow the blind control of the analytical quality. Each sampling site was regularly described for spatial coordinates, soil and air temperature, local geology, type and main properties of soils, land use, and any additional detail related to anthropic activities in the surroundings.

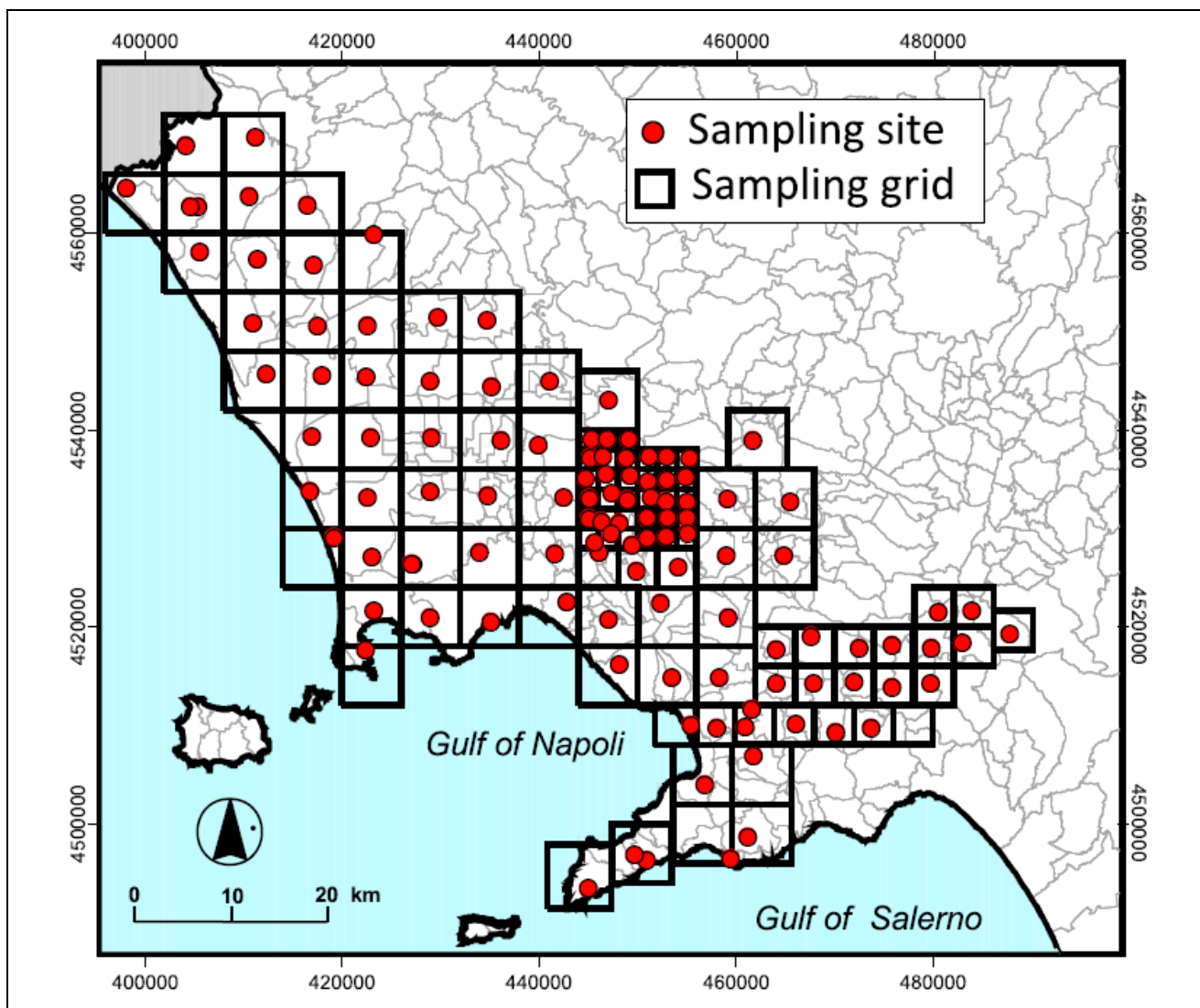


Fig. 2 - Sampling grid and sample site locations.

At 25 selected sites additional soil samples were also collected as representatives of the soil units of the study area to determine their physicochemical properties (Grain size, pH, Organic Carbon). All the samples were stored in plastic bags and kept at a temperature of 4° C by means of a portable cooler during the transport from the collection site to the Environmental Geochemistry Laboratory (LGA) at University of Naples Federico II. The 119 samples collected for PAHs analyses, packed in polystyrene boxes together with dry ice pellets (to keep temperature of samples conveniently low) were sent to the Key Laboratory of Biogeology and Environmental Geology of

Ministry of Education at China University of Geosciences in Wuhan for PAHs analyses and the 25 samples collected for physicochemical analyses were sent to the Agricultural and Environmental Analytical Laboratory of the Agricultural Department of the University of Naples Federico II.

3.2 Chemical analyses

Chemicals

16 USEPA priority PAHs standards (including naphthalene, acenaphthylene, acenaphthene, fluorene, phenanthrene, anthracene, fluoranthene, pyrene, benz[a]anthracene, chrysene, benzo[b]fluoranthene, benzo[k]fluoranthene, benzo[a]pyrene, indeno[1,2,3-cd]pyrene, dibenz[a,h]anthracene, and benzo[g,h,i]perylene) in a mixture, deuterated recovery surrogates standard consisting of naphthalene-D8; acenaphthene-D10; phenanthrene-D10; chrysene-D12 and perylene-D12, were obtained from Ultra Scientific Inc. (North Kingston, RI, USA). The internal standard (hexamethylbenzene) was acquired as a solid of 99% purity (Aldrich Chemical, Gillingham, Dorset, USA).

Dichloromethane and n-hexane were purchased from Tedia Co., USA. Acetone was purchased from Fisher Scientific, USA. All organic solvents were better than spectrum grade and were redistilled in a glass system before use. Neutral silica gel (80-100 mesh) and alumina (100-200 mesh) were Soxhlet-extracted for 48h in dichloromethane (DCM) solvent. Upon drying at room temperature, silica gel and alumina were baked at 180°C and 240°C for 12h, respectively. After cooling down, purified water (3% of the reagent weight) was added to reduce activity. Sodium sulfate was baked at 450°C and stored in sealed containers.

The glass wares were cleaned with detergent, $K_2Cr_2O_7$ - H_2SO_4 solution, tap water and deionized water, respectively and finally baked at 180°C for 4 h and rinsed by some solvent twice and three times before use.

Extraction and Clean up

In the Key Laboratory of Biogeology and Environmental Geology, soil samples were homogenized and freeze-dried. 10 g of dried soil from each sample were spiked with 1000 ng ($5\mu l$ of 200 mg l^{-1}) of recovery surrogates (naphthalene-D8; acenaphthene-D10; phenanthrene-D10; chrysene-D12 and perylene-D12) and were Soxhlet-extracted (4-6 cycles/h) with dichloromethane

for 24 h. Elemental sulfur was removed by adding activated copper granules to the collection flasks.

The sample extract was concentrated and solvent-exchanged to hexane and further reduced to 2-3 ml by a rotary evaporator (Heidolph 4000). A 1:2 (v/v) alumina/silica gel column (both 3% deactivated with H₂O) was used to cleanup the extract and PAHs were eluted with 30 ml of dichloromethane/hexane (3:7). The eluate was then concentrated to 0.2 ml under a gentle nitrogen stream and 1000 ng (5 μ l of 200 mg l⁻¹) of hexamethylbenzene were added as an internal standard prior to gas chromatography- mass spectrometry (GC- MS) analysis.

PAHs analysis

A HP6890N gas chromatograph equipped with a mass selective detector (5975MSD) was used for detecting the levels of polycyclic aromatic hydrocarbons (PAHs) in the soil samples. The capillary column used for the analysis was a DB-5MS (30.0 m \times 250 μ m \times 0.25 μ m film thickness). It was coupled with a HP-5975 mass selective detector operated in the electron impact mode (EI mode, 70 eV). The chromatographic conditions were as follows: injector and detector temperatures were of 270 °C and 280 °C, respectively; oven temperature program started at 60 °C for 5 min and increased to 290 °C at a rate of 3 °C min⁻¹ and then was kept at 290 °C for 40 min. The carrier gas was highly pure helium at a constant flow rate of 1.5 ml min⁻¹. The mass spectrometer operated in the selected ion monitoring (SIM) mode and was tuned with perfluorotributylamine (PFTBA) according to the manufacturer criteria. Mass range between 50 and 500 m/z was used for quantitative determinations. Data acquisition and processing were made by a HP Chemstation data system. Chromatographic peaks of samples were identified by mass spectra and by comparison with the standards. An aliquot of 1 μ l of the purified sample was injected into the GC-MSD for the analysis, conducted in splitless/split mode with a solvent delay of 5 min. A six point response factor calibration was established to quantify the target analyses.

Quality assurance and quality control (QA/QC)

Procedure types used for QA/ QC were: method blank control (procedural blank samples), parallel sample control (duplicate samples), solvent blank control and basic matter control. In order to ensure the validity of the analyses during the experiment, different reagents and procedures were used:

(1) 1000 ng of naphthalene-D8, acenaphthene-D10, phenanthrene-D10, chrysene-D12 and perylene-D12 were used as recovery surrogates, and 1000 ng of hexamethylbenzene were added in the purified extracts as internal standard. The spike recoveries of PAHs using composite standards were of $49.9\% \pm 14.5\%$ for naphthalene-D8, $74.2\% \pm 9.4\%$ for acenaphthene-D10, $91.5\% \pm 11.6\%$ for phenanthrene-D10, $87.1\% \pm 8.5\%$ for chrysene-D12 and $89.2\% \pm 11.0\%$ for perylene-D12, respectively;

(2) An internal standard method was used for quantification, a six-point calibration curve was established according to the results from the PAHs-16 standard reagents with concentration of 10 mg l^{-1} , 5 mg l^{-1} , 2 mg l^{-1} , 1 mg l^{-1} , 0.5 mg l^{-1} and 0.2 mg l^{-1} , and the target compounds were identified on the basis of the retention times and selected quantitative ion;

(3) During the pretreatment, a procedural blank and a parallel sample consisting of all reagents was run to check for interferences and cross contaminations in every set of samples (about 16 samples). Only low concentrations of few certain target compounds can be detected in procedural blank samples. For more than 96% of target compounds in parallel samples, the relative error (RE, %) of concentrations are less than 50%, which is acceptable for *Specification of Multi-purpose Regional Geochemical Survey* and *Guidelines for samples analysis of Multi-purpose Regional Geochemical Survey* recommended by China Geological Survey (DD2005-1 and DD2005-3);

(4) During the GC-MS analysis period, a solvent blank sample and a PAHs-16 standard reagent with a concentration of 5 mg l^{-1} was injected every day before analyzing the soil samples. The target compounds were not detectable in the solvent blank samples;

(5) Multi-injections were used for precision or accuracy. The samples of different concentrations were injected continually for 10 times, and the relative standard deviation (RSD) was calculated. RSD for all the target compounds ranged from 3.2% to 7.9%.

The final concentrations of PAHs in all the samples were corrected according to the recovery of the surrogates and were subtracted of the values of blank samples.

3.3 Physicochemical analyses

Particle size distribution of samples was determined by the pipette method (Gee and Bauder 1986), soil pH was measured in water, and soil organic carbon (OC) content was measured according to the Walkley-Black method and converted to organic matter (OM) by multiplying for 1.724 (Nelson and Sommers 1996) (Table 1).

Table 1 - Main physical-chemical properties of a selection of the soil samples collected across the study areas.

Samples	Coarse sand g kg ⁻¹	Fine sand g kg ⁻¹	Silt g kg ⁻¹	Clay g kg ⁻¹	OC g kg ⁻¹	OM g kg ⁻¹	pH
3	73	127	238	562	14.4	24.8	8.00
6	210	446	275	69	21.6	37.3	6.53
7	252	374	247	127	22.6	38.9	7.82
13	86	562	182	170	20.8	35.8	7.96
16	34	515	201	250	13.7	23.5	8.13
21	249	413	267	71	19.7	34.0	7.74
24	190	379	361	70	15.9	27.4	7.09
35	455	420	110	15	22.6	39.0	7.50
36	528	380	73	19	11.1	19.1	7.96
38	214	615	156	15	18.5	31.9	7.65
40	279	462	211	49	16.1	27.7	7.32
42	335	557	98	9	17.8	30.7	6.18
44	549	358	86	7	22.8	39.4	6.95
52	559	362	65	14	24.4	42.1	6.71
55	452	468	63	16	15.1	26.0	7.82
57	462	471	60	7	25.1	43.2	7.09
60	214	418	258	110	7.1	12.2	6.95
SAR-O-3	301	429	229	42	9.5	16.3	6.31
SAR-O-9	500	336	141	24	19.7	34.0	7.64
SAR-O-13	190	468	260	83	24.0	41.4	7.69
SAR-O-17	353	441	171	36	19.6	33.9	7.59
SAR-O-20	417	440	131	12	25.3	43.6	6.96
ACE-O-6	388	383	194	34	16.8	29.0	7.79
ACE-O-21	263	461	229	47	15.5	26.7	7.27
ACE-O-24	228	518	217	38	14.4	24.9	7.76

3.4 Statistics, soil classification and geochemical mapping

An univariate statistical analysis was performed on the chemical data (Table 2; Fig. 3) which were, subsequently, georeferenced and mapped by means of a geochemistry dedicated GIS software named GEODAS (Cheng 2003).

Table 2 - Statistic parameters for the analyzed PAHs compounds (values expressed in ng g⁻¹).

Compound	Min	Max	Mean	Geom. Mean	Median	St. Dev.	Skewness	Kurtosis
Naphthalence	1.25	135.27	10.30	7.40	6.65	13.96	6.59	55.30
Acenaphthylene	0.18	157.65	8.35	2.76	2.715	17.86	5.87	44.29
Acenaphthene	0.1	11.07	1.05	0.59	0.46	1.62	3.96	18.80
Fluorene	0.39	19.85	2.15	1.55	1.4	2.54	4.46	25.29
Phenanthrene	1.48	539.19	31.18	13.66	11.45	63.47	5.52	37.90
Anthracene	0.07	104.36	5.99	1.85	1.865	13.22	5.12	31.34
Fluoranthene	0.69	1249.48	74.95	21.21	22.58	159.77	5.02	30.92
Pyrene	0.63	1064.31	66.34	19.59	21.66	139.67	4.98	29.97
Benzo[a]anthracene	0.12	1195.05	56.24	13.77	15.01	133.56	6.12	46.87
Chrysene	2.02	2984.11	210.39	65.39	67.85	411.24	4.43	23.68
Benzo[b]fluoranthene	0.6	2964.48	180.17	49.56	58.26	363.89	4.90	31.02
Benzo[k]fluoranthene	0.19	1149.35	93.16	27.38	32.23	172.04	3.83	17.45
Benzo[a]pyrene	0.15	4277.61	259.15	62.12	76.595	541.51	4.79	28.73
Indeno[1,2,3-d]pyrene	0.84	3386.81	213.67	56.25	74.65	425.10	4.62	28.05
Dibenzo[a,h]anthracene	0.03	552.41	34.37	8.99	10.81	68.29	4.80	30.52
Benzo[g,h,i]perylene	0.59	1537.15	144.22	43.32	42.07	264.92	3.53	13.98

Interpolated map for each of the analyzed PAHs compound and for the sum of the low molecular weight (LMW, 2-3 aromatic rings) and the high molecular weight (HMW, 4 and more aromatic rings) PAHs were produced (Fig. 4, 5, 6); specifically, fluoranthene (Fla), pyrene (Pyr), benzo[a]anthracene (BaA), chrysene (Chr), benzo[b]fluoranthene (BbF), benzo[k]fluoranthene (BkF), benzo[a]pyrene (BaP), indeno[1,2,3-cd]pyrene (IcdP), dibenzo[a,h]anthracene (DahA), benzo[g,h,i]perylene (BghiP) are classified as HMW-PAHs and naphthalene (Nap), acenaphthylene (Acy), acenaphthene (Ane), fluorene (Flo), phenanthrene (Phe) and anthracene (Ant), are classified as LMW-PAHs.

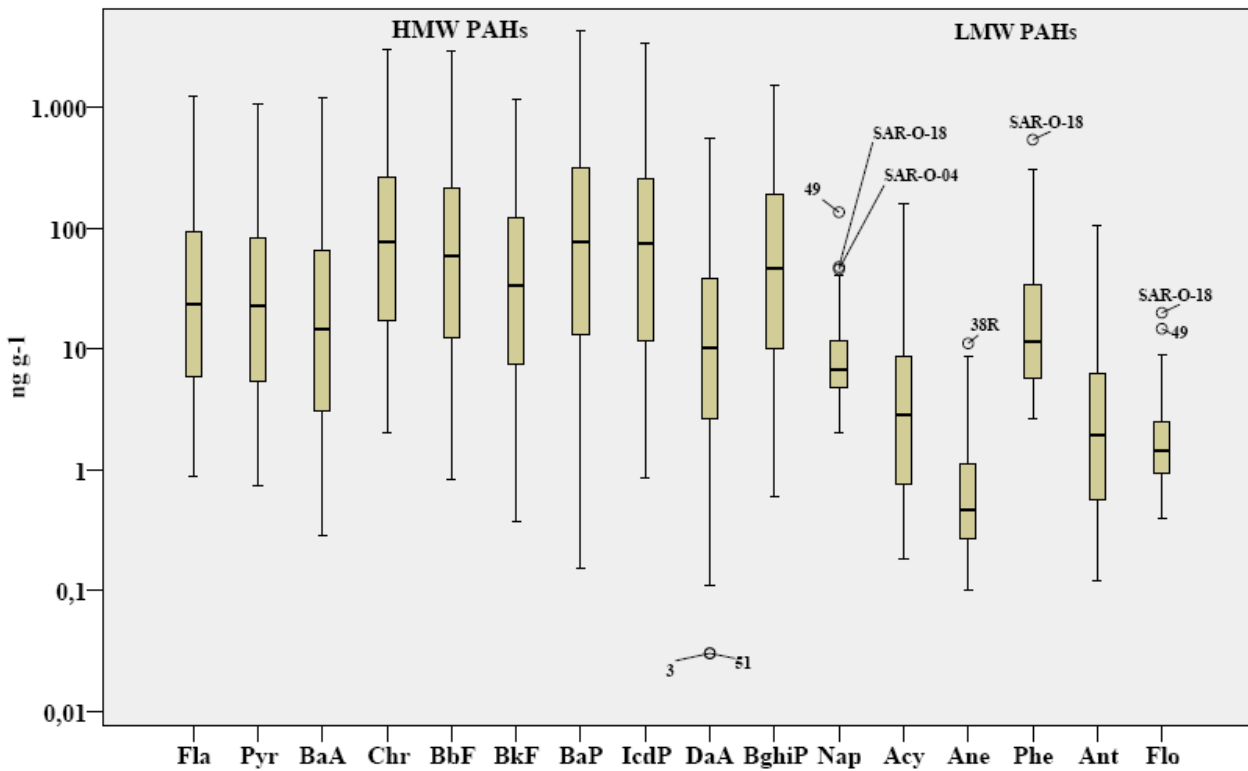


Fig. 3 - Box plots of PAHs concentrations.

Spatial interpolation process was based on a classical IDW (Interpolated Weighted Distance) algorithm enhanced by the application of some principles of fractal geometry (Multifractal IDW) (Cheng 2003). Furthermore, the map of PAHs potential contaminated areas was produced by extracting from the interpolated grid of each PAHs compound the pixels whose value exceeded the trigger limit established by the Italian environmental law (D. Lgs. 152/2006) for the residential use of soils (Table 2); overlapping and summing all the reclassified layers, a unique grid was obtained showing all the areas where at least one PAHs compound was found to be exceeding its corresponding

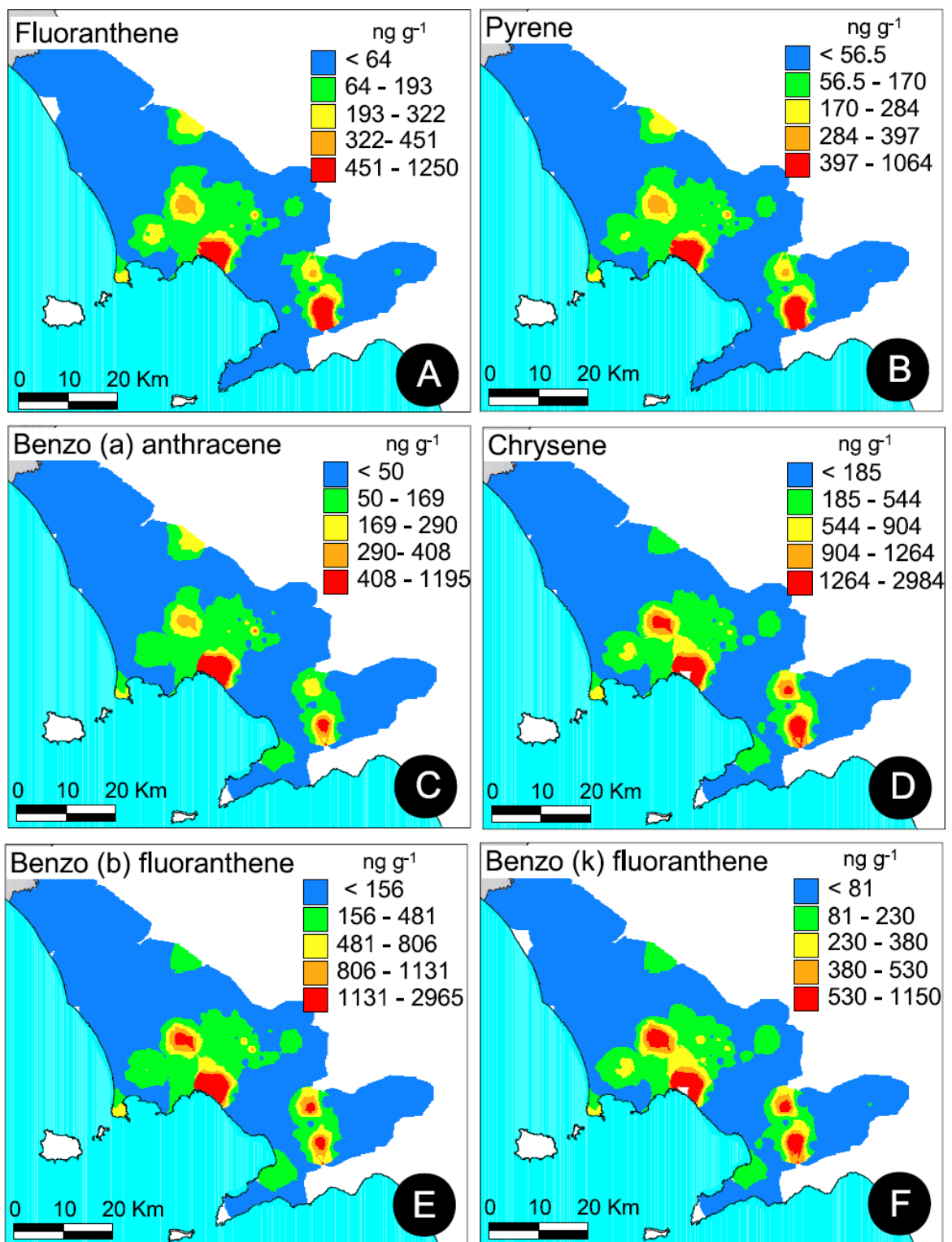


Fig. 4 - Distribution pattern of PAHs in the study area.

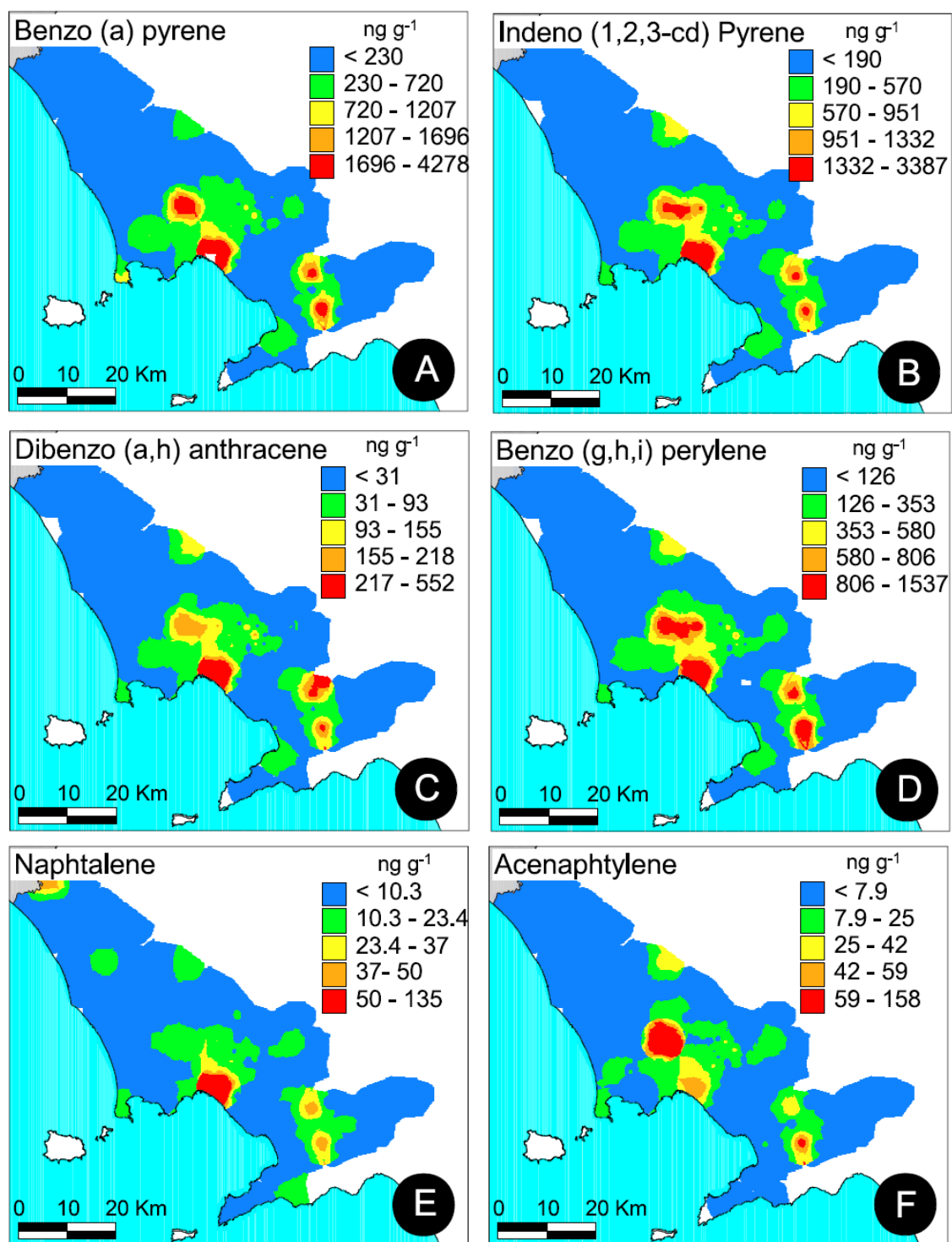


Fig. 5 - Distribution pattern of PAHs in the study area.

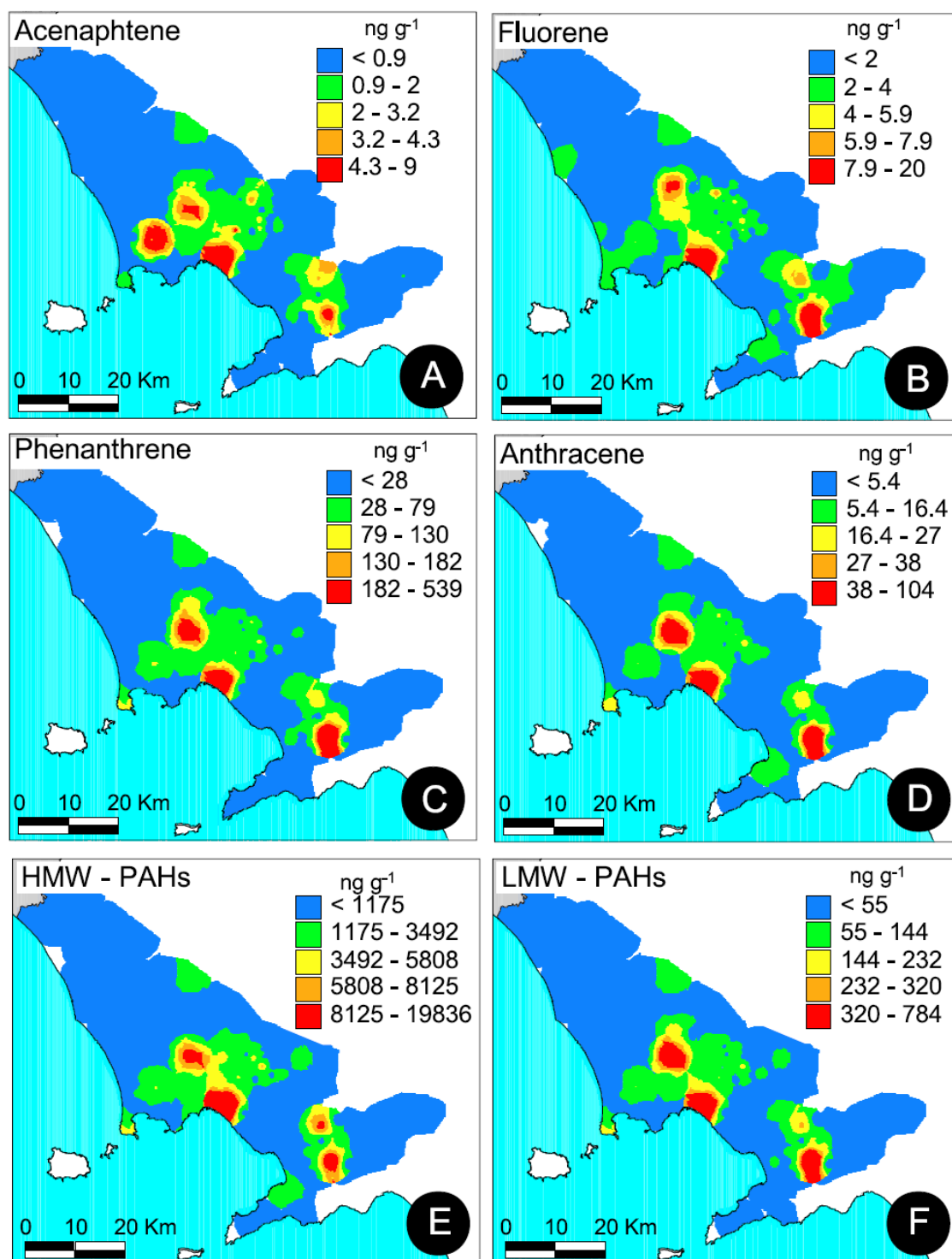


Fig. 6 - Distribution pattern of PAHs in the study area.

Table 3 - Soil trigger limits (expressed as ng g^{-1}) for residential (Column A) and industrial (Column B) land use as established for a selection of PAHs compounds by the Italian environmental law (D.Lgs. 152/2006); PAHs toxic equivalency factors (TEFs) with respect to BaP are reported in Column C (Nisbet and LaGoy 1992).

Compound	A	B	C
Benzo[a]anthracene	500	10000	0.1
Benzo[a]pyrene	100	10000	1
Benzo[b]fluoranthene	500	10000	0.1
Benzo[k]fluoranthene	500	10000	0.1
Benzo[g,h,i]perylene	100	10000	0.1
Chrysene	5000	50000	0.01
Dibenzo[a,e]pyrene	100	1000	1
Dibenzo[a,l]pyrene	100	1000	100
Dibenzo[a,h]pyrene	100	1000	1
Dibenzo[a,h]anthracene	100	1000	1
Indeno[1,2,3-cd]pyrene	100	5000	0.1
Pyrene	5000	50000	0.001

trigger limits (Fig. 7).

Moreover, maps of the spatial distribution of pH and OC (Fig. 8) were generated and grain size data were plotted on a USDA textural triangle (Fig. 9) to show the spatial variability of the physicochemical properties of the soil in the study area and to define their textural features, respectively.

3.5 Preliminary Quantitative Risk Assessment (PQRA)

A Preliminary Quantitative Risk Assessment (PQRA) focused on a residential exposure scenario was run in general accordance with the guidances released by the Environmental Protection Agencies of USA and Canada (Health Canada 2010b; USEPA 1991). Three different pathways (direct ingestion, dermal absorption, inhalation of fugitive dust outdoors) were considered in order to calculate the Incremental Lifetime Cancer Risk (ILCR) generated by the presence of PAHs in the soil (USEPA 2002) and the following equations (Health Canada 2010a) were applied for calculating the doses of contaminants assumed by human receptors through the different routes of exposure:

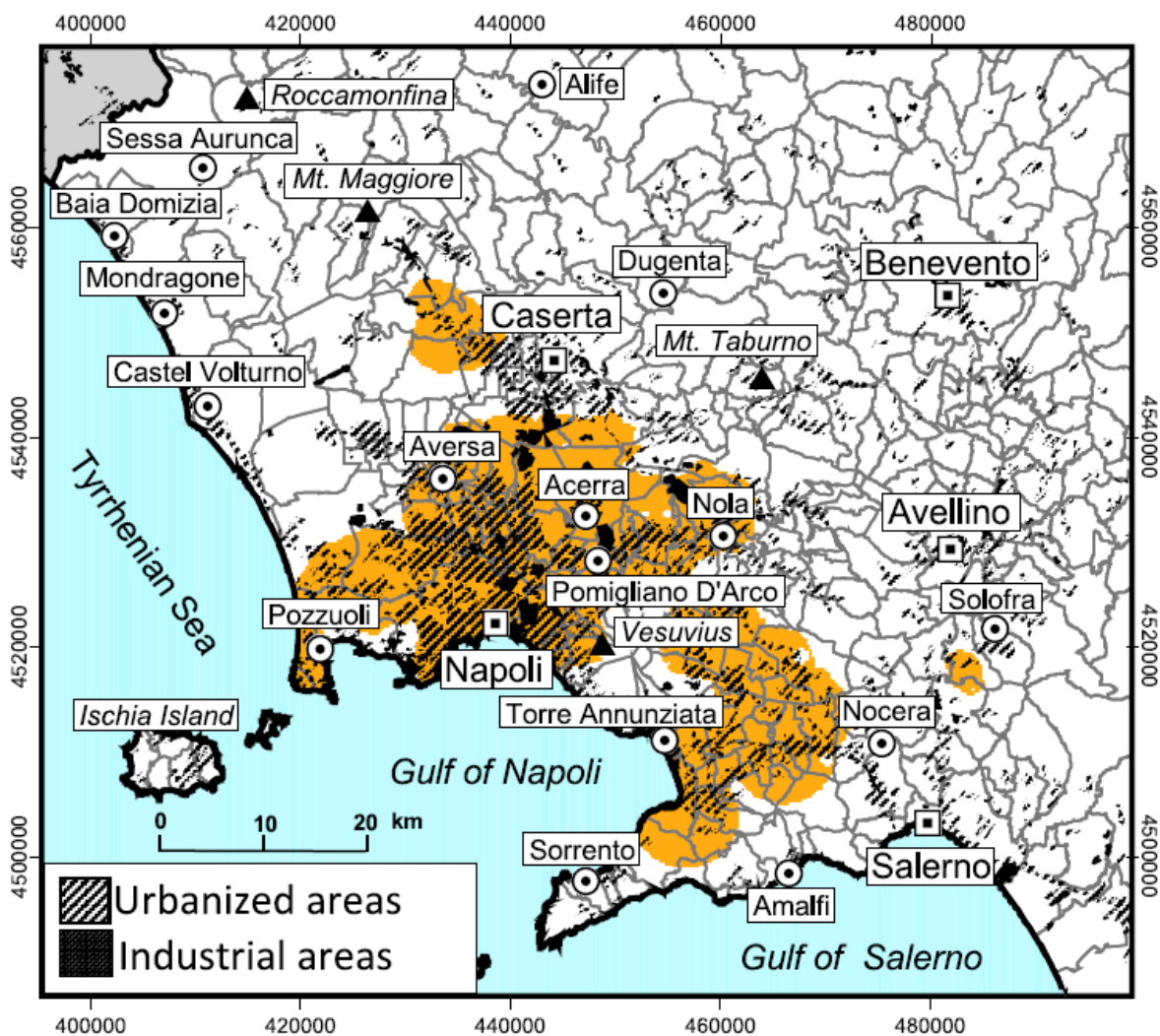


Fig. 7 - Map of the PAHs potential contaminated areas showing all the areas where at least one PAH compound was found to be exceeding its corresponding trigger limits as established for soils by the Italian environmental law (D. Lgs. 152/2006).

Eq. 1

$$Dose_{ing} = \frac{C_s * IR_s * RAF_{oral} * D_{hours} * D_{days} * D_{weeks} * D_{years}}{BW * LE}$$

Eq. 2

$$Dose_{inh} = \frac{C_s * P_{air} * IR_a * RAF_{inh} * D_{hours} * D_{days} * D_{weeks} * D_{years}}{BW * LE}$$

Eq. 3

$$Dose_{derm} = \frac{C_s * SA_h * SL_h * RAF_{derm} * EF * D_{days} * D_{weeks} * D_{years}}{BW * LE}$$

Where:

Dose_{ing} (mg/kg-day) = Accidental soil ingestion dose;

Dose_{inh} (mg/kg-day) = Particulate inhalation dose;

Dose_{derm} (mg/kg-day) = Dermal contact dose;

C_s (mg/kg) = Concentration of contaminant in soils;

IR_s (kg/day) = Accidental soil ingestion rate;

IR_a (m³/hour) = Air inhalation rate;

RAF_{oral} (unitless) = Relative Absorption Factor for the gastrointestinal tract;

RAF_{inh} (unitless) = Relative Absorption Factor for the lungs;

RAF_{derm} (unitless) = Relative Absorption Factor for the skin;

P_{air} (kg/m³) = Concentration of particles in the air;

D_{Hours} = Hours per day with exposure. 0 - 16 / 16 hours for accidental ingestion of soil; 0 - 24 / 24 hours for soil particulate inhalation;

D_{Days} = Days in a week with exposure (0 - 7) / 7 days;

D_{Weeks} = Weeks in a year with exposure (0 - 52) / 52 weeks ;

D_{Years} = Total of years with exposure;

SA_h (cm²) = Surface area of hands (Assuming that only hands are exposed);

SL_h (kg/cm² - event) = Soil loading rate to exposed skin;

EF (event/day) = Number of dermal exposure per day;

BW (kg) = Body weight of receptor;

LE = Life expectancy. The number of year that a person is likely to live;

Table 4 - Default values used for the calculation of the doses assumed by human receptors through

the exposure pathways considered in this study.

Parameter	Unit	Toddler	Adult	Reference
Body weight (BW)	kg	16.5	70.7	Richardson (1997)
Ingestion rate (IR _s)	kg/day	8.00E-05	2.00E-05	CCME (2006); MassDEP (2002)
Inhalation rate (IR _a)	m ³ /hour	0.36	0.69	Allan et al. (2008)
Oral Relative Absorption Factor (RAF _{oral})	-	1	1	Health Canada (2010a)
Life Expectancy (LE) (years)	years	80	80	Health Canada (2010b)
Concentration of particles in air (P _{air})	kg/m ³	7.6E-10	7.6E-10	USEPA (1991)
Inhalation Relative Absorption Factor (RAF _{inh})	-	1	1	Health Canada (2010a)
Surface area of hands (SA _h)	cm ²	430	890	Richardson (1997)
Soil loading rate to exposed skin (SL _n)	kg/cm ² - event	1.00E-07	1.00E-07	Kissel et al. (1996)
Years of exposure (D _{years})	years	5	60	Health Canada (2010a)
Dermal Relative Absorption Factor (RAF _{derm})*	-	0.148	0.148	Moody et al. (2007)
Oral Slope Factor (SF _{ing})*	kg - day/mg	2.3	2.3	Health Canada (2010a)
Inhalation Slope Factor (SF _{inh})*	kg - day/mg	0.13	0.13	Health Canada (2010a)
Dermal Slope Factor (SF _{derm})*	kg - day/mg	25	25	Knafla et al. (2006)

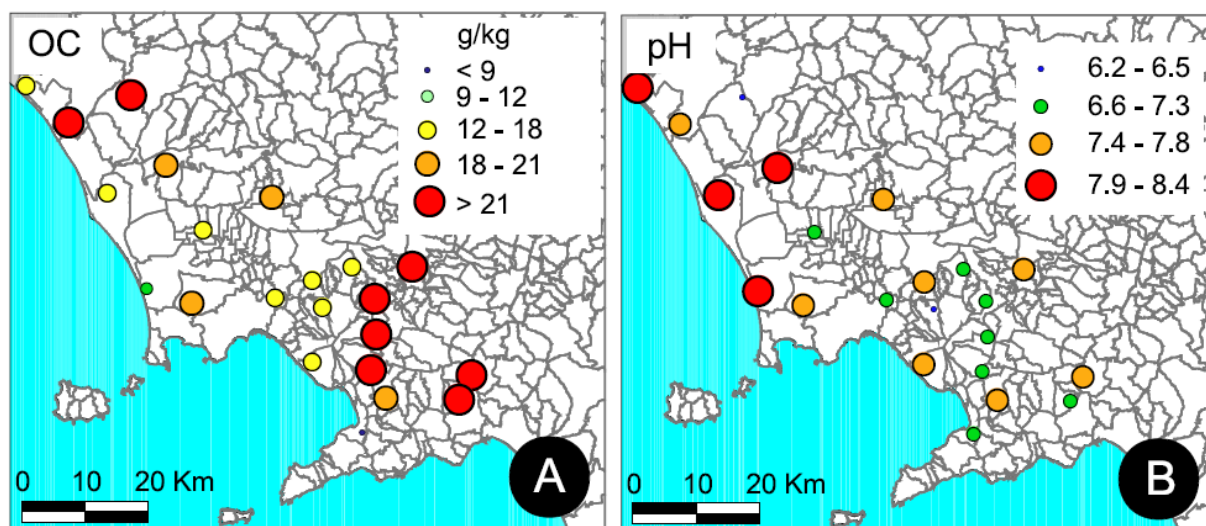


Fig. 8 - Spatial variability of OC (A) and pH (B) in 25 selected samples collected across the study area.

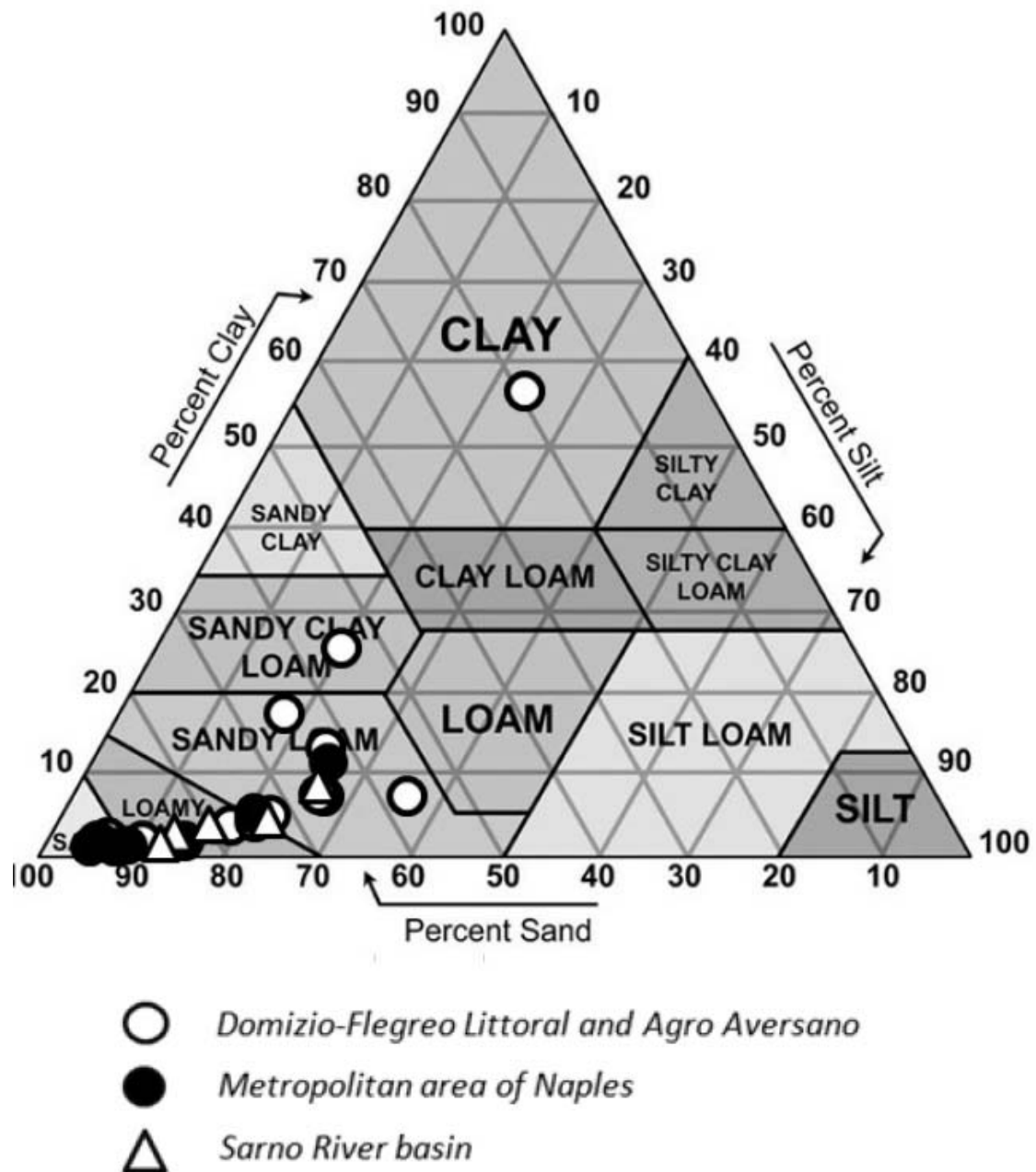


Fig. 9 - USDA textural triangle reporting the textural features of 25 selected samples collected across the study area.

The PQRA was focused on toddler (from 7 monthly to 4 years old) and adult (>20 years old) receptors (Knafla et al. 2006; Health Canada 2010b) and, for some of the parameters in the above

equations (Eq. 1, Eq. 2, Eq. 3), default values, borrowed from literature, were applied (Table 4).

The concentrations of each PAH compound were converted to the corresponding BaP toxic equivalent concentrations by using the Toxic Equivalency Factor (TEF) (Nisbet and LaGoy 1992) reported in Table 3 and for each sample the total PAHs concentration was determined by summing the BaP toxic equivalents calculated per each compound.

The interpolated map of total PAHs (Fig. 10A) was carried out by means of a multifractal IDW, as well, and, subsequently, it was reduced to a vector format reporting the administrative boundaries of each municipality as a polygon.

Specifically, the maximum total PAHs value among those of all the pixels falling into the boundaries of each polygon (Fig. 10A) was associated to the respective municipality (Fig. 10B) to provide a reference value to be used as C_s to calculate the reasonable maximum exposure (RME) doses of contaminants by means of the equations presented above (Eq. 1, Eq. 2, Eq. 3).

To calculate the ILCR, the following general equation (Health Canada 2010a) was applied and the "municipality-based" maps of ILCR for both toddlers and adults were carried out (Fig. 11A; Fig. 11B):

Eq. 4

$$ILCR = (Dose_{ing} * SF_{ing}^I) + (Dose_{inh} * SF_{inh}^I) + (Dose_{derm} * SF_{derm}^I)$$

Where:

ILCR (unitless) = Incremental Life Cancer Risk;

SF_{ing} (kg-day/mg) = Oral Slope factor (chemical specific) (Table 4);

SF_{inh} (kg-day/mg) = Inhalation Slope factor (chemical specific) (Table 4);

SF_{derm} (kg-day/mg) = Dermal Slope factor (chemical specific) (Table 4);

4. Results and discussions

The OC and, consequently, the OM content resulted moderately low for the soils of the metropolitan area of Naples, the Phlegrean Fields and the Regi Lagni basin and moderately enriched for the soil of the northern sector of the Volturno River basin and of the Sarno river basin (Table 1; Fig. 8A).

In accordance with the USDA classification criteria (Soil Survey Division Staff 1993), the pH

varied from slightly acid, in the soils of the eastern sector of the Mt. Vesuvius complex, to moderately alkaline (Table 1) in the soils of the Domizio-Flegreo littoral and Agro Aversano area (Fig. 8B).

The soil texture of most of selected soils varied from sandy to sandy-loamy with an average content of silt in the range between 10 and 30 % (Table 1; Fig. 9).

The comparison between spatial distribution of physicochemical and PAHs data did not show any interesting correlation even at a qualitative level.

The distribution of PAHs concentrations was, generally, positively skewed and leptokurtic for all the considered compounds and HMW-PAHs are more enriched in soils than LMW-PAHs (Table 2).

Among HMW-PAHs, BaP and IcdP, ranging from 0.15 to 4227 ng g⁻¹ and from 0.84 to 3386 ng g⁻¹, respectively, showed the highest concentrations followed in the order by Chr, BbF, BghiP, Fla, BaA, BkF, Pyr, DahA (Table 2, Fig. 3); these compounds are mostly concentrated in the eastern and northern sector of Naples and in the Sarno River plain (Figs. 5 A-F; 6 A-D)

Among the LMW-PAHs the most abundant compound was Phe, ranging from 1.48 ng g⁻¹ to 539 ng g⁻¹, followed by Acy and Nap, ranging from 0.18 to 157.65 ng g⁻¹ and from 1.25 to 135.27 ng g⁻¹, respectively and, in the order, by Ant, Flo, Ace (Table 2).

Phe (Fig. 6C), which has as the main emission source the combustion of fossil fuels, traffic and exhausts from industry, was mostly concentrated in correspondence with the eastern sector of Naples urban area, the municipal area of Aversa and the alluvial plain of the Sarno River.

Likewise, Nap (Fig. 5E), originating from vehicle exhausts, evaporated gasoline, moth and pest repellants, and Acy (Fig. 5F), commonly used to make dyes, plastics and pesticides, was more concentrated in areas near Aversa and Nocera, were abundant only in the Naples area.

In urban and anthropized areas, often, the high values of HMW-PAHs in soils may be attributed to both a massive deposition from atmosphere, mostly generated from fossil fuels combustion (Dai et al. 2008; Maliszewska-Kordybach et al. 2009) and to a general small degradation rate of these compounds (as compared to LMW-PAHs), that causes a slow desorption from soot particles favoring the accumulation in soil (Krauss et al. 2000).

Furthermore, it has to be taken into account that LMW-PAHs are characterized by a greater volatility in respect to the HMW-PAHs. As a matter of the fact, they are more prone to be transported to remote sites than the HMW-PAHs which are mainly associated with soil particles and are easily

deposited close to source sites (Lohmann et al. 2007).

In the eastern sector of Naples urban area, the large concentrations of PAHs could be easily related to the presence of both chemical industries and refineries and the presence of a complex road network characterized by an intense car traffic generated by commuters daily moving to the city from the province. This hypothesis is also supported by the results obtained by Cicchella et al. (2005) and De Vivo et al. (2006) who showed that the eastern sector of the Naples urban area is characterized by the high scores of an elemental factor association including Pb-Zn-Ag-Hg-Au-Cd-Cr-Cu which is generally explained by the presence of human activities and industrial settlements.

In the northern sector of the metropolitan area of Naples, from Acerra to Aversa, in the Agro Aversano area, PAHs presented a peculiar distribution. In fact, the greatest concentrations were found in correspondence with the densely populated municipal area of Aversa, where dairies, producing buffalo mozzarella cheese, and some manufacturing companies, mostly dedicated to textile and footwear production, are the main productive activities. Therefore, it could be inferred that the most important source of PAHs in this area should be the illegal burning of urban and special wastes dispersed in the open countryside and continuously burned to reduce their volume and to hide their presence.

In the Sarno River basin, PAHs relevant concentrations were found in the alluvial plain in correspondence with two main sections (A3 and A30) of the national highway network that is intensely busy by commercial and personal motor vehicles, daily moving in and from Naples and Salerno.

In many cases, across the study area, BaA, BbF, BkF, IcdP, DahA, BghiP, and BaP showed values above the soil trigger limits established by the Italian environmental law (D.Lgs. 152/2006) for the residential land use (Table 3) and, despite the large population density, the whole metropolitan area of Naples, the Agro Aversano and, partly, the Sarno River basin, should be considered potentially contaminated since, in these areas, at least one PAH compound of those considered in this study, exceeded its corresponding trigger limit (Fig. 7). Thus, for people living in the Campania Plain, PAHs represent a relevant environmental problem posing the need of evaluating if there is an effective risk for public health.

The results of the PQRA carried out for the present study area, based on both default values and very conservative assumptions to characterize exposure pathways (Table 4), do not represent a

definitive assessment of the human health risk; however, the PQRA shows that, for the sole exposure to PAHs in soil, the city of Naples is characterized by an ILCR of 1.7×10^{-5} for toddlers (Fig. 11A) and of 2.9×10^{-5} for adults (Fig. 11B) which are both above the threshold value of 1×10^{-5} deemed to be "essentially negligible" (Health Canada 2010b). As a matter of the fact, the latter data can be interpreted as the possibility that an increase of the baseline cancer incidence could occur in the resident population up to 2 units per 100,000 exposed toddlers and up to 3 units per 100,000 exposed adults over an exposure time of 6 and 60 years, respectively. Given that in 2012 in Naples the adults were around 750,000 and the toddlers were around 50,000 (Comune di Naples 2011), and supposing that they were all likewise exposed to PAHs in soil for the respective exposure time, a reliable prediction could be to expect an overall increase in gastric (Knauf and Rice 1992) and respiratory tract (Thyssen et al. 1981) cancer incidence of 23 units for adults and of 1 unit for toddlers.

For the exposed adults, the PQRA revealed a "not-negligible" situation for carcinogenic risk ($ILCR \geq 1 \times 10^{-5}$) also for some municipalities in the surroundings of Naples metropolitan area and in the Sarno River alluvial plain (Fig. 11A; 11B); specifically, in addition to Naples, the small villages of Portici and San Giorgio a Cremano, densely populated, are the municipalities with the highest ILCR across the whole study area.

Conclusion

The results obtained by the PQRA in this study together with the epidemiological evidence of an increased incidence of some cancer types in Campania (Comba et al. 2006; Senior and Mazza 2004; Albanese et al. 2013b; Albanese et al. 2008) pose the need of developing a detailed and multi-media based geochemical characterization of the regional territory to define, at least at regional scale, a conceptual model considering all the exposure pathways followed by contaminants to reach the human target from the emitting source. Soil, water, air, food should be taken into account and concentrations of metals and organic compound, such as PAHs, should be determined within these media to allow the development of a environmental risk analysis based on the effective concentrations of contaminant likely to come into contact with humans.

Although, in case of an objective risk to human health, little could be done to clean up the soils of a territory covering more than $1,000 \text{ km}^2$, the location and the control of the sources of emission of contaminants could be of crucial importance to recover the environment in the long term and the

results of a risk assessment could be used, at least, to establish a priority order in the implementation of safety measures and remediation plans consistent with the available resources.

Acknowledgment

This work was supported by grant from the Ministero dell'Università e della Ricerca Scientifica -Industrial Research Project "Integrated agro-industrial chains with high energy efficiency for the development of eco-compatible processes of energy and biochemicals production from renewable sources and for the land valorization (EnerbioChem)" PON01_01966, funded in the frame of Operative National Programme Research and Competitiveness 2007–2013 D. D. Prot. n. 01/Ric. 18.1.2010.

References

- Albanese, S., Cicchella, D., De Vivo, B., Lima, A., Civitillo, D., Cosenza, A., et al. (2011). Colour Composite Maps and Results from an Urban Brownfield Site. In C. C. Johnson, A. Demetriades, Juan Locutura, & R. T. Ottesen (Eds.), *Mapping the Chemical Environment of Urban Areas* (pp. 410-423): John Wiley & Sons, Ltd.
- Albanese, S., De Luca, M. L., De Vivo, B., Lima, A., & Grezzi G. (2008). Relationships between heavy metals distribution and cancer mortality rates in the Campania Region, Italy. In B. H. E. De Vivo B., Lima A. (Ed.), *Environmental Geochemistry: Site characterization, Data analysis and Case histories* (pp. 391-404). Amsterdam: Elsevier.
- Albanese, S., De Vivo, B., Lima, A., Cicchella, D., Civitillo, D., & Cosenza, A. (2010). Geochemical baselines and risk assessment of the Bagnoli brownfield site coastal sea sediments (Naples, Italy). *Journal of Geochemical Exploration*, 105(1-2), 19-33.
- Albanese, S., Iavazzo, P., Adamo, P., Lima, A., & De Vivo, B. (2013a). Assessment of the environmental conditions of the Sarno river basin (south Italy): a stream sediment approach. *Environmental Geochemistry and Health*, 35(3), 283-297.
- Albanese, S., Taiani, M. V. E., De Vivo, B., & Lima, A. (2013b). An environmental epidemiological study based on the stream sediment geochemistry of the Salerno province (Campania region, Southern Italy). *Journal of Geochemical Exploration*, 131, 59-66.
- Allan, M., Richardson, G. M., & Jones-Otazo, H. (2008). Probability density functions describing 24-hour inhalation rates for use in human health risk assessments: an update and comparison. *Human and Ecological Risk Assessment*, 14, 372–391.
- Bove, M. A., Ayuso, R. A., De Vivo, B., Lima, A., & Albanese, S. (2011). Geochemical and isotopic study of soils and waters from an Italian contaminated site: Agro Aversano (Campania). *Journal of Geochemical Exploration*, 109(1-3), 38-50.
- CCME (2006). A Protocol for the Derivation of Environmental and Human Health Soil Quality Guidelines. Winnipeg, MB.
- Cheng, Q. (2003). *GeoData Analysis System (GeoDAS) for mineral exploration and environmental assessment, user's guide (GeoDAS Phase III)*. Toronto, Ontario, Canada: York University.
- Cicchella, D., De Vivo, B., & Lima, A. (2005). Background and baseline concentration values of elements harmful to human health in the volcanic soils of the metropolitan and provincial areas of Naples (Italy). *Geochemistry-Exploration Environment Analysis*, 5, 29-40.
- Comba, P., Bianchi, F., Fazzo, L., Martina, L., Menegozzo, M., Minichilli, F., et al. (2006). Cancer

- mortality in an area of Campania (Italy) characterized by multiple toxic dumping sites. *Annals of the New York Academy of Sciences*, 1076, 449-461.
- Comune di Naples (2011). Popolazione residente per sesso, singole età e cittadinanza - Comune di Naples - Dati definitivi del 15° Censimento della popolazione (9 ottobre 2011). <http://www.comune.Naples.it/flex/cm/pages/ServeBLOB.php/L/IT/IDPagina/21423>. Accessed 1 Dec 2013.
- Conte, P., Zena, A., Pilidis, G., & Piccolo, A. (2001). Increased retention of polycyclic aromatic hydrocarbons in soils induced by soil treatment with humic substances. *Environmental Pollution*, 112(1), 27-31.
- Dai, J., Li, S., Zhang, Y., Wang, R., & Yu, Y. (2008). Distributions, sources and risk assessment of polycyclic aromatic hydrocarbons (PAHs) in topsoil at Ji'nan city, China. *Environmental Monitoring and Assessment*, 147(1-3), 317-326.
- De Vivo, B., Cicchella, D., Lima, A., & Albanese, S. (2006). *Atlante geochimico-ambientale dei suoli dell'area urbana e della Provincia di Naples / Geochemical Environmental Atlas of the urban and provincial soils of Naples*. Roma: Aracne editrice.
- De Vivo, B., Rolandi, G., Gans, P. B., Calvert, A., Bohron, W. A., Spera, F. J., et al. (2001). New constraints on the pyroclastic eruptive history of the Campanian volcanic Plain (Italy). *Mineralogy and Petrology*, 73(1-3), 47-65.
- Enzminger, J. D., & Ahlert, R. C. (1987). Environmental Fate of Polynuclear Aromatic-Hydrocarbons in Coal-Tar. *Environmental Technology Letters*, 8(6), 269-278.
- Froehner, S., Maceno, M., & Machado, K. S. (2011). Predicting bioaccumulation of PAHs in the trophic chain in the estuary region of Paranagua, Brazil. *Environmental Monitoring and Assessment*, 174(1-4), 135-145.
- Gee, G. W., & Bauder, J. W. (1986). Particle-size analysis. In A. Klute (Ed.), *Methods of Soil Analysis, Part 1* (2nd Edition ed.). Madison, Wisconsin, USA: Soil Science Society of America.
- Grezzi, G., Ayuso, R. A., De Vivo, B., Lima, A., & Albanese, S. (2011). Lead isotopes in soils and groundwaters as tracers of the impact of human activities on the surface environment: The Domizio-Flegreo Littoral (Italy) case study. *Journal of Geochemical Exploration*, 109(1-3), 51-58.
- Health Canada (2010a). *Federal Contaminated Site Risk Assessment in Canada, Part II: Health Canada Toxicological Reference Values (TRVs) and Chemical-Specific Factors. Version 2.0*. Ottawa, ON: Health Canada.
- Health Canada (2010b). *Federal Contaminated Site Risk Assessment in Canada. Part I: guidance on Human Health Preliminary Quantitative Risk Assessment (PQRA). Version 2.0*. Ottawa, ON.: Health Canada.
- ISTAT (2011). Censimento generale dell'industria e dei servizi. Roma, Italy. <http://censimentoindustriaeservizi.istat.it/>. Accessed 1 Dec 2013.
- Kissel, J. C., Richter, K. Y., & Fenske, R. A. (1996). Field measurement of dermal soil loading attributable to various activities: implications for exposure assessment. *Risk Analysis*, 16(1), 115-125.
- Knafla, A., Phillipps, K. A., Brecher, R. W., Petrovic, S., & Richardson, M. (2006). Development of a dermal cancer slope factor for benzo[a]pyrene. *Regulatory Toxicology and Pharmacology*, 45(2), 159-168.
- Knauf, L., & Rice, G. (1992). *Statistical Evaluation of Several Benzo[a]pyrene Bioassays*.

Memorandum to R. Schoeny. Cincinnati, OH: U.S. EPA.

- Krauss, M., Wilcke, W., & Zech, W. (2000). Polycyclic aromatic hydrocarbons and polychlorinated biphenyls in forest soils: depth distribution as indicator of different fate. *Environmental Pollution*, 110(1), 79-88.
- Lohmann, R., Breivik, K., Dachs, J., & Muir, D. (2007). Global fate of POPs: current and future research directions. *Environmental Pollution*, 150(1), 150-165.
- Mai, B. X., Qi, S. H., Zeng, E. Y., Yang, Q. S., Zhang, G., Fu, J. M., et al. (2003). Distribution of polycyclic aromatic hydrocarbons in the coastal region off Macao, China: Assessment of input sources and transport pathways using compositional analysis. *Environmental Science & Technology*, 37(21), 4855-4863.
- Maliszewska-Kordybach, B., Smreczak, B., & Klimkowicz-Pawlas, A. (2009). Concentrations, sources, and spatial distribution of individual polycyclic aromatic hydrocarbons (PAHs) in agricultural soils in the Eastern part of the EU: Poland as a case study. *Science of the Total Environment*, 407(12), 3746-3753.
- Masih, A., & Taneja, A. (2006). Polycyclic aromatic hydrocarbons (PAHs) concentrations and related carcinogenic potencies in soil at a semi-arid region of India. *Chemosphere*, 65(3), 449-456.
- MassDEP (2002). Technical Update: Calculation of Enhanced Soil Ingestion Rate. Boston, MA.
- Means, J. C., Wood, S. G., Hassett, J. J., & Banwart, W. L. (1980). Sorption of polynuclear aromatic hydrocarbons by sediments and soils. *Environmental Science & Technology*, 14(12), 1524-1528.
- Moody, R. P., Joncas, J., Richardson, M., & Chu, I. (2007). Contaminated soils (I): In vitro dermal absorption of benzo[a]pyrene in human skin. *Journal of Toxicology and Environmental Health, Part A*, 70(21), 1858-1865.
- Murphy, E. M., Zachara, J. M., & Smith, S. C. (1990). Influence of Mineral-Bound Humic Substances on the Sorption of Hydrophobic Organic-Compounds. *Environmental Science & Technology*, 24(10), 1507-1516.
- Nam, J. J., Song, B. H., Eom, K. C., Lee, S. H., & Smith, A. (2003). Distribution of polycyclic aromatic hydrocarbons in agricultural soils in South Korea. *Chemosphere*, 50(10), 1281-1289.
- Nelson, D. W., & Sommers, L. E. (1996). Total carbon, organic carbon, and organic matter. In P. A. Sparks DL, Helmke PA, Loeppert RH, Soluanpour PN, Tabatabai, MA, Johnston CT, Sumner ME (Ed.), *Methods of soil analysis part 3: Chemical methods* (pp. 961-1010.). Madison, Wisconsin, USA: Soil Science Society of America, Inc. and American Society of Agronomy, Inc., .
- Nisbet, I. C. T., & LaGoy, P. K. (1992). Toxic equivalency factors (TEFs) for polycyclic aromatic hydrocarbons (PAHs). *Regulatory Toxicology and Pharmacology*, 16(290-300).
- Richardson, G. M. (1997). *Compendium of Canadian Human Exposure Factors for Risk Assessment*. Ottawa, ON: O'Connor Associates Environmental Inc.
- Senior, K., & Mazza, A. (2004). Italian "triangle of death" linked to waste crisis. *Lancet Oncology*, 5(9), 525-527.
- Shuttleworth, K. L., & Cerniglia, C. E. (1995). Environmental aspects of PAH biodegradation. *Applied Biochemistry and Biotechnology*, 54(1-3), 291-302.
- Soil Survey Division Staff (1993). *Soil survey manual (Handbook 18)*. Washington, DC: U.S. Department of Agriculture.

- Sun, J. H., Wang, G. L., Chai, Y., Zhang, G., Li, J., & Feng, J. (2009). Distribution of polycyclic aromatic hydrocarbons (PAHs) in Henan Reach of the Yellow River, Middle China. *Journal of Toxicology and Environmental Health, Part A*, 72(5), 1614-1624.
- Thyssen, J., Althoff, J., Kimmerle, G., & Mohr, U. (1981). Inhalation studies with benzo[a]pyrene in Syrian golden hamsters. *Journal of the National Cancer Institute*, 66, 575-577.
- USEPA (1991). Risk Assessment Guidance for Superfund: Volume I - Human Health Evaluation Manual (Part B, Development of risk-based preliminary remediation goals). Washington, DC: US EPA (United States Environmental Protection Agency).
- USEPA (2002). Supplemental guidance for developing soil screening levels for Superfund sites. Washington, DC: US EPA (United States Environmental Protection Agency).
- USEPA (2013). Priority Pollutants. <http://water.epa.gov/scitech/methods/cwa/pollutants.cfm>. Accessed 1 Dec 2013.
- Weissenfels, W. D., Klewer, H. J., & Langhoff, J. (1992). Adsorption of polycyclic aromatic hydrocarbons (PAHs) by soil particles: influence on biodegradability and biotoxicity. *Applied Microbiology and Biotechnology*, 36(5), 689-696.

SECTION 2.4

Investigation on Inorganic Pollution Level in Surface Sediments of Naples and Salerno Bay

*Paper published in Computational Water, Energy, and Environmental Engineering, Volume 2,
Pages 36-40*

Investigation on inorganic pollution level in surface sediments of Naples and Salerno bay*

Menghan Wang, Benedetto De Vivo ,Stefano Albanese, Annamaria Lima

Dipartimento di Scienze della Terra
Università di Naples Federico II, Naples, Italy
Via Mezzocanone 8. menghan.wang@unina.it

Wanjun Lu

Department of Marine Science, Faculty of Earth Resource
China University of Geosciences, Wuhan, China

Flavia Molisso and Marco Sacchi

C.N.R. Istituto Geomare Sud, Naples, Italy

Abstract

In this study, superficial marine sediments collected from 96 sampling sites were analyzed for 53 inorganic elements. Each sample was digested in aqua regia and analyzed by ICP-MS. A developed multifractal inverse distance weighted (IDW) interpolation method was applied for the compilation of interpolated maps for both single element and factor scores distributions. R-mode factor analysis have been performed on 23 of 53 analyzed elements. The 3 factor model, accounting 84.9 % of data variability, were chosen, The three elemental associations obtained have been very helpful to distinguish anthropogenic from geogenic contribution. The aim of this study is to distinguish distribution patterns of pollutants on the sea floor of Naples and Salerno bays. In general, local lithologies, water dynamic and anthropogenic activities determine the distribution of the analyzed elements. To estimate pollution level in the area, Italian guidance, Canadian sediment quality guidance and Long's criteria are chosen to set the comparability. As the results shows, arsenic and lead may present highly adverse effect to living creatures.

Keywords: Pollution level; Compositional data analysis; Factor analysis; Naples and Salerno Gulf.

1. Introduction

Naples bay is a 10-mile wide Gulf located in the south western coast of Italy, while Salerno bay is a Gulf of Tyrrhenian Sea and separated from Naples bay by Sorrento Peninsula. Industrial complexes, intense commercial and transport activities insist on this area, which makes it potentially a heavily polluted coastal district and in need of remediation activities. Sediments are considered as a suitable medium to distinguish contamination and geochemical background of marine environment, since they are the pool of different deposition source and are a more stable medium than sea water. Moreover, toxic contaminants prefer to adsorb on sediments surface especially hydrophobic organics such as PAHs and PCBs. The aim of this study is to accomplish a comprehensive investigation of inorganic elements concentration on sediment surface and illustrate their distribution patterns.

2. Materials and method

2.1. Sampling

Surface sediment samples (following the directives of the national program for assessment of marine pollution of highly contaminated Italian coastal areas) were collected from 96 locations (Fig. 1) of Naples and Salerno bays in May 2000. A differential global positioning system (DGPS) was used to identify each location precisely. 23 samples were collected using a box-corer with an inner diameter of 25 cm, of which we have used the superficial sediments to be analyzed. 63 samples were collected by grab. Each sample was divided into three and stored in 4°C freezer.

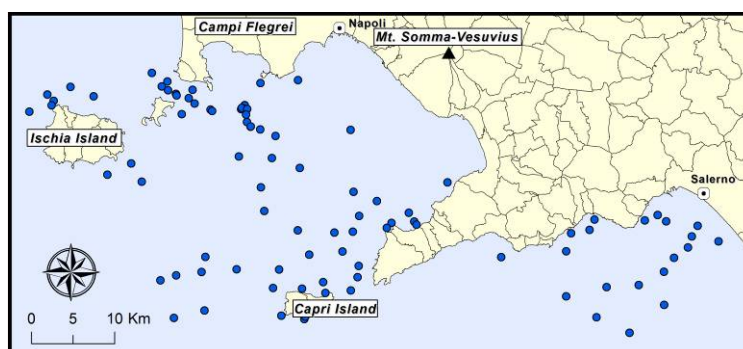


Fig.1 Study area and samples locations

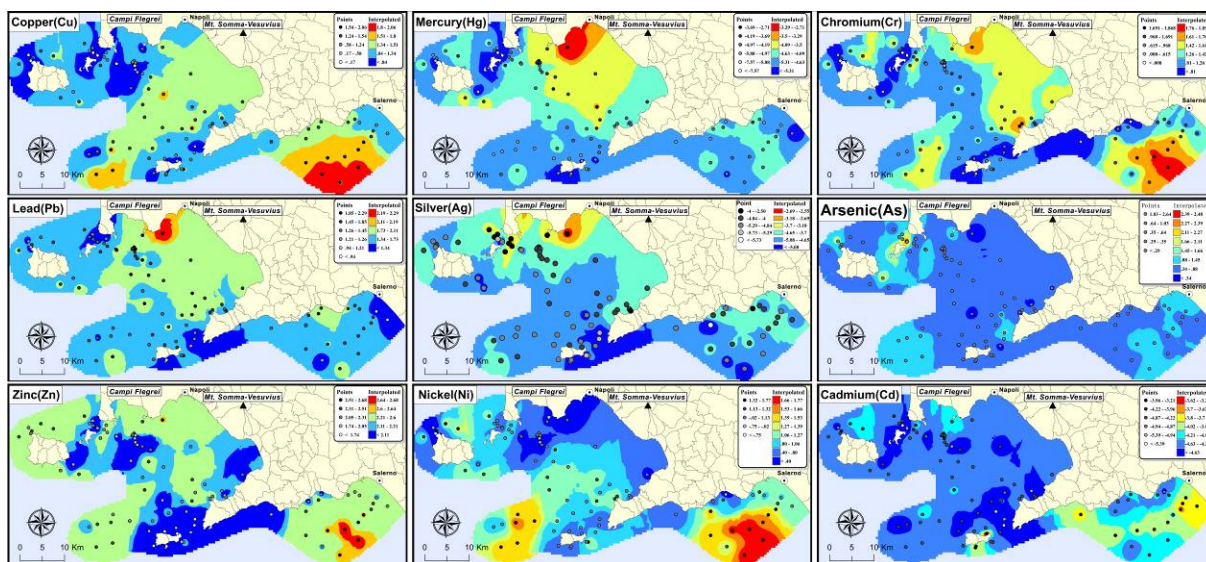
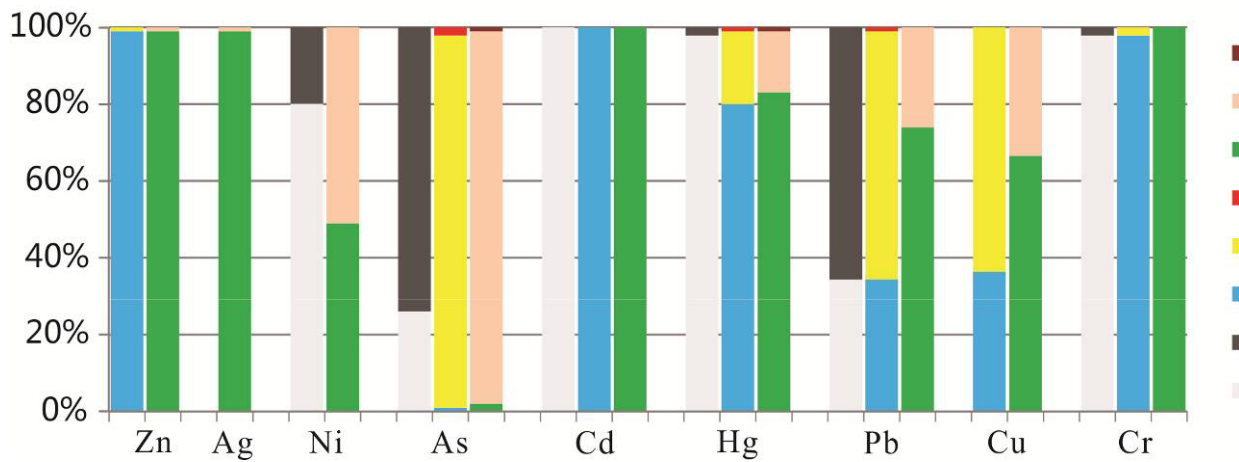


Figure.3 Single elements distribution in Naples and Salerno Gulf

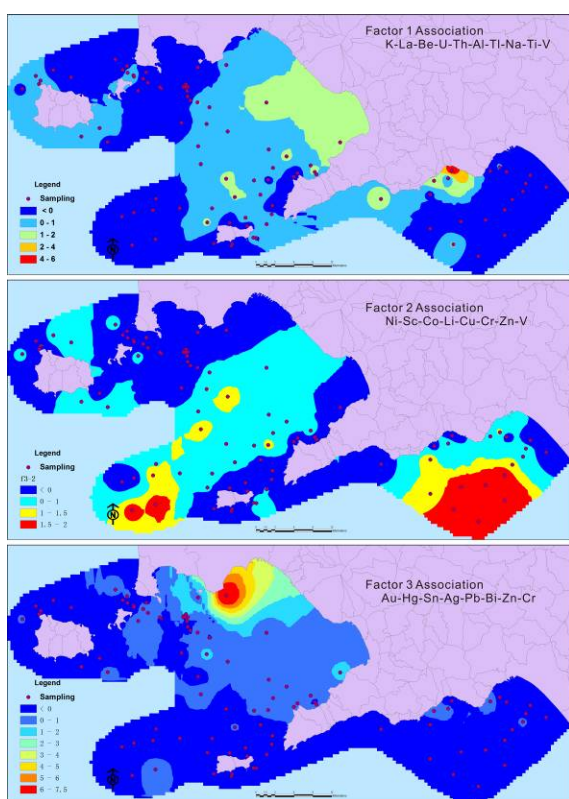


Figure.4 Factor score association maps

2.2. Chemical analyses and quality control

The all air-dried sediment samples were sieved and 30 g of the $<150 \mu\text{m}$ fraction was retained for analysis of 53 elements (Table 1). Analyses were carried out by Acme Analytical Laboratories Ltd. (Vancouver, Canada), through its Italian affiliate (Norwest Italia Srl, Naples). Each sample was digested in a modified aqua regia solution and analyzed by inductively coupled plasma–mass spectrometry (ICP-MS) and atomic emission spectrometry (ICP-AES). Specifically, a 15-g split of the pulp was digested in 45 ml of the aqua regia mixture (1 part concentrated hydrochloric acid to 1 part nitric acid to 1 part deionised water) at 90°C for 1 h. The solution was taken to a final volume of 300 ml with 5% HCl. Aliquots of sample solution were aspirated into a Jarrel Ash Atomcomp 975 ICP-Emission Spectrometer

and a Perkin Elmer Elan 6000 ICP-Mass Spectrometer.

2.3. Statistical and spatial analysis

For single element interpreting, all the data should be transformed with proper log-ratio method to avoid negative effect of compositional property (Reimann et al., 2012). All the information was managed in a GIS

Table 1. Rotating component matrix

Element	Component		
	1	2	3
Cu	.424	.786	.345
Pb	.392	.299	.788
Zn	.251	.655	.676
Ag	-.005	-.141	.838
Ni	-.006	.981	.035
Co	.167	.920	.063
U	.884	-.161	.122
Au	.105	-.048	.944
Th	.853	.307	.147
Bi	.126	.408	.781
V	.609	.541	.163
La	.894	-.056	.122
Cr	.024	.671	.665
Ti	.722	-.309	.015
Al	.846	.483	.116
Na	.808	.196	.147
K	.916	.133	.134
Sc	-.033	.946	.005
Tl	.824	.353	.257
Hg	.163	.104	.927
Sn	.293	.086	.878
Be	.891	.279	.207
Li	.186	.900	.090

georeferenced environment, using ArcGis 9.3 software package. Geodetic reference system is the Universal Transverse Mercator (fuse 33) projection on the ellipsoid World Geodetic System (WGS, 1984). All the geochemical maps were generated using the Multifractal Inverse Distance Weighted (IDW) algorithm as

an interpolation method. Factor analysis performed with the IBM SPSS Statistics 19 software package was applied to reduce the number of dimensions and extracting synthetic information about the distribution of elements in the studied environment (Albanese et al., 2007; Cicchella, 2003)

3. Results and Discussion

Heavy metals concentrations of study area were compared to 3 different marine sediment quality guidelines (CCME, 2002; Long et al., 1998; Long et al., 1995; Sprovieri et al., 2007) with the purpose of illustrating contamination level of Naples and Salerno bays (Table 2). Long (Long et al., 1995) initializes the estimation of adverse biological effect by collect and summary publications. In his work, ERL represents effect-range low which means below it rarely adverse effects, and ERM represents effect-range median which means above it frequently associated with adverse effects. Canadian sediment quality guidelines (CCME, 2002), shares same idea with Long, and include results recently. In CCME's guideline, IQSG represents interim marine sediment quality guideline and PEL represent probably effect level. Italian 367 (Albanese et al., 2010) set the environment tolerated value based on Italian law.

Pollution levels are compared in Fig.2 by presenting percentage of different category samples. Concentrations of Zn, Ag, Cd and Cr in sediment seldom exceed adverse effect thresholds in the area, while Ni, Hg, Pb and Cu have median polluted value which may cause adverse effect to living creatures as well as human beings. Only Arsenic shows values highly dangerous, reflecting probably mostly influence of volcanic sediments from Neapolitan volcanoes (Vesuvius, Campi Flegri, Ischia Island) rather than anthropogenic source.

Figure 3 shows the distribution pattern of selected analyzed elements. Most of heavy toxic metals have a similar distribution. Ag, Hg and Pb aggregates close to Naples metropolitan area, indicating that intense industrial, agricultural

and commercial activities affect these elements distribution pattern. Arsenic is mostly concentrated around Pozzuoli bay, where hydrothermal activity related to Campi Flegrei is documented as being very rich in As (Albanese et al., 2010). The distributions of Ni, Zn, and Cu indicate the water energy decrease from coastal to deep sea and cause finer sediment deposit off Gulf. Distribution pattern of Chromium indicate combination of anthropogenic effect and water energy effect.

To understand the distribution modes of the different heavy metals and discriminate the different sources, R-mode factor analysis (FA) on 23 of 53 analyzed elements was carried out. The factor model three, accounting 84.9 % of data variability, have been chosen. The elements are considered to describe effectively the composition of factors if the loading is over 0.51. The associations of the three-factor model are F1 (K, La, Be, U, Th, Al, Tl, Na, Ti, V) accounted for 32.5% of data variability, F2 (Ni, Sc, Co, Li, Cu, Cr, Zn, V) accounted for 27.4% of data variability and F3 (Au, Hg, Sr, Ag, Pb, Bi, Zn, Cr) accounted for 24.9% of data variability. Figure 4 shows the distribution pattern of the three association factor scores.

F1 association represents the elements whose distribution is mostly of geogenic source, meaning that human activities have little control on their behavior in Naples and Salerno bays. F2 represents elements mainly influenced by water energy. F3 is the most anthropogenic factor, showing intense human activities of the Naples metropolitan area as the main source for this 9 elements distribution patterns. The latter is in agreement with the results obtained by Cicchella et al., 2005 for volcanic soils of the metropolitan and provincial areas of Naples.

4. Acknowledgements

Authors thank the C.N.R. Istituto Geomare Sud a Naples to provide samples and corresponding data, and Dr. Monica Capodanno for sediment storage and disposal. This preliminary study is part of a

more comprehensive PhD program of M. Wang, aimed at the study as well of Persistent Organic Pollutants (POP), such as PAH and PCBs, by SERS laboratory and in situ experimental researchs to understand the behaviour of POP with time.

REFERENCES

- [1] Albanese, S., De Vivo, B., Lima, A., Cicchella, D., 2007. Geochemical background and baseline values of toxic elements in stream sediments of Campania region (Italy). *Journal of Geochemical Exploration*, 93(1): 21-34.
- [2] Albanese, S. et al., 2010. Geochemical baselines and risk assessment of the Bagnoli brownfield site coastal sea sediments (Naples, Italy). *Journal of Geochemical Exploration*, 105(1-2): 19-33.
- [3] Cicchella, D., 2003. Palladium and platinum concentration in soils from the Naples metropolitan area, Italy: possible effects of catalytic exhausts. *The Science of The Total Environment*, 308(1-3): 121-131.
- [4] Cicchella D., De Vivo B. & Lima A., 2005 - Background and baseline concentration values of elements harmful to human health in the volcanic soils of the metropolitan provincial area of Naples (Italy). *Geochemistry: Exploration-Environment-Analyses*, 5: 29-40.
- [5] CCME, C.C.C.o.M.o.t., 2002. Canadian sediment quality guidelines for the protection of aquatic life. *Canadian Environmental Quality Guidelines*. In: Environment, C.C.o.M.o.t. (Editor). MB, Winnipeg.
- [6] Long, E.R., Field, L.J., MacDonald, D.D., 1998. Predicting toxicity in marine sediments with numerical sediment quality guidelines. *Environmental Toxicology and Chemistry*, 17(4): 714-727.
- [7] Long, E.R., MacDonald, D.D., Smith, S.L., Calder, F.D., 1995. Incidence of adverse biological effects within ranges of chemical concentrations in marine and estuarine sediments. *Environmental management*, 19(1): 81-97.
- [8] Reimann, C. et al., 2012. The concept of compositional data analysis in practice - Total major element concentrations in agricultural and grazing land soils of Europe. *Science of the Total Environment*, 426: 196-210.
- [9] Sprovieri, M. et al., 2007. Heavy metals, polycyclic aromatic hydrocarbons and polychlorinated biphenyls in surface sediments of the Naples harbour (southern Italy). *Chemosphere*, 67(5): 998-1009.

Table 2. Heavy metals concentration comparison with different environmental guidelines

	Cu(ppm)	Pb(ppm)	Zn(ppm)	Ag(ppb)	Ni(ppm)	Cr(ppm)	Hg(ppb)	As(ppm)	Cd(ppm)
Average	26.4	39.24	68.56	103.28	20.29	26.28	97.65	16.85	0.1
10.00%	7.61	20.13	35.64	31	6.98	8.92	21.7	9.68	0.05
25.00%	14.45	26.18	63.23	46.5	11.8	16	42.25	12	0.07
50.00%	26.62	35.5	71	71	21.6	27.8	79	14.35	0.09
75.00%	37.81	47.47	84.43	109.5	27.7	35.75	116.25	17.45	0.11
Median	29	69.7	106	519	7.5	38.6	435	12.3	0.11
MAD	12	34.4	35.8	450	14.1	12.6	356	3.05	0.03
Minimum	3	9	16	17	2	3	3	5	0.02
Maximum	72	128	178	1012	40	74	864	74	0.19
ER-L	34	46.7	150	1000	20.9	81	150	8.2	1.2
ER-M	270	218	410	3700	51.6	370	710	70	9.6
ISQG	18.7	30.2	124			52.3	130	7.24	0.7
PEL	108	112	271			160	700	41.6	4.2
Italian 367		30			30	50	300	12	0.3

Investigation on Inorganic Pollution Level in Surface Sediments of Naples and Salerno Bay

Menghan Wang¹, Benedetto De Vivo¹, Stefano Albanese¹, Annamaria Lima¹,
Wanjun Lu², Flavia Molisso³, Marco Sacchi³

¹Dipartimento di Scienze della Terra Università di Napoli Federico II, Napoli, Italy

²Department of Marine Science, Faculty of Earth Resource, China University of Geosciences, Wuhan, China

³C.N.R. Istituto Geomare Sud, Napoli, Italy

Email: menghan.wang@unina.it

Received 2013

ABSTRACT

In this study, superficial marine sediments collected from 96 sampling sites were analyzed for 53 inorganic elements. Each sample was digested in aqua regia and analyzed by ICP-MS. A developed multifractal inverse distance weighted (IDW) interpolation method was applied for the compilation of interpolated maps for both single element and factor scores distributions. R-mode factor analysis has been performed on 23 of 53 analyzed elements. The 3 factor model, accounting 84.9% of data variability, were chosen. The three elemental associations obtained have been very helpful to distinguish anthropogenic from geogenic contribution. The aim of this study is to distinguish distribution patterns of pollutants on the sea floor of Naples and Salerno bays. In general, local lithologies, water dynamic and anthropogenic activities determine the distribution of the analyzed elements. To estimate pollution level in the area, Italian guidance, Canadian sediment quality guidance and Long's criteria are chosen to set the comparability. As the result shows, arsenic and lead may present highly adverse effect to living creatures.

Keywords: Pollution Level; Compositional Data Analysis; Factor Analysis; Napoli and Salerno Gulf

1. Introduction

Naples bay is a 10-mile wide gulf located in the south western coast of Italy, while Salerno bay is a gulf of Tyrrhenian Sea and separated from Naples bay by Sorrento Peninsula. Industrial complexes, intense commercial and transport activities insist on this area, which makes it potentially a heavily polluted coastal district and in need of remediation activities. Sediments are considered as a suitable medium to distinguish contamination and geochemical background of marine environment, since they are the pool of different deposition source and are a more stable medium than sea water. Moreover, toxic contaminants prefer to adsorb on sediments surface especially hydrophobic organics such as PAHs and PCBs. The aim of this study is to accomplish a comprehensive investigation of inorganic elements concentration on sediment surface and illustrate their distribution patterns.

2. Materials and Method

2.1. Sampling

Surface sediment samples (following the directives of the national program for assessment of marine pollution of

highly contaminated Italian coastal areas) were collected from 96 locations (Figure 1) of Naples and Salerno bays in May 2000. A differential global positioning system (DGPS) was used to identify each location precisely. 23 samples were collected using a box-corer with an inner diameter of 25 cm, of which we have used the superficial sediments to be analyzed. 63 samples were collected by grab. Each sample was divided into three and stored in 4°C freezer.

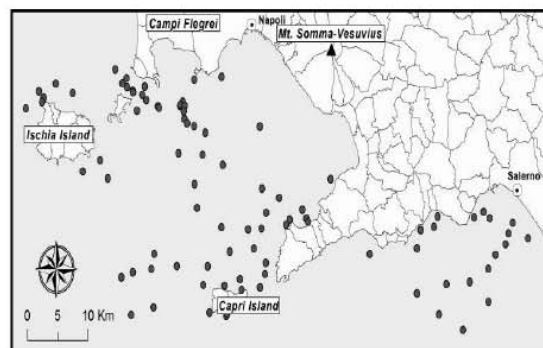


Figure 1. Study area and samples locations.

CHAPTER 3

LABORATORY RAMAN *IN SITU* RESEARCHES

OF FLUID SYSTEMS AND IRON MINERALS

CHANGES

*This chapter is about the application of in situ Raman apparatus to geochemical experiments.
Content of this paper has been also used for Master Thesis (China University of Geosciences Wuhan).*

SECTION 3.1

In situ Raman spectroscopic study of diffusion coefficients of methane in liquid water under high pressure and wide temperatures

*Paper published in **Fluid Phase Equilibrium**, 2013, Volume 360, Pages 274-278*

In situ Raman spectroscopic study of diffusion coefficients of methane in liquid water under high pressure and wide temperatures

Guo Huirong¹, Chen Ying¹, Lu Wanjun^{2*}, Li Lanlan¹, Wang Menghan²

¹ School of Environmental Studies, China University of Geosciences,
Wuhan 430074, China

² State Key Laboratory of Geological Processes and Mineral Resources,
China University of Geosciences, Wuhan 430074, China

Abstract

Methane is commonly found in sedimentary basin at temperatures of at least 473 K. Accurate values of diffusion coefficients for methane in water at high pressure and elevated temperature are essential to our understanding of transport behavior of methane in pore spaces at reservoir conditions. However, the experimental data are limited to conditions at low temperatures and pressures. In this study, diffusion coefficients of methane in water were determined under high pressures (up to 40 MPa) and wide temperature range (from 273 K to 473 K) via Raman spectroscopic method. The relationship between diffusion coefficient of methane in water [$D(\text{CH}_4)$ in m^2/s] and temperature (T in K) was derived with Speedy-Angell power-law approach as:

$$D(\text{CH}_4) = D_0 [T/T_s - 1]^m$$

Where, $D_0 = 15.95 \times 10^{-9} \text{ m}^2/\text{s}$, $T_s = 229.8 \text{ K}$, $m = 1.8769$. At constant temperature, pressure has rather small effect on the diffusion coefficients. The diffusion coefficients of methane in water are found to be slightly increasing with pressure below 20 MPa, but decreasing with pressure above 20 MPa.

Keywords: methane; water; diffusion coefficient; Raman spectrum; high pressure;

1. Introduction

Methane is commonly found in sedimentary basin at temperatures of at least 473 K [1]. Diffusion coefficients of methane in water at high pressure and high temperature near the reservoir conditions are fundamental quantities in the calculations of the rates of transport caused by

* Author to whom correspondence should be addressed (luwanjuncug@126.com); Tel.: +86 18062051972; fax: +86 27 6788 3051

concentration gradients, especially in unfractured clay, shale, and other geological materials having low permeability [2, 3]. However, most experimental studies on the diffusion coefficients of methane in water were performed at temperature below 353 K and at one atmosphere or rather low pressures, due to the difficulties of accurate measurement on the concentration of gas in the liquid at higher temperatures and high pressures. In the last decades, some indirect methods were developed by measuring the changing properties of diffusing gas such as volume, pressure, without measuring the liquid compositions [4], e.g., the gas pressure decay method [3], the dissolved gas volume method [5]. These indirect methods have some advantages, for example, they are simple and easy. But these indirect methods need to correlate the measured changes of gas pressure or volume to the composition dissolved in the liquid to obtain the diffusion coefficient, which might be introduced some uncertainties. The gas pressure decay method can perform at relatively high pressure, e.g., 35 MPa [3], but it is not performed at constant pressure, thus it is not able to reveal clearly the pressure effect to the diffusion coefficient of methane in water.

Raman spectroscopy has been used for quantitative analysis for several decades [6]. At constant temperature the concentration of dissolved methane is proportional to the Raman band intensity ratio of methane and water [7-10]. Thus, we can use the quantitative Raman spectroscopic method to monitor *in situ* the concentration changes during methane diffusion in water under high pressure and elevated temperature. We have previously applied such quantitative Raman spectroscopic methods to determining the diffusion coefficients of methane in water at room temperature and under two pressures [9]. In this study, the work was extended to the wider temperature and pressure ranges, from 273 to 473 K and from 5 to 40 MPa, to study the temperature and pressure effects on the diffusion coefficients of methane in water.

2. Experimental

The experimental setting (Fig. 1) and procedures for study of methane diffusion at high pressures and wider temperatures are extended from our Raman spectroscopic observation at room temperature [9]. The main improvement is that the capillary high pressure optic cell was mounted inside a Linkam

CAP500 heating-cooling stage (for details, see [11]), so that the diffusion process can be observed at a constant temperature from 273 to 473 K with precisions of ± 0.1 K from 273 to 373 K, and ± 0.3 K from 373 to 473 K [12]. The water used in the experiments is second de-ionized with resistivity of $18.24 \text{ M}\Omega \cdot \text{cm}$. Methane was from Air Products with a purity of 99.99%.

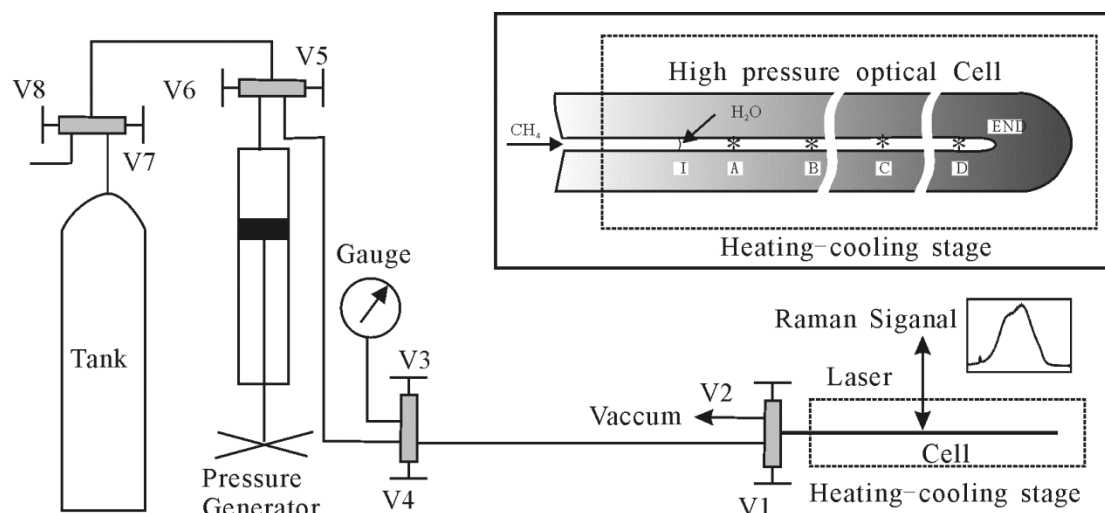


Figure 1. A schematic diagram of system for in situ Raman spectroscopic study of diffusion of gas in liquid water at high-temperature and high-pressure. All valves (shaded) are three-way/two-stem combination taper-seal valves from High Pressure Equipment Co. (Cat. No.15-15AF1). The insert is a schematic diagram showing a section of water pressurized by methane in the high-pressure optical cell, the gas/water interface (I), and four sample spots at A, B, C, and D (*) for the collection of Raman spectra in diffusion experiments.

During the experiment, a section of distilled deionized water was loaded into the close end of the optical cell (Fig. 1), and then the open end of the cell was connected to the high-pressure valve in the line for evacuating the air and loading and pressurizing methane (99.99%, Air Products) in the cell. The pressure was read from a Setra 204D digital pressure transducer with Datum 2000TM manometer (69 MPa full scale; accurate to $\pm 0.14\%$). After the water section in the cell was pressurized by methane under constant pressure, methane was eventually dissolved and diffused into water from the gas-water interface, driven by the gradient of chemical potential along the interface to liquid water at the end of the cell.

The diffusion of methane in water was monitored by a JY/Horiba LabRam HR Raman system, using 532.06 nm (frequency doubled Nd:YAG) laser excitation, a 50x Olympus objective with 0.5 numerical aperture, a 300-groove/mm grating with a spectral resolution of about 4 cm^{-1} .

Time-dependent Raman spectra (Fig. 2) of the solution at several different spots along the one dimensional diffusion path were collected one by one sequentially. The distance of each spot to the end of the cell was measured by an automated motorized x - y translation stage controlled by a computer, with an accuracy of one micrometer. The Raman band intensity ratios (Peak Height Ratio, HR) of methane and water were calculated, and the varying composition profiles of the solution in the diffusion experiments were obtained (Fig. 3).

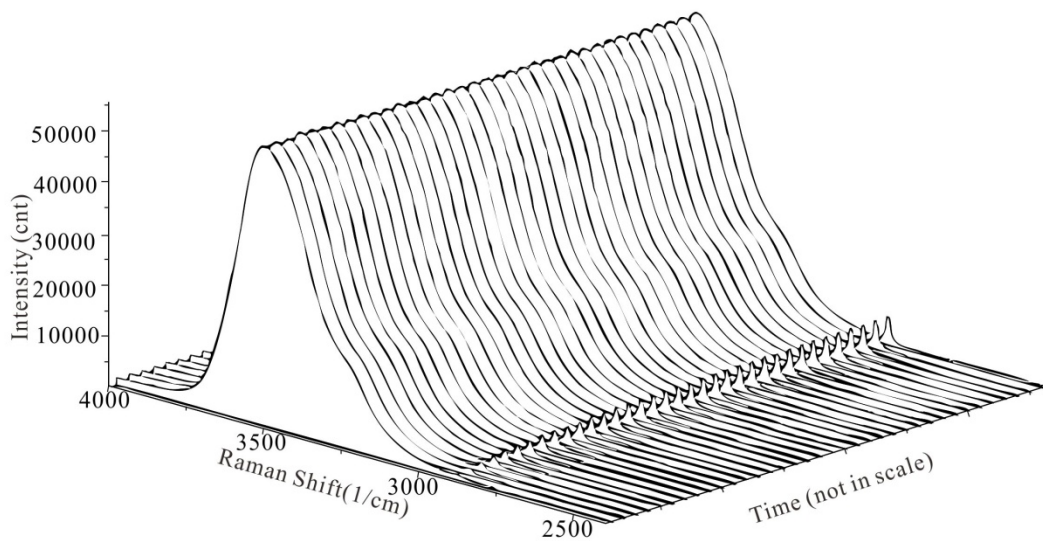


Figure 2. Time-dependent Raman spectra of dissolved methane (CH_4 , around 2910 cm^{-1}) and water (H_2O , around 3520 cm^{-1}) collected at the spot B (3.000 mm away from the spot A, and 14.911 mm away from the end of the tube), at different times after the water was pressurized by methane at 20 MPa and 473 K.

3. Results and discussion

Diffusion of methane in water was observed at the wider temperature and pressure ranges, from 273 to 473 K and from 5 to 40 MPa. The concentration of methane in water in the diffusion cell changes as a function of time and distance (Fig. 3). At the spot near the interface (usually observed within 10 micrometers to the gas- liquid interface), the observed concentrations are always close to the equilibrium values.

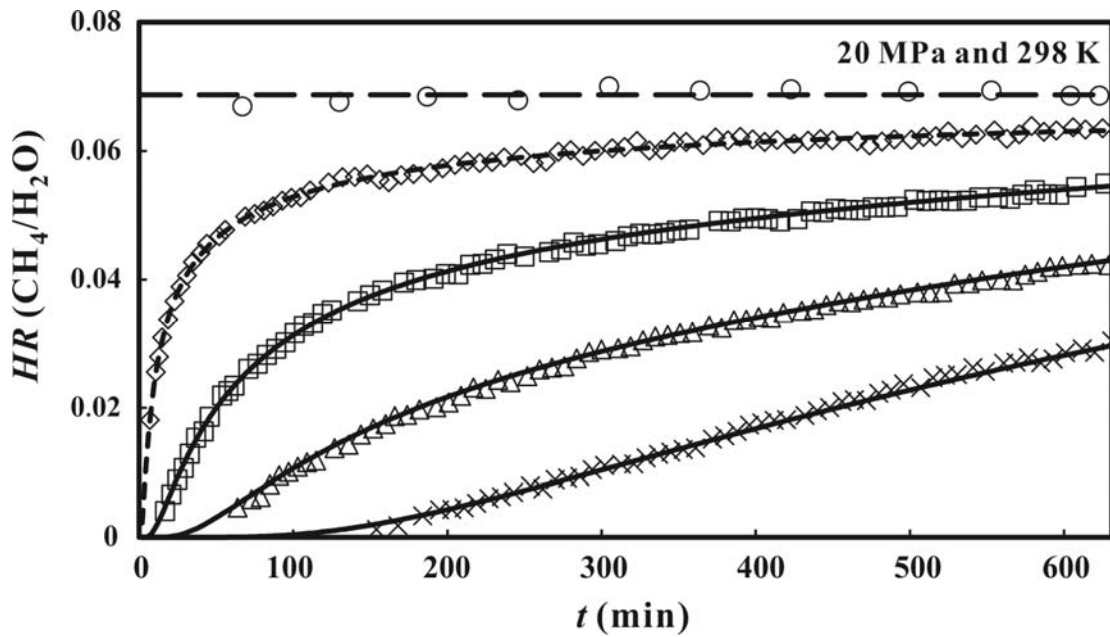


Figure 3. Raman peak intensity ratios for $\text{CH}_4/\text{H}_2\text{O}$ (equivalent to the concentration of dissolved methane in water), as a function of time t near the gas-water interface (I, circle) and at spots A (diamond), B (square), C (triangle), and D (plus), after water was pressurized by methane at specific temperature and pressure, e.g., 20 MPa and 298 K. The dash lines represent the $\text{CH}_4/\text{H}_2\text{O}$ ratios near the gas/water interface. The dotted curves represent the least-squares fit of the data at spot A. The solid curves represent calculated values at positions B, C, and D, assuming the left boundary condition is defined by the dotted curve and for the diffusion coefficient listed in Table 1 for that particular temperature-pressure condition. These diffusion coefficients give the best fit of the observed concentration profiles.

3.1. Calculated diffusion coefficients

The transport of methane in the water was treated as a one-dimensional diffusion process. The initial methane concentration in the solution at every point is zero, and during the diffusion process the concentration at the water-gas interface is constant (theoretically equal to the solubility of methane in the water at the specific temperature and pressure), while at the end of the diffusion cell the concentration flux is zero. With these initial conditions and two boundary conditions along the diffusion path, diffusion coefficients can be estimated by the least-squares method by comparing the numerically simulated results based on Fick's Second Law, with experimentally measured concentrations at specific times and sample positions (see [9, 12] for details). The root-mean-square deviations of the methane concentrations between the experimental and simulated

values for each experimental spot were calculated with the diffusion coefficients fixed at values ranging from $0.5 \times 10^{-9} \text{ m}^2\text{s}^{-1}$ to $20.0 \times 10^{-9} \text{ m}^2\text{s}^{-1}$ (e.g., Fig. 4). The D values with the least deviations (v) were then obtained. The diffusion coefficients in between D_A and D_B of the values correlated to the deviations less than the double of least deviation ($2v$) are within 95% confidence. We repeated some observations to check the repeatability for some pressure and temperature conditions, and found that the average deviations of the estimated diffusion coefficients (about 2%) at same pressure and temperature are much less than the uncertainties with 95% confidence.

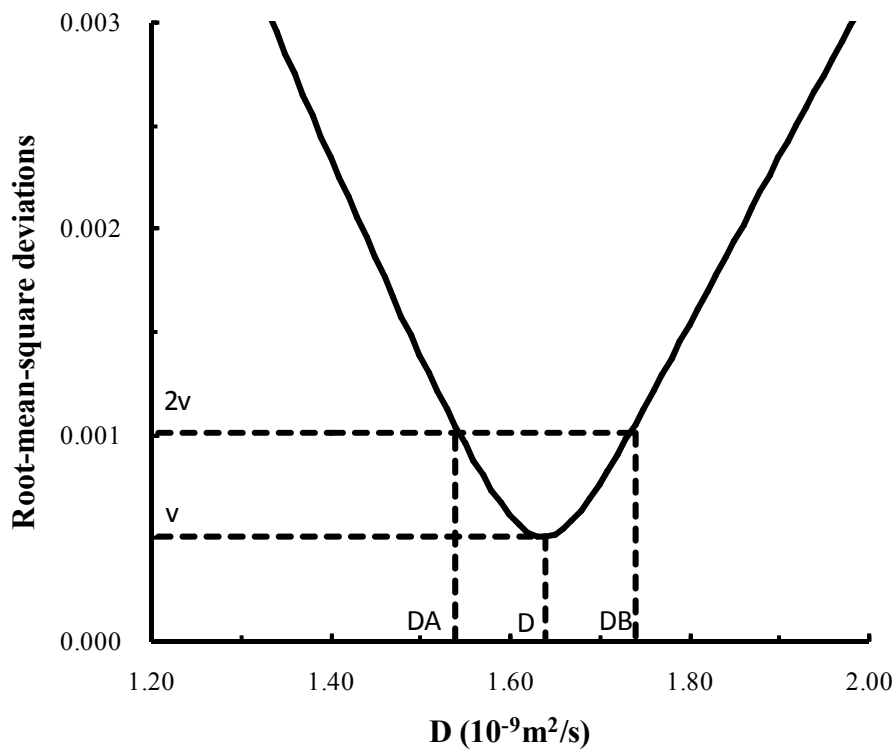
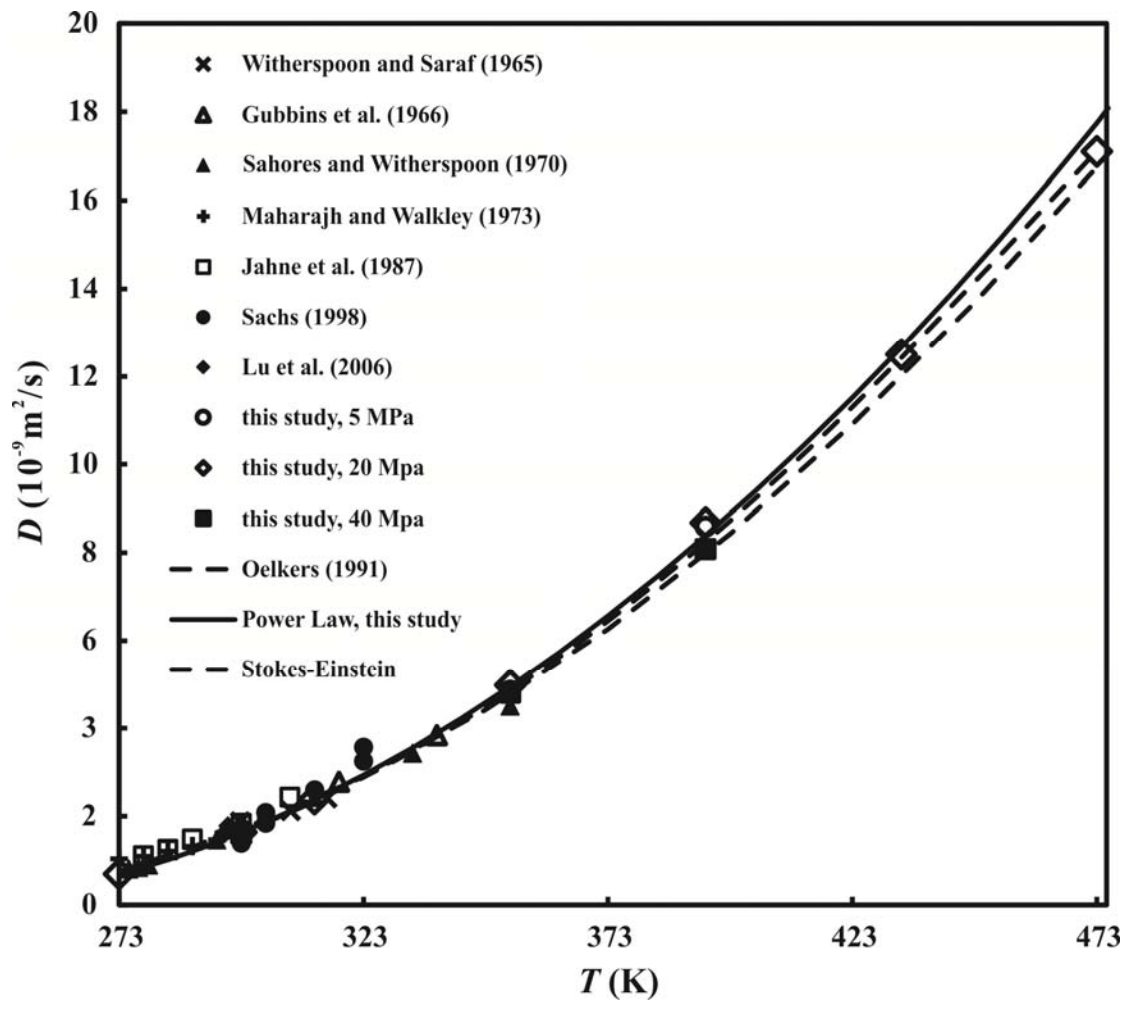


Figure 4. The root-mean-square deviation of the methane concentration between the experimental and the simulated values versus the tested diffusion coefficients for each experimental spot at 20 MPa and 298 K. The diffusion coefficient D was determined at the least deviation (v). The diffusion coefficients in between D_A and D_B of the values correlated to the double of least deviation ($2v$) are within 95% confidence. The uncertainties of diffusion coefficient was determined from $(D_A - D_B)/2$.



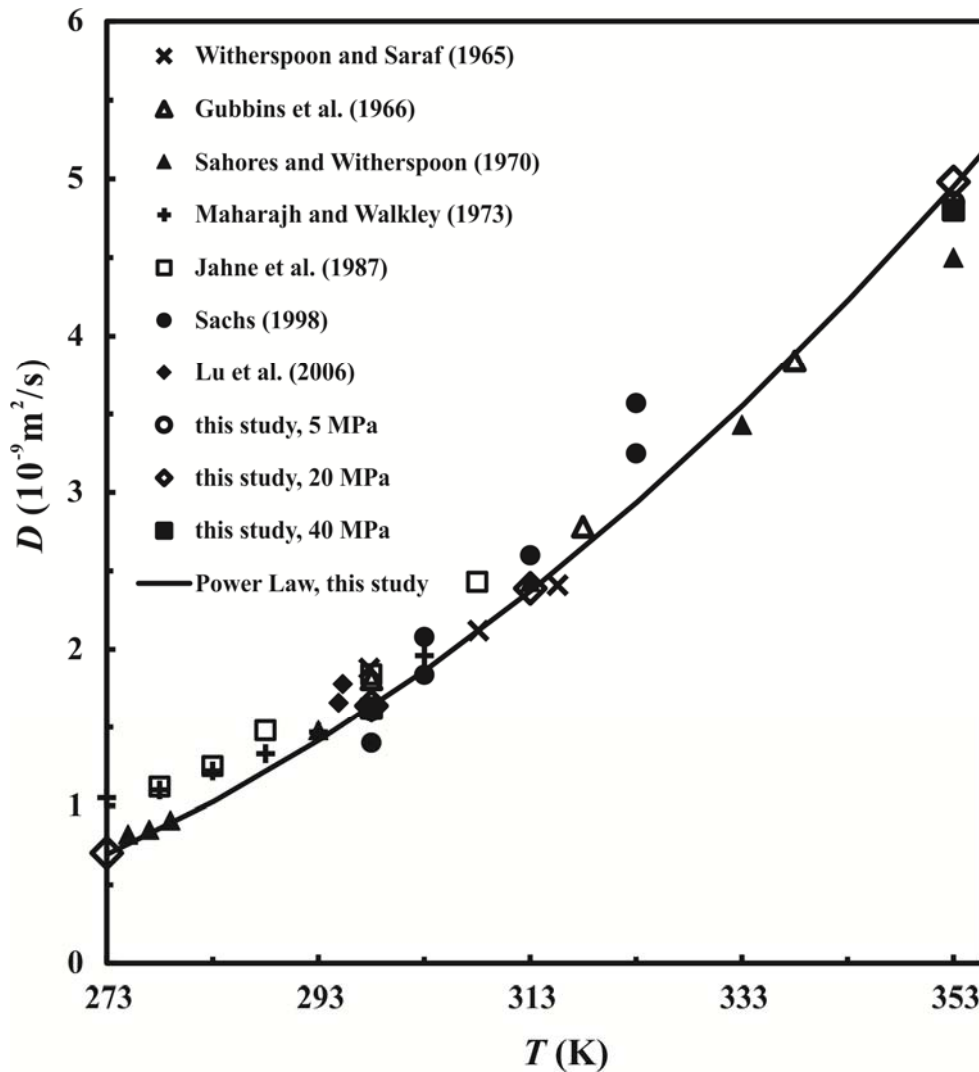


Figure 5. Comparison of our results with previously measured or calculated data on the diffusion coefficients of methane in water as a function of temperature from 273 to 473 K (a), and enlarged from 273 to 353 K (b).

Diffusion coefficients and their uncertainties with 95% confidence were estimated (Table 1, Fig. 5). The estimated uncertainties increase with decreasing pressure and increasing temperature. Diffusion coefficients obtained in this study are in good agreement with previous measurements of Witherspoon and Saraf [13] and Sahores and Witherspoon [14] by the capillary-cell method, Gubbins [15] by the diaphragm-cell method, and the theoretical study of Oelkers [2]. The data obtained with the moving boundary method by Maharajh and Walkley [16] near 298 K are close to ours, and data obtained with the diaphragm-cell method by Jähne [17] are about 10 % larger than ours. The value that Pratt et al. [18] measured at 290 K is about 17 % less than ours.

TABLE 1. Diffusion coefficients (D s) of methane in pure water measured in this study at specific pressure (p) –temperature (T) conditions. ^a

p (MPa)	T (K)	D (10^{-9} m ² /s)	Uncertainties of D (10^{-9} m ² /s)
5	298	1.61	0.26
5	353	4.85	0.22
5	393	8.59	2.40
10	298	1.63	0.13
10	353	5.00	0.72
10	393	8.70	0.83
20	273	0.702	0.07
20	298	1.64	0.10
20	313	2.39	0.21
20	353	4.98	0.34
20	393	8.68	0.66
20	433	12.5	0.80
20	473	17.1	0.90
30	298	1.60	0.13
30	353	4.79	0.38
30	393	8.45	0.74
40	298	1.62	0.11
40	353	4.80	0.33
40	393	8.08	0.66

^a Standard uncertainties u are $u(T) = 0.1$ K for 273 K $<T<$ 373 K, $u(T) = 0.3$ K for 373 K $<T<$ 573 K, $u(p) = 0.097$ MPa, and the uncertainties of diffusion coefficients (D) are estimated for each measurement at the T and p condition (0.95 level of confidence).

According to the Stokes-Einstein relation, the product of viscosity (η) and diffusion coefficient (D) is simply proportional to the absolute temperature T [19].

$$D = k_B T / (6\pi\eta r_s) \quad (1)$$

where k_B is the Boltzmann constant and r_s is the hydrodynamic radius. Assuming r_s does not change with temperature, the diffusion coefficient (D) at temperature T can be calculated with the viscosity (η) at T , the viscosity (η_{298}) and the diffusion coefficient (D_{298}) at 298 K:

$$D = D_{298} * \eta_{298} * T / (\eta * 298) \quad (2)$$

where the $D_{298} = 1.64 \times 10^{-9} \text{ m}^2/\text{s}$ was measured in this study, the viscosity (η) can be calculated from the ‘‘IAPWS Formulation 2008’’ released by the International Association for the Properties of Water and Steam [20]. It can be seen from Fig. 5, the Stokes-Einstein relation can reproduce well the diffusion coefficients data measured in this study over the temperature range from 273 to 473 K, with an average absolute deviation about 2.9%.

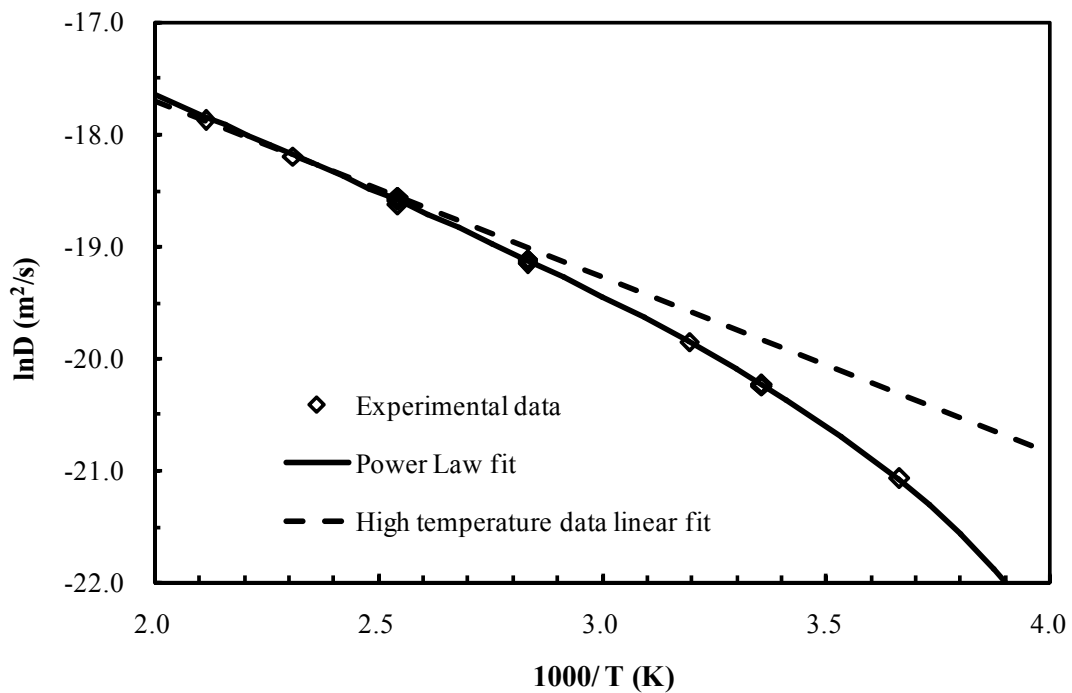


Figure 6. Logarithms of the diffusion coefficients of methane in water as a function of reciprocal absolute temperature. The diamonds represent the data measured in this study. The dash-dot line is the linear fit of the three high temperature data points at 20 MPa. The solid lines of power law fitting are also plotted.

3.2. The effect of temperature on diffusion coefficient

Fig. 6 shows the Arrhenius plot of logarithms of the diffusion coefficients of methane in water as a function of reciprocal absolute temperature. It can be seen that, below 353 K, the slope of the curve becomes more negative at lower temperatures, while the data show Arrhenius behavior only at higher temperatures.

The temperature dependence of D can be represented by Speedy-Angell [21] power-law (Fig. 6), which has the following form:

$$D(\text{CO}_2) = D_0 [T/T_s - 1]^m \quad (3)$$

where $D_0 = 15.95 \times 10^{-9} \text{ m}^2/\text{s}$, $T_s = 229.8 \text{ K}$, $m = 1.8769$.

3.3. The effect of pressure on diffusion coefficient

The effect of pressure on gas diffusion coefficient in liquid water has not been well investigated. Based on study with the pressure-decay method, Sachs [3] suggested that, the diffusion coefficient of methane in water might be considerably pressure-dependent. However, comparing the values that we measured at five pressures at 298, 353, and 393 K, we found that the pressure effect on the diffusion coefficients of methane in water is rather small (Table 1, Fig. 7).

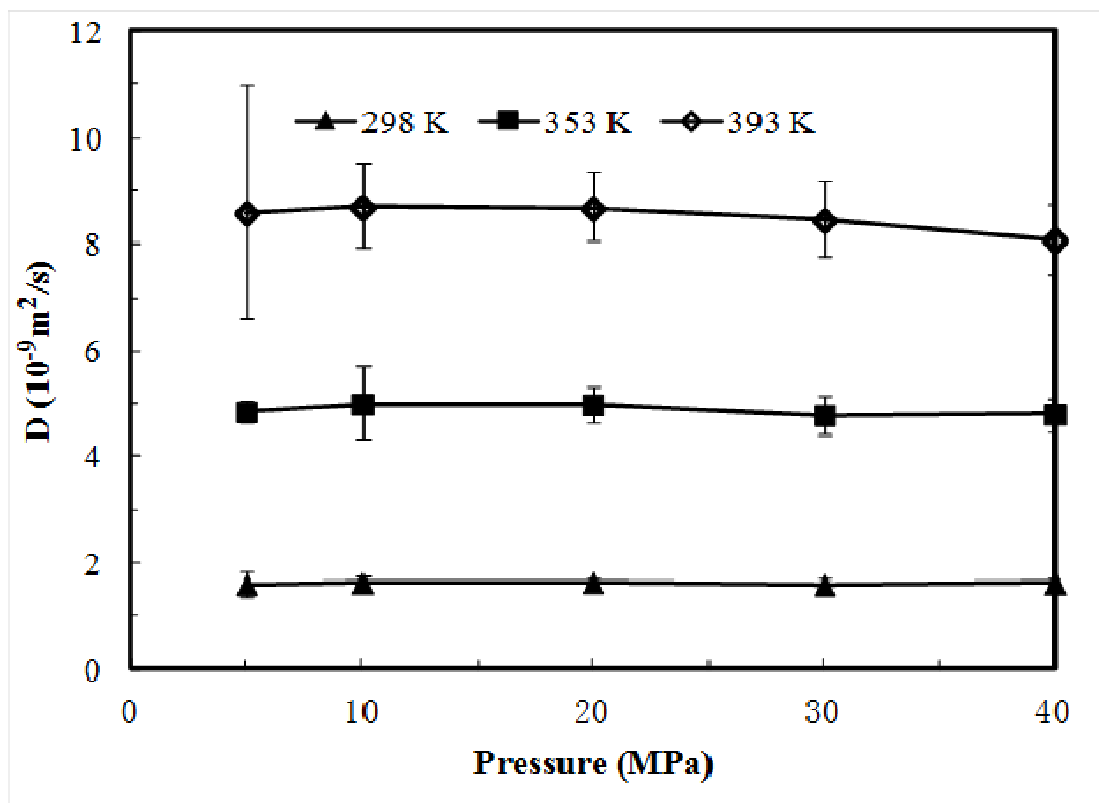


Figure 7. The diffusion coefficients of methane in water as a function of pressure at 298, 353, and 393 K.

It can also be seen that, the diffusion coefficients of methane in water show maxima near 20 MPa at constant temperature, they increase slightly with pressure below 20 MPa and decrease with pressure above 20 MPa.

4. Conclusions

Diffusion of methane in liquid water was studied with quantitative Raman spectroscopy under high pressure and wide temperatures, 19 data of the diffusion coefficients of methane in water were obtained from 273 to 473 K, and from 5 to 40 MPa. It is concluded that, diffusion coefficients of methane in water show Arrhenius behavior only at higher temperatures, the temperature dependence of the diffusion coefficients of methane in water can be fitted with Speedy-Angell power-law. The pressure effect is small, the diffusion coefficients of methane in water are found to be increasing with pressure below 20 MPa, but decreasing with pressure above 20 MPa. To our knowledge, this is the first systematically experimental study on gas diffusion coefficients in liquid water at wide temperature and pressure ranges to reveal the transport process under geological environments. Observation of gases diffusion transport in complex systems with brine and/or with gas hydrate will be done in the near future.

Acknowledgments

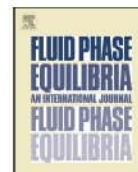
We thank Drs. I-Ming Chou and R.C. Burruss for their kind help and guidance for many years on the Raman spectroscopic research on Geo-fluids. We are grateful to Dr. Rui Sun, and two anonymous reviewers for their critical reviews and helpful comments. This work was partly supported by the National Basic Research Program of China (the 973 Program, Grant No. 2009CB219503), National Sciences Foundation of China (No. 41102154), and the Fundamental Research Funds for National University, China University of Geosciences (Wuhan).

Appendix

Supplementary data associated with this article can be found, in the online version.

References

- [1] B.P. Tissot, D.H. Welte, Petroleum formation and occurrence, 2nd ed., Springer- Verlag, New York, 1984.
- [2] E.H. Oelkers, *Geochim. Cosmochim. Ac.* 55 (1991) 3515-3529.
- [3] W. Sachs, *J. Petrol. Sci. Eng.* 21 (1998) 153-164.
- [4] N. Policarpo, P. Ribeiro, *Braz. J. Petro. Gas* 5 (2011) 171-188.
- [5] M. Jamialahmadi, M. Emadi, H. Muller-Steinhagen, *J. Petrol. Sci. Eng.* 53 (2006) 47-60.
- [6] M.J. Pelletier, *Appl. Spectrosc.* 57 (2003) 20-42.
- [7] D. Guillaume, S. Teinturier, J. Dubessy, J. Pironon, *Chem. Geol.* 194 (2003) 41-49.
- [8] J. Pironon, J.O.W. Grimmer, S. Teinturier, D. Guillaume, J. Dubessy, *J. Geochem. Explor.* 78 (2003) 111-115.
- [9] W. Lu, I.M. Chou, R.C. Burruss, M.Z. Yang, *Appl. Spectrosc.* 60 (2006) 122-129.
- [10] W.J. Lu, I.M. Chou, R.C. Burruss, *Geochim. Cosmochim. Ac.* 72 (2008) 412-422.
- [11] W. Lu, H. Guo, I.M. Chou, R.C. Burruss, L. Li, *Geochim Cosmochim Ac.* 115 (2013) 183-204.
- [12] I.M. Chou, R.C. Burruss, W.J. Lu, in: J. Chen, Y. Wang, T.S. Duffy, G. Shen, L.F. Dobrzhinetskaya (Eds.) *Advances in High-Pressure Technology for Geophysical Applications*, Elsevier, Amsterdam, 2005, pp. 475-485.
- [13] P. Witherspoon, D. Saraf, *J. Phys. Chem.* 69 (1965) 3752-3755.
- [14] K.J. Sahores, P.A. Witherspoon, in: G.D. Hobson, G.C. Spears (Eds.) *Advances in Organic Geochemistry*, Pergamon, Oxford, 1970, pp. 219-230.
- [15] K.E. Gubbins, K.K. Bhatia, R.D. Walker, *AIChE J.* 12 (1966) 548-552.
- [16] D.M. Maharajh, J. Walkley, *Can. J. Chem.* 51 (1973) 944-952.
- [17] B. Jähne, G. Heinz, W. Dietrich, *J. Geophys. Res.* 92 (1987) 10767-10776.
- [18] K.C. Pratt, D.H. Slater, W.A. Wakeham, *Chem. Eng. Sci.* 28 (1973) 1901-1903.
- [19] A. Einstein, *Investigations on the theory of the Brownian movement*, Courier Dover Publications, New York, 1956.
- [20] M.L. Huber, R.A. Perkins, A. Laesecke, D.G. Friend, J.V. Sengers, M.J. Assael, I.N. Metaxa, E. Vogel, R. Mareš, K. Miyagawa, *J. Phys. Chem. Ref. Data* 38 (2009) 101-125.
- [21] R. Speedy, C. Angell, *J. Phys. Chem.* 65 (1976) 851.



In situ Raman spectroscopic study of diffusion coefficients of methane in liquid water under high pressure and wide temperatures



Huirong Guo^a, Ying Chen^a, Wanjun Lu^{b,*}, Lanlan Li^a, Menghan Wang^b

^a School of Environmental Studies, China University of Geosciences, Wuhan 430074, China

^b State Key Laboratory of Geological Processes and Mineral Resources, China University of Geosciences, Wuhan 430074, China

ARTICLE INFO

Article history:

Received 6 April 2013
Received in revised form
20 September 2013
Accepted 23 September 2013
Available online 2 October 2013

Keywords:

Methane
Water
Diffusion coefficient
Raman spectrum
High pressure

ABSTRACT

Methane is commonly found in sedimentary basin at temperatures of at least 473 K. Accurate values of diffusion coefficients for methane in water at high pressure and elevated temperature are essential to our understanding of transport behavior of methane in pore spaces at reservoir conditions. However, the experimental data are limited to conditions at low temperatures and pressures. In this study, diffusion coefficients of methane in water were determined under high pressures (up to 40 MPa) and wide temperature range (from 273 to 473 K) via Raman spectroscopic method. The relationship between diffusion coefficient of methane in water [$D(\text{CH}_4)$ in m^2/s] and temperature (T in K) was derived with Speedy–Angell power-law approach as:

$$D(\text{CH}_4) = D_0 \left[\frac{T}{T_s} - 1 \right]^m$$

where $D_0 = 15.95 \times 10^{-9} \text{ m}^2/\text{s}$, $T_s = 229.8 \text{ K}$, $m = 1.8769$. At constant temperature, pressure has very small effect on the diffusion coefficients.

© 2013 Elsevier B.V. All rights reserved.

1. Introduction

Methane is commonly found in sedimentary basin at temperatures of at least 473 K [1]. Diffusion coefficients of methane in water at high pressure and high temperature near the reservoir conditions are fundamental quantities in the calculations of the rates of transport caused by concentration gradients, especially in unfractured clay, shale, and other geological materials having low permeability [2,3]. However, most experimental studies on the diffusion coefficients of methane in water were performed at temperature below 353 K and at one atmosphere or rather low pressures, due to the difficulties of accurate measurement on the concentration of gas in the liquid at higher temperatures and high pressures. In the last decades, some indirect methods were developed by measuring the changing properties of diffusing gas such as volume, pressure, without measuring the liquid compositions [4], e.g., the gas pressure decay method [3], the dissolved gas volume method [5]. These indirect methods have some advantages, for example, they are simple and easy. But these indirect methods need to correlate the measured changes of gas pressure or volume to the composition dissolved in the liquid to obtain the diffusion coefficient, which

may introduce some uncertainties. The gas pressure decay method can perform at relatively high pressure, e.g., 35 MPa [3], but it is not performed at constant pressure, thus it is not able to reveal clearly the pressure effect to the diffusion coefficient of methane in water.

Raman spectroscopy has been used for quantitative analysis for several decades [6]. At constant temperature the concentration of dissolved methane is proportional to the Raman band intensity ratio of methane and water [7–10]. Thus, we can use the quantitative Raman spectroscopic method to monitor in situ the concentration changes during methane diffusion in water under high pressure and elevated temperature. We have previously applied such quantitative Raman spectroscopic methods to determining the diffusion coefficients of methane in water at room temperature and under two pressures [9]. In this study, the work was extended to the wider temperature and pressure ranges, from 273 to 473 K and from 5 to 40 MPa, to study the temperature and pressure effects on the diffusion coefficients of methane in water.

2. Experimental

The experimental setting (Fig. 1) and procedures for study of methane diffusion at high pressures and wider temperatures are extended from our Raman spectroscopic observation at room temperature [9]. The main improvement is that the capillary high pressure optical cell was mounted inside a Linkam CAP500

* Corresponding author. Tel.: +86 18062051972; fax: +86 27 6788 3051.

E-mail addresses: luwanjuncug@126.com, wjlu@cug.edu.cn (W. Lu).

SECTION 3.2

Pressure and temperature dependence of the Raman peak intensity ratio of asymmetric stretching vibration (ν_3) and asymmetric bending overtone ($2\nu_2$) of methane

Paper accepted by Applied Spectroscopy (in press)

Pressure and temperature dependence of the Raman peak intensity ratio of asymmetric stretching vibration (ν_3) and asymmetric bending overtone ($2\nu_2$) of methane

Wang Menghan^{1,2}, Lu Wanjun^{1*}, Li Lanlan¹, Qiao Shaohua¹

¹State Key Laboratory of Geological Processes and Mineral Resources,
Wuhan 430074, China

²Dipartimento di Scienze della Terra, della Ambiente e delle Risorse, Università degli Studi di
Naples Federico II, Via Mezzocannone 8, 80134 Naples, Italy

ABSTRACT

Raman peaks of asymmetric stretching vibration (ν_3) and asymmetric bending overtone ($2\nu_2$) of methane were studied at elevated pressures and temperatures, from 3 to 51 MPa, and 298.15 to 473.15 K. The peak intensity ratio of ν_3 and $2\nu_2$ were calculated and the relationship among peak intensity ratio, temperature, and pressure/density were derived with numerical equations. With such relationships, geologists can determine the pressure and density of methane fluid inclusions by Raman spectroscopic measurement of the peak intensity ratios of ν_3 and $2\nu_2$.

Keywords: Asymmetric vibrations, Raman peak intensity ratio, Temperature, Pressure, Methane

INTRODUCTION

Raman spectroscopy became a powerful tool to study the properties of fluid inclusions in minerals since 1980s¹. Many parameters were derived from the Raman spectra of fluid to determinate the pressure and composition in the fluid inclusion, such as peak position²⁻⁵, peak width ratio^{3,4}, peak intensity ratio^{3,4,6} and peak area ratio⁷⁻¹². For methane in inclusions, the peak position of the C-H symmetric stretching band (ν_1) of methane shifts to lower wavenumbers as pressure increases^{2-5, 13}. To date, ν_1 shifting is the most wide-used quantitative Raman scattering method

*Author to whom correspondence should be addressed (luwanjuncug@126.com); Tel.: +86 18062051972; fax:+86 27 6788 3063

regardless of interior label. However, the determination of inner pressure in methane-bearing inclusion is only reliable when the composition is well acknowledged, because ν_1 shifting could be significantly affected by the presence of other gases^{3,4}.

Besides the most intensified C-H symmetric stretching band (ν_1), asymmetric stretching band (ν_3) and asymmetric bending band overtone ($2\nu_2$) are two primary bands with mediate intensity (~2% intensity of ν_1). Peak intensity ratio (PIR) of ν_3 and $2\nu_2$ is found to systematically change with pressure at room temperature and the relationship between PIR and pressure seems to be independent to composition of natural gas¹⁴. It is worthy to know how the relationship between the PIR and pressure is affected by temperature and the composition of the fluid samples, when we use PIR to accurately determine the pressure of methane-bearing fluid inclusion.

In this study, the PIR is studied for pure methane system at elevated pressures and temperatures. The relationship among peak intensity ratio, temperature, and pressure/density were derived with numerical equations. As a demonstration, the inner pressure and density of two methane inclusions were determined by Raman spectroscopic measurement of the peak intensity ratios of ν_3 and $2\nu_2$.

METHOD

1) Experimental apparatus and procedures

The apparatus and procedures are similar to those we used recently for the study of carbon dioxide diffusion in water^{11, 15}. A capillary high pressure optical cell (CHPOC) was used for loading methane under high pressure. The pressure was read from a Setra 204D digital pressure transducer with Datum 2000TM manometer (69 MPa full scale; accurate to $\pm 0.14\%$). The CHPOC was put into the slot in the silver plate of the Linkam CAP500 heating-cooling stage for temperature control. This device can control temperatures between ~83 and 773 K with precisions of ± 0.2 K from 298 to 373 K, and ± 0.5 K from 373 to 573 K¹⁶.

Raman spectroscopic measurement of the peak intensity ratios of ν_3 and $2\nu_2$ at constant temperature and pressure was conducted with the following procedure: (1) insert the cell horizontally into the heating-cooling stage, which was mounted on an X-Y-Z stage under a microscope for

observations and Raman analyses. (2) evacuate the pressure line and the cell and then load it with methane (99.99%, Air Products); (3) repeat procedure (2) twice; (4) use the pressure generator to adjust the pressure in the cell; (5) adjust the sample temperature by heating-cooling stage.

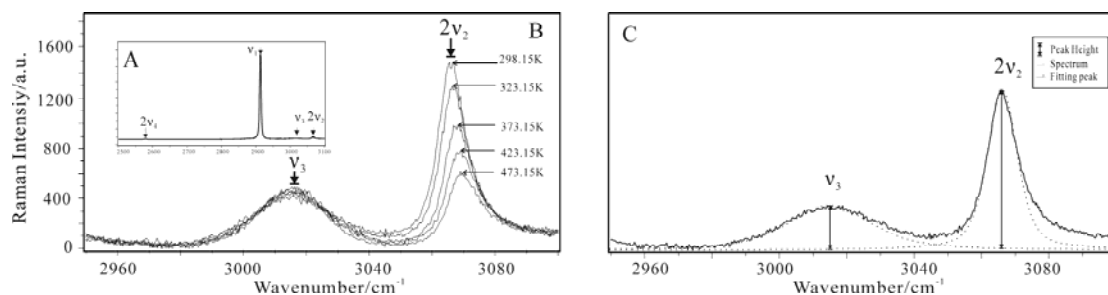


Figure 1. Raman spectra of methane under 30 MPa at temperature from 298.15 K to 473.15 K. A: Spectrum is acquired in the range of 2500 cm^{-1} to 3100 cm^{-1} , covering four bands of methane. B: When temperature increases, intensity of $2\nu_2$ changes (decreases) more significantly than intensity of ν_3 . The ratio of peak intensities ($\nu_3/2\nu_2$) varies along with temperature. C: Peak intensities of ν_3 and $2\nu_2$ are measured according to fitted peaks which are calculated with built-in software (*Labspec 5.28.25*).

2) Spectra collection and calibration of methane peak heights

Spectra of methane were acquired by a JY/Horiba LabRam HR Raman system, using 532.06 nm (frequency doubled Nd:YAG) laser excitation, a 50x Olympus objective with 0.5 numerical aperture, a 1800-groove/mm grating with a resolution of about 0.65 cm^{-1} ; $\sim 15\text{ mW}$ laser light was focused on a central level of the horizontal cell during the measurement. Spectra were collected at each sample spot sequentially covered 2500 cm^{-1} to 3100 cm^{-1} , which covered the stretching and bending overtone of methane (the asymmetric bending overtone $\sim 2580\text{ cm}^{-1}$, the symmetric stretching band at $\sim 2910\text{ cm}^{-1}$, the asymmetric stretching band at $\sim 3020\text{ cm}^{-1}$ and the asymmetric bending overtone band at $\sim 3070\text{ cm}^{-1}$), for 60 to 200 seconds with two accumulations per spectrum. Before each acquisition, single window shot for one second was repeated until the peak height of symmetric stretching band (ν_1 , Fig.1) steadily reaches maximum. This step was to make sure the maximum peaks height obtained and spectra were comparative.

Each spectrum was extracted to the range from 2950 cm^{-1} to 3100 cm^{-1} . After reducing the

background, no further modification of spectrum was needed. Obtained spectra were fitted and PIR were calculated with the built-in software (*Labspec 5.28.25*).

For comparison, the shifting of ν_1 with pressure was also studied. For ν_1 shifting experiments, a lightened Neon lamp was placed below objective stage of microscope. Measured ν_1 peak position was corrected from Neon lamp reference shifts, as following equation¹⁷:

$$\frac{\nu_{\text{true}} - 2836.988806}{\nu_1 - \text{Ne}_1} = \frac{3008.12744 - 2836.988806}{\text{Ne}_2 - \text{Ne}_1} \quad (1)$$

where ν_{true} was the corrected wavenumber of symmetric stretching bands, and ν_1 was the acquired wavenumber along with Neon lamp reference. Ne_1 and Ne_2 were two bands corresponding to Neon lamp scattering bands of 2836.99 cm^{-1} (at 626.65 nm wavelength) and 3008.13 cm^{-1} (at 633.44 nm wavelength) respectively.

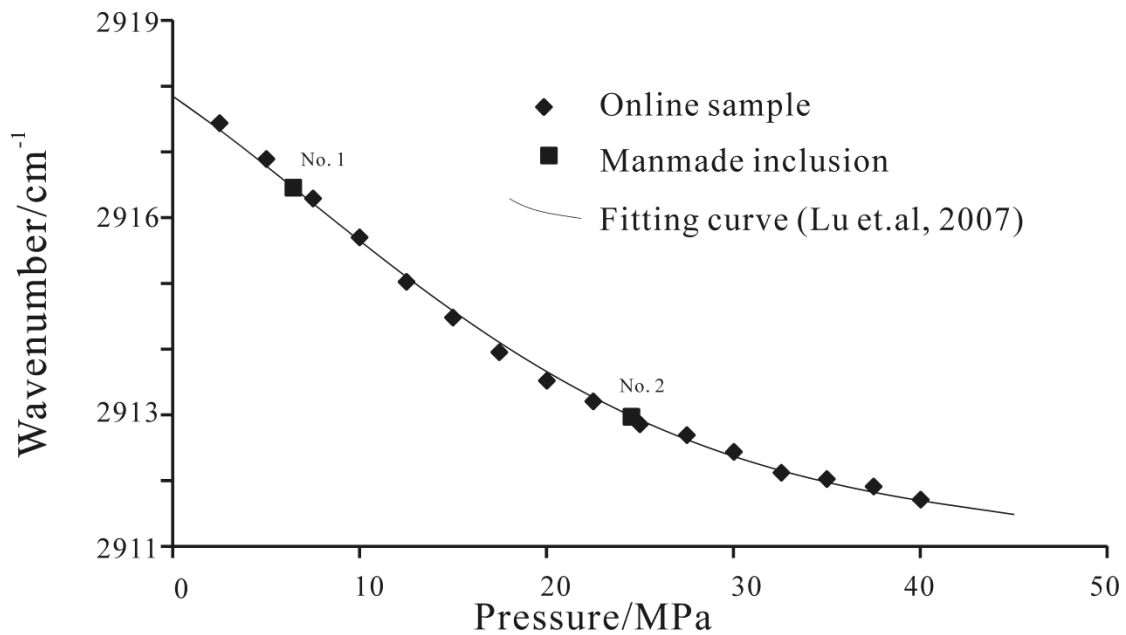


Figure 2. The fitting curve (solid line) followed the form of calculating methane vapor pressure with ν_1 peak position⁴. Least square method is used to fit the laboratory standard ν_0 , which is determined as 2917.849 cm^{-1} . The corrected ν_1 peak position of manmade methane inclusions (solid squares) are 2916.456 cm^{-1} and 2912.972 cm^{-1} for No.1 and No.2 methane inclusion respectively. Followed Eq. 3, inner pressures of inclusions are 6.45 MPa and 24.54 MPa, respectively.

Followed the procedure of Lu's work⁵, the lab reference shift, ν_0 , was determined by least square method using MATLAB R2012b package when fitting the following equation (Fig. 2):

$$v_{\text{true}} = v_0 + (2.8095 \times 10^{-8}P_1^5 - 5.2333 \times 10^{-6}P_1^4 + 3.2622 \times 10^{-4}P_1^3 - 5.5116 \times 10^{-3}P_1^2 - 1.9228 \times 10^{-1}P_1) \quad (2)$$

where P_1 is pressure in MPa.

The fitted v_0 is 2917.849 cm^{-1} , with R^2 equals to 0.997787. The pressure (MPa) of methane inclusion can be calculated from the following equation:

$$P = -0.0148 \times (v_{\text{true}} - v_0)^5 - 0.1791 \times (v_{\text{true}} - v_0)^4 - 0.8479 \times (v_{\text{true}} - v_0)^3 - 1.765 \times (v_{\text{true}} - v_0)^2 - 5.876 \times (v_{\text{true}} - v_0) \quad (3)$$

3) Regression procedures of peak heights ratio

To find a quantitative relationship for PIR, temperature, and pressure/density, one thousand functions were automatic tested with 1STOPT15 package using Levenberg-Marquardt method combined universal global optimization method. Optimum fitting curves were depicted as follows:

$$R = F(T, P) = (p_1 + p_2 \times T + p_3 \times T^2 + p_4 \times P + p_5 \times P^2 + p_6 \times P^3) / (1 + p_7 \times T + p_8 \times T^2 + p_9 \times P + p_{10} \times P^2 + p_{11} \times P^3) \quad (4);$$

$$P = F(T, R) = (p_1 + p_2 \times T + p_3 \times T^2 + p_4 \times P + p_5 \times P^2 + p_6 \times P^3) / (1 + p_7 \times T + p_8 \times T^2 + p_9 \times P + p_{10} \times P^2 + p_{11} \times P^3) \quad (5);$$

$$D = F(T, R) = (p_1 + p_2 \times T + p_3 \times T^2 + p_4 \times P + p_5 \times P^2 + p_6 \times P^3) / (1 + p_7 \times T + p_8 \times T^2 + p_9 \times P + p_{10} \times P^2 + p_{11} \times P^3) \quad (6);$$

where, R is the peak heights ratio between v_3 and $2v_2$, p_i are the fitting parameters, T is the temperature in K, P is the pressure in MPa, D is the density in g/cm^3 , calculated from the equation of state of Duan^{18,19} (Table I).

Table I. Observation intensity ratio ($H_{\nu_3}/H_{2\nu_2}$) and spectrum acquired temperature and pressure. The density is calculated based on equation of state of Duan.

T (K)	P (bar)	Observed Ratio	Density (g/cm^3)*	T (K)	P (MPa)	Observed Ratio	Density (g/cm^3)*	T (K)	P (MPa)	Observed Ratio	Density (g/cm^3)*
298.15	2.95	1.45	2.00E-02	323.15	30.23	0.34	1.90E-01	423.15	10.09	1.23	4.67E-02
298.15	5.16	1.06	3.64E-02	323.15	39.81	0.29	2.26E-01	423.15	15.05	0.97	6.95E-02
298.15	7.10	0.85	5.17E-02	323.15	51.45	0.24	2.57E-01	423.15	20.00	0.84	9.14E-02
298.15	10.09	0.67	7.67E-02	373.15	2.95	2.11	1.55E-02	423.15	30.23	0.61	1.32E-01
298.15	15.05	0.51	1.19E-01	373.15	5.16	1.48	2.74E-02	423.15	39.81	0.50	1.64E-01
298.15	20.00	0.38	1.57E-01	373.15	7.10	1.28	3.81E-02	423.15	51.45	0.41	1.96E-01
298.15	30.23	0.28	2.14E-01	373.15	10.09	1.01	5.47E-02	473.15	2.95	2.47	1.20E-02
298.15	39.81	0.24	2.49E-01	373.15	15.05	0.81	8.22E-02	473.15	5.16	1.92	2.10E-02
298.15	51.45	0.21	2.78E-01	373.15	20.00	0.65	1.08E-01	473.15	7.10	1.65	2.89E-02
323.15	2.95	1.68	1.82E-02	373.15	30.23	0.48	1.56E-01	473.15	10.09	1.40	4.10E-02
323.15	5.16	1.19	3.27E-02	373.15	39.81	0.39	1.90E-01	473.15	15.05	1.17	6.07E-02
323.15	7.10	1.00	4.59E-02	373.15	51.45	0.32	2.23E-01	473.15	20.00	1.00	7.96E-02
323.15	10.09	0.78	6.71E-02	423.15	2.95	2.35	1.35E-02	473.15	30.23	0.77	1.16E-01
323.15	15.05	0.61	1.03E-01	423.15	5.16	1.79	2.38E-02	473.15	39.81	0.63	1.45E-01
323.15	20.00	0.45	1.36E-01	423.15	7.10	1.49	2.89E-02	473.15	51.45	0.53	1.75E-01

*:calculated from equation of state of Duan¹⁷

RESULTS

1) Dependent relations between peak heights ratio with pressure, temperature and density.

PIR is affected by methane pressure, temperature and density. Quasi-polynomial lines are fitted to isothermal pressure-ratio scatter diagrams (Fig.3). For temperature-ratio scatter diagrams, a series of quasi-linear relations are fitted and with decreasing slopes towards increasing pressure (Fig.4). Based on the calculated densities¹⁸, quasi-powered lines are fitted to isothermal ratio-density scatter diagrams (Fig. 5).

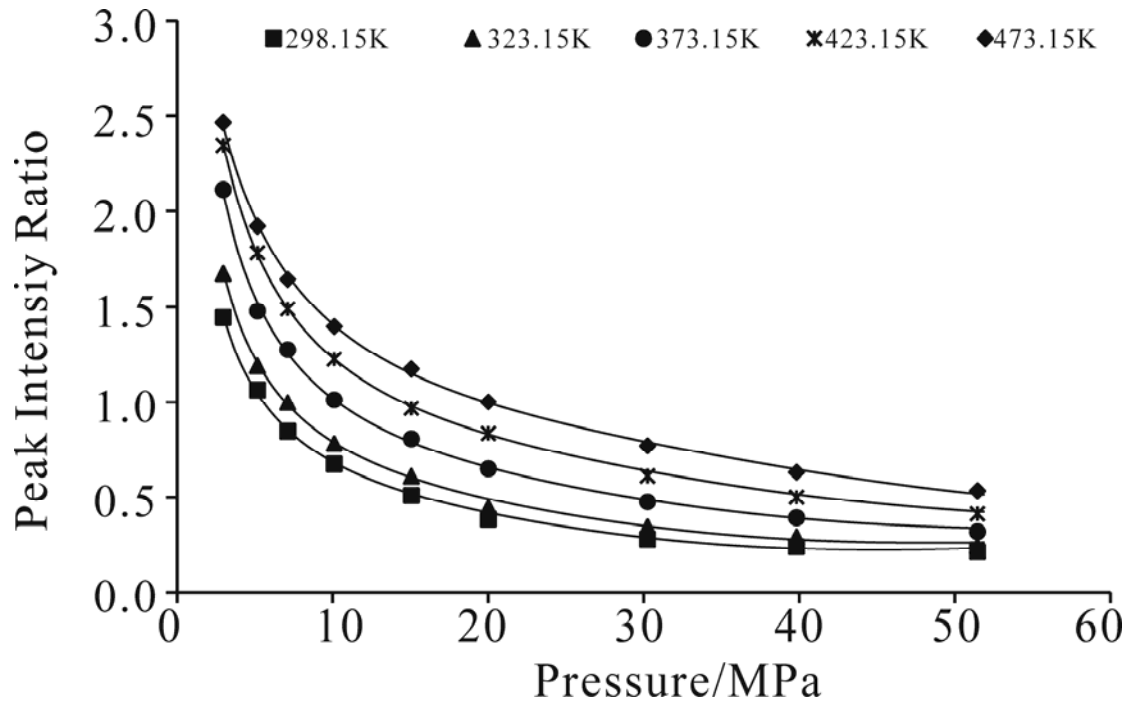


Figure 3. Isothermal intensity ratio (H_{v3}/H_{2v2}) as function of pressure in MPa, pressure ranges in 3-51 MPa. Symbols represent average value of experimental results at same temperature and pressure (Table.1), while solid lines indicate fitting result of Eq.4; parameter of Eq.4 is shown in Table.2. The fact that solid lines traverse symbols supports the effectiveness of fitting function.

2) Fitting functions

Calculated with 1STOPT15 package, the functions are depicted as Eqs. 4 to 6. Parameters and coefficients of the function are listed in Table II.

Goodness of fit is evaluated by four different parameters: correlation coefficient, determination coefficient, root mean square error (RMSE) and chi-square coefficient (Table II). Correlation coefficient and determination coefficient reflect effectiveness of fitting functions, while RMSE and chi-square coefficient indicate normal distribution of error and accuracy. All the parameters indicate

the reliability of fitting functions.

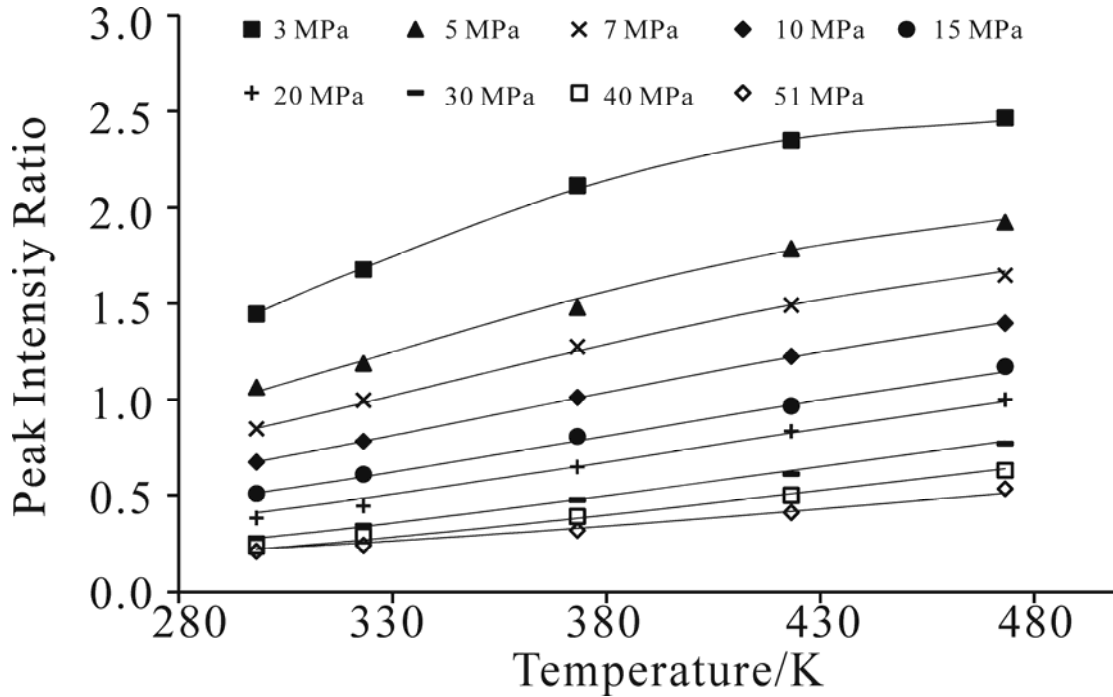


Figure 4. Isobaric intensity ratio (H_{v3}/H_{2v2}) as function of temperature in K, temperature range 298.15 K to 473.15 K. Symbols represent average value of experimental results at same temperature and pressure (Table.1), while solid lines indicate fitting result of Eq. 4; parameter of Eq. 4 is shown in Table.2. The fact that solid lines traverse symbols supports the effectiveness of fitting function.

3) Application on methane-bearing fluid inclusions

With the above equations, the inner pressure of methane inclusion can be determined when the PIR is obtained at a strictly controlled temperature. To test this method, two methane inclusions were synthesized following the procedures of Chou et al.²⁰. No.1 inclusion has 0.65 mm outer diameter and 0.3 mm inner diameter. No.2 inclusion has 0.3 mm outer diameter and 0.15 mm inner diameter. The results are listed in Table III and Table IV. Densities are determined as 0.046483 g/cm³ and 0.185141 g/cm³ for No.1 and No.2 inclusions respectively, calculated from measured ν_1 shift.

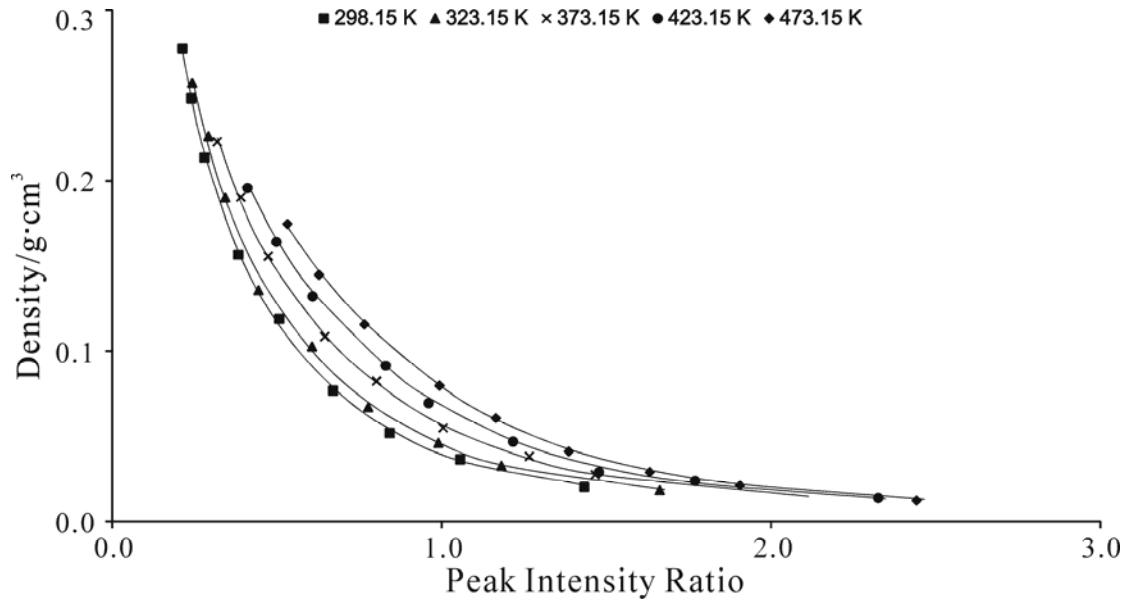


Figure 5. Isothermal density in g/cm^3 as function of intensity ratio (H_{v3}/H_{2v2}). Symbols represent average value of experimental results at same temperature and pressure (Table.1), while solid lines indicate fitting result of Eq. 6; parameter of Eq.6 is shown in Table.2. The fact that solid lines traverse symbols supports the effectiveness of fitting function.

PIR of these two synthetic inclusions were obtained at elevated temperatures, the inner pressures were calculated for each temperature condition. The calculated densities using the pressure derived from Eq. 5 along combined with Duan's equation (Table III and Table IV) exhibit $\pm 2.65\%$ and $\pm 3.55\%$ of uncertainties for No.1 and No.2 inclusions respectively. If densities are calculated from Eq. 6, the uncertainties for No.1 and No.2 inclusions are $\pm 4.21\%$ and $\pm 3.48\%$ respectively. Average densities calculated from PIR are compared with densities derived of v_1 shifting. Less than 5% difference exists between the densities determined from two methods.

Remarkable temperature effect on PIR may introduce error in pressure calculation when the Raman spectra were collected at room temperature without accurate temperature controlling. Room temperature varies, for example, from 20°C to 25°C at different labs in different seasons. When inner density of methane inclusion varies between 0.0166 g/cm^3 and 0.0935 g/cm^3 , the calculation error of density exceed 2% of the result.

Table II. Goodness of fitting coefficients and parameters of Eq. 4-6 to calculate intensity ratio, pressure and density respectively.

		Ratio: Eq.4	Pressure: Eq.5	Density: Eq.6
Correlation Coefficient		0.99963	0.99947	0.99955
Determination Coefficient		0.99926	0.99894	0.99909
Root Mean Square Error		0.01593	0.51981	2.303E-03
Chi-Square Coefficient		0.00865	0.30236	1.157E-03
Parameters	p₁	5.710E-01	1.878E+01	1.018E+00
	p₂	-3.259E-03	-1.843E-02	3.622E-03
	p₃	1.049E-05	-2.336E-04	3.656E-07
	p₄	7.312E-04	-1.725E+01	-3.134E+00
	p₅	-7.978E-06	1.544E+01	1.913E+00
	p₆	1.312E-08	-4.812E+00	-2.775E-01
	p₇	-5.395E-03	-3.826E-03	7.279E-04
	p₈	8.408E-06	5.232E-06	3.627E-06
	p₉	8.823E-03	-2.662E+00	2.501E+01
	p₁₀	-2.666E-05	1.114E+00	-3.294E+01
	p₁₁	3.661E-08	-1.301E+00	2.243E+01

CONCLUSIONS

Raman peaks of asymmetric stretching vibration (ν_3) and asymmetric bending overtone ($2\nu_2$) of methane were studied at elevated pressures and temperatures. The peak intensity ratio (PIR) decreases with increasing pressure and decreasing temperature. We demonstrated that such PIR can be used to determine the pressure and density of pure methane inclusions. Even the composition of such inclusions is detectable when combined with other Raman parameters, such as ν_1 position shifting or those parameters regarding to interior standard. In the future, more experiments should be performed to know how the PIR is affected by additional components in the fluid inclusion.

Table III. Calculated pressure and density of No.1 manmade methane inclusion from intensity ratio ($H_{\nu_3}/H_{2\nu_2}$).

T (K)	Ratio	P (MPa) ^a	D(g/cm ³) ^b	D(g/cm ³) ^c
283.15	0.92	5.80	0.04456	0.04392
298.15	0.96	6.16	0.04417	0.04281
308.15	0.98	6.46	0.04439	0.04199
323.15	1.02	6.86	0.04431	0.04262

348.15	1.07	7.73	0.04548	0.04440
373.15	1.12	8.55	0.04610	0.04520
423.15	1.24	9.82	0.04544	0.04469
473.15	1.36	11.05	0.04484	0.04506
Density stdev.			0.00069	0.00122
Average Density			0.04491	0.04384
Uncertainty			±2.65%	±4.21%

^a Calculated from Eq.5

^b Calculated from the temperature and pressure shown in this table using equation of state of Duan¹⁷

^c Calculated from Eq.6

^d Based on ν_1 peak position, the pressure at 298.15 K is 6.4531 MPa. Calculated with equation of state of Duan¹⁷, the density at 298.15 K is 0.046483 g/cm³.

Table IV. Calculated pressure and density of No.2 manmade methane inclusion from intensity ratio (H_{ν_3}/H_{ν_2}).

T (K)	Ratio	P (MPa) ^a	D(g/cm ³) ^b	D(g/cm ³) ^c
283.15	0.33	21.32	0.18187	0.18007
293.15	0.33	23.78	0.18605	0.18521
298.15	0.33	24.33	0.18390	0.18352
308.15	0.34	26.46	0.18558	0.18559
323.15	0.36	28.04	0.18010	0.18034
348.15	0.38	32.85	0.18186	0.18169
373.15	0.42	35.33	0.17511	0.17440
448.15	0.50	47.43	0.17472	0.17467
Density stdev.			4.33E-03	4.31E-03
Average Density			1.81E-01	1.81E-01
Uncertainty			3.55%	3.48%

^a Calculated from Eq.5

^b Calculated from the temperature and pressure shown in this table using equation of state of Duan¹⁷

^c Calculated from Eq.6

^d Based on ν_1 peak position, the pressure at 298.15 K is 24.5425 MPa. Calculated with equation of state of Duan¹⁷, the density at 298.15 K is 0.185141g/cm³.

Acknowledgments

We thank Drs. I-Ming Chou and R.C. Burruss for their kind help and guidance for many years on the Raman spectroscopic research on Geo-fluids. This work was partly supported by the Key Project of Chinese Ministry of Education (No. 109108), the National Basic Research Program of China (Grant

REFERENCE

1. B. Wopenka and J. D. Pasteris. "Limitations to Quantitative-Analysis of Fluid Inclusions in Geological Samples by Laser Raman Microprobe Spectroscopy". *Appl Spectrosc* 1986. **40**(2). 144-151.
2. D. Fabre, Couty, R. " Investigation on the density effects in the Raman spectrum of methane up to 3.000 bar. Application to the determination of pressure in fluid inclusions trapped in minerals". *Comptes rendus de l'Académie des sciences. Série 2, Mécanique, Physique, Chimie, Sciences de l'univers, Sciences de la Terre* 1986. **303**(14). 4.
3. J. C. Seitz, J. D. Pasteris, and I.-M. Chou. "Raman spectroscopic characterization of gas mixtures. I. Quantitative composition and pressure determination of CH₄, N₂, and their mixtures". *American Journal of Science* 1993. **293**. 297-297.
4. J. C. Seitz, J. D. Pasteris, and I.-M. Chou. "Raman spectroscopic characterization of gas mixtures. II. Quantitative composition and pressure determination of the CO₂-CH₄ system". *American Journal of Science* 1996. **296**(6). 577-600.
5. W. J. Lu, I. M. Chou, R. C. Burruss, and Y. C. Song. "A unified equation for calculating methane vapor pressures in the CH₄-H₂O system with measured Raman shifts". *Geochim Cosmochim Acta* 2007. **71**(16). 3969-3978.
6. T. Azbej, M. J. Severs, B. G. Rusk, and R. J. Bodnar. "In situ quantitative analysis of individual H₂O-CO₂ fluid inclusions by laser Raman spectroscopy". *Chem Geol* 2007. **237**(3-4). 255-263.
7. J. Dubessy, S. Buschaert, W. Lamb, J. Pironon, and R. Thiéry. "Methane-bearing aqueous fluid inclusions: Raman analysis, thermodynamic modelling and application to petroleum basins". *Chem Geol* 2001. **173**(1-3). 193-205.
8. J. Dubessy, A. Moissette, R. J. Bakker, J. D. Frantz, and Y. G. Zhang. "High-temperature Raman spectroscopic study of H₂O-CO₂-CH₄ mixtures in synthetic fluid inclusions: first insights on molecular interactions and analytical implications". *Eur J Mineral* 1999. **11**(1). 23-32.
9. D. Guillaume, S. Teinturier, J. Dubessy, and J. Pironon. "Calibration of methane analysis by Raman spectroscopy in H₂O-NaCl-CH₄ fluid inclusions". *Chem Geol* 2003. **194**(1-3). 41-49.
10. W. J. Lu, I. M. Chou, and R. C. Burruss. "Determination of methane concentrations in water in equilibrium with sl methane hydrate in the absence of a vapor phase by in situ Raman spectroscopy". *Geochim Cosmochim Acta* 2008. **72**(2). 412-422.
11. W. J. Lu, I. M. Chou, R. C. Burruss, and M. Z. Yang. "In situ study of mass transfer in aqueous solutions under high pressures via Raman spectroscopy: A new method for the determination of diffusion coefficients of methane in water near hydrate formation conditions". *Appl Spectrosc* 2006. **60**(2). 122-129.
12. J. Pironon, J. O. W. Grimmer, S. Teinturier, D. Guillaume, and J. Dubessy. "Dissolved methane in water: temperature effect on Raman quantification in fluid inclusions". *J Geochem Explor* 2003. **78-9**. 111-115.
13. F. Lin. "Experimental Study of the PVTX Properties of the System H₂O-CH₄". Dissertation, Virginia Polytechnic Institute and State University, Virginia. 2005.
14. S. B. Hansen, R. W. Berg, and E. H. Stenby. "How to determine the pressure of a methane-containing gas mixture by means of two weak Raman bands, $\nu(3)$ and $2\nu(2)$ ". *Journal of Raman Spectroscopy* 2002. **33**(3). 160-164.
15. W. Lu, H. Guo, I. M. Chou, R. C. Burruss, and L. Li. "Determination of diffusion coefficients of carbon dioxide in water between 268 and 473 K in a high-pressure capillary optical cell with in situ Raman spectroscopic measurements". *Geochim Cosmochim Acta* 2013. **115**(0). 183-204.
16. I. M. Chou, "Optical cells with fused silica windows for the study of geological fluids", in

Applications of Raman spectroscopy to Earth sciences and cultural heritage, J. Dubessy, M. C. Caumon and F. Rull, Eds. (EMU Notes in Mineralogy, 2012).

17. S. B. Kim, R. M. Hammaker, and W. G. Fateley. "Calibrating Raman Spectrometers Using a Neon Lamp". *Appl. Spectrosc.* 1986. **40**(3). 412-415.
18. Z. Duan, N. Møller, and J. H. Weare. "A general equation of state for supercritical fluid mixtures and molecular dynamics simulation of mixture PVTX properties". *Geochim Cosmochim Ac* 1996. **60**(7). 1209-1216.
19. Z. Duan, N. Møller, and J. H. Weare. "Accurate prediction of the thermodynamic properties of fluids in the system H₂O–CO₂–CH₄–N₂ up to 2000 K and 100 kbar from a corresponding states/one fluid equation of state". *Geochim Cosmochim Ac* 2000. **64**(6). 1069-1075.
20. I. M. Chou, Y. Song, and R. C. Burruss. "A new method for synthesizing fluid inclusions in fused silica capillaries containing organic and inorganic material". *Geochim Cosmochim Ac* 2008. **72**(21). 5217-5231.

Pressure and Temperature Dependence of the Raman Peak Intensity Ratio of Asymmetric Stretching Vibration (ν_3) and Asymmetric Bending Overtone ($2\nu_2$) of Methane

Menghan Wang,^{a,b} Wanjun Lu,^{a,*} Lanlan Li,^a Shaohua Qiao^a

^a China University of Geosciences, State Key Laboratory of Geological Processes and Mineral Resources, Wuhan 430074, P.R. China

^b Università degli Studi di Napoli Federico II, Dipartimento di Scienze della Terra, della Ambiente e delle Risorse, Via Mezzocannone 8, 80134 Napoli, Italy

Raman peaks of the asymmetric stretching vibration (ν_3) and the asymmetric bending overtone ($2\nu_2$) of methane were studied at elevated pressures and temperatures, from 3 to 51 MPa and from 298.15 to 473.15 K. The peak intensity ratios of ν_3 and $2\nu_2$ were calculated, and the relationship among peak intensity ratio, temperature, and pressure/density were derived using equations. Such relationships allow geologists to determine the pressure and density of methane fluid inclusions using Raman spectroscopic measurements of the peak intensity ratios of ν_3 and $2\nu_2$.

Index Headings: Asymmetric vibrations; Raman peak intensity ratio; Temperature; Pressure; Methane.

INTRODUCTION

Since the 1980s, Raman spectroscopy has become a powerful tool used to study the properties of fluid inclusions in minerals.¹ Many parameters were derived from the Raman spectra of fluids to determine the pressure and composition of the fluid inclusion, such as peak position,^{2–5} peak width ratio,^{3,4} peak intensity ratio,^{3,4,6} and peak area ratio.^{7–12} For methane in inclusions, the peak position of the C–H symmetric stretching band (ν_1) of methane shifts to lower wavenumbers as pressure increases.^{2–5,13} To date, ν_1 shifting is the most widely used quantitative Raman scattering method regardless of interior label. However, the determination of the inner pressure of a methane-bearing inclusion is reliable only when its composition is well known because ν_1 shifting can be significantly affected by the presence of other gases.^{3,4}

Compared to the most intense C–H symmetric stretching band (ν_1) for methane, the asymmetric stretching band (ν_3) and asymmetric bending overtone ($2\nu_2$) are two primary bands with intermediate intensity (~2% of the intensity of ν_1). The peak intensity ratio (PIR) of ν_3 and $2\nu_2$ has been found to systematically change with changes in pressure at room temperature, and the relationship between the PIR and pressure seems to be independent of the composition of natural gas.¹⁴ It is important to know how the relationship between the PIR and pressure is affected by temperature and the composition of the fluid samples when we use the PIR

($H_{\nu_3}/H_{2\nu_2}$) to accurately determine the pressure of methane-bearing fluid inclusions.

In this study, we examined the PIR of a pure methane system at elevated pressures and temperatures, and we derived the relationships among PIR, temperature, and pressure/density using equations. To demonstrate the method, we determined the inner pressure and density of two methane inclusions using Raman spectroscopic measurements of the PIRs.

METHOD

Experimental Apparatus and Procedures. The apparatus and procedures were similar to those we used recently for the study of methane and carbon dioxide diffusion in water using a HORIBA LabRam-HR spectrometer.^{11,15} A capillary high-pressure optical cell (CHPOC) was used for loading the methane under high pressure. The pressure was read using a Setra 204D digital pressure transducer with Datum 2000TM manometer (69 MPa full-scale; accurate to $\pm 0.14\%$). The CHPOC was put into the slot in the silver plate of the Linkam CAP500 heating–cooling stage for temperature control. This device can control temperatures between ~ 83 and 773 K with a precision of ± 0.2 K from 298 to 373 K and of ± 0.5 K from 373 to 573 K.¹⁶

Raman spectroscopic measurements of the PIRs of ν_3 and $2\nu_2$ at constant temperature and pressure were conducted using the following procedure. (1) We inserted the cell horizontally into the heating–cooling stage, which was mounted on an XYZ stage under a microscope for observations and Raman analyses. (2) We evacuated the pressure line and the cell and then loaded it with methane (99.99%; Air Products). (3) We repeated step 2 twice. (4) We used the pressure generator to adjust the pressure in the cell. (5) We adjusted the sample temperature using the heating–cooling stage.

Spectra Collection and Calibration of Methane Peak Heights. The spectra of methane were acquired using a JY/Horiba LabRam HR Raman system with 532.06 nm (frequency-doubled neodymium-doped yttrium aluminum garnet [Nd : YAG]) laser excitation, a 50 \times Olympus objective with 0.5 numerical aperture, and a 1800 groove/mm grating with a resolution of about 0.65 cm^{-1} ; an ~ 15 mW laser light was focused on a central level of the horizontal cell during the measurement. The spectra were collected from 2500 to 3100 cm^{-1} , which covered the stretching and bending overtone of methane

Received 8 October 2013; accepted 18 December 2013.

* Author to whom correspondence should be sent. E-mail: luwanjuncug@126.com.
DOI: 10.1366/13-07316

Volume 68, Number 5, 2014

0003-7028/14/6805-0000/0
© 2014 Society for Applied Spectroscopy

APPLIED SPECTROSCOPY

SECTION 3.3

The effects of CH₄ and CO₂ on the sulfidization of goethite and magnetite – an in-situ Raman spectroscopic study in the high-pressure capillary optical cells at room temperature

Paper submitted to European Journal of Mineralogy

The effects of CH₄ and CO₂ on the sulfidization of goethite and magnetite – an in-situ Raman spectroscopic study in the high-pressure capillary optical cells at room temperature

Wang Menghan^{1&2}, Chou I-Ming³, Lu Wanjun¹ and De Vivo Benedetto²

1 Department of Marine Science and Engineering, China University of Geosciences, Wuhan 430074, China

2 Dipartimento di Scienze della Terra, dell' Ambiente e delle Risorse, Università di Naples Federico II, 80134 Naples, Italy

3 Laboratory for Experimental Study Under Deep-sea Extreme Conditions, Sanya Institute of Deep-sea Science and Engineering, Chinese Academy of Sciences, Sanya 572000, China

Abstract

Reactions of goethite and magnetite with sulfide solutions under CH₄ and/or CO₂ atmospheres were monitored *in situ* with Raman spectroscopy in the high-pressure capillary optical cells (HPOCs) at room temperature. Isolated systems were created in the enclosed HPOCs for the study of the mineral-solution interactions to prevent oxidation during the experiments. We observed that iron (oxyhydr) oxide minerals were inert to sulfide solution under CH₄ atmosphere, and that the addition of CO₂ to this system triggered the sulfidization reactions; iron monosulfide (mackinawite) was identified in the solution after six hours and pyrrhotite in the vapor phase after 5 days. The iron monosulfide was metastable, which dissolved after about ten days. In submarine environments, these processes might occur above the sulfate-methane interface, where CO₂ was produced by oxidation of methane. Sulfidization of iron (hydroxyl) oxide may play a key role for the dissolution of iron into interstitial water.

Keywords: goethite, magnetite, sulfidization, mackinawite, pyrrhotite, methane, carbon dioxide, Raman spectroscopy

Introduction

Iron sulfide minerals include a diverse group of solids, many of which play the key roles in low temperature marine environments and in biogeochemical processes (Canfield et al., 2000; Canfield et al., 1992; Rickard and Luther, 2007; Schoonen, 2004). Pyrite is the most abundant iron sulfide mineral on the Earth's surface layer (Haese et al., 1998; Li et al., 2011; Morgan et al., 2011), followed by mackinawite and greigite, whereas troilite and pyrrhotite are less abundant (Rickard and Luther,

2007).

Various valences of iron sulfide minerals commonly appear at the transient depth between the iron oxide reduction zone and the sulfate reduction zone in marine sediments. The conversion of iron oxide minerals to sulfides is solely ascribed to various crystal structures (Poulton et al., 2004). However, large discrepancy of reaction rate exists between different studies (Canfield et al., 1992; Poulton et al., 2004), and this discrepancy was assumed to be resulted from different interstitial compositions and geochemical environments. For example, organoclastic iron sulfides reflect high concentrations of S and Fe in pore water (Haese et al., 1997), whereas methanotrophic iron sulfides indicate high concentrations of methane and carbon dioxide in pore water (Lim et al., 2011; Sassen et al., 2004; Wehrmann et al., 2011).

The reaction mechanisms of iron sulfide minerals have been extensively studied (Luther, 1991; Morse, 1999; Morse and Wang, 1997; Poulton et al., 2004; Rickard, 1997; Theberge, 1997; Wang, 1995; Wilkin and Barnes, 1996). Most of these studies investigated the reactions between sulfide solution and synthesized iron monosulfide minerals. Sol-gel approach (Wang, 1995) was used to simulate anoxic sediment and successfully synthesized crystalline pyrite. Freeze-drying method was used (Rickard, 1997) to protect FeS from oxidation during the study the kinetics of pyritization. Recently, Raman spectroscopy was used to identify and characterize the conversion of iron sulfide minerals (Bourdoiseau et al., 2011; Bourdoiseau et al., 2008).

The main obstacle in the study of iron sulfide minerals is their extreme sensitivity to oxygen (Csákberényi-Malasics et al., 2012). In this study, high pressure capillary optical cell (HPOC) was used to prevent oxidation of these minerals during experiments. Also, *in-situ* monitoring of reactions allows us to reveal the processes and the controlling factors for the transformation of these minerals.

Materials and Methods

Syntheses of the starting iron (hydroxyl) oxide and iron monosulfides

Goethite and magnetite were synthesized from the following reagent grade compounds (greater than 98.5% purity): $\text{Fe}(\text{NO}_3)_3 \cdot 9\text{H}_2\text{O}$, KOH, $\text{FeSO}_4 \cdot 7\text{H}_2\text{O}$, KNO_3 and $\text{Na}_2\text{S} \cdot 9\text{H}_2\text{O}$, purchased from

Sinopharm Chemical Reagent Co., Ltd. CH₄ and CO₂ were purchased from Air Products and Chemicals, Inc. USA, with purities of more than 99.99%.

Goethite and magnetite were synthesized following the procedures of (Schwertmann and Cornell, 2007a, b). To achieve pure goethite, 100 mL of Fe(NO₃)₃ solution was poured into a 2 L polyethylene flask, followed by rapid addition of 180 mL solution of KOH with constant stirring. Immediately after the precipitation of the red-brown 2-line ferrihydrite, the suspension was diluted to 2 L with distilled water in a closed polyethylene flask and stored at 70 °C for 60 hrs. Note that the preparation was carried out in a polyethylene vessel instead of a glass bottle, because silicate glass dissolves considerably in strong alkaline solution. During the heating stage (at 70 °C), the voluminous, red-brown suspension of ferrihydrite was converted to a compact yellow brown precipitate of goethite. At the end, the reaction vessel was removed from the oven the goethite precipitate was centrifuged, washed, and dried.

To produce pure magnetite, 80 g of FeSO₄·7H₂O was dissolved in 560 mL of deionized water (previously flushed with N₂) in a 1 L glass beaker, which was closed with an air tight plastic lid with holes for gas inlet and a thermometer. The beaker was placed in a water bath (i.e., a 3 L beaker filled with water at 90 °C), with a thermometer in place and connected to an N₂ gas inlet for the purging of the sample chamber. Once the desired temperature was reached, 240 mL of an oxygen-free solution containing 6.46 g of KNO₃ and 44.9 g of KOH was added dropwise for approximately five minutes. The obtained solution was heated at 100 °C for another half to one hour, and then cooled overnight to room temperature. The black precipitate was washed and dried. No protection against air oxidation is needed once the black precipitate was formed.

In order to compare the Raman spectra of our experimental products with iron monosulfide minerals, these minerals were first produced by mixing FeSO₄ solution with Na₂S solution, and the precipitates were immediately loaded in a fused silica capillary tube followed by sealing both ends of the tube with a hydrogen-oxygen flame to form a fused silica capillary capsule (FSCC) (Chou et al., 2008) to prevent oxidation. Note that the sulfide solution was prepared by dissolving 12 g of Na₂S·9H₂O in 100 mL of deionized water (previously flushed with N₂) in a 100 mL volumetric flask.

Experimental apparatus and procedures

A high-pressure optical cell (HPOC) was used as the reaction chamber (Chou, 2005; Lu et al., 2008; Lu et al., 2006). The HPOC was made of 15 cm long silica capillary tube (0.3 mm ID and 0.66 mm OD) with one end sealed with a hydrogen-oxygen flame. Sulfide solution of 0.5 M was sucked into the tube, and several grains of iron oxide solids were loaded into the tube. After the solid and solution were centrifuged to the enclosed end, the open end of the tube was connected to the gas line. The tube and the gas line were vacuumed and then loaded with methane, and this vacuum-gas loading procedure was repeated several times to remove residual air before loading the desired gas in the HPOC. The cell was then mounted on an X-Y-Z stage under a microscope for observation and Raman analyses. A schematic diagram of the *in-situ* Raman spectroscopic measurement system is shown in Fig. 1. The room temperature was kept around 20 °C. The pressure was read from a Setra 204D digital pressure transducer with Datum 2000TM manometer (69 MPa full scale; accurate to $\pm 0.14\%$). Seven experimental runs were performed with different initial conditions (Table 1).

Characterization of iron minerals and in-situ monitoring with Raman spectroscopy

Raman analyses were carried out with a Jobin Yvon-Horiba, high-resolution Raman spectrometer (LabRAM HR-800) equipped with a microscope and a Peltier-cooled charge coupled device (CCD) detector. Excitation was provided by a Nd:YAG laser (532.08 nm), and its power was adjusted between 1.94 and 0.07 mW on the outer wall of HPOC in order to prevent excessive heating of the samples. The sample spot diameter was $\sim 4 \mu\text{m}$ under a 50x objective lens. A grating of 600 gr/mm was used, and most of the spectra for the samples in the HPOC were collected between 100 and 4000 cm^{-1} wavenumbers to cover the bands of iron (hydroxyle) oxide and sulfide minerals, CO_2 , CH_4 , H_2O , S , CO_3^{2-} , HCO_3^- and SO_4^{2-} (Table 2). The spectra were recorded with a resolution of $\sim 2 \text{cm}^{-1}$.

In our control run, Raman spectra of iron monosulfide precipitates from mixture of FeSO_4 solution and Na_2S solution were obtained. Repeatable bands near 250 and 312 cm^{-1} represented the species of black iron sulfide precipitates (Fig. 2).

Table 1. Initial conditions and final products of experimental runs

Run No.	Gas		Na ₂ S Solution		Iron oxide	Location	Products	pH	pe
	CH ₄ Partial Pressure (MPa)	CO ₂ Partial Pressure (MPa)	Concentration (M)	Length (cm)					
1	10	0	0.5	3.14	Goethite	Liquid	-	12.803	-11.522
2	10	0	0.5	1.12	Goethite	Gas	-	12.803	-11.457
3	0.7	6.3	0.5	0.5	Magnetite	Gas	Pyrrhotite Sulfur Carbonate	5.8099	-2.4712
4	0.7	6.3	0.5	2.27	Magnetite	Gas	Pyrrhotite Sulfur Carbonate	5.9498	-2.6915
4	0.7	6.3	0.5	2.27	Magnetite	Liquid	Mackinawite Sulfur Carbonate	5.9498	-2.6915
5	3.2	3.8	0.5	0.92	Goethite	Liquid	Mackinawite Sulfur Carbonate	6.0782	-2.8572
6	0.7	6.3	0.5	1.14	Goethite	Liquid	Mackinawite Sulfur Carbonate	5.8312	-2.513
7	0.7	6.3	0.5	1.21	Goethite	Liquid	Mackinawite Sulfur Carbonate	5.8312	-2.513

Table 2. Raman peak positions for minerals, aqueous species, and gases in the experiments

Substances	Phase	Peak positions (cm ⁻¹)			
Goethite	solid	247	301	391	479
Magnetite	solid	211	272		
Mackinawite	solid	245-251	300-311		
Pyrrhotite	solid	330	363-372		
Sulfur	solid	153	220	473	
S ²⁻ /HS ⁻	aqueous	2575			
CO ₃ ²⁻ /HCO ₃ ⁻	aqueous	1013	1362		
CH ₄	aqueous	2911			
H ₂ O	aqueous		Around 3395		
H ₂ S	gas	2581			
CH ₄	gas	2917			
CO ₂	gas	1285	1389		
SO ₄ ²⁻	aqueous	1010			

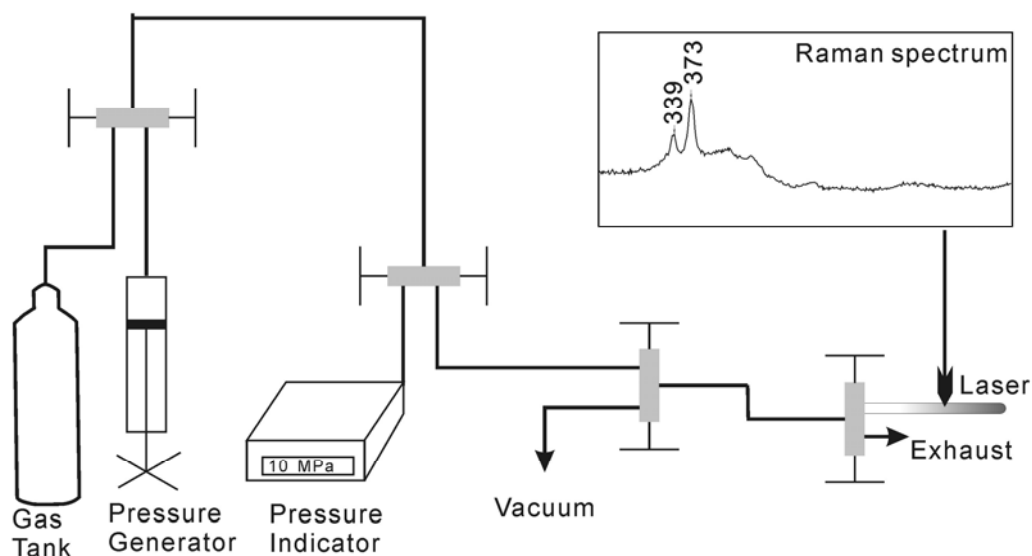


Figure 1 A. schematic diagram of the experimental set up for collecting in situ Raman spectra of the sample in an HPOC. The example Raman spectrum was derived from pyrrhotite, which was converted from magnetite exposed to the CH₄-CO₂ vapor phase in the presence of a sulfide solution (for detail, see text).

Results and discussions

Experimental results were listed in Table 1. Goethite was reacted with Na₂S solution under CH₄ gas (run nos. 1 and 2) and under CH₄-CO₂ gas mixture (runs nos. 5, 6, and 7). Magnetite was reacted with CH₄-CO₂ gas mixture (runs nos. 3 and 4).

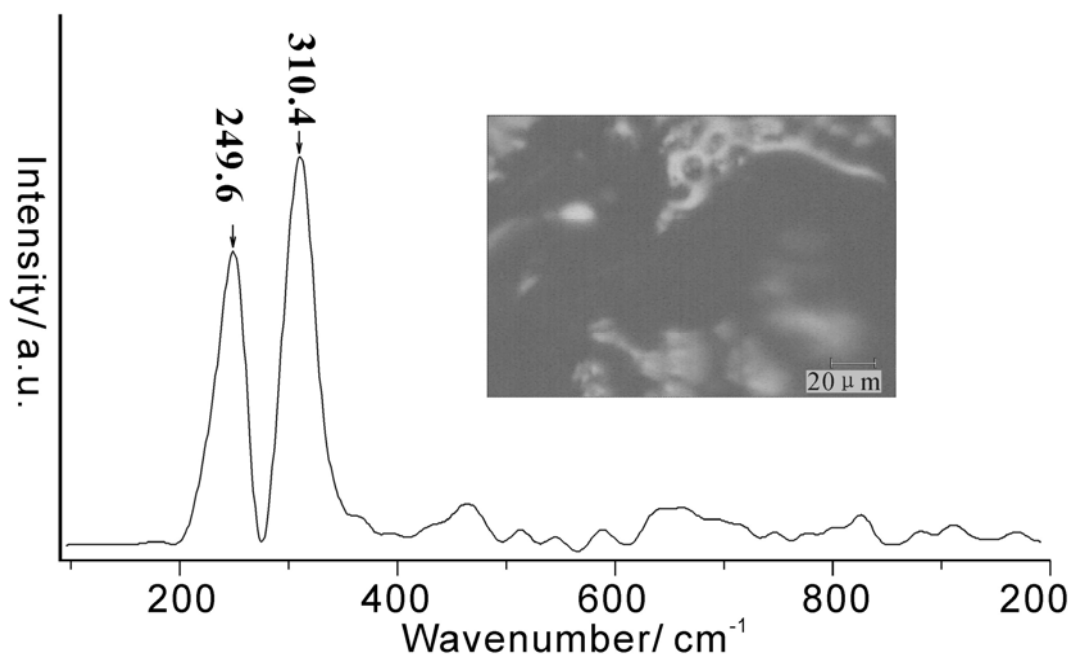


Figure 2. Raman spectra and photo of instant precipitate produced by mixing FeSO_4 solution and Na_2S solution. Repeatable Raman bands at $\sim 250 \text{ cm}^{-1}$ and 310 cm^{-1} indicate iron sulfide precipitations.

Goethite and Na_2S solution under CH_4 atmosphere

In run no. 1, goethite was immersed in the solution near the sealed end of the cell (Fig. 3), whereas in run 2, it was exposed to the vapor phase (Fig. 4). Raman spectra of the samples were collected daily for a period of fifteen days. Peak positions and intensities of goethite ($245, 298, 386,$ and 480 cm^{-1}) remained constant, indicating no reaction occurred. This was also supported by the appearance of the goethite in the cell, showing no obvious changes in either shape or color. Similarly, in run no. 2, Raman spectra and appearance of goethite that exposed to methane gas phase remained the same as those at the initial state (Fig. 3). Our results showed that goethite did not react with sulfide solution under CH_4 atmosphere.

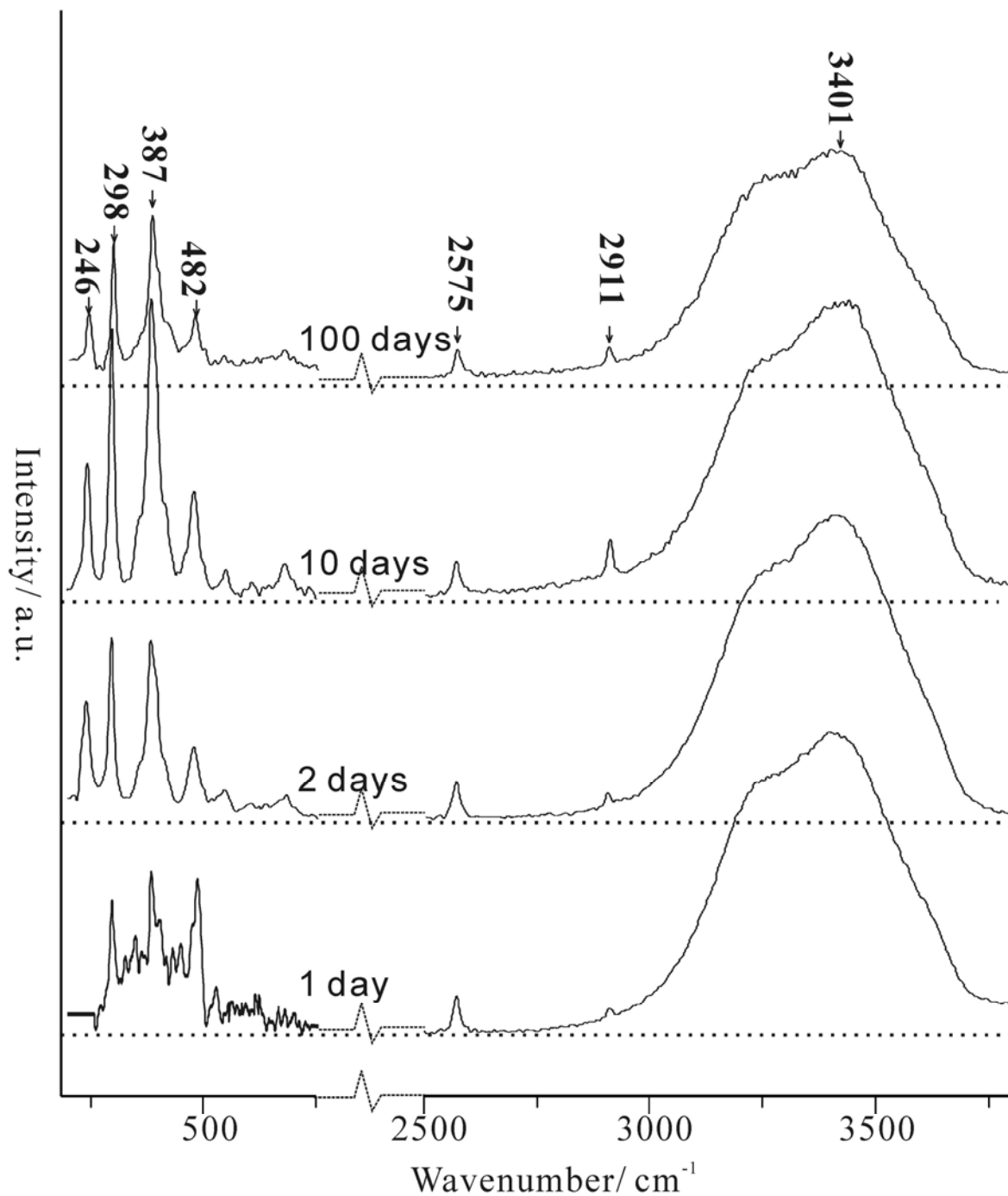


Figure 3. Raman spectra of the sample in run no. 1 collected in situ at various time, showing the coexistence of goethite and sulfide solution for up to 100 days under 10 MPa of methane at 20 °C with no reactions detected. The peaks indicated in the top spectrum are for water (3401 cm^{-1}), aqueous methane (2911 cm^{-1}), dissolved sulfide ions (2575 cm^{-1}) and goethite (246 cm^{-1} , 298 cm^{-1} , 387 cm^{-1} and 482 cm^{-1}).

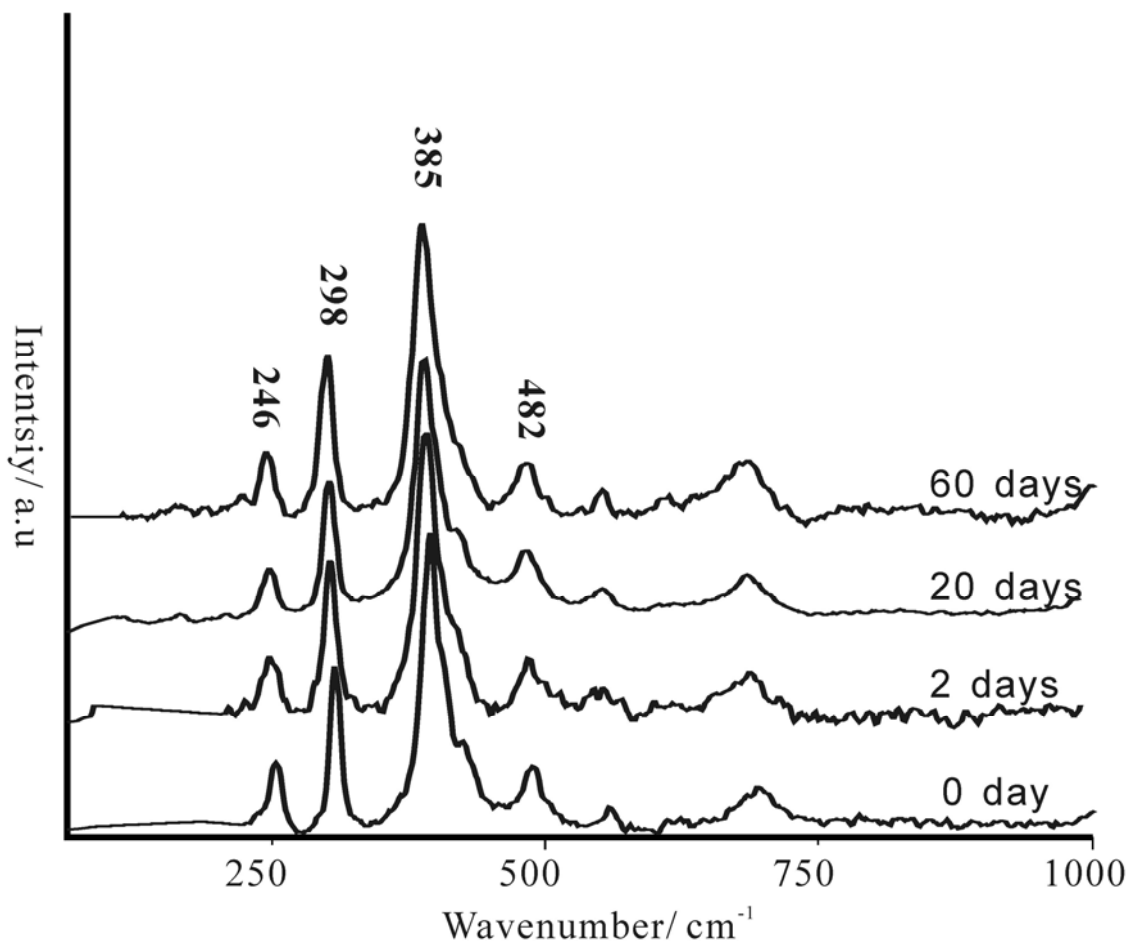


Figure 4. Run no.2: Coexistence of goethite and sulfide solution for more than 60 days in the vapor phase, under 10 MPa methane atmosphere, 20 ° C. The peaks indicated in the top spectrum were from goethite.

Iron minerals (goethite or magnetite) and Na₂S solution under CO₂-CH₄ atmosphere

When the medium gas was a mixed CO₂-CH₄, sulfide ions in the aqueous phase reacted with both goethite (run no. 4) and magnetite (run nos. 5, 6, and 7; Figs. 5 and 6) to form mackinawite, sulfur, and an unknown liquid, which was fluorescent and could be the organic sulfur compounds identified by Heinen and Lauwers (1996) produced by the reactions of FeS, H₂S, and CO₂ at elevated temperature. However, the primary product of these experiments was elemental sulfur, which was in the needle shape. On the other hand, when magnetite was exposed to the vapor phase (run nos. 3 and 4), instead of mackinawite, pyrrhotite was produced (Figs. 7 and 8) with sulfur in rod shape. No observations were made for goethite exposed to the vapor phase in this study, but will be made in the near future.

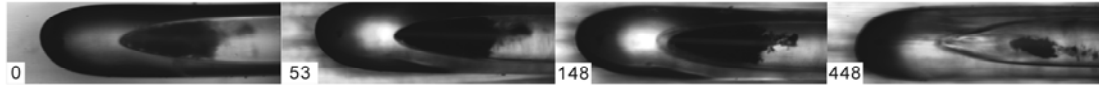
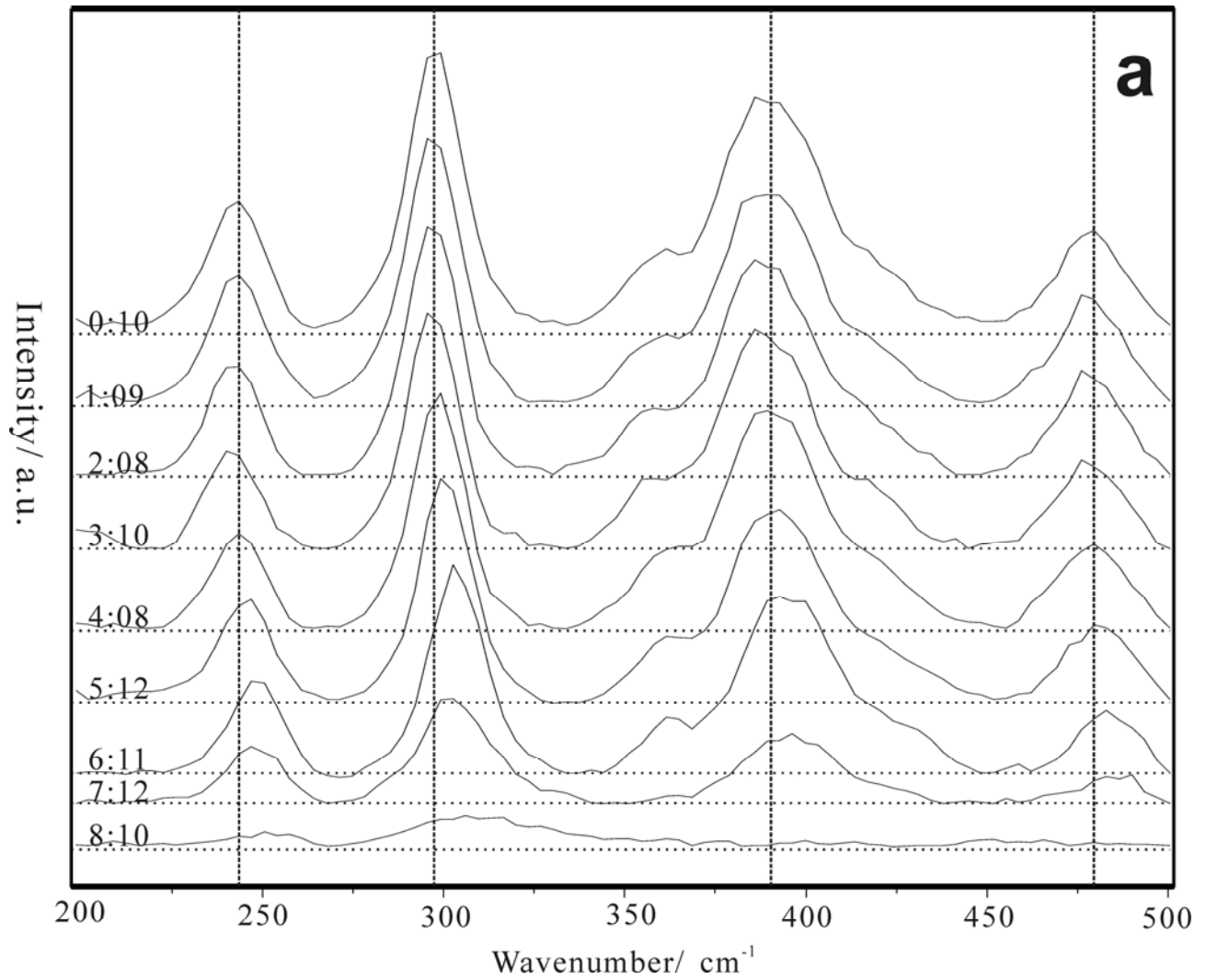


Figure 5. Images of goethite in the HPOC for run no. 5 under $\text{CH}_4\text{-CO}_2$ pressure from 0 to 448 hours. Iron sulfide minerals appeared before 53 hours, and the intensity of Raman signals decreased after 53 hours and became undetectable at 448 hours, indicating the dissolution of the newly formed iron sulfides.



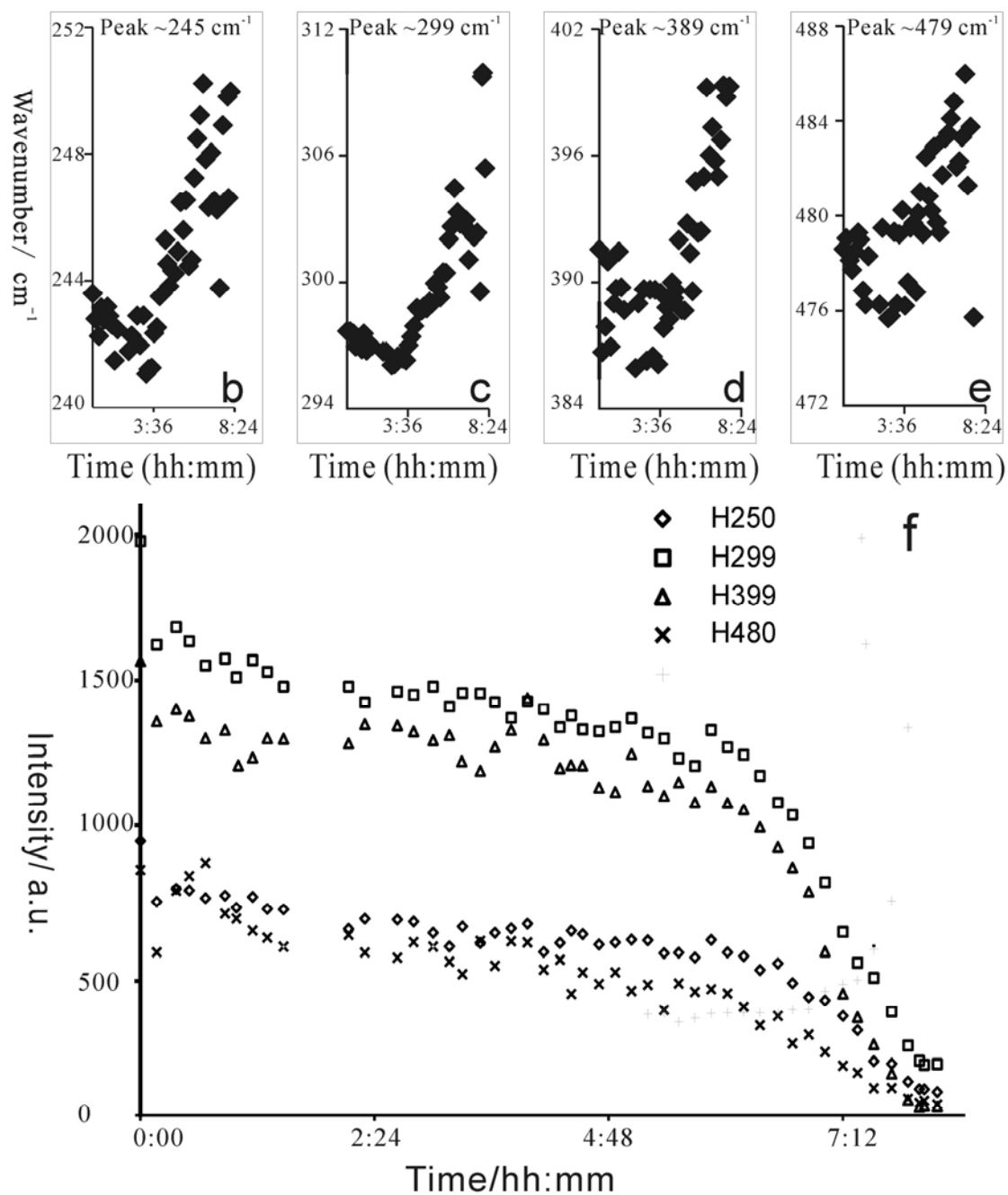


Figure 6 (a). In situ Raman spectra for the solid phases in run no. 7 for the first 8.2 hours, showing the shift of the peak positions after 4.08 hours and the reduction of the signals after 6.11 hours. The shift of the peak positions at about 245, 299, 389, and 479 cm^{-1} are shown in (b), (c), (d), and (e), respectively. The reversal points near 3:36 for all of these peaks indicate the transformation of goethite to mackinawite. The reduction of Raman signals after 6.11 hours shown in (a) was resulted from the dissolution of these newly formed mackinawite, and this reduction of Raman signals was clearly shown in (f).

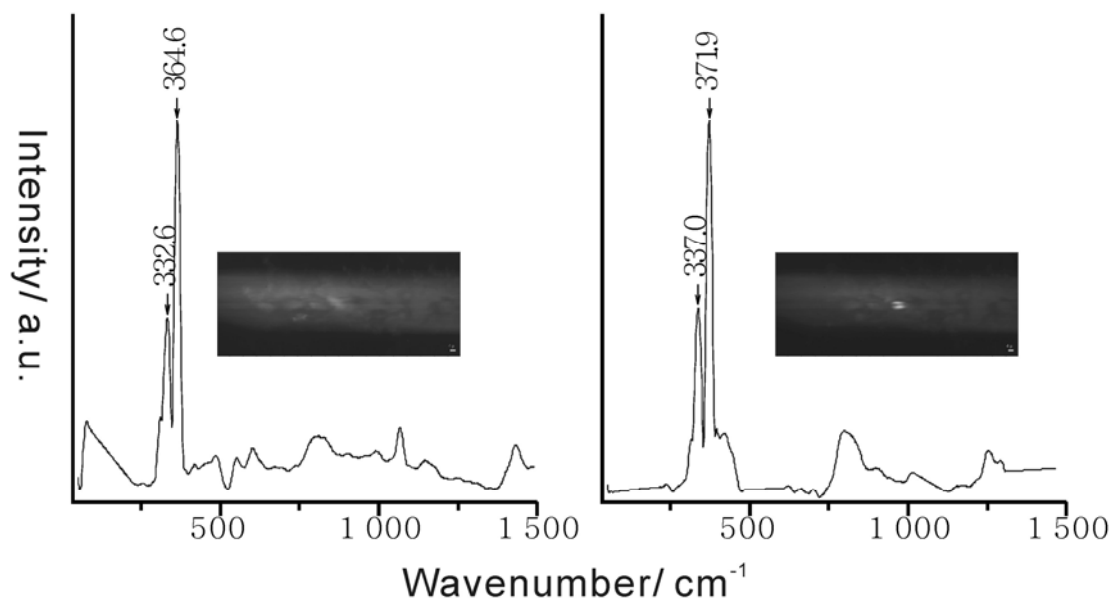


Figure 7. Raman spectra of iron sulfide minerals in run no. 3. Peaks at ~ 333 cm^{-1} and ~ 363 cm^{-1} (a), or 337 cm^{-1} and ~ 372 cm^{-1} (b) indicate the occurrence of pyrrhotite. The white sample spot shined after excited by laser.

Sulfidization of goethite and mineral dissolution

The transition process from goethite to iron monosulfide was clearly indicated by the evolution of Raman spectra in the changes of the number of peaks, peak heights, and peak positions. In Fig. 6(a), in-situ Raman spectra for the solid phases in run no. 7 are shown for the first 8.2 hours. It shows the shift of the peak positions after 4.08 hours and the reduction of the signals after 6.11 hours. The shift of the peak positions at about 245, 299, 389, and 479 cm^{-1} are shown in (b), (c), (d), and (e), respectively. The reversal points near 3 hr 36 min for all of these peaks indicate the transformation of goethite to mackinawite. This is in agreement with Bourdoiseau et al. (2011), who reported the peak shifts at 251 and 306 cm^{-1} corresponding to the formation of mackinawite. Also, Bourdoiseau et al. (2008) reported the shift of peak positions from 283 (± 1) cm^{-1} to 297 (± 1) cm^{-1} , and from symmetric to asymmetric peak. In our control run, repeatable bands near 250 and 312 cm^{-1} were observed for the species of black iron sulfide precipitates (Fig. 2).

The reduction of Raman signals after 6.11 hours shown in Fig. 6(a) was resulted from the dissolution of this newly formed mackinawite, and this process may take more than 10 days, depending on how far away goethite was from the vapor-aqueous phase boundary; the further way from the interface, the slower the reaction, indicating that the reaction was regulated by the mass transfer of CO_2 from the gas into the sulfide solution.

In comparative observations, goethite showed no obvious change in more than 30 days when

they were loaded in pure water with 5 MPa CO₂ as medium gas without methane.

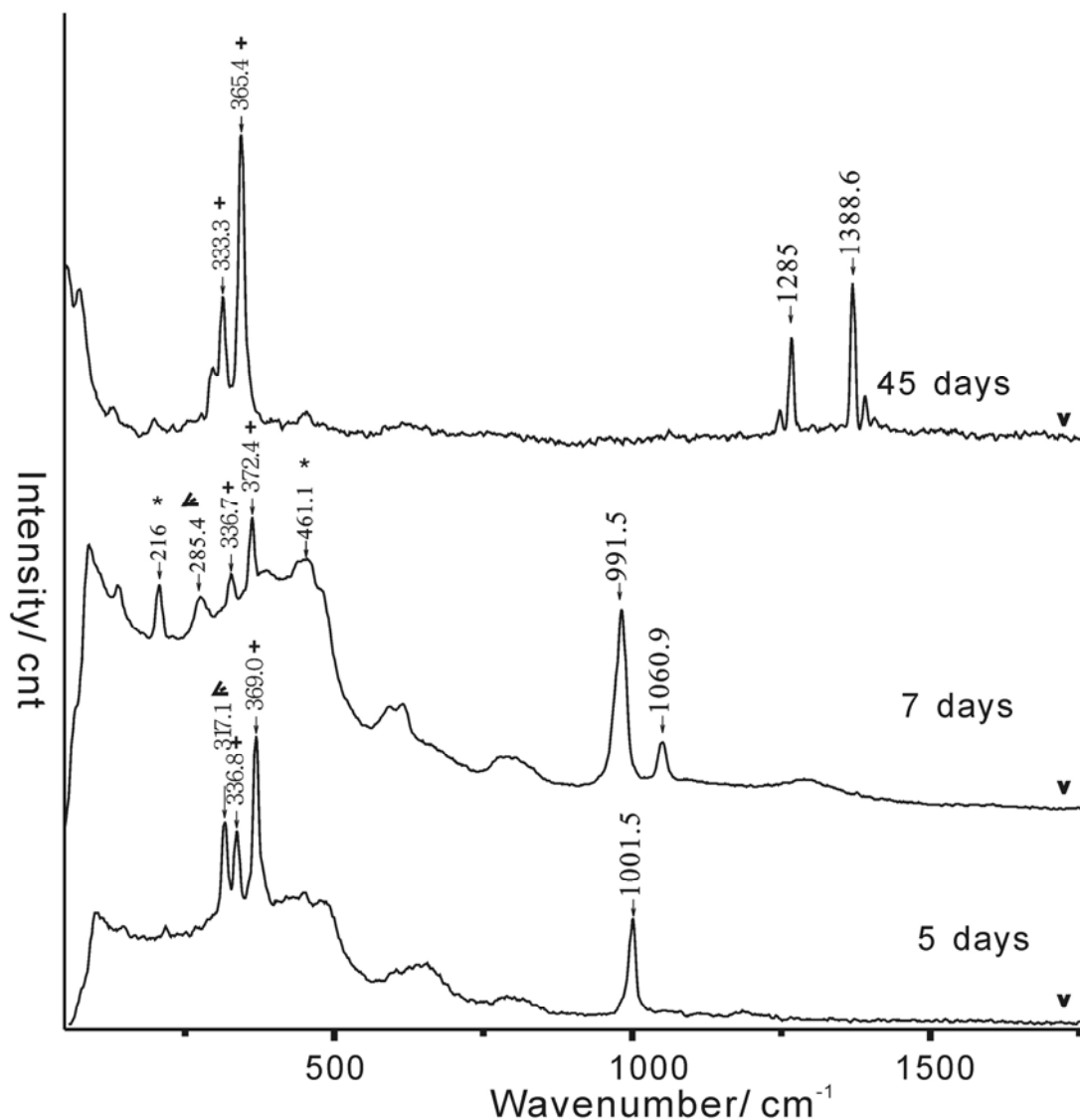


Figure 8. Raman spectra of iron sulfide minerals collected in run no. 4. Peaks at 333 (or 336) cm⁻¹ and 369 (or 372, 365) cm⁻¹ indicate the occurrence of pyrrhotite. Bands of ~101 cm⁻¹, ~148 cm⁻¹, 216 cm⁻¹ and 460 cm⁻¹ are related to elemental sulfur. Bands of 317 cm⁻¹ (5 days) and 285 cm⁻¹ (7 days) are corresponding to metastable iron minerals. Peaks of elemental sulfur was marked by a star (*), those for pyrrhotite by a plus sign (+), and those for metastable sulfide minerals by an arrow (←).

Minerals exposed to the vapor phase

Pyrrhotite, a thermodynamically stable iron sulfide, was produced when synthesized magnetite was exposed to the CH₄-CO₂ vapor phase.

Authoritative worldwide Raman spectra databases were checked to identify products of run nos. 3 and 4 (Table 3). Spectra of these databases were obtained from various natural minerals or synthetic material, and disturbances of lattice defects or drop-in were also reflected on the various peaks for the

same minerals/material. In our case, the primary peaks of the experimental products were at 335 (± 2) and 369 (± 4) cm^{-1} , indicating the presence of pyrrhotite rather than pyrite (Table 4).

Table 3. Collection of Raman peak positions for iron sulfide minerals from worldwide databases

Minerals	Raman peak position (cm^{-1})			database
pyrite	342	377	428	1
pyrite	343	378	430	2
pyrite	343	379	430	2
pyrite	345	383		3
pyrite	342	380		3
pyrite	336	371		3
pyrite	341	365	320	3
pyrite	344	380		3
pyrite	349	381		4
marcasite	325	386		2
marcasite	320		535	4
marcasite	324	385	657	3
pyrrhotite	335	376	665	4
pyrrhotite	341	375		3

¹: Free database 2000-2013 Laboratoire de géologie de Lyon ENS-Lyon France

²: Free database 2007 Physics Department University of Parma

³: The RRUFF™ Project database

⁴: Raman database from donors of SFMC (Société Française de Minéralogie et de Cristallographie)

Table 4 Raman peak positions of iron sulfide minerals produced in the experiments

Run No.	Raman peak position of stable minerals (cm^{-1})		Raman peak position of metastable minerals (cm^{-1})
3	333	363	
3	333	372	
3	337	374	
4	338	369	317
4	336	372	285
4	333	365	

Conclusions

The processes of sulfidization of goethite and magnetite in Na_2S solution under CH_4/CO_2 atmospheres were observed in high-pressure capillary optical cells (HPOCs) and characterized in-situ with Raman spectroscopy at room temperature. No obvious sulfidization reactions were observed

when the assemblages were under CH₄ pressure. However, the addition of CO₂ to the sample assemblages promoted the sulfidization reaction. The main product was elemental sulfur and mackinawite when goethite or magnetite was immersed in the Na₂S solution, and pyrrhotite was produced when magnetite was exposed to the vapor phase; no observations were made for goethite exposed to the vapor phase. The produced mackinawite was not stable, which dissolved gradually.

Near the sulfate-methane interface in submarine sediment, CO₂ and sulfide are the major products of sulfate-methane redox reactions, especially in the high methane flux venting system. The high methane flux often leads to the precipitation of sedimentary pyrite in the sulfate-methane transition zone. The mackinawite and pyrrhotite produced from sulfidization of goethite or magnetite observed in this study may well be the precursors of pyrite, and their formation mechanisms derived from this study enhanced our understanding of the micro environment of iron-sulfide-carbon system in deep sea sediments and associated geochemical reactions.

Acknowledgments

This work was partly supported by the National Sciences Foundation of China (No. 41102154), the National Basic Research Program of China (No. 2009CB219503), the Program for New Century Excellent Talents in University by Ministry of Education (NCET-08-0830), and the Knowledge Innovation Program of Chinese Academy of Sciences (SIDSSE-201302). This work is also part of the Ph.D. Program of M. Wang with Università degli studi di Naples Federico II (Italy).

References

- Bourdoiseau, J. A., Jeannin, M., Remazeilles, C., Sabota, R., and Refait, P., 2011, The transformation of mackinawite into greigite studied by Raman spectroscopy: *Journal of Raman Spectroscopy*, v. 42, no. 3, p. 496-504.
- Bourdoiseau, J. A., Jeannin, M., Sabot, R., Rémazeilles, C., and Refait, P., 2008, Characterisation of mackinawite by Raman spectroscopy: Effects of crystallisation, drying and oxidation: *Corrosion Science*, v. 50, no. 11, p. 3247-3255.
- Canfield, D. E., Habicht, K. S., and Thamdrup, B., 2000, The Archean sulfur cycle and the early history of atmospheric oxygen: *Science*, v. 288, no. 5466, p. 658-661.
- Canfield, D. E., Raiswell, R., and Bottrell, S., 1992, The Reactivity of Sedimentary Iron Minerals toward Sulfide: *American Journal of Science*, v. 292, no. 9, p. 659-683.
- Chou, I. M., Burruss R.C. and Lu W.J. , A new optical cell for spectroscopic studies of geologic fluids at pressures up to 100MP. , *in Proceedings Advances in High-pressure Technology for Geophysical Applications*, Amsterdam, 2005, Elsevier, p. 11.
- Chou, I. M., Song, Y., and Burruss, R. C., 2008, A new method for synthesizing fluid inclusions in fused silica capillaries containing organic and inorganic material: *Geochimica Et Cosmochimica Acta*, v. 72, no. 21, p. 5217-5231.
- Csákberényi-Malasics, D., Rodriguez-Blanco, J. D., Kis, V. K., Rečnik, A., Benning, L. G., and Pósfai, M., 2012, Structural properties and transformations of precipitated FeS: *Chemical Geology*, v. 294, p. 249-258.
- Haese, R. R., Petermann, H., Dittert, L., and Schulz, H. D., 1998, The early diagenesis of iron in pelagic sediments: a multidisciplinary approach: *Earth and Planetary Science Letters*, v. 157, no.

3-4, p. 233-248.

- Haese, R. R., Wallmann, K., Dahmke, A., Kretzmann, U., Muller, P. J., and Schulz, H. D., 1997, Iron species determination to investigate early diagenetic reactivity in marine sediments: *Geochimica Et Cosmochimica Acta*, v. 61, no. 1, p. 63-72.
- Heinen, W., and Lauwers, A. M., 1996, Organic sulfur compounds resulting from the interaction of iron sulfide, hydrogen sulfide and carbon dioxide in an anaerobic aqueous environment: *Origins of Life and Evolution of the Biosphere*, v. 26, no. 2, p. 131-150.
- Kleppe, A., and Jephcoat, A., 2004, High-pressure Raman spectroscopic studies of FeS₂ pyrite: *Mineralogical Magazine*, v. 68, no. 3, p. 433-441.
- Li, X., Cutter, G. A., Thunell, R. C., Tappa, E., Gilhooly III, W. P., Lyons, T. W., Astor, Y., and Scranton, M. I., 2011, Particulate sulfur species in the water column of the Cariaco Basin: *Geochimica Et Cosmochimica Acta*, v. 75, no. 1, p. 148-163.
- Lim, Y. C., Lin, S., Yang, T. F., Chen, Y.-G., and Liu, C.-S., 2011, Variations of methane induced pyrite formation in the accretionary wedge sediments offshore southwestern Taiwan: *Marine and Petroleum Geology*, v. 28, no. 10, p. 1829-1837.
- Lu, W. J., Chou, I. M., and Burruss, R. C., 2008, Determination of methane concentrations in water in equilibrium with sl methane hydrate in the absence of a vapor phase by in situ Raman spectroscopy: *Geochimica Et Cosmochimica Acta*, v. 72, no. 2, p. 412-422.
- Lu, W. J., Chou, I. M., Burruss, R. C., and Yang, M. Z., 2006, In situ study of mass transfer in aqueous solutions under high pressures via Raman spectroscopy: A new method for the determination of diffusion coefficients of methane in water near hydrate formation conditions: *Applied Spectroscopy*, v. 60, no. 2, p. 122-129.
- Luther, G. W., 1991, Pyrite synthesis via polysulfide compounds: *Geochimica Et Cosmochimica Acta*, v. 55, no. 0, p. 2839-2849.
- Lutz, H. D., and Müller, B., 1991, Lattice vibration spectra. LXVIII. Single-crystal Raman spectra of marcasite-type iron chalcogenides and pnictides, FeX₂ (X=S, Se, Te; P, As, Sb): *Physics and Chemistry of Minerals*, v. 18, no. 4, p. 265-268.
- Mernagh, T. P., and Trudu, A. G., 1993, A laser Raman microprobe study of some geologically important sulphide minerals: *Chemical Geology*, v. 103, no. 1-4, p. 113-127.
- Morgan, B., Burton, E. D., and Rate, A. W., 2011, Iron monosulfide enrichment and the presence of organosulfur in eutrophic estuarine sediments: *Chemical Geology*.
- Morse, J. W., 1999, Sulfides in sandy sediments: New insights on the reactions responsible for sedimentary pyrite formation: *Aquatic Geochemistry*, v. 5, no. 1, p. 75-85.
- Morse, J. W., and Wang, Q. W., 1997, Pyrite formation under conditions approximating those in anoxic sediments .2. Influence of precursor iron minerals and organic matter: *Marine Chemistry*, v. 57, no. 3-4, p. 187-193.
- Poulton, S. W., Krom, M. D., and Raiswell, R., 2004, A revised scheme for the reactivity of iron (oxyhydr)oxide minerals towards dissolved sulfide: *Geochimica Et Cosmochimica Acta*, v. 68, no. 18, p. 3703-3715.
- Rickard, D., 1997, Kinetics of pyrite formation by the H₂S oxidation of iron (II) monosulfide in aqueous solutions between 25 and 125 degrees C: The rate equation: *Geochimica Et Cosmochimica Acta*, v. 61, no. 1, p. 115-134.
- Rickard, D., and Luther, G. W., 2007, Chemistry of iron sulfides: *Chemical Reviews*, v. 107, no. 2, p. 514-562.
- Sasaki, K., 1997, Raman study of the microbially mediated dissolution of pyrite by *Thiobacillus ferrooxidans*: *The Canadian Mineralogist*, v. 35, no. 4, p. 999-1008.
- Sassen, R., Roberts, H. H., Carney, R., Milkov, A. V., DeFreitas, D. A., Lanoil, B., and Zhang, C. L., 2004, Free hydrocarbon gas, gas hydrate, and authigenic minerals in chemosynthetic

- communities of the northern Gulf of Mexico continental slope: relation to microbial processes: *Chemical Geology*, v. 205, no. 3-4, p. 195-217.
- Schoonen, M., 2004, Mechanisms of sedimentary pyrite formation: *Geological Society of America*, v. 379, p. 18.
- Schwertmann, U., and Cornell, R. M., 2007a, Goethite, *Iron Oxides in the Laboratory*, Wiley-VCH Verlag GmbH, p. 67-92.
- , 2007b, Magnetite, *Iron Oxides in the Laboratory*, Wiley-VCH Verlag GmbH, p. 135-140.
- Theberge, S. M., and Luther, G.W., 1997, Determination of the electro-chemical properties of a soluble aqueous FeS species present in sulfidic solutions: *Aquatic Geochemistry*, v. 3, p. 21.
- Wang, Q. a. M., J.W., 1995, laboratory simulation of pyrite formation in anoxic sediment, *in* Vairavamurthy, M. A., and Schoonen, M.A.A., ed., *Geochemical Transformations of Sedimentary Sulfur*, Volume 612: Washington, D.C., American Chemical Society Symposium Series, p. 18.
- Wehrmann, L. M., Templer, S. P., Brunner, B., Bernasconi, S. M., Maignien, L., and Ferdelman, T. G., 2011, The imprint of methane seepage on the geochemical record and early diagenetic processes in cold-water coral mounds on Pen Duick Escarpment, Gulf of Cadiz: *Marine Geology*, v. 282, no. 1-2, p. 118-137.
- Wilkin, R. T., and Barnes, H. L., 1996, Pyrite formation by reactions of iron monosulfides with dissolved inorganic and organic sulfur species: *Geochimica Et Cosmochimica Acta*, v. 60, no. 21, p. 4167-4179.

CHAPTER 4

SURFACE ENHANCED RAMAN SCATTERING

APPLIED TO *IN SITU* GEOCHEMISTRY

Section 4.1

In situ extraction and SERS analysis of organic compounds

This section describes SERS experiments in detail, including content of Crystal Violet detection.

Parts of the results of such experiments are reported in paper n.8

***In situ* extraction and SERS analysis of organic compounds**

Wang Menghan¹, De Vivo Benedetto¹, Lu Wanjun² and Muniz-Miranda Maurizio³

1. Dipartimento di Scienze della Terra, dell'Ambiente e delle Risorse (DiSTAR), Università di Naples Federico II, 80134 Naples, Italy.
2. Department of Marine Science and Engineering, China University of Geosciences (CUGW), Wuhan 430074, China.
3. Dipartimento di Chimica, Università di Firenze, Firenze, Italy

Abstract

Rapid development of human society releases abundant harmful and new material into natural environment. A demanding of innovative approach to detect organic contaminants encourages various researches on *in-situ* techniques. Up to date, Raman scattering and other optic spectroscopic technologies are anchored with hope on substituting laboratorial procedures, such as GC-MS.

A new substrate embedding silver nanoparticles into siloxane polymer is used as a platform to generate Surface-Enhanced Raman scattering (SERS). Polymer serves as supporting material of silver nanoparticles as well as a stationary phase. After a short period of extraction, certain partition of organic compounds from aqueous solution accumulates into polymer. When silver nanoparticles is in touch with organic compounds, $10^4\sim 10^6$ degree of magnification Raman scattering can be obtained. Because of these two-steps amplification, SERS, which is typical accompany with strict lab condition, could compromise to apply for field survey.

Crystal violet (CV) is chosen to evaluate extraction properties of polymer. Color "transferring" indicates effective extraction of crystal violet into polymer. Intensive Raman bands include SERS effects and resonance scattering of CV. Low concentration of 4-nitrophenol (PNP) and 4-nitroaniline (PNA) (as low as 10^{-7} M) are dropped onto substrate and generate SERS fingerprint. After subtraction Raman bands of polymer and silver salts, clear evidence indicates availability of macro SERS spectra. Micro SERS testifies compounds penetrating as depth as 200 μ m from the surface.

In the future, a suitable substitution of silver salts is supposed to expand the application of such techniques to more compounds. At the present stage, detection of trace concentration PNP and PNA is applicable.

Introduction

Intense development of industries during last century has created thousands of synthetic organic compounds, such as plastics, lubricants, fuels, pesticides and etc. All of these compounds, along with organic byproducts and residues, constitute a new category of contaminants to natural environment. Among all the organic contaminants, persistent organic pollutants (POPs) are believed to be the most harmful compounds (Jones and De Voogt, 1999). POPs include variety of pesticides (OCPs), chlorobenzene species (PCBs and HCBs) and polyaromatic hydrocarbons (PAHs). POPs exhibit following four characteristics. 1) high toxicity: small quantity of POPs may cause severe damage; 2) persistency: POPs are resistant to photolysis, chemolysis and biolysis; 3) accumulation: POPs are

hydrophobic and lipophilic; this helps POPs accumulate in soil, sediment and biological adipose tissue; 4) mobility: most POPs are semi volatile and easily migrate in the atmosphere.

Clean water, which is free from toxic chemicals, is essential to both human health and economic development, when considering its different uses, as (1) drinking water, (2) water for agriculture, (3) water for zoo-technique, (4) water for industrial systems. Moreover, the demand for pure water is continuously rising due to the global industrialization and the socio-economical growth of emerging countries. Unfortunately, aquifers as sources of drinking water can undergo pollution, due to (1) atmospheric contamination, (2) discharge of liquid contaminants and/or (3) percolation from contaminated soils. At the same time, water pollution can provoke soil contamination, by accumulating both heavy metals and toxic or carcinogenic compounds in marine and fluvial sediments. In marine waters, as well as in flow waters and aquifers, chemical compounds, usually used as herbicides, pesticides and antibacterial agents in agriculture and zoo-prophylaxis, can be present. Many of these have molecular structures similar to natural products and are degraded naturally or through their own chemical or photochemical instability. On the other hand, when these compounds are stable, they can alter the ecosystem, accumulating in living organisms or diffusing through the environment by volatilization, dissolution or percolation from contaminated soils. As a consequence, the effects of the pollution can manifest themselves very far from the original site.

Concentration of POPs in soils, sediments and aquarium are commonly measured with proven technique Gas Chromatography (GC) (Chen et al., 2011; Fu et al., 2003). Samples are washed and then concentrated with stationary phase, such as hexane. Extracted POPs are heated and pass through a GC column, in which each gas moves through the column at a different rate. Combined with mass spectrometry (MS), different POPs could be determined quantitatively at the same time. However, demanding of in-situ detection techniques requires substitute technologies of GC-MS. The next generation technology should be rapid, non-destructive and portable. Spectroscopic approaches, such as infrared absorption, Raman and fluorescence, are the most suitable alternatives. Among the most recent techniques that have been proposed to recognize pollutants, Raman spectroscopy is one that allows the identification of different molecules on the basis of their vibrational bands, providing an unambiguous molecular fingerprint. However, the low sensitivity of Raman scattering, along with possible spectral interference due to fluorescence emission, impairs the use of this technique for the recognition of molecular traces. In these cases one can use the SERS (surface-enhanced Raman scattering) effect, which is able to enhance the Raman intensity of molecules adsorbed on metal substrates by many orders of magnitude and to promote a drastic quenching of fluorescence. Huge

magnifications of the Raman signal are observed when a molecule adheres to nanostructured surfaces of metals with high optical reflectivity, such as Ag, Au and Cu. The SERS enhancement factors are generally up to 10^7 with respect to the Raman intensities of non-adsorbed molecules. By means of experimental procedures that combine microscopy and spectral observation beyond the light diffraction limit, 10^{14} - 10^{15} enhancement factors are reached, thus ensuring single-molecule detection. Thanks to its peculiar properties, SERS spectroscopy, since its discovery at the beginning of the seventies, has achieved a leading role in the analytical investigation of very low traces of contaminants, allowing the spectroscopic detection at subpicogram level. Actually, aromatic nitroderivatives could be identified by means of SERS spectroscopy when adsorbed on silver nanoparticles, as demonstrated in the literature by observing strong enhancements of their Raman bands (Muniz-Miranda, 2013).

Determination of POPs and other organic contaminants in marine environment inspires the study of in-situ detection approaches. An intension of applying such advanced techniques into field survey is consistent with the object of environmental geochemistry. Integration of field survey, rapid analysis and geochemical mapping extends the future of geochemistry and serves effectively to governing and management.

In this study, an integrated approach of surface enhanced Raman scattering (SERS) and solid phase extraction (SPE) is considered. Organic pollutants were firstly concentrated into solid phase with silver nanoparticles embedded, and following micro (macro) Raman detection of SERS spectrum.

Technique background

Raman scattering and surface enhanced Raman scattering (SERS)

Raman scattering is an inelastic scattering related to vibrational, rotational and low-frequency modes in a system. Since discovery by Sir C. V. Raman in 1928 (Raman and Krishnan, 1928), Raman spectroscopy developed enormously.

When a sample is illuminated by a laser beam, usually in the range from near infrared to ultra violet, Raman scattering, filtered out Rayleigh scattering, is collected and dispersed onto a detector. The Raman effects root in interactions between incident light and molecule. A photon excites the molecule from the ground state to virtual energy state. When molecule returns to a different state, this difference leads to a shift in emitted photon's frequency from incident photon's. In another word the shift is Raman effect. Raman scattering commonly refers to the Stokes bands, whose wavenumbers

are downshifted with respect to the incident radiation. The amount of the polarizability change determines intensity of Raman scattering while the pattern of shifted frequencies is determined by the vibrational normal modes (Gardiner et al., 1989; Le Ru and Etchegoin, 2008) (Fig. 1).

Raman spectroscopy detects unique information of chemical bonds and symmetry of molecules, which provide fingerprint of chemicals. The detection with Raman technique requires minimum sample preparation and causes negligible damage to samples. However, compared with other approaches, the normal Raman scattering is very weak. Valuable Raman signal requires certain quantity of samples in the irradiated area. If Raman scattering is applied to a complex system, fluorescence interruptions from surroundings are always to be taken in the consideration (Matousek et al., 2002).

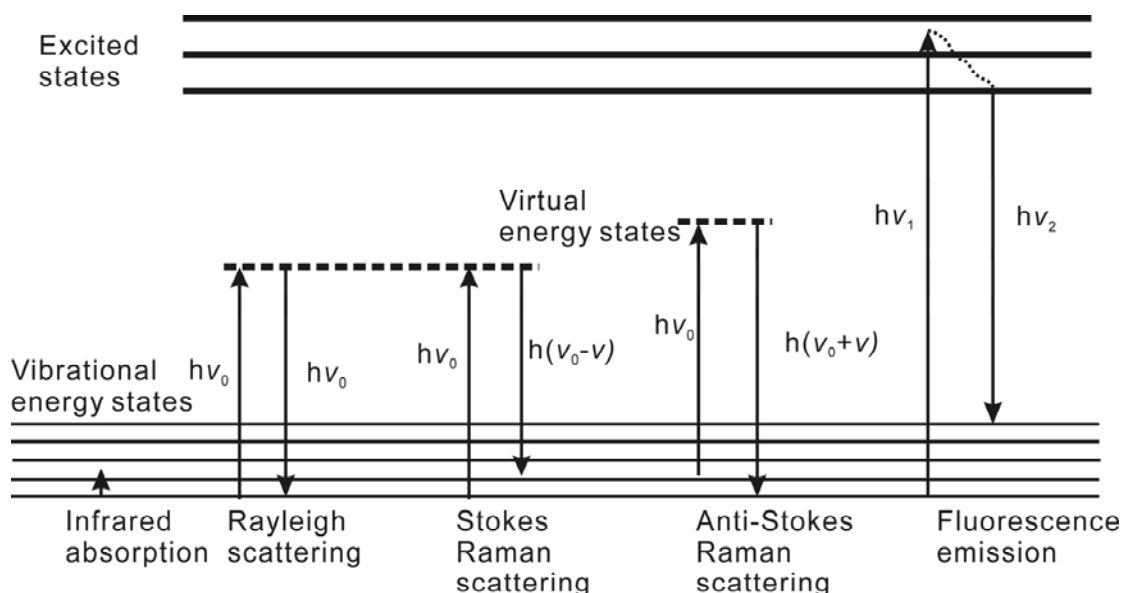


Figure 1. Schematic introduction to Raman scattering and other related optical effects.

Raman spectroscopy is a typical approach in chemistry to determine material properties, such as discrimination of SiO, Si₂O₂ and Si₃O₃ (Khanna, 1981). Besides conventional chemistry application, Raman is also important in studies of physics, biology and geology. For instance, mineralogists utilize Raman spectroscopy to identify minerals and furthermore mineral evolutions (Bourdoiseau et al., 2011).

In the last several decades, developments of Raman techniques give birth to several advanced techniques, including surface enhanced Raman (SERS) (Le Ru and Etchegoin, 2008), resonance Raman (RRS) (Martin and Falicov, 1983), tip enhanced Raman (Hermann et al., 2011), coherent

anti-Stokes Raman (CARS) (Tolles et al., 1977) and so on. Among all the branches of Raman, SERS is the most suitable technique to improve the sensitivity and for in-situ applications.

In 1973, Martin Fleischman, Patrick J. Hendra and A. James McQuillan surprisingly noticed orders of Raman amplification of pyridine adsorbed on electrochemically roughened silver (Fleischmann et al., 1974). Until 1973, Jeanmaire and Van Duyne proposed that an electromagnetic (EM) effect should account for the enormous enhancement (Jeanmaire and Van Duyne, 1977), while Albrecht and Creighton ascribed the effect to charge-transfer effect (Albrecht and Creighton, 1977). Up to date, electromagnetic effect based on plasmon resonance could be served as explanation to majority of SERS phenomena (Stiles et al., 2008).

Raman cross-section, which determines the Raman spectrum, is derived from the molecular polarizability and the magnitude of incident EM field. When the EM wave, such as monochromatic laser beam, interacts with a surface, the fields at the surface are different. Material and morphology of surface determine the change of EM field. For rough noble metal surface, such as silver and gold, the enhancement of EM occurs due to the happening of localized surface plasmon resonance (LSPR) (Fig. 2). Because Raman scattering approximately scales as E^4 , the EM enhancement factor is in order of biquadrate as LSPR enhancement. This EM enhancement is estimated in order of 10^{14} . Although EM enhancement account for the SERS effect, chemical attachment of molecule to noble metal nanoparticles is essential to involve the molecule into the enhanced EM (Le Ru and Etchegoin, 2008; Stiles et al., 2008), contributing to another enhancement factor up to 10^2 .

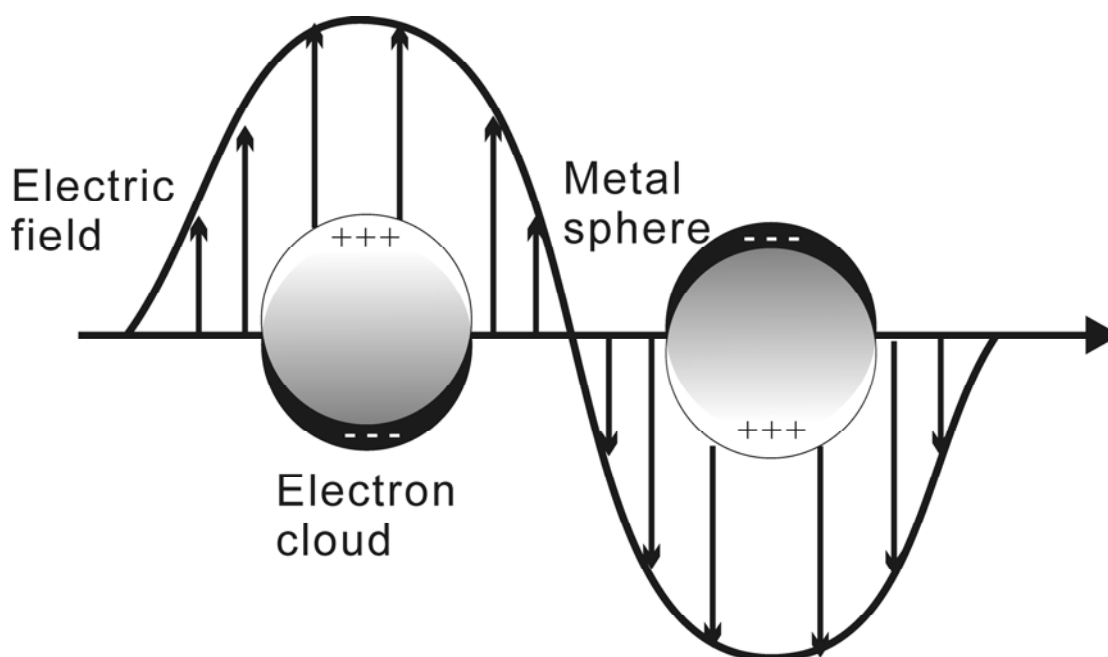


Figure 2. Schematic amplification of electromagnetic field due to localized surface plasmon resonance effect.

SERS draws attentions from chemists, physicians, biologists and other scientists mainly because of its amplification of conventional Raman signal. Raman is believed to be useful to most scientific branches but limited by its weak intensity. Most attractive application of SERS happens in the realm of single molecular detection (Lim, 2010; Sheridan et al., 2007), with enhancement factors reaching 10^{14} - 10^{15} . SERS provide a more precise, detailed option of single molecular detection. Served for theoretical physics, SERS itself provides information of material structure on molecular level. Many biological applications use SERS probes as substitutes to probes based on fluorescence. Numerous researches focus on applying SERS as an analytical approach in chemistry, biochemistry, food research, geochemistry, etc (Ciolla et al., 2012). The application to detect organic pollutants (POPs) is also included.

The organic compounds are the typical analytes for SERS verification, from pyridine at the very beginning of SERS history to the currently most used dyes (Lendl and Leopold, 2003). However, only last 15 years started the attempts of SERS as pollutants detection approach (Li et al., 1999). This delay could be ascribed to a semi-quantitative of the technique, as well as the reproducibility problem of substrates. Along with development in fabricating suitable substrates, researchers produced several forms of in-situ setups of SERS.

An optical research group in Technique University of Berlin dedicates to in-situ SERS probes since the end of 1990s (Kwon et al., 2013; Leyton, 2004; Lucht et al., 2000; Murphy, 1999, 2000; Nguyen, 2004; Schmidt, 2004). Detection of PAHs in sea water was their primary goal. The approach included sol-gel fabrication of substrate with noble nanoparticle embedded. A prototype of in-situ SERS probe could be concluded from their experiments: a portable micro Raman system, structure material to fix noble metal nanoparticles on the cell surface, a capture chemical to trap target from sea water. Because PAHs are unable to attach metal nanoparticles, a capture chemical is inevitable for PAHs detection. Lucigenin, diquat, humid acid, cyclodextrin and calixarene (Guerrini et al., 2009a, b; Leyton, 2004; Leyton et al., 2008; Xie et al., 2010) have been demonstrated as available capture chemicals. An alternative of portable Raman system is the optical fiber SERS sensor. Different from Kronfeldt's prototype, modified fiber head is immersed in the solution or seawater (Lucotti and Zerbi, 2006). A recent development is the attempt of combination SERS with solid phase extraction (SPE) (Lai et al., 2013).

The endeavor combination of SPE and conventional Raman could be dated back to 1995, when Wittkamp tried to detect benzene, toluene, ethylbenzene and xylene (BTEX) (Wittkamp and Tilotta,

1995) with solid phase microextraction (SPME) and Raman spectroscopy. After that, sporadic publications concerned about Raman detection on SPME fiber.

Solid phase extraction (SPE) and related techniques

Solid phase extraction (SPE) is a separation process by which compounds are separated from mixtures due to absorption or adsorption mechanisms. The solid in SPE acts as stationary phase to concentrate desired molecular. A common application of SPE is in the analysis of organic pollutants. The extracted pollutants are released to GC-MS for quantitative determination.

Developments and modifications to SPE create several innovative separation approaches. SPME (Arthur et al., 1992a; Arthur et al., 1992b; Arthur and Pawliszyn, 1990; Gao et al., 1990) is one commercially available approach based on SPE. The microextraction refers to micro volume of stationary phase as well as easy handed process. Another alternative of SPE is stir bar sorptive extraction (SBSE) (Baltussen et al., 1999), in which process stirring is a significant step of extracting molecular. SBSE expands range of compounds that SPE could be used to.

MATERIALS AND METHODS

Schematic design of substrate

The idea of design is similar to the researches ongoing in China (Lai et al., 2013) at the same period: the combination of SERS and SPE. Solution containing organic contaminants was injected into a column contained propanethiol modified with silver dendrites. After solution was force to get through the propanethiol, some contaminant molecular was attached to silver dendrites which were ready to generate SERS spectrum. However, there are several differences in our designation. Firstly, idea in this study is based on embedded silver nanoparticles rather than superficial silver dendrites. SERS signal are generated from the silver particles at the surface also inside of stationary phase. Moreover, the extraction prototype is based on SPME rather than SPE. SPME is an automatic extraction process compared with various others, and has the potential to apply for in situ investigation, such as sea water and sea sediment.

The design is schematically introduced in Fig. 3. During the formation of polymer from monomer, a suitable dispersive silver salts were added to the matrix. The curing agent in polymer kit could polymerize the monomers and reduce silver salts to silver nanoparticles at the same time. The suitable silver salts should disperse or solute in the nonpolar solvent which could commixture with polymer.

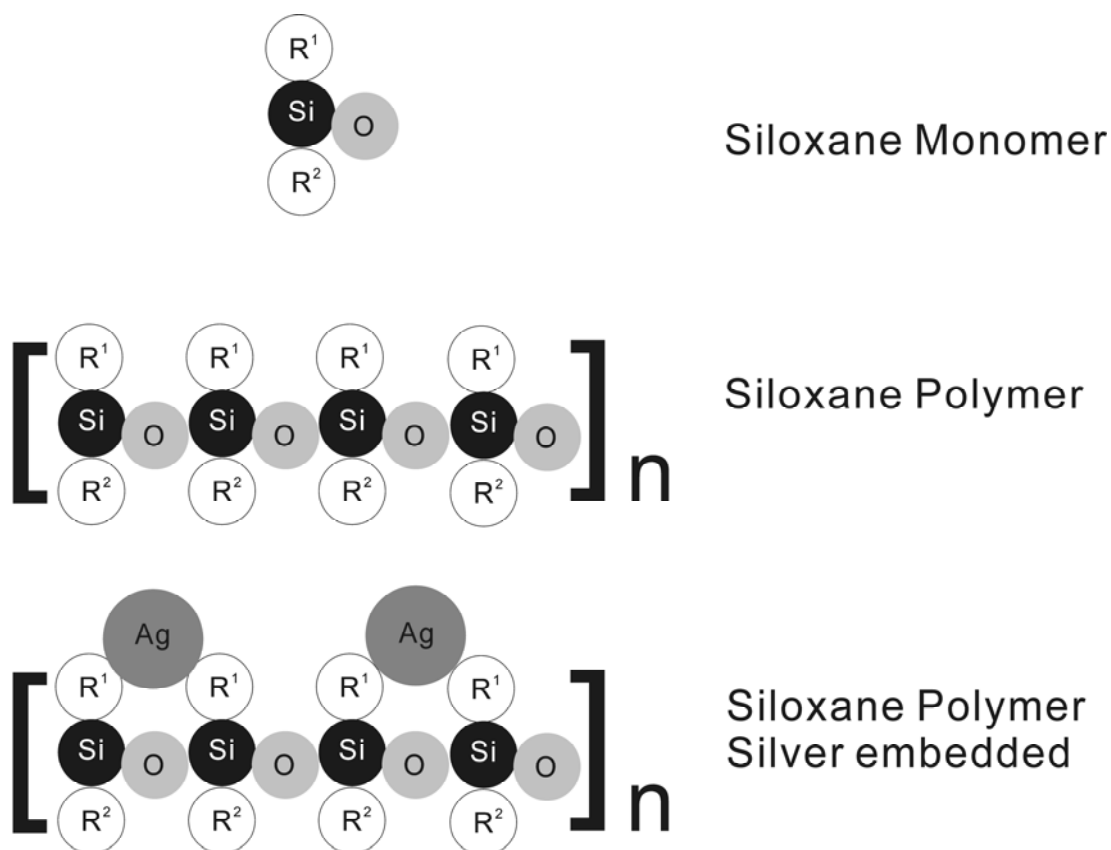


Figure 3. Procedure and schematic concepts of silver embedded polymer. During the process of monomers curing to polymer, a suitable dispersive silver salts was added to matrix. Because curing agent could serve as reductant to silver salts, as the consequence silver nanoparticles were formed during curing process.

Embedding nanoparticles is a proven technique in the realm of polymer nanoscience, obtaining nanocomposites as called by polymer scientists. The idea is primarily proposed to modify physical properties of polymer material, which helps polymer to serve well in various applications.

Chemicals and Extraction media

PDMS elastomer kits (Sylgard 184, Dow Corning) and silver benzoate (Sigma–Aldrich) were used as received. The kit contains the elastomer (PDMS) and the curing agent which is composed of dimethyl, methylhydrogen siloxane, dimethyl siloxane, dimethylvinylated, and trimethylated silica, tetramethyl-tetravinyl cyclotetrasiloxane, and ethyl benzene.

4-nitrophenol, 4-nitroaniline, and crystal violet (Sigma-Aldrich) were analytical grade, and the solutions were prepared with high-purity water from a Milli-QPLUS ultrapure water system.

Nitrophenols are a class of pollutants arousing relevant environmental alarm, because are responsible for severe damages to the vegetation. These products can derive from combustion or, to a

greater extent, from reactions in atmosphere by nitration or oxidation. 4-Nitrophenol is one of the most studied pollutants, because it is readily absorbed and accumulated in soils, dramatically modifying the humus pH. In this way, this pollutant cannot be degraded, contaminating flow waters, aquifers and marine waters.

4-nitroaniline (PNA), as well as PNP (4-nitrophenol) is a nitroaromatic compound, slightly soluble in water. For this reason it can be considered, as well as PNP, a possible contaminant of the aqueous environment. 4-nitroaniline is commonly used in the synthesis of dyes, antioxidants and pharmaceuticals, in gum inhibitors, poultry medicines, and as a corrosion inhibitor. The compound is toxic, particularly harmful to all aquatic organisms, and can cause long-term damage to the environment if released as a pollutant.

Preparation of silver embedded PDMS

Preparation of silver embedded PDMS (Ag-PDMS) was followed the procedure of Goyal (Goyal et al., 2009). Elastomer (8 g) was mixed thoroughly with the curing agent in the weight ratio of 10:1 and then degassed under vacuum to remove entrapped air bubbles. Silver benzoate (3 ml, 5×10^{-3} M solution in hexane) was added to the polymer and sonicated for 15 min to obtain a homogeneous mixture. Subsequently, the color of the mixture changed to brown. It was then casted on glass slides and cured under vacuum at room temperature.

Extraction of crystal violet and 4-nitrophenol

Crystal violet (CV) extraction was similar to a reported procedure (Manzo et al., 2013). A 250mL volume of the water sample containing CV with concentrations $0.16 \mu\text{g.L}^{-1}$, $0.8 \mu\text{g.L}^{-1}$, $20 \mu\text{g.L}^{-1}$, 20mg.L^{-1} was poured into a beaker, and potassium hydroxide was used to adjust the pH value to 14. The cover glass with coated siloxane polymer was placed inside the beaker, and the stir was rotated at 1250 rpm for 30 min at 70°C .

Neutral carbinol CV was functioned with hydroxide in base media. Hydrogen atom of such C-OH bond formed hydrogen bonds with oxygen from PDMS, which resulted in efficient extraction of CV. 4-nitrophenol was supposed to be easily extracted to PDMS due to C-OH bond existence. Ag-PDMS was immersed in 5 ml 10^{-5} M 4-nitrophenol overnight at room temperature. Before SERS detection, the surface of Ag-PDMS was thoroughly washed with high-purity water.

Instrumentation

UV–vis absorption spectra of Ag-PDMS were obtained in the 200–800 nm region by using a Cary 5 Varian spectrophotometer.

Macro-Raman spectra were performed by using a Jobin-Yvon HG-2S monochromator, a cooled RCA-C31034A photomultiplier, and the 514.5 nm exciting line supplied by an Ar⁺ laser with a power of 50 mW. A defocused laser beam and a rotating device were adopted to impair thermal effects. Micro-Raman spectra were measured by a Renishaw RM2000 instrument, equipped with an Ar⁺ laser emitting at 514.5 nm. Sample irradiation was accomplished by using the 50x microscope objective of a Leica Microscope DMLM. The backscattered Raman signal was fed into the monochromator through 40 m slits and detected by an air-cooled CCD (2.5 cm⁻¹ per pixel) filtered by a double holographic Notch filters system. Spectra were calibrated with respect to a silicon wafer at 520 cm⁻¹.

RESULTS

PNA has a polar group (amino group) that can strongly interact with the polysiloxane polymer, as well as PNP that can interact with the hydroxyl group. For this reason both compounds can be adsorbed on the polymer, in close contact with the Ag nanoparticles embedded in it. Hence, these compounds can be easily detected in water by SERS effect by depositing drops on the polymer surface. The Limit of Detections (LODs) for these compounds can reach 10⁻⁷ M concentrations or less; consequently, this procedure can be considered a sensitive method for detecting these pollutants in waters or in soil, if wetted by contaminated waters.

The absorbance center maximum moves from 410 nm to 425 nm in the UV-visible spectra of Ag-PDMS. This absorbance is due to the surface plasmon excitation of silver nanoparticles and confirms the nanoparticle formation. Changes of absorbance spectra are due to different density of nanoparticles in PDMS. Higher absorbance center and higher intensity of spectrum corresponds to PDMS with more nanoparticles (Fig. 4).

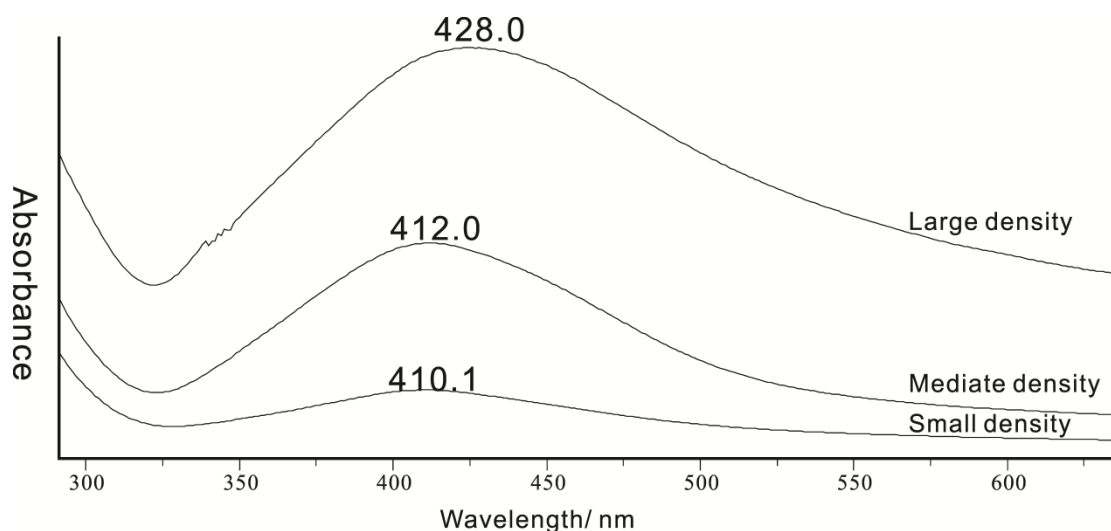


Figure 4 UV-vis absorption spectra of Ag-PDMS with different density of Ag nanoparticles.

PDMS and silver benzoate has several strong Raman bands. The primary step of SERS application with Ag-PDMS is to recognize and eliminate bands of polymer and benzoate. These bands are listed in Table 1 and shown in Fig. 5.

Table 1 Raman bands of polymer background, benzoate silver, 4-nitrophenol and crystal violet.

PDMS	Ag-PDMS	Nitrophenol SERS	Nitrophenol crystal	Crystal Violet SSERS	Crystal Violet SERS(literature 633nm)
493	491	646		730	726
619	617	856	870		745.5
711	711	1112	1112	762	761
792	795.1	1166	1172	808	806
	842	1244	1218	916	916
	1005		1284	940	940.5
1126	1126	1326	1326		978.5
1265	1265		1338	1178	1174.5
1411	1413	1570	1586	1296	1298
	1601				1349
				1372	1387
				1446	1448
				1478	1473.5
				1538	1541
				1590	1588.5
				1622	1620

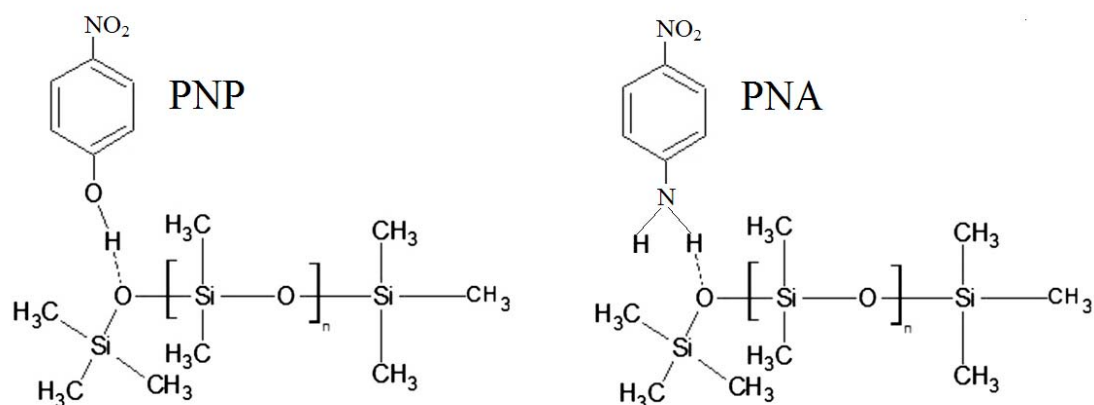


Figure 5. Chemical structures of PNP and PNA integrated with siloxane polymers.

To demonstrate the SERS activity of Ag-PDMS, crystal violet (CV) is chosen as the initiative target because of its resonant contribution to the SERS effect. As shown previously, PDMS effectively concentrates CV from alkalinity aqueous solution. An Ag-PDMS is immersed into 250 ml heated alkalinity CV solution with concentration of 5×10^{-8} M. Transparent polymer is colorized to pale violet after extraction for half an hour. A SERRS (Surface Enhanced Resonant Raman Scattering) spectra of CV in Ag-PDMS exhibit fingerprint band at cm^{-1} when laser power is as low as 50 mW. Sample carbonization is easily triggered when increasing laser power, with consequent disappearing of SERRS spectra.

Ag-PDMS is immersed in 5 ml 10^{-5} M PNP solution overnight to demonstrate the usefulness of experimental set to contaminants detection. The surface of polymer is thoroughly washed with high-purity water to eliminate non-absorbed PNP molecules. Laser beam is focused onto silver aggregates under micro Raman spectroscopy at different depth of polymer (Fig. 6). Effective spectra is achieved until 200 μm depth from polymer surface. When focus on deeper silver aggregates, inevitable photoreaction of benzoate occurs in the sample, evidenced by the appearing of the broad bands of amorphous carbon. SERS spectra of PNP at different depth demonstrate the extracting and SERS efficiency of Ag-PDMS (Fig. 7).

Macro SERS spectra of dropped PNP and PNA onto Ag-PDMS is shown in Fig. 8 and Fig. 9. Different from micro Raman, macro Raman shares laser power averagely onto the substrate avoiding possible photoreaction. Subtracted SERS spectra of PNP and PNA exhibit peaks attributed to both contaminants.

FUTURE IMPROVEMENTS

The results indicate a bright future for in situ pollutants determination with this new approach. However, a few problems need to be solved before field availability.

The need of dispersive in nonpolar solvent determines the use of benzoate silver as the qualified chemical. But the SERS bands of benzoate are always present, impairing an immediate detection of target contaminants. Most of organic pollutants have benzene ring, which is also in the structure of benzoate. In this case, the Raman bands belonging to benzene ring of these compounds are hard to be detected. As well, too many bands presents in benzoate spectra which leave over only limited “space” on the spectra to detect pollutants. Other disadvantages of benzoate, as well as of other organic functional groups, are the fluorescence effect and possible photoreaction. As illustrated in Fig. 6,

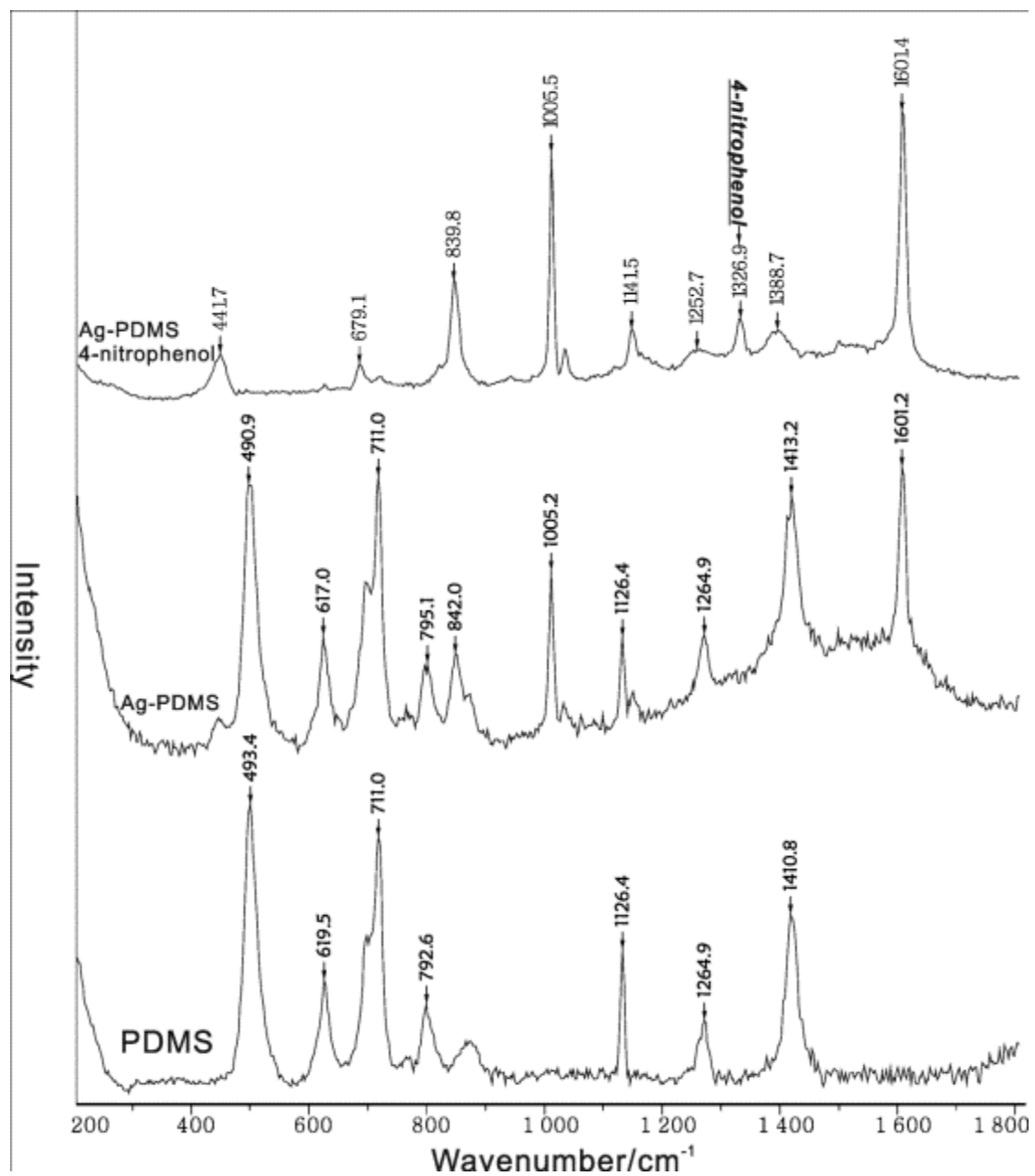


Figure 6. Micro Raman spectrum of PDMS and micro SERS spectra of Ag-PDMS and Ag-PDMS with extracted 4-nitrophenol.

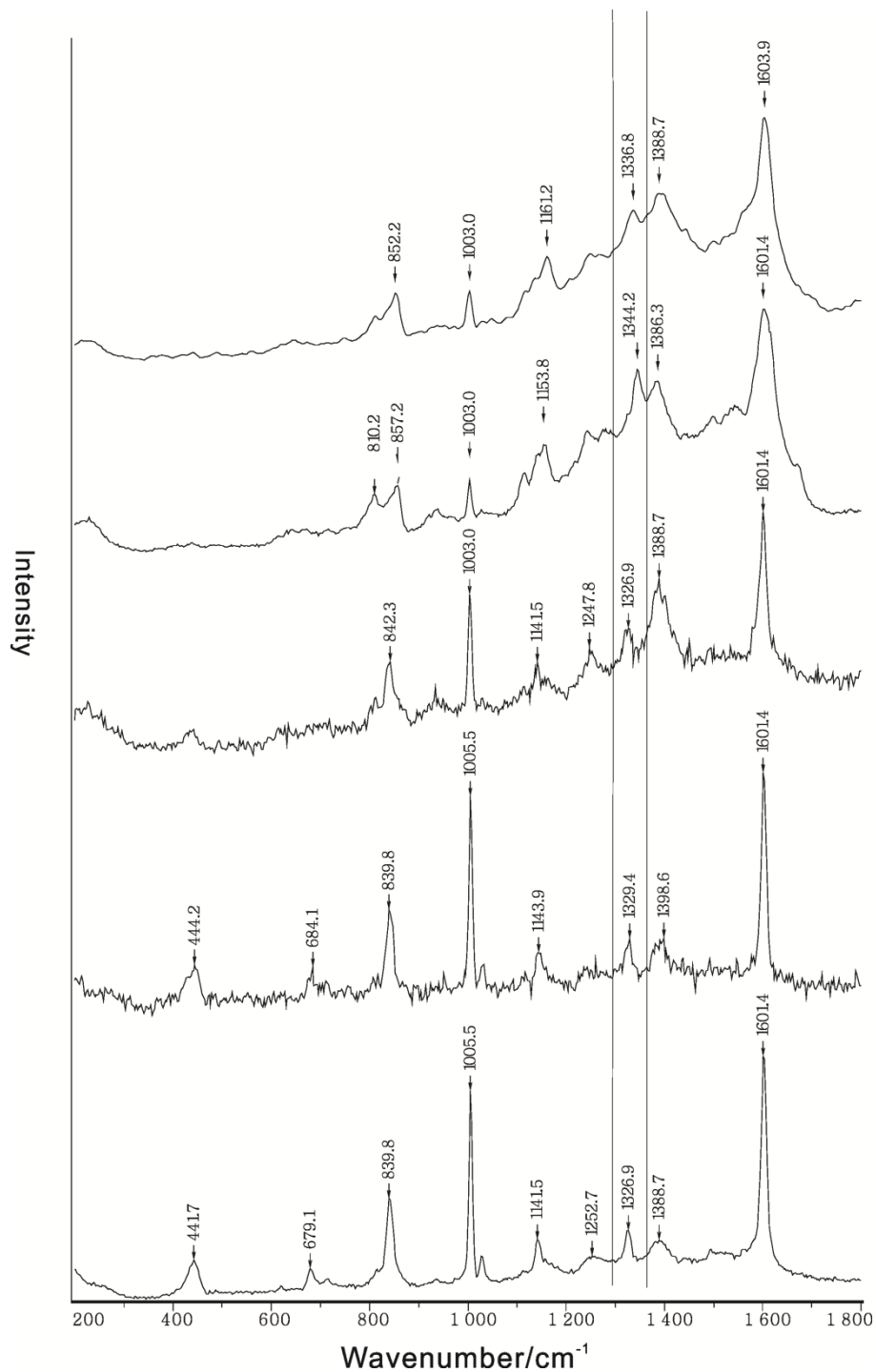


Figure 7. Micro SERS spectra of 4-nitrophenol with increasing depth inside Ag-PDMS. The optimum spectrum is acquired at the surface of substrate. As depth increasing, carbonized photoreaction of benzoate creates interfering bands from 1000 to 1700 cm⁻¹. Effective spectrum could be acquired until 200 μ m into PDMS.

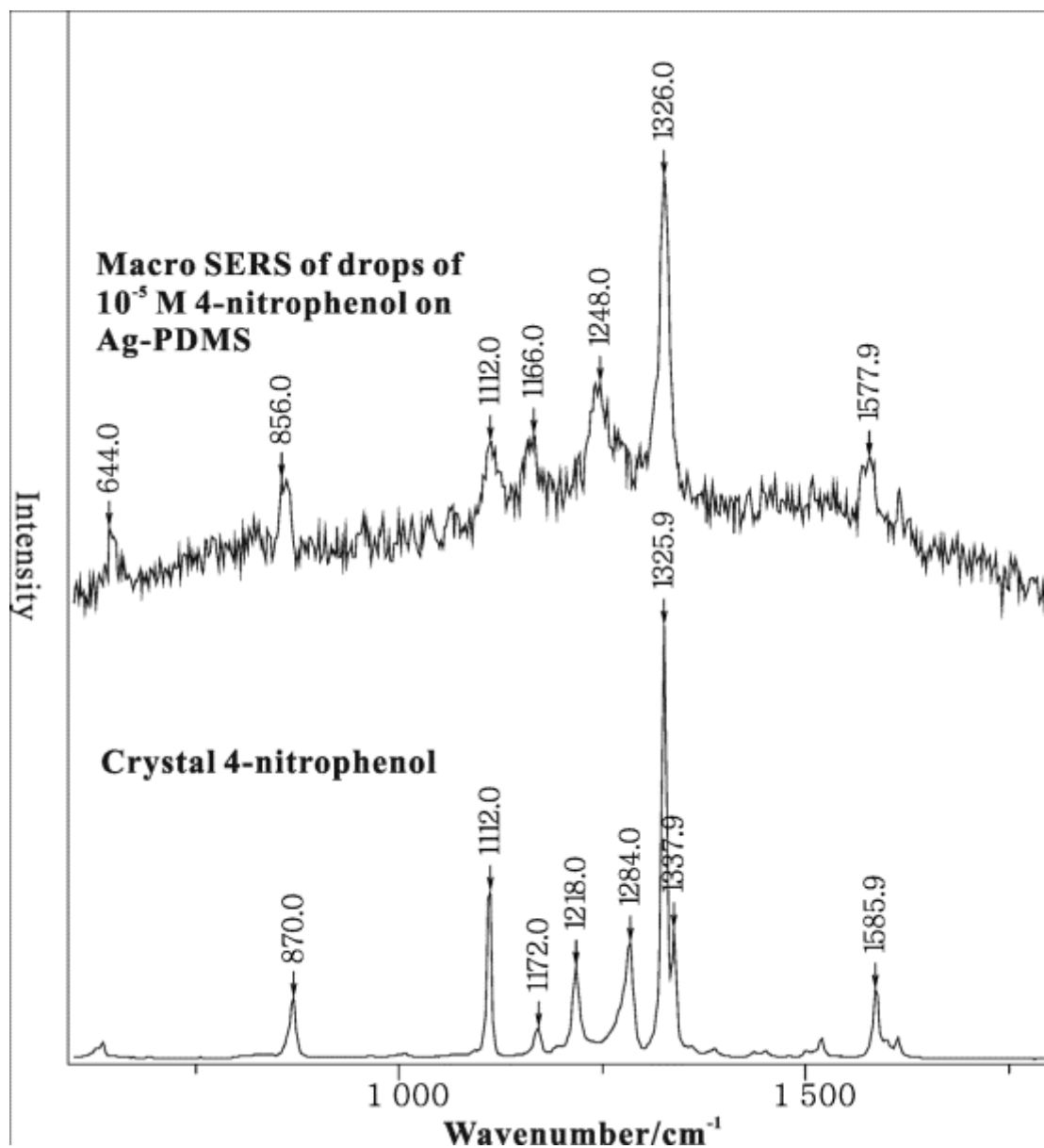


Figure 8. Macro SERS spectra of 4-nitrophenol after subtracted with Ag-PDMS SERS spectrum. Several bands are corresponding to macro Raman spectrum of crystal 4-nitrophenol.

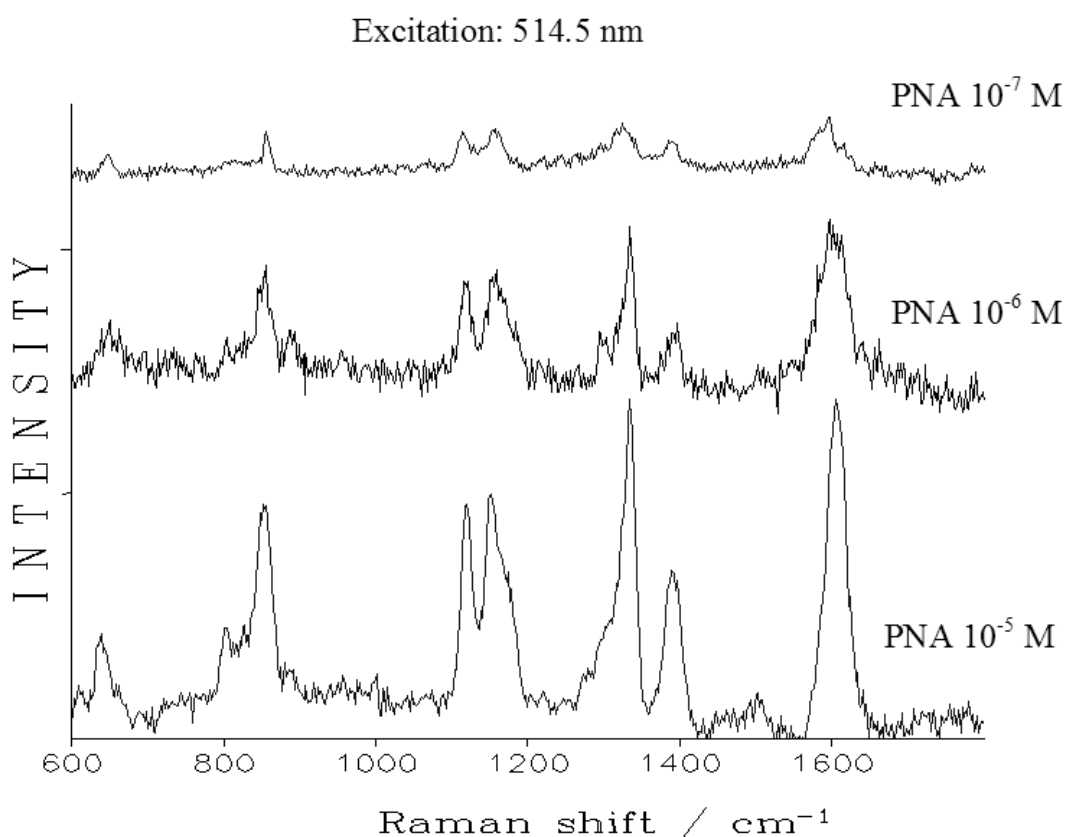


Figure 9. Macro SERS spectra of PNA after subtracted with Ag-PDMS SERS spectrum.

effective spectrum could be obtained only as depth as 200 μm from polymer surface. As focus goes deeper, the background due to carbonized reaction increases and masks the bands of nitro group. A substitute of benzoate silver should possess following properties: dispersivity in nonpolar solvent, absence of benzene ring and photoreactions. Besides replacement of silver compounds, a more suitable stationary phase should be developed. The current polymer, Sylgard 184, is commercially available and easy handed. However, Sylgard 184 is not specifically designed as stationary phase for organic extraction. An ideal polymer should have same effectiveness as those used on SPME fibers.

REFERENCE

- Albrecht, M.G., Creighton, J.A., 1977. Anomalously intense Raman spectra of pyridine at a silver electrode. *J Am Chem Soc* 99, 5215-5217.
- Arthur, C.L., Killam, L.M., Buchholz, K.D., Pawliszyn, J., Berg, J.R., 1992a. Automation and Optimization of Solid-Phase Microextraction. *Anal Chem* 64, 1960-1966.
- Arthur, C.L., Killam, L.M., Motlagh, S., Lim, M., Potter, D.W., Pawliszyn, J., 1992b. Analysis of

- Substituted Benzene Compounds in Groundwater Using Solid-Phase Microextraction. *Environ Sci Technol* 26, 979-983.
- Arthur, C.L., Pawliszyn, J., 1990. Solid phase microextraction with thermal desorption using fused silica optical fibers. *Anal Chem* 62, 2145-2148.
- Baltussen, E., Sandra, P., David, F., Cramers, C., 1999. Stir bar sorptive extraction (SBSE), a novel extraction technique for aqueous samples: Theory and principles. *Journal of Microcolumn Separations* 11, 737-747.
- Bourdoiseau, J.A., Jeannin, M., Remazeilles, C., Sabota, R., Refait, P., 2011. The transformation of mackinawite into greigite studied by Raman spectroscopy. *J Raman Spectrosc* 42, 496-504.
- Chen, W., Jing, M., Bu, J., Ellis Burnet, J., Qi, S., Song, Q., Ke, Y., Miao, J., Liu, M., Yang, C., 2011. Organochlorine pesticides in the surface water and sediments from the Peacock River Drainage Basin in Xinjiang, China: a study of an arid zone in Central Asia. *Environmental monitoring and assessment* 177, 1-21.
- Cialla, D., Marz, A., Bohme, R., Theil, F., Weber, K., Schmitt, M., Popp, J., 2012. Surface-enhanced Raman spectroscopy (SERS): progress and trends. *Anal Bioanal Chem* 403, 27-54.
- Fleischmann, M., Hendra, P., McQuillan, A., 1974. Raman spectra of pyridine adsorbed at a silver electrode. *Chem Phys Lett* 26, 163-166.
- Fu, J., Mai, B., Sheng, G., Zhang, G., Wang, X., Peng, P., Xiao, X., Ran, R., Cheng, F., Peng, X., 2003. Persistent organic pollutants in environment of the Pearl River Delta, China: an overview. *Chemosphere* 52, 1411-1422.
- Gao, X.P., Davies, J.P., Weaver, M.J., 1990. A Test of Surface Selection-Rules for Surface-Enhanced Raman-Scattering - the Orientation of Adsorbed Benzene and Monosubstituted Benzenes on Gold. *J Phys Chem-Us* 94, 6858-6864.
- Gardiner, D.J., Graves, P.R., Bowley, H.J., 1989. *Practical Raman Spectroscopy*. Springer-Verlag Heidelberg, Germany.
- Goyal, A., Kumar, A., Patra, P.K., Mahendra, S., Tabatabaei, S., Alvarez, P.J.J., John, G., Ajayan, P.M., 2009. In situ Synthesis of Metal Nanoparticle Embedded Free Standing Multifunctional PDMS Films. *Macromol Rapid Comm* 30, 1116-1122.
- Guerrini, L., Garcia-Ramos, J.V., Domingo, C., Sanchez-Cortes, S., 2009a. Nanosensors Based on Viologen Functionalized Silver Nanoparticles: Few Molecules Surface. Enhanced Raman Spectroscopy Detection of Polycyclic Aromatic Hydrocarbons in Interparticle Hot Spots. *Anal Chem* 81, 1418-1425.
- Guerrini, L., Garcia-Ramos, J.V., Domingo, C., Sanchez-Cortes, S., 2009b. Sensing Polycyclic Aromatic Hydrocarbons with Dithiocarbamate-Functionalized Ag Nanoparticles by Surface-Enhanced Raman Scattering. *Anal Chem* 81, 953-960.
- Hermann, P., Hermelink, A., Lausch, V., Holland, G., Möller, L., Bannert, N., Naumann, D., 2011. Evaluation of tip-enhanced Raman spectroscopy for characterizing different virus strains. *Analyst* 136, 1148-1152.
- Jeanmaire, D.L., Van Duyne, R.P., 1977. Surface Raman spectroelectrochemistry: Part I. Heterocyclic, aromatic, and aliphatic amines adsorbed on the anodized silver electrode. *Journal of Electroanalytical Chemistry and Interfacial Electrochemistry* 84, 1-20.
- Jones, K.C., De Voogt, P., 1999. Persistent organic pollutants (POPs): state of the science. *Environmental Pollution* 100, 209-221.
- Khanna, R., 1981. Raman-spectroscopy of oligomeric SiO species isolated in solid methane. *Journal of Chemical Physics*. doi 10.
- Kwon, Y.-H., Kolomijeca, A., Kronfeldt, H.-D., Ossig, R., Hubenthal, F., 2013. Naturally Grown Ag Nanoparticle SERS Substrate As Chemical Sensor in Fresh Water Applying 488 nm Microsystem Laser Diode. *International Journal of Offshore and Polar Engineering* 23.

- Lai, Y., Cui, J., Jiang, X., Zhu, S., Zhan, J., 2013. Combination of solid phase extraction and surface-enhanced Raman spectroscopy for rapid analysis. *Analyst* 138, 2598-2603.
- Le Ru, E., Etchegoin, P., 2008. Principles of Surface-Enhanced Raman Spectroscopy: and related plasmonic effects. Access Online via Elsevier.
- Lendl, B., Leopold, N., 2003. A new method for fast preparation of highly surface-enhanced Raman scattering (SERS) active silver colloids at room temperature by reduction of silver nitrate with hydroxylamine hydrochloride. *J Phys Chem B* 107, 5723-5727.
- Leyton, P., 2004. Selective Molecular Recognition of Polycyclic Aromatic Hydrocarbons (PAHs) on Calix[4]arene-Functionalized Ag Nanoparticles by Surface-Enhanced Raman Scattering. *J. Phys. Chem. B* 108, 7.
- Leyton, P., Córdova, I., Lizama-Vergara, P.A., Gómez-Jeria, J.S., Aliaga, A.E., Campos-Vallette, M.M., Clavijo, E., García-Ramos, J.V., Sanchez-Cortes, S., 2008. Humic acids as molecular assemblers in the surface-enhanced Raman scattering detection of polycyclic aromatic hydrocarbons. *Vib Spectrosc* 46, 77-81.
- Li, Y.-S., Lin, X., Cao, Y., 1999. Using a sol-gel process for the fabrication of surface-enhanced Raman scattering active substrates. *Vib Spectrosc* 20, 95-101.
- Lim, D.-K., 2010. Nanogap-engineerable Raman-active nanodumbbells for single-molecule detection. *Nature materials* 9, 8.
- Lucht, S., Murphy, T., Schmidt, H., Kronfeldt, H.D., 2000. Optimized recipe for sol-gel - based SERS substrates. *J Raman Spectrosc* 31, 1017-1022.
- Lucotti, A., Zerbi, G., 2006. Fiber-optic SERS sensor with optimized geometry. *Sensor Actuat B-Chem* 121, 9.
- Manzo, V., Navarro, O., Honda, L., Sánchez, K., Inés Toral, M., Richter, P., 2013. Determination of crystal violet in water by direct solid phase spectrophotometry after rotating disk sorptive extraction. *Talanta* 106, 305-308.
- Martin, R., Falicov, L., 1983. Resonant raman scattering, *Light scattering in Solids I*. Springer, pp. 79-145.
- Matousek, P., Towrie, M., Parker, A., 2002. Fluorescence background suppression in Raman spectroscopy using combined Kerr gated and shifted excitation Raman difference techniques. *J Raman Spectrosc* 33, 238-242.
- Muniz-Miranda, M., 2013. SERS monitoring of the catalytic reduction of 4-nitrophenol on Ag-doped titania nanoparticles. *Applied Catalysis B: Environmental*.
- Murphy, T., 1999. Use of sol-gel techniques in the development of surface-enhanced Raman scattering (SERS) substrates suitable for in situ detection of chemicals in sea-water. *J. Phys. Chem. B* 69, 4.
- Murphy, T., 2000. Surface-enhanced Raman scattering (SERS) system for continuous measurements of chemicals in sea-water. *J. Raman Spectrosc.* 31, 6.
- Nguyen, T.P., 2004. Surface-enhanced Raman Scattering (SERS) for in-situ Analysis of Mixture of Polycyclic Aromatic Hydrocarbons (PAHs) in Sea-water. *Mathematik und Naturwissenschaften der Technischen Universität Berlin, Berlin*.
- Raman, C., Krishnan, K., 1928. A new type of secondary radiation. *Nature* 121, 501-502.
- Schmidt, H., 2004. Detection of PAHs in seawater using surface-enhanced Raman scattering (SERS). *Mar Pollut Bull* 49, 229-234.
- Sheridan, E., Inya-Agha, O., Keyes, T., Forster, R., 2007. Electrodeposited noble metal SERS: Control of single nanoparticle size and control of array interparticle spacing - art. no. 64500U, in: VoDinh, T., Lakowicz, J.R. (Eds.), *Plasmonics in Biology and Medicine IV*, pp. U4500-U4500.
- Stiles, P.L., Dieringer, J.A., Shah, N.C., Van Duyne, R.P., 2008. Surface-Enhanced Raman Spectroscopy. *Annual Review of Analytical Chemistry* 1, 601-626.

- Tolles, W.M., Nibler, J., McDonald, J., Harvey, A., 1977. A review of the theory and application of coherent anti-Stokes Raman spectroscopy (CARS). *Appl Spectrosc* 31, 253-271.
- Wittkamp, B.L., Tilotta, D.C., 1995. Determination of BTEX Compounds in Water by Solid-Phase Microextraction and Raman-Spectroscopy. *Anal Chem* 67, 600-605.
- Xie, Y., Wang, X., Han, X., Song, W., Ruan, W., Liu, J., Zhao, B., Ozaki, Y., 2010. Selective SERS detection of each polycyclic aromatic hydrocarbon (PAH) in a mixture of five kinds of PAHs. *J Raman Spectrosc*, n/a-n/a

Section 4.2

Sensitive SERS Detection of Nitroaromatic Pollutants in Water

*Paper is accepted by **Applied Spectroscopy** (in press)*

Easy and Sensitive SERS Detection of Nitroaromatic Pollutants in Water

Wang Menghan¹, De Vivo Benedetto¹, Lu Wanjun², Muniz-Miranda Maurizio³*

- [1] *Dipartimento di Scienze della Terra, dell'Ambiente e delle Risorse (DISTAR), Università Federico II, 80134 Naples, Italy*
- [2] *Department of Marine Science and Engineering, China University of Geosciences (CUGW), Wuhan 430074, China*
- [3] *Dipartimento di Chimica "Ugo Schiff", Università di Firenze, V. Lastruccia 3 Sesto Fiorentino, 50019 Italy; * corresponding author, E-mail: muniz@unifi.it*

Abstract

The increasing and urgent demand for clean water requires new approaches for identifying possible contaminants. In the present work, polymer substrates with embedded silver nanoparticles are employed for revealing the presence of traces of nitroaromatic compounds in water, on the basis of the SERS (surface-enhanced Raman scattering) effect. These platforms provide an easy and sensitive detection of these organic pollutants with low concentrations in contaminated water.

Keywords: SERS, silver nanoparticles, pollutant, aromatic nitro-derivatives, water

1. Introduction

Clean water, which is free from toxic chemicals, is essential to both human health and economic development, when considering its different uses, as (1) drinking water, (2) water for agriculture, (3) water for zoo-technique, (4) water for industrial systems. Moreover, the demand for pure water is continuously rising due to the global industrialization and the socio-economical growth of emerging countries. Unfortunately, aquifers as sources of drinking water can undergo pollution, due to (1) atmospheric contamination, (2) discharge of liquid contaminants and/or (3) percolation from contaminated soils. At the same time, water pollution can provoke soil contamination, by accumulating both heavy metals and toxic or carcinogenic compounds in marine and fluvial sediments. In marine waters, as well as in flow waters and aquifers, chemical compounds, usually used as herbicides, pesticides and antibacterial agents in agriculture and zoo-prophylaxis, can be present. Many of these have molecular structures similar to natural products and are degraded naturally or through their own chemical or photochemical instability. On the other hand, when these compounds are stable, they can alter the ecosystem, accumulating in

living organisms or diffusing through the environment by volatilization, dissolution or percolation from contaminated soils. As a consequence, the effects of the pollution can manifest themselves very far from the original site. Nitrophenols are a class of pollutants arousing relevant environmental alarm, as responsible for severe damages to the vegetation^{1,2}. These products can derive from combustion or, to a larger extent, from reactions in atmosphere by nitration or oxidation. 4-Nitrophenol is one of the most studied pollutants, because it is readily absorbed and accumulated in soils, dramatically modifying the humus pH. In this way, this pollutant cannot be degraded, contaminating flow waters, aquifers and marine waters^{3,4}.

Also nitroanilines are aromatic compounds that may entail severe risks to the environment and therefore to the human health. 4-Nitroaniline, in particular, is commonly used in the synthesis of dyes, antioxidants and pharmaceuticals, in gum inhibitors, poultry medicines, and as a corrosion inhibitor. The compound is toxic, particularly harmful to all aquatic organisms, and can cause long-term damage to the environment⁵. For this reason it has been stipulated as priority pollutant by the Environmental Protection Agencies (EPAs) of many countries.

Among the most recent techniques that were proposed to recognize pollutants, Raman spectroscopy is one that allows the identification of different molecules on the basis of their vibrational bands, providing an unambiguous molecular fingerprint. However, the low sensitivity of Raman scattering, along with possible spectral interference due to fluorescence emission, impairs the use of this technique for the recognition of molecular traces. In these cases one can use the SERS (surface-enhanced Raman scattering) effect [6], which is able to enhance the Raman intensity of molecules adsorbed on metal substrates by many orders of magnitude and to promote a drastic quenching of fluorescence. Huge magnifications of the Raman signal are observed when a molecule adheres to nanostructured surfaces of metals with high optical reflectivity, such as Ag, Au and Cu. The SERS enhancement factors are generally up to 10^7 with respect to the Raman intensities of non-adsorbed molecules. By means of experimental procedures that combine microscopy and spectral observation beyond the light diffraction limit, 10^{14} - 10^{15} enhancement factors are reached, thus ensuring single-molecule detection. Thanks to its peculiar properties, SERS spectroscopy, since its discovery at the beginning of the seventies, has achieved a leading role in the analytical investigation of very low traces of contaminants, allowing the spectroscopic detection at subpicogram level. Actually, aromatic nitroderivatives could be identified by means of SERS spectroscopy when adsorbed on silver nanoparticles, as demonstrated in the literature⁷⁻¹¹ by observing strong enhancements of their Raman bands. In this work we propose the employment of

SERS platforms constituted by silver nanoparticles embedded into a polymeric matrix for identifying traces of 4-nitrophenol and 4-nitroaniline in waters.

2. Experimental

Polydimethylsiloxane (PDMS) elastomer kits (Sylgard 184, Dow Corning) and silver benzoate (Sigma-Aldrich) were used as received. The kit contains the elastomer (PDMS) and the curing agent which is composed of dimethyl, methylhydrogen siloxane, dimethyl siloxane, dimethylvinylated, and trimethylated silica, tetramethyl-tetravinyl cyclotetrasiloxane, and ethyl benzene. 4-nitrophenol (PNP) and 4-nitroaniline (PNA) (Sigma-Aldrich) were analytical grade, and the solutions were prepared with high-purity water from a Milli-QPLUS ultrapure water system.

A SERS-active substrate was prepared according to the procedure of Goyal¹², constituted by a polymer matrix with embedded Ag nanoparticles (Ag-PDMS). Elastomer (8 g) was mixed thoroughly with the curing agent in the weight ratio of 10:1 and then degassed under vacuum to remove entrapped air bubbles. Silver benzoate (3 ml, 5×10^{-3} M solution in hexane) was added to the polymer and sonicated for 15 min to obtain a homogeneous mixture. Subsequently, the color of the mixture changed to brown. It was then casted on glass slides and cured under vacuum at room temperature.

UV-vis absorption spectra of Ag-PDMS were obtained in the 200–800 nm region by using a Cary 5 Varian spectrophotometer.

Macro-Raman spectra were performed by using a Jobin-Yvon HG-2S monochromator, a cooled RCA-C31034A photomultiplier, and the 514.5 nm exciting line supplied by an Ar⁺ laser with a power of 50 mW. A defocused laser beam and a rotating device were adopted to impair thermal effects. Micro-Raman spectra were measured by a Renishaw RM2000 instrument, equipped with an Ar⁺ laser emitting at 514.5 nm. Sample irradiation was accomplished by using the 50x microscope objective of a Leica Microscope DMLM. The backscattered Raman signal was fed into the monochromator through 40 μ m slits and detected by an air-cooled CCD (2.5 cm^{-1} per pixel) filtered by a double holographic Notch filters system. Spectra were calibrated with respect to a silicon wafer at 520 cm^{-1} .

3. Spectroscopic characterization of the Ag-PDMS substrate

The Ag-PDMS substrate has been characterized by UV-visible absorption and Raman spectroscopy (**Fig. 1** and **Fig. 2**, respectively). The occurrence of a surface plasmon resonance band around 400 nm indicates the formation of silver nanoparticles embedded in the polymeric matrix. The absorbance center moves from 410 nm to 428 nm (**Fig. 1**), by increasing the content of silver

benzoate and, consequently, the density of the silver nanoparticles. PDMS and silver benzoate have several strong Raman bands. The primary step of the SERS applications with Ag-PDMS is to recognize and eliminate the Raman bands of both polymer and benzoate. As shown in **Fig. 2**, strong and sharp bands occur around 1000 and 1600 cm^{-1} , due to the ring vibrations of benzoate, intensified by the SERS effect promoted by the silver nanoparticles.

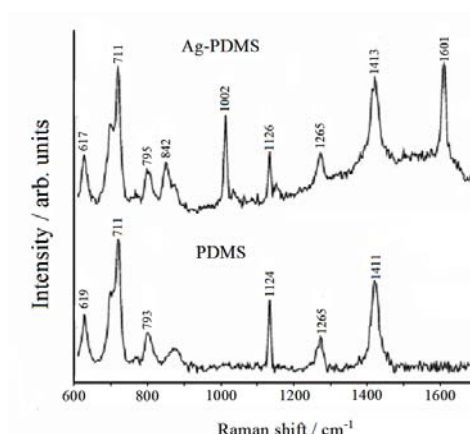
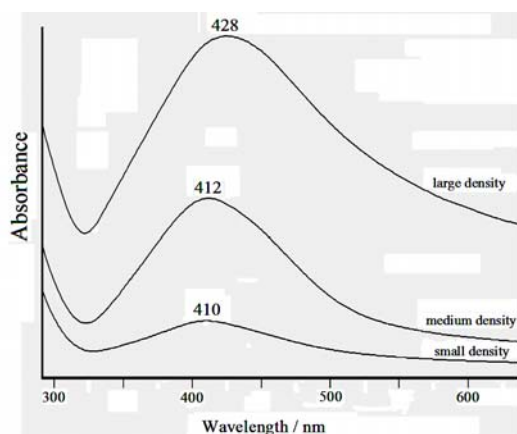


Fig. 1 – UV-vis extinction of Ag-PDMS samples with different metal density.

Fig. 2 – Raman spectra of PDMS and Ag-PDMS. Excitation: 514.5 nm.

4. SERS Spectra of PNP and PNA

4-Nitrophenol (PNP) and 4-nitroaniline (PNA) are nitroaromatic compounds that are toxic by ingestion, inhalation and absorption, with cumulative effects. No tolerability limit in potable water is known and, consequently, no detection limit can be fixed. They exhibit sizeable solubilities in water (PNP: 3.2 g/L, pH 5-6; 5.0 g/L, pH 7; PNA: 1.9 g/L, pH 5-7; Temp: 25°C). Hence, they represent potential pollutants of the aqueous environment, both wastewaters and aquifers, and consequently of the soil, if wetted by contaminated waters. PNP and PNA have polar groups (hydroxyl and amino group, respectively) that can strongly interact with PDMS, as shown in **Fig. 3**, leaving the nitrogroups free to interact with the Ag nanoparticles embedded in the polymer matrix. Hence both compounds can be adsorbed on the Ag/polymer substrate and easily detected by SERS effect by simply depositing drops of aqueous solution on the polymer surface and drying them at room temperature.

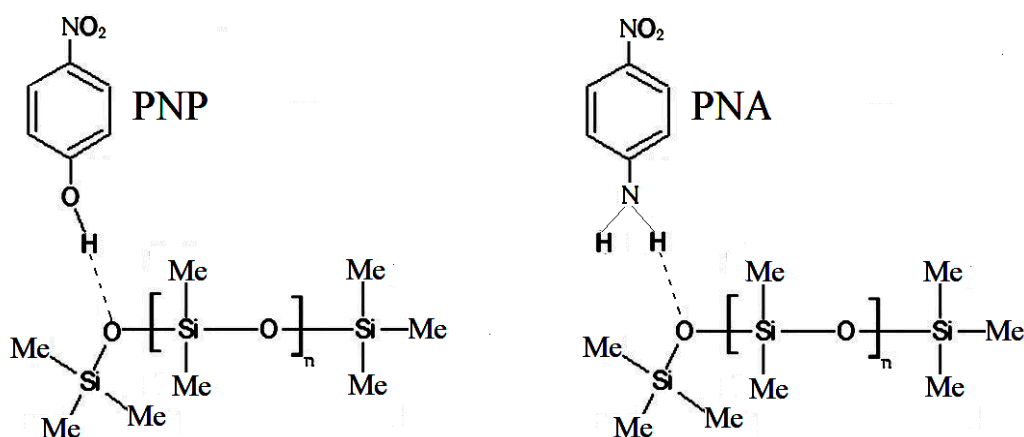


Fig. 3 – Interaction scheme of PNP and PNA with PDMS.

In addition, both compounds show a very strong Raman band in the 1300-1350 cm^{-1} region (see Fig. 4), due to the symmetric stretching mode of the nitrogroup, where no band of benzoate and polysiloxane, as constituents of the polymer matrix, occurs (see Fig. 2). Consequently, the presence of these aromatic derivatives can be clearly evidenced by the occurrence of the marker band of the nitrogroup, as shown in Fig. 5.

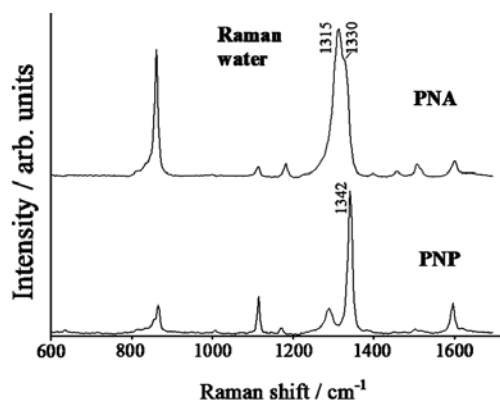


Fig. 4 – Raman spectra of PNP and PNA in aqueous solutions. Excitation: 514.5 nm.

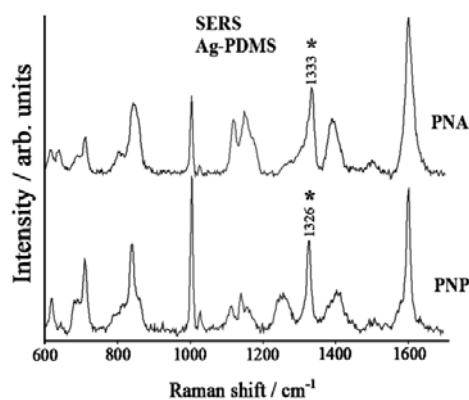


Fig. 5 – SERS spectra of PNP of Ag-PDMS with PNP and PNA. Excitation: 514.5 nm.

To obtain the SERS spectra of Fig. 5, it has been sufficient to deposit drops of much diluted solution of PNP or PNA on the polymer surface. The ligand molecules result strongly bound to the Ag-PDMS matrix, because the SERS spectra can be observed without loss of intensity after long washing in running solvent. Finally, the Raman signal of Ag-PDMS can be subtracted to the observed SERS spectra, obtaining the difference spectra reported in Fig. 6 and Fig. 7 for adsorbed PNP and

PNA, respectively. The SERS spectra closely correspond to those reported in the literature for both compounds adsorbed on silver colloidal particles^{11,13,14}, when nitrogroups interact with the metal surface. By employing a rotating device for the sample and defocalized laser beam, SERS spectra can be obtained without the occurrence of spurious bands due to thermal effects. As shown in these figures, the Limit of Detection (LOD) for these compounds can reach 10^{-7} M concentrations or less; consequently, this procedure can be considered a sensitive method for detecting these pollutants in waters or in soil, if wetted by contaminated waters. The SERS sensitivity could be further increased by shifting the Raman excitation wavelength to the maximum of the plasmon resonance band of the Ag nanoparticles. Actually, this could be obtained by using exciting lines as those at 457.9 nm and 488.0 nm, as furnished by an Ar⁺ laser, instead of that at 514.5 nm. In addition, the Raman intensity is expected to increase by using shorter wavelength radiations, due to the λ^{-4} dependence of the scattering intensities.

Finally, this procedure is not only able to reveal the presence of nitroderivatives in water, but also to identify specific nitrophenols and nitroanilines by the assignment of the observed SERS bands.

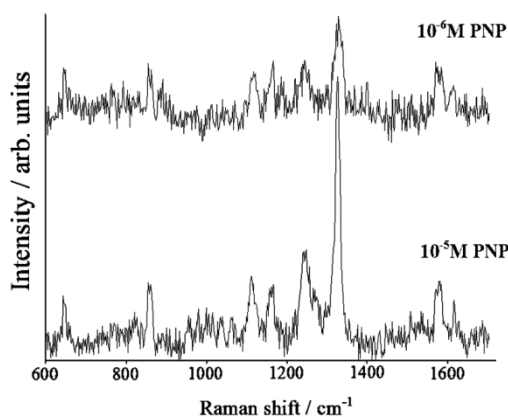


Fig. 6 – SERS spectra of PNP by subtracting Ag-PDMS. Excitation: 514.5 nm.

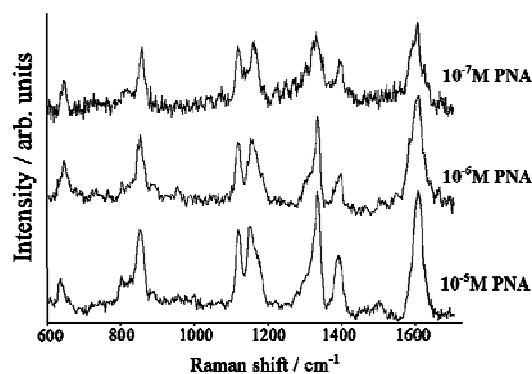


Fig. 7 – SERS spectra of PNA by subtracting Ag-PDMS. Excitation: 514.5 nm.

Similar results can be obtained by using micro-Raman apparatus and the same laser exciting line (514.5 nm). Laser beam is focused onto silver aggregates under micro Raman spectroscopy at different depths of polymer after immersing polymer in PNP solution (10^{-6} M concentration). After long washing in running water, effective spectra are achieved until 200 μ m depth from the polymer surface, demonstrating that PNP molecules are extracted from the aqueous solution and enter into the polymer matrix. The optimum spectrum with adsorbed PNP is, however, acquired at the surface of substrate (**Fig. 8**). When focus is set on deeper silver aggregates, instead, inevitable photoreaction of

benzoate occurs. As shown in **Fig. 8**, the background signal increases with the polymer depth by fluorescence emission, while instead, the marker band of benzoate around 1000 cm^{-1} strongly decreases. Moreover, large and broad bands appear in the high-frequency region, at about 1380 and 1580 cm^{-1} , due to the Raman bands of amorphous carbon produced during the laser irradiation.

5. Conclusions and discussion

We prepared SERS platforms constituted by silver nanoparticles embedded in a polymer matrix to reveal the presence of traces of nitroaromatic compounds as dangerous pollutants of flow waters, aquifers, fluvial and marine waters. The advantages of the SERS recognition of these molecules can be thus summarized:

- 1) Very high sensitivity due to the giant enhancement of the Raman signal;
- 2) Fluorescence quenching due to the molecule/metal chemical interaction;
- 3) Possibility to identify the molecular sites of interaction with metal by observing changes of band frequencies and intensities.

These properties are very important for obtaining a rapid and sensitive identification of different aromatic nitroderivatives with significant advantages in terms of time necessary for the analytical determination. The use of Ag nanoparticles embedded in PDMS results more efficient with respect to other SERS substrates, because it allows a quite sensitive detection of nitroaromatics without any sample manipulation, extraction from solvent or concentration procedures, because the pollutant molecules are capped by the polymer matrix when enter in contact with the substrate. This can be obtained by simple immersion in contaminated water or depositing drops of the aqueous sample. Moreover, contrary to usual Ag colloidal dispersions, these SERS substrates are stable in time; hence, it is not necessary to use them as freshly prepared. Finally, their preparation is quite simple and not expensive.

The occurrence of ions or organic compounds in contaminated waters could interfere in the SERS detection of nitroaromatics, but the following points are to be taken into account: (a) at the normal pH values of aquifers, the title contaminants are capped into the polymeric matrix, as shown in the paper, by chemical interaction with polysiloxane, with enhanced SERS response; (b) inorganic anions, eventually present in contaminated waters, are not expected to impair the chemical interaction of the title nitroaromatics with the polymer, because they are not specifically adsorbed on polysiloxane; (c) the SERS spectra of nitroaromatics show the occurrence of a very strong band,

attributable to nitrogroup, in the 1300-1350 cm^{-1} spectral region, where inorganic ions do not have bands and other organic compounds do not exhibit strong Raman bands.

In the future the present technique will be employed to identify the presence in water environment of other important pollutants as nitroimidazoles. They are present in drugs used for farm animals (cows, poultry and pigs), promoting genetic mutations and tumor modifications if present in aquifers, and previously were identified by different chromatographic methods¹⁵⁻¹⁷, which contemplated complex extraction procedures.

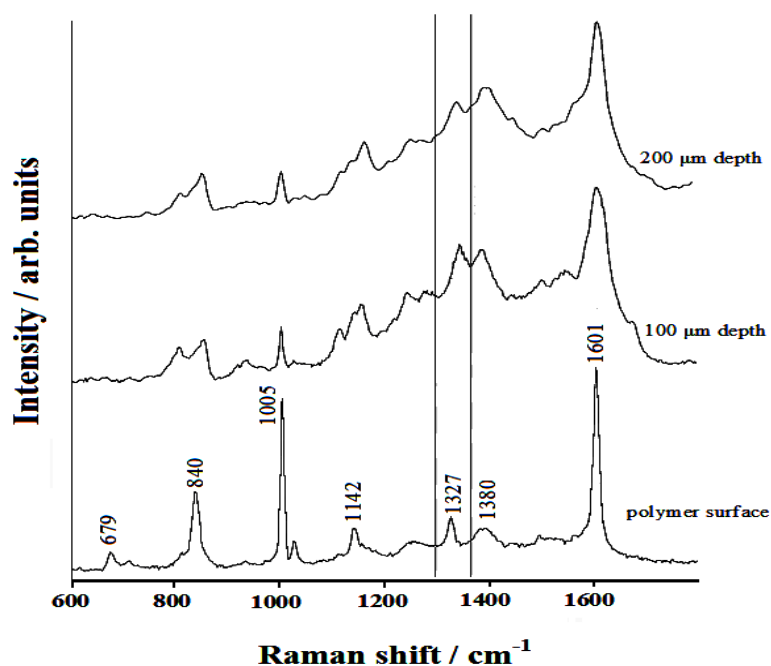


Fig. 8 – Micro-SERS spectra of Ag-PDMS with PNP. Excitation: 514.5 nm.

References

1. United States Environmental Protection Agency (US EPA). "Ambient Water Quality Criteria for Nitrophenols". Office of Water Regulations and Standards, Criteria and Standards Division. Washington, DC: EPA 440/5-80-063, 1980.
2. Agency for Toxic Substances Disease Registry (ATSDR). "Toxicological Profile for Nitrophenols: 2-Nitrophenol and 4-Nitrophenol". U.S. Department of Health and Human Services, Public Health Service. Atlanta, GA: 1992 (104 pp.).
3. D.K. Richards, W.K. Shiehs. "Biological fate of organic priority pollutants in the aquatic environment". *Water Res.* 1986. 20: 1077–1090.
4. R.C. Loehr, R. Krishnamoorthy. "Terrestrial bioaccumulation potential of phenolic compounds". *Hazard. Waste Hazard. Mater.* 1988. 5: 109–119.
5. L. Zhu, B. Lou, K. Yang, B. Chen. "Effects of ionizable organic compounds in different species on the sorption of p-nitroaniline to sediment". *Water Research* 2005. 39: 281–288.
6. S. Schlücker, editor. *Surface-Enhanced Raman Scattering: Analytical, Biophysical and Life Science Applications*. Weinheim, Germany: Wiley-VCH, 2011.

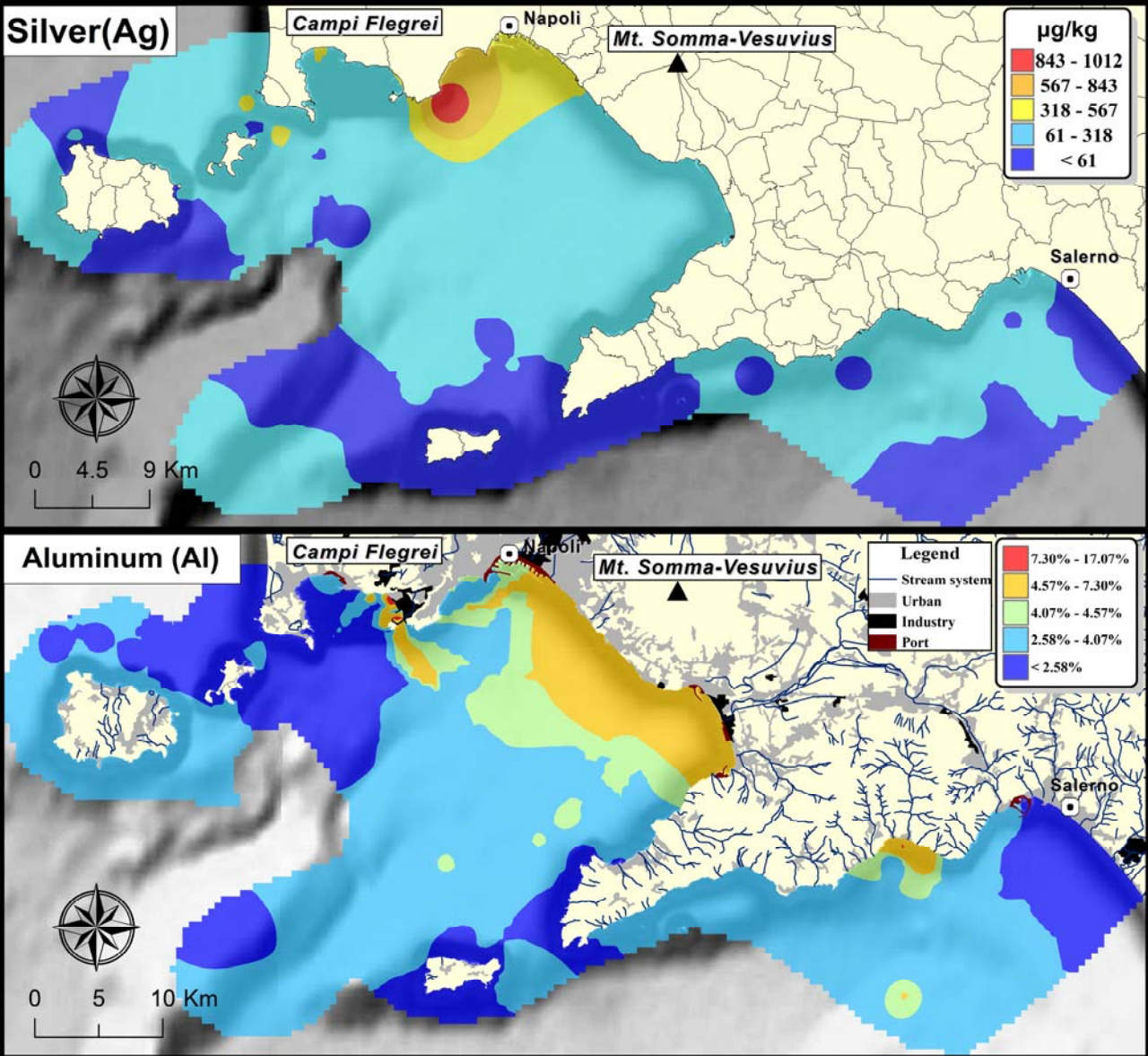
7. M. Muniz-Miranda. "SERS monitoring of the catalytic reduction of 4-nitrophenol on Ag-doped titania nanoparticles". *Appl. Catal. B: Environ.* 2013. 146: 147-150.
8. M. Muniz-Miranda, B. Pergolese, A. Bigotto. "Surface-enhanced Raman scattering and density functional theory study of 4-nitrobenzonitrile adsorbed on Ag and Ag/Pd nanoparticles". *J. Phys. Chem. C* 2008. 112: 6988-6992.
9. M. Muniz-Miranda, B. Pergolese, A. Bigotto. "SERS and DFT study of nitroarenes adsorbed on metal nanoparticles". *Vibr. Spectrosc.* 2007. 43: 97-103.
10. M. Muniz-Miranda. "Adsorption mechanism of 2-amino,5-nitropyrimidine on silver substrates, as detected by surface-enhanced Raman scattering". *Vibr. Spectrosc.* 2002. 29: 229-233.
11. M. Muniz-Miranda. "pH dependence of the surface-enhanced Raman scattering of p-nitroaniline adsorbed on silver sols". *J. Raman Spectrosc.* 1997. 28: 205-210.
12. Goyal, A. Kumar, P. K. Patra, S. Mahendra, S. Tabatabaei, P. J. J. Alvarez, G. John, P. M. Ajayan. "In situ synthesis of metal nanoparticle embedded free standing multifunctional PDMS films". *Macromol. Rapid Comm.* 2009. 30: 1116-1122.
13. T. Tanaka, A. Nakajima, A. Watanabe, T. Ohno, Y. Ozaki. "Surface-enhanced Raman scattering of pyridine and p-nitrophenol studied by density functional theory calculations". *Vibr. Spectrosc.* 2004. 34: 157-167.
14. D. A. Perry, H. J. Son, J. S. Cordova, L. G. Smith, A. S. Biris. "Adsorption analysis of nitrophenol isomers on silver nanostructures by surface-enhanced spectroscopy". *J. Coll. Interface Sci.* 2010. 342: 311-319.
15. R. Zeleny, S. Harbeck, H. Schimmel. "Validation of a liquid chromatography-tandem mass spectrometry method for the identification and quantification of 5-nitroimidazole drugs and their corresponding hydroxy metabolites in lyophilised pork meat". *J. Chromatogr. A* 2009. 1216: 249-256.
16. H-W. Sun, F-C. Wang, L-F. Ai. "Simultaneous determination of seven nitroimidazole residues in meat by using HPLC-UV detection with solid-phase extraction". *J. Chromatogr. B* 2007. 857: 296-300.
17. D. Hurtaud-Pessel, B. Delepine, M. Laurentie. "Determination of four nitroimidazole residues in poultry meat by liquid chromatography-mass spectrometry". *J. Chromatogr. A* 2000. 882: 89-98.

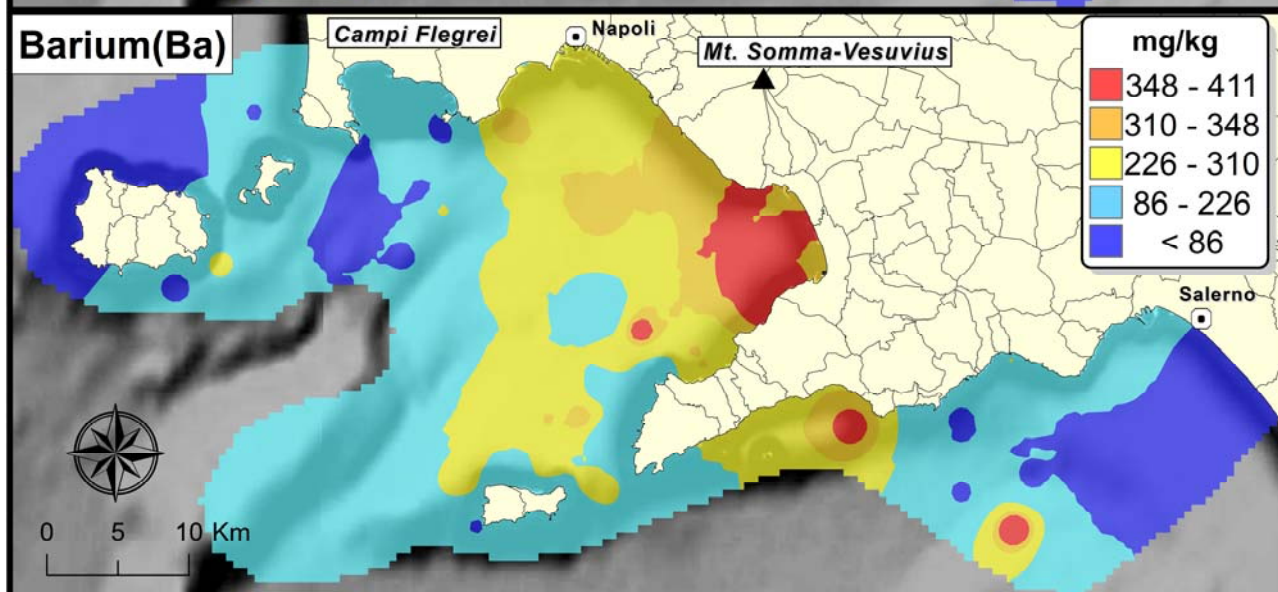
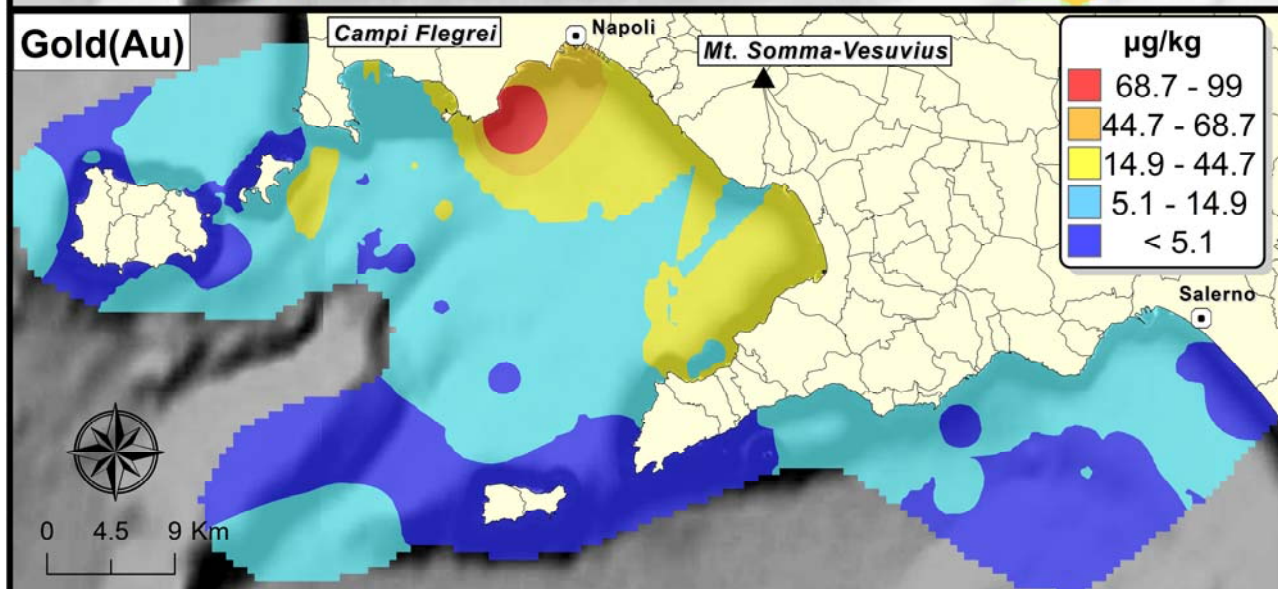
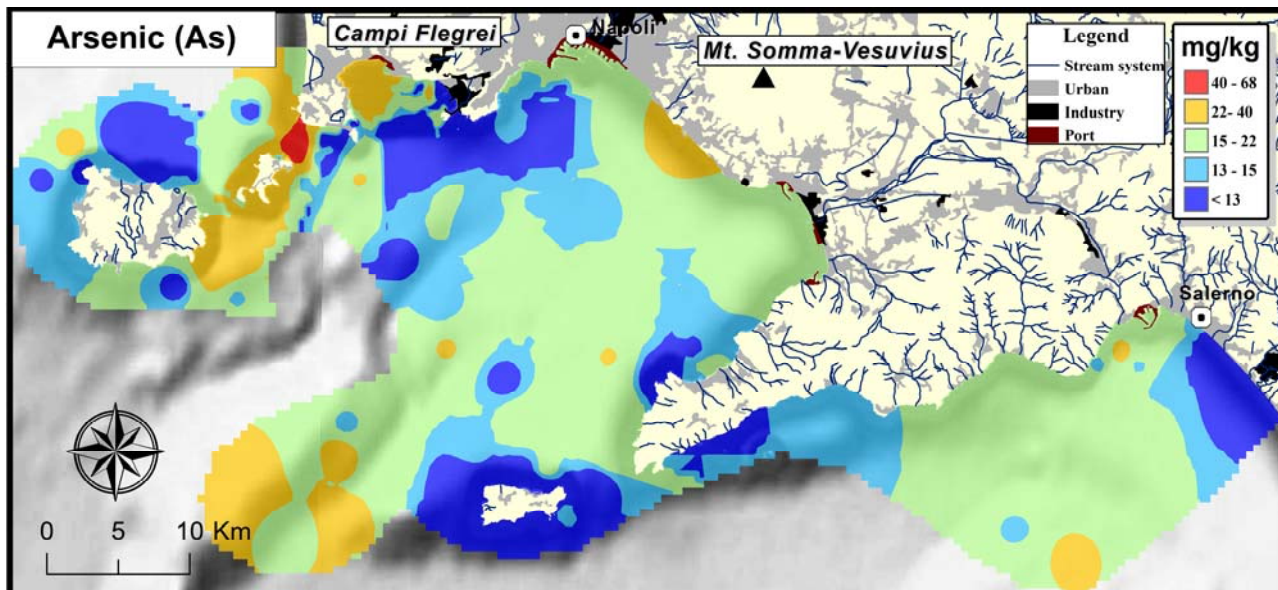
Appendix A

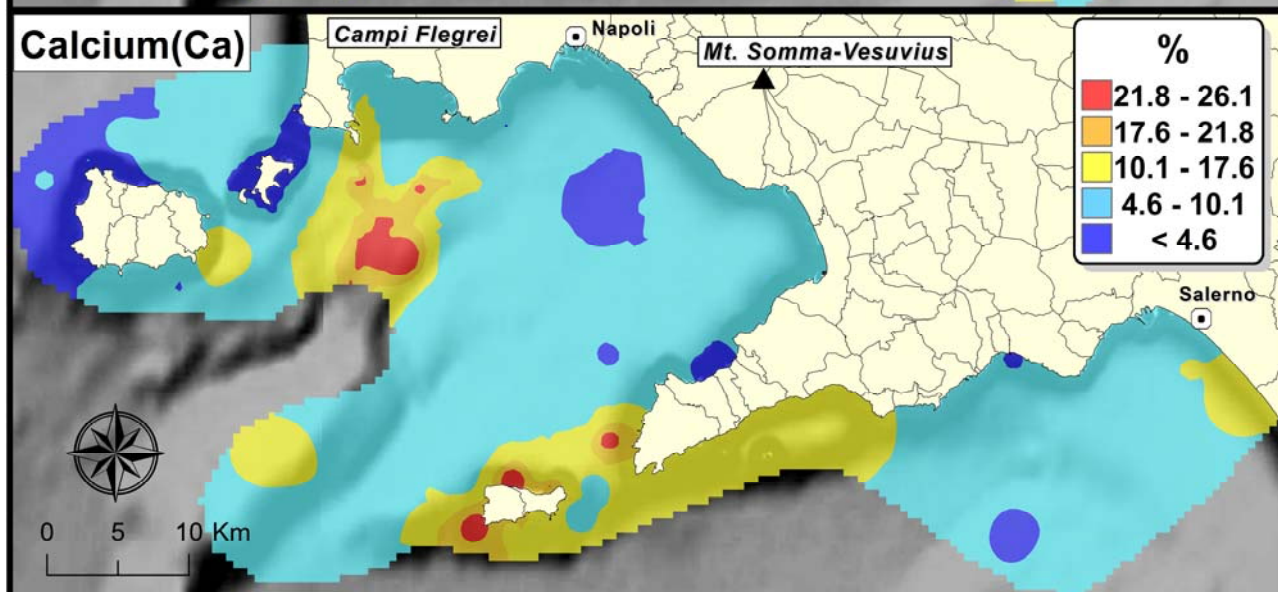
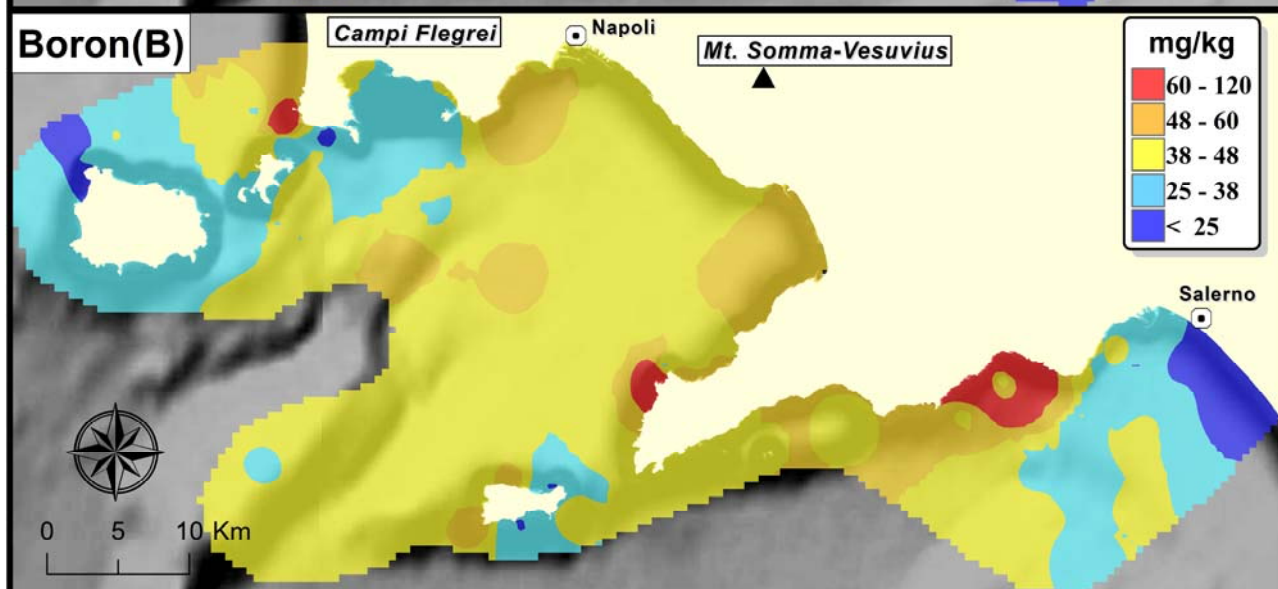
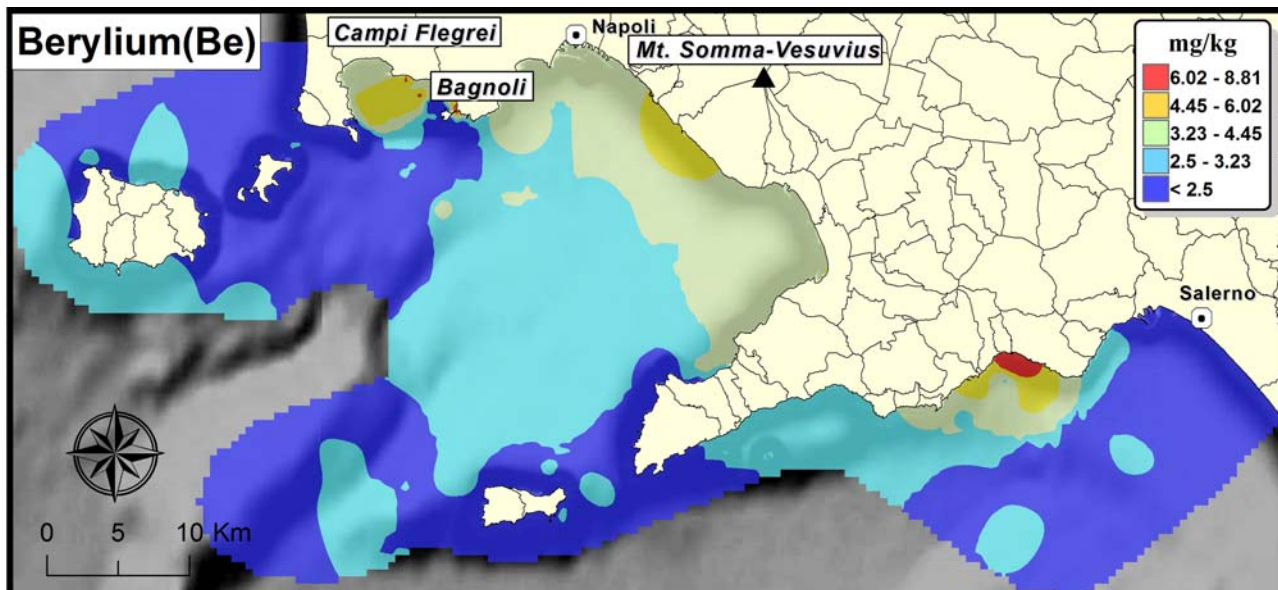
Maps of inorganic elements distribution in the Naples and Salerno Gulfs

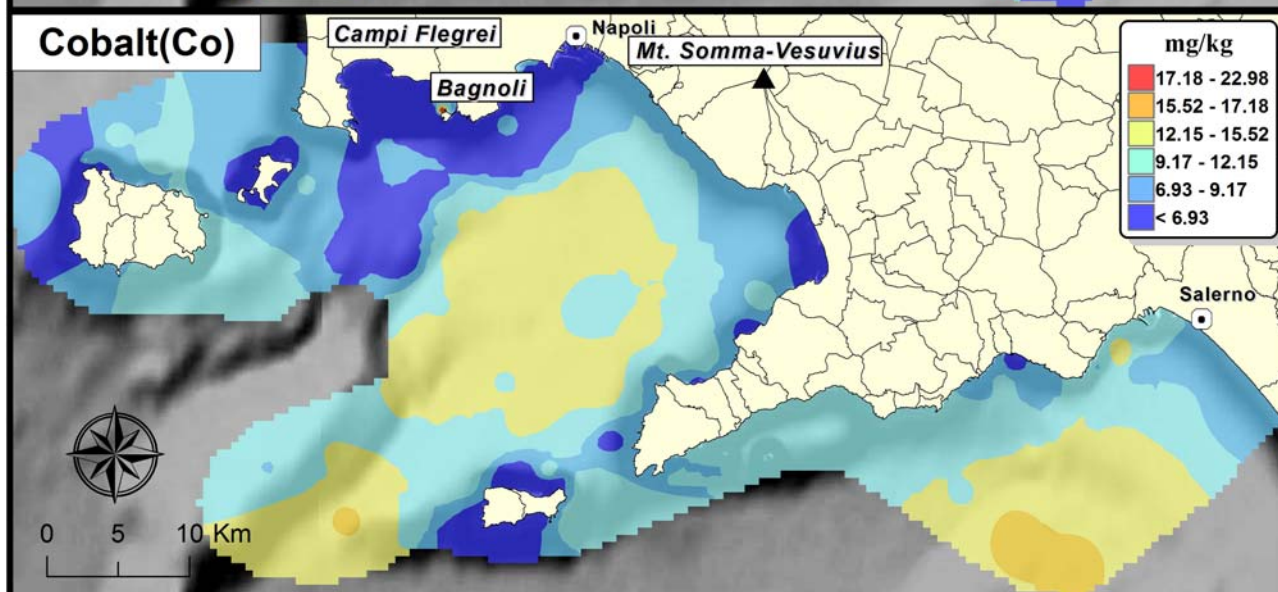
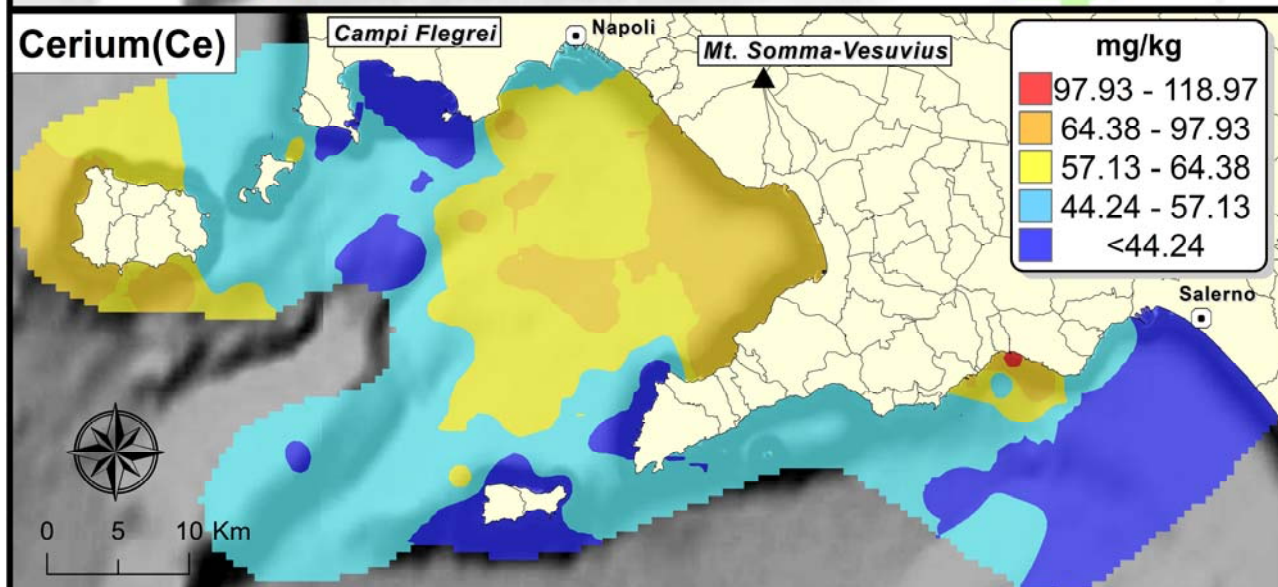
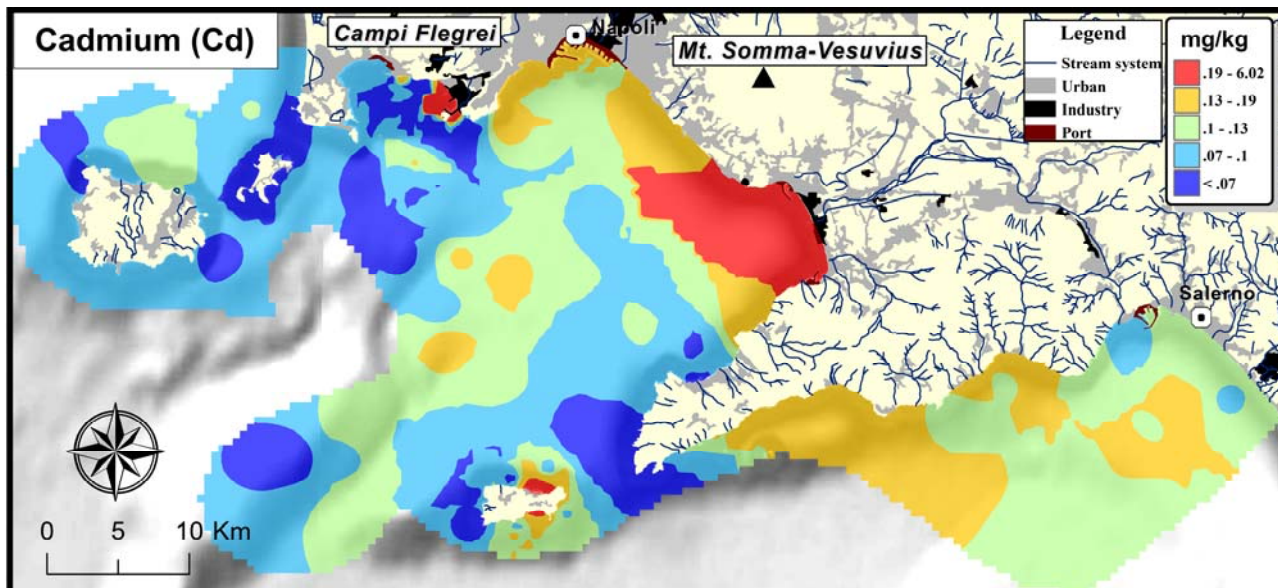
Interpolated concentration maps

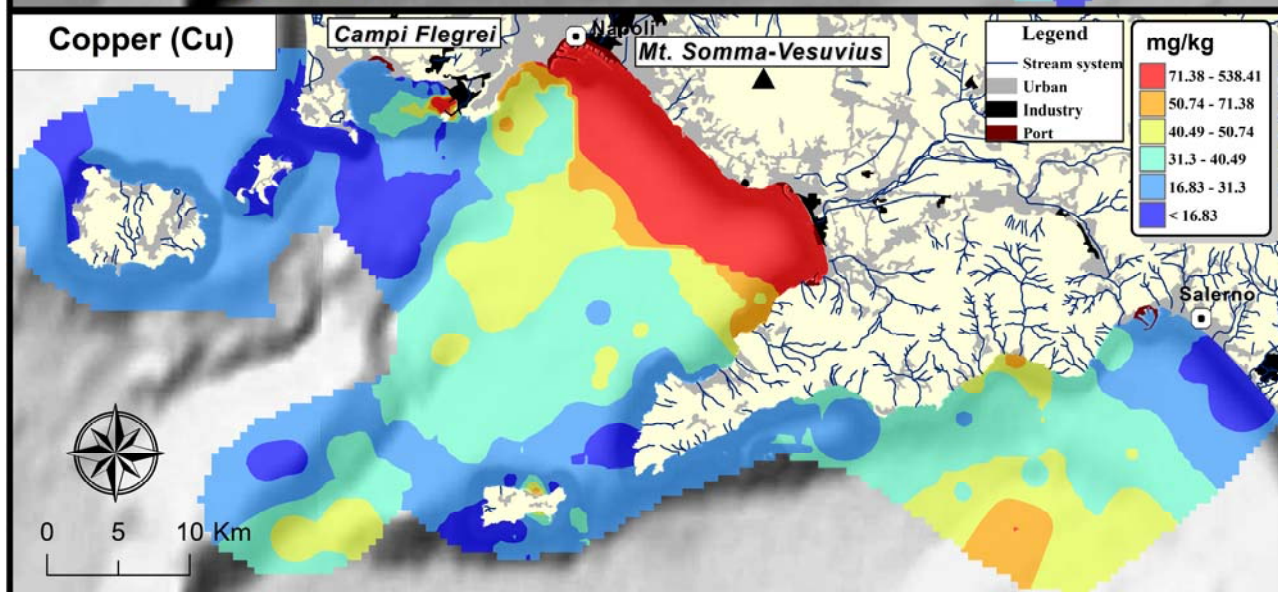
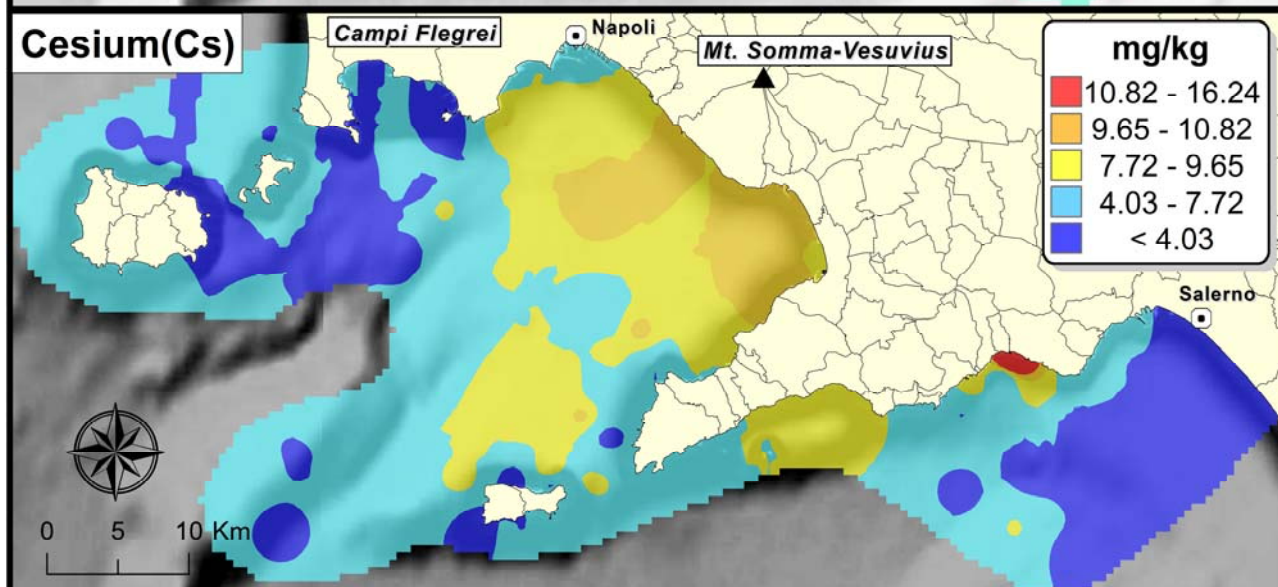
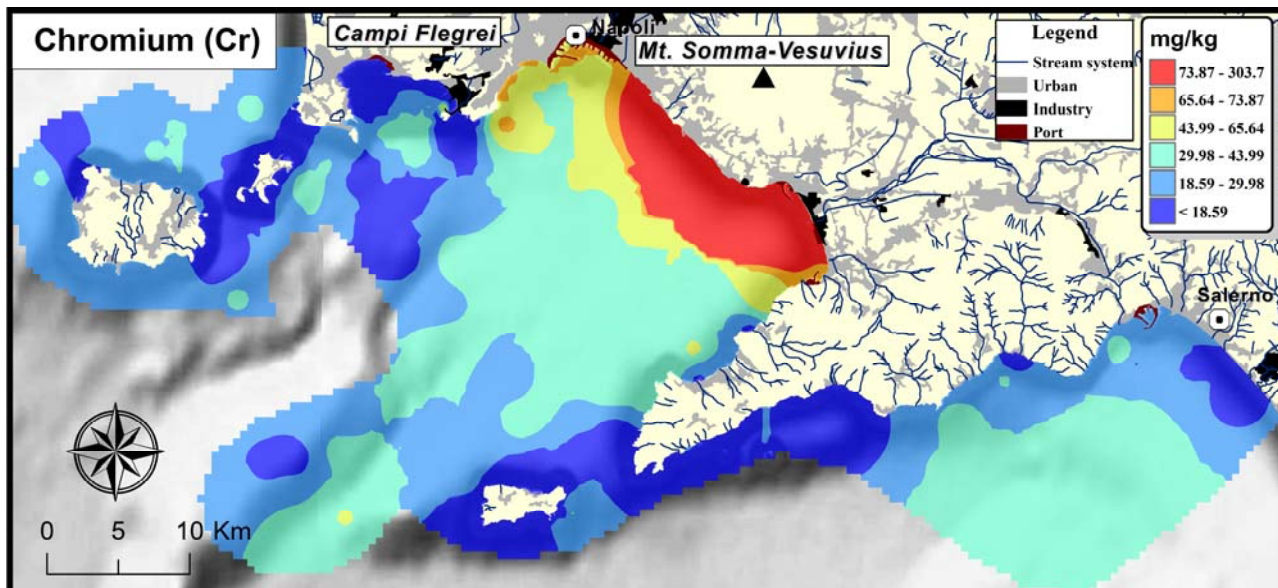
Interpolated concentration maps (page 208-223)

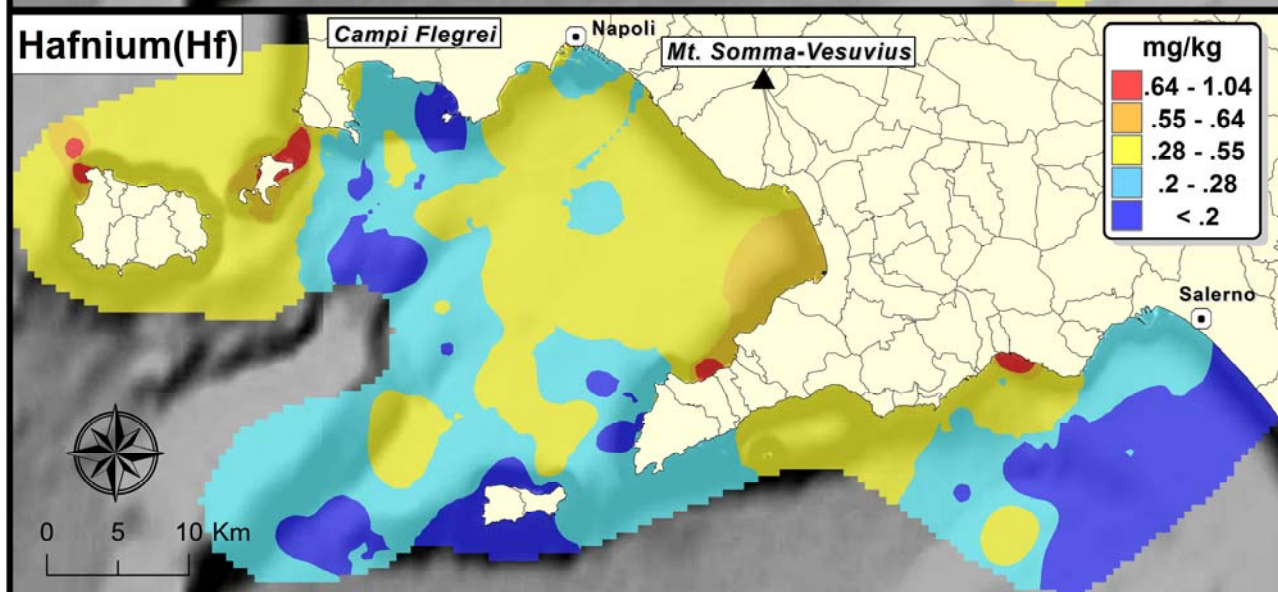
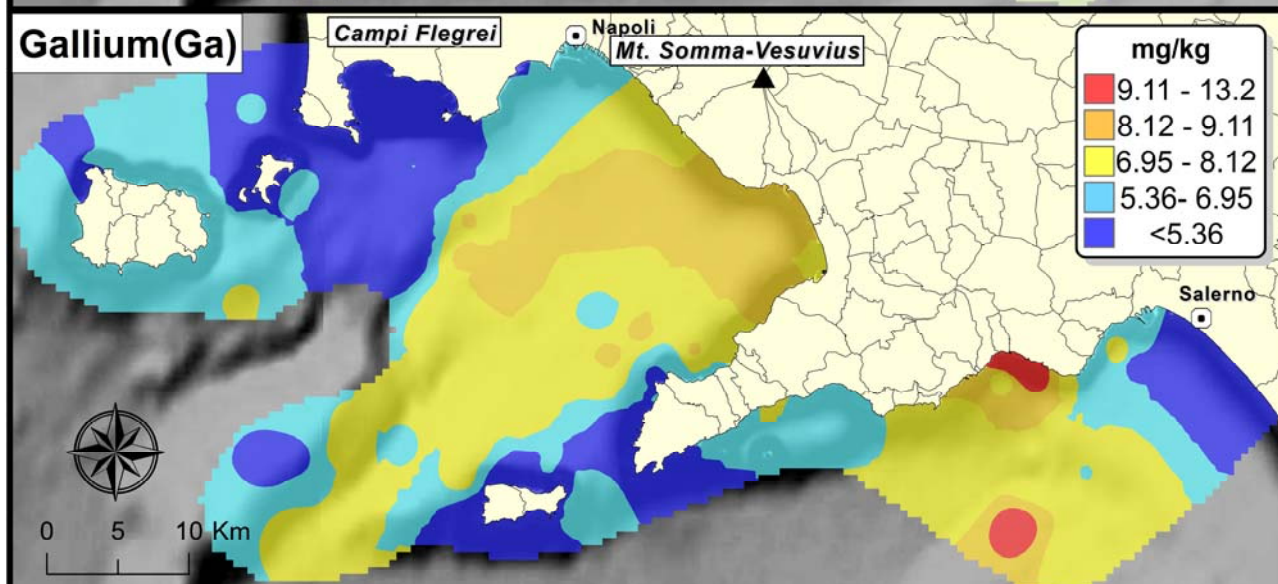
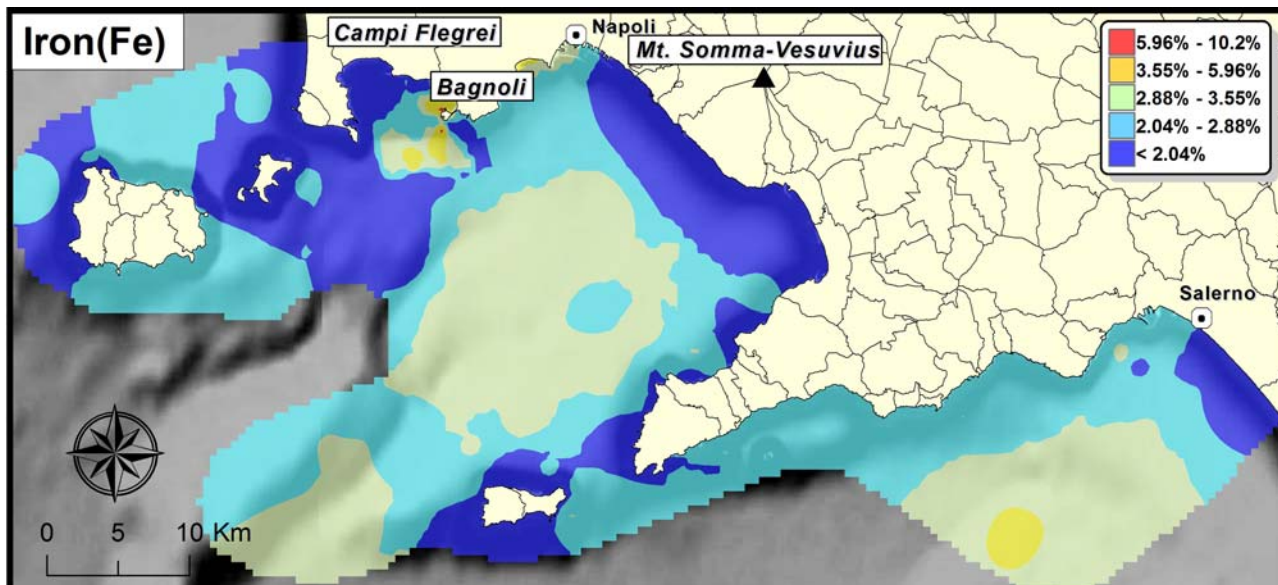


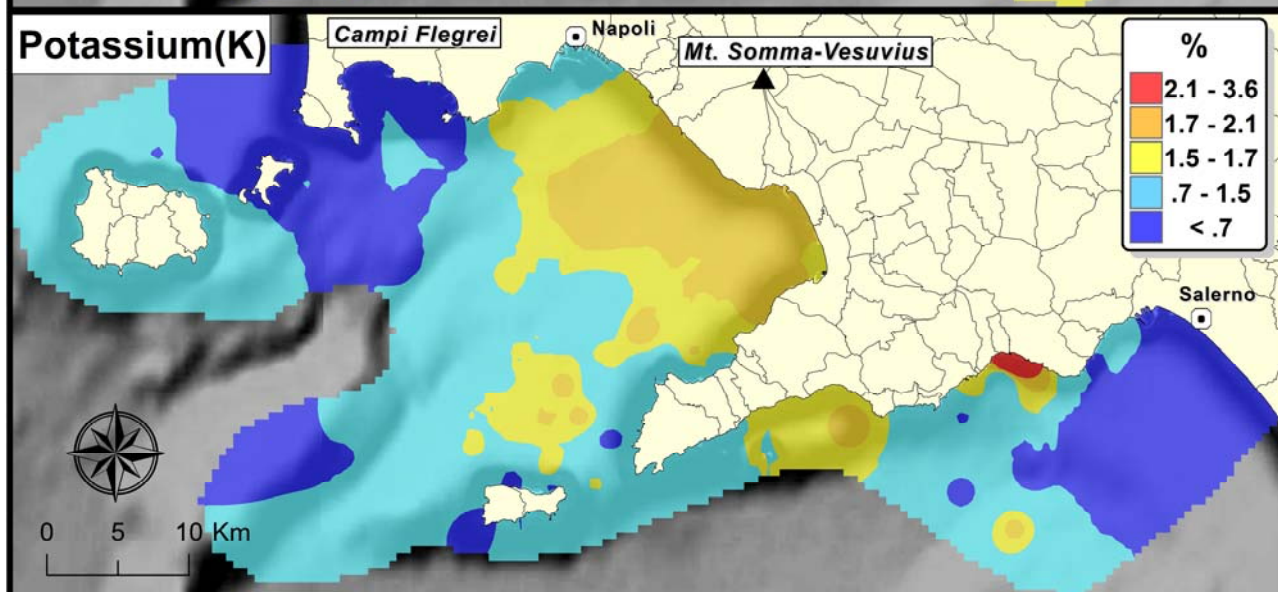
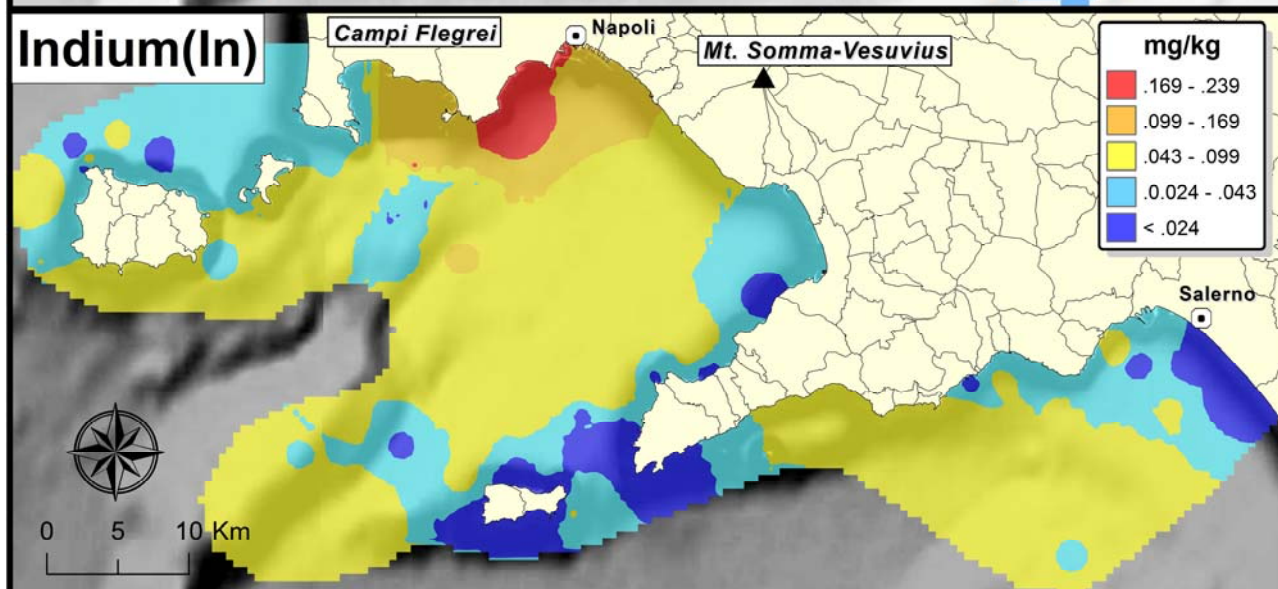
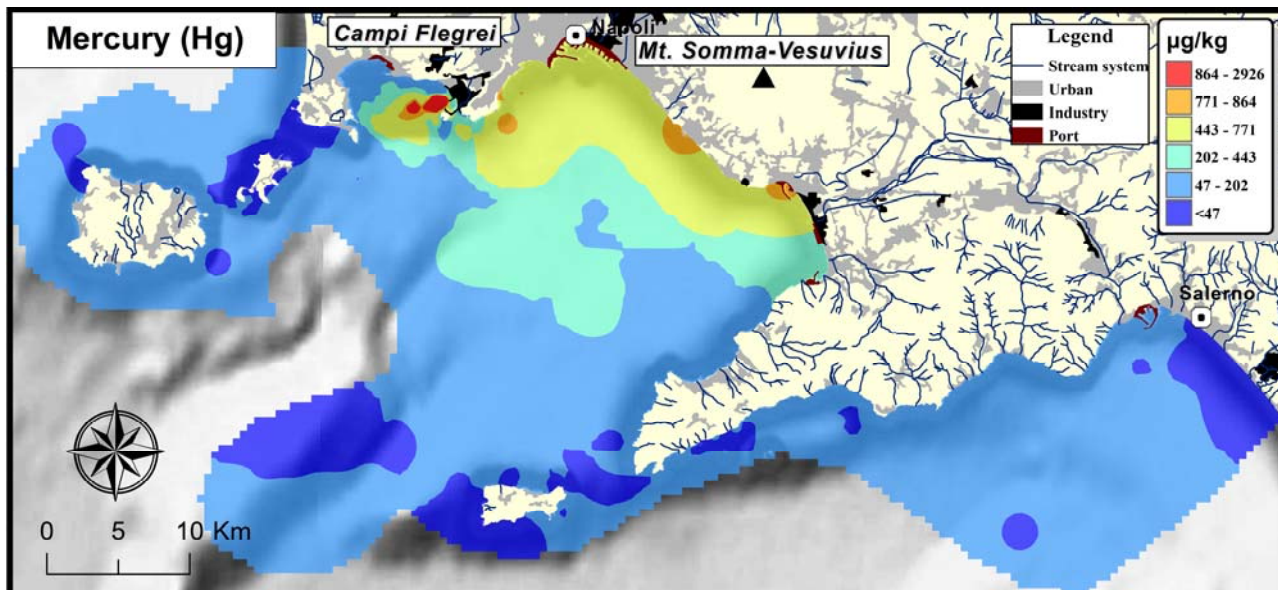


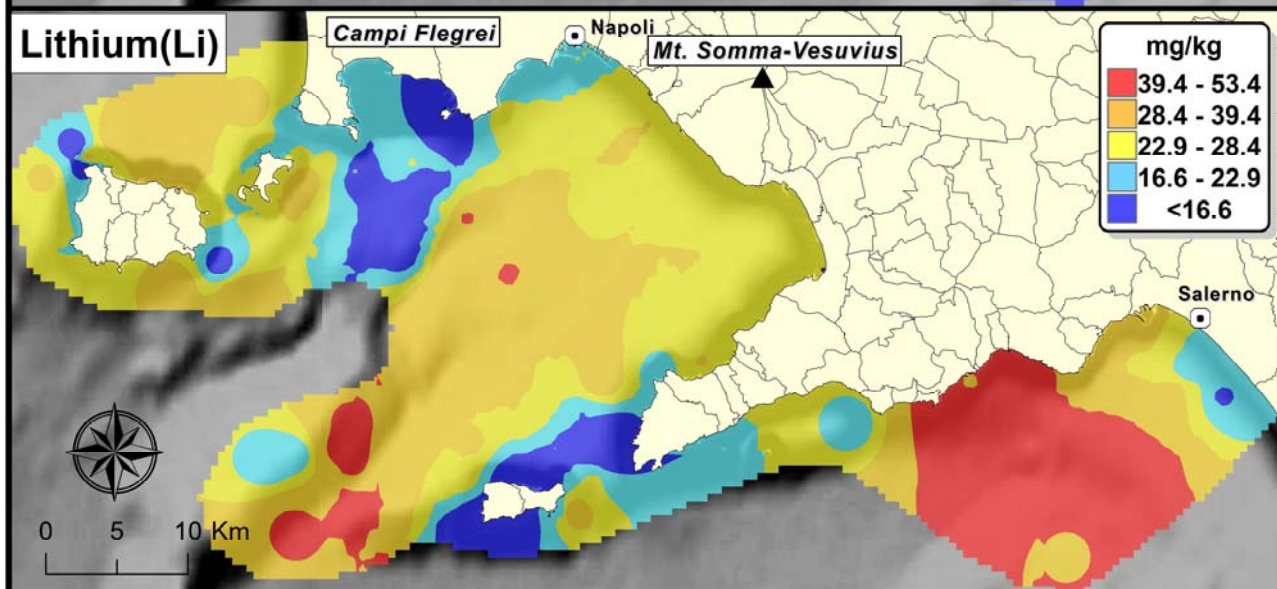
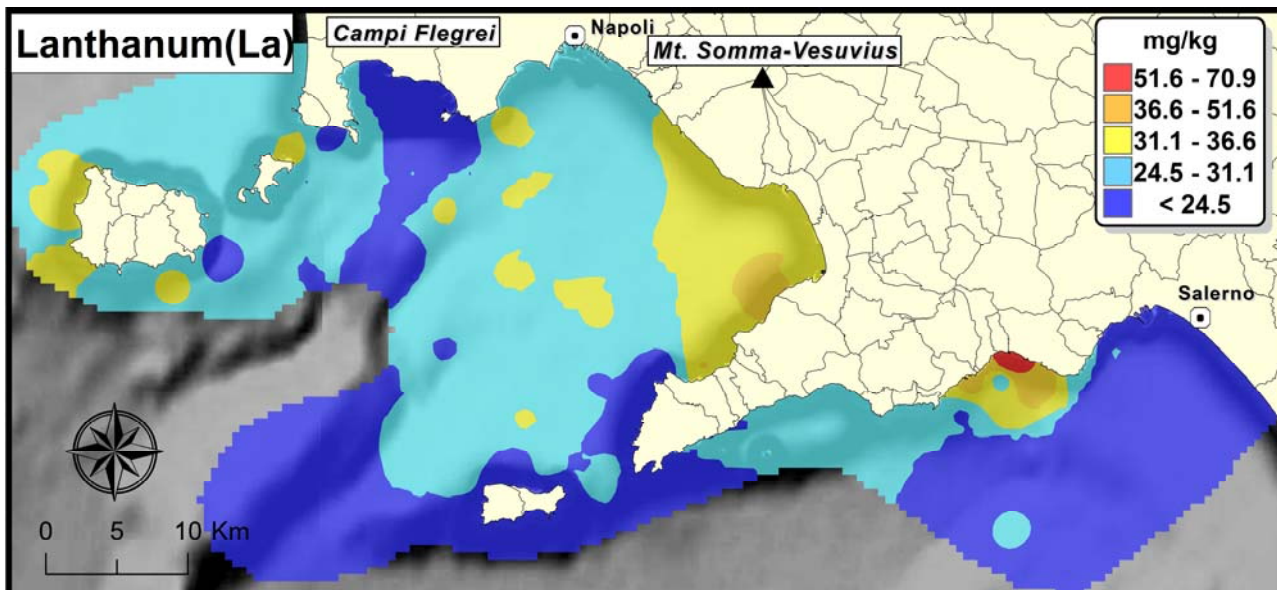


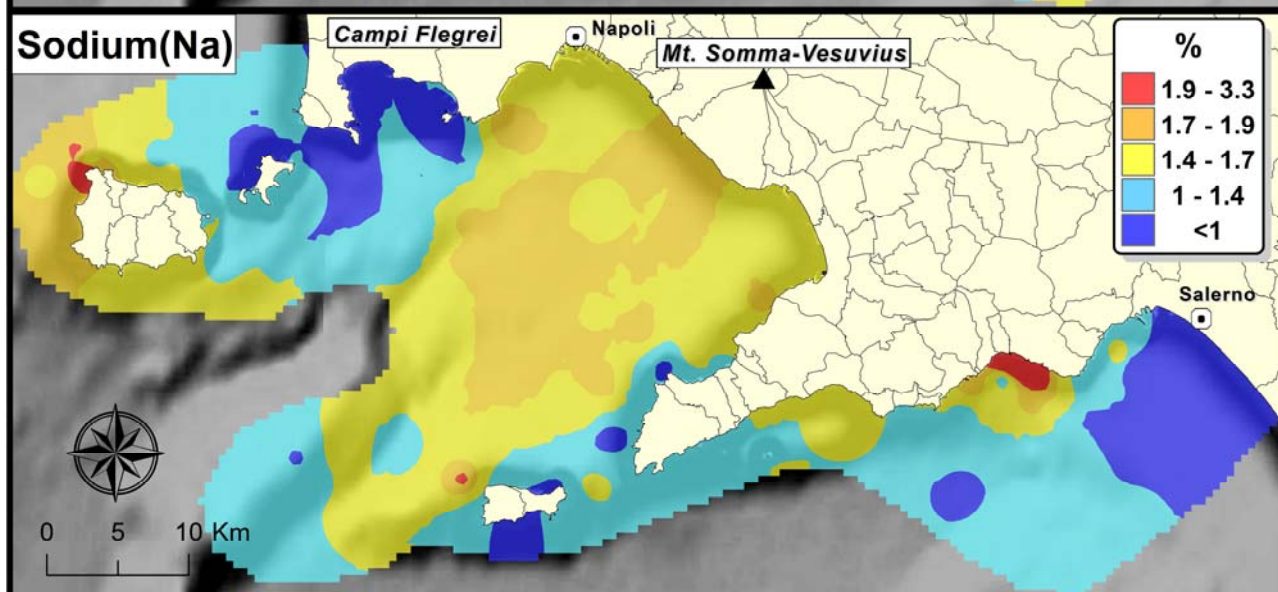
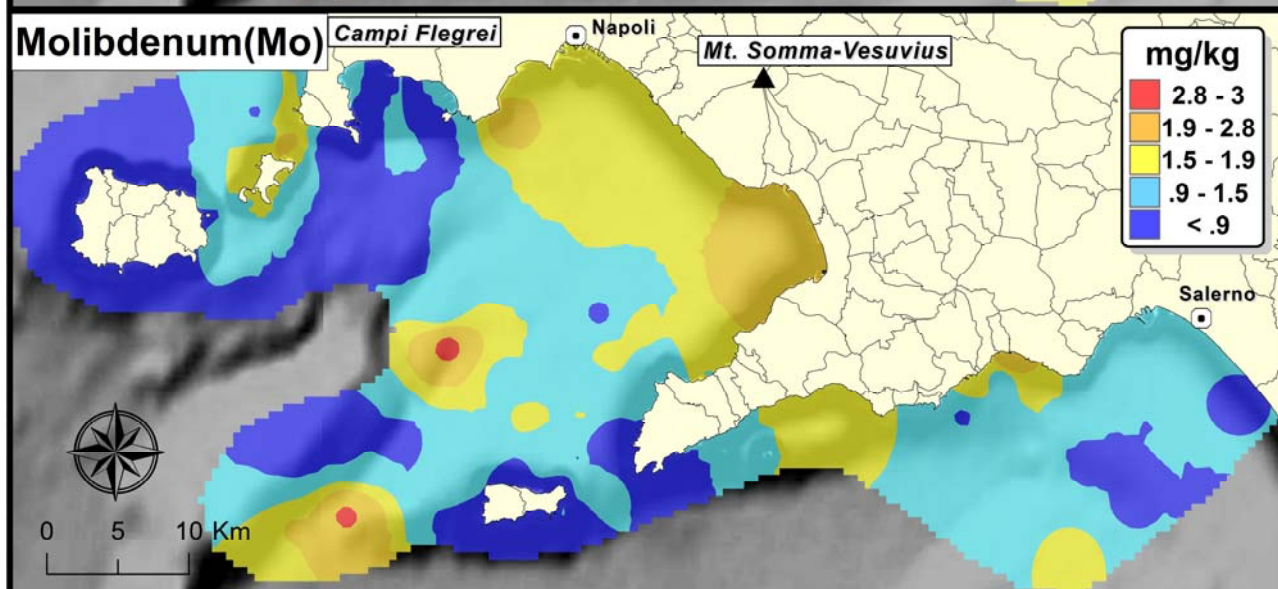
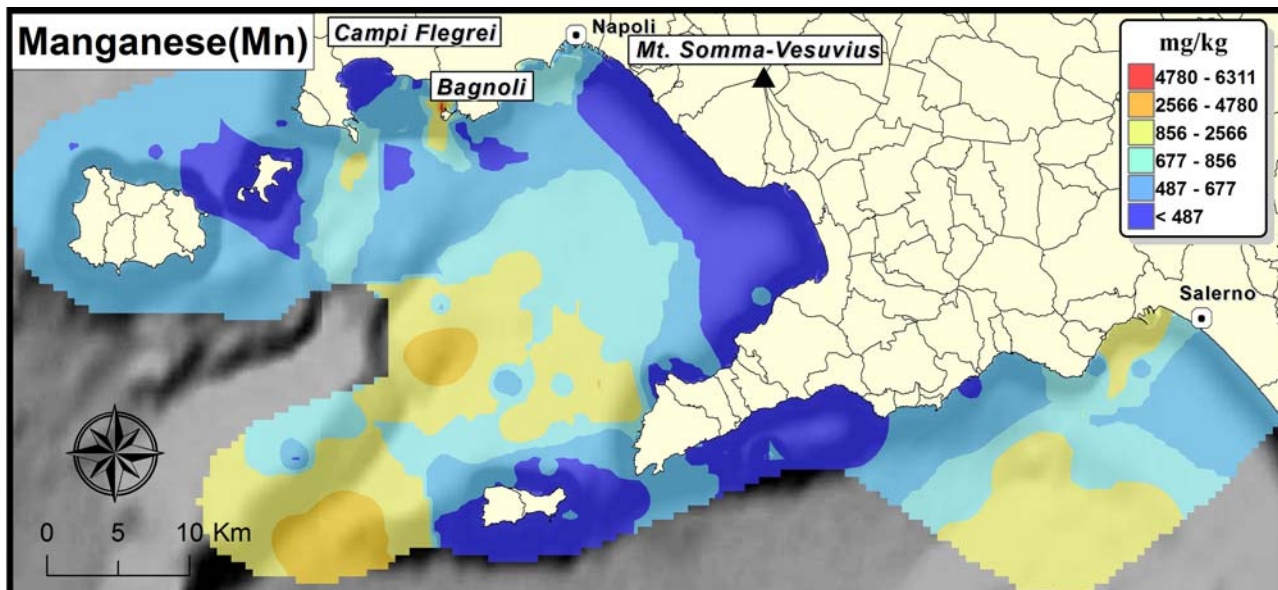


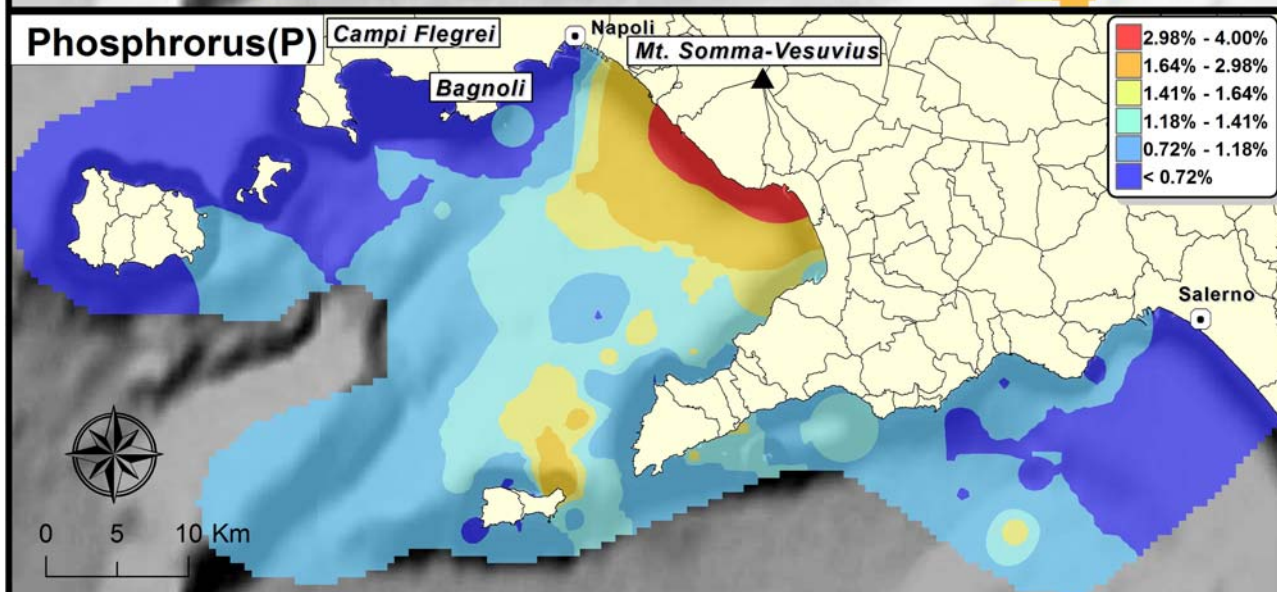
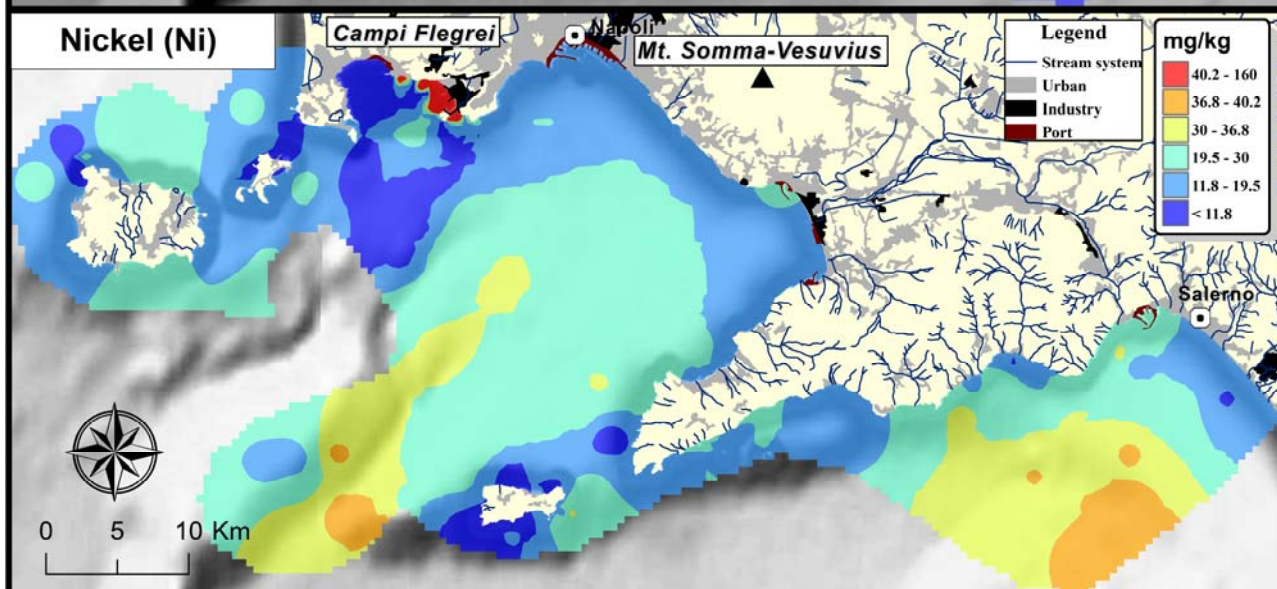
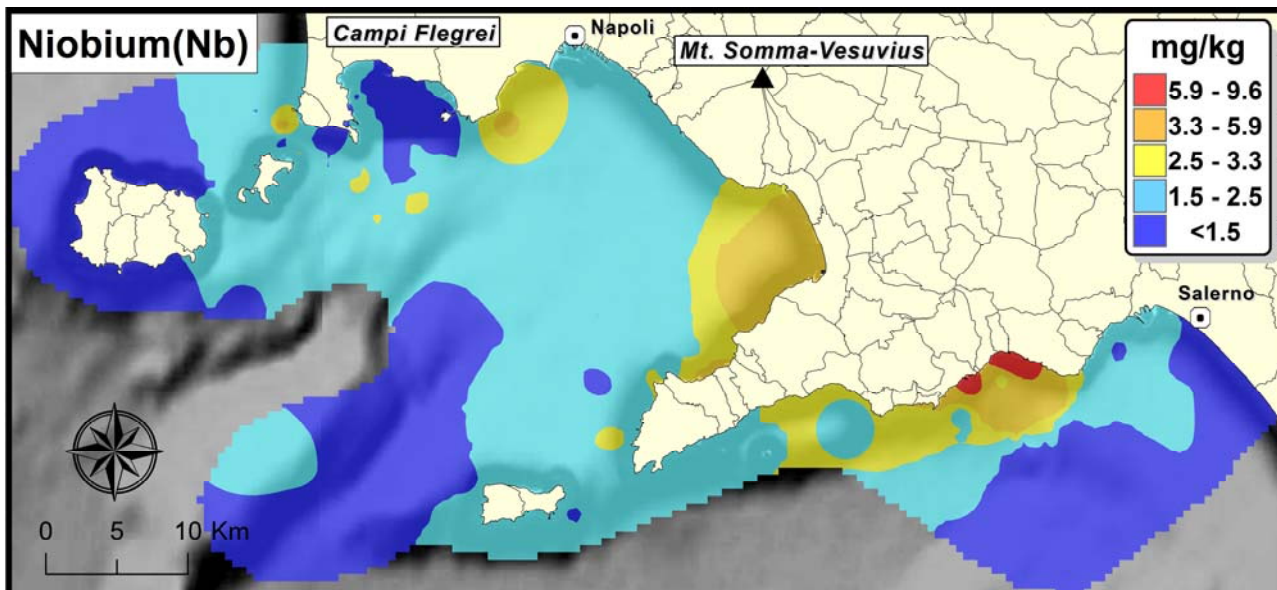


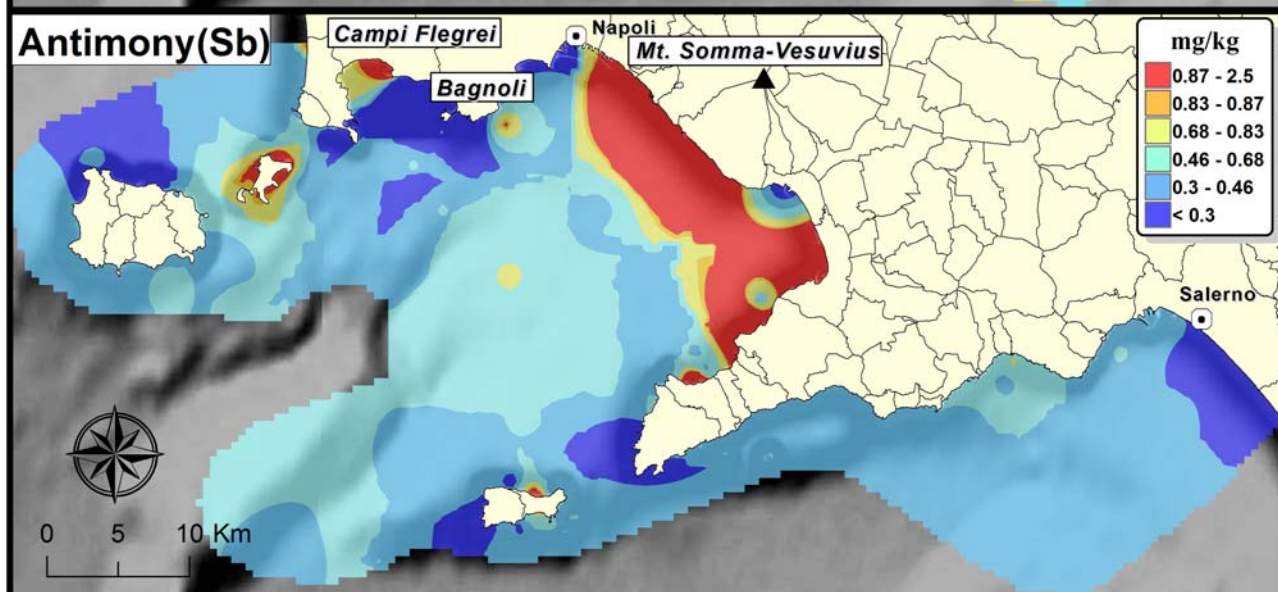
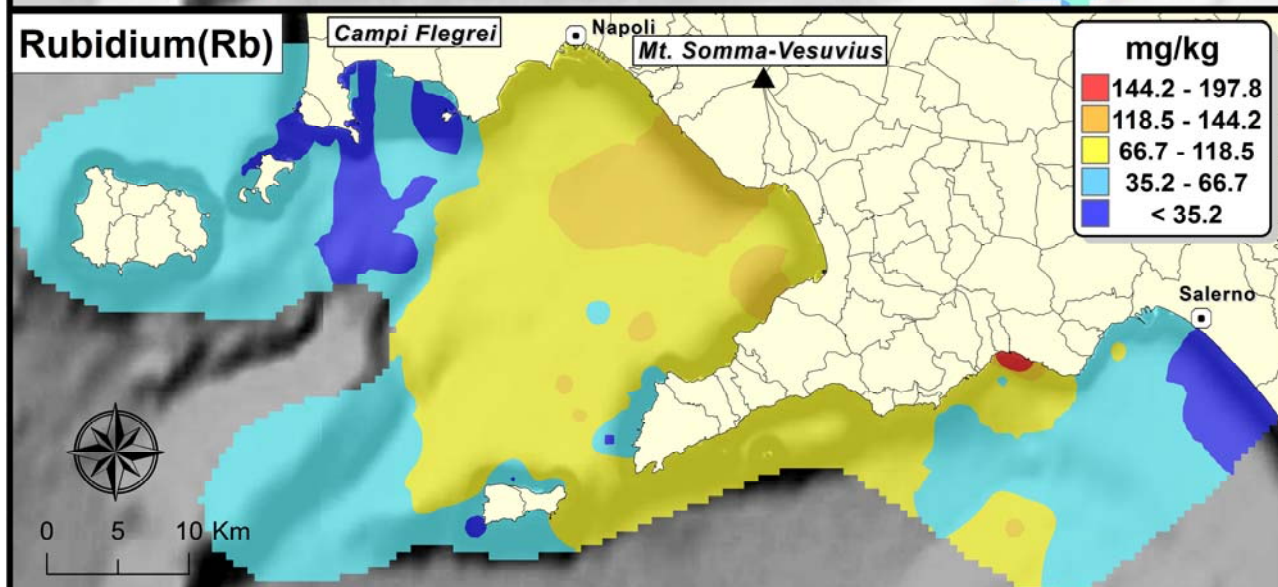
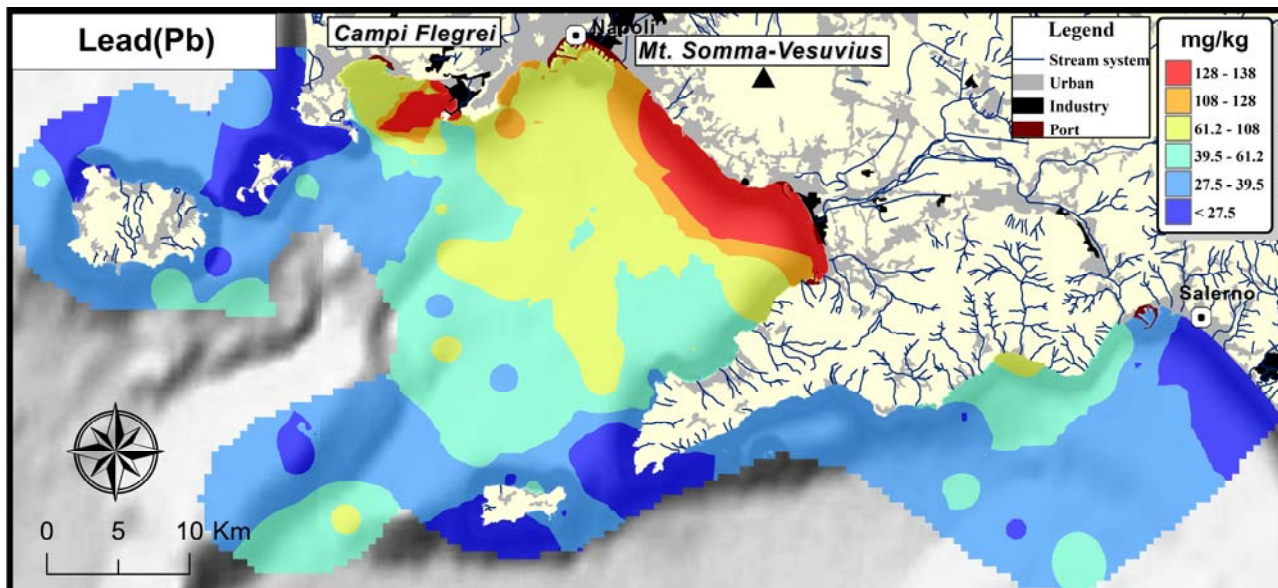


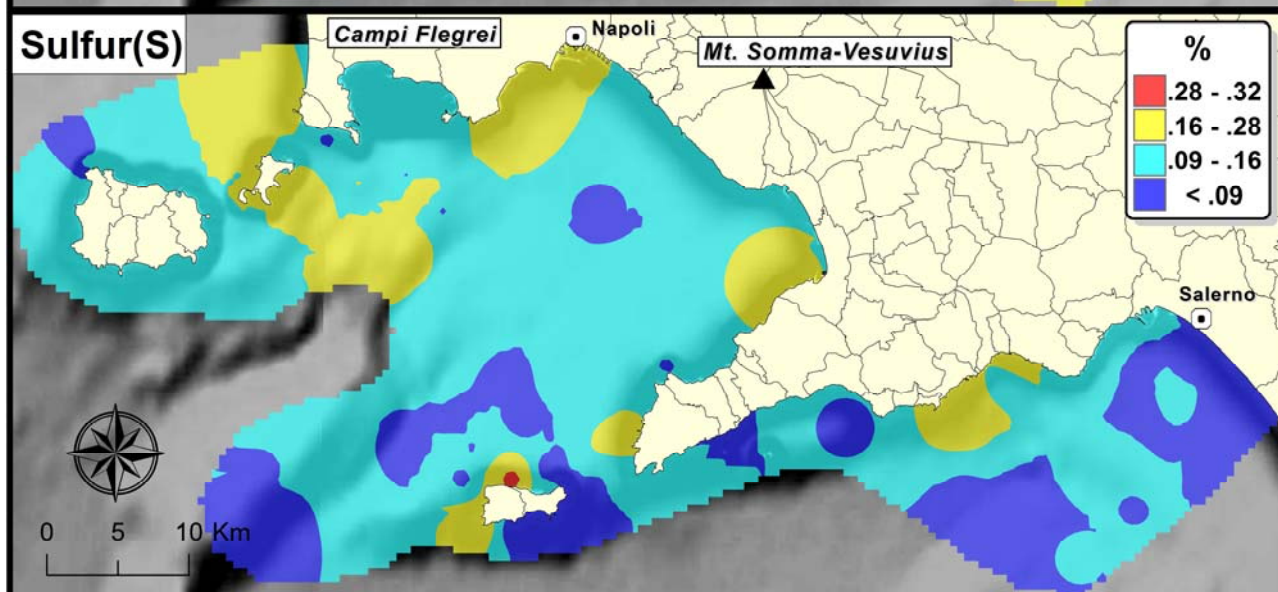
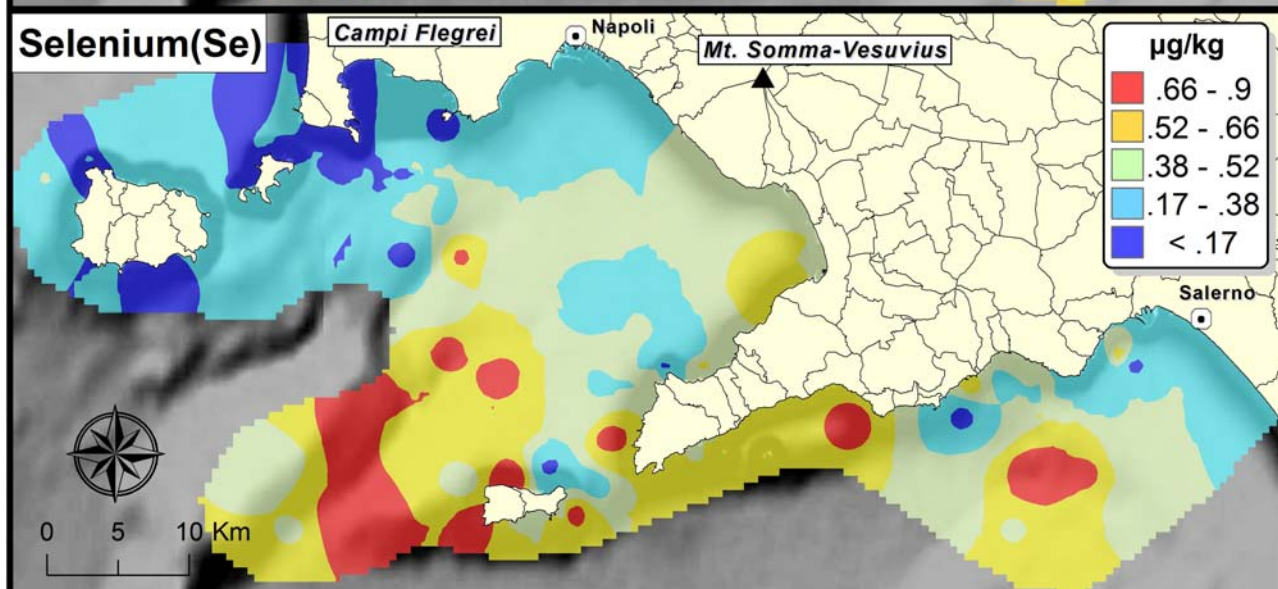
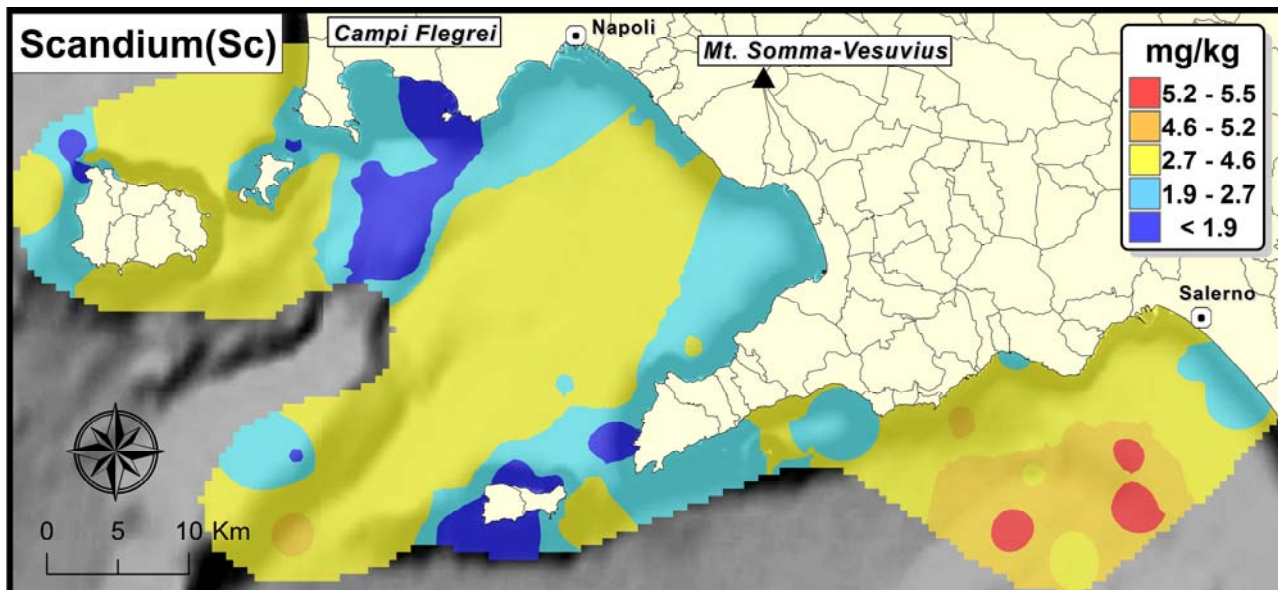


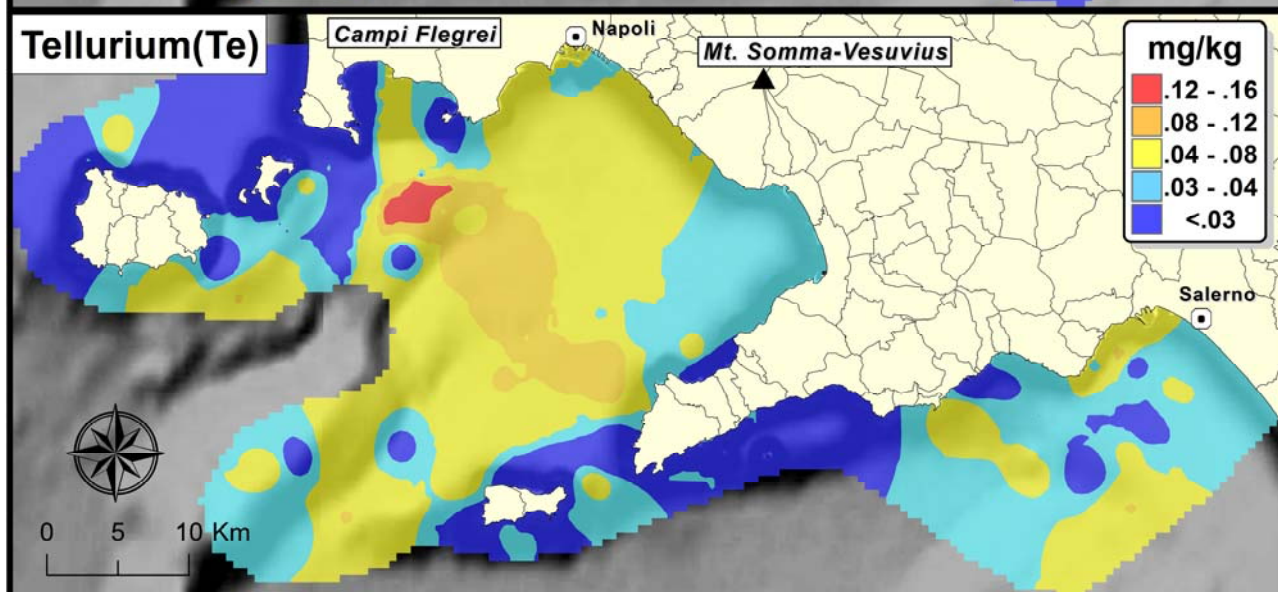
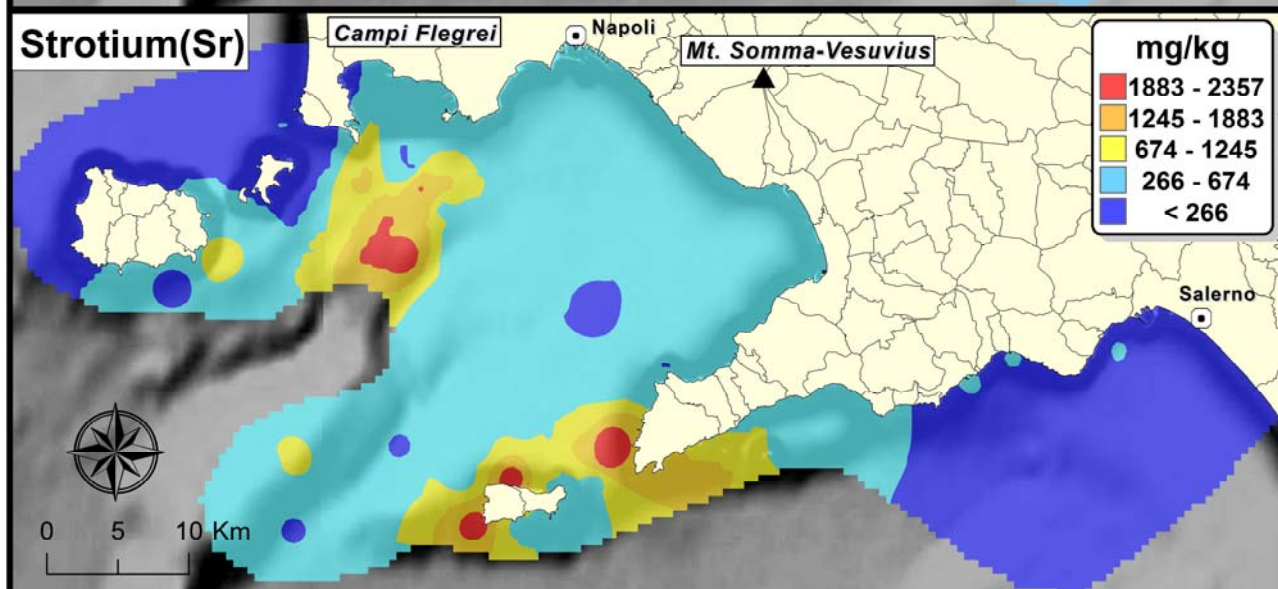
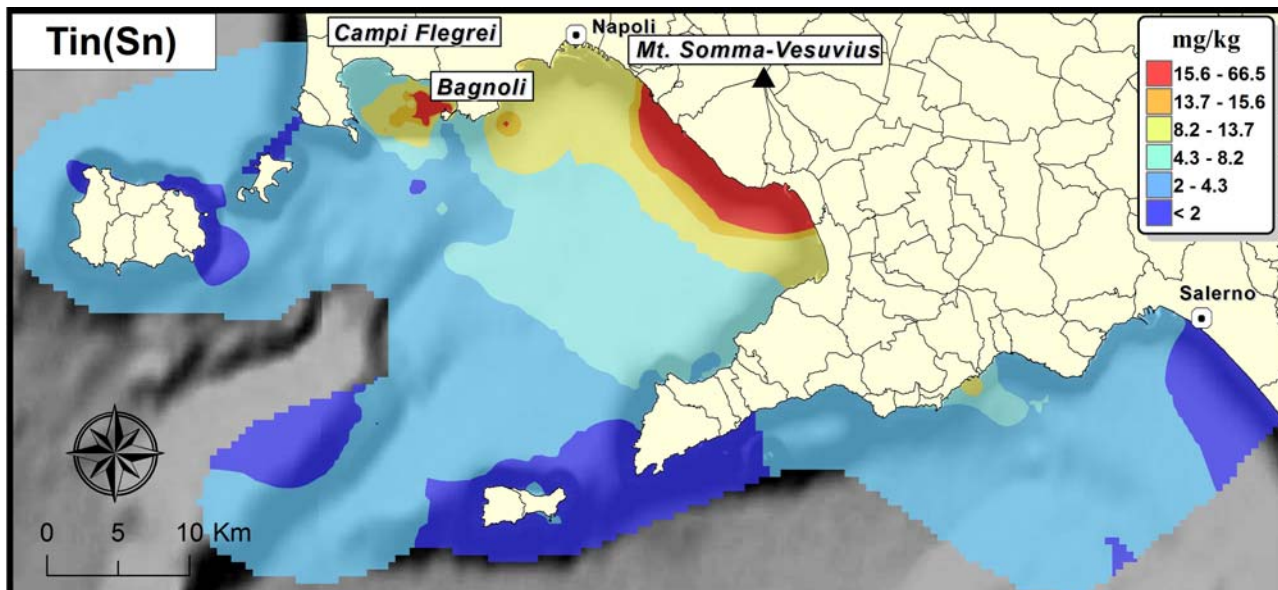


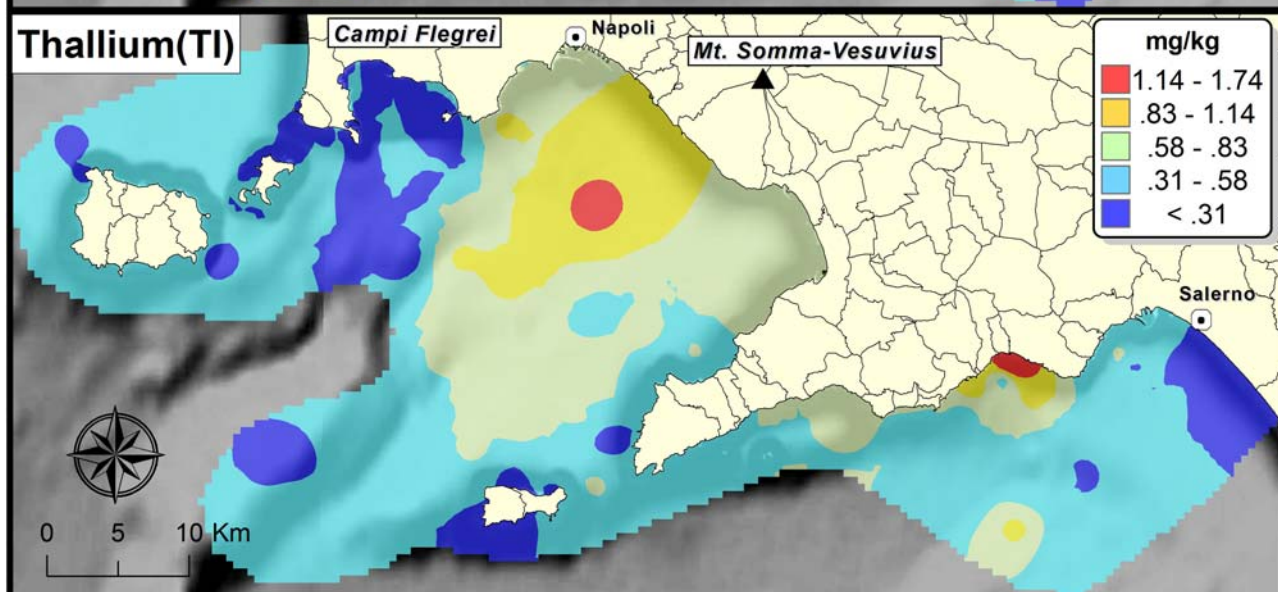
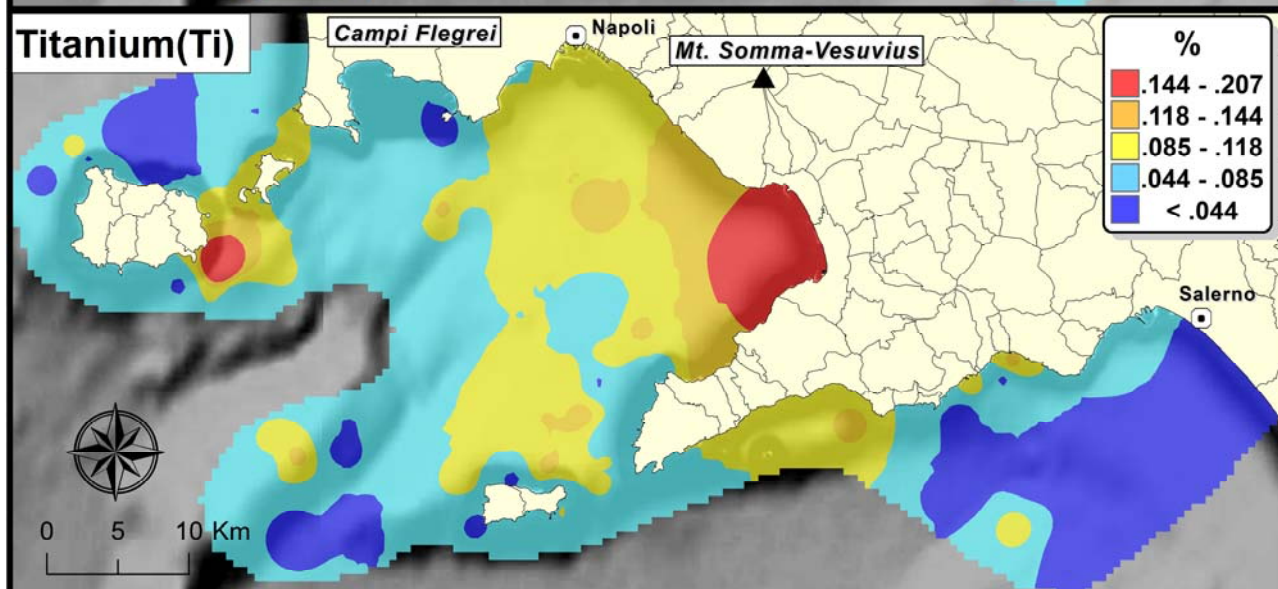
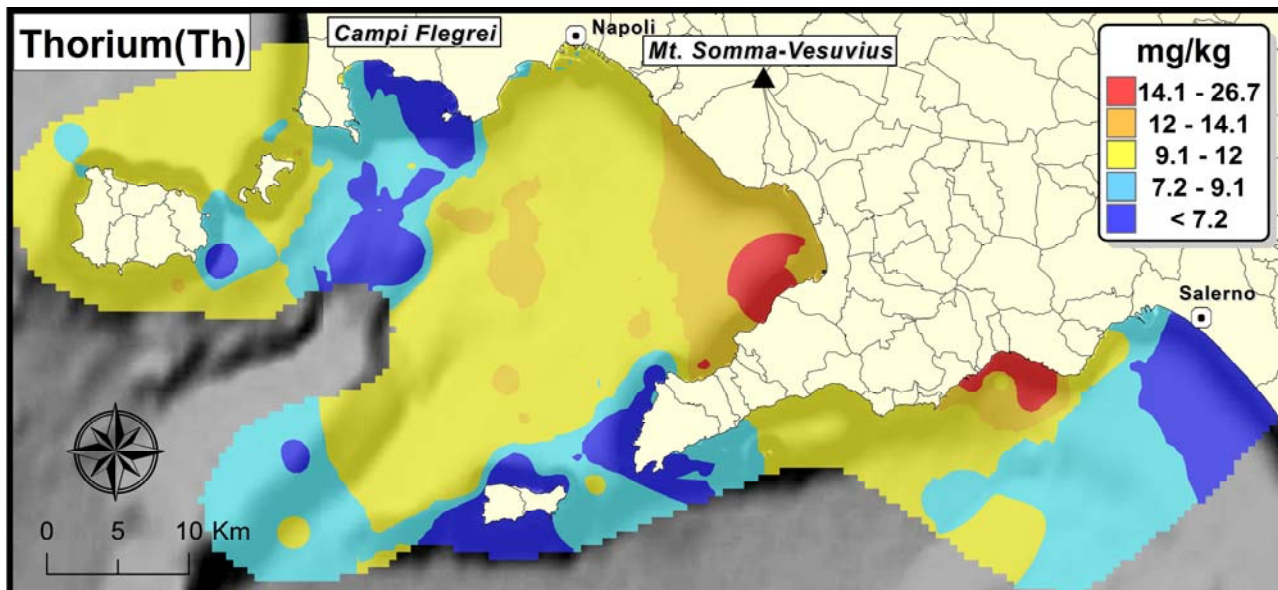


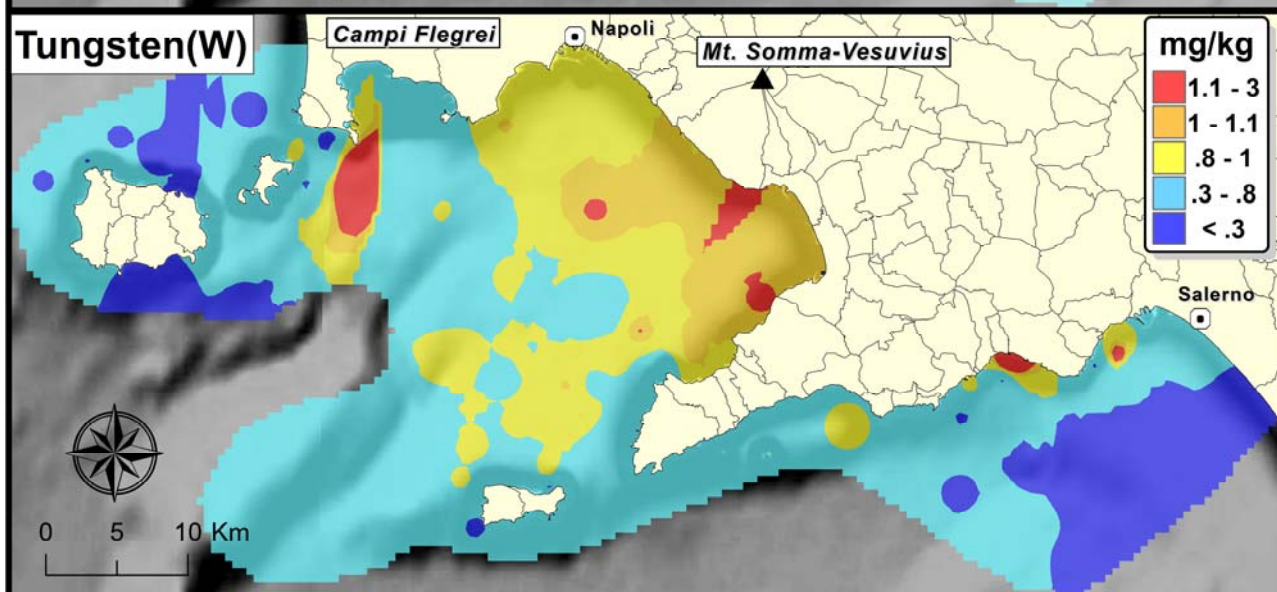
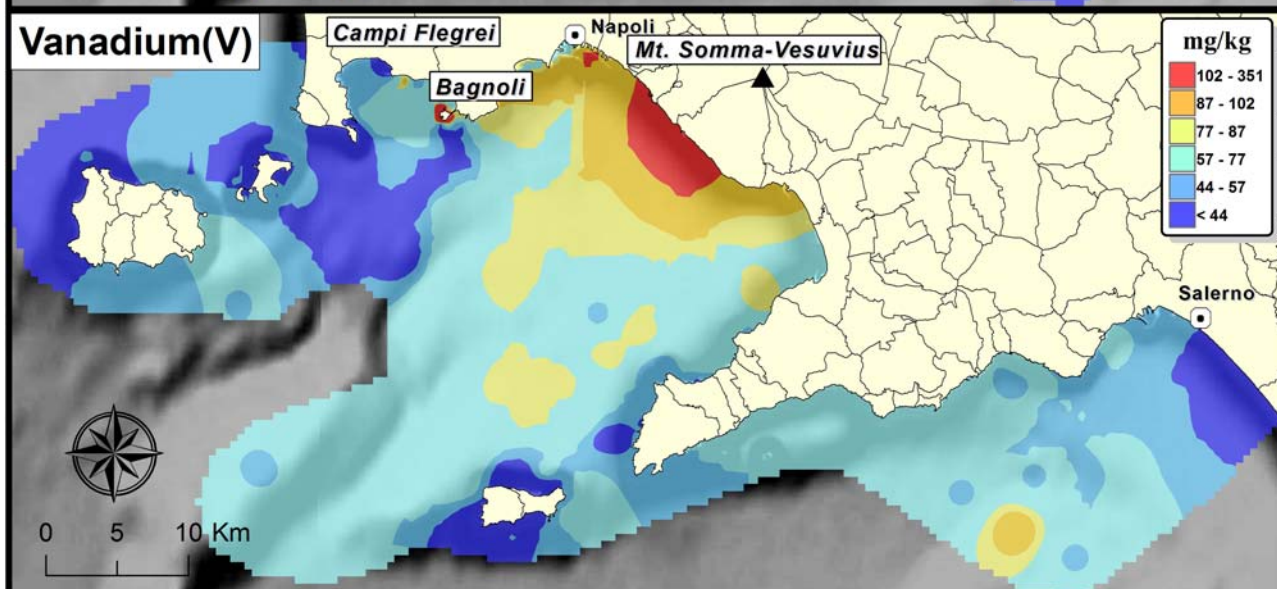
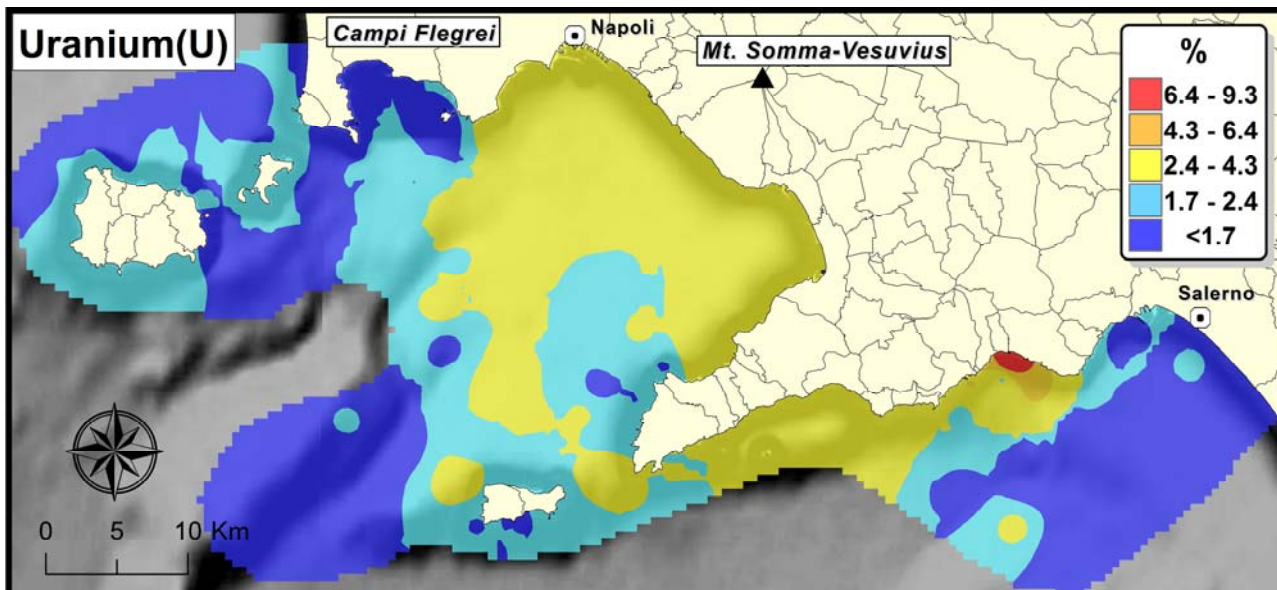


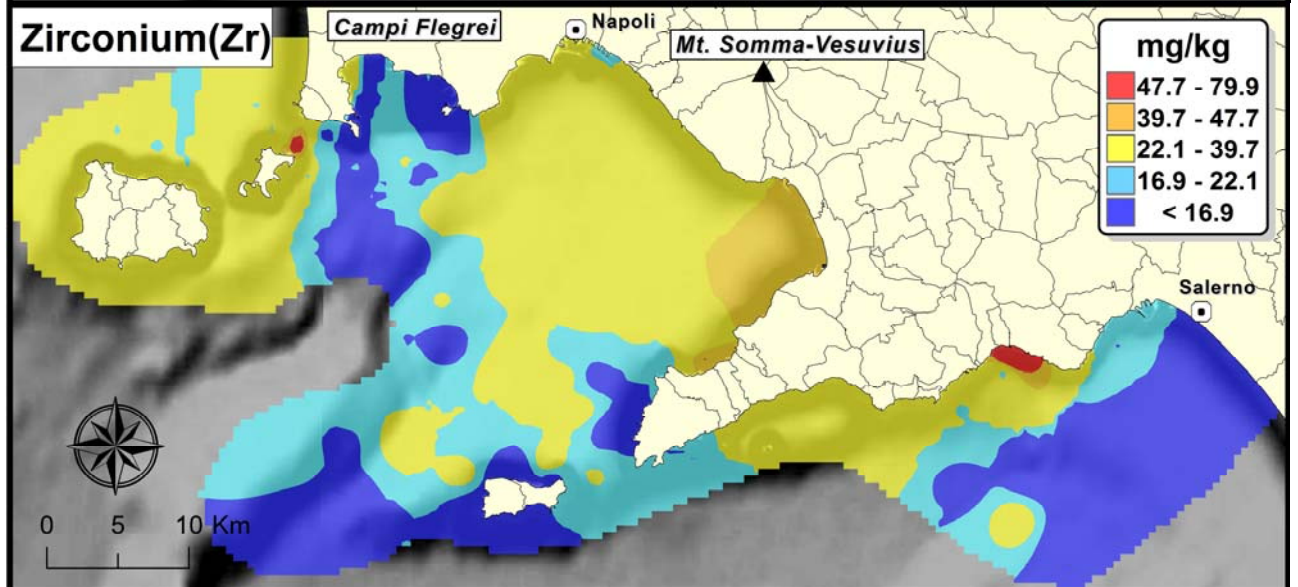
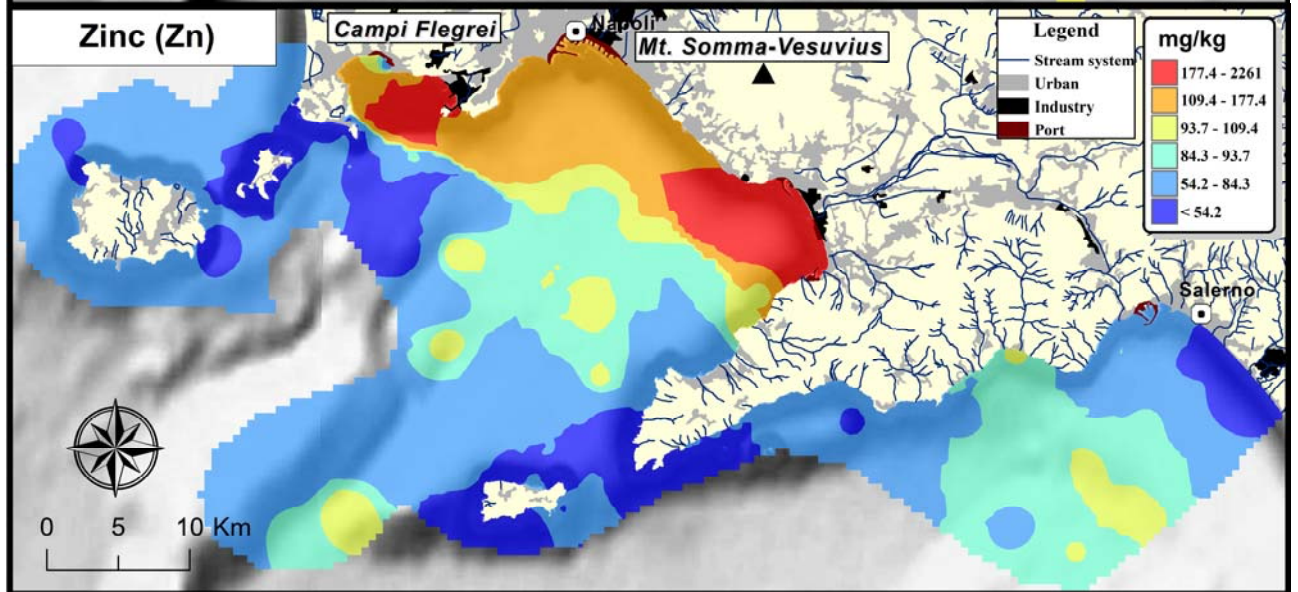
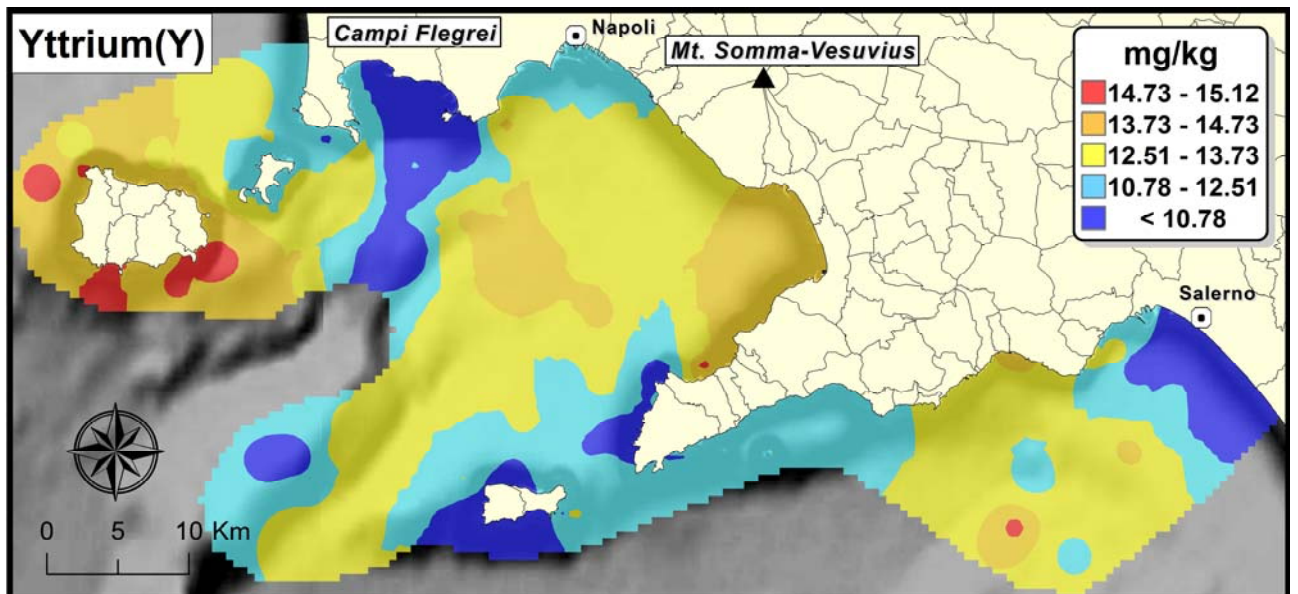




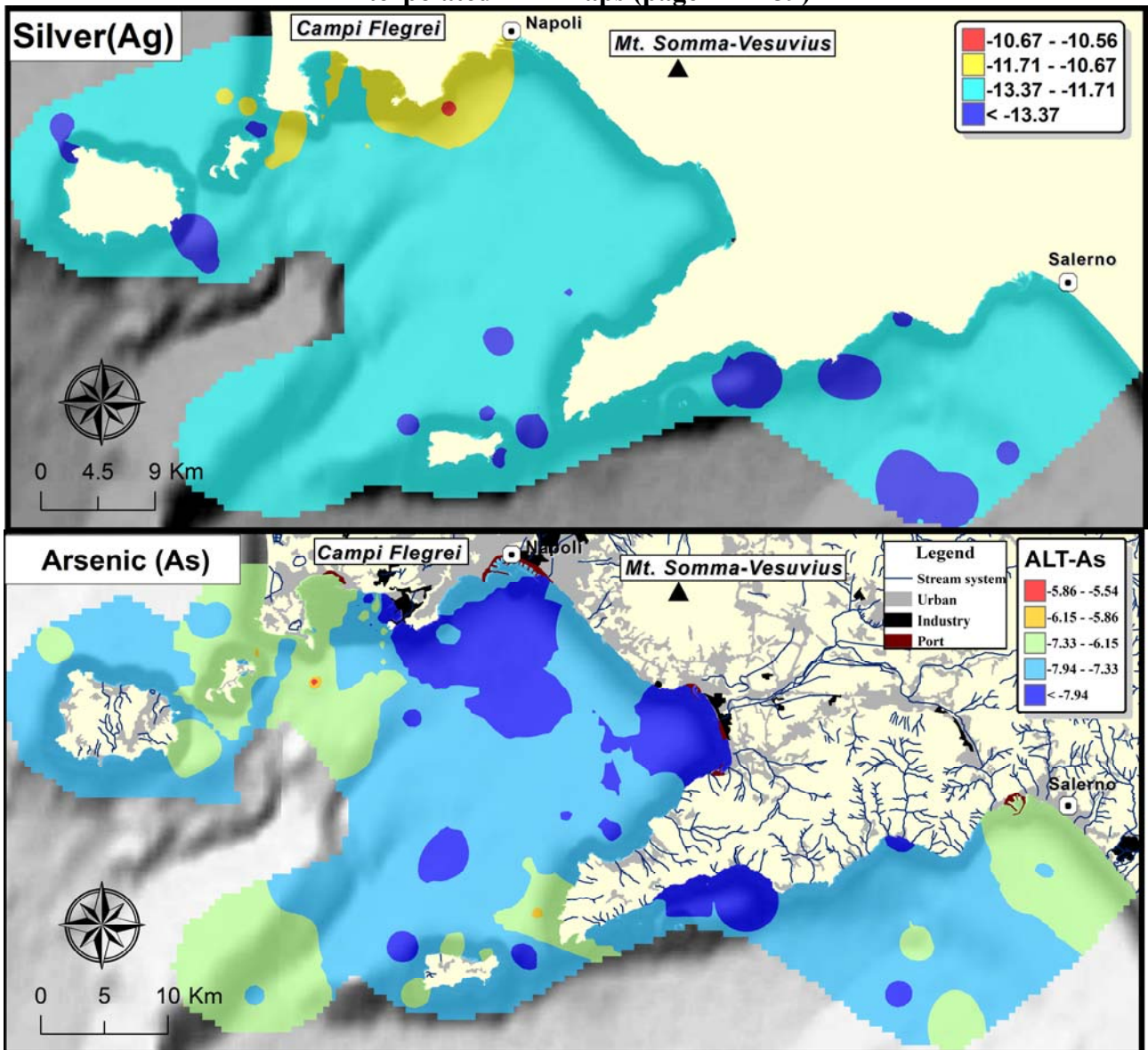


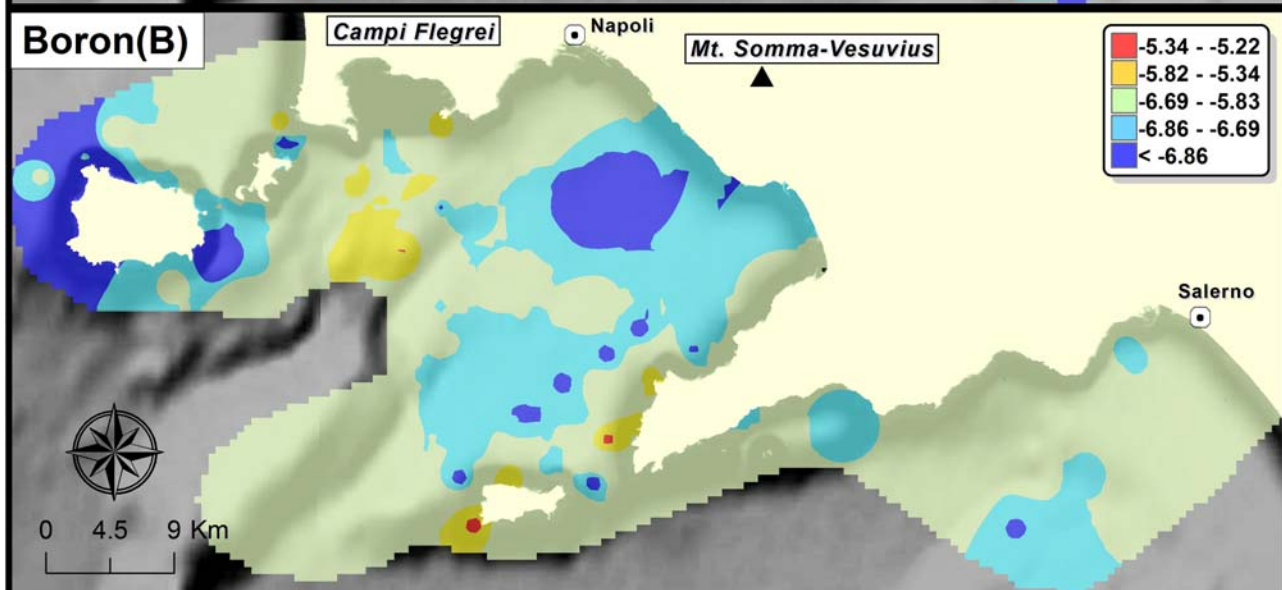
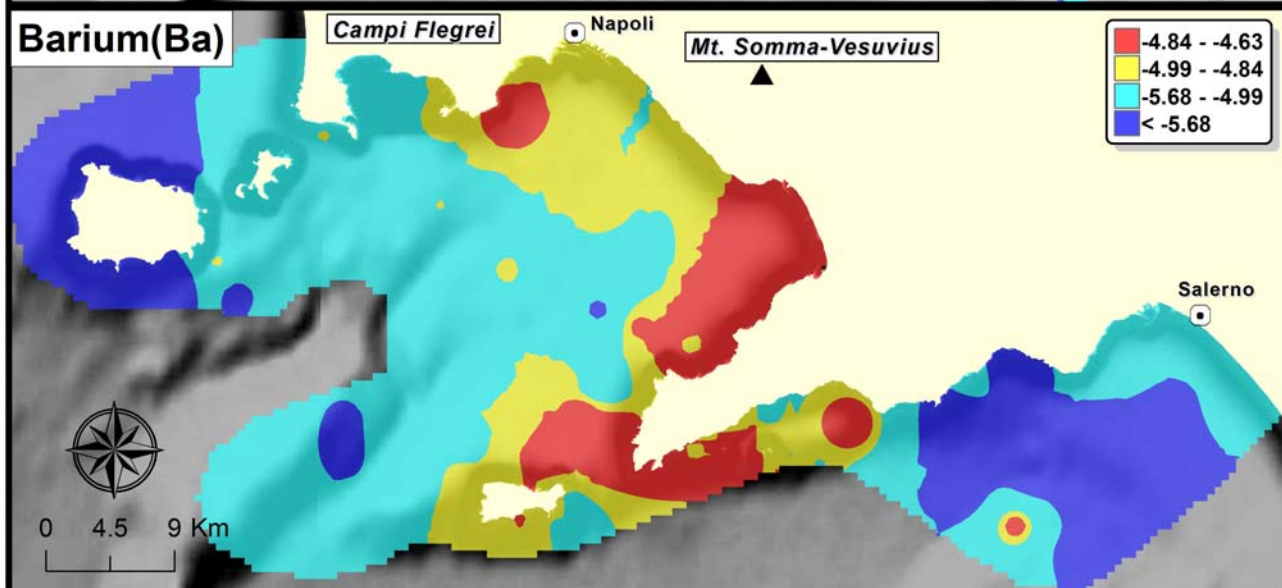
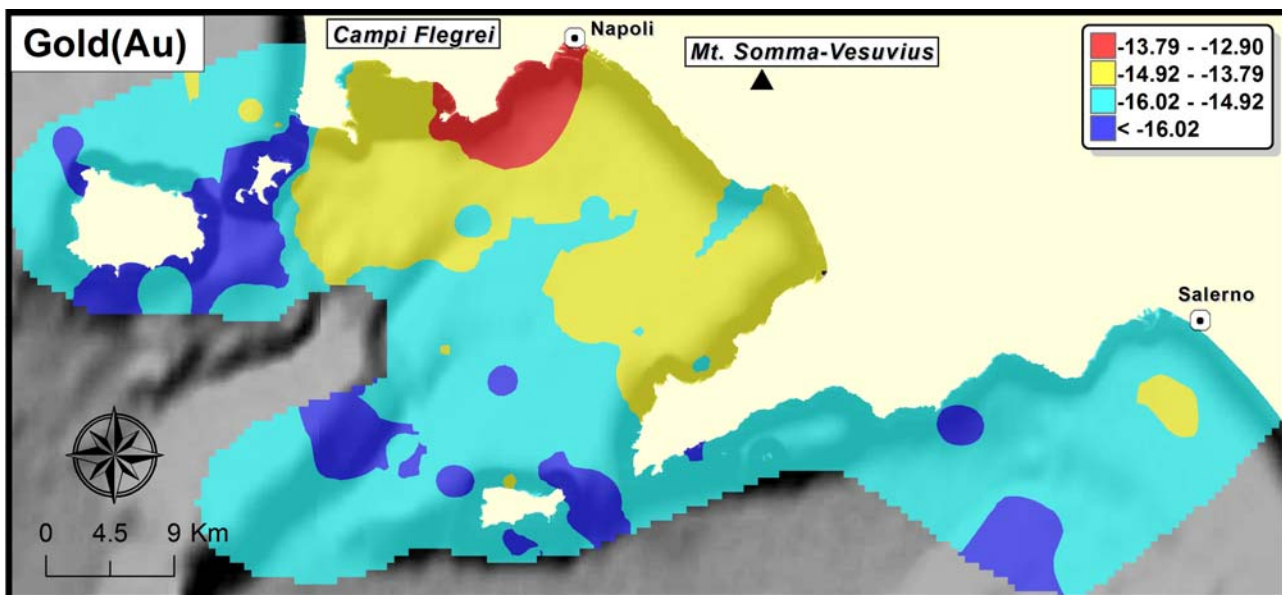


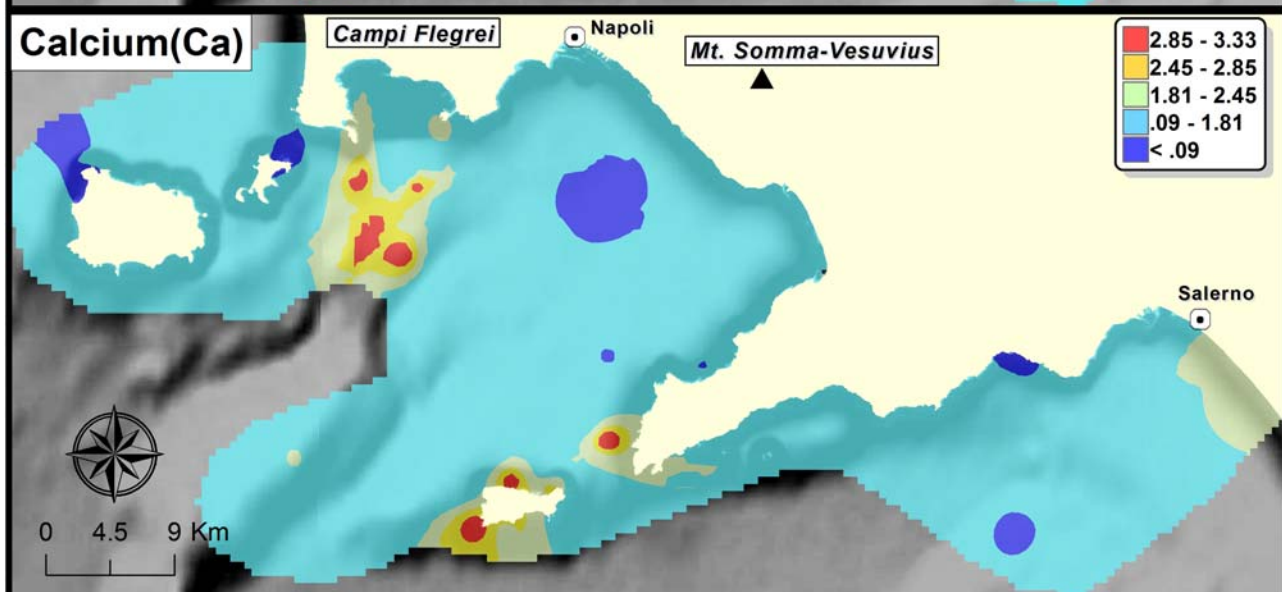
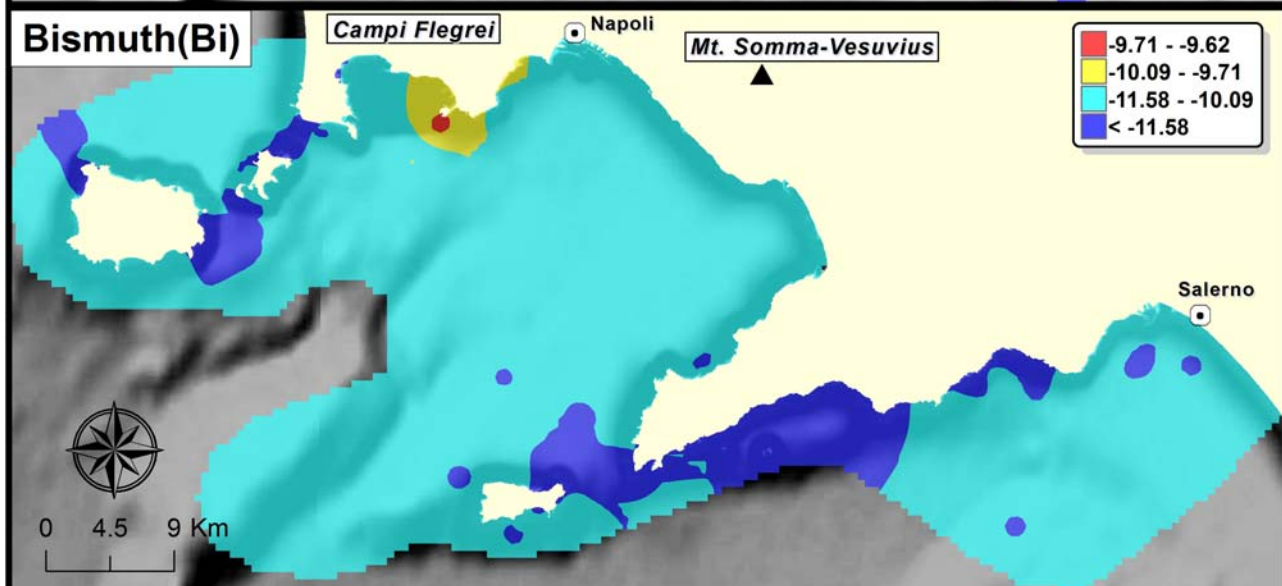
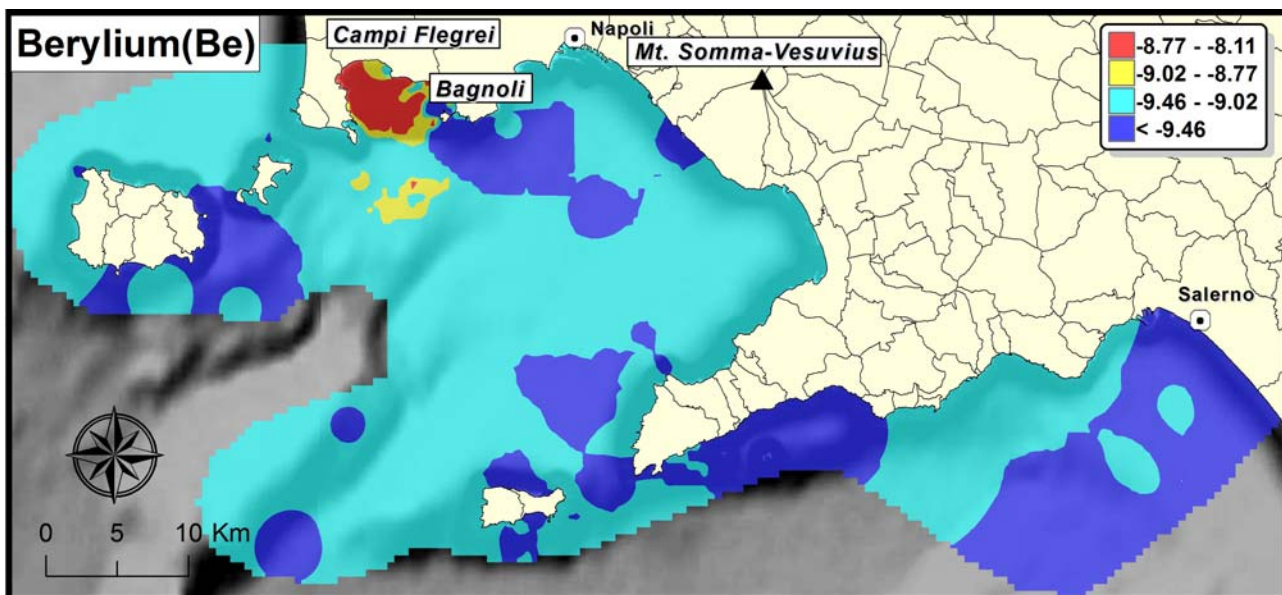


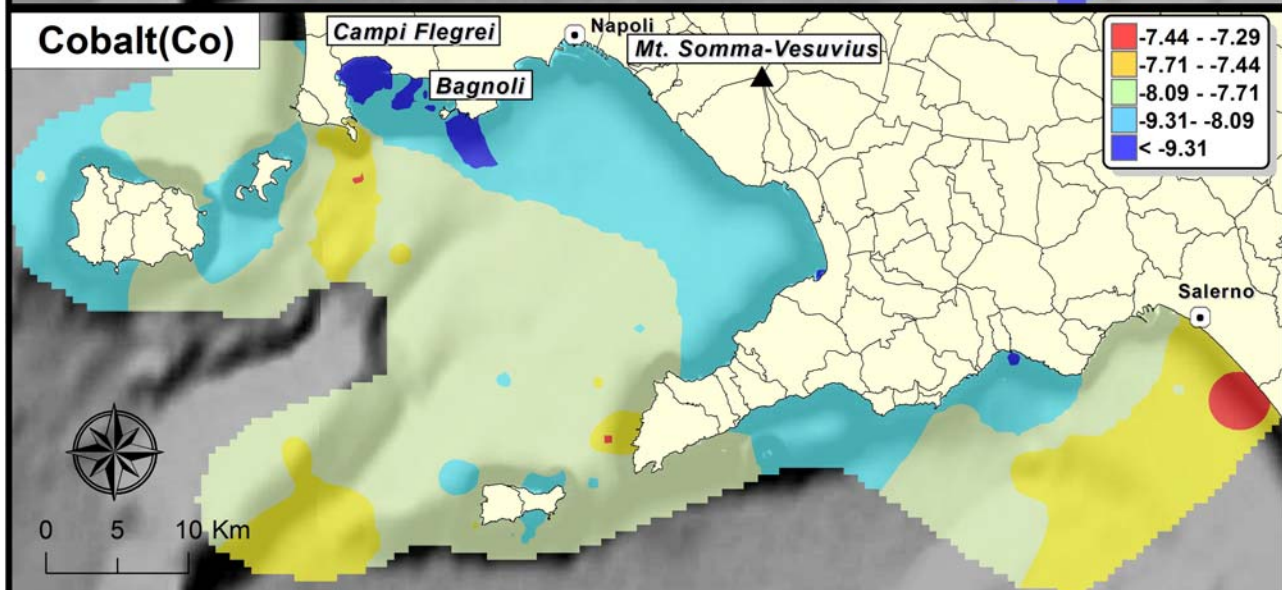
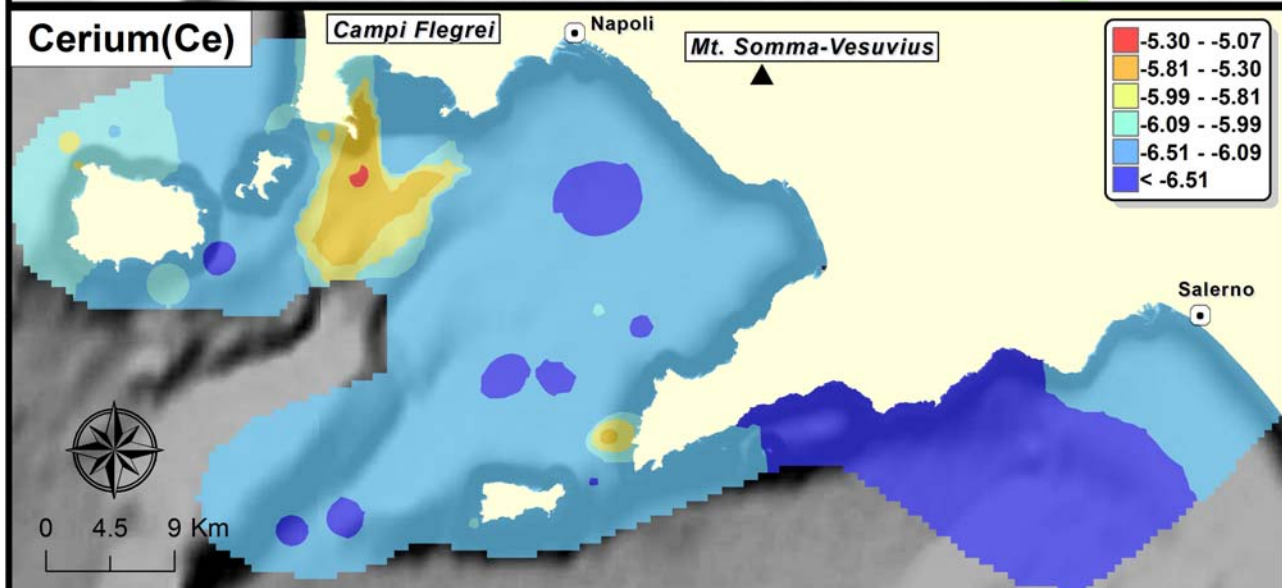
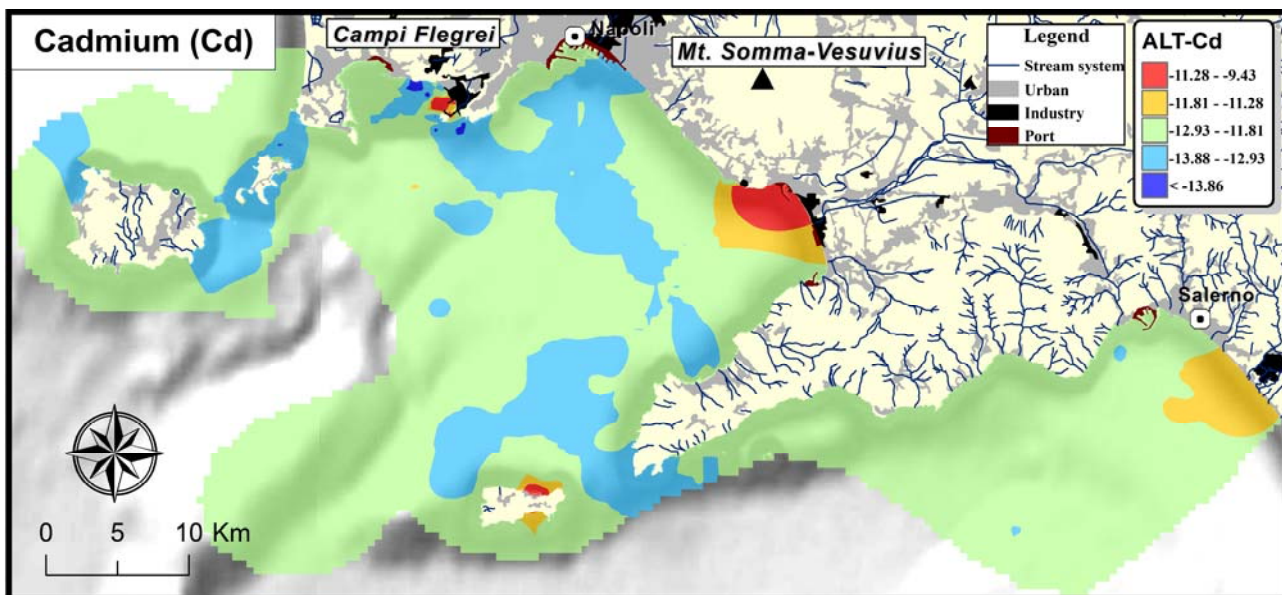


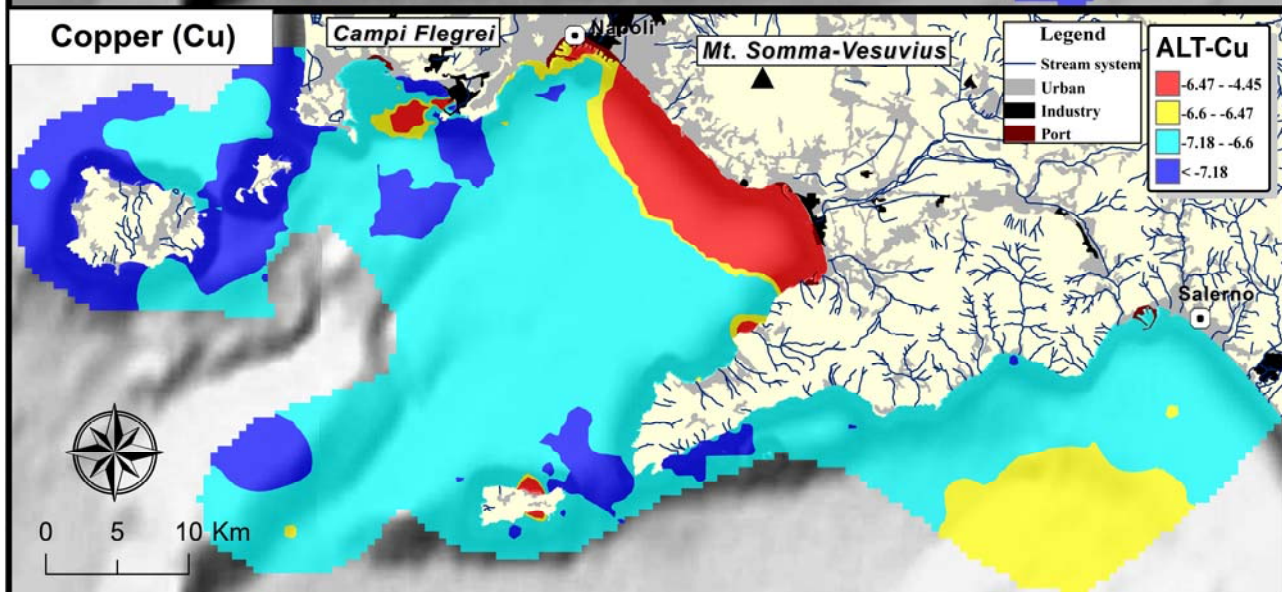
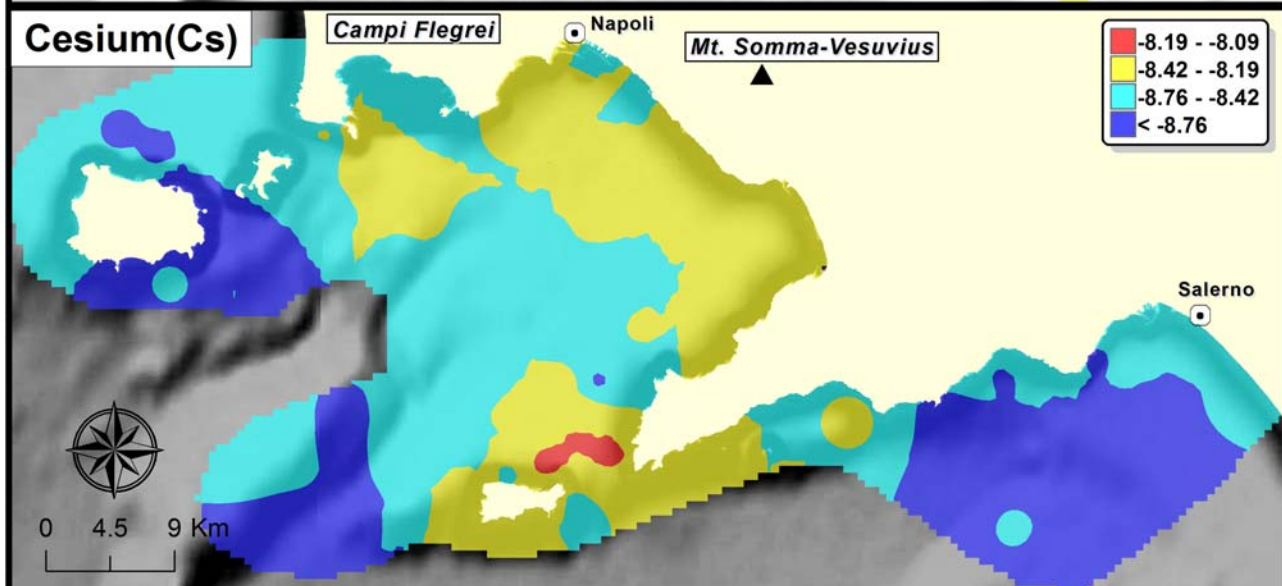
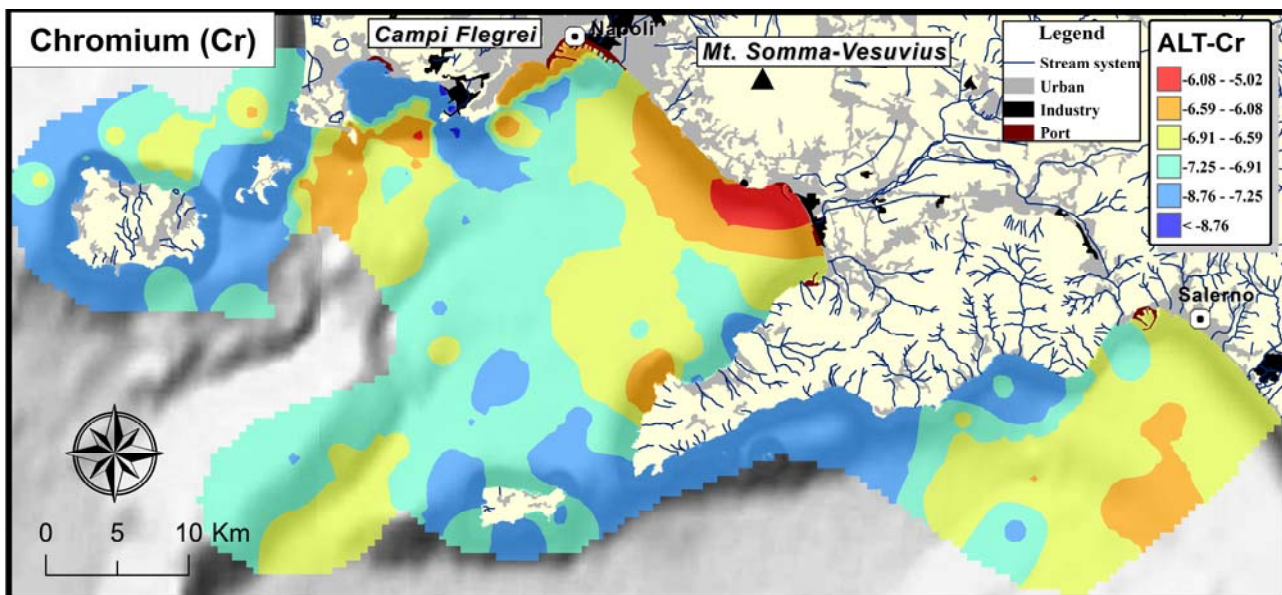
Interpolated ALT maps (page 224-239)

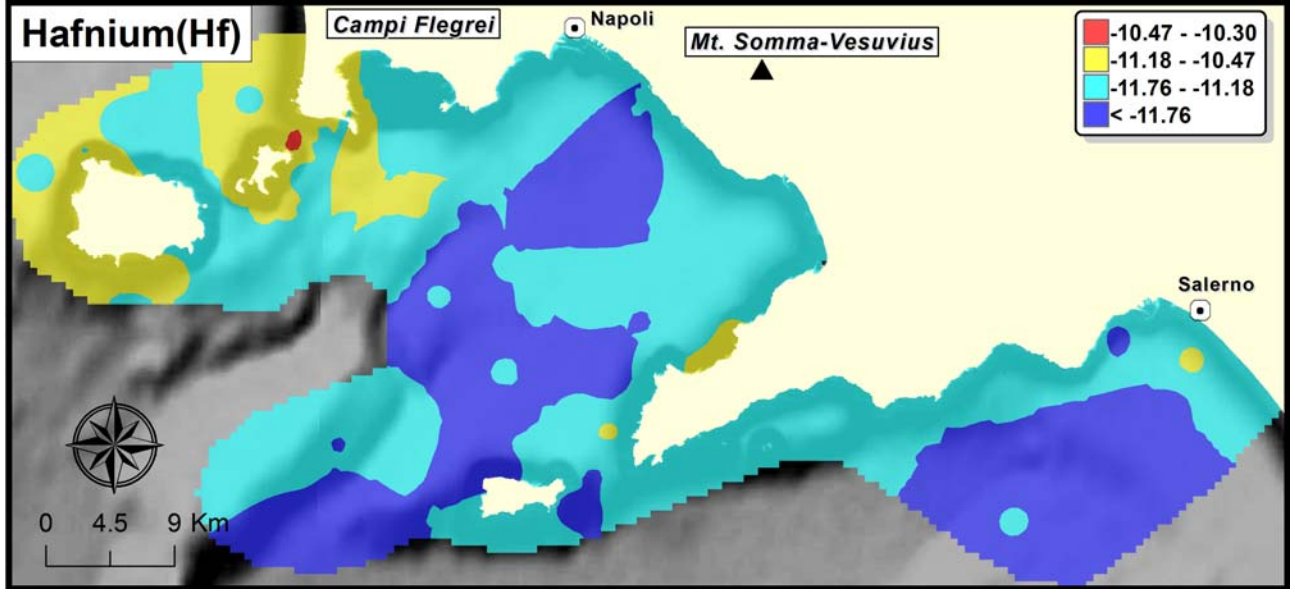
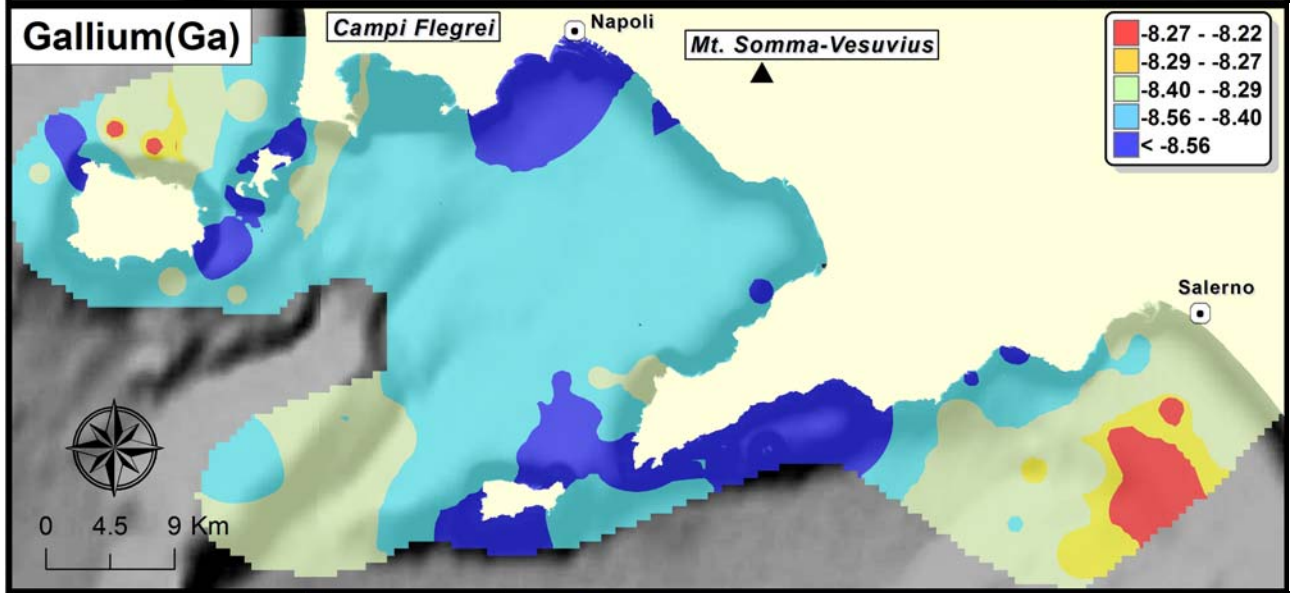
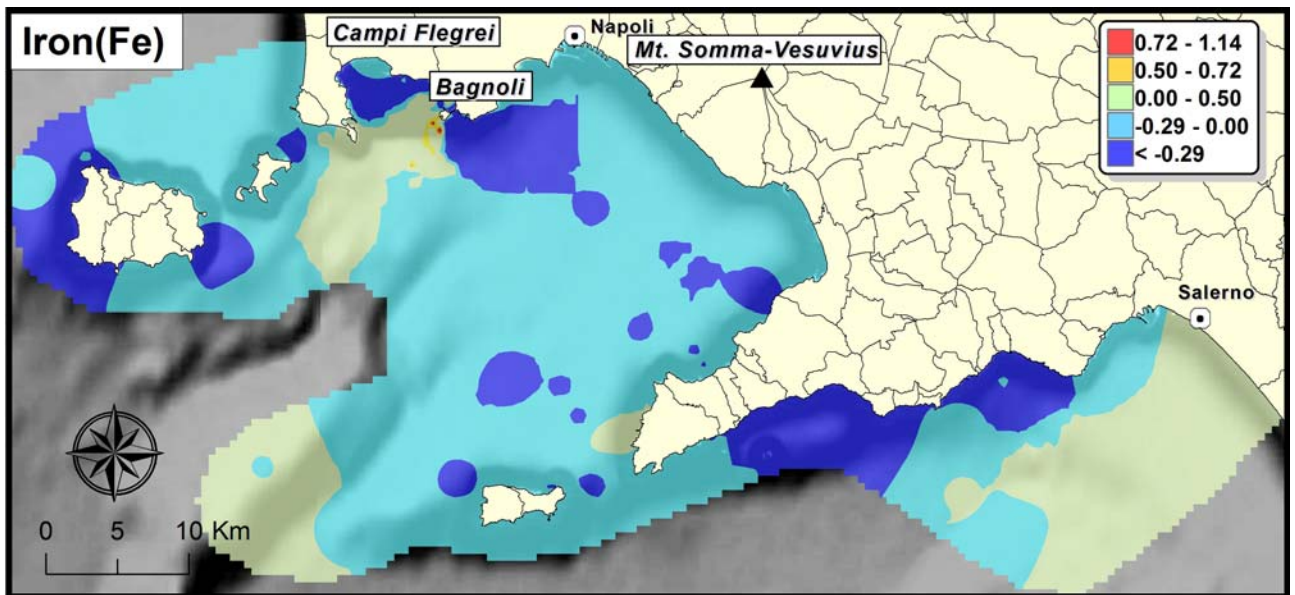


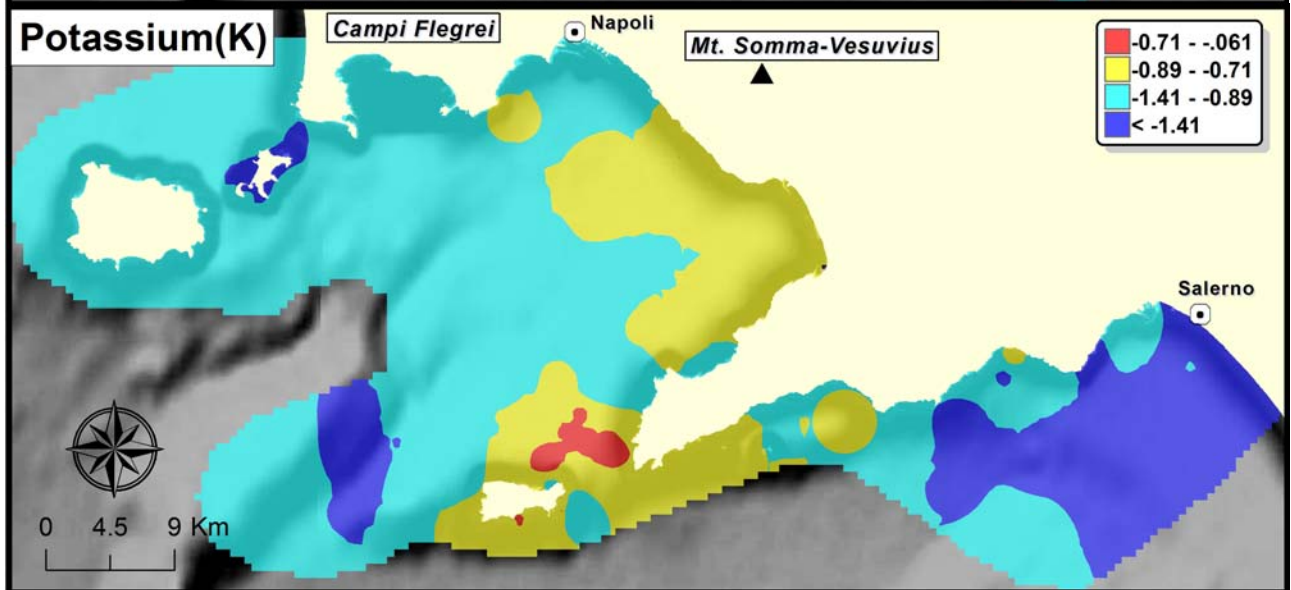
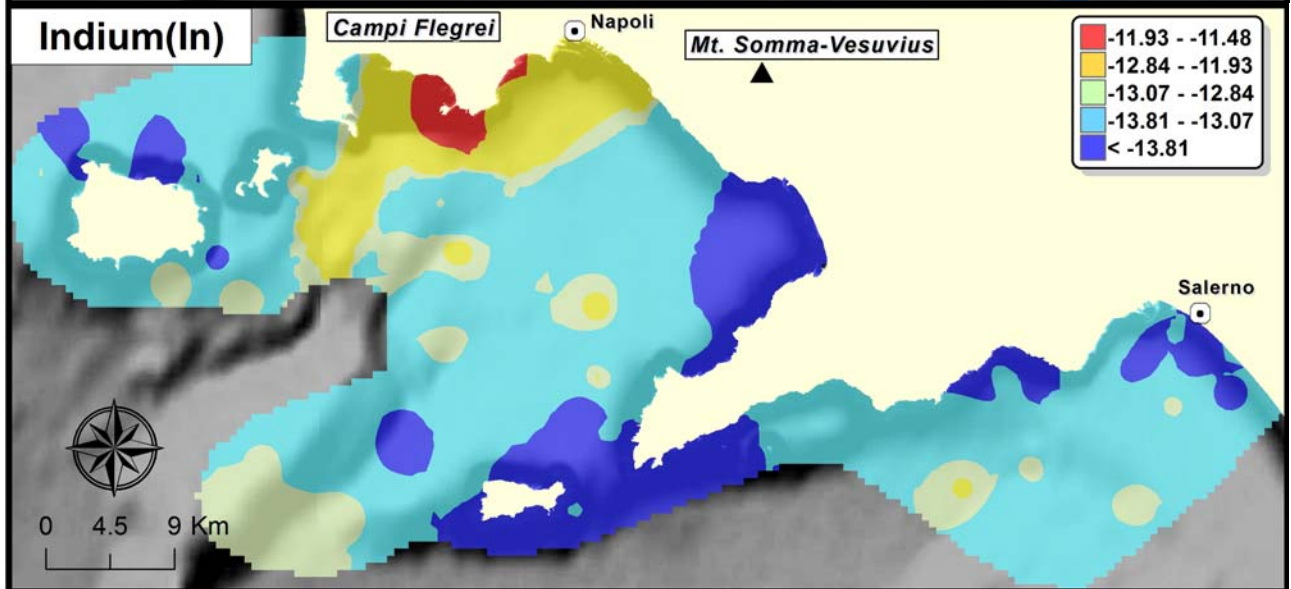
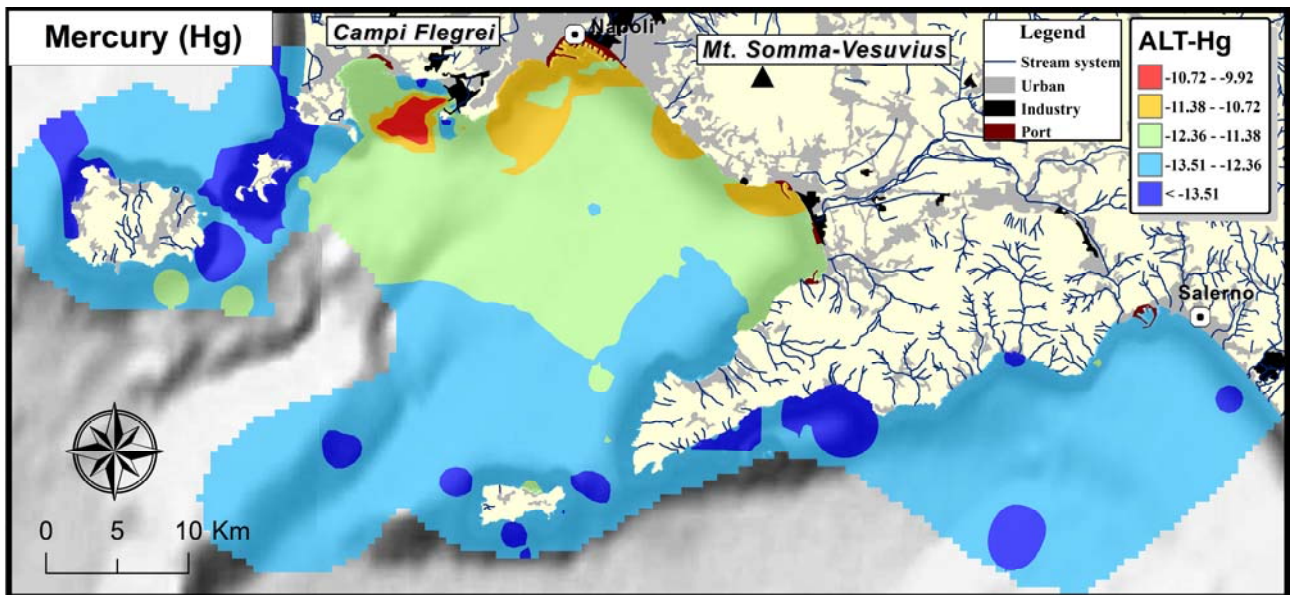


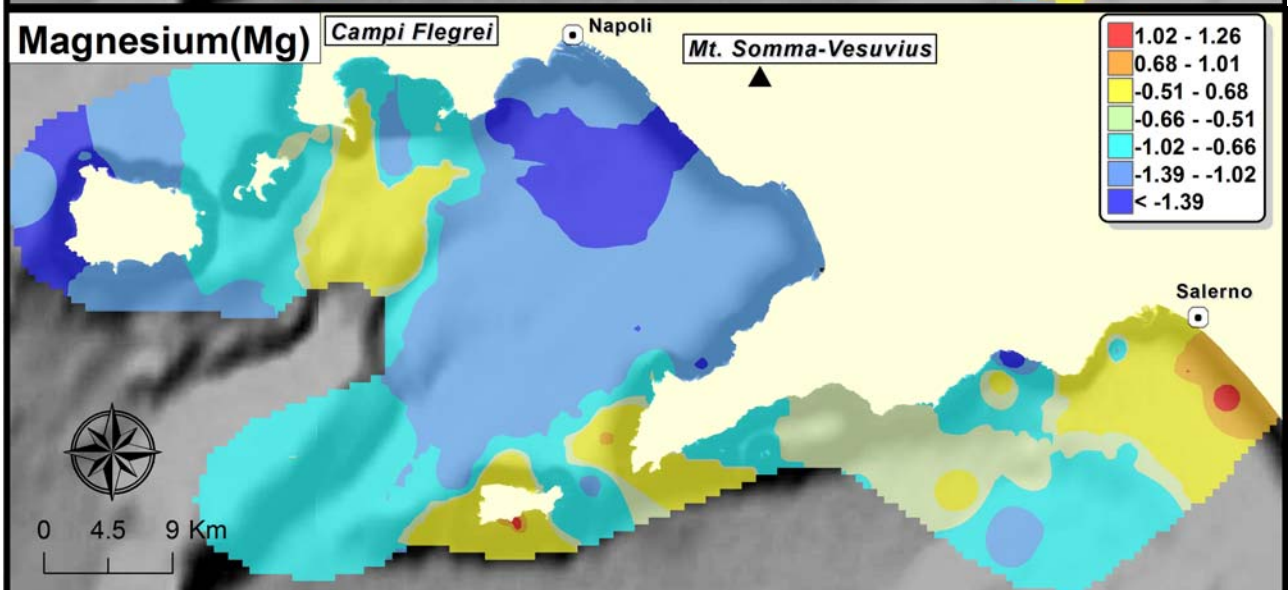
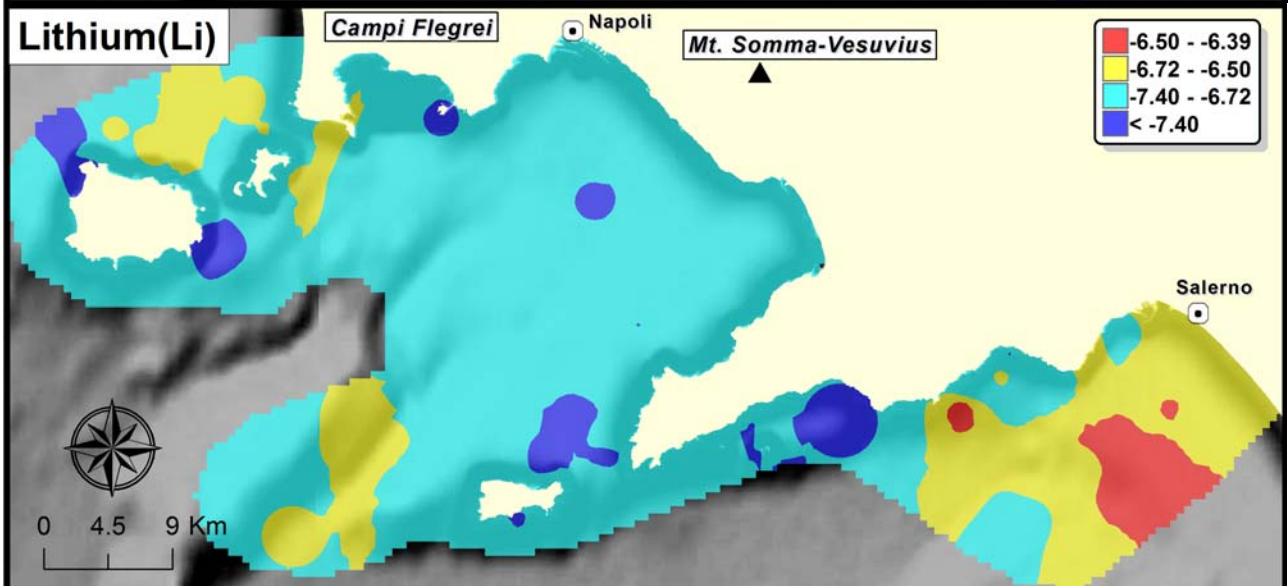
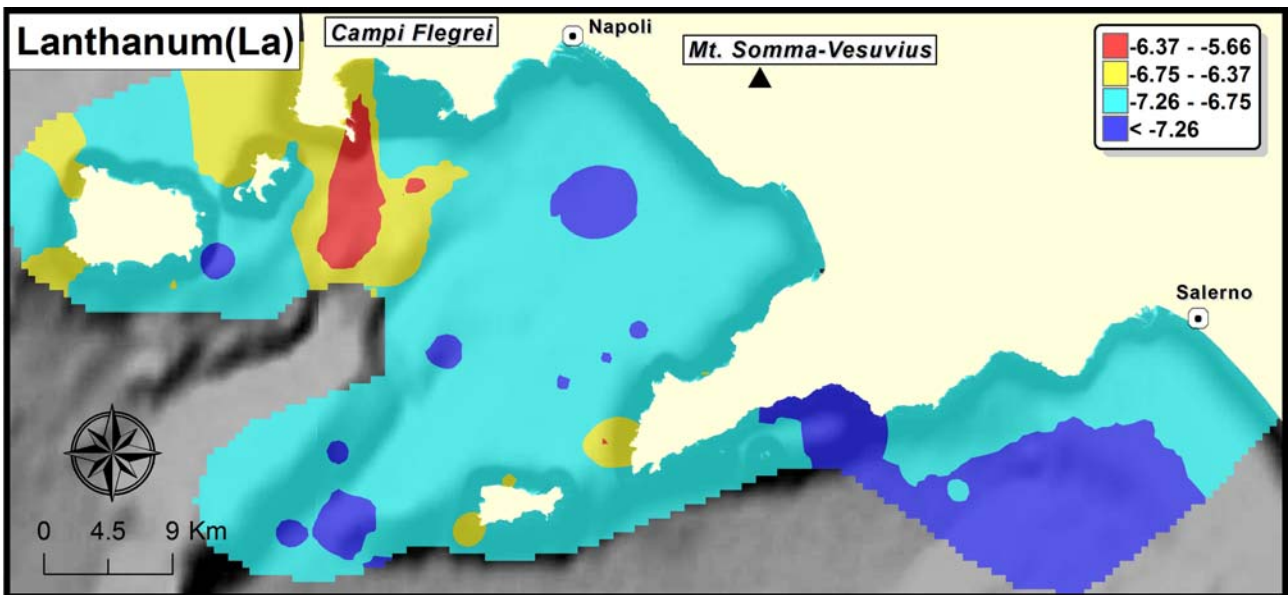


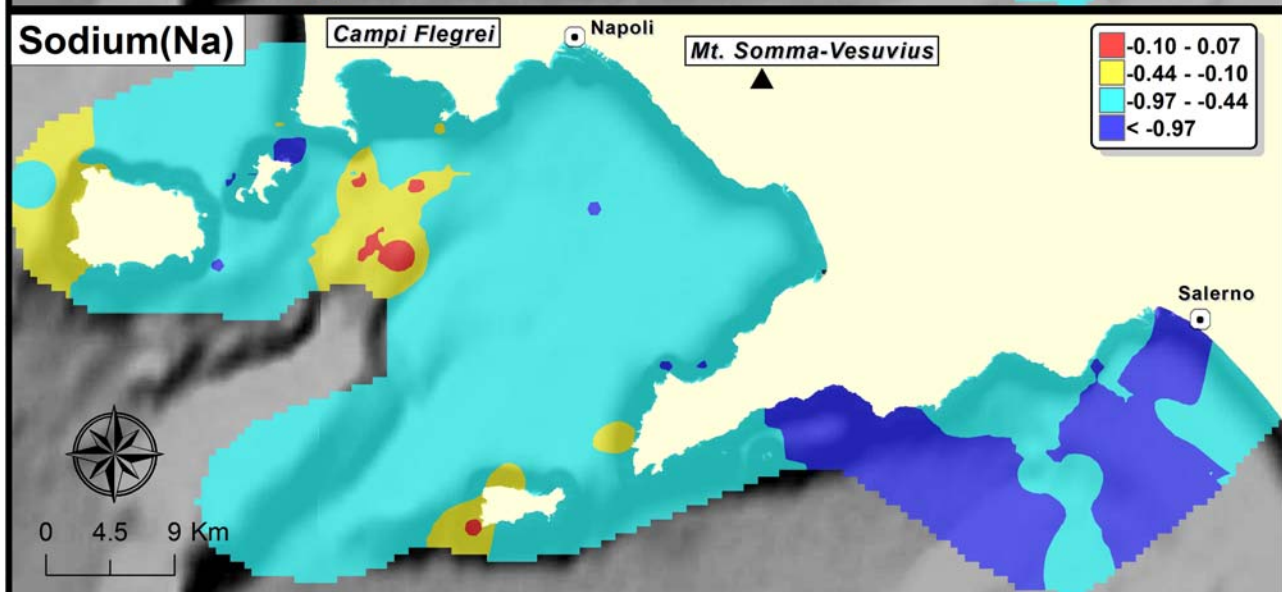
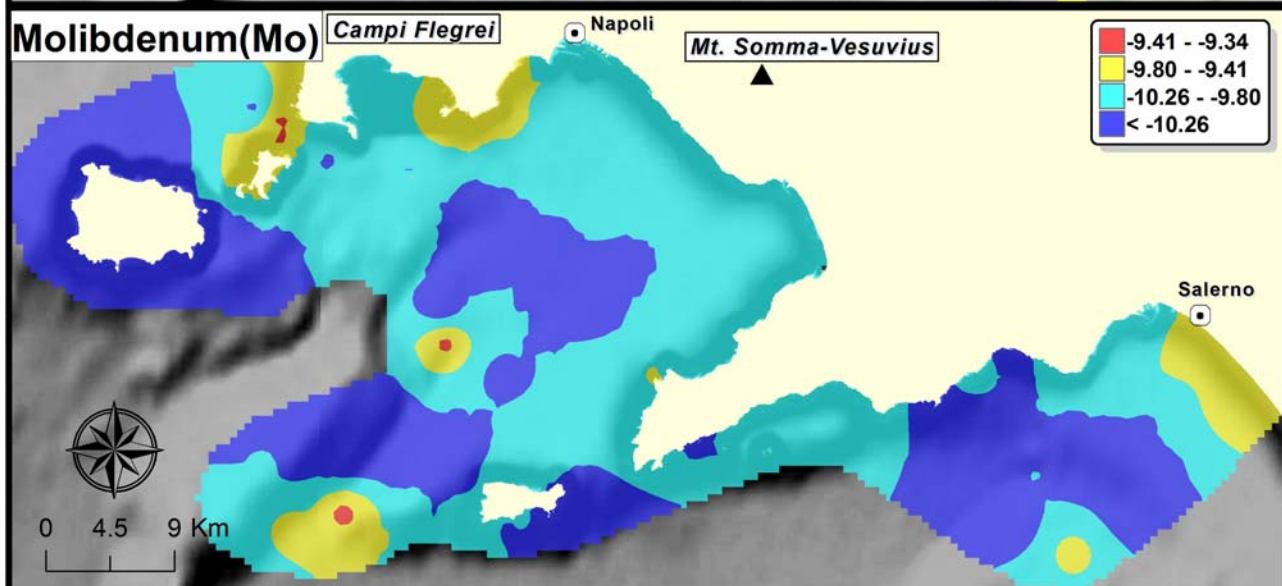
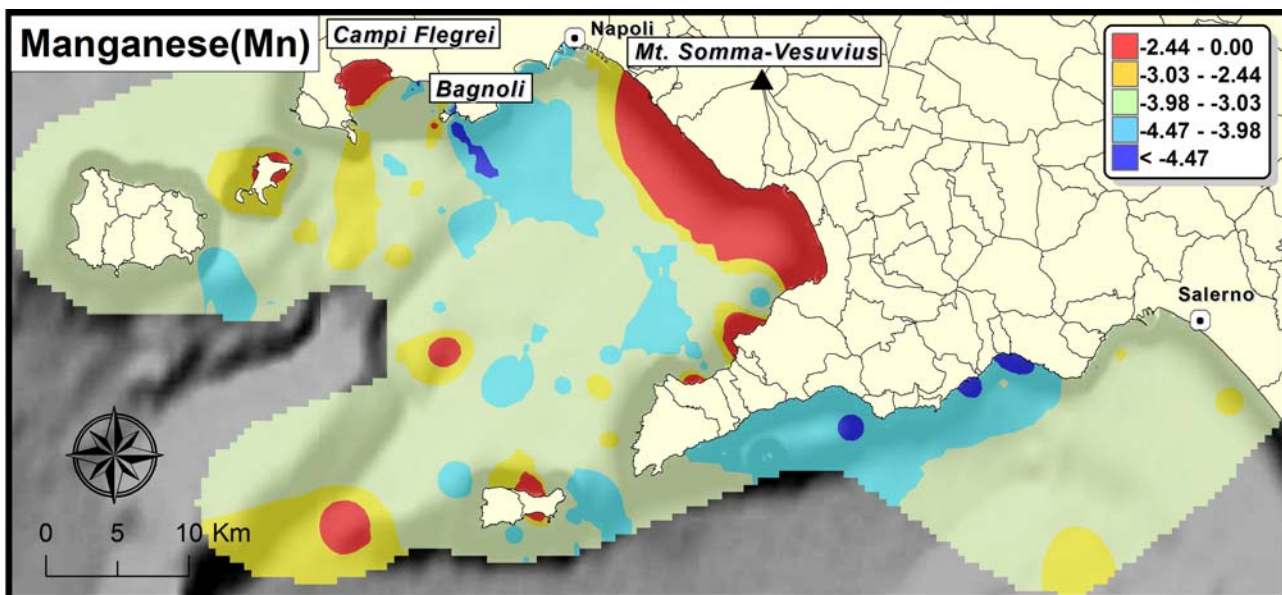


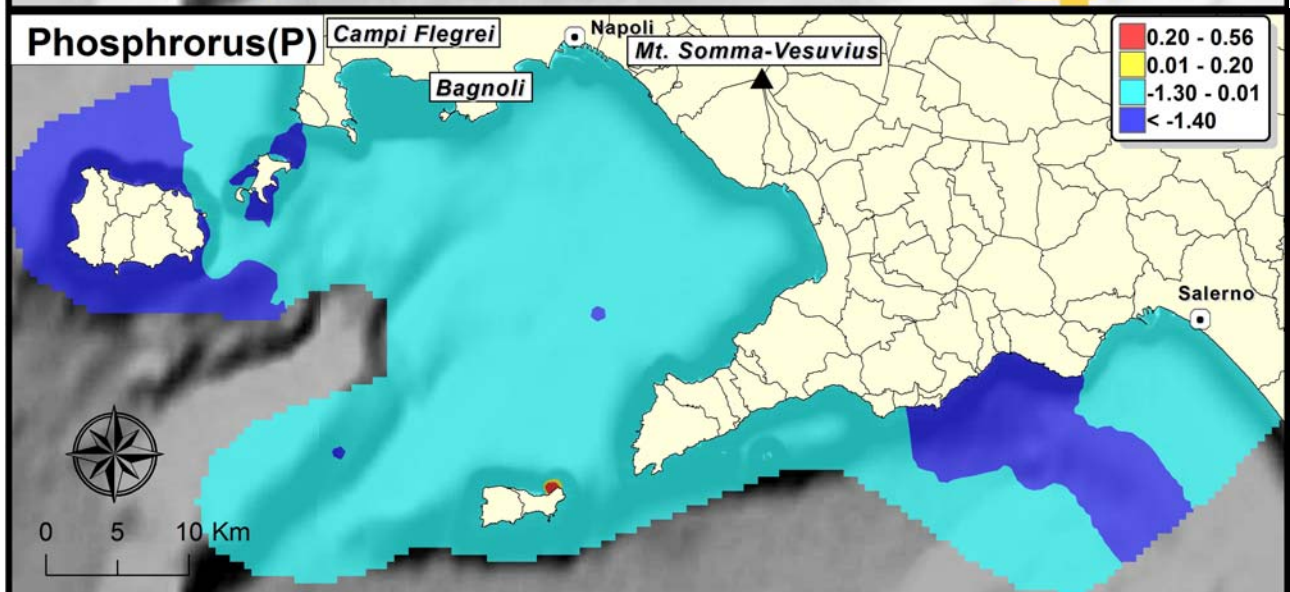
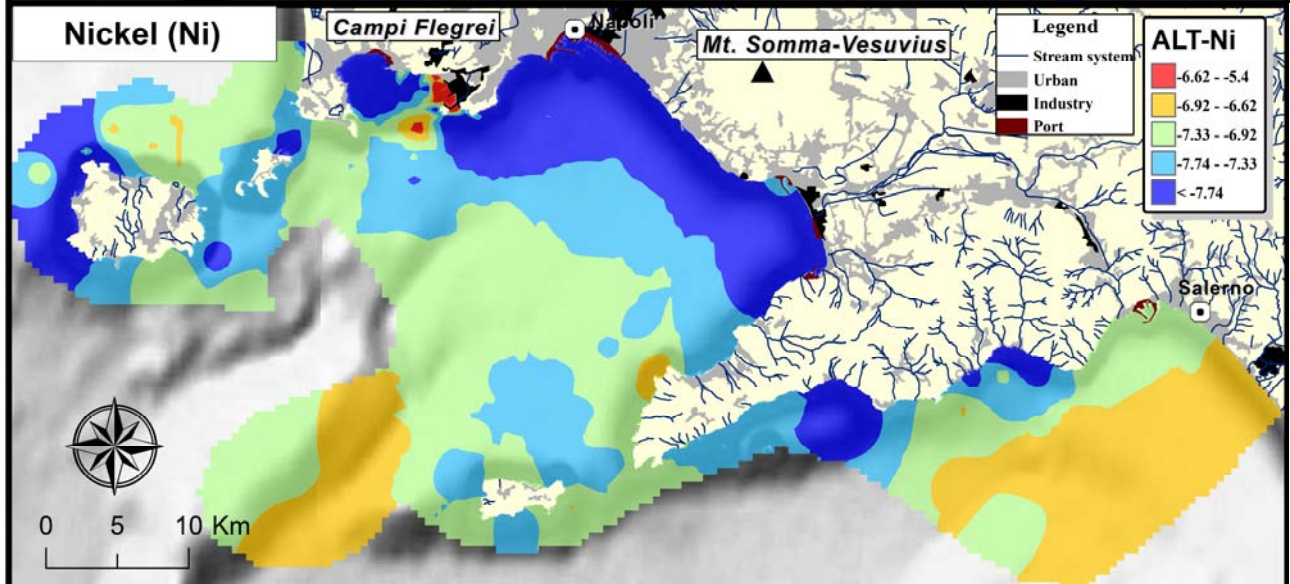
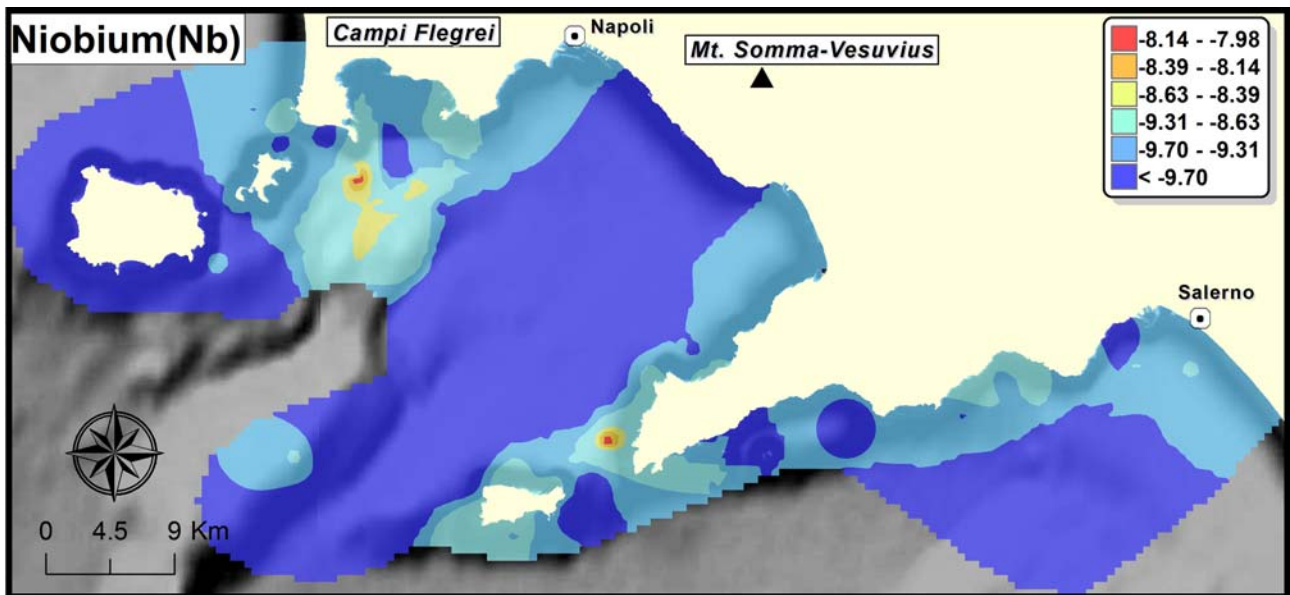


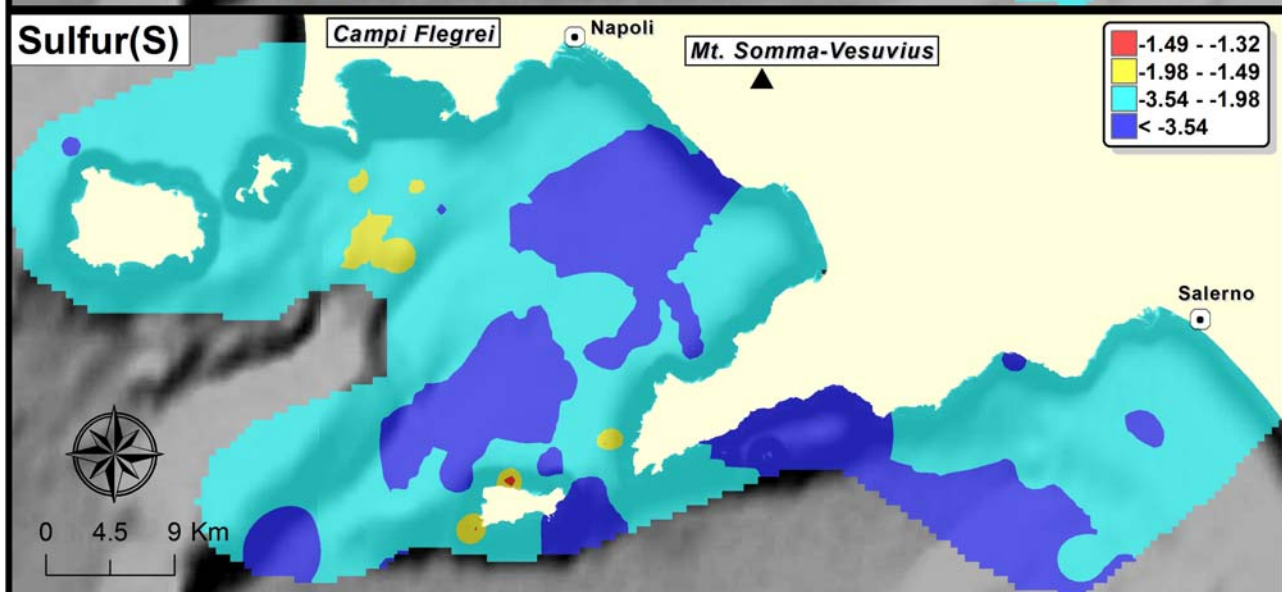
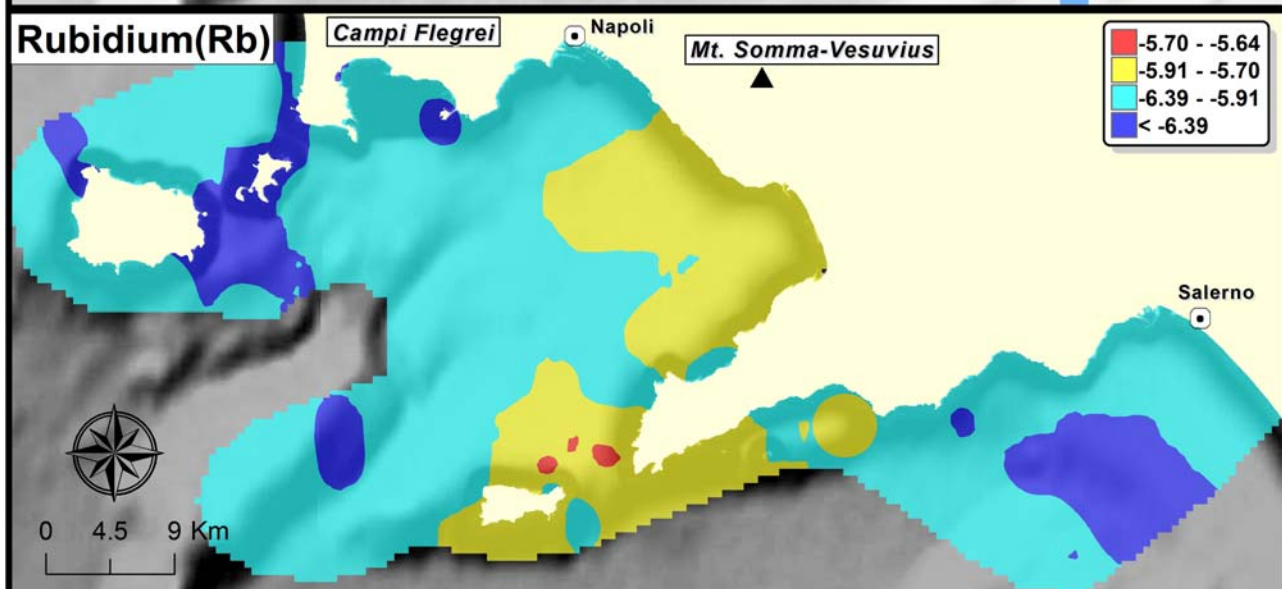
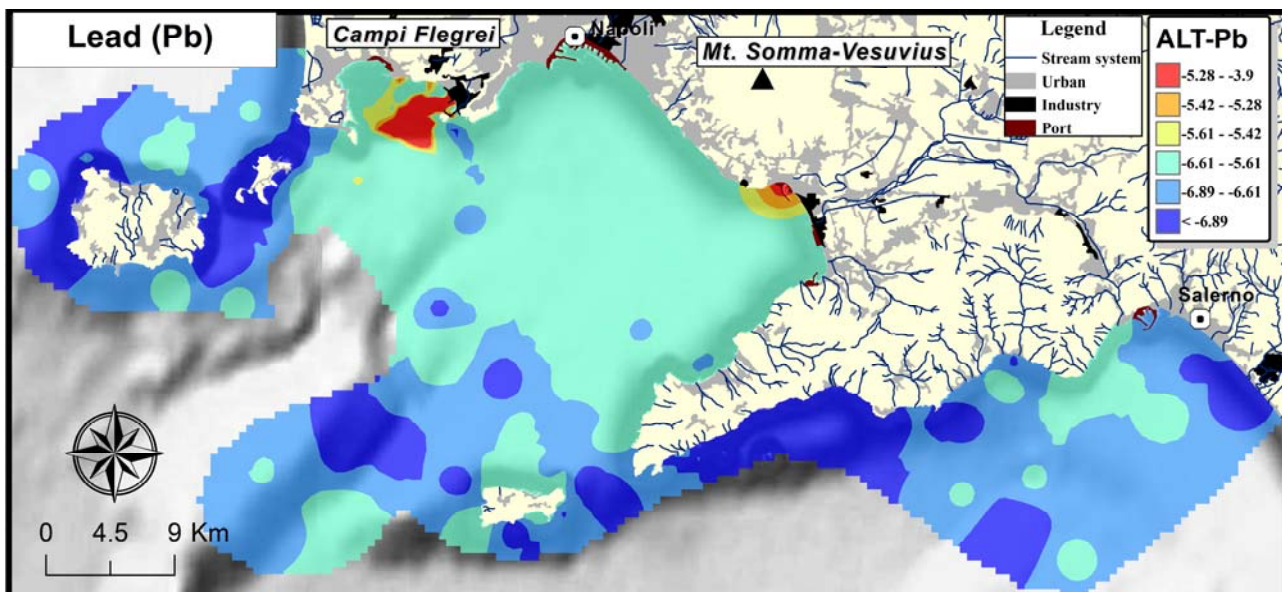


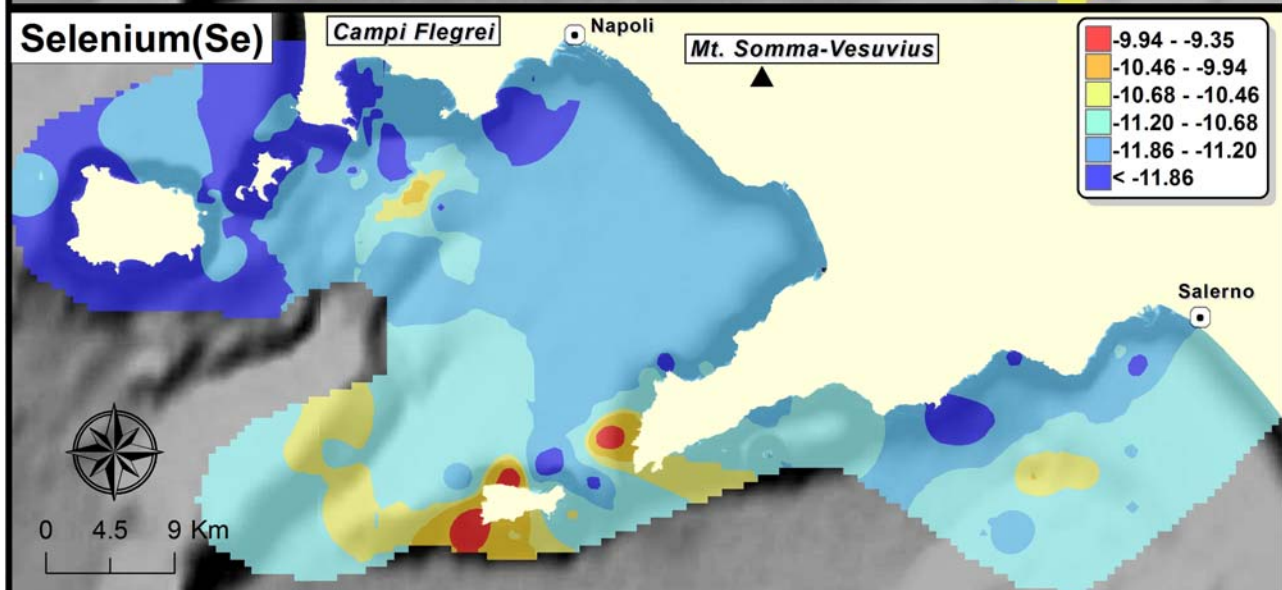
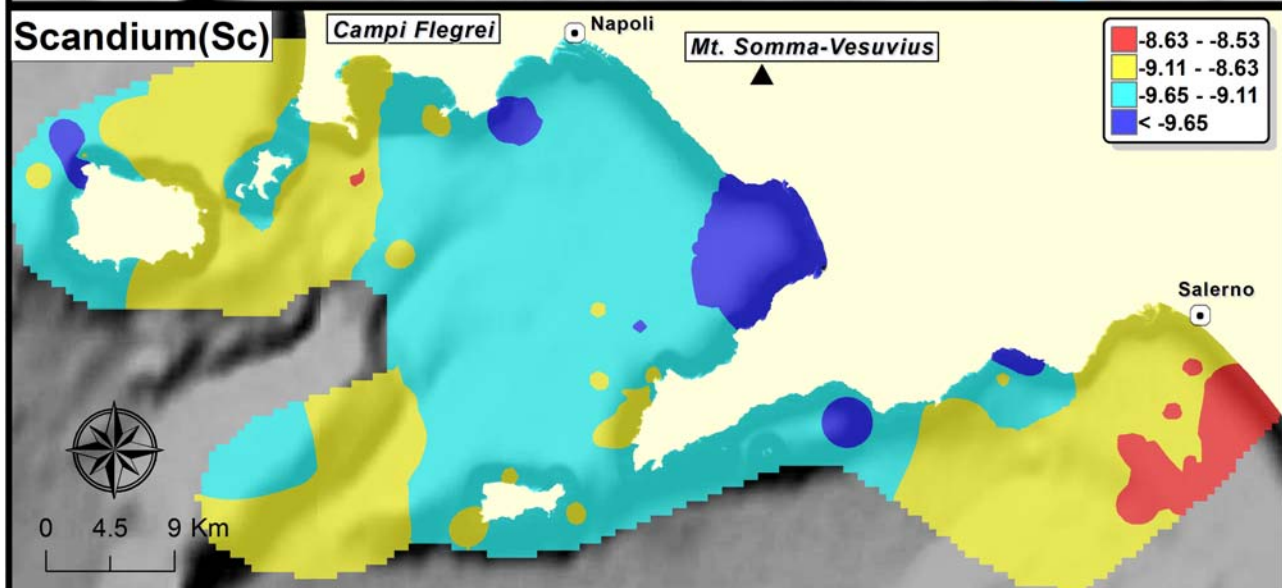
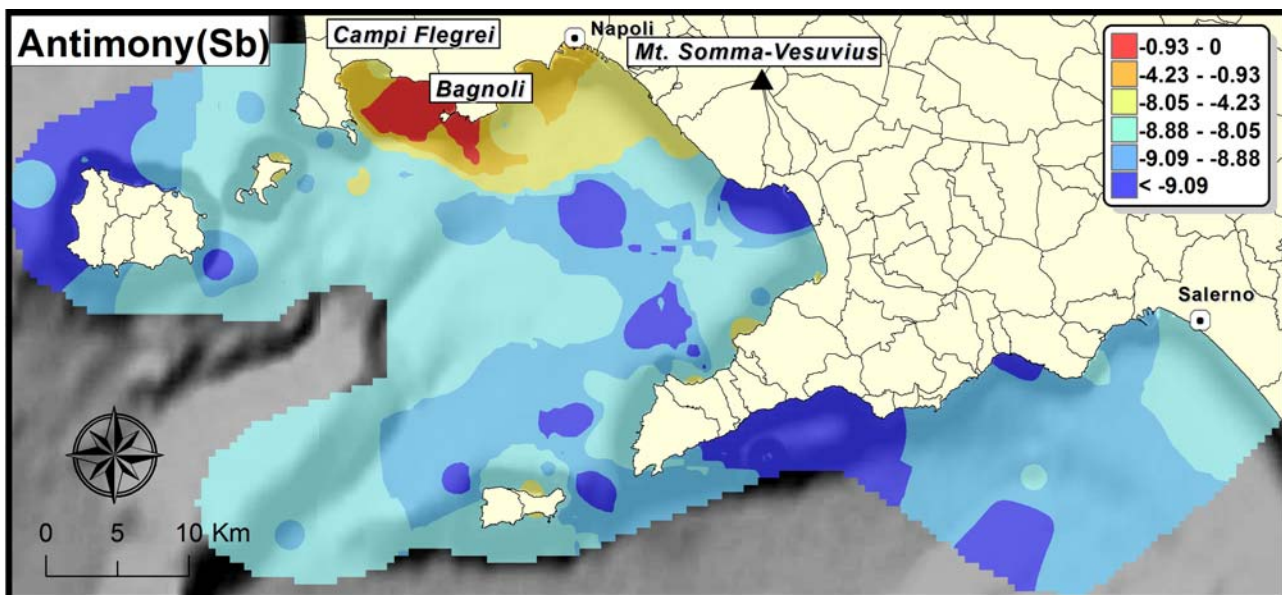


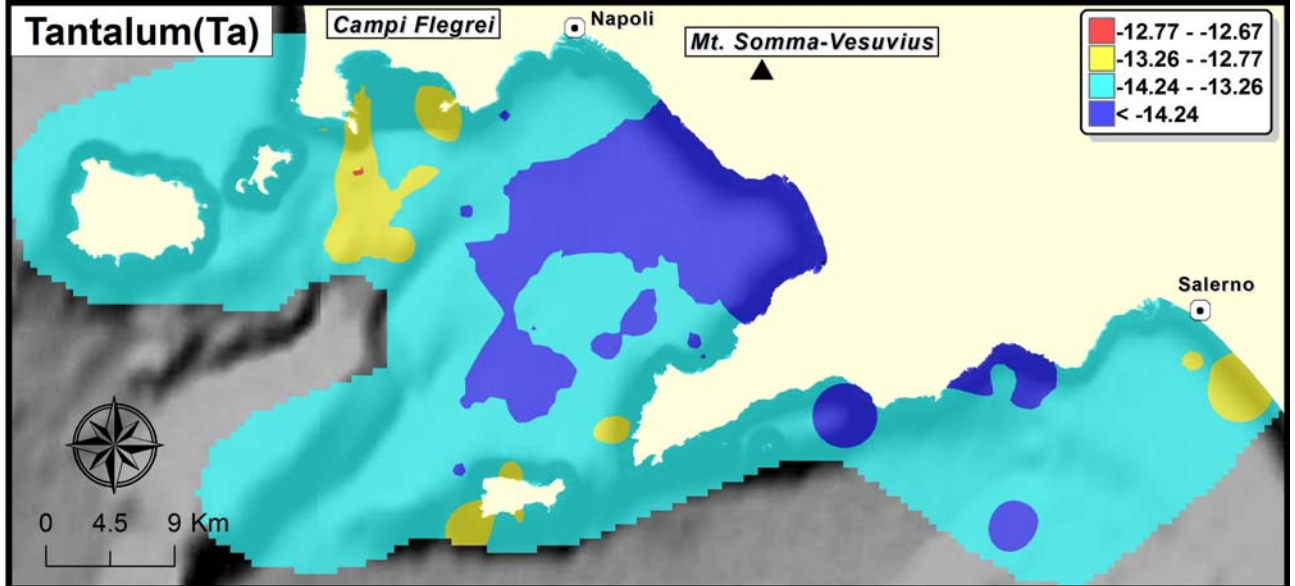
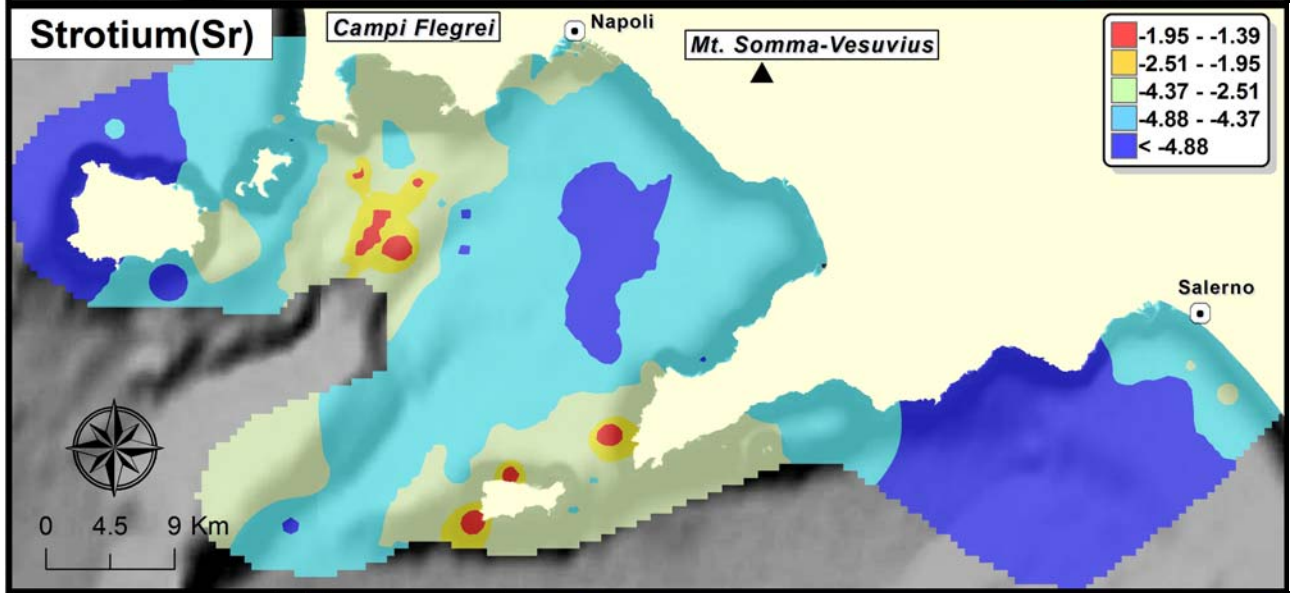
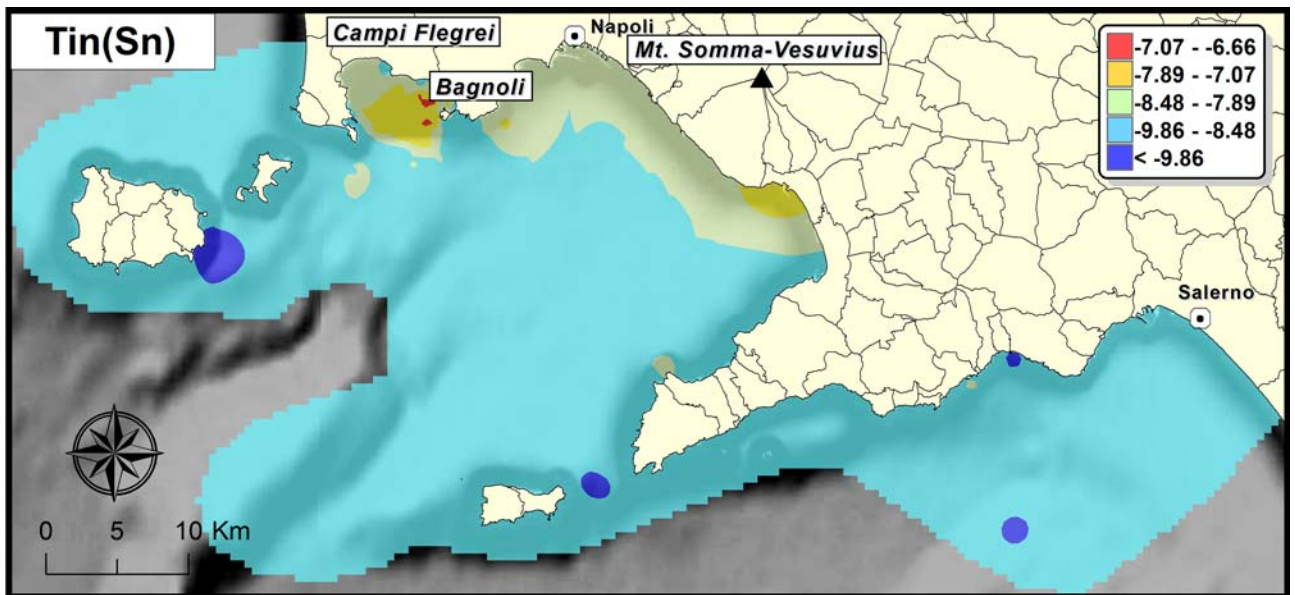


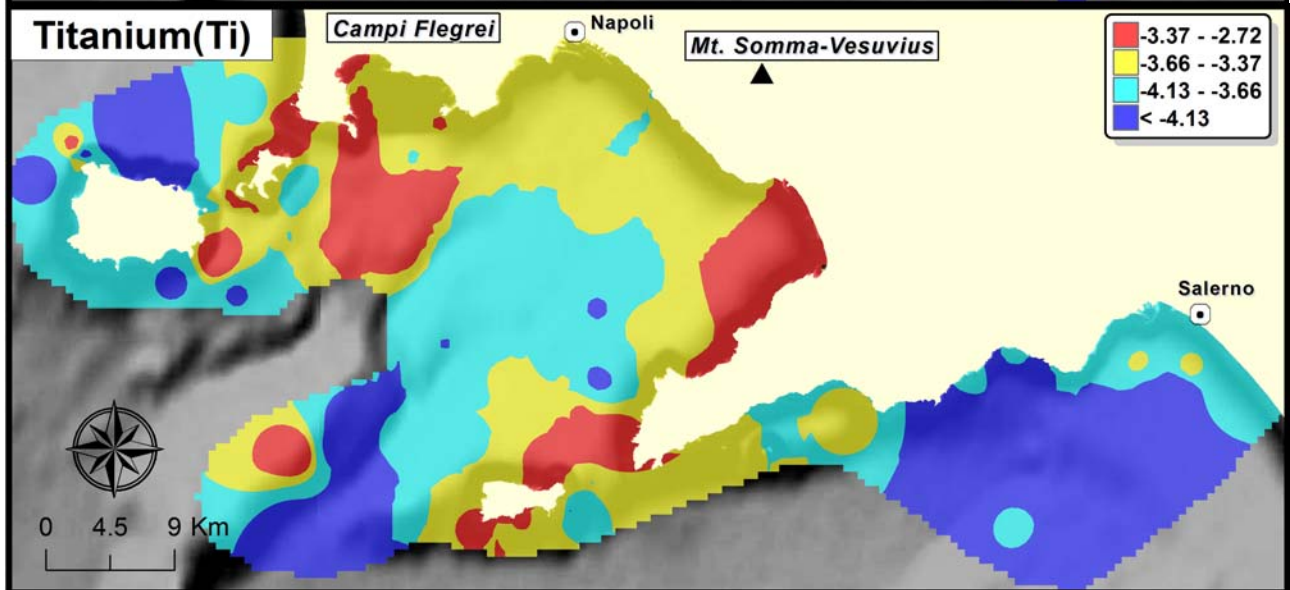
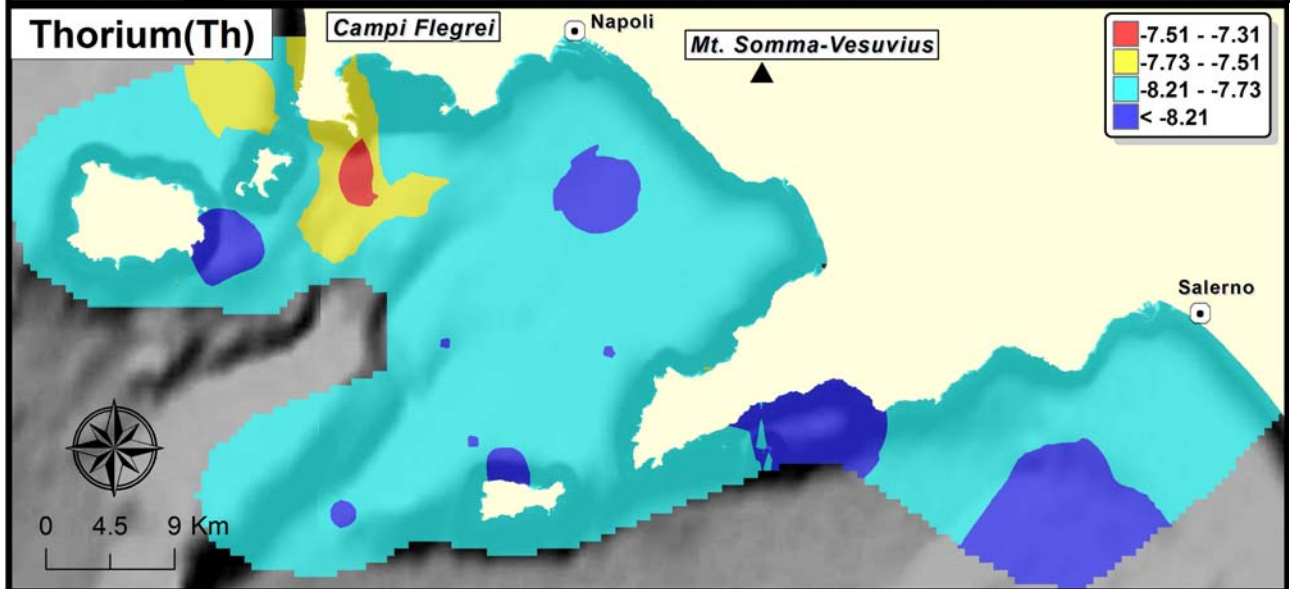
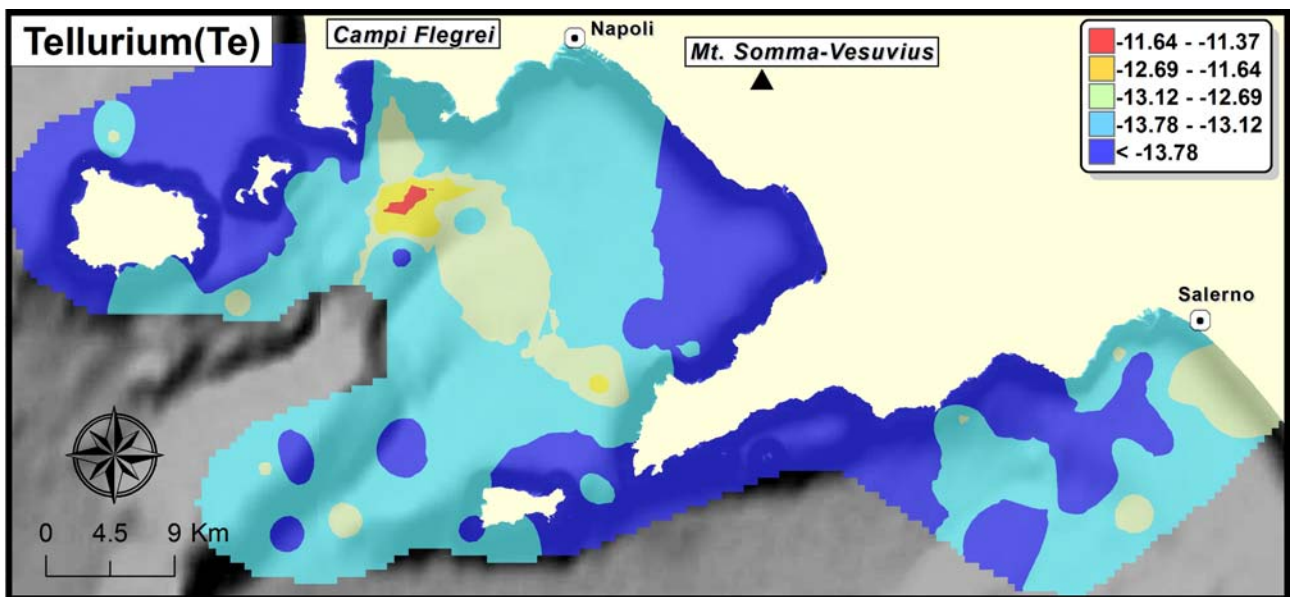


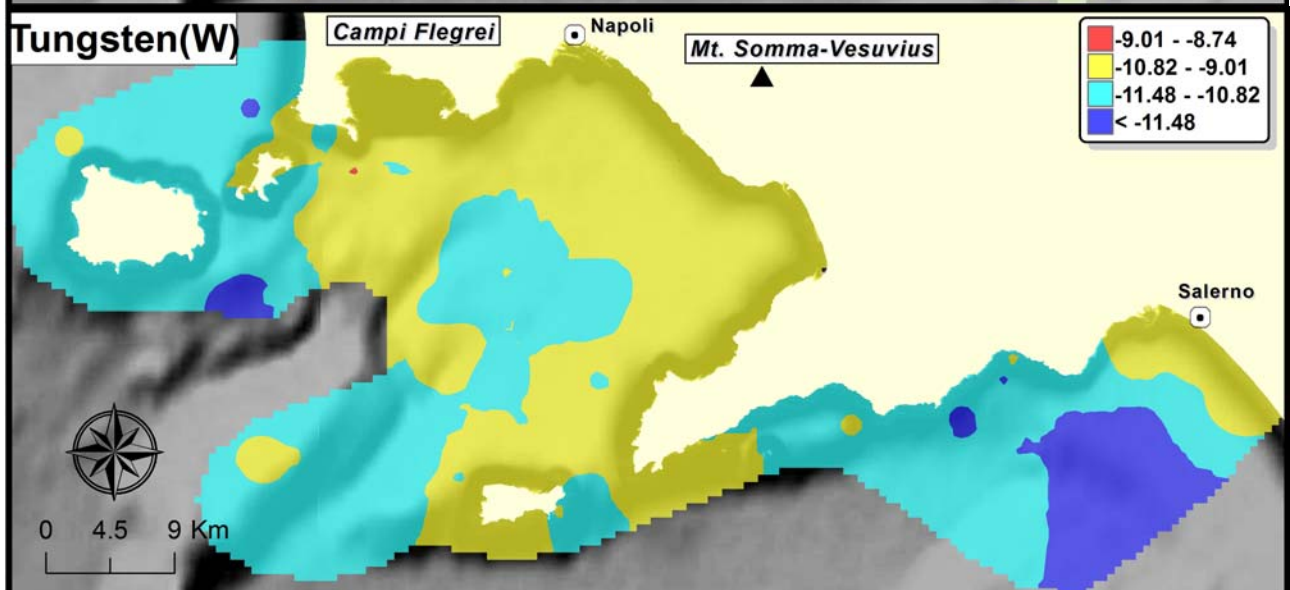
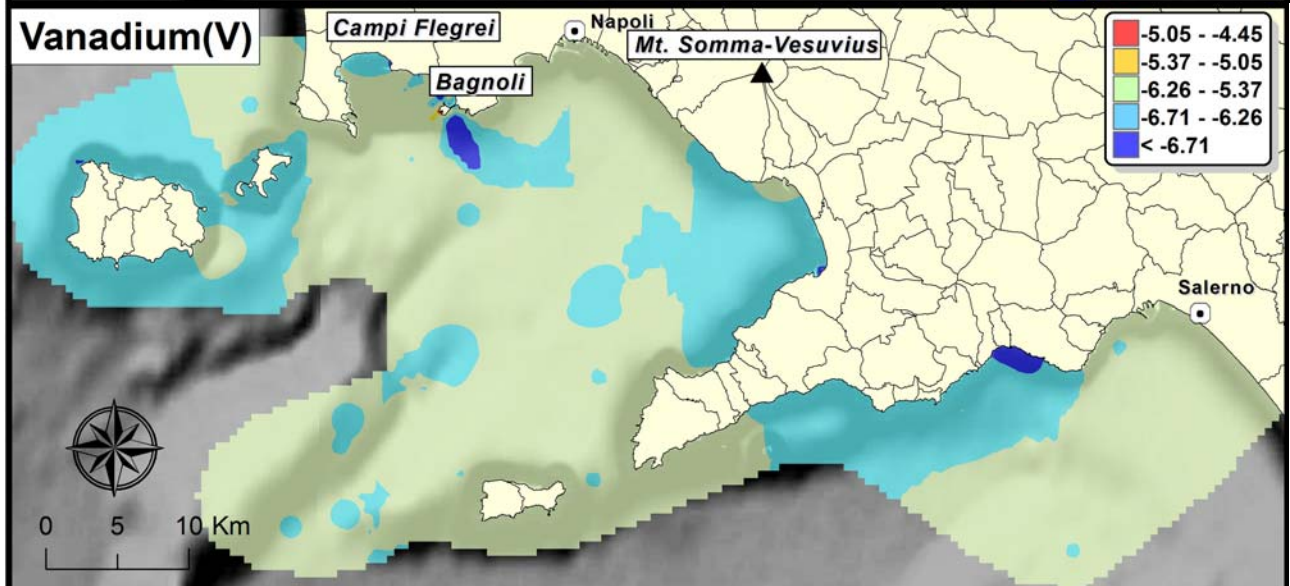
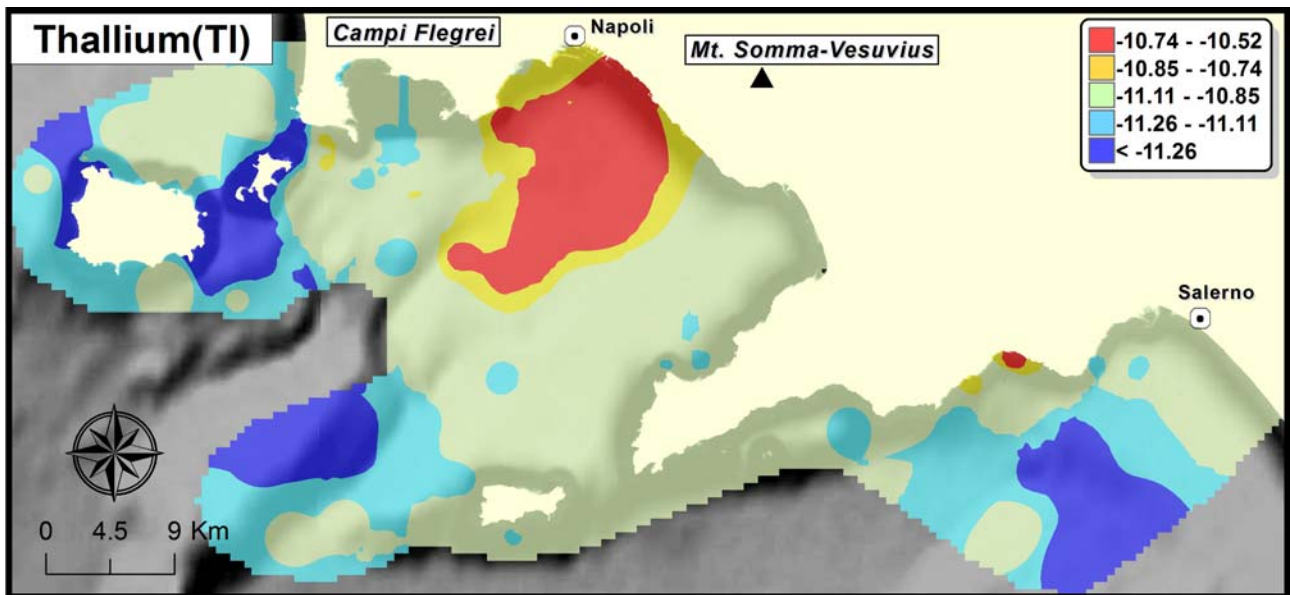


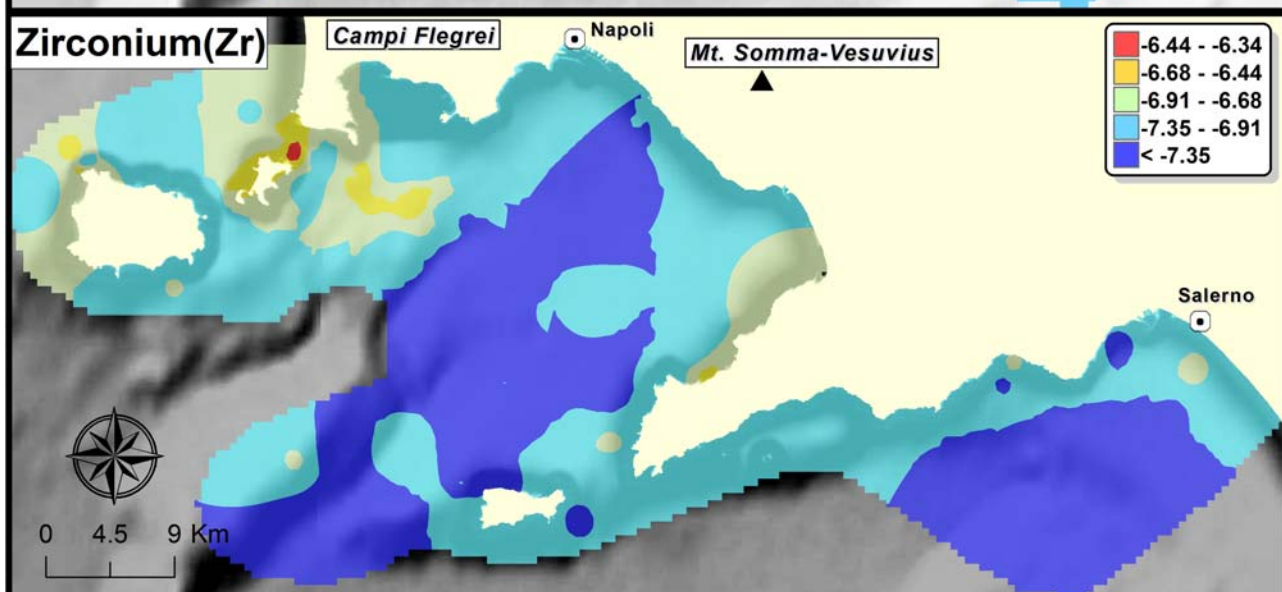
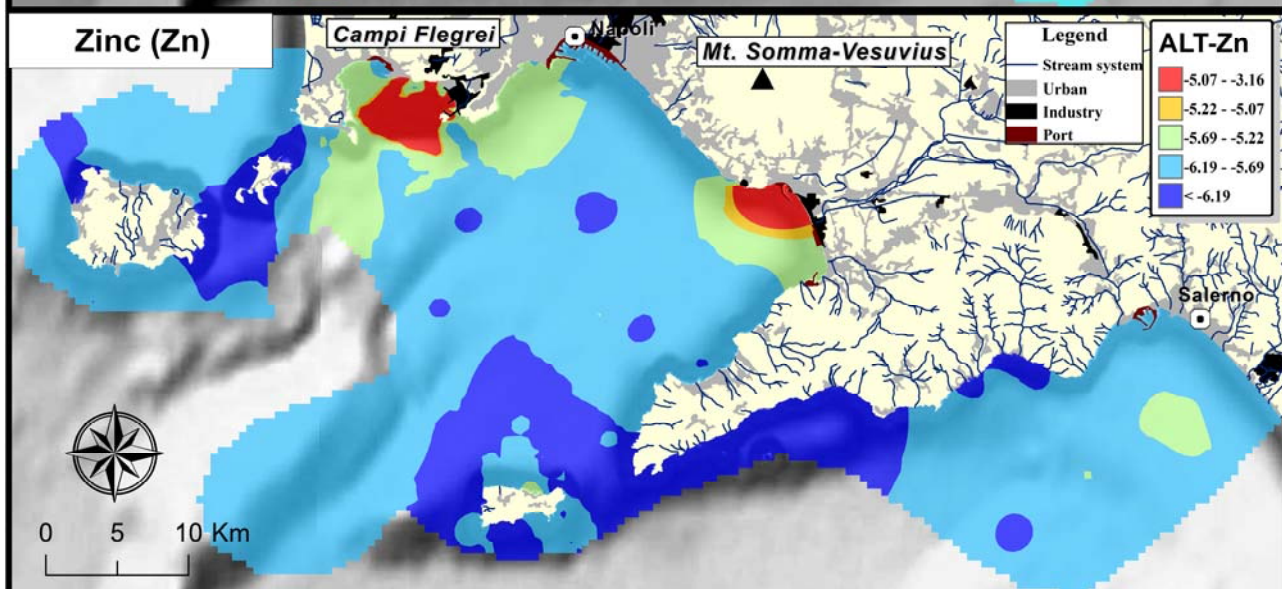
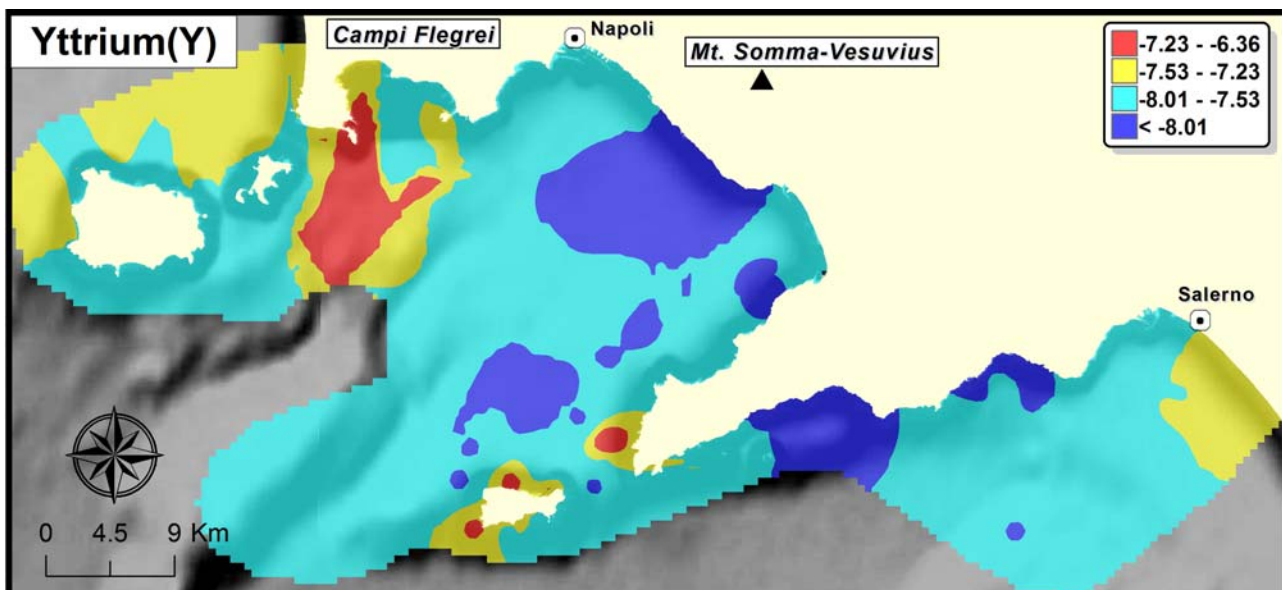








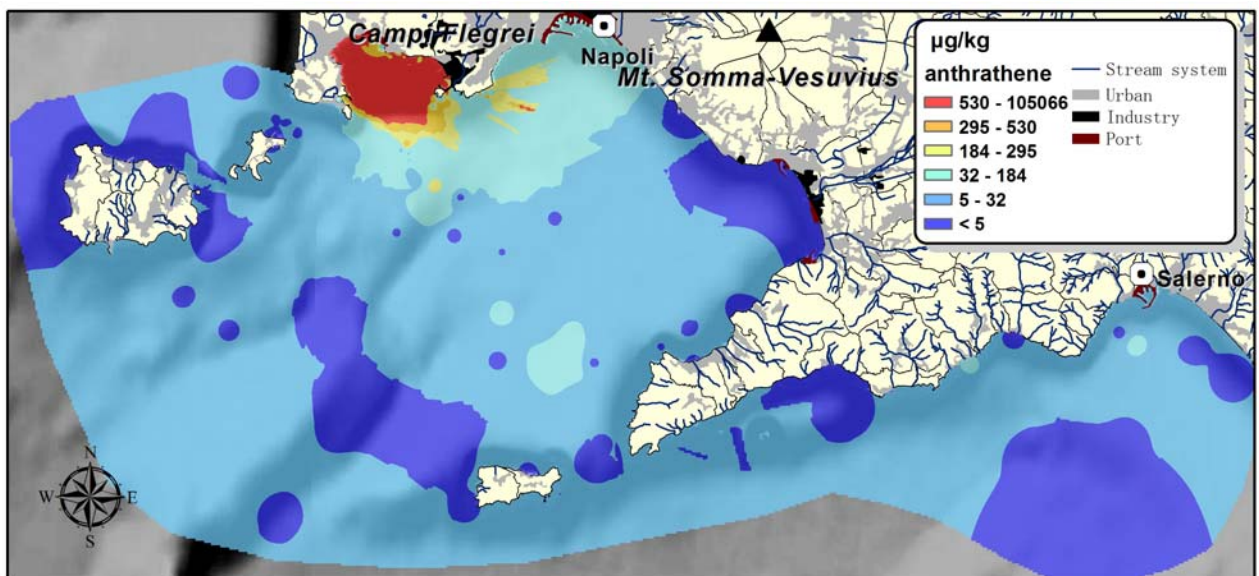
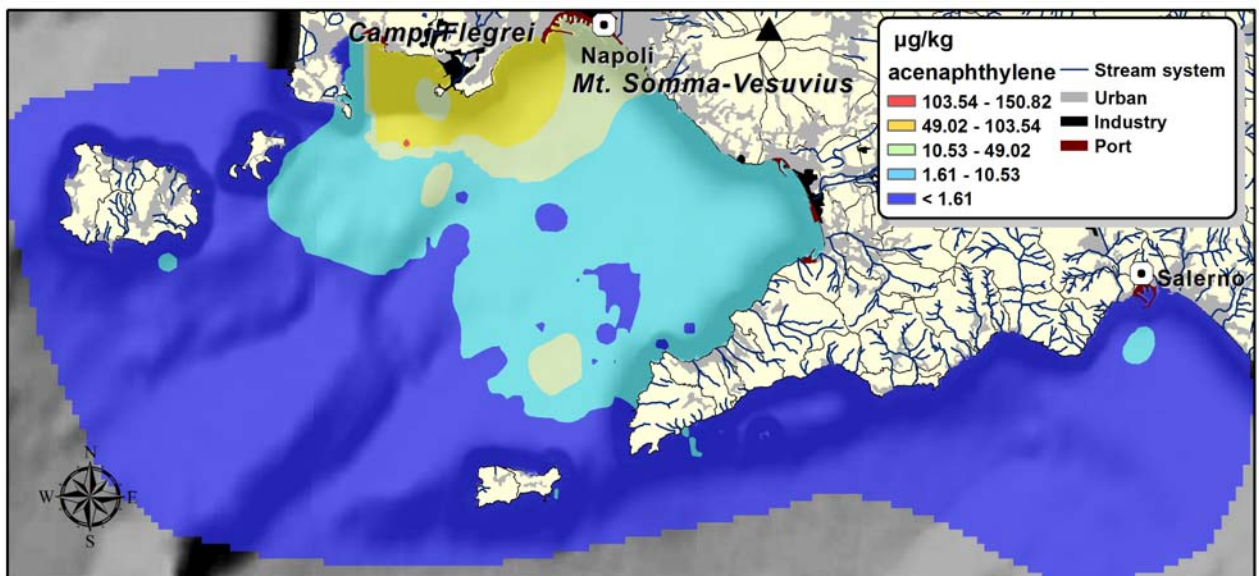
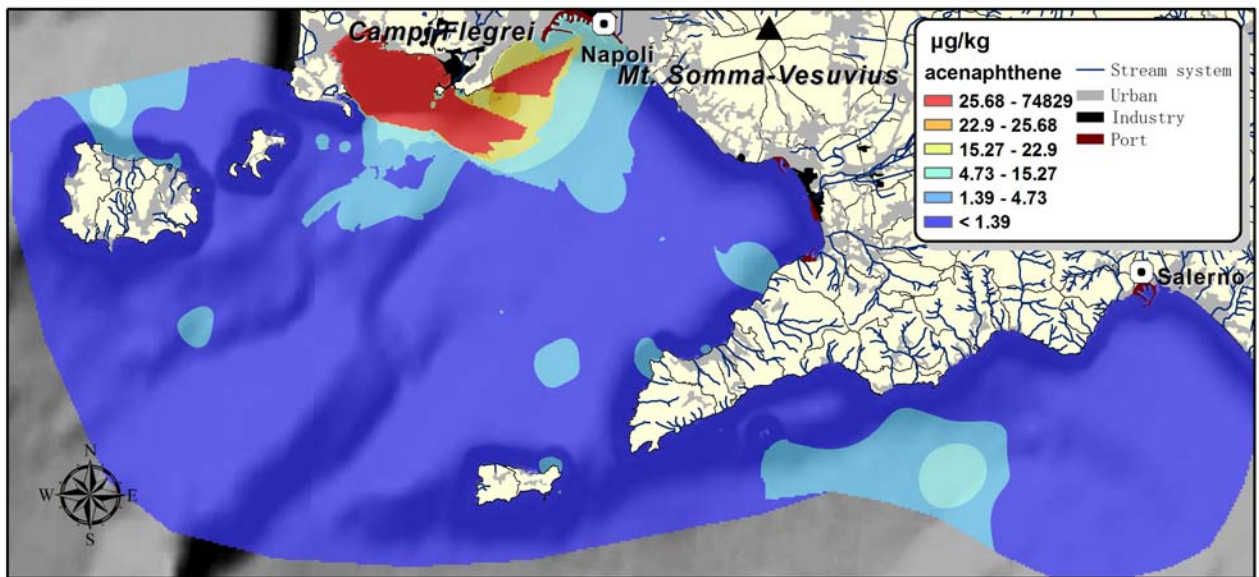


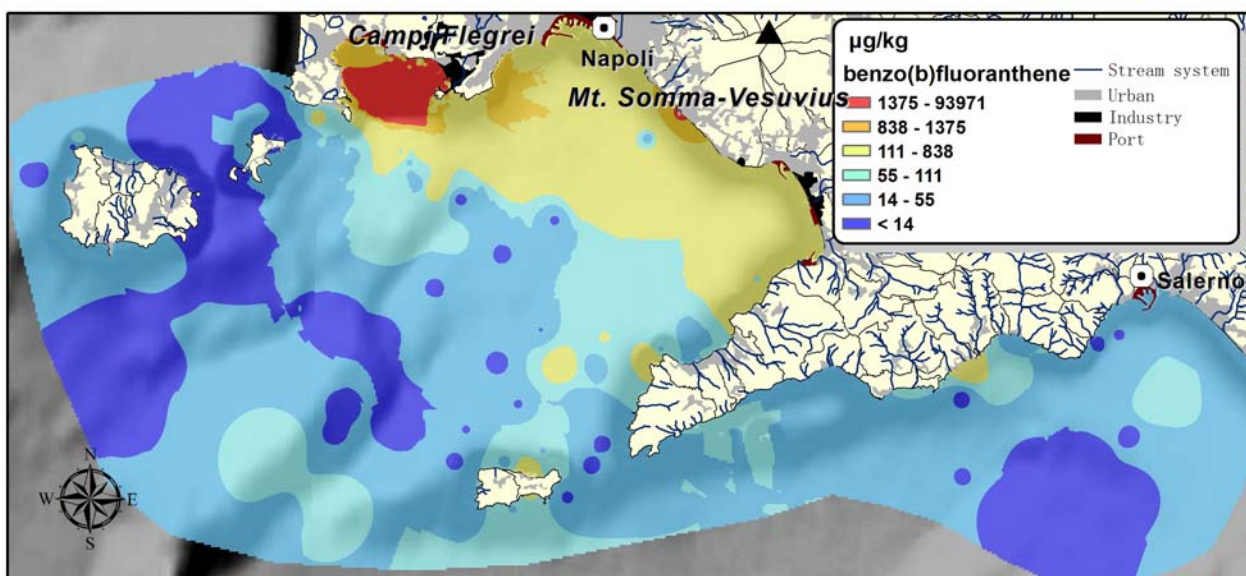
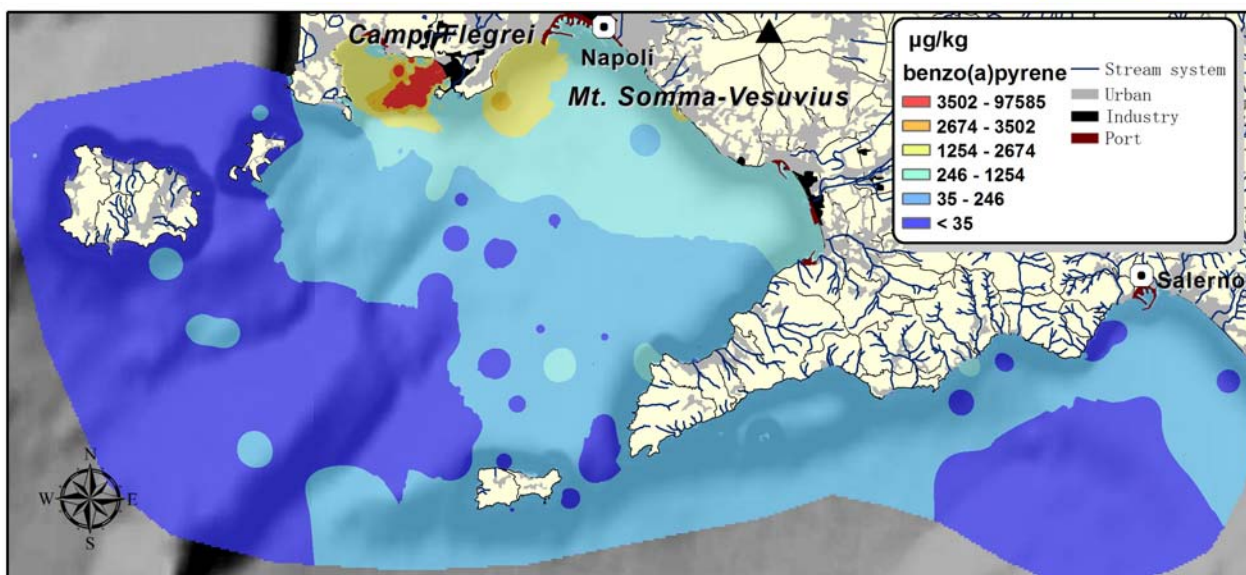
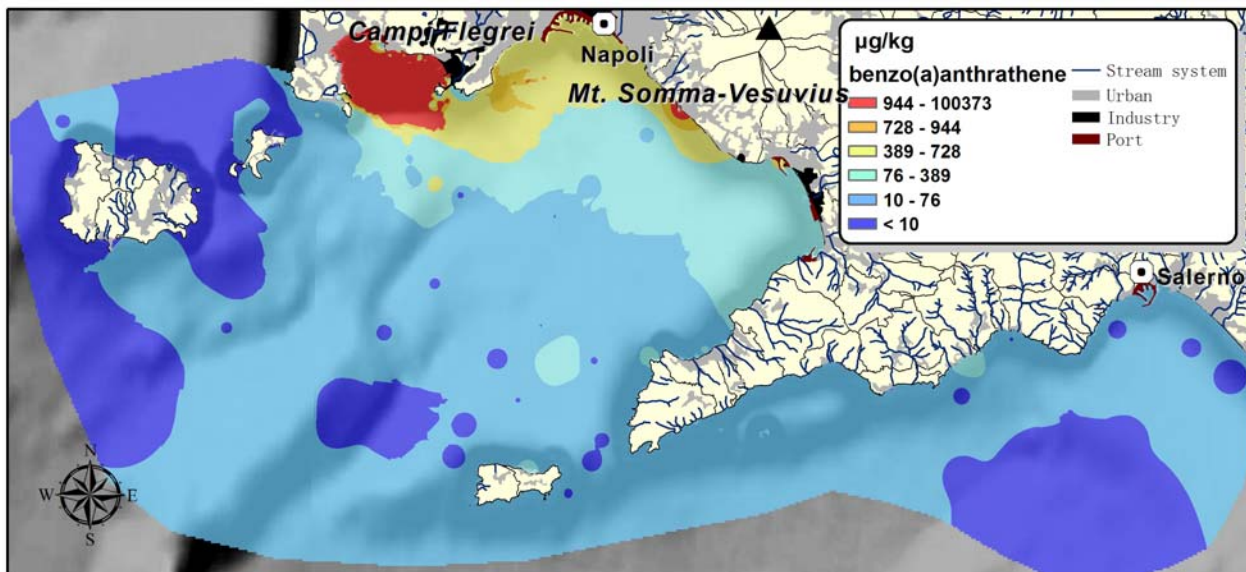


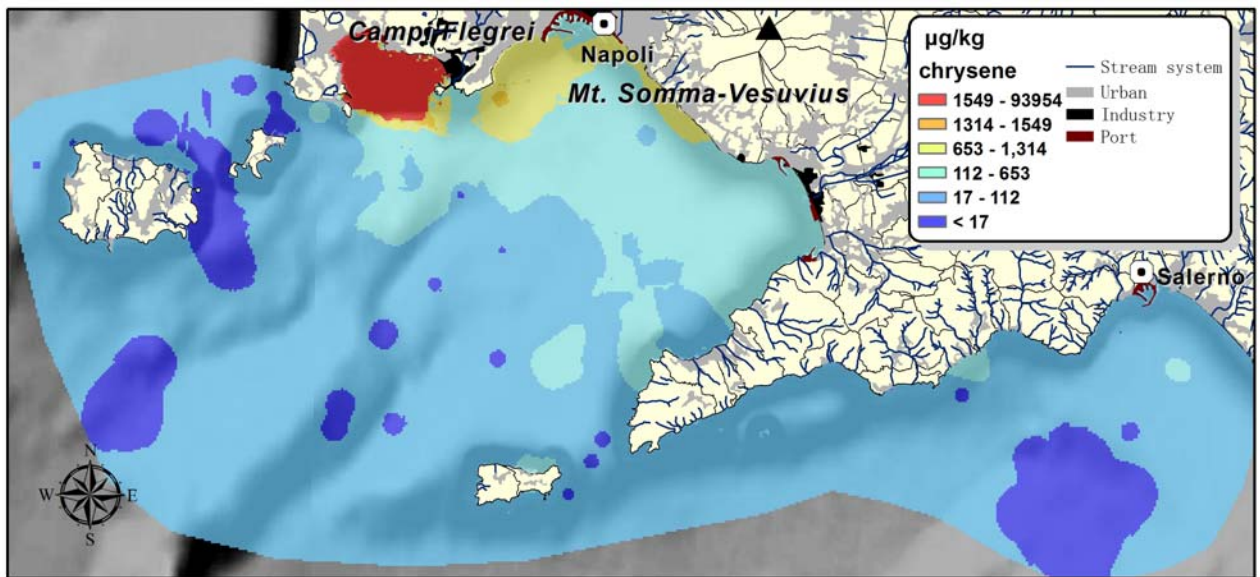
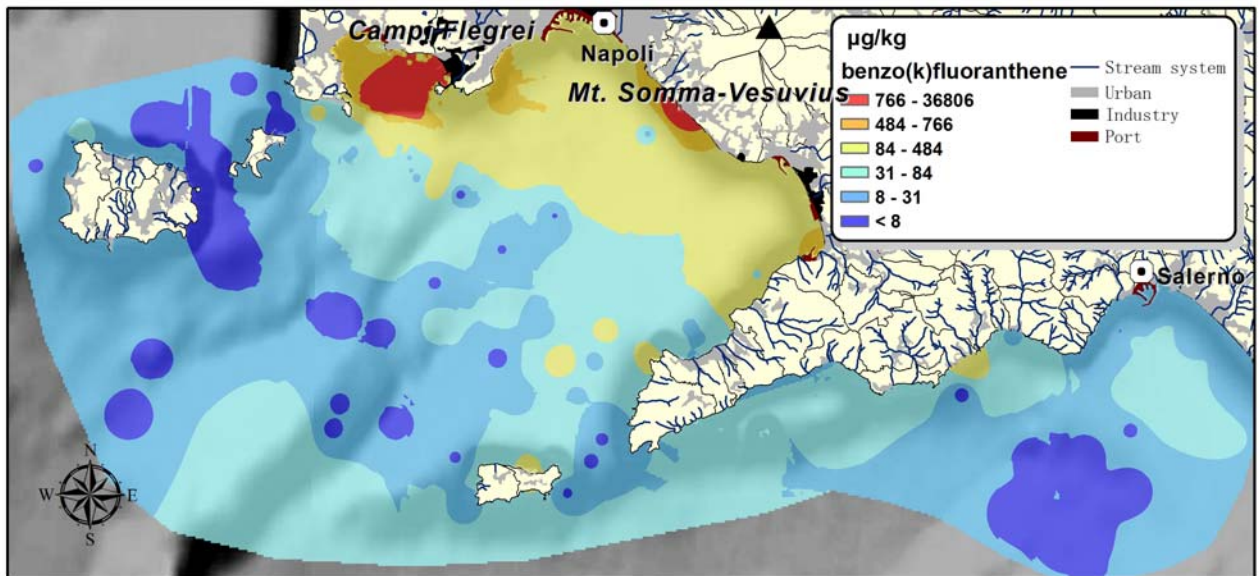
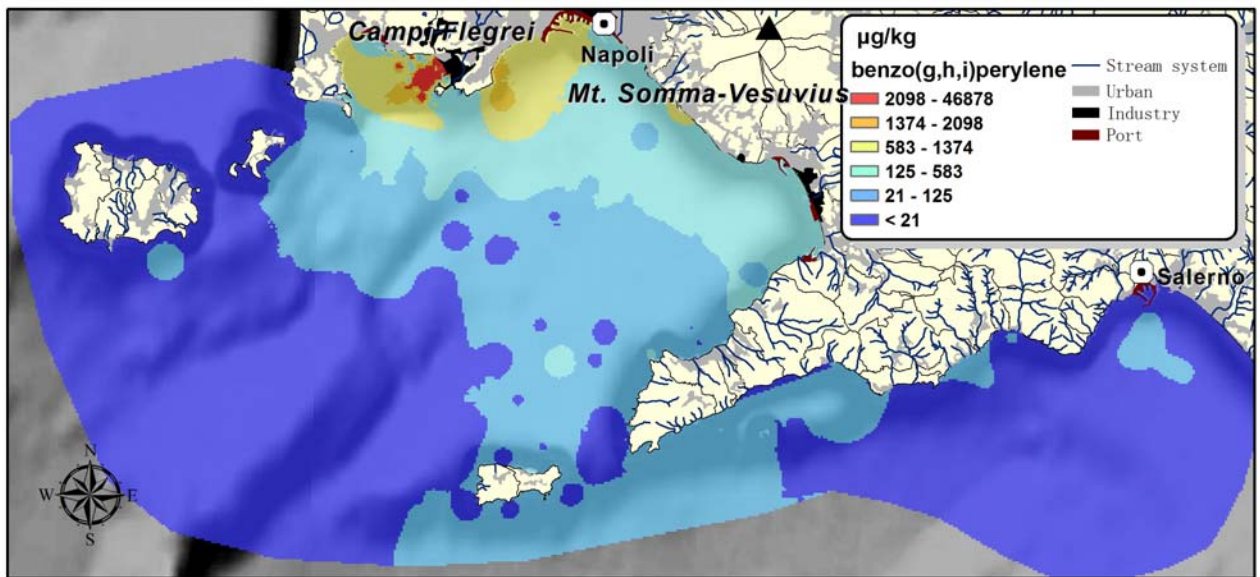
Appendix B

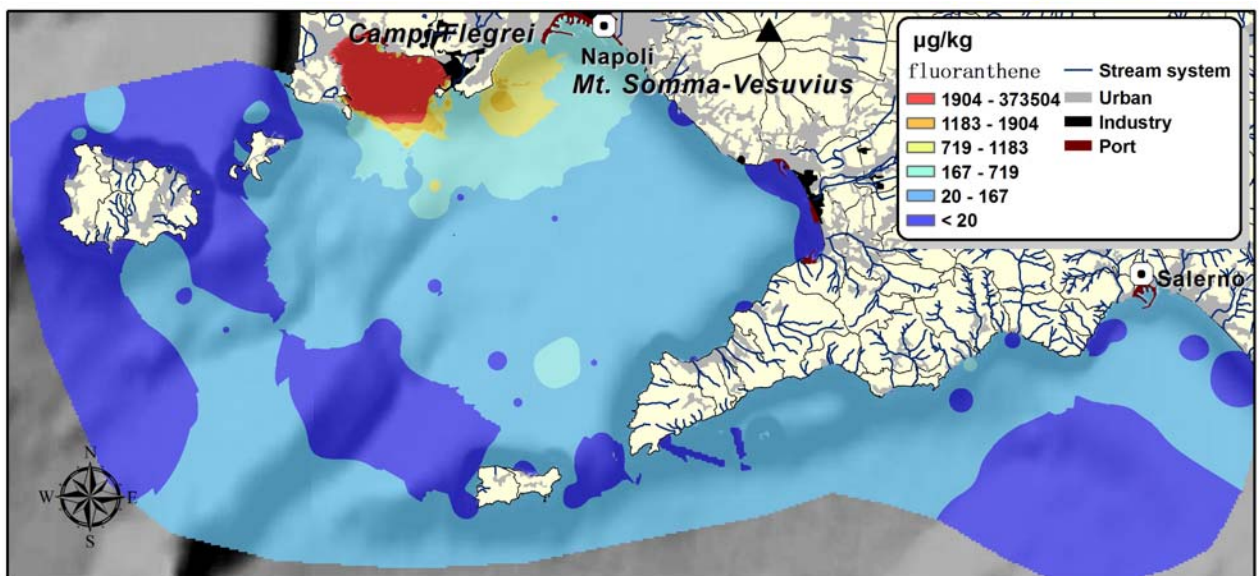
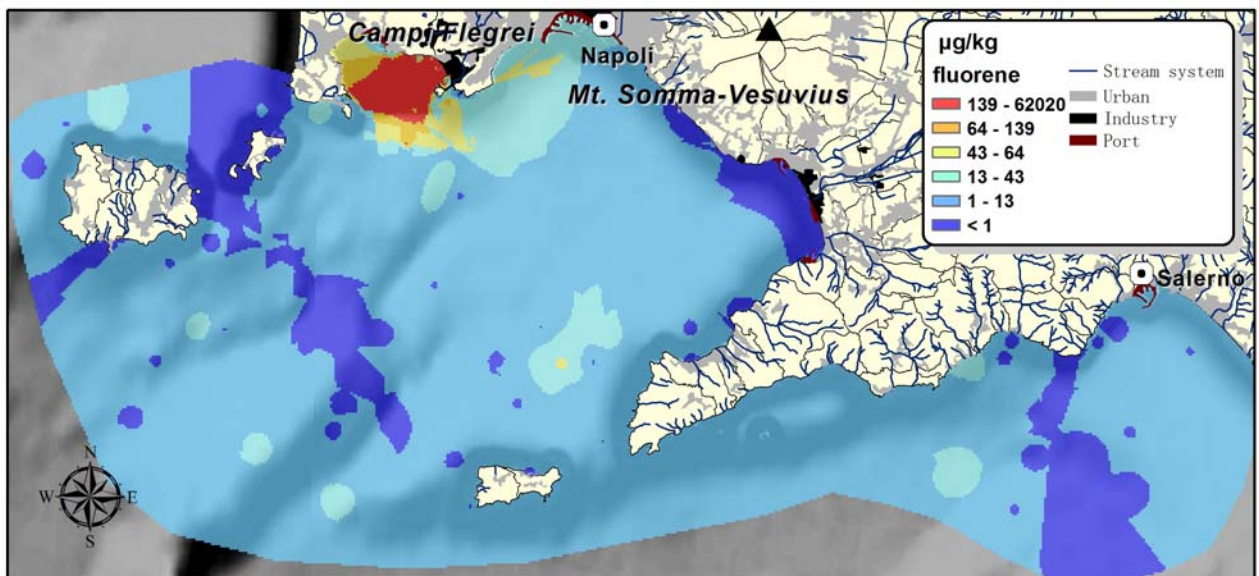
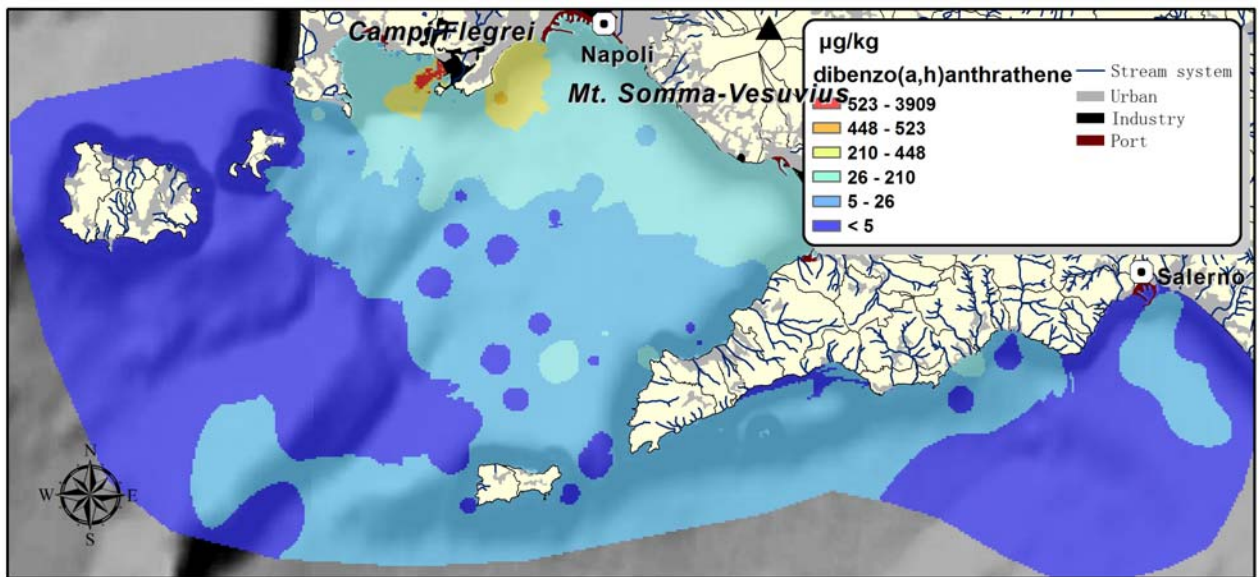
Maps of PAH (Polycyclic Aromatic Hydrocarbons) distribution in the Naples and Salerno Gulfs

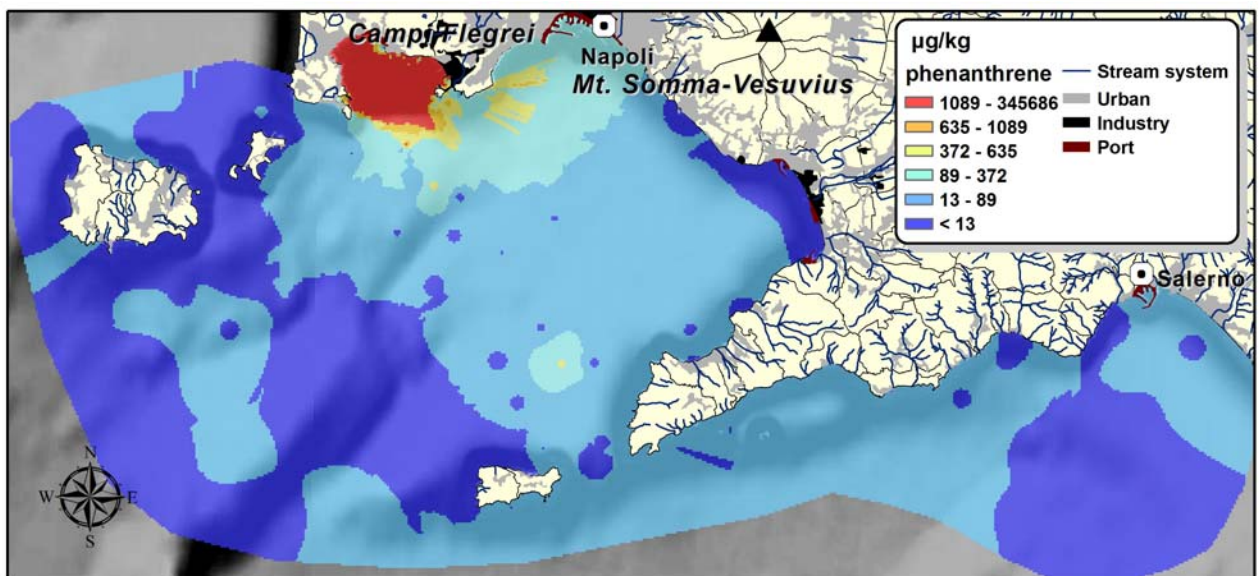
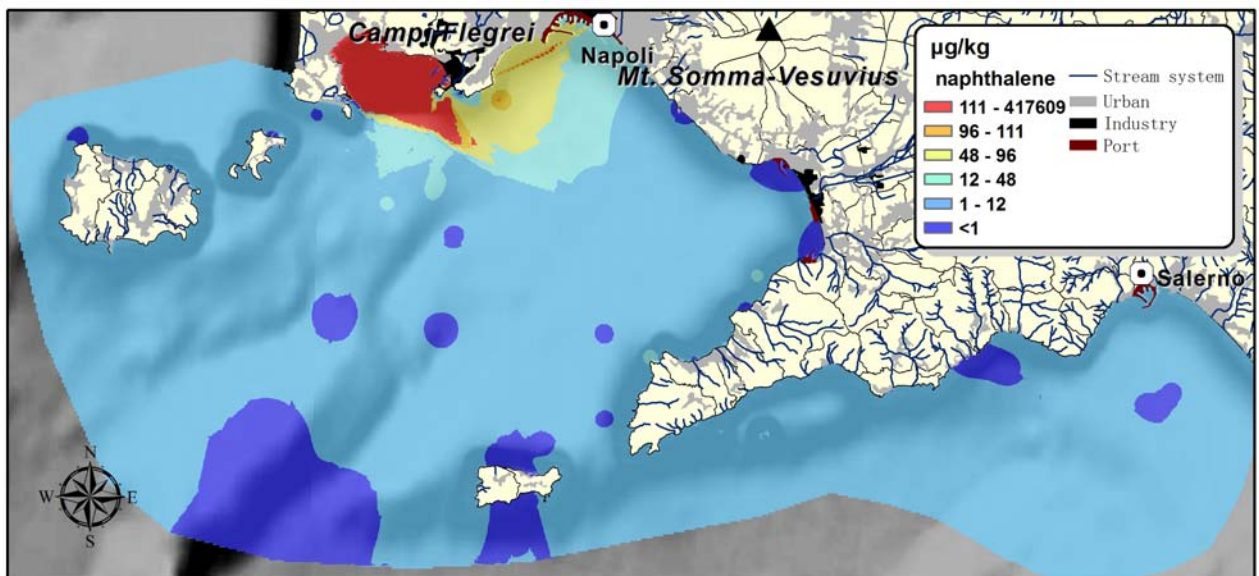
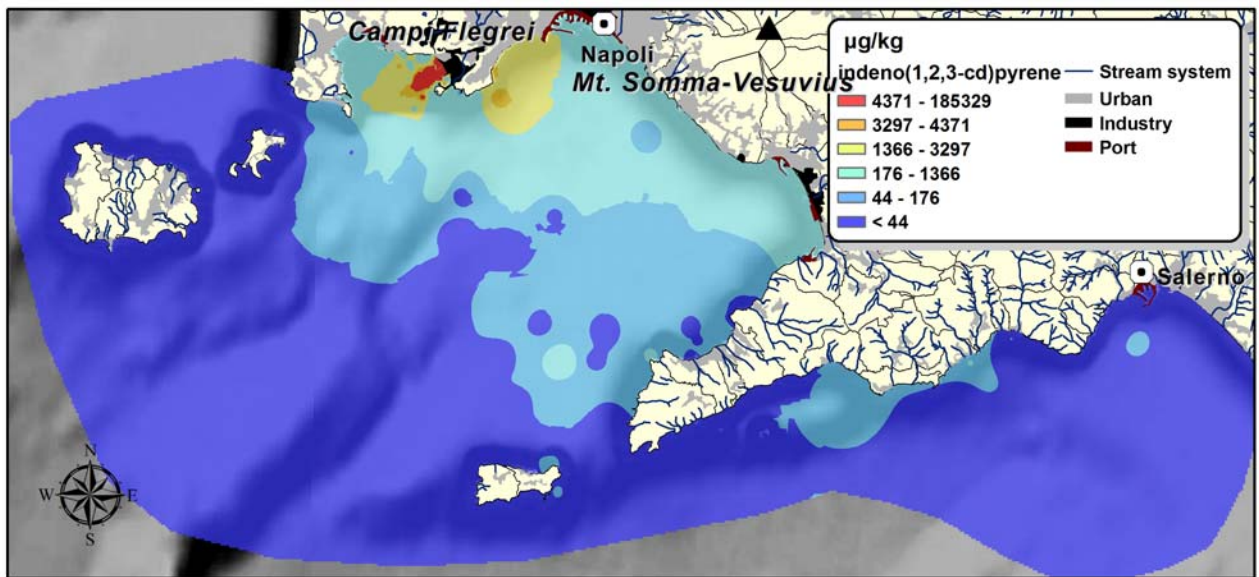
Interpolated concentration maps

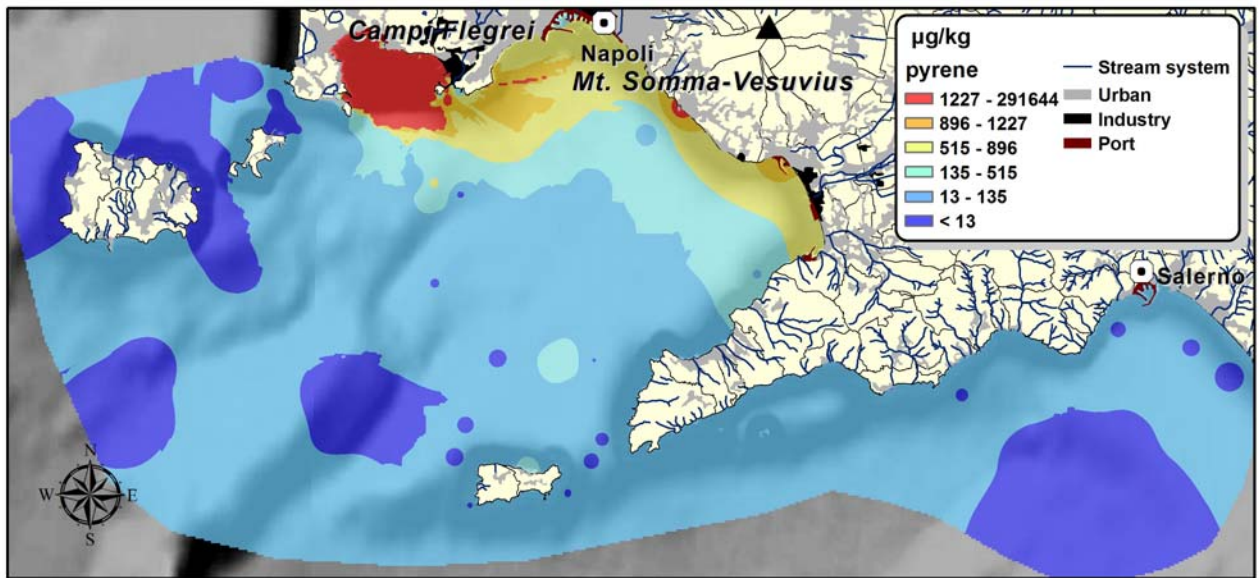








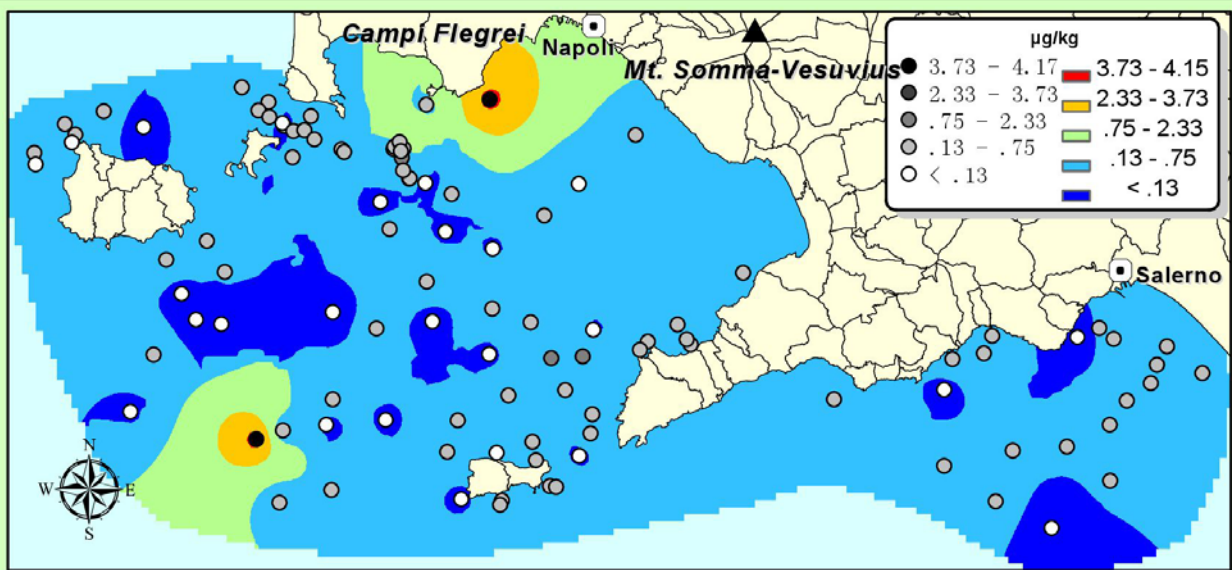




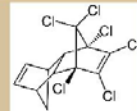
Appendix C

Maps of OCPs (Organochlorinated Pesticides) in the Naples and Salerno Gulfs

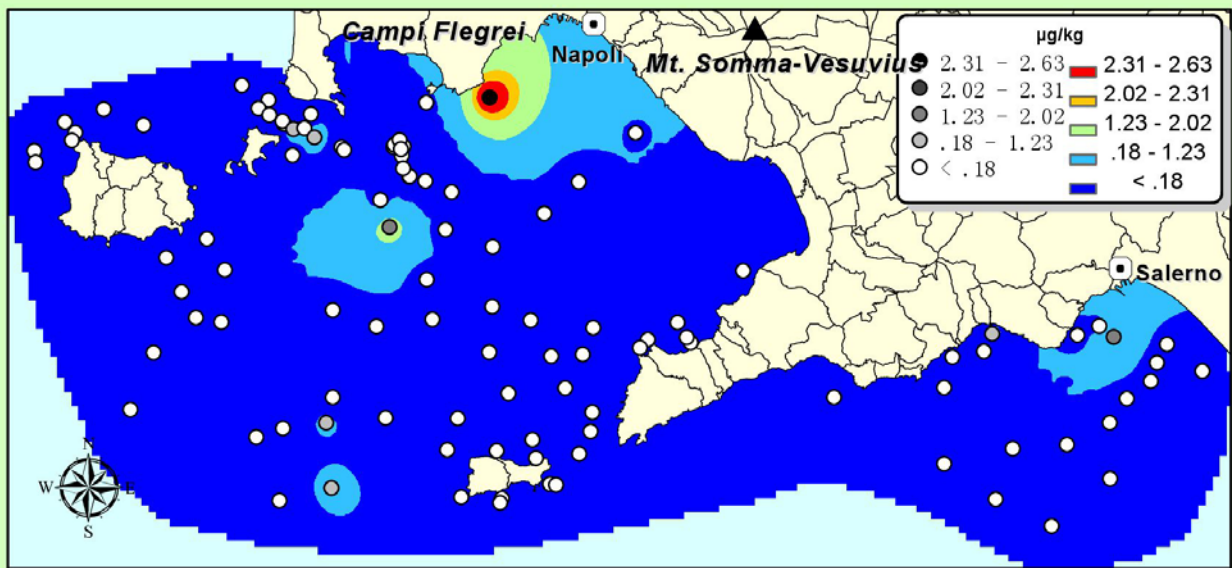
Interpolated concentration maps



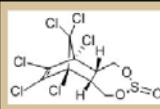
Aldrin



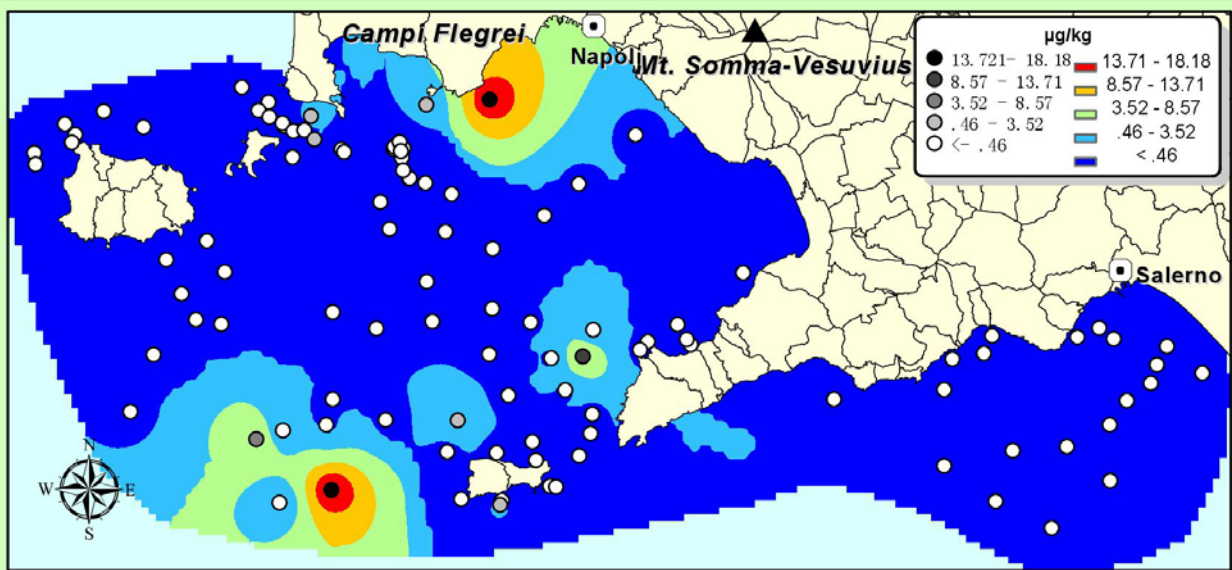
0 5 10Km



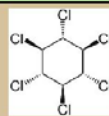
b-Endosulfan



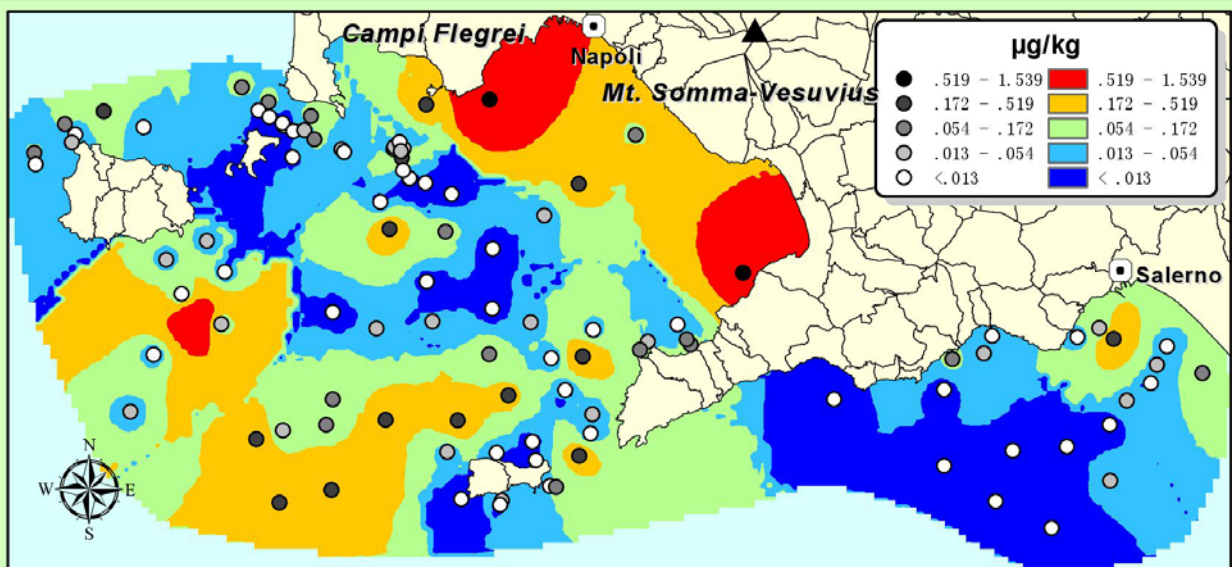
0 5 10Km



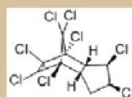
beta-Hexachlorocyclohexane
β-HCH



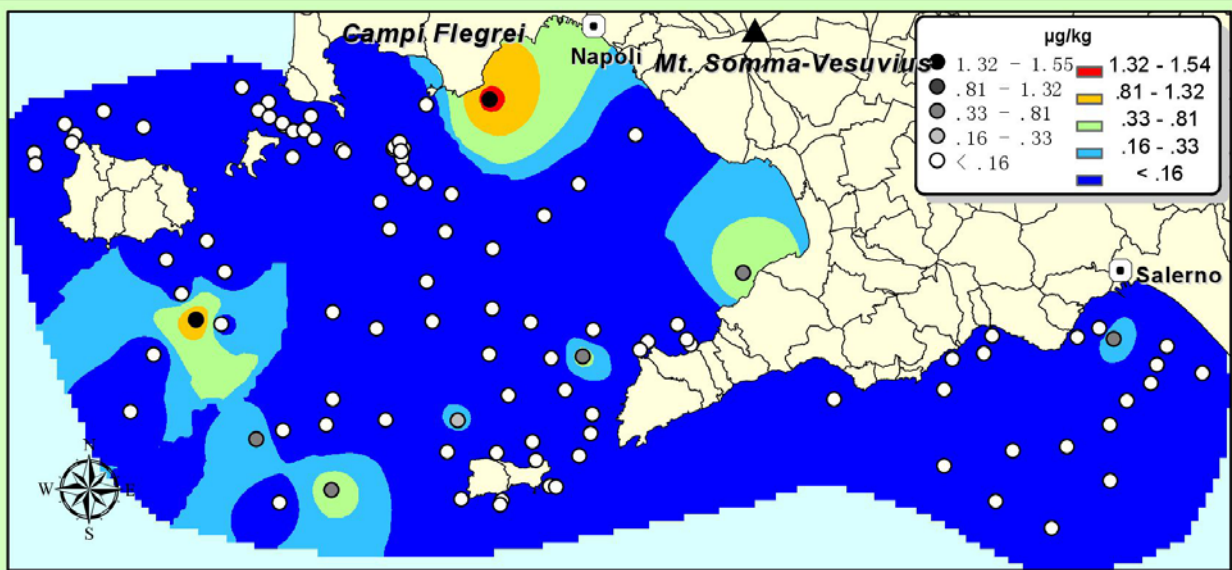
0 5 10Km



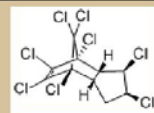
Chlordane



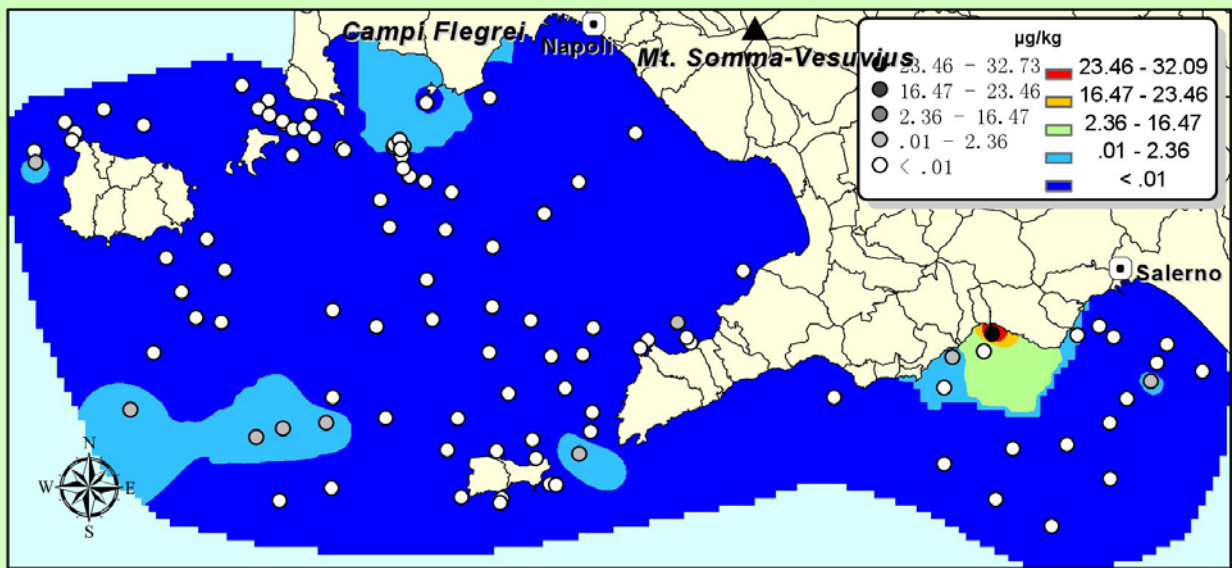
0 5 10Km



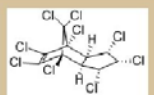
cis-Chlordane



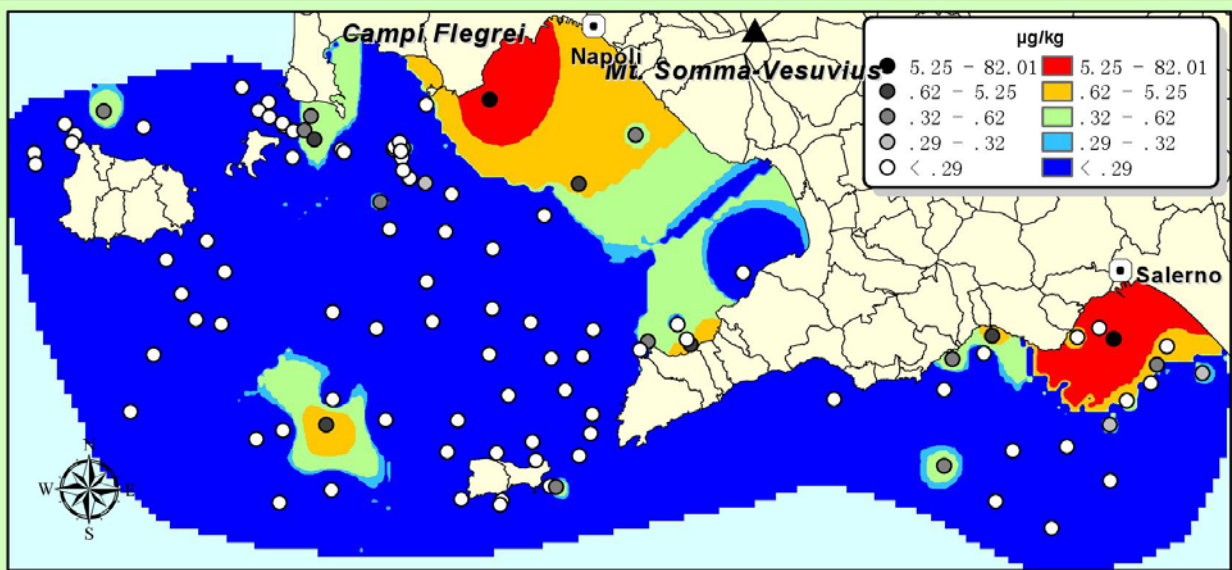
0 5 10Km



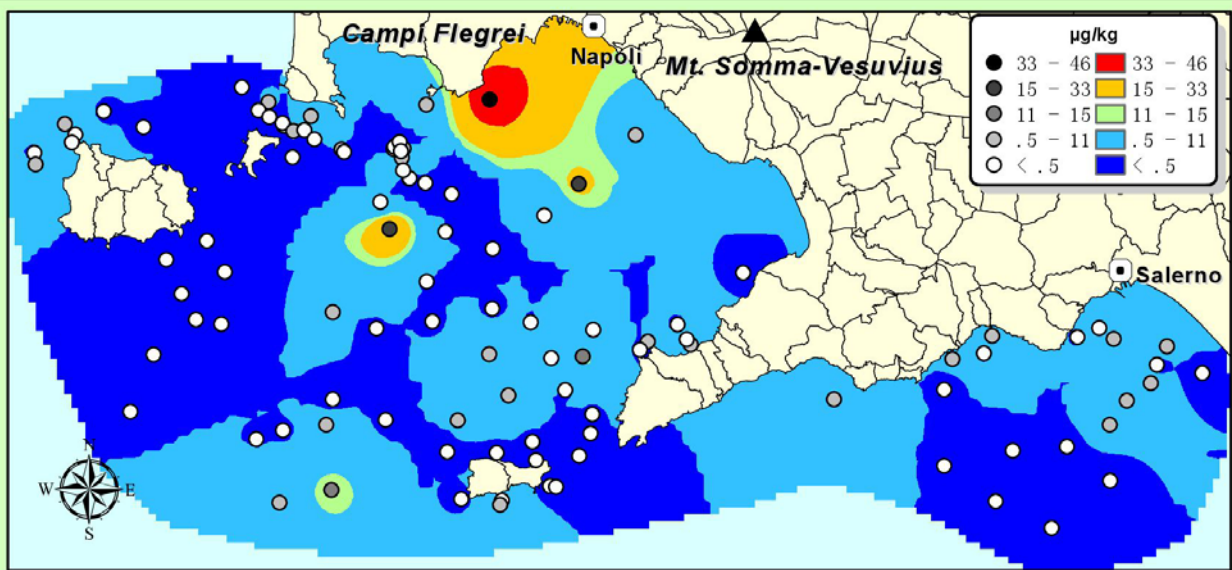
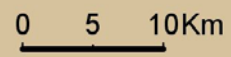
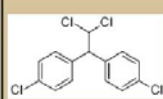
cis-Nonachlor



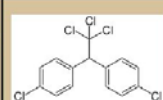
0 5 10Km

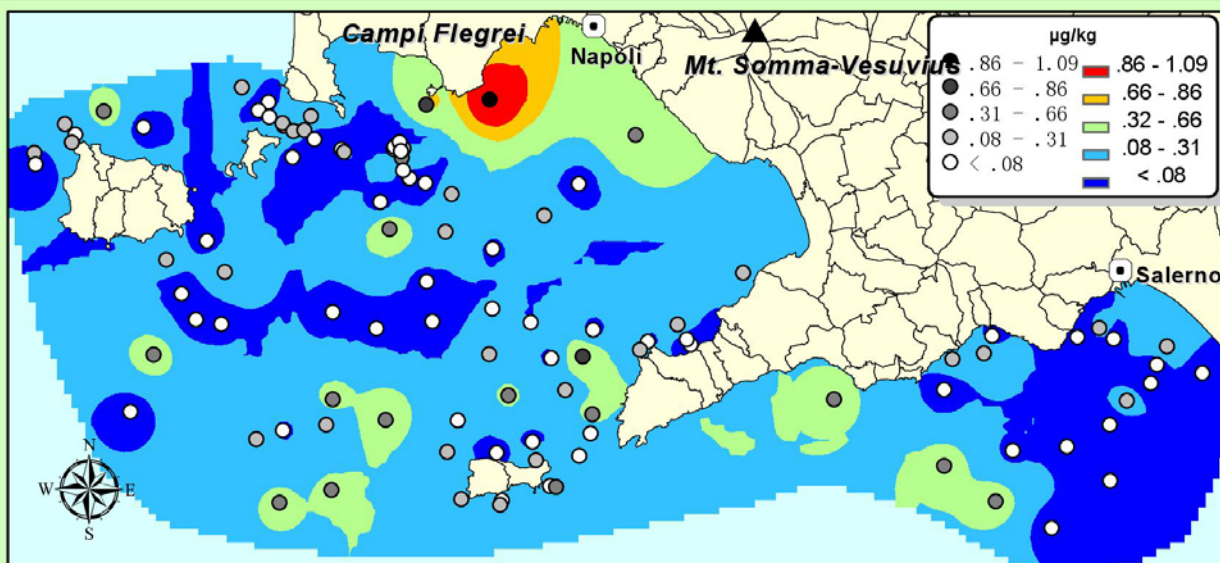


**Dichlorodiphenyldichloroethane
 DDD**

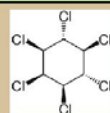


**Dichlorodiphenyltrichloroethane
 DDT**

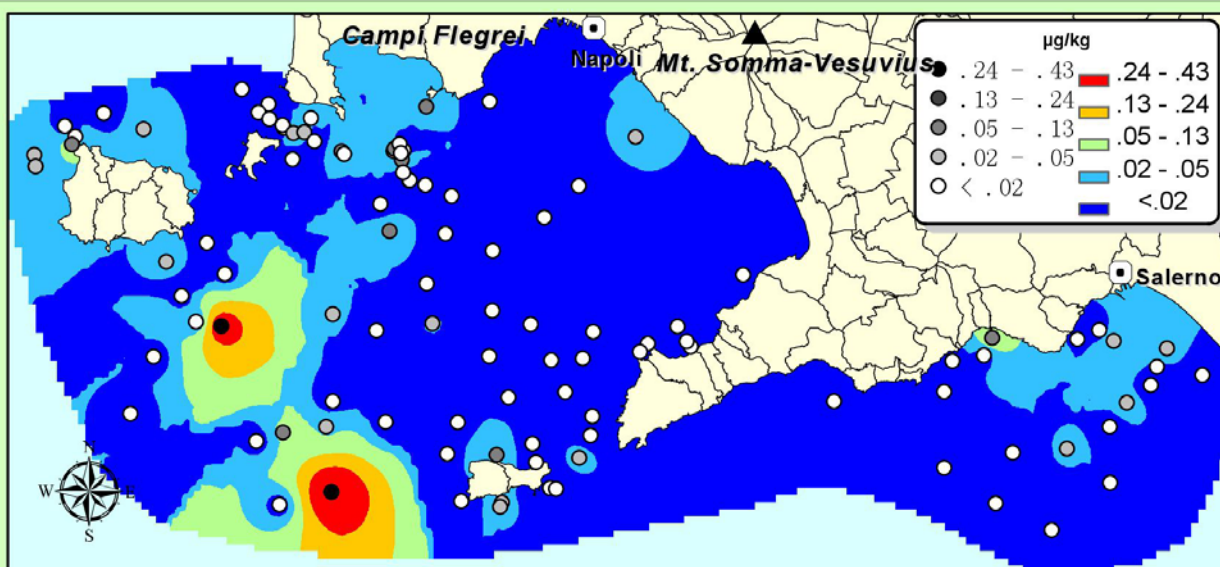




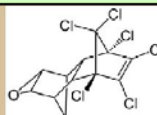
delta-Hexachlorocyclohexane
δ-HCH



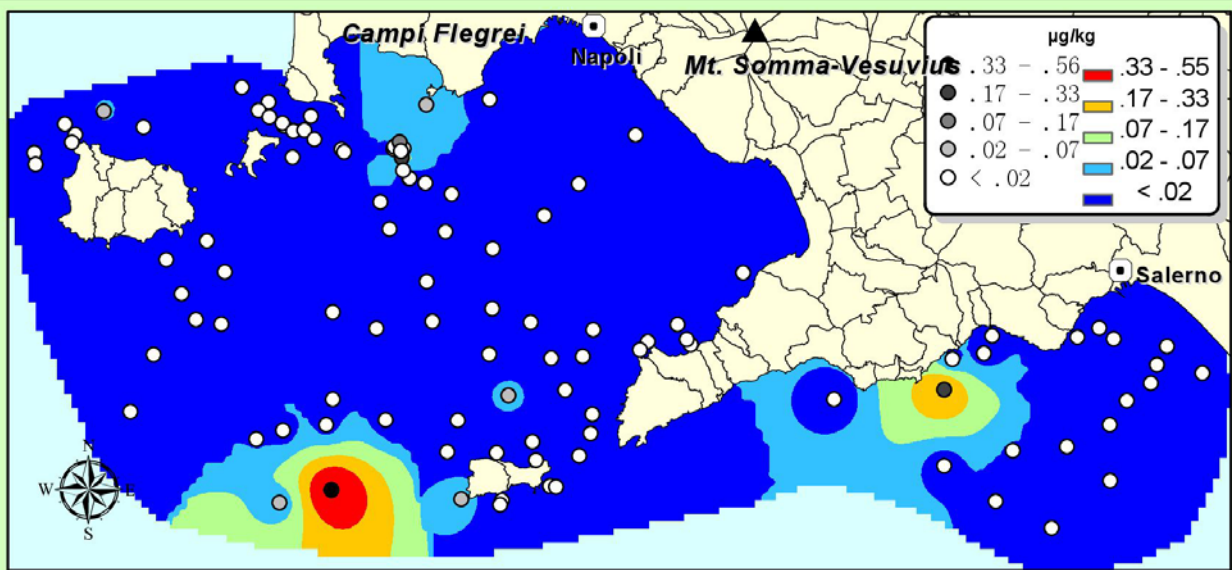
0 5 10Km



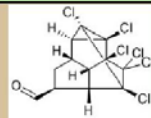
Dieldrin



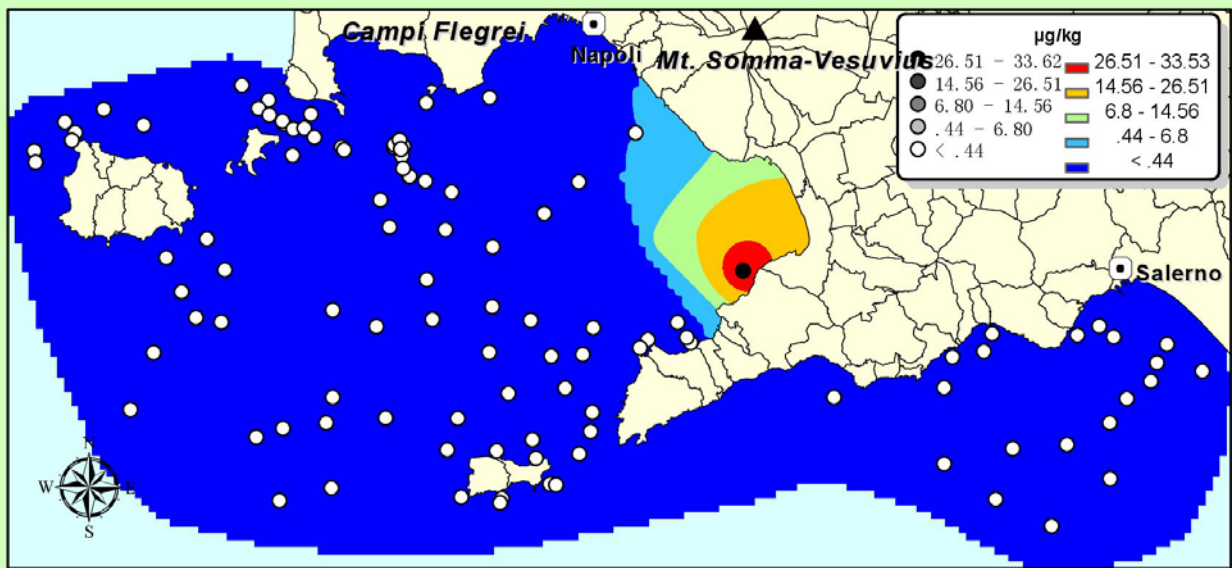
0 5 10Km



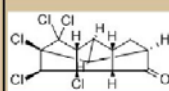
Endrin aldehyde



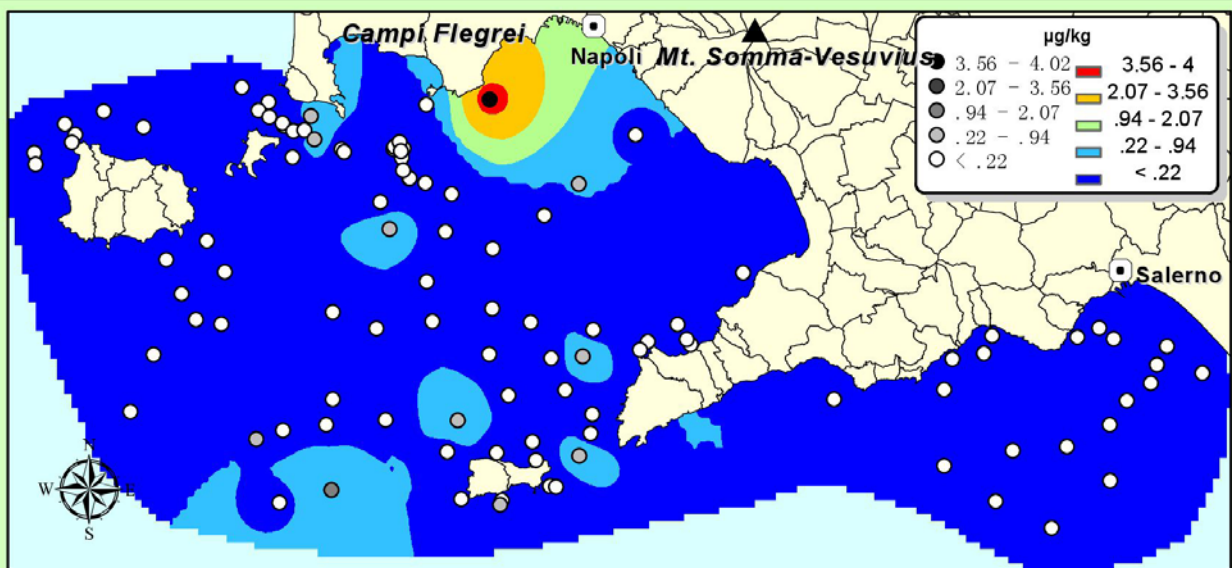
0 5 10Km



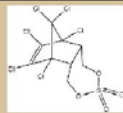
Endrin ketone



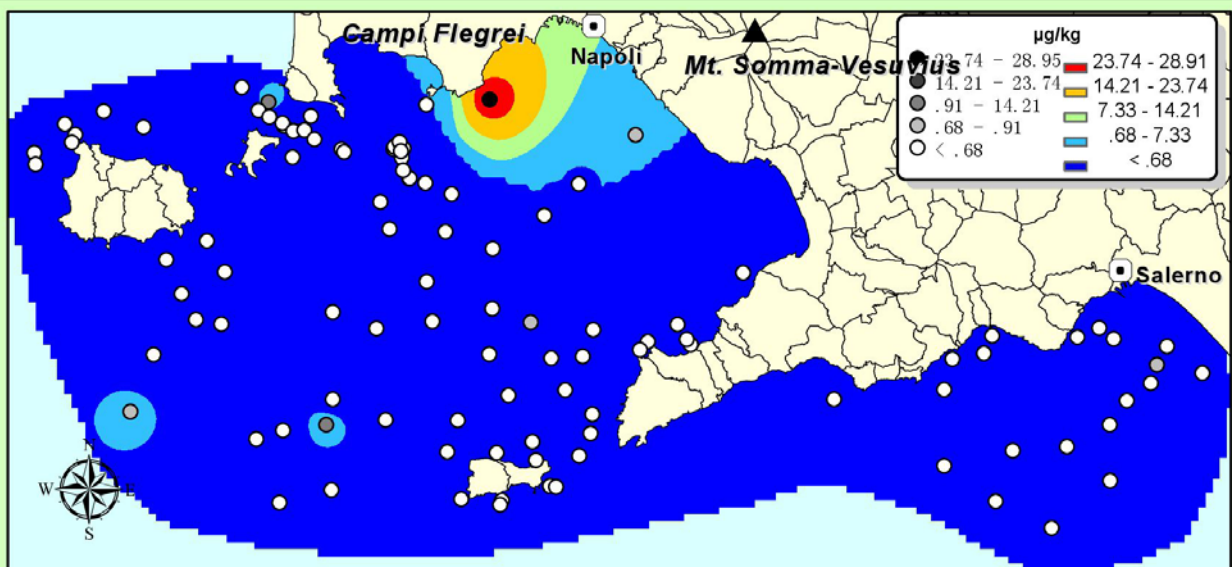
0 5 10Km



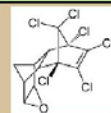
Endosulfan sulfate



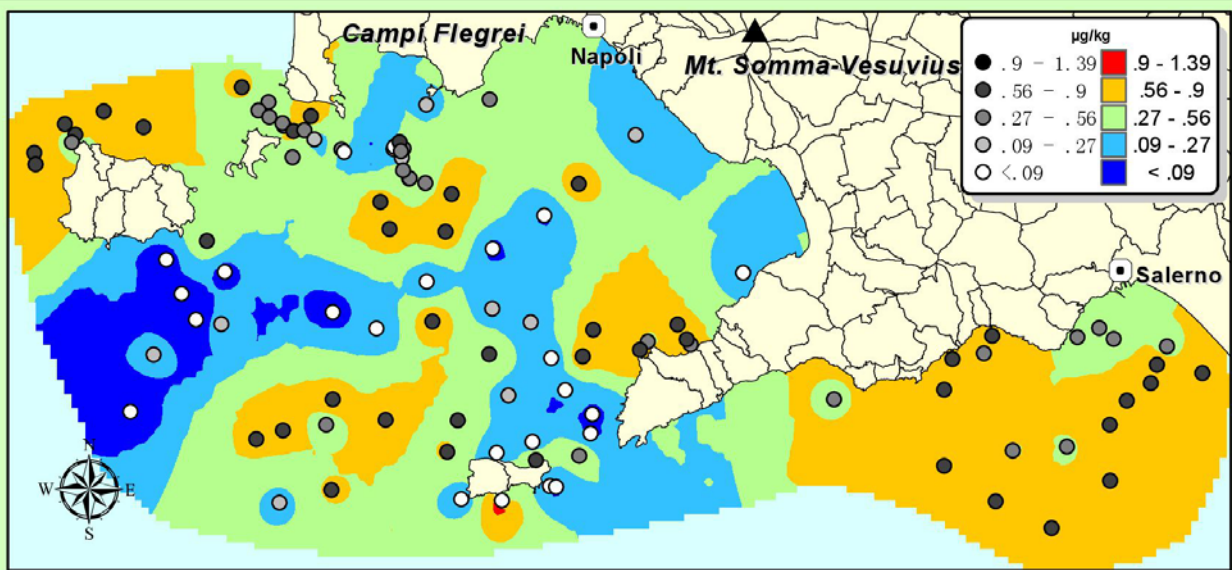
0 5 10Km



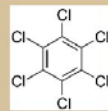
Endrin



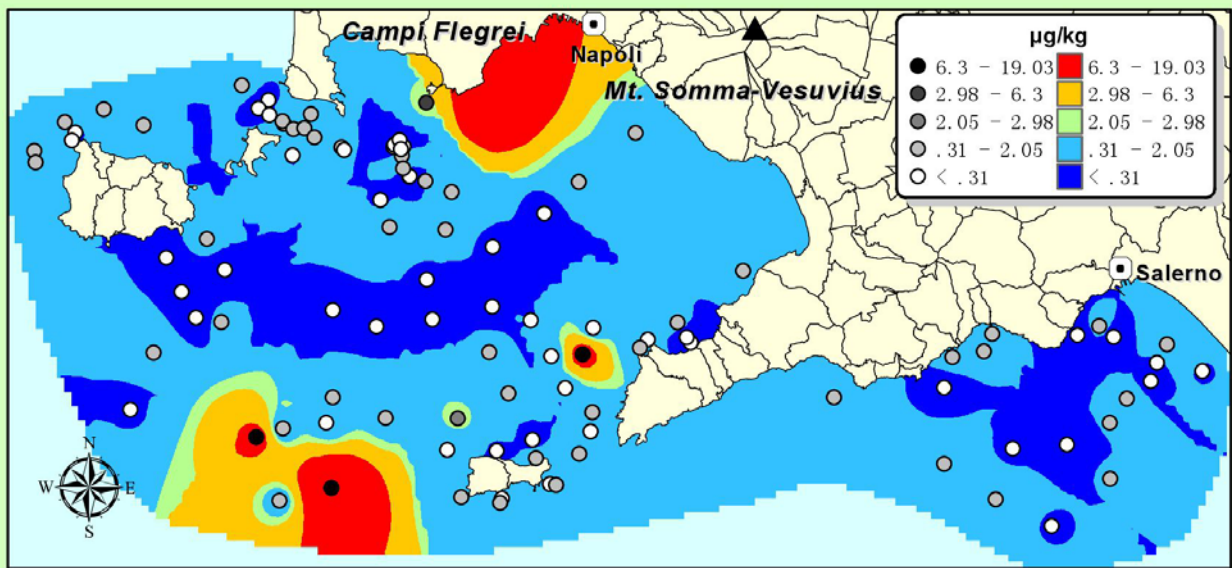
0 5 10Km



**Hexachlorobenzene
HCB**

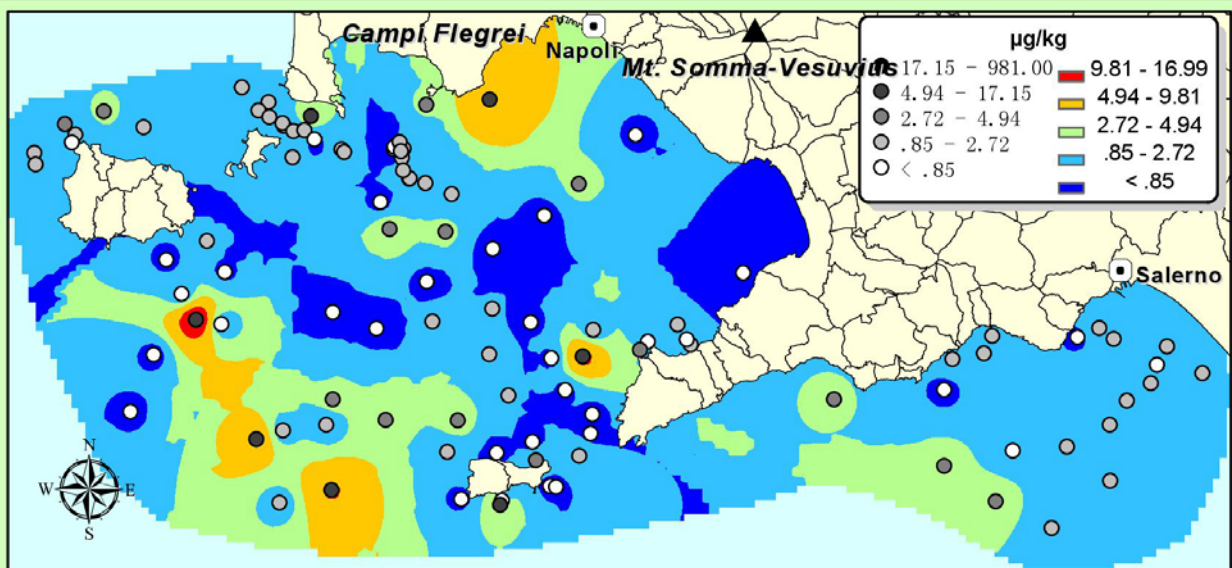


0 5 10Km

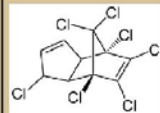


Hexachlorocyclohexane

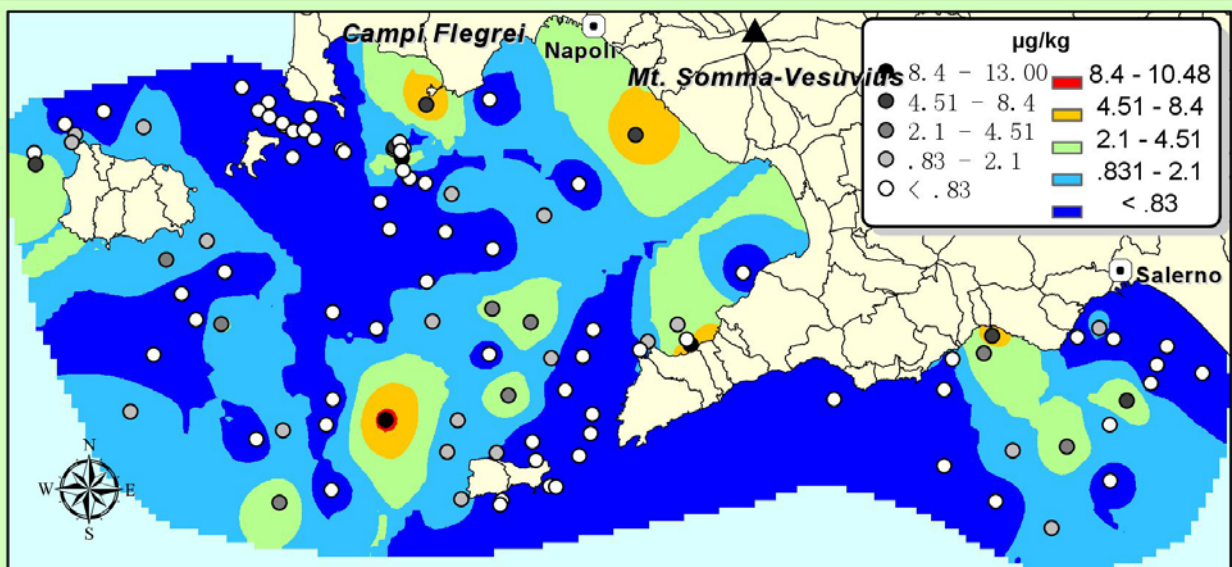
0 5 10Km



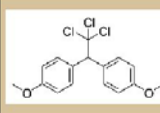
Heptachlor



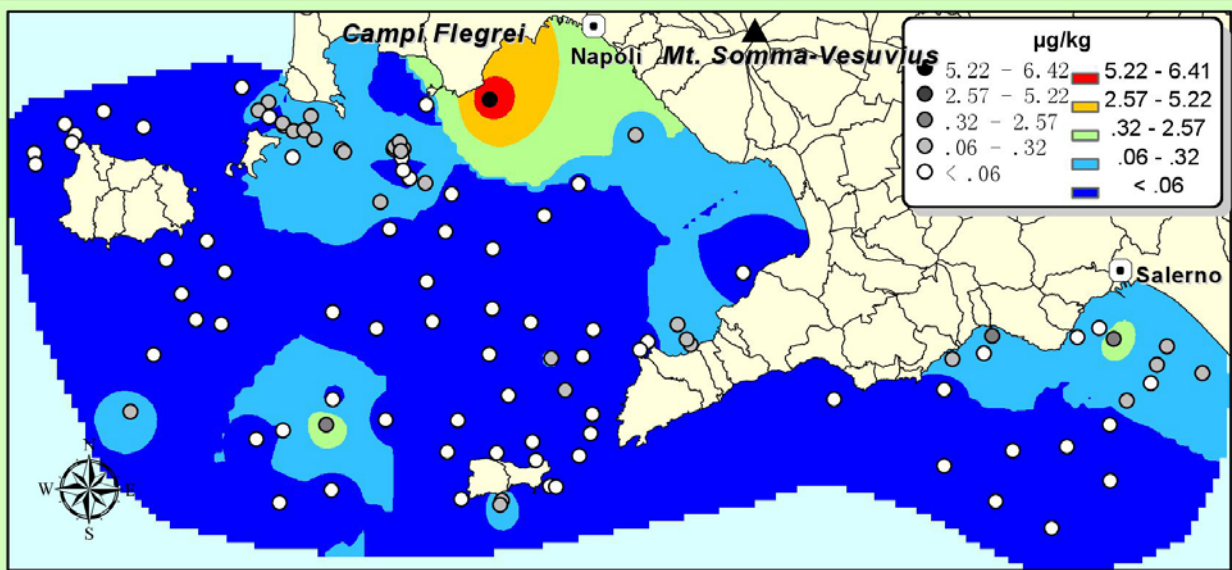
0 5 10Km



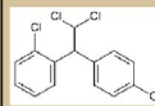
Methoxychlor



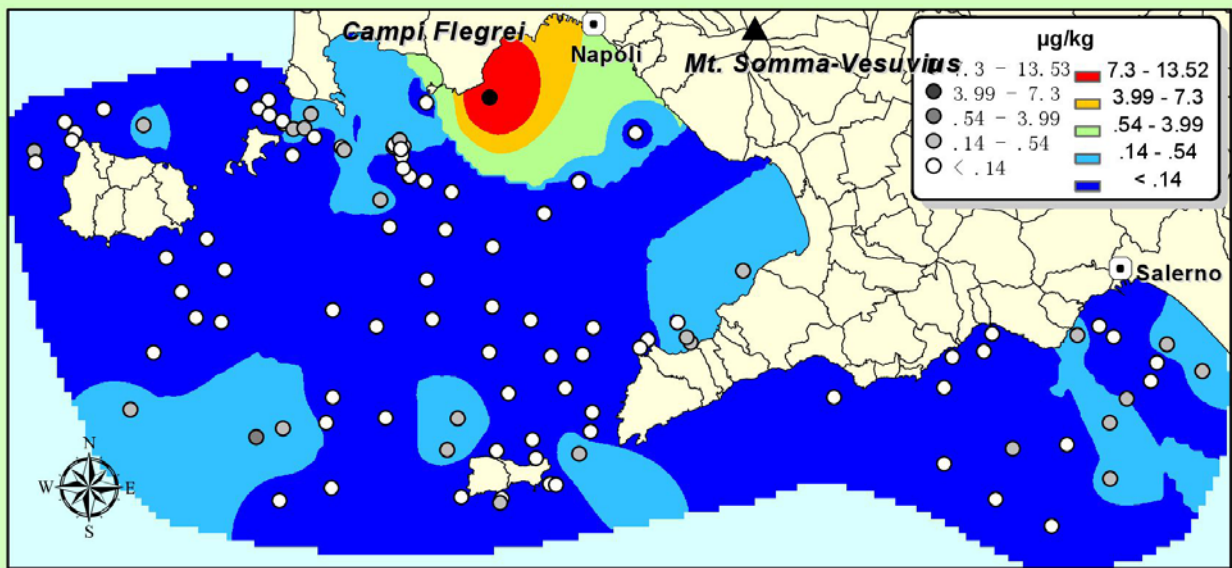
0 5 10Km



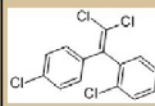
o,p'-Dichlorodipenyldichloroethane
o,p'-DDD



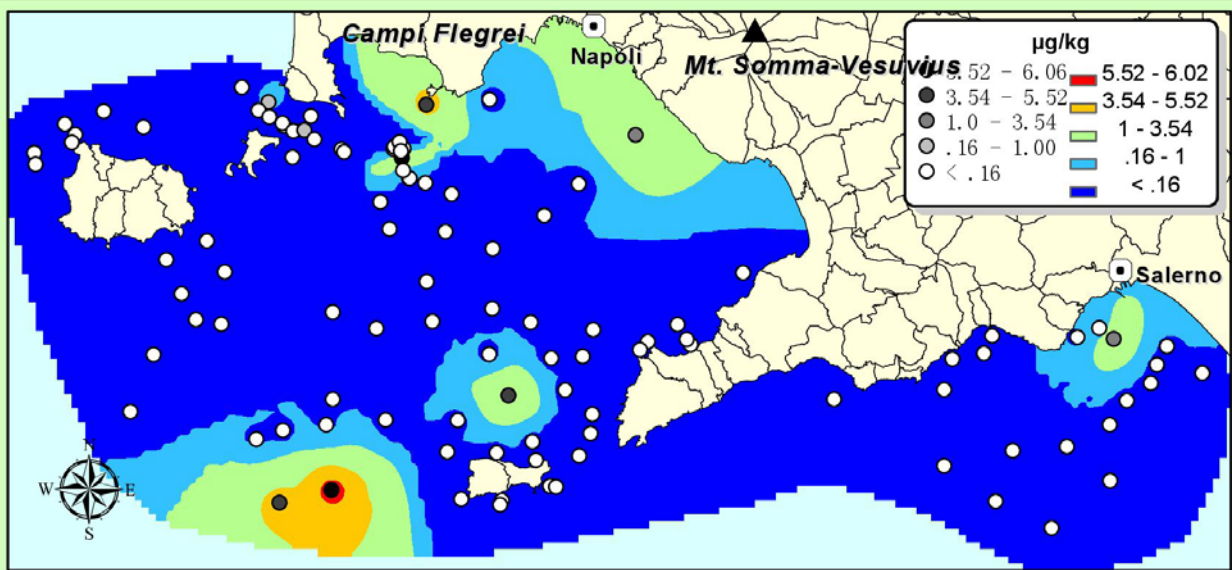
0 5 10Km



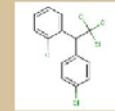
o,p'-Dichlorodipenyldichloroethylene
o,p'-DDE



0 5 10Km



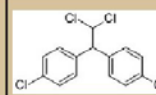
o,p'-Dichlorodiphenyltrichloroethane
o,p'-DDT



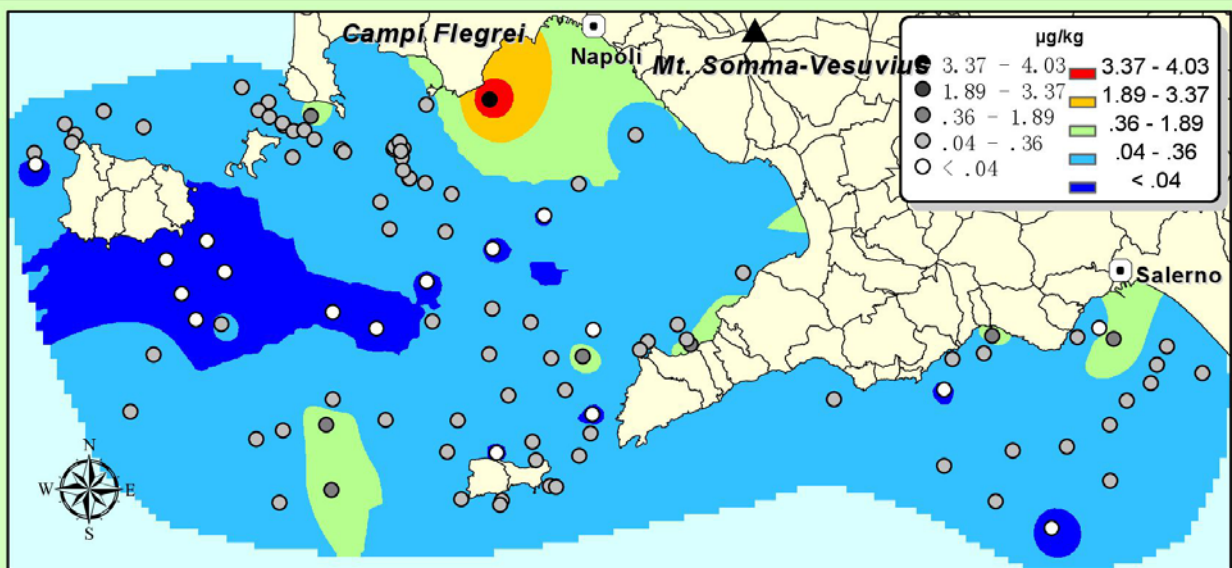
0 5 10Km



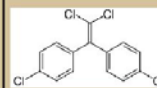
p,p'-Dichlorodiphenyldichloroethane
p,p'-DDD



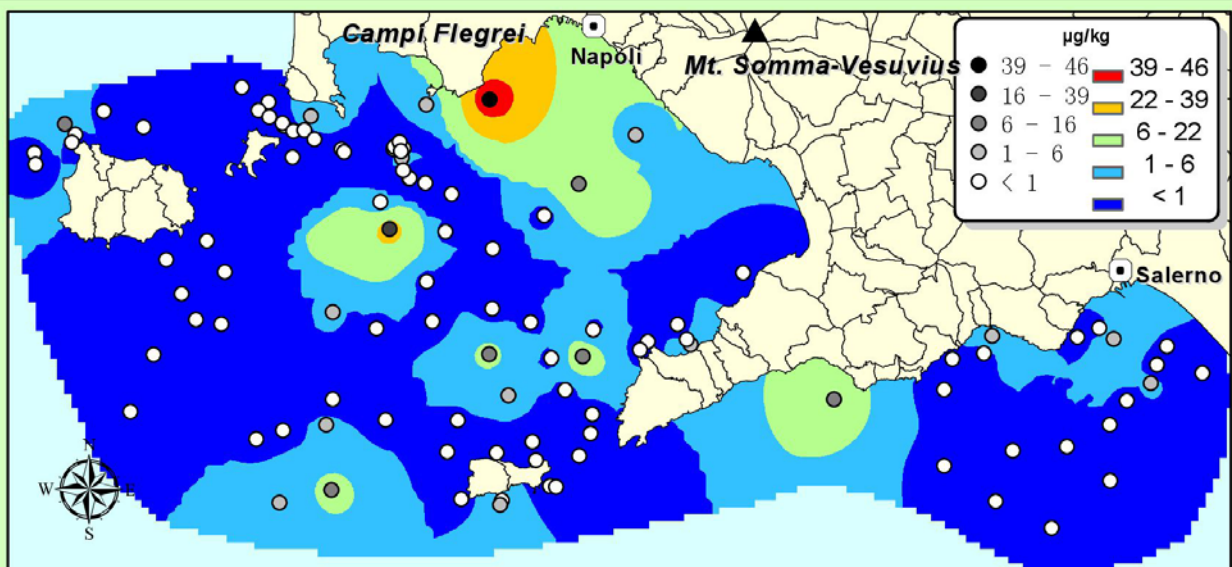
0 5 10Km



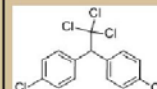
p,p'-Dichlorodipenyldichloroethylene
p,p'-DDE



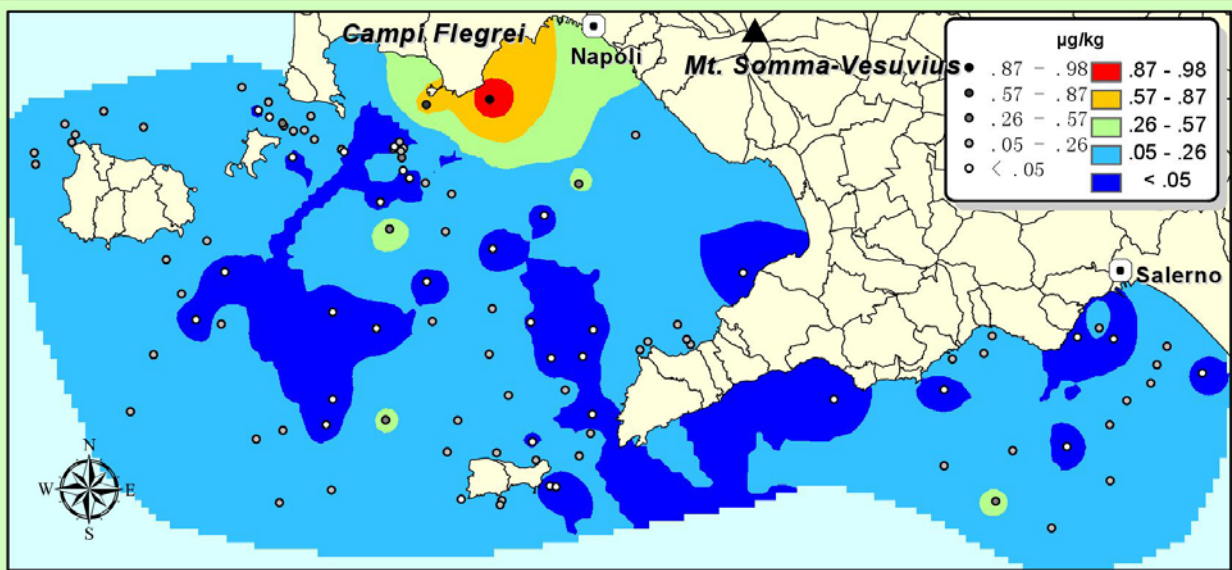
0 5 10Km



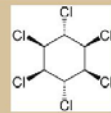
p,p'-Dichlorodiphenyltrichloroethane
p,p'-DDT



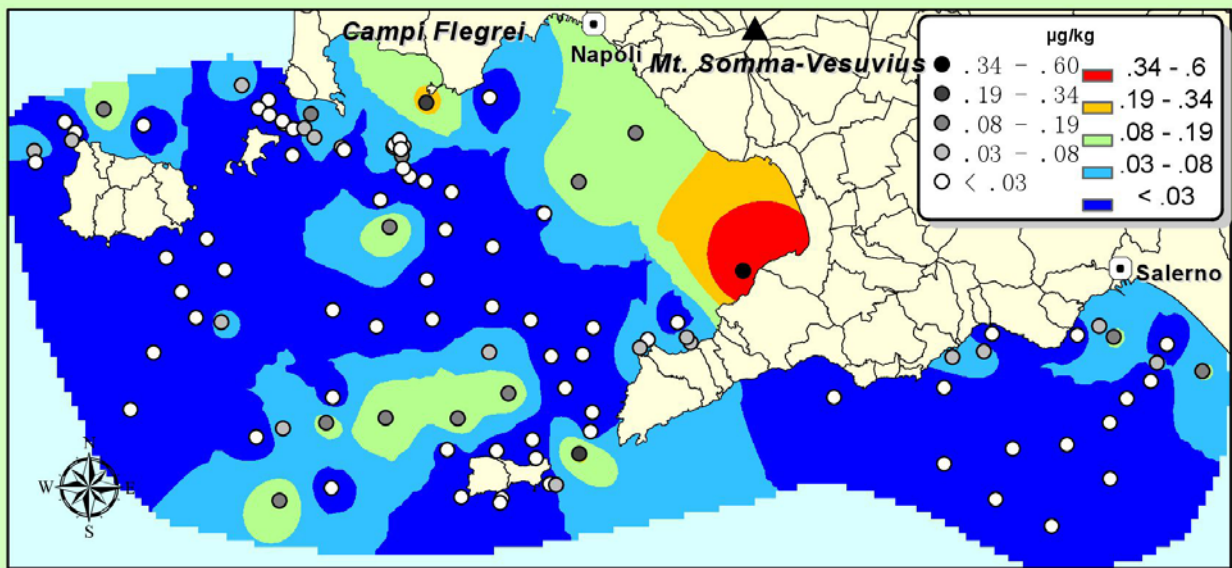
0 5 10Km



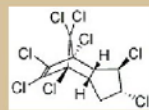
**gamma-Hexachlorocyclohexane
γ-HCH**



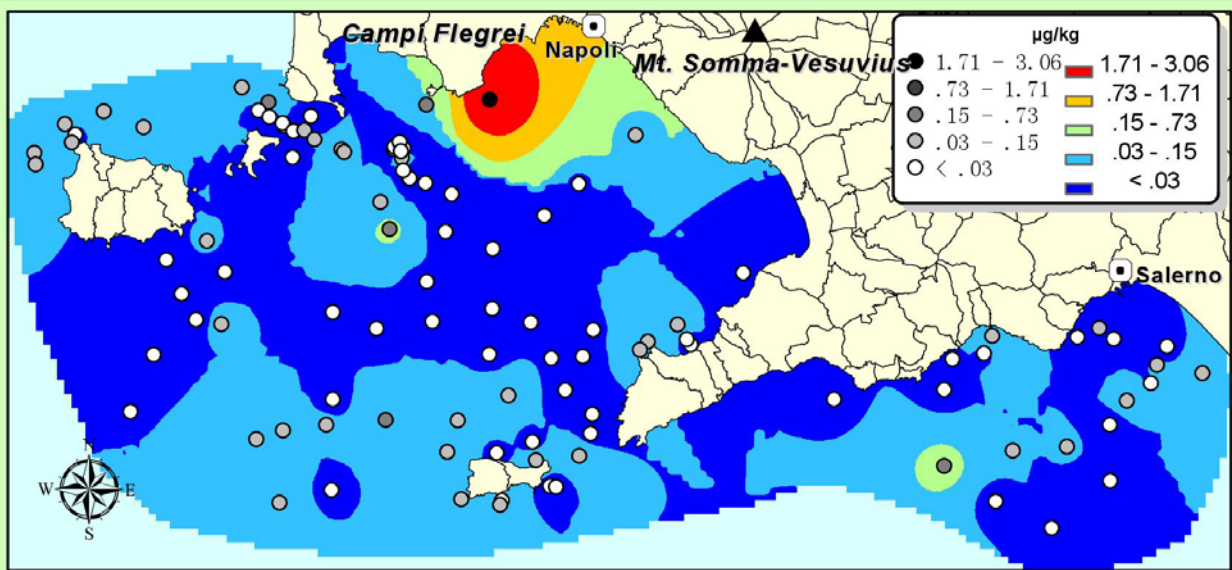
0 5 10Km



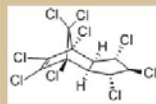
trans-Chlordane



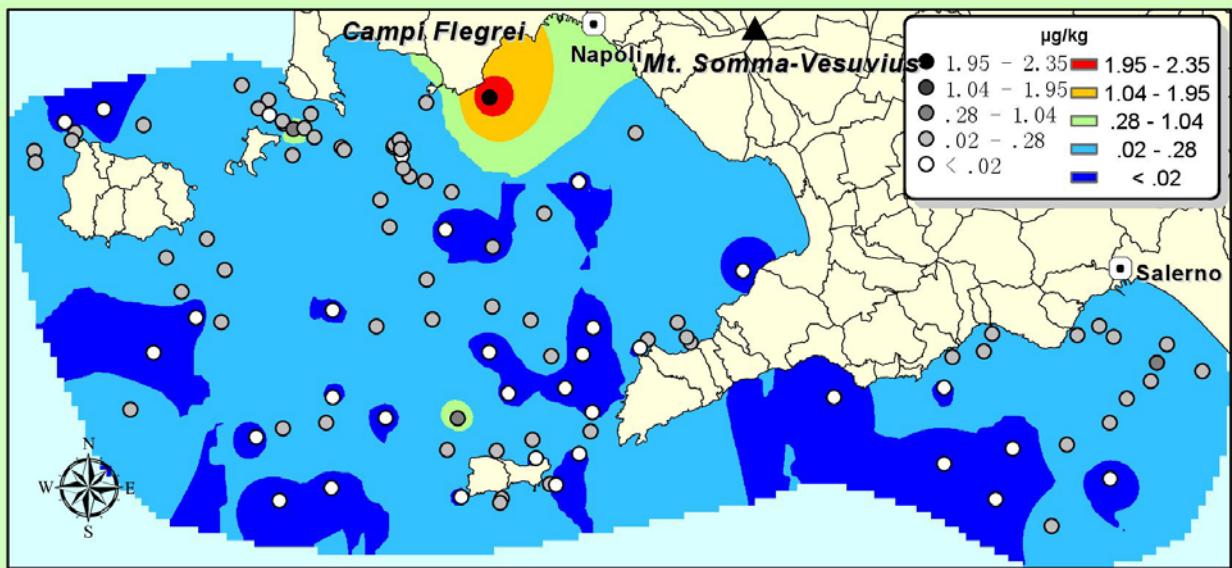
0 5 10Km



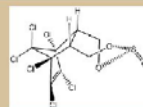
trans-Nonachlor



0 5 10Km



α-Endosulfan



0 5 10Km

